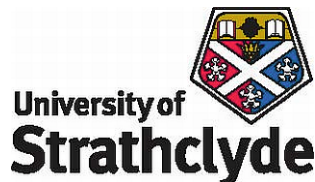


University of Strathclyde
Department of Naval Architecture & Marine
Engineering



Development of Physiological Motion Sickness Model
for the Contemporary Marine Vessels

by

Hassan Khalid

A thesis presented in fulfilment of the requirements for the degree of
Doctor of Philosophy

2010

This thesis is the result of the author's original research. It has been composed by the author and has not been previously submitted for examination which has led to the award of a degree.

The copyright of this thesis belongs to the author under the terms of the United Kingdom Copyright Acts as qualified by University of Strathclyde Regulation 3.50. Due acknowledgement must always be made of the use of any material contained in, or derived from, this thesis.

Signed: Hassan Khalid

Date: 23 September 2010

DEDICATION

This thesis is dedicated to Khalid, Nasim, and Saeed.

ACKNOWLEDGEMENT

Firstly I would like to express my cordial gratitude to Dr. Osman Turan for all the things that would require a volume thicker than this to enlist. I feel my vocabulary is not enough to articulate my feelings of gratefulness. Thank you very much for everything and for introducing me to the fascinating world of Human Factors.

I would also like to express my thankfulness to the researchers and staff of the Department for their assistance and friendships; especially, to Mr Iraklis Lazakis, Mr Rafet Emek Kurt and Mr Keith Lonsdale for helping me with the full scale trials.

I would also take this opportunity to express my heartiest appreciation to the anonymous ferry operator for not only allowing me to carry out field trials on their vessel, but also for providing me with all the, much needed, support.

I am deeply indebted to Samina, Abshar and Ozair, for making my life meaningful and the least of all, tolerating my physical and mental absence for seemingly countless years.

Last but not least, I must thank the National University of Science and Technology (Pakistan) for providing me the opportunity to pursue my PhD under their scholarship.

CONTENTS

CONTENTS	ii
LIST OF MAIN TEXT FIGURES	xi
LIST OF MAIN TEXT TABLES	xxi
ABSTRACT	xxiv
Chapter 1. INTRODUCTION	1
1.1 Chapter Overview	1
1.2 General Perspectives	1
1.3 Specific Issue	4
1.4 Layout	8
1.5 Chapter Summary	8
Chapter 2. RESEARCH QUESTION, AIMS, & OBJECTIVES OF THE PROJECT 9	
2.1 Chapter Overview	9
2.2 Research Question	9
2.3 Aims & Objectives	9
2.4 Chapter Summary	10
Chapter 3. LITERATURE REVIEW	11
3.1 Chapter Overview	11
3.2 Historical Backdrop	11
3.3 What is Motion Sickness?	13
3.4 Susceptibility to Motion Sickness	14
3.4.1 Gender	15
3.4.2 Age	16
3.4.3 Personal Traits	16

3.4.4	Sleep Deprivation.....	16
3.4.5	Psychological Features.....	16
3.4.6	Activity.....	17
3.4.7	Physiological Aspects	17
3.4.8	Temporal Aspects	18
3.5	Habituation	18
3.6	Brief Review of Motion Sickness Theories.....	20
3.6.1	Vestibular Overstimulation Theory	22
3.6.2	Sensory Conflict Theory	26
3.6.3	Reafference Principle.....	32
3.6.4	Neural Mismatch Hypothesis and Habituation / Adaptation	34
3.6.5	Weakness of Sensory Conflict Theory.....	37
3.6.6	Postural Instability Theory.....	39
3.6.7	Subjective Vertical Conflict (SV-Conflict) Theory	41
3.7	Existing Methods & Standards of Motion Sickness Prediction for Ships... 45	
3.7.1	O’Hanlon & McCauley’s (1974) MSI Method.....	46
3.7.2	McCauley et al. (1976) Method	49
3.7.3	ISO 2631-3:1985.....	55
3.7.4	Lawther & Griffin (1986, 1987 and 1988) Method	56
3.7.5	BS 6841:1987 and ISO 2631-1:1997	65
3.8	COMPASS Project and its Findings	68
3.8.1	Laboratory Tests in Motion Simulators	70
3.8.2	Development of Susceptibility and Motion Sickness Models	72
3.9	Effects of Motion Sickness on Crew Performance.....	75
3.10	Subjective Measures of Motion Sickness and Wellbeing	78
3.11	Research Gap.....	82

3.12	Chapter Summary	83
Chapter 4.	APPROACH ADOPTED.....	85
4.1	Overview of the Chapter	85
4.2	Mind Map of the Approach Adopted	85
4.3	Review of the Vestibular System and Its Models	86
4.4	Development of Theoretical & Mathematical Framework	86
4.5	Calibration and Validation of the Model.....	87
4.6	Field Trials for Further Validation of the Model.....	88
4.7	Comparison of the Motion Sickness Models	90
4.8	Chapter Summary	90
Chapter 5.	VESTIBULAR SYSTEM AND ITS MODELS	92
5.1	Overview of the Chapter	92
5.2	Role of Vestibular System in Motion Sickness Etiology	92
5.3	Human Inertial Guidance System–The Vestibular Apparatus	93
5.4	Morphology of Vestibular System	93
5.4.1	Anatomy of Vestibular Hair Cells.....	95
5.4.2	Anatomy of Semicircular Canals	96
5.4.3	Anatomy of Otolith Organs.....	98
5.5	Physiology and Biomechanics of Vestibular Organs	100
5.5.1	Physiology of Semicircular Canals	100
5.5.2	Biomechanics of Semicircular Canals	102
5.5.3	Velocity Storage Mechanism and Adaptation.....	117
5.5.4	Physiology of Otoliths	118
5.5.5	Biomechanics of Otoliths.....	120
5.6	Neural Processing of Vestibular Cues.....	132
5.7	Vestibular Response Models	136

5.7.1	Classical Model for Spatial Orientation.....	137
5.7.2	Optimal Models for VOR and Spatial Orientation	140
5.7.3	Vestibular-Visual Interaction Models	143
5.8	Internal Models and Observer Theory from Physiologic Perspectives	143
5.8.1	Physiologic ‘Internal Models’	144
5.8.2	Physiologic Observers.....	147
5.9	Oman’s Sensory Conflict Model for Motion Sickness.....	150
5.10	TNO’s Subjective Vertical Model for Motion Sickness	155
5.11	NAME’s Subjective Vertical Model for Motion Sickness.....	157
5.12	Other Physiological Models for Orientation / Motion Sickness	170
5.13	Chapter Summary	171
Chapter 6.	THEORETICAL AND MATHEMATICAL FRAMEWORK	173
6.1	Overview of the Chapter	173
6.2	Laboratory Studies – Pure Horizontal Oscillations’ Induced Sickness.....	173
6.2.1	Studies on Fore-and-Aft Oscillations.....	173
6.2.2	Studies on Lateral Oscillations	176
6.3	Anomalies of Existing SV-Conflict Models.....	178
6.4	Existing Solution of the (SV-Conflict) Model Anomalies	180
6.5	Proposed Solution of the (SV-Conflict) Model Anomalies	182
6.6	Hybrid Subjective Vertical Horizontal Conflict Model for Motion Sickness 183	
6.6.1	Orientation / Motion Perception Part.....	183
6.6.2	Emetic Part	191
6.7	Calculation of Frequency Weightings	197
6.8	Chapter Summary	199
Chapter 7.	CALIBRATION AND VALIDATION OF THE MODEL.....	201

7.1	Overview of the Chapter	201
7.2	Model Calibration and Validation Techniques.....	201
7.2.1	Typical Model Types	201
7.2.2	Calibration and Validation of Models for Engineering Processes	202
7.2.3	Calibration and Validation of Models for Natural Processes	203
7.3	Calibration Procedure for SVH-Conflict Model	205
7.4	Selection of Model Parameters.....	207
7.5	Statistical Testing of Model Fitness	208
7.5.1	Exact Binomial Test of Significance.....	210
7.5.2	Calculation of the Exact Binomial Test Significances (<i>p-values</i>)	211
7.5.3	Accounting for the ‘Multiple Hypotheses Testing’	212
7.6	Selection of Objective Function	213
7.7	Selection of Calibration Data	214
7.8	Estimation of Model Parameters	218
7.8.1	Available Field Trial Data.....	218
7.8.2	Selection of Parameter Values	222
7.8.3	Procedure used for the Parameter Estimation	224
7.8.4	Identification of the Optimised Parameter Values	233
7.9	Validation of SVH-Conflict Model.....	236
7.9.1	Step-1: Filtering of Motion Histories.....	237
7.9.2	Step-2: Calculation of Passenger Zone Motions.....	237
7.9.3	Step-3: Calculation of Motion Sickness Incidences.....	238
7.9.4	Step-4: Statistical Testing of Model Fitness to Individual Trial	238
7.9.5	Step-5: Statistical Testing of Model Fitness to all Validation Field Trials	241
7.10	Comparison with Other Models	242

7.10.1	Time Domain Calculation of Motion Sickness Incidences.....	243
7.10.2	Frequency Domain Calculation of Motion Sickness Incidences	243
7.10.3	Testing Statistical Fitness to Individual Trials.....	246
7.10.4	Testing Statistical Fitness to all Trials of the Considered Vessels.....	251
7.11	Chapter Summary	251
Chapter 8.	FIELD TRIALS FOR THE FURTHER VALIDATION.....	253
8.1	Overview of the Chapter	253
8.2	Full Scale Trials for the Further Validation of SVH-Conflict Model	253
8.2.1	Vessel Features Considered for the Field Trials	254
8.2.2	Brief Descriptions of the Vessels and Operation Area	256
8.3	Field Trial Procedure.....	258
8.3.1	Description of Survey Questionnaire.....	259
8.3.2	Details of Ferry MH-I Trial Procedure	265
8.3.3	Details of RHIB-J Trial Procedure.....	269
8.4	Summary of the Passenger Participation / Weather Condition / Vessel Motions.....	272
8.5	Analysis of the Field Trial Results Using SVH-Conflict Model.....	273
8.5.1	Step-1: Filtering of Motion Histories.....	274
8.5.2	Step-2: Calculation of Passenger Zone / Sitting Position Motions	276
8.5.3	Step-3: Calculation of Motion Sickness Incidences.....	277
8.5.4	Steop-4: Statistical Fitness Testing	277
8.6	Comparison with Other Models	278
8.6.1	Calculation of Motion Sickness Incidences	279
8.6.2	Statistical Fitness Testing.....	280
8.7	Statistical Analyses of MH-I Questionnaires	282
8.7.1	Summary Statistics – Frequency Tables	284

8.7.2	Cross Tabulations - Significant Dependencies	290
8.7.3	Cross Tabulation – Measures of Association.....	294
8.7.4	Measures of Association / Effects for the Dichotomous Variables ...	296
8.7.5	Measures of Association for the Nominal Variables	307
8.7.6	Measures of Association for the Ordinal Variables	310
8.8	Statistical Analyses of RHIB-J Questionnaires.....	313
8.8.1	Summary Statistics – Frequency Tables	314
8.8.2	Cross Tabulations - Significant Dependencies	318
8.9	Salient Observations of Statistical Analyses	318
8.10	Chapter Summary	319
Chapter 9. DISCUSSIONS & RECOMMENDATIONS FOR FUTURE RESEARCH 321		
9.1	Overview of the Chapter	321
9.2	A Brief Recap of the Thesis and Its Novelties	321
9.3	Contributions & Achievement of Research Objectives.....	324
9.3.1	Main Contributions	324
9.3.2	Further Contribution to Existing Knowledge.....	325
9.3.3	Research Objectives Achieved.....	326
9.4	Underlying Simplifications /Limitations of the Model	327
9.4.1	Modelling of the Limited Sense Modalities.....	327
9.4.2	Model being Partly Statistical	328
9.4.3	Usage of Observers	329
9.4.4	Consideration of Passive Motions Only.....	329
9.4.5	Layout of Emetic Brain.....	330
9.4.6	Consideration of Habituation	330
9.4.7	Limited Representation of Comfort	331

9.4.8	Frequency Response for Pure Horizontal Motions	332
9.4.9	Limited Improvement over the SV-Conflict Models	332
9.5	Recommendations for Future Research.....	333
9.6	Chapter Summary	335
Chapter 10.	CONCLUSIONS	336
10.1	Overview of the Chapter	336
10.2	Concluding Statements.....	336
	REFERENCES	338
Appendix A.	Data Pertaining to Calibration of SVH-Conflict Model.....	361
A.1	Raw and Filtered Motion Histories of WP-G	361
A.2	Trip-Wise Predicted Overall MSI for WP-G.....	369
A.3	Trip-Wise Exact Binomial Test P-Values for WP-G.....	381
A.4	Magnitude of the Objective Function for WP-G	394
Appendix B.	Data Pertaining to Validation of SVH-Conflict Model.....	412
B.1	Raw and Filtered Motion Histories.....	412
B.2	Passenger Zones Layout	436
B.3	Passenger Zones Position Vectors	438
Appendix C.	Data Pertaining to Further Validation of SVH-Conflict Model	441
C.1	Raw and Filtered Motion Histories of MH-I.....	441
C.2	Cross Tabulation – MH-I.....	443
C.3	Cross Tabulation – RHIB-J	480
Appendix D.	Details of Motion Reference Unit	483
D.1	Description of Motion Reference Unit (MRU).....	483
Appendix E.	Model Comparison	492
E.1	Overview of the Appendix.....	492

E.2	Individual Field Trial Based Comparison.....	492
E.3	Vessels-wise Comparison	498
E.4	Overall Comparison of the Motion Sickness Models.....	511
E.5	Summary.....	512

LIST OF MAIN TEXT FIGURES

Figure 1.1:Trends in passenger transportation;(A)by rail;(B)by private cars;(C)by bus and coach [EU: Europe; OECD: OECD member countries; ITF: ITF member countries], (OECD/ITF 2009)	1
Figure 1.2: Transport service index (TSI); land and air transportation (RITA/BTS 2009)	2
Figure 1.3: International passenger movement between UK and Europe: (solid line) short sea shipping; (dashed line) channel tunnels (Eurostar and Le Shuttle) transportation (Dft 2010)	3
Figure 3.1. Percentage of people vomiting (MSI%) over time for a population exposed to ship motions [Crossland 1998].	19
Figure 3.2. Percentage of race participants vomiting on one or more occasion during training and as function of race leg [Turner & Griffin 1995].	19
Figure 3.3. Conceptual model of factors possibly involved in causation of motion sickness [Griffin 1990].....	21
Figure 3.4. Illustrative model of the multiple pathways through which a motion environment is perceived: (a) for a driver of a car and (b) for a passenger in the same car reading a book [Mansfield 2004]	28
Figure 3.5. The basic structural components of the neural mismatch model [Reason 1978b]	34
Figure 3.6. Diagram illustrating the effects and after-effects of sensory rearrangement as predicted by the neural mismatch model. [Reason 1975].....	36
Figure 3.7. (A) Motion sickness incidence (%) after 2h of endured motion versus frequency and acceleration [O'Hanlon & McCauley 1974] (B) MSI (%) predicted using SV-Conflict model after 2h of vertical sinusoidal motion versus frequency and acceleration [Bos & Bles 1998].	44
Figure 3.8. MSI for combined sway (A: 0.5 ms^{-2} , B: 1.5ms^{-2}) and roll (A: 10° ; B: 2°) (Bos et al. 2002a)	45
Figure 3.9. Motion Sickness Incidence (within 2 hours) as a function of log average acceleration (\bar{a}) for each wave frequency (f) [O'Hanlon & McCauley, 1974].....	48

Figure 3.10. Empirically derived relationship of MSI (percent emesis within 2 hours) to wave frequency and average acceleration imparted during each half-wave cycle for vertical sinusoidal motion [O'Hanlon & McCauley, 1974].....	48
Figure 3.11. Incidence of vomiting associated with exposure to various magnitudes and frequencies of vertical oscillation [McCauley et al. (1976)].....	50
Figure 3.12. Motion sickness incidence variation with exposure time at the vertical oscillation frequency of 0.25Hz [McCauley et al. (1976)].	51
Figure 3.13. Mathematical model describing MSI(%) after 2 hours of endured motion versus frequency and acceleration [McCauley et al. (1976)].....	52
Figure 3.14. ISO 2631-3:1985 "Severe Discomfort Boundaries" [International Organisation for Standardization, 1985].....	56
Figure 3.15. Acceleration time histories for the six degrees of freedom motion of a ship [Griffin 1990].	57
Figure 3.16. Acceleration power spectral densities for the six degrees of freedom ship motions: frequency resolution 0.01Hz; duration 4hours [Griffin 1990].	58
Figure 3.17. (A) Acceleration effects of 20min exposure at four frequencies [Alexander et al. 1947] (B) Acceleration effects of 2hrs exposure at three frequencies [McCauley et al. 1976] (C) Acceleration effects of 2hrs exposures on board ships with dominant frequency around 0.2Hz [Lawther & Griffin 1988b] [adopted from Lawther & Griffin 1987].....	59
Figure 3.18. The effects of frequency on normalized vomiting incidence for 2h exposures [McCauley et al. 1976], with suggested asymptotic frequency weighting (solid lines) and approximate weightings using an analog/digital filter (dashed line) [adopted from Lawther & Griffin 1987].	60
Figure 3.19. The effects of motion dose, using results from Alexander et al. (1947), McCauley et al. (1976), and Lawther & Griffin (1986) [Lawther & Griffin 1987]. .	62
Figure 3.20. Vomiting incidence variations with weighted RMS acceleration magnitudes (A) Results from McCauley et al. (1976) (B) Results from Lawther & Griffin (1988b) [Lawther & Griffin 1987].....	62
Figure 3.21. W_f frequency weightings for the prediction of vomiting incidences on passenger ferries as defined by BS 6841:1987 [Mansfield (2004)]......	66

Figure 3.22. ISO 2631-1:1997 frequency weighting curve W_f (circles) and quasi-least square filter approximations: second order (dot), third order (dash), fourth order (solid), and fifth order (dash-dot) [Zuo & Nayfeh (2003)].	68
Figure 3.23. Asymptotic and realizable frequency weightings for lateral acceleration, derived from the normalized mild nausea incidence, compared with the weighting for vertical acceleration, W_f , as defined in BS 6841. All weightings are normalized such that their maximal values are 1.0. Asymptotic weighting = solid thick line; realizable weighting = dotted line; normalized mild nausea incidence: black triangles = points at which values differ significantly from static condition, open triangles = points at which values not significantly different from static condition; W_f = solid thin line [Donohew & Griffin, 2004].	72
Figure 3.24. Percentage crew (all ships) with fail factor of 0 and its inverse 1 variation with MISC. The dotted line is the best fit polynomial.	78
Figure 3.25. Relationship between average MSI and MISC as observed in 12 experimental studies at TNO (Bos 2004).	81
Figure 4.1. Mind map of the approach adopted	85
Figure 5.1. Overview of ear and vestibular system; 1 Pinna; 2 Auditory duct; 3 Ear drum; 4 Lateral canal ; 5 Posterior canal; 6 Anterior canal; 7 Cochlea; 8 Auditory nerve; 9 Eustachian tube [downloaded and adopted from www.bartleby.com].	94
Figure 5.2. The labyrinth and its innervations [Purves et al. 2004].	94
Figure 5.3. Morphological polarisation of vestibular hair cells [adopted from Perlmutter 2008].	95
Figure 5.4. Polarization of hair cells in sensory epithelium of semicircular canal ampullae, the utricular and saccular maculae [Purves et al. 2004].	96
Figure 5.5. (A) Schematic representation of the semicircular canals; (B) Enlarged view of ampulla and crista [adopted from Perlmutter 2008].	96
Figure 5.6. Arrangement of canals in pairs. The two horizontal canals form a pair; the right anterior canal and left posterior canal form a pair and vice versa [downloaded and adopted from scienceblogs.com].	97
Figure 5.7. Responses of lateral canals during head rotation in horizontal plane [adopted from Perlmutter 2008].	98

Figure 5.8. Cross section of utricular macula showing hair bundles projecting into gelatinous membrane when head is tilted [adopted from Perlmutter 2008].	99
Figure 5.9. Morphological polarization of hair cells in the utricular and saccular maculae [Purves et al. 2004].	100
Figure 5.10. Response of axon innervated to semicircular canal; A Rotational stimulus used; B Discharge rate of vestibular nerve axon innervating anterior canal of a squirrel monkey [adopted from Goldberg & Fernandez, 1971].....	101
Figure 5.11. Free-body diagram of a short section of endolymph within a semicircular canal showing pressure acting within the fluid and shear stresses acting tangent to the curved centreline of the duct. These stresses act on their respective areas to generate forces that accelerate or decelerate the endolymph in inertial space [Rabbitt et al. 2004].	102
Figure 5.12. Time response of lateral semicircular canal to unit step change of angular velocity.....	107
Figure 5.13. Bode diagram of lateral semicircular canal transfer function $(0.00071s/(s^2+166.7s+12.63))$ as per the hydrodynamic canal model of Rabbitt et al. 2004.....	108
Figure 5.14. Bode diagram of semicircular canal transfer function $(s/(s^2+76.97s+3.846))$ as per the hydrodynamic model of Steinhausen 1931; time constants as estimated by Mayne 1974.	109
Figure 5.15. Semicircular response to unit step acceleration; A Cupular / Endolymph volumetric displacement [Rabbitt et al. 2004]; B Endolymph angular displacement [Steinhausen 1931; Mayne 1974].....	111
Figure 5.16. Bode diagram of semicircular canal transfer function $[540s^2/(18s+1)(30s+1)]$ as per the subjective perception model of Ormsby & Young 1977.....	113
Figure 5.17. Bode diagram of semicircular canal transfer function $[(0.574s(s+100))/(s+0.1)(s+0.033)]$ as per the vestibular afferent model by Borah et al. 1988 also used by Elias et al. 2008 for modelling sensory conflict in artificial gravity.	114

Figure 5.18. Bode diagram of semicircular canal transfer function $[(80s/(1+80s))((1+0.049s)/(1+5.7s)(1+0.03s))]$ as per the electrophysiological recordings in squirrel monkey by Fernandez & Goldberg 1971.....	115
Figure 5.19. Bode diagram of afferent based semicircular canal transfer function $(s/(s+1/5.7))$ Merfeld et al. 1993 & Merfeld & Zupan 2002.....	116
Figure 5.20. Displacement of utricular otolithic membrane during upright, tilted and under translational acceleration conditions [adopted from Purves et al. 2004].	118
Figure 5.21. Response of vestibular nerve axon from utricular macula; A stimulating force-trapezoid; B discharge rate for excitatory force; C discharge rate for inhibitory force [after Fernandez & Goldberg 1976].....	120
Figure 5.22. Schematic layout of otolith organs [after Igarashi 1966].	121
Figure 5.23. Lumped-parameter model of otolith with free-body diagram of the otoconial layer showing the various forces acting on the layer [after Rabbitt et al. 2004].	122
Figure 5.24. Bode diagram of otolith transfer function $(0.631/(s^2+5.1s+0.5))$ as per the hydrodynamic otolith model of Rabbitt et al. 2004.	126
Figure 5.25. Time response of otoliths to: A unit step change of linear velocity; B unit step change of linear gravito-inertial acceleration.	126
Figure 5.26. Bode diagram: A regular unit B: irregular unit. (Gains: circle and solid curves; phases: squares and dashed curves; filled symbol: excitatory; open symbol: inhibitory sinusoids; curves: as fitted to transfer function) [Fernandez & Goldberg 1976c].....	128
Figure 5.27. Bode diagrams of otolith transfer function as per Raphan et al. (1996); A regular afferents; B irregular afferents.....	130
Figure 5.28. Bode diagrams comparing regular otolith afferents' transfer function suggested by Fernandez & Goldberg 1976c (solid lines), by a simpler transfer function (dashed line), and by a pure delay of 36 ms (dotted line) [Crane & Demer 1999].	131
Figure 5.29. Bode diagram for subjective tilt transfer function of otoliths as per Young 1969.....	132
Figure 5.30. Neural processing of complex stimuli: A motion stimuli; B net polarization of otolith hair bundles during motions; C instantaneous firing rate (IFR)	

of primary otolith afferent; D IFR of central vestibular nucleus neuron [Angelaki & Cullen 2008].....	135
Figure 5.31. Principal planes and reference axes of human body [downloaded and adapted from http://www.brianmac.co.uk/bodyaxis.jpg].....	137
Figure 5.32. 2D spatial orientation model by Mayne 1974.....	138
Figure 5.33. Optimal theory based vestibular response models: A schematic diagram of 3D VOR model by Merfeld; B schematic diagram of 3D orientation model by Glasauer [Glasauer & Merfeld 1997].....	141
Figure 5.34. A simple servomechanism to control body motions	144
Figure 5.35. Sub-division of internal models for sensory and motor processing [MacNeilage et al. 2008].....	146
Figure 5.36. Role of observer in a control system [Ellis 2002].	147
Figure 5.37. Traditional physiological observer model [MacNeilage et al. 2008]. .	148
Figure 5.38. Orientation brain model: A schematic diagram [Oman 1990]; B mathematical realization [Oman 1982].....	151
Figure 5.39. Emetic brain model: A schematic diagram; B mathematical realization [Oman 1990].	154
Figure 5.40. Spatial orientation and motion sickness model [Bos et al. 2008].....	156
Figure 5.41. Subjective vertical conflict model for six degrees of freedom ship motions [Ververiotis 2004].	158
Figure 5.42. Reference axes with respect to head (Π) & space (Σ) [Mayne 1969]..	159
Figure 5.43. Bode plot of estimated to actual GIA transfer function with $K_f = 5$ (solid line) and $K_f = 100$ (dashed line).	165
Figure 5.44. Bode plot of SV-conflict transfer function with $K_f = 5$ (solid line) and $K_f = 100$ (dashed line).....	166
Figure 5.45. Post processing of subjective vertical conflict into motion sickness incidence [Ververiotis 2004].	167
Figure 5.46. Hill function plot (solid line: $b = 2.5$, $n = 1$; dotted line: $b = 0.7$, $n = 2$).	168
Figure 6.1. Effect of frequency of fore-and-aft sinusoidal oscillation on motion sickness incidence for a 30-min exposure. Results are normalized by division of the raw incidence data by the peak acceleration. Data are from Golding and Markey,	

1996 (3.6 m/s ² peak acceleration, moderate nausea, -x-); Golding et al., 1997 (3.6 m/s ² peak acceleration, moderate nausea, -O-); Golding et al., 2001 (1 m/s ² peak acceleration, moderate nausea, -□-) and from Griffin and Mills, 2002 (0.5 m/s peak velocity, moderate nausea, —◇—) [Mansfield 2004].....	175
Figure 6.2. Effect of frequency of lateral sinusoidal oscillation on motion sickness incidence for a 30-min exposure. Results are normalized by division of the raw incidence data by the peak acceleration. Data are from Lobb, 2001 (1 m/s peak velocity at frequencies below 0.315 Hz, 0.5 m/s peak velocity at 0.315 Hz, mild nausea, -x-) and from Griffin and Mills, 2002a (0.5 m/s peak velocity, mild nausea -•-; moderate nausea, -O-) [Mansfield, 2004]	176
Figure 6.3. Asymptotic and realizable frequency weightings for lateral acceleration, derived from the normalized mild nausea incidence, compared with the weighting for vertical acceleration, W _f , as defined in BS 6841. All weightings are normalized such that their maximal values are 1.0. Asymptotic weighting = solid thick line; realizable weighting = dotted line; normalized mild nausea incidence: black triangles = points at which values differ significantly from static condition, open triangles = points at which values not significantly different from static condition; W _f = solid thin line [Donohew & Griffin, 2004].	177
Figure 6.4. Normalized orientation (dotted line) and magnitude (circles) differences of the subjective vertical conflict under the sinusoidal sway and heave oscillations, respectively	181
Figure 6.5. Schematic diagram of 'orientation / motion perception' part of the hybrid subjective vertical horizontal (SVH) conflict model of motion sickness.	184
Figure 6.6. Time responses of first order SCC neurons (solid green line) and VS-observer (dotted orange line) to a step angular velocity (dashed blue line).....	189
Figure 6.7. Frequency response of SH-conflict before (solid line) and after (dotted line) low pass filtering.....	194
Figure 6.8. Magnitudes of sensory conflicts for unit RMS accelerations (before the hill functions): SV-conflict (dashed line); SH-conflict (solid line)	194
Figure 6.9. Magnitudes of sensory conflicts for unit RMS accelerations (after the hill functions): SV-conflict (dashed line); SH-conflict (solid line).....	195

Figure 6.10. Schematic diagram of 'emetic brain' part of the hybrid subjective vertical horizontal (SVH) conflict model of motion sickness.....	196
Figure 6.11. Normalized frequency weighting for pure horizontal (lateral) oscillations (unit RMS accelerations); SVH-conflict model (solid line); SV-conflict model (diamonds); Donohew & Griffin [2004] (dotted line).	198
Figure 6.12. Normalized frequency weighting for pure vertical (heave) oscillations (unit RMS acceleration); SVH-conflict model (solid line); SV-conflict model (diamonds); Lawther & Griffin [1987] (dotted line).....	199
Figure 7.1. Flowchart showing the major steps of calibrating a model and using it to make predictions [Hill & Tiedeman 2007].	204
Figure 7.2. Schematic diagram of calibration procedure adopted for SVH-conflict model.....	206
Figure 7.3. Passenger zones of WP-G.....	217
Figure 7.4. Inertial (OXYZ) and body (Gxyz) frame of references for the vessel motions.....	219
Figure 7.5. Raw motion history of WP-G at MRU position during Trip-1; linear accelerations (A) longitudinal (B) lateral (C) vertical; angular velocities (D) roll (E) pitch (F) yaw.	224
Figure 7.6. Filtered motion history of WP-G at MRU position during Trip-1; linear accelerations (A) longitudinal (B) lateral (C) vertical; angular velocities (D) roll (E) pitch (F) yaw.	225
Figure 7.7. Motion history of WP-G during Trip-1 at MRU; linear accelerations (A) longitudinal (B) lateral (C) vertical; angular velocities (D) roll (E) pitch (F) yaw; and Zone-A; linear accelerations (G) longitudinal (H) lateral (I) vertical.....	227
Figure 7.8. Predict MSI for zone A during the WP-G Trip-1 ($K_h = 1/2$, $b_{CH} = 1.5$, $n_{CH} = 2.0$); (A) simple sum (B) Pythagoras approach.	228
Figure 7.9. (A) Minimum χ^2 and (B) maximum overall P-value variations with K_h for WP-G.	234
Figure 7.10. Schematic diagram of ISO 2631-1:1997/BS 6841:1987 time domain implementation.....	243

Figure 7.11. Linear acceleration PSDs of WP-G at MRU position during Trip-1; non-weighted (A) longitudinal (B) lateral (C) vertical; weighted (D) longitudinal (E) lateral (F) vertical;.....	244
Figure 8.1. Rigid Hull Inflatable Boat: (A) layout (B) hullform.	257
Figure 8.2. Field trial area of RHIB [map downloaded from http://maps.google.com/maps].	258
Figure 8.3. Passenger comfort survey questionnaire.	261
Figure 8.4. MRU installation arrangement aboard Ferry-I: (A) installation details (B) powering & connection details.....	267
Figure 8.5. MRU installation arrangement aboard RHIB: (A) installation details; (B) seating arrangements.	270
Figure 8.6. Questionnaire used onboard RHIB: (A) during and (B) after the trial..	271
Figure 8.7. Motion history (upper-row; lower-filtered) of MH-I at MRU position during Trip-1; linear accelerations (A) longitudinal (B) lateral (C) vertical; angular velocities (D) roll (E) pitch (F) yaw.....	274
Figure 8.8. Motion history (upper-row; lower-filtered) of RHIB-J at MRU position during Trip-1; linear accelerations (A) longitudinal (B) lateral (C) vertical; angular velocities (D) roll (E) pitch (F) yaw.....	275
Figure 8.9. Passenger zones layout of MH-I.....	276
Figure 8.10: Frequency statistics of Q1	284
Figure 8.11: Frequency statistics of Q2	284
Figure 8.12: Frequency statistics of Q3	284
Figure 8.13: Frequency statistics of Q4	285
Figure 8.14: Frequency statistics of Q5	286
Figure 8.15: Frequency statistics of Q6	286
Figure 8.16: Frequency statistics of Q7	287
Figure 8.17: Frequency statistics of Q8	287
Figure 8.18: Frequency statistics of Q9	287
Figure 8.19: Frequency statistics of Q10	288
Figure 8.20: Frequency statistics of Q11	288
Figure 8.21: Frequency statistics of Q12 and 13	289
Figure 8.22: Frequency statistics of Q14	289

Figure 8.23: Frequency statistics of Q15	290
Figure 8.24: Frequency statistics of Q16 to Q19	290
Figure 8.25: Frequency statistics of Q2 and Q3.....	314
Figure 8.26: Frequency statistics of Q4	315
Figure 8.27: Frequency statistics of Q5	315
Figure 8.28: Frequency statistics of Q6 & Q7	316
Figure 8.29: Frequency statistics of Q8	316
Figure 8.30: Frequency statistics of Q9	317
Figure 8.31: Frequency statistics of Q10 & Q11	317

LIST OF MAIN TEXT TABLES

Table 3.1: Categories & types of sensory conflict along with some examples of various provocative stimuli (adapted from Griffin, 1990; 1991).....	30
Table 3.2: Characteristic parameters describing the susceptibility according to Equation(3.17), based on the observed illness ratings ($0 \leq IR \leq 3$) for different groups of passengers (Bos et al. 2007).	73
Table 3.3: COMPASS seasickness model parameters (Pescetto 2006).....	75
Table 3.4. Misery Scale (MISC) (Bos et al. 2005).....	80
Table 5.1. Model parameters for lateral canals in humans [Rabbitt et al.(2004)]....	107
Table 5.2. Median parameters of otolith transfer function-Fernandez & Goldberg (1976c)	129
Table 5.3: Transfer functions and other parameters of NAME's SV-conflict model	169
Table 6.1. Hill function and leaking integrator parameters.	197
Table 7.1: Summary of field trials used for the model calibration and subsequent validation.....	216
Table 7.2: Summary of full scale field trials for WP-G.....	217
Table 7.3: Values of unknown parameters considered for searches.	223
Table 7.4: Relative position vectors \mathbf{r} (meters) of WP-G's passenger zones.	227
Table 7.5: Overall MSI (simple sum), for the various combinations of hill function shape parameters and $K_h = 1$, during the WP-G Trip-1.	229
Table 7.6: Overall MSI (Pythagoras-type approach), for the various combinations of hill function shape parameters and $K_h = 1$, during the WP-G Trip-1.	229
Table 7.7: Exact binomial test <i>p-values</i> for the predicted overall MSIs (simple sum), under various combinations of hill function shape parameters and $K_h = 1$, for the WP-G Trip-1.	230
Table 7.8: Exact binomial test <i>p-values</i> for the predicted overall MSIs (Pythagoras-type approach), under various combinations of hill function shape parameters and $K_h = 1$, for the WP-G Trip-1.	231
Table 7.9: Magnitude of the objective function for $K_h=1$, while the total MSI being calculated as simple sum (minimum value in bold).....	232

Table 7.10: Magnitude of the objective function for $K_h=1$, while the total MSI being calculated using Pythagoras-type approach (minimum value in bold).....	233
Table 7.11: Minimum values of the objective function for the various considered values of feedback gain (K_h) and the associated magnitudes of the hill function shape parameters.	234
Table 7.12: Optimised combinations of SVH-conflict model parameters for the Pythagoras-type approach.	235
Table 7.13: Overall Chi-statistics and P-values for the optimum combinations of model parameters (see Table 7.12).	236
Table 7.14: Observed and predicted MSIs along with the exact binomial test <i>p-values</i>	239
Table 7.15: Chi-square goodness-of-fit test result for SVH-conflict model.....	241
Table 7.16: Predicted and observed MSI along with the exact binomial test <i>p-values</i>	247
Table 7.17: Model-wise chi-square goodness-of-fit results – validation vessels (including WP-G).....	251
Table 8.1: Approximate particulars of the vessels used for further validation field trials.....	257
Table 8.2: Online weather forecast resources.	266
Table 8.3: Summary of the field trial weather conditions and reply rates.	272
Table 8.4: Summary of the RMS translational accelerations and rotational velocities (averaged over passenger zone / seating position) of MH-I and RHIB-J.	273
Table 8.5: Relative position vectors \mathbf{r} (meters) of passenger zones (aboard Ferry-I) and sitting positions (aboard RHIB-J).	276
Table 8.6: Observed MSI and the exact binomial test <i>p-values</i> for MH-I and RHIB-J	278
Table 8.7: Chi-square goodness-of-fit test result for SVH-conflict model.....	278
Table 8.8: Motion sickness calculation models/methods used for comparison with SVH-conflict model	279
Table 8.9: Predicted and observed MSI along with the exact binomial test <i>p-values</i>	280

Table 8.10: Model-wise chi-square goodness-of-fit results – vessels enlisted in Table 8.1.....	281
Table 8.11: Type and categories of statistical data.	282
Table 8.12: Binning of continuous variables	283
Table 8.13: Significant dependencies amongst comfort survey queries based on FDR approach with $q=0.05$ (orange cells represent significant interactions)	293
Table 8.14: Measures of association for cross tabulation (Garson 2008b).....	294
Table 8.15: Measures of association selected for assessing the strength and direction of significant dependencies of survey questionnaires	295
Table 8.16: Measures of association (percent differences) for dichotomous variables (red cells: $\%d > +1\%$; blue: $\%d < -1\%$; green: $-1\% < \%d < +1\%$).....	299
Table 8.17: Measures of association (Goodman-Kruskal Tau) for the nominal variables	308
Table 8.18: Measures of association (Goodman-Kruskal Gamma) for the ordinal variables	310

ABSTRACT

Developing on sensory conflict theory (Reason & Brand 1975) and the heuristic model (Oman 1982), Bles et al.(1998) proposed the subjective vertical (SV-conflict) theory of motion sickness. They postulated that motion sickness is elicited in all situations that lead to a difference between the sensed and subjective verticals. Sensed vertical is Earth's gravity as perceived by the human's sense modalities, while subjective vertical is also Earth's gravity but in accordance with the 'expectations' of central nervous system based on past interactions with spatial environment. This theory radically simplifies the original sensory conflict theory and gives the heuristic model a pragmatic approach. The motion sickness models developed under the SV-conflict theory, have successfully been used by Bos & Bles (2000), Ververiotis & Turan (2002b), Bos et al. (2002a) and Dallinga et al. (2002) to predict seasickness incidences aboard high speed passenger ferries. A recent EU project COMPASS (Turan 2006), indicated that the role of horizontal accelerations in the elicitation of motion sickness on board contemporary vessels is stronger than perceived before.

After defining an alternate statement of the SV-conflict theory, this research project is proposing a further elaboration of a physiological model for predicting seasickness by explicitly incorporating the effects of horizontal accelerations (normal to gravity) experienced aboard contemporary vessels. It is hypothesised that explanation of motion sickness variability may be improved by considering the combined effects of the subjective vertical and subjective horizontal conflicts. The later, alike SV-conflict is defined as the difference between sensed and 'expected' horizontal accelerations. A 'hybrid subjective vertical-horizontal (SVH) conflict' model is successfully developed and applied to 68 field trials of 10 different vessels. The percent commuters getting seasick (i.e. motion sickness incidences, MSIs), recorded during the field trials, are statistically compared with the values predicted by the physiologic (SVH and SV) as well as the existing prominent descriptive sickness prediction models. In general, SVH-conflict model is outperforming the regression-based models and displaying reasonable improvement over the SV-conflict model.

Chapter 1. INTRODUCTION

1.1 Chapter Overview

This chapter briefly presents the general (§1.2) and specific (§1.3) background reasoning for the initiation and pursuance of this research work. It concludes by outlining the layout (§1.4) of this writing to improve its readability.

1.2 General Perspectives

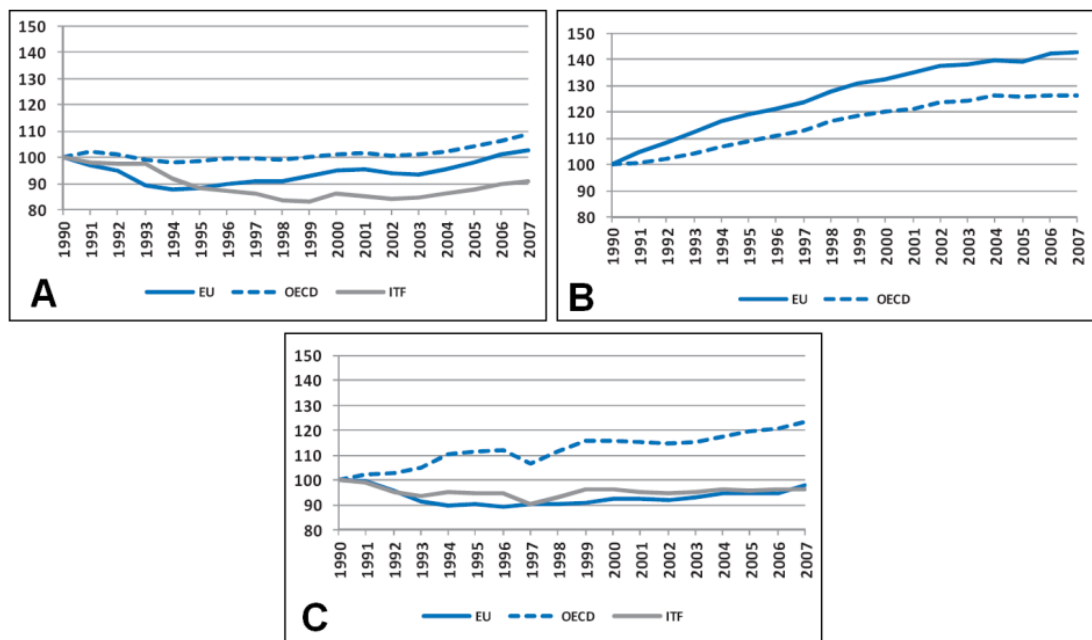


Figure 1.1: Trends in passenger transportation; (A) by rail; (B) by private cars; (C) by bus and coach [EU: Europe; OECD: OECD member countries; ITF: ITF member countries], (OECD/ITF 2009)

Over the past few decades, the economic globalisation has led to an increase in the world transportation activities (Janelle & Beuthe 2002). This worldwide increase in the people-travelling can be seen in the statistics (based on passenger-kilometres) shown in Figure 1.1, for the various modes of land transportation. These transportation statistics were jointly prepared by the Organisation for Economic Co-operation & Development (OECD) and the International Transport Forum (ITF)

(OECD/ITF 2009). The transportation data pertains to the years between 1990 and 2007 (inclusive) with the 1990 transport level treated as the datum (=100).

A similar rising trend could be seen in the TSI (Transport Service Index) statistics depicted in Figure 1.2, which represent the passenger-miles / number of passenger travelling in a given month using the land as well as air means of transportation. These statistics are estimated by the USA Research and Innovative Technology Administration (RITA) and the Bureau of Transport Statistics (BTS) on monthly basis (RITA/BTS 2009). The indexes shown are for the years starting Jan 1990 till December 2009 (inclusive); the TSI of year 2000 is used as the datum (=100) level.

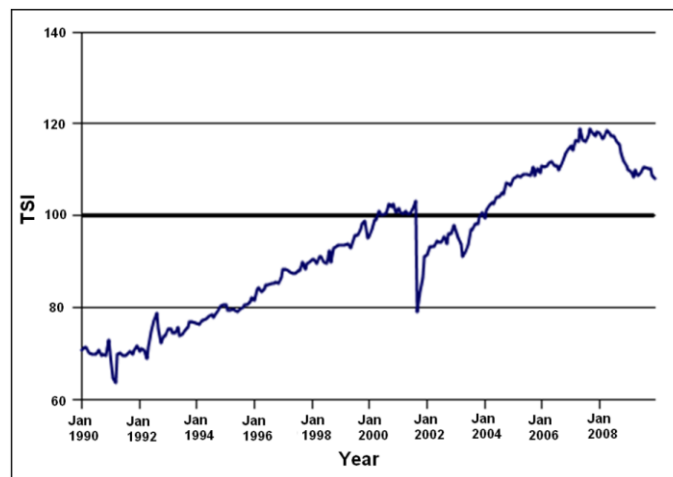


Figure 1.2: Transport service index (TSI); land and air transportation (RITA/BTS 2009)

In addition to the economic globalisation, the regional freedom of movement statutes like the recent EU legislation allowing the citizens of member states to freely move and reside in any member state (EC 2004) have further boosted the public transportation activities. These commuting activities are likely to increase in the foreseeable future, leading to a natural competition between the various modes of travel.

An example of the land transportation competing with the sea mode of travel can be observed from Figure 1.3. This figure is depicting the transport statistics of the passengers travelling from UK to other European countries using either the short sea

shipping (passenger ferries) or the channel tunnels (Eurostar and Le Shuttle ; using cars, busses, coaches etc.). According to the Department for Transport (Dft) UK, “Since 1997, there has been downward trend in (short sea) passenger journeys with only 2002 and 2007 experiencing growth” (Dft 2010). As such the cost of travelling is almost half on the passenger ferries as compared to Le Shuttle, however, with some extra journey time (almost an hour). Given the aforesaid, the decline in short sea passenger transportation in this sea-link may partly be attributed to the perceived / actual discomfort associated with a ferry travel.

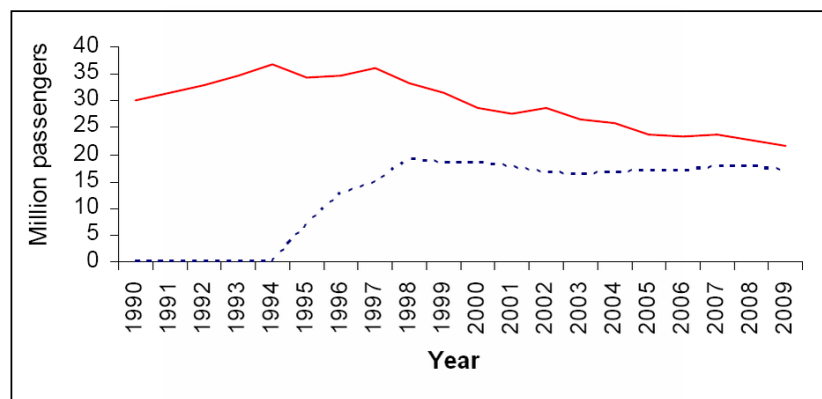


Figure 1.3: International passenger movement between UK and Europe: (solid line) short sea shipping; (dashed line) channel tunnels (Eurostar and Le Shuttle) transportation (Dft 2010)

The ever increasing commuter expectations of high travel-comfort, in conjunction with the abovementioned stimuli, have pressurised the ship designers and builders to provide commuting means that should be economical, fast and above all ‘comfortable’. In this regard, classification societies have played very effective role in providing detailed guidance and ensuring their implementation to achieve high levels of onboard ergonomic standards (lighting, noise, vibration, air quality etc.). Consequently, seasickness remains the primary, if not the only, source of nuisance for sea travel. This is the reason, motion sickness is considered to be one of the most important design criteria for passenger vessels (Dallinga et al. 2002; Sariöz & Sariöz 2005; Turan 2006; Arribas & Pineiro 2007) and is a growing concern of world navies (Stevens & Parsons 2002; McCauley et al. 2007; Colwell et al. 2008).

1.3 Specific Issue

Motion sickness is not a medical or pathological condition; rather it is the natural and very much normal response of a wide range of animal species' physiological systems, including that of humans, towards the non-volitional, real or virtual, motions. Its persistence may ultimately require treatment for dehydration and counselling regarding the loss of will to survive, but in itself it is not as fatal as the acute sufferer might wish it to be. Until the end of 18th century this issue was restricted to sailors, animal (camels) and animal fetched coach riders; however, the rapid growth of the modes of transportation since the beginning of 19th century has multiplied the situations where a person could experience motion sickness. Moreover, the increased affordability of travel by the multitude of vehicle types has given a significant boost to the incidences of travel sicknesses.

Despite having a primeval nature, the theoretical and practical understanding of motion sickness causation has still not been fully matured and research continues to improve knowledge base on this otherwise commonly encountered issue. Alike any other scientific discipline of similar abstraction, the focus of research on motion sickness has found two (fundamentally) different directions. One approach attempts to understand and model the underlying physiological mechanism responsible for the elicitation of sickness symptoms(Irwin 1881; Reynolds 1884; Quix 1922; Brooks 1939; Tyler & Bard 1949; de Wit 1953; Reason 1969; Money 1970; Reason 1970; Dobie 1974; Reason & Brand 1975; Oman 1978; Reason 1978b; Oman 1982; 1990; Bles et al. 1998; Bos & Bles 1998b; Oman 1998; Benson 1999; Bos & Bles 2002; Verveniotis & Turan 2002a; Verveniotis & Turan 2002b; Turan et al. 2003; Verveniotis 2004; Bos et al. 2008).

The other school of thought focuses on the development of descriptive statistical models capable of predicting proportion of people likely to suffer sickness symptoms under given (mostly passive) motion environments(Alexander et al. 1945a; 1945c; 1945b; 1945d; O'Hanlon & McCauley 1974; McCauley et al. 1976; Lawther & Griffin 1986; 1987; 1988b; Griffin 1990; Golding & Kerguelen 1992; Golding et al.

1995; Golding & Markey 1996; Golding et al. 1997; Golding et al. 2001; Lobb 2001; Matsangas 2004; Turan et al. 2005).

Although Alexander et al. (1945a; 1945c; 1945b; 1945d) carried out a number of laboratory experiments, but those by O'Hanlon & McCauley (1974) and McCauley et al. (1976) were the first ever systematic endeavours to establish the role of amplitude and frequencies of pure (sinusoidal) vertical motions onto the occurrence of motion sickness. They exposed over 500 young college male students to vertical sinusoidal motions with twenty-five combinations of ten frequencies (from 0.083 to 0.7Hz) and various (RMS) magnitudes (from 0.27 to 5.5 m/s²). They were able to define mathematical models capable of predicting proportion of people vomiting (termed as Motion Sickness Incidence, MSI) under pure sinusoidal vertical motions of known magnitudes (accelerations) and frequencies. McCauley et al.(1976) also studied the effects of roll and pitch oscillations in isolation as well as in combination with the vertical motions. However, they did not find any considerable effects of the rotational motions (roll and pitch) onto the elicitation of motion sickness.

Later on, Lawther & Griffin(1986; 1988a) carried out field trials aboard six monohull, two hovercraft and one hydrofoil vessel operating around the British Isles. They recorded almost 300 hours of six degrees of freedom vessel motions in 114 voyages ranging from half an hour to six hours duration. By integrating the laboratory experiment studies undertaken at the Wesleyan University (Alexander et al. 1945a; 1945c; 1945b; 1945d), the Human Factors Research Incorporation, HFRI, (O'Hanlon & McCauley 1974; McCauley et al. 1976) and their own field trials, they proposed yet another descriptive approach for the prediction of vomiting incidences using vertical motions of monohull vessels(Lawther & Griffin 1987). Their work eventually determined the sole standards (BS 6841:1987(BSI 1987) and ISO 2631-1:1997(ISO 1997)) of marine industry for predicting comfort qualities of any vessels regarding seasickness.

The descriptive approach offers many advantages from simplicity and a practical application view point. Yet it remains scarce on explaining the underlying

mechanism responsible for the elicitation of sickness symptoms. As Lawther & Griffin(1987) put it “The mathematical descriptions of the effects of the variables are not intended to reflect the underlying mechanisms that cause motion sickness, but are merely a pragmatic approach to a problem with a clearly defined scope”.

On the other end of the spectrum, the most comprehensive theory of motion sickness relying on the morphology and physiology of human’s motion sensors is the ‘sensory conflict’ theory. Although, originated and refined over a long period of time(Irwin 1881; Quix 1922; Brooks 1939; Tyler & Bard 1949; de Wit 1953; Reason 1969; Money 1970; Reason 1970; Dobie 1974; Reason & Brand 1975; Oman 1978; Reason 1978b), Reason(Reason & Brand 1975) may rightly be considered as the reformer of modern version of this theory. The essence of this theory is summarised by Wertheim(1998) as: “The labyrinthine receptors provide the brain with information about self motions that is incongruent with the sensations of motion generated by other sensory systems such as visual or proprioceptive (somatic) systems and / or the information does not match with what is expected from previous transaction with the motion environment.”

Sensory conflict theory is very successful in identifying the sickness provocative environments, but suffers one fundamental drawback – being ‘qualitative’ in nature, it cannot translate the cause into proportion of people likely to suffer sickness(Griffin 1990). Oman(1982) tried addressing this issue by integrating the physiological aspects of the theory with optimal control engineering. He proposed using ‘observers’ to replicate the functional features of ‘neural mismatch hypothesis’(Reason 1978b), for predicting the ‘expected’ sense modalities using recent transaction with the spatial environment. This concept forms the cornerstone of all pragmatic physiological models of motion sickness. However, a mathematical description of the human sensory system ascribed by Oman(1982) remains unsorted.

Simplifying the large set of possible sensory conflicts professed by ‘sensory conflict’ theory and developing on the heuristic model of Oman(1982), Bos & Bles(Bles et al. 1998; Bos & Bles 1998a; 1998b; 2002) postulated their ‘subjective vertical’ theory of motion sickness. Effectively, they restated the “neural mismatch

hypothesis”(Reason 1978b) that formed the basis of Oman’s(1982) heuristic model. They redefined these theories as: “All situations which provoke motion sickness are characterised by a condition in which the ‘sensed vertical’(sensed gravity) as determined on the basis of integrated information from the eyes, the vestibular system and the non-vestibular proprioceptors is at variance with the ‘subjective vertical’ (expected gravity) as predicted on the basis of previous experience.”(Bles et al. 1998)

Using the ‘subjective vertical’ theory, Verveniotis & Turan (2002a; 2002b; Turan et al. 2003) developed their version of SV-conflict model of motion sickness involving the vestibular system only. They used their model to successfully predict motion sickness observed (through passenger survey) aboard high speed crafts (a catamaran and a Deep-V monohull), using the relevant motion histories of the vessels(Verveniotis 2004). Interestingly, atypical to monohull, they found significantly high levels of lateral accelerations exhibited by these vessels. Moreover the findings of a recent EU project COMPASS(Turan 2006), indicate a greater role of horizontal accelerations in the elicitation of motion sickness aboard contemporary vessels than perceived before.

Though the mathematical implementations of SV-conflict theory (Bos et al. 2001; 2002; Bos et al. 2002c; Verveniotis & Turan 2002a; 2002b; Turan et al. 2003; Verveniotis 2004; Bos et al. 2008; Turan et al. 2009) are capable of predicting multi-dimensional (rotational velocities, linear accelerations, and gravities) sensory conflict vectors. However, so far only the conflict pertaining to the gravity differences (sensed and expected), termed as SV-conflict, has been used to predict motion sickness under passive motion environments. This research project investigates potential improvement of the existing SV-conflict models by explicitly considering the conflicts between the sensed and expected horizontal linear accelerations for predicting seasickness.

1.4 Layout

Next chapter presents the research question, aims and objectives of this research project. Chapter 3 reviews the literature relevant to motion sickness. Thereafter, Chapter 4 explains the research methodology adopted for this work. Chapter 5 presents detailed account of the vestibular system and its models. Chapter 6 briefly discusses the theoretical premise and outlines the development of proposed motion sickness model. Calibration (search for appropriate parameters) and validation of the hybrid model using field trials' data available at NAME are covered in Chapter 7. Further validation of the model through full scale trials, specifically organized for this study, is presented in Chapter 8. Findings of this study are discussed in details in Chapter 9 and the scope for further research is also discussed therein. Finally, Chapter 10 concludes this work.

As far as the appendices are concerned, the data pertaining to the calibration of new model is given in Appendix A. The validation and further validation data are respectively outlined in Appendix B and Appendix C respectively. The technical aspects of the motion reference unit, used for recording motion histories of the vessels for the sickness studies of this work, are presented in Appendix D. Finally, the detailed statistical comparisons of the new model with the prominent physiologic and descriptive motion sickness models are given in Appendix E

1.5 Chapter Summary

The chapter has presented the factors for pursuing this research in general as well as specific terms. It also summarised the layout of the thesis to smoothen the reading flow.

The next chapter is outlining the research question, aim and objectives of this project.

Chapter 2. RESEARCH QUESTION, AIMS, & OBJECTIVES OF THE PROJECT

2.1 Chapter Overview

This is a very brief chapter that presents the research question along with the aims and objectives of this work.

2.2 Research Question

The research question of this study may be put together as:

“Can we improve accuracy of the ‘subjective vertical conflict’ physiologic motion sickness model by explicitly incorporating the effects of horizontal accelerations?”

2.3 Aims & Objectives

The primary aim of this study is to investigate potential improvement in statistical accuracy of the 'subjective vertical (SV) conflict' motion sickness model developed at NAME for predicting seasickness incidences aboard contemporary vessels. This is to be carried out by appropriately incorporating the effects of ‘subjective horizontal (SH) conflict’, defined as the vector difference of the sensed and expected (subjective) horizontal accelerations. The sensed and subjective horizontal accelerations are, respectively, the components of gravito-inertial accelerations (in body frame of reference) normal to the sensed and expected verticals. The aforementioned aim of this research is pursued through following objectives:

- To critically review the literature relevant to ‘motion sickness’, in an endeavour to identify the descriptive and physiological models available for seasickness prediction aboard marine vessels.

- To propose and develop a physiological ‘motion sickness’ model, by extending the existing ‘subjective vertical’ model with the explicit inclusion of horizontal accelerations experienced onboard contemporary vessels.
- To calibrate, i.e. identify the unknown parameters of, the ‘hybrid model’ through statistical fitting of field trials of a reference vessel.
- To validate the calibrated ‘hybrid model’ using full scale data measured onboard various vessels by NAME alone and as part of COMPASS project.
- To undertake afresh full scale trials onboard passenger vessels for the further validation of the proposed ‘hybrid model’.
- To statistically compare the performance of physiological and descriptive models of motion sickness for predicting seasickness aboard contemporary and classical vessels.

2.4 Chapter Summary

This chapter has dwelled upon identifying the research question along with the aims and objectives of this study.

The next chapter is reviewing the literature related to various aspects of motion sickness.

Chapter 3. LITERATURE REVIEW

3.1 Chapter Overview

This chapter presents a brief history of ‘motion sicknesses’ as relevant to maritime environments (§3.2), following to that the typical symptoms of this malaise are discussed (§3.3). The chapter then discusses phenomena like 'susceptibility' (§3.4) and 'habituation' (§3.5). Current standards and procedure for motion sickness evaluations (§3.7) are discussed after summarizing the existing motion sickness theories (§3.6). The salient aspects and important findings of the COMPASS projects (§3.8) are presented, before outlining the research gaps (§3.11) towards the end.

3.2 Historical Backdrop

The history of ‘motion sickness’ is probably as ancient as the humans’ experience of riding floating objects (tree trunks etc.) on streams, lochs, rivers, seas and, perhaps, while traversing on tamed animals. However its most notorious form, namely ‘seasickness’ also called ‘nausea’, does find it’s deserved place in written records as far back as the ancient Greeks (Reason & Brand 1975). It is believed that the term ‘nausea’ has its roots in the Greek mythological word ‘naus’ meaning ‘ship’, which indicates the primordial nature of motion sickness and its association with the sea travel. Griffin (1991b), Dobie (2000), Stevens & Parsons (2002), and Benson (2002) discuss various studies on seasickness as part of their review of motion sickness history pertaining to marine vessel, a few of which are summarized below:

- Hill (1936), reports that more than 90% of inexperienced passenger suffered seasickness during the first two or three days of journeys in severe sea states, whereas moderate sea conditions resulted into 25 to 30% people becoming sick.

- Chinn (1951), highlights that almost 20 to 30% of the passengers become motion sick during the first two or three days of an Atlantic crossing on liners in a moderate sea state.
- Handford et al.(1953), found that 34% of military personnel suffered seasickness during their crossing of Atlantic onboard a military transport ship.
- Bruner (1955), carried out a questionnaire survey of 699 men aboard a destroyer assigned with escort duty in the US Navy. He found that 39% of personnel never got seasick, 39% suffered occasional sickness, 10% got frequently sick and remaining 13% were almost always seasick.
- Trumbull et al.(1960), observed that 8.5 to 22.1% of military troops suffered vomiting incidence aboard naval ships during their crossings of Atlantic on three different occasions.
- Pethybridge et al.(1978), while investigating the vomiting incidence amongst naval personnel aboard 2 UK Royal Navy ships, found that 67 and 73% of the respective crew experienced seasickness during their career. Of the same crew, 42 and 56% individuals had been sick during the past year, whereas during sea trials of five days in rough weather, 38 and 47% of the personnel got sick at least once.
- In another similar study on naval crewmembers, Pethybridge et al. (1982) report that 10 to 30% of personnel become seasickness during the commonly encountered sea conditions and this number rises to between 50 and 90% in rough weather.
- Lawther & Griffin (1986; 1987; 1988b; 1988a), recorded vomiting incidences amongst the passengers of six monohull, two hovercraft and one hydrofoil vessel operating around the British Isles and, depending on the sea conditions, found it to be as high as 70%.
- Attias et al. (1987), in a study on the effectiveness of an anti-sickness medicine onboard a 300 tonne vessel, observed that 53% of the control subjects became seasick in sea state 2 and 3 during the first two days and 23% suffered the malaise on day 3.

- Dobie (2000), referring to the database of Navy Medical Information Management Centre (US), reports that 489,266 new recruits in the Navy were diagnosed with motion sickness between 1980 and 1992, also there were revisits of 106,932 during the same period.

It is self-evident from the terse account of history given in above, that the ‘motion sickness’ is a very common issue in maritime environment and, therefore, warrants a serious attention to improve the comfort levels of unaccustomed passengers. Its prevalence amongst the naval personnel also requires concerted efforts for its quantification and subsequent minimization to enhance the operational efficiency of Navy and alike departments. The primary focus of the research present herein is on the passenger vessels, nevertheless, proposed model may be modified for the Navy personnel by introducing a habituation function similar to the one proposed by Colwell (1994; 2009).

3.3 What is Motion Sickness?

‘Motion sickness’ is a group of common nausea syndrome that is experienced by most of the travellers irrespective of the mode of transportation. Depending upon the nature of transport, it is termed as ‘seasickness’, ‘coach-sickness’, ‘car-sickness’, ‘airsickness’, and even ‘space-sickness’. Motions of the vehicle play key role to initiate the feelings of dizziness, bodily warmth, sweating, drowsiness, yawning, changing of mouth dryness level, headache, stomach awareness, nausea and finally the emesis (vomiting). But the story does not end here; if the provoking motions are not eliminated then the cycle repeats itself – though with decreased severity. It is interesting to note that the presence of physical motions is not an essential requirement as the visually perceived motions, like those in the virtual environment, are equally capable of producing the undesirable symptoms, usually termed as ‘Cinerama’ or ‘simulator-sickness’.

Motion sickness is not a medical condition rather it is the natural and very much normal response of human body towards the non-volitional, real or virtual, motions. Its persistence may ultimately require treatment for dehydration, but in itself it is not

as fatal as the acute sufferer might wish it to be. Until the end of 18th century, this issue was restricted to sailors, animal and animal fetched coach riders; however, the rapid growth in the modes of transportation since 19th century has multiplied the situations where a person could experience motion sickness. Moreover, the increased affordability of travel by the multitude types of vehicles has also given a significant boost to the incidences of travel sicknesses.

The past couple of decades have shown an increased demand and rapid development of short sea cargo and passenger transportation within EU countries and other places in the world, with similar geographical features. This has not only pressed the ship designers and builders to produce greater number of ships, but also to substantially increase their speeds to cut down on travel time. Developments in the material and propulsion technologies have broadened the possibilities of designing lightweight non-conventional ships customised for speeds in excess of 40knots with very high payload displacement fractions. These peculiar hullforms have generally been designed and evaluated for their performance features like passenger comforts using techniques developed for the conventional ships (Verveniotis 2004).

Susceptibility to Motion Sickness

‘Susceptibility’, refers to the inclination of an individual to become motion-sick in a given provoking environment. According to Griffin (1990), a wide variation in ‘susceptibility’ can be seen between different individuals (called inter-subject variability), and even the same person may exhibit different levels of susceptibility on different occasions (intra-subject variability). Primary contributors to these variations include psychological factors like individuals’ past experience, adaptability and personality. Physiological factors like functioning of vestibular, visual and somatosensory systems also play key role towards the inclination of a person to suffer motion sickness or otherwise. People of all ages, genders, and past experience are vulnerable and may experience motion sickness once or more during their lives, if exposed to provoking combination of real / virtual motion environments. Nevertheless, certain biasness features to this vulnerability have been

identified by the researchers in the past as outlined in the following (Stevens & Parsons 2002):

3.4.1 Gender

Lawther & Griffin (1986) and Benson (1999), found higher susceptibility to motion sickness amongst female than males. In a recent study Bos et al. (2007), found that females are 1.5 times more prone to motion sickness than males of similar age and previous history. The anatomical and hormonal differences between the two genders might be responsible for the observed difference in the susceptibility (Reason & Brand 1975).

Generally the terms sex and gender are treated as synonyms in the research literature. However, it is interesting to note that the Institute of Medicine (IOM, USA) has identified a subtle but important difference between the two terms for the human beings (Wizemann & Pardue 2001). IOM recommend using the term sex for the classification of humans and non-human animals on the basis of reproductive organs and the functions that derive from the sex chromosomes. Whereas, the term gender is recommended to be used to refer to a person's self representation as a male or female, or how that person is responded to by social institutions on the basis of the individual's gender presentation (Torgrimson & Minson 2005). Briefly, sex is a biological difference between the human beings while gender is more of a self-identity and/or social/cultural representation of a person.

In the context of motion sickness research, this difference appears to be more of a gender type rather than the sex; as the "...women (in general are) willing to express their (sickness) feelings openly while men pretend there are fewer problems, especially in public" (Bos et al. 2005). This may result into a biased motion sickness data as the males are shy to express their illness feelings while females don't. Consequently, despite the abovementioned general findings, there might not be any real difference between the two sexes as far as the susceptibility to motion sickness is concerned.

3.4.2 Age

Age plays statistically significant role in susceptibility; children below the age of two years show the highest tolerance. Susceptibility, then rapidly increases with a peak around 11 years in females and 21 years in males (Bos et al. 2007); tolerance level gradually increases throughout life (Lawther & Griffin 1986; Wertheim 1998; Benson 1999). It is important to note that dotage does not make a person immune and according to Benson (1999), 22% of seasickness sufferers travelling onboard Channel Island Ferry (English Channel) were over the age of 59 years.

3.4.3 Personal Traits

Motion sickness is found to be a permanent trait, in that some individuals remain immune, while others experience it in a range of real and virtual motion environments with little or no age-dependent abatement (Guedry 1991a). Interestingly, in the study carried out by Bos et al. (2007), people with previous history of motion sickness (on ships and other modes of transportation) felt twice as much uncomfortable aboard ships than those who did not suffer seasickness before. Guedry (1991a) also highlights that individual's personality and past motion experiences have bearings on their future attempts to expose themselves to provoking motion environment and attempting to defeat their symptoms.

3.4.4 Sleep Deprivation

Dowd (1974), reported a rise in motion sickness levels amongst aircraft pilots induced by sleep deprivation, also interfering with the vestibular habituation process. This phenomenon is amplified in the maritime environment, where the sleeping conditions on board marine vessels are often not very favourable for a relaxing sleep.

3.4.5 Psychological Features

Collins & Lentz (1976), found significant relationship between the susceptibility to motion sickness and the psychological features of the individuals e.g. subjects with higher anxiety are more inclined to get motion sick. Similarly, researchers found that introverts tend to exhibit greater motion sickness (Kottenhoff & Lindahl 1960; Reason & Graybiel 1972), this is probably due to them being slower adaptors.

Resistance to emesis shown by some people, considering it to be a major event, leads them to the state of increased misery with little or no relief. Whereas, those who are willing to vomit as part of their body's natural reflexivity towards non-volitional motions with little efforts do get some, albeit temporary, relief and show greater tendency to adapt to provoking environment (Guedry 1991a).

3.4.6 Activity

The nature of activity being carried out by the persons exposed to provoking environment also plays an important role in their susceptibility to motion sickness. Benson (1999), reports that given the time for relaxation and contemplation, individuals concentrate more on the non-volitional motions they are exposed to and that leads to motion sickness. On the other hand studies carried out aboard ships and aircraft indicate that individuals involved in activities requiring mental concentration on a particular task have reduced tendency to become sick (Wiker et al. 1979).

3.4.7 Physiological Aspects

Reason & Brand (1975) hypothesised that the rate at which the internal model (residing inside Central Nervous System) of motion environment updates its expectation of the physical environment, governs the susceptibility to motion sickness. They proposed the following three characteristics that would influence this rate of synchronisation:

- **Receptivity.** This is the ability of a person to internally amplify motion stimulus or range of motion stimuli that would cause the undesirable affects. In this regard, some people remain unaffected by a given stimuli due to high internal damping, whereas others readily amplify the signal.
- **Adaptability.** It is defined as the rate at which the internal model adjusts itself to the new provoking motion environment; commonly referred to as the process of getting one's 'sea legs'. People with high receptivity may display higher level of adaptability and thereby suffer lesser motion sickness as the sensory mismatch (see §3.6.2) may abate before the threshold level of

neurochemical link is achieved. Thus adaptability may not be positively associated with receptivity.

- **Retentiveness.** This refers to long term storage (inside the neural store) of the mismatch environment to which a person is repeatedly exposed. It results in reduced susceptibility to motion stimuli for which an impression could be extracted by the internal model from the neural store (see §3.6.4). A common observation in favour of this characteristic is returning to sea after spending several days in port and not getting motion sick.

3.4.8 Temporal Aspects

Some of the temporal aspects are also found to affect the predisposition of a person to motion sickness (Guedry 1991a). These include, but not limited to, headaches (due to reasons other than motion sickness), inflammation of inner ear, excessive consumption of alcohol, and gastrointestinal disorder. Fear of getting motion sick and its associated anxiety also make a person more conscious of provoking environment leading to increased susceptibility.

3.5 Habituation

The process of acquiring one's 'sea legs', which would occur in almost 95% of the population from a few hours to several days of exposure is termed as habituation or adaptation (Stevens & Parsons 2002). Duly influenced by the susceptibility factors identified in §3.4, the time to habituate is a function of the type of wave movement (Wertheim 1998). The time to reach the stage of emesis by a susceptible person may range from a few seconds or minutes, while being exposed to provoking stimuli in a laboratory or fairground apparatus, to several hours aboard an aircraft, a ship, or a vehicle of similar motions (Griffin 1990). The habituation process could be seen to take place in the motion sickness incidences (MSI) recorded by Crossland (1998), while studying the motion sickness amongst the population exposed to ship motions, as shown in Figure 3.1. It is important to note that this figure gives the impression that all people travelling aboard ships would become immune to motion sickness after 2.5 days at sea. However, this is not correct due to the fact that almost 5% of the

population remain immune to the habituation process (see Colwell 1989 for more details).

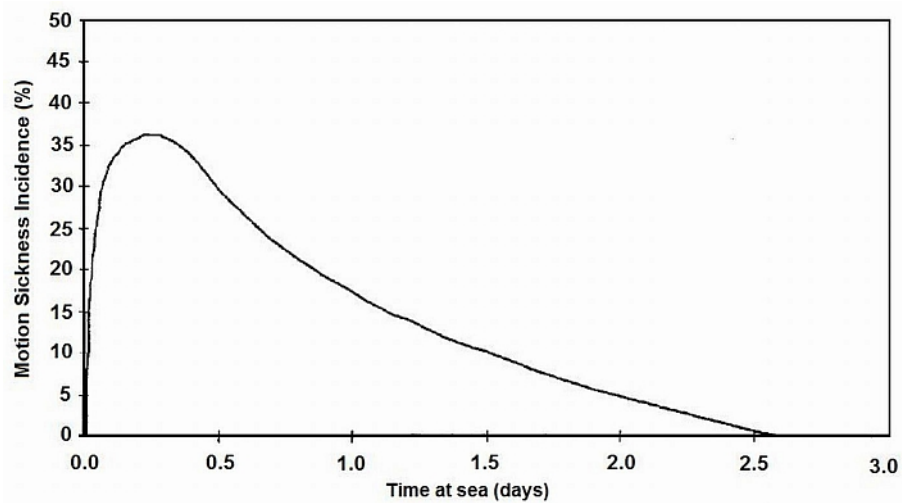


Figure 3.1. Percentage of people vomiting (MSI%) over time for a population exposed to ship motions [Crossland 1998].

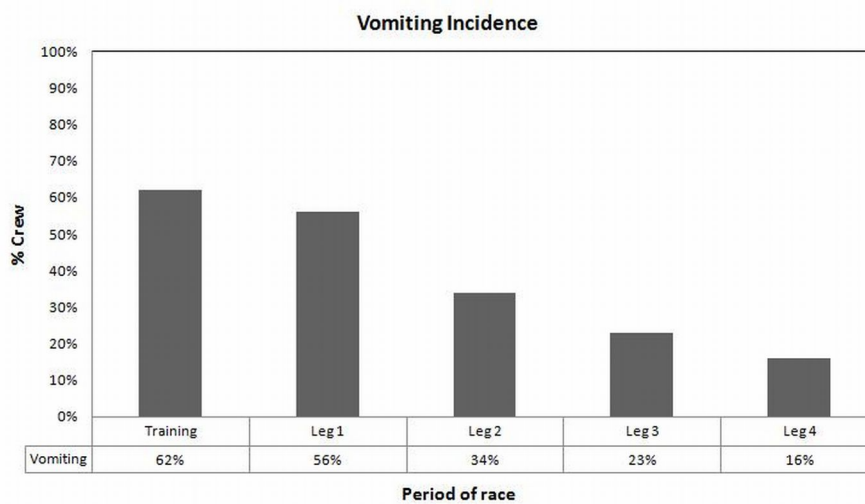


Figure 3.2. Percentage of race participants vomiting on one or more occasion during training and as function of race leg [Turner & Griffin 1995].

Turner & Griffin (1995) recorded motion sickness incidences, as percentage of participants who vomited, during various phases of a round the world yacht race. Excluding the training sessions, this race was divided into four legs and a significant reduction in vomiting incidences were reported by the participants ($\chi^2 = 14.64$; p -

value < 0.01; 3 d.o.f), as the race progressed towards final phases (see Figure 3.2). This also demonstrates the manifestation of habituation or adaption phenomenon.

3.6 Brief Review of Motion Sickness Theories

In the past, researchers have been trying to explain the motion sickness using a variety of psychological and physiological theories (Mansfield 2004). Fear formed the core part of psychological versions and “overstimulation” of stomach was the crucial element of physiological hypotheses. These theories, though seemed logical, failed to explain all types of motion sicknesses (sea, air, space, simulator, Cinerama, etc.). This led to the development of more tangible theory that combines the physiological and psychological aspects of human beings, called “sensory conflict” or “sensory rearrangement” theory (Reason & Brand 1975).

During the studies concerning postural stability, Stoffregen (1985) found the subjects opting for discontinuation of experiment complained and reported symptoms of motion sickness. Based on these observations, Stoffregen & Ricco (1991) proposed the “postural instability” theory of motion sickness. Similarly, considering the outcome of a series of studies related to optokinetic drum (Bles 1981), human centrifugation (Bles et al. 1995), and ship motion simulator (Wertheim et al. 1998), Bos & Bles (1998; Bos & Bles 1998b; Bos & Bles 1998a; Bos & Bles 2002; Bos et al. 2008) redefined the “sensory rearrangement” theory as “subjective vertical conflict” theory. All of these pertinent theories of motion sickness are briefly discussed in this section and its sub-sections.

A range of factors implicated in the causation of motion sickness have been identified by Griffin (1990) as illustrated in Figure 3.3. The details of these factors may lead to a false impression that motion sickness is something insightfully understood, but it’s the symptoms that are well comprehended rather than the mechanism (Stevens & Parsons 2002). Money (1970) asserts that one of the major milestones in understanding the etiology of motion sickness was, “...the decision to study motion sickness independently of its most obvious organic localization, the stomach; it was decided to seek its genesis in the recondite areas of the organs

governing equilibrium. Today it appears logical that motion sickness should be studied in connection with the organs responsible for equilibrium, but years ago it seemed only a remote possibility, since the predominant tendency in the historical evolution of Medicine has always been to begin the study of an illness in the area of its principle symptom”.

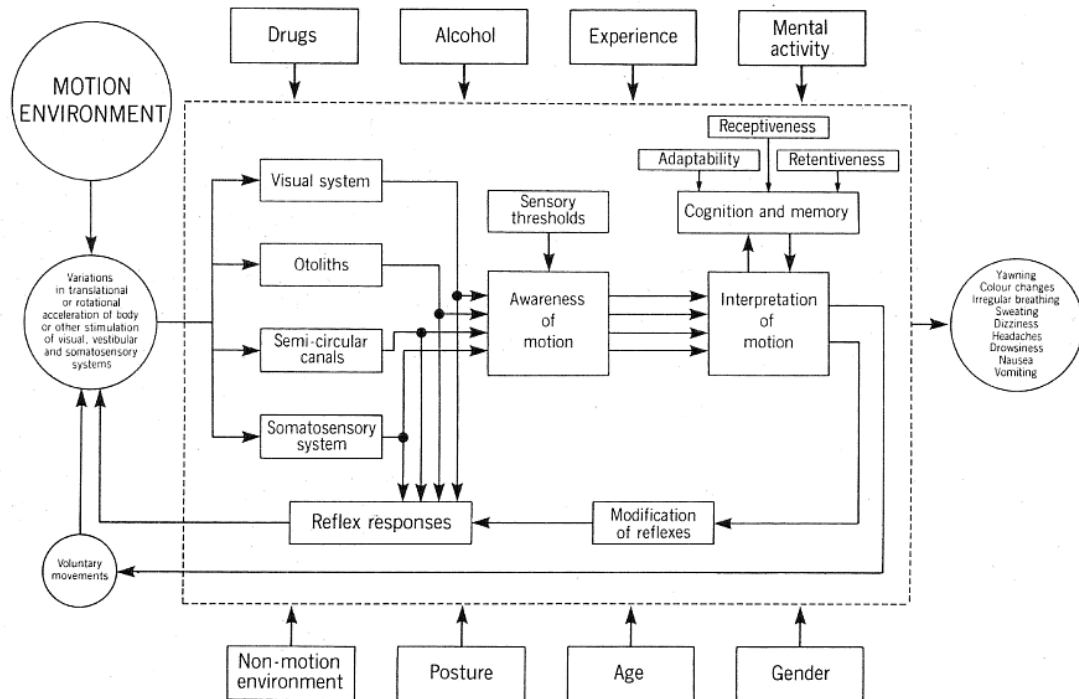


Figure 3.3. Conceptual model of factors possibly involved in causation of motion sickness [Griffin 1990]

The vestibular system is, arguably, considered to be one of the oldest sensory system that exists in vertebrates enabling them to sense and control their own movements (Highstein et al. 2004). The most significant function of this system is to detect motions of head relative to the earth. This labyrinthine apparatus comprises of semicircular canals and otolith organs that have similar structure across the extent of vertebrate phyla. As the vertebrates translate and rotate through space, vestibular system senses and reports the linear and angular motion magnitudes with direction (relative to head) to the central nervous system (Moore et al. 2001). CNS combines these signals with the information generated by other sensory systems like visual and somato-sensory to compute a central estimate of position and motion vectors of head

and body called gravito-inertial vector (Gizzi et al. 1994; Cohen et al. 2001; Imai et al. 2001). This vectorial information is then used by CNS to generate reflexive motor activity that assists controlling the motion of vertebrates (Guedry 1991b).

Tyler & Bard (1949), in their extensive review on motion sickness, indicate that the idea of vestibular system's involvement in motion sickness dates back to 1870, originated by Glotz. Involvement of the vestibular system in the onset of motion sickness was established with the discovery of the fact that people without functioning vestibular systems (Labyrinthine Defective, LDs) are immune to motion sickness in the real provoking motion environment (Tyler & Bard 1949; Benson 1999). LD may either be caused by some disease (e.g. meningitis, etc.) or inherited e.g. deaf mutes. Such an immunity was introduced in animals by labyrinthectomy prior to their testing for motion sickness e.g. Sjöber (1931) found that all four of the highly susceptible dogs he was experimenting on, failed to get motion sick after the bilateral destruction of their labyrinths. Later on Money & Friedberg (1964), also experimenting on dogs, reported similar findings. Detailed description of the vestibular system and its mathematical models are presented in Chapter 5. At this point, the following two most important theories of motion sickness (Money 1970) are briefly presented:

- Vestibular Overstimulation Theory
- Sensory Conflict Theory

3.6.1 Vestibular Overstimulation Theory

According to Money (1970), this theory considers the source of motion sickness as an overstimulation or irritation that causes a shift in the neural activity from equilibrator centre (vestibular system) to the one that produces the signs and symptoms of motion sickness (Brooks 1939). During the first half of nineteenth century, the researchers had concluded that vestibular system plays a key role in the aetiology of motion sickness (Reason & Brand 1975). As a result, a significant era (up to 1960s) got dominated by the notion that motion sickness results from the overstimulation of vestibular system by the non-physiological vehicular motions imposed on a rider's head. This approach practically excluded the role played by

other sensory systems like visual and non-vestibular proprioceptors. At that point in time, investigations into motion sickness focused on deciding the primary receptor system (semicircular canals or otoliths) responsible for the undesirable symptoms.

Tyler & Bard (1949) point out “There are three schools of thought.....: One believes that both groups of receptors, the cristae of the semicircular canals and the maculae of the otolith organs, are involved; another school maintains that only the maculae are concerned; a third group holds that the otolith organs are not essentially involved and that motion sickness is caused chiefly, if not solely, by stimulation of the cristae”. In simpler words this theory predicts either of the following labyrinthine overstimulation:

- Semicircular canals only.
- Otoliths only.
- Semicircular canals and otoliths.

The view that considered overstimulation of “canals-only”, had its roots in the work of Irwin (1881), Reynold (1884) and those who were not fully aware of the functional differences between otoliths and canals at that time (Reason & Brand 1975). Benson and Brand (1968) mention that “de Wit (1953) suggested that individual differences in susceptibility to motion sickness were related to the sensitivity of semicircular canal receptors, for he (de Wit) found that a group of subjects who were habitually seasick had longer after-sensations and lower sensory thresholds to angular stimuli than a group who did not suffer from this disability”. However, Reason (1968) and later on Dobie (1974) could not confirm the relationship proposed by de Wit (1953) for post-rotary after-sensations and the impulsive stimulus. By 1975, the exclusive involvement of semicircular canals in the causation of motion sickness was mostly ruled out.

The unnatural or excessive stimulation of “otoliths-only” enjoyed its support from the observations made by Quix (1922), that the rotational ship motions are insufficient to stimulate semicircular canals. According to Reason & Brand (1975),

there were following four primary evidences in favour of the otoliths' dominance in the onset of motion sickness:

- Linear accelerations of provoking vehicles (aircrafts and ships) were thought to dominate rotational ones; thus otoliths (sensors for linear motions) get over-stimulated while threshold levels of canals (sensors for rotational motions) do not get exceeded.
- Nystagmus (rapid, involuntary, oscillatory motion of the eyeballs) was not observed during sea or airsickness.
- Pure linear accelerations could apparently lead to motion sickness symptoms.
- Significant reduction in motion sickness is observed by adopting the supine position or by simply tilting the head back.

Fallaciousness of the first supportive argument is attributable to the inaccurate (higher) thresholds levels determined for the semicircular canals. Mach (1875) and Dodge (1923) established the angular acceleration detection threshold level as $2^\circ/\text{sec}^2$, which was rarely exceeded by the angular motions imposed on the passengers by the ship's motions (Quix 1922). Whereas, the studies carried out by Clark & Stewart (1968) using perception and oculogyral illusion (an illusion occurring in angular acceleration in which the position of fixed light appears to drift) as indicator found the mean threshold value as low as $0.10^\circ/\text{sec}^2$. Furthermore, the studies attempting to quantify the accelerations received by the labyrinthine receptors failed to take account of the independent head movements (Morales 1949). The association of independent head movements in the elicitation of motion sickness reported by Johnson et al.(1951) further invalidated the overstimulation of otoliths as the sole cause of motion sickness.

The second evidence has also been rejected by the experiments conducted to study the generation of nystagmus during Off-Vertical Axis constant-velocity Rotation, OVAR (i.e. about the Earth's horizontal). According to Wood (2002), "The continuously varying orientation of the head and body relative to gravity during OVAR, however, stimulates the otoliths ". It is well established now that stimuli

of these experiments do not only cause nystagmus, but are also highly provocative of motion sickness symptoms (Denise et al. 1996). Thus absence of nystagmus while the symptoms of motion sickness appear is no longer a valid argument.

The third claim had its genesis in the beliefs linked to the first evidence that the rotational motions of ships and aircrafts are not strong enough to stimulate canals. Therefore, de Wit (1953), a strong supporter of “canal-only” overstimulation theory, concluded that “Seasickness is caused by the overstimulation of the otolith system. The part played by the other organs in the determination of the position of the body is only secondary”. Moreover, the extensive series of studies organized by Wendt et al. (Alexander et al. 1945a; 1945c; 1945b; 1945d) using a vertical accelerator called “Wave Machine” to correlate motion sickness with pure vertical motions augmented this view point. The shortcoming of these studies, highlighted by Reason & Brand (1975), are “these experiments suffered from the serious flaw that the subjects’ head were not restrained so this means that we cannot discount the possibility that sickness was due to the independent angular head movements....”. In addition, the study involving restraining of head (Fraser & Manning 1950) while replicating the linear component of otherwise highly provocative swing motions could not elicit the motion sickness, which also negates the third evidence.

The fourth evidence is the only one that cannot be rejected on the basis of scientific observations, as supine position does provide relieving effects to the motion sickness sufferer (Manning & Stewart 1949). But these relieving effects of the supine position can be explained by theories other than the otolithic overstimulation (Reason & Brand 1975). Furthermore, it could be argued that in such an orientation the head becomes (practically) restrained, preventing angular motions and sickness, as the rotational motions do play a significant role in its elicitation.

In addition to the weaknesses of “otolith-only” theory highlighted in the above, Reason & Brand (1975) argued that the overstimulation theory in general and the otolithic excessive stimulation in particular fails to explain the following: Motion sickness induced by the visual effects (simulator sickness) such as Cinerama

and in a virtual environment like those of “flight-simulators” and more recently by the 3D video games referred to as “3D sickness” amongst the game players (Ujike et al. 2004).

- The “Coriolis vestibular reaction”, in which the otolithic stimuli are almost identical to a static tilt while a person moves the head about an axis different from the axis of rotation. This should not elicit sickness under the overstimulation theory as the otolithic overstimulation is absent.
- Sickness induced by the “zero-gravity” or space-sickness does not involve any overstimulation of otoliths. In absence of gravity no otolithic stimulus exists except during the translational movements of the head in space. Yet the space-sickness prevails amongst the astronauts while in space or when being subjected to artificial gravity (Crampton 1990).
- Partial elimination of any labyrinthine receptors in general and otoliths in particular (Igarashi & Nagaba 1962) does not introduce immunisation to motion sickness.
- “Habituation” or “adaptation” phenomenon, especially the “mal de débarquement” i.e. “land sickness” that occurs on cessation of the provocative motion stimuli after a long journey aboard a ship or after a long exposure to Coriolis accelerations cannot be explained by the overstimulation theory.

All of the arguments presented in above clearly indicate that the overstimulation theory cannot, but explain a few of the occurrences of motion sickness; that too with dubious if not incorrect evidences in its favour. No wonder why this theory was abandoned by most of the researchers by the early 1960s and focus was diverted towards the development of “sensory conflict” or “sensory rearrangement” theory, briefly presented next.

3.6.2 Sensory Conflict Theory

“Sensory conflict” (Reason & Brand 1975) is currently the most widely accepted theory for motion sickness. It is also referred to by other names such as “conflict mismatch theory”, “sensory rearrangement theory” (Reason 1978a) and “neural

mismatch theory (see §3.6.4)” (Benson 1999). According to Wertheim (1998), the core essence of all these theories may be summarised as “The labyrinthine receptors provide the brain with information about self motions that is incongruent with the sensations of motion generated by other sensory systems such as visual or proprioceptive (somatic) systems and / or the information does not match with what is expected from previous transaction with the motion environment.” As highlighted at the beginning of §3.6, involvement of vestibular apparatus is inevitable in any theory attempting to explain motion sickness, therefore it also plays a key part in the sensory conflict theory.

Mansfield (2004) argues that in certain cases individuals might have control over the provocative stimuli, referred to as pseudo-sense of “control”, that would augment other sensory systems to produce a more consistent model of the moving environment. A person driving a vehicle is less likely to suffer motion sickness as compared to the passengers and this may be attributed to synergising effects of pseudo-sense of “control” with the other sense modalities. On the other hand, a car passenger engaged in reading a book while the driver turns the car round a corner, will experience a mismatch between the visual and vestibular feedback of the moving environment. The eyes, focused on (relatively stationary) book, would be reporting a motionless environment, while the canals and otoliths of labyrinthine apparatus would sense the angular and translational accelerations. The somatic system will also be sensing a variation of pressure across the body. Since, the passenger is lacking the pseudo-sense of “control”; hence, the net cognitive model of the motion environment would receive incongruent information that may lead to the symptoms of motion sickness. This is pictorially illustrated in Figure 3.4.

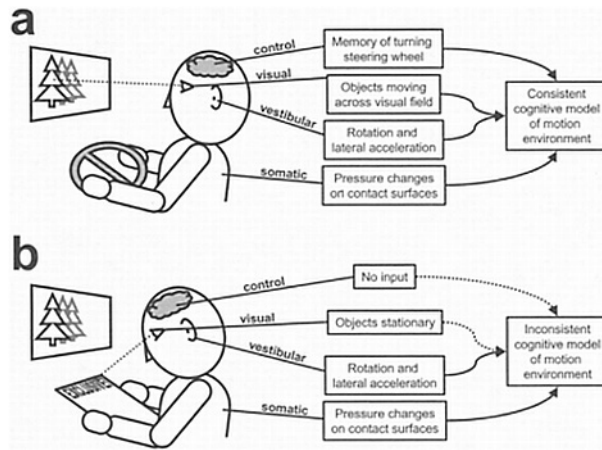


Figure 3.4. Illustrative model of the multiple pathways through which a motion environment is perceived: (a) for a driver of a car and (b) for a passenger in the same car reading a book [Mansfield 2004]

Another example of “sensory mismatch” phenomenon would be of a person inside a ship’s cabin at sea with no visual access to outside environment. In this case the vestibular and somatic system would be sensing motions, while the visual cues would register a ‘no motion’ scenario. This would thus lead to a conflict between the different sensory systems, causing seasickness. It may be interesting to note that for the previous example, the car passengers susceptible to motion sickness are advised to look ahead through the wind screen, while those aboard a ship feel somewhat relieved by looking at a stationary horizon, as seen from a weather deck or through a window (porthole).

Reason & Brand (1975) mention that the origin of “sensory conflict” theory dates back to Irwin (1881) when he wrote: “In the visual vertigo of seasickness there appears to be a discord between the immediate or true visual impressions and a certain visual habit or visual sense of the fitness and order of things, which passes into consciousness as distressing feeling of uncertainty, dizziness and nausea”. Here, Irwin is displaying his clear understanding of the “sensory conflict”, while he realises that presence of a variance between the otherwise congruous sources of spatial environment leads to a conflict between what is reported now and what is expected on the basis of previous experience. This very concept of “exposure history” forms the basis of “sensory rearrangement” theory proposed by Held (1961). He concluded

that during the initial pre-adapted stages of rearrangement of sensory cues (created in laboratory) a conflict exists between the sensory input and the pattern expected on the basis of past experience.

Influenced by the “reafference principle” (see §3.6.3) of Von Holst & Mittelstaedt (1950) and the “sensory rearrangement” experiments conducted by Held(1961), Reason (Reason 1969; Reason 1970; Reason & Brand 1975; Reason 1978a) formalized the “sensory rearrangement” theory. He proposed that “... all situations which provoke motion sickness are characterised by a condition of sensory rearrangement in which the motion signals transmitted by the eyes, the vestibular system and the non-vestibular proprioceptors are at variance not only with one another, but also – and this is the crucial factor – with what is expected on the basis of past experience or exposure history”. He asserts that presence of vestibular apparatus in any elicitation of motion sickness is mandatory, be it directly or indirectly. The provoking sensory conflicts are divided into two major categories:

- “Visual(Eyes) - Inertial(vestibular and non-vestibular proprioceptive) Rearrangement”, which represents the conflict *between* the sensory systems, also referred to as “inter-sensory conflict” (Stevens & Parsons 2002). In this case the signals from the visual and vestibular systems are at variance with each other and further classified into two types:
 - Type 1: Signals from both the visual and vestibular system are present but are of incongruent nature and do not accord with the expectations arising from previous experience.
 - Type 2: Either the visual or vestibular cues are absent in the presence of the other.
- “Canal-Otolith Rearrangement” also called “intra-sensory conflict” (Stevens & Parsons 2002); this is the conflict that prevails when one of the peripheral labyrinthine receptor registers signal incongruent with the signal generated by the other. An example would be sensing of linear accelerations by the otoliths during off-vertical axis rotation at constant velocity, in which case the canals

afferents would be absent. Once again, this category can be subdivided into two types:

- Type 1: Presence of both the canal and otolithic signals but incompatible with each other.
- Type 2: Either canal or otolithic signals are present in the absence of the cues from other (complementary) vestibular receptor.

A summary of these categories and types along with some commonly observed examples (Griffin 1990; Griffin 1991a) are depicted in Table 3.1.

Table 3.1: Categories & types of sensory conflict along with some examples of various provocative stimuli (adapted from Griffin, 1990; 1991)

Type of Conflict	Category of Conflict	
	Inter-sensory Conflict (Visual–Vestibular)	Intra-sensory Conflict (Canal–Otolith)
Type I	<p>Definition: Visual and vestibular systems simultaneously signal different (i.e. contradictory or uncorrelated) information.</p> <p>Examples: Watching waves from a ship. Use of binoculars in a moving vehicle. Making head movements when vision is distorted by optical device. “Pseudo Coriolis” stimulation.</p>	<p>Definition: Canals and otoliths simultaneously signal different (i.e. contradictory or uncorrelated) information.</p> <p>Examples: Making head movements whilst rotating (Coriolis or cross-coupled stimulation). Making head movements in an abnormal acceleration environment which may be constant (hyper- or hypo-gravity) or fluctuating (linear oscillation). Space-sickness. Vestibular disorders (e.g.</p>

Type of Conflict	Category of Conflict	
	Inter-sensory Conflict (Visual–Vestibular)	Intra-sensory Conflict (Canal–Otolith)
		Ménière’s disease, acute labyrinthitis, and trauma labyrinthectomy).
Type IIa	<p>Definition: Visual system signals in the absence of an expected vestibular signal.</p> <p>Examples: Cinerama sickness. Simulator sickness. ‘Haunted Swing’. Circularvection.</p>	<p>Definition: Canals signal in the absence of an expected otolith signal.</p> <p>Examples: Positional alcohol nystagmus. Caloric stimulation of semicircular canals. Vestibular disorders (e.g. pressure vertigo, cupulolithiasis).</p>
Type IIb	<p>Definition: Vestibular system signals in the absence of an expected visual signal.</p> <p>Examples: Looking inside moving vehicle without external reference (e.g. below deck in a boat). Reading in a moving vehicle.</p>	<p>Definition: Otoliths signal in the absence of an expected canal signal.</p> <p>Examples: Low-frequency (<0.5 Hz) translational oscillation Rotating linear acceleration vector (“barbeque spit” rotation, rotation about an off-vertical axis)</p>

When we move around in our daily life, the labyrinthine receptors work in harmony with each other and in coordination with visual and non-vestibular proprioceptive cues. Thus, the overall cognitive model of natural self-propulsion is highly correlated within various sensory cues. On the other hand when we expose ourselves to atypical

motion environment, such as that of a vehicle, we get subjected to passive motions that are otherwise absent in the natural environment. This leads to an artificial disruption of the harmony amongst the signals being produced by the orientation sensors and what is expected from our previous transaction with the motion environment. This conflict between our current sense of spatial environment and what is held in our neural store (from our recent past experience) is considered to be the causation of motion sickness. Reason & Brand (1975) have outlined a great deal of experimental studies and their correlation with the involved sensory rearrangements.

3.6.3 Reafference Principle

As already mentioned (§3.6.2), the core concept of “sensory rearrangement” theory derives its stimulus from the “reafference principle”, proposed by von Holst & Mittelstaedt (1950). This principle was hypothesised to answer the following two questions:

- Animals have built in reflex system to compensate for the involuntary motions; in the presence of such a system how can they perform intentional movements?
- How the central nervous system is able to distinguish the sensory cues reporting motions generated by self-propulsion and those imposed by the forced (passive) environment, such as that of a vehicle.

According to Varjú (1990), the notion of this principle can be summarized as: “...the motor commands (efference copy) are compared to the sensory afference in order to discriminate between passive and active motions”. The model proposed by von Holst & Mittelstaedt(1950) comprised of a closed-loop feedback system. A motor command producing efference for some muscle initiates the system and leaves a “self-image” in the CNS, called “efference-copy”, carrying information about the stimulus. The effector (muscle, gland, or organ) reacts to the incoming stimulus and generates a feedback signal called “re-afference”. The “re-afference” signal is then compared by CNS with the “efference-copy” it had retained earlier on; if the two

signals match then the “self-image” is erased and no further activity takes place. If, however, the “re-afference” differs from the “efference-copy”, a mismatch signal is produced, which would either manipulate the movement through further motor activity or raises itself to a higher centre producing the illusory perception. The idea of “reafference principle” is brilliant, but is very difficult to implement mathematically, as Varjú (1990) puts it: “The reafference principle was formulated in very general terms not suited for mathematical analysis”. Furthermore, information on how CNS generates the “efference-copy” and compares it with the “re-afference” in spatial and time domains was also not provided in their original model (Oman 1982).

While attempting to explain (using sensory rearrangement) the effects and after-effects of prism distortion in long duration exposures, Held (1961) introduced an important modification to the reafference principle referred to as “correlation storage”. He says: “The Correlation Storage acts as a kind of memory which retains traces of previous combinations of concurrent efferent and reafferent signals. The currently monitored efferent signal is presumed to select the trace combinations containing the identical efferent part and to reactivate the reafferent trace combined with it”. The current afferent signal is then compared with the traces of afferent signal retrieved from the “correlation storage” in a “comparator” device. The difference between the two would lead to the addition of the revised afferent impression in the “correlation storage” and the future selection of the new afferent trace would depend on its age. As Held (1961) puts it: “...the selection from storage by the currently monitored efferent must be weighted by the recency of the trace combinations when alternatives are available. Thus, for example, if the conditions that make for typical combinations of signals are systematically changed, as they are by rearrangement, the new combinations will be stored. The same monitored efferent signal may now revive either an old or a new reafferent trace or both. We will assume that this ambiguity is gradually eliminated by weighting in favour of more recent combinations”. This means that on abatement of the rearrangement conditions, a certain amount of time would still be required to identify the usual combinations of the efferent and their corresponding afferents (Reason & Brand 1975).

3.6.4 Neural Mismatch Hypothesis and Habituation / Adaptation

Inspired by the work of Held (1961) for “correlation storage” (see §3.6.3) and the “sensory conflict” hypothesis of motion sickness proposed by Claremont (1931) and advanced by various researchers (Hill 1936; Morales 1946; Kirkner 1949; Lansberg 1960; Steele & Major 1961; Guedry 1964; Gillingham 1966; Guedry 1968; Reason 1969; Reason 1970), Reason (Reason & Graybiel 1972; Reason & Brand 1975; Reason 1978b) proposed the “neural mismatch” hypothesis to explain the etiology of motion sickness and its adaptation process. Reason (1978b) noted that it is not appropriate to conclude that the CNS carries out a direct comparison of inter-sensory signals. This is because the “normal” behaviour (response) and whether they conflict or not would depend on coding, context and previous sensory-motor experience.

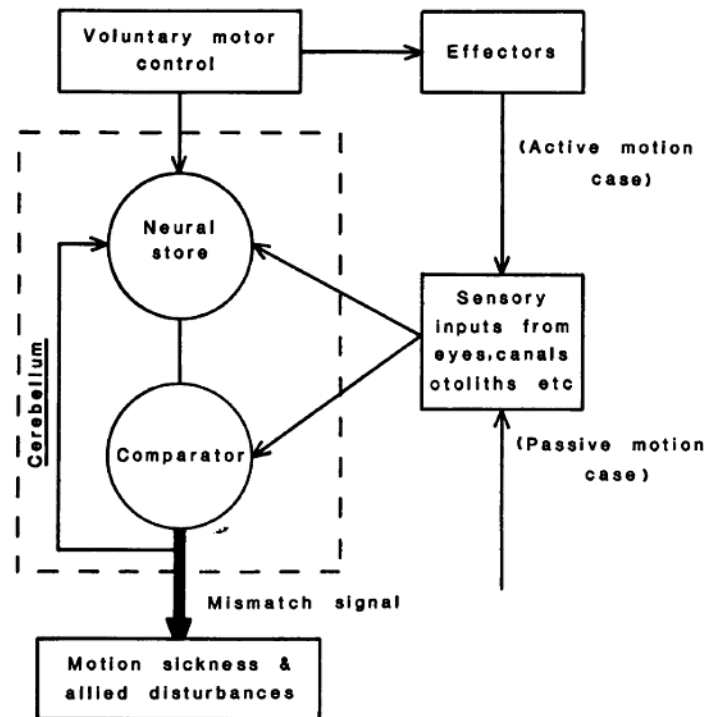


Figure 3.5. The basic structural components of the neural mismatch model [Reason 1978b]

Reason observed that the existence of “sensory conflict” itself is not sufficient to cause motion sickness as a continued interaction with the otherwise provoking stimuli leads to a gradual dilution and eventual disappearance of the symptoms (of course it may not happen in the rare 5% of the population, see §3.5). He argues

(Reason 1978b): “It is this crucial temporal comparison between present and past patterns of spatial stimulation that provides the necessary explanatory link between the sensory rearrangement notion and protective adaptation”. The two fundamental components of his model, as depicted in Figure 3.5, are:

- A “neural store” unit that retains the important information relating the characteristics of the sensory cues generated by the spatial sensors during their previous transaction with the motion environment.
- A “comparator” unit meant to compare the existing contents of the “neural store”, with the incoming sensory signals of the motion sensors.

The model depicted in Figure 3.5, is an extended version of the initial model (Reason & Graybiel 1972; Reason & Brand 1975), as it distinguishes between the adaption process of “voluntary” and “in voluntary” (passive) movements. The rate of adaptation for the active self-propelled motions is much higher than the one acquired on exposure to the passive non-volitional movements. The working of this model for the passive motions (we are interested in the motion sickness induced by the vehicular motions while the passengers are assumed to be seated and not executing any volitional movements) may be explained as follows:

- Whenever an individual is exposed to a novel motion environment in which visual and vestibular cues are at variance or there exists intra-sensory conflict, the information recorded in the “neural store” (for the typical environment) would be significantly different from the incoming sensory signals. The “comparator” unit would detect this discrepancy and generates a mismatch signal representing magnitude and direction of the mismatch. Since the magnitude of the mismatch would be initially very high, it will ascend to higher centres initiating the neurophysiological and biochemical mechanism responsible for the elicitation of motion sickness. It is important to note that only those mismatch signals that implicate the labyrinthine receptors would lead to motion sickness, as direct or indirect involvement of vestibular system in the incidence of motion sickness is indispensable (see beginning of §3.6)

- If the exposure to unnatural (rearranged) motion environment continues for some time, then (depending upon the susceptibility level of the individual) records of the “neural store” are gradually updated. This would put the characteristic information of the newer motion environment on top in the store and their likelihood of being selected for comparison with the incoming sensory cues would increase with passage of time. If the stimulus continues to prevail, then at some point in time the “comparator” would be receiving traces of the rearranged afferences for comparison from the “neural store”. When this happens, the individual is said to be habituated / adapted to the atypical environment as long as it is maintained.
- Essentially, on return to the previous natural environment the records of “neural store” would be in dissonance with the prevailing conditions and that would again generate the mismatch signal causing motion sickness (“mal de débarquement” phenomenon). However, the re-adaption period for the typical environment would be shorter due to well-established (over-learned) afferent traces retained by the store (Reason & Graybiel 1969).

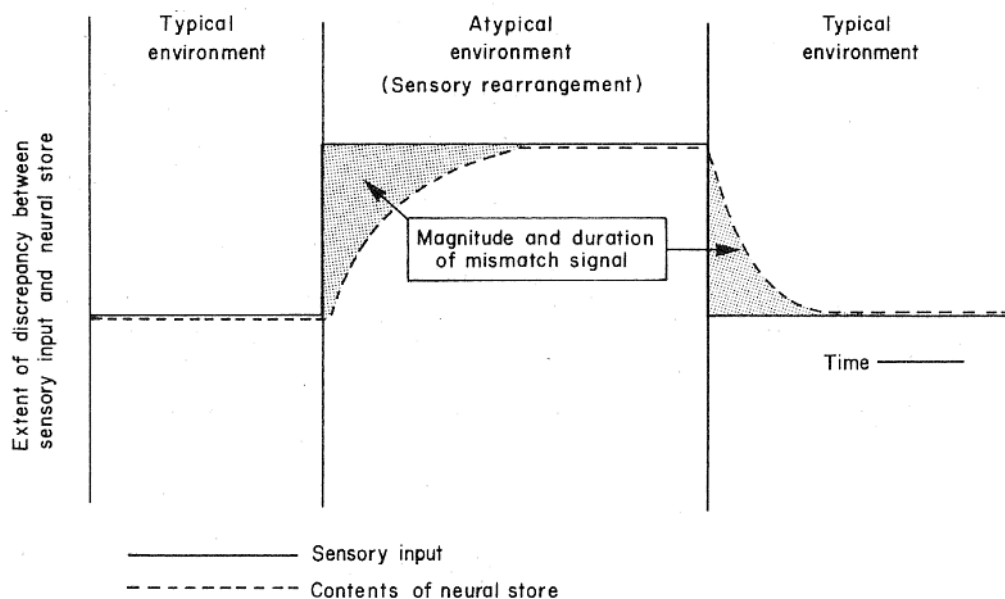


Figure 3.6. Diagram illustrating the effects and after-effects of sensory rearrangement as predicted by the neural mismatch model. [Reason 1975]

A diagram depicting the “neural mismatch” adaptation process is shown in Figure 3.6. It is important to see the unique way “neural mismatch” hypothesis is defining elicitation of motion sickness. Though it is driving its roots from the “sensory rearrangement” theory, but the distinguishing feature is the involvement of “neural store” that maintains records of previous sensory-motor experience. The “inter- or intra-modality” conflict alone is not enough for the causation of motion sickness as it should also be at variance with what is recorded in the “neural store”.

3.6.5 Weakness of Sensory Conflict Theory

Considering the theoretical details it provides, the “sensory conflict theory” is very useful to understand the underlying mechanism for the elicitation of motion sickness symptoms. It may be used to qualitatively predict the nauseogenicity of the known combinations of motion stimuli (Stevens & Parsons 2002). However, it does not provide the methodology to quantify the “sensory conflict” and thereby the proportion of population expected to suffer motion sickness under a given motion environment. As Griffin (1990) puts it: “...but it cannot be used to predict the extent of any symptoms, or how they depend on the magnitude of motion, the type of motion or the duration of motion. The sensory conflict theory must owe some of its success to the difficulty of conceiving an experiment which could disprove the theory”.

Oman (1982) argues that it is not obvious how “sensory rearrangement” could be used to explain nauseogenicity of certain stimuli such as passive vertical low frequency linear accelerations, as the model is primarily qualitative rendering simulation and quantitative prediction beyond its reach. Commenting on “neural mismatch” hypothesis, he raises many important questions, such as:

- “How should a trace (neural record) be represented analytically?”
- “If it is the neural memory of the time history of a previously experienced efferent or afferent signal, must it have a beginning and an end? If so, what determines the duration of this epoch?”
- “How can we represent the neural store in a more functional way?”

In a later study Oman (1990) asserts: “The model did not really address the question of why the CNS should have to compute a sensory conflict signal, other than to make one sick, or what functional properties conflict signals might have such that they could be indentified in a physiological experiment.”

It is our opinion that the stance of Griffin (Griffin 1990; 1991a) and similar criticism by others (Guedry 1968; Oman 1978; 1982) undermines the fact that so far no evidence is available in literature that would disprove the “sensory conflict” theory. It’s not just the matter of conceiving an experiment that would render the “sensory conflict” theory useless, rather it’s the lack of appreciation that “(it is the) suitability of this theory in the context of motion sickness that no experiment can disprove it” (Verveniotis 2004). We believe that even some aspects of this theory may not prove to be as important / relevant (de Graaf et al. 1998), yet it would continue to provide the necessary platform for the development of theories relying on human sensors of motion. An important finding in this regard is that of Mittelstaedt (1983; Mittelstaedt et al. 1989) who, theoretically related motion sickness with the body orientation in space. He stated that a conflict between vestibular and visceral graviceptor signals regarding “body orientation” may lead to motion sickness during vertical motions.

This is why building on the “neural mismatch” hypothesis (Reason 1978a), and making use of “observer theory” from control engineering, Oman (1978; 1982; 1990; 1991) developed the “heuristic mathematical model for the dynamics of sensory conflict and motion sickness”. Though his model was also qualitative in nature, yet it helped in blending the mathematics and neurophysiological notions of sensory conflict and motion sickness. Inspired by this model and findings of others (Stott 1986; Benson 1988; Guedry 1991b) Bos & Bles (1998; Bos & Bles 1998b; Bos & Bles 1998a; Bos & Bles 2002; Bos et al. 2008) have developed a new variant of sensory conflict theory called “subjective vertical conflict” theory for motion sickness. This theory forms the primary source of inspiration for this work and is briefly presented in §3.6.7 .

3.6.6 Postural Instability Theory

During their studies concerning postural stability (not supposed to elicit motion sickness), Stoffregen (1985; Stoffregen et al. 1999) found that the participants opting for discontinuation of experiment complained and reported symptoms of motion sickness. This came as a surprise for them as there was no real or virtual motion involved in their studies. These observations coupled with the similar findings reported by Lishman & Lee (1973), encouraged Stoffregen & Ricco (1991) to review and subsequently reject the “sensory conflict” theory from ecological perspectives. They concluded that the “sensory rearrangement” and “neural mismatch” hypotheses were unable to explain the elicitation of motion sickness attributable to very small amplitude of self-induced spontaneous sway motions. According to “sensory conflict” paradigm, low-magnitude sensory conflicts (such as resulting from spontaneous sway) are a common, if not necessary, feature of mundane behaviour and should not cause motion sickness symptoms (Reason 1978b; Oman 1982).

Another important observation was regarding the level of spontaneous sway motions (displacement and velocity) in the “sick” group, which showed significantly higher magnitudes as compared to the “well” group. Based on these findings Riccio & Stoffregen (1991) postulated a new hypothesis of motion sickness called “postural instability theory”. This theory relies on postural control defined as: “the coordinated stabilisation of all body segments” and the postural stability: “the state in which uncontrolled movements of the perception and action systems are minimised”. The fundamental proposal of this theory is: “...prolonged postural instability is the cause of motion sickness”; in other words “degradation in the ability to actively control the postural motions of the body and its part (leads to the motion sickness, Stoffregen & SmartJr 1998)”. They (Riccio & Stoffregen 1991) have also identified some corollary hypotheses, the most important of which are:

- “(Motion sickness) Symptoms may...scale directly to the magnitude of instability”.

- “Reductions in demands on postural control should reduce the incidence or severity of motion sickness”.

They substantiate above corollaries by giving the example of a supine person or the one resting his / her head is able to attenuate or even eliminate the symptoms of motion sickness. In their later studies, Stoffregen and co-workers demonstrated (by either measuring the postural sway or recording the centre of pressure displacements) that the subjects experiencing motion sickness symptoms exhibit increased levels of postural instability. They have applied and validated their theory for the visually induced motions while the subjects were either sitting or standing on earth-fixed platforms (Stoffregen et al. 2000; Bonnet et al. 2006; Faugloire et al. 2007; Villard et al. 2008). They have also tested the “postural instability” hypothesis for the cases where no motion was induced, but the subjects were partially restrained (Bonnet et al. 2008). However, they have not conducted any “postural instability” study for motion sickness that uses real motions of a moving platform. Perhaps the difficulties involved in differentiating the postural motions from those induced by the vehicular motions are the discouraging factors.

Interestingly, there are very few (known) studies in the literature attempting to disprove the “postural instability” theory. Warwick-Evan & Beaumont (1995) conducted a twofold study aiming to; firstly test the “sensory conflict” hypothesis that motion sickness is exacerbated with increased level of sensory conflict. Secondly, to evaluate that reducing demands on postural control will reduce motion sickness as predicted by the “postural instability” hypothesis. They exposed their sitting participants to the two levels of (visual-vestibular) sensory conflict by displaying a video film at two speeds (normal and 20% fast), which was recorded at eye-level perspective of someone walking inside and outside a building. In order to reduce demands on postural control all subjects were asked to sit on hard chair designed to minimise their postural movements. The results were:

- Motion sickness was widespread; unaffected by the restraints

- There was significantly greater motion sickness associated with the lower sensory conflict.

The abovementioned study was thus not supporting the hypothesis of either theory i.e. increased sickness with increased conflict or reduced sickness with reduced demands on postural stability. Since only one condition of posture (restrained sitting) was considered, this study faced criticism that it could not be used to verify if restraining (hence postural stability) had any effects on motion sickness. This led Warwick-Evans et al. (1998), to run another similar study in which they subjected the participants to two different levels of sensory-conflict (again visual-vestibular) under two levels of postural restraints (standing and lying down on a coach). Once again they could not verify the hypothesis of “postural instability” regarding reduction in motion sickness under restrained condition; also the subsidiary proposition of the “sensory conflict” (increased sickness with increased conflict) remained inconsistent.

On a more fundamental basis this theory lacks vestibular basis, which plays the pivotal role in motion sickness etiology(Benson 2002). Consequently, it is unable to explain why LDs do not become motion sick in an environment otherwise taxing on postural control. Furthermore, underlying mechanism of the phenomenon like habituation / adaptation remains unexplained by the theory

3.6.7 Subjective Vertical Conflict (SV-Conflict) Theory

In their studies concerning human centrifugation, Bles et al.(1995) observed that after prolonged centrifugation the motion sickness is elicited only by those head movements that alter head orientation relative to Earth’s gravity. In that the roll and pitch motions of head were provocative in the upright sitting subjects, whereas yaw movement would only induce motion illusions without any associated sickness. Likewise, in supine position motion sickness appeared while executing yaw and pitch head movements, but the roll motion was not nauseating. They also noted that studies related to optokinetic circularvection rarely report motion sickness symptoms (Bles 1981). Interestingly, in such studies subjects would focus onto an

optokinetic drum (a black and white striped cylinder which rotates in front of a seated, stationary subject) that stimulates the visual illusionary sensation of self rotation (circularvection), which is in direct contradiction with the sensory cues generated by the vestibular system. According to “sensory rearrangement” theory (Reason 1970; Reason & Brand 1975; Reason 1978b) and the heuristic model of “neural mismatch” proposed by Oman (1982), such a conflict should be highly provocative, whereas it was not the case. The optokinetic circularvection does exhibit nauseogenic characteristic but it is when the head is tilted, in which case it is referred to as pseudo-Coriolis effects (Bos & Bles 2004; 2006; Bos et al. 2008).

These observations coupled with earlier studies attempting to explain elicitation of motion sickness through (sensory conflict generated) illusionary disorientation (Guedry 1991b; Guedry et al. 1998), encouraged Bos & Bles (1998; Bos & Bles 1998b; Bos & Bles 1998a; Bos & Bles 2002; Bos et al. 2008) to redefine the “sensory rearrangement” theory. Effectively, they have restated the “neural mismatch hypothesis” (Reason 1978b) that formed the basis of Oman’s (1982) heuristic model. They re-postulate these theories as: “All situations which provoke motion sickness are characterised by a condition in which the ‘sensed vertical’ as determined on the basis of integrated information from the eyes, the vestibular system and the non-vestibular proprioceptors is at variance with the ‘subjective (expected) vertical’ as predicted on the basis of previous experience” (Bles et al. 1998). The original version of “sensory rearrangement” theory identifies various inter and intra-sensory conflicts between and within the spatial sensory systems respectively (see Table 3.1 in §3.6.2). Whereas, the “neural mismatch” hypothesis links these sensory conflicts with “expectations” as the existence of conflicts themselves are not sufficient enough to elicit a sustained motion sickness (see §3.6.4).

The primary question that concerns “subjective vertical, SV” theory, as Bles et al. (1998) put it, is: “...whether the conflict categories as described by several authors (Reason & Brand 1975; Oman 1982; Griffin 1991a; Guedry 1991b) can be restricted to only this conflict, or, in other words, is the SV-conflict theory sufficient to account for the different forms of motion sickness?” Bearing in mind this fundamental

question, they discuss some of the most important and commonly observed sickness provoking laboratory / real life motion scenarios. In the same work, they have qualitatively demonstrated that SV-conflict is sufficient to explain the nauseogenicity of Coriolis effects, seasickness, micro & hyper-gravity, air & car sickness, simulator sickness and clinical vertigo. It is generally accepted that passively induced motions are primarily responsible for the elicitation of motion sickness as active motions form part of the locomotion (natural way to move around) that are rarely sickness provoking. Interestingly enough, despite having similar sensory conflict, not all passively induced real / virtual motion situations are nauseogenic. Since, not all passive motions lead to a conflict between the sensed and expected vertical i.e. SV-conflict, hence "...this might explain why people get sick in one situation and not in the other, despite the fact that sensory conflict (as per neural hypothesis) is large in both situations" (Bles et al. 1998).

Bles et al.(1998; 2000) report that the passive motions varying body orientation with respect to gravity are far more provocative than those which do not alter gravity; this also substantiates the SV-conflict hypothesis. An obvious example is the level of motion sickness elicited while people are rotated in yaw direction (without any head tilt to avoid Coriolis effects) about their z-axis (directed from feet to head) in a lit room. If this rotation is about the Earth's vertical (an axis perfectly aligned with gravity) than almost no one would get motion sick. Whereas, if they are rotated about an off-vertical axis (in a barbeque fashion) then most of the people find it highly nauseating (Bos & Bles 1998a). In the first instance, when the axis of rotation is aligned with Earth's vertical, there will be no signal of angular velocity after a while due to the dynamics of semicircular canals. Hence no SV-conflict will be produced, though the visual-vestibular conflict would still exist as per the general sensory conflict theory (which should be highly provocative). In the later case, the rotating gravity vector would give rise to a conflict between the sensed and expected vertical that should lead to motion sickness in accordance with the SV-conflict theory (which does take place). Another natural aspect of living organisms that supports SV-conflict theory is their dependence on Earth's gravity to establish their orientation for an upright posture.

Though, the qualitative explanation provided by the general sensory conflict theories (“sensory rearrangement” and “neural mismatch hypothesis”) are very detailed, rationale and comprehensive. Nevertheless, the “Only one provocative conflict?” paradigm proposed by SV-conflict theory appears to be very pragmatic and highly successful in explaining the elicitation of motion sickness under most of the encountered provoking situations. Furthermore, the mathematical model of SV-conflict theory (Bles 1998), primarily involving the vestibular system (Bos & Bles 1998b; Bos & Bles 1998a), has successfully been used to predict the results of past laboratory experiments on motion sickness (O’Hanlon & McCauley 1974; McCauley et al. 1976) as shown in Figure 3.7.

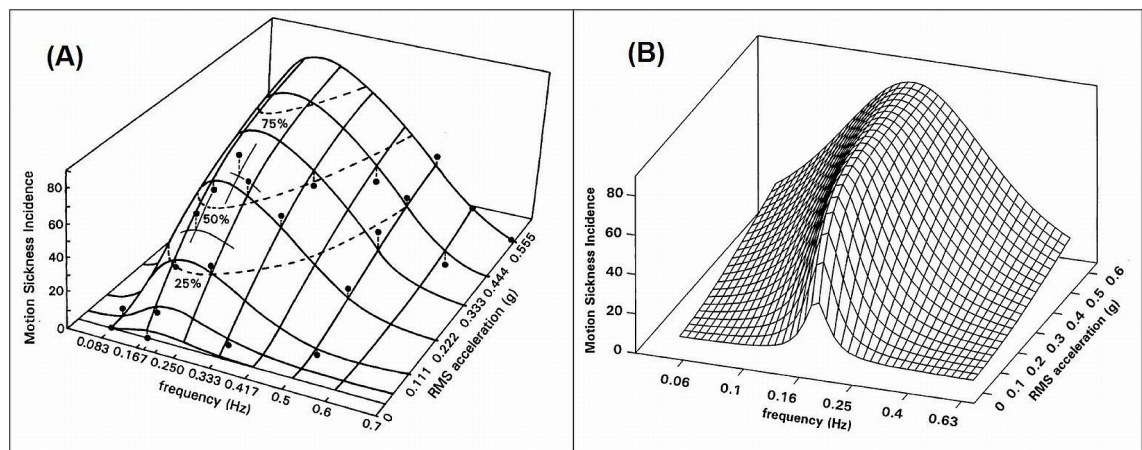


Figure 3.7. (A) Motion sickness incidence (%) after 2h of endured motion versus frequency and acceleration [O’Hanlon & McCauley 1974] (B) MSI (%) predicted using SV-Conflict model after 2h of vertical sinusoidal motion versus frequency and acceleration [Bos & Bles 1998].

In a later work, Bos et al.(2002a) extended their SV-conflict model to predict sickness under six degrees of freedom motions, however, the sensory conflict was still limited to the differences between the sensed and expected (subjective) verticals. They suggested splitting the SV-conflict vectors into magnitude and orientation effects, wherein the orientation effects would be zero under pure vertical oscillations. The magnitude effects were attributable to the changes in gravitoinertial accelerations, therefore, leading to a ‘slow’ accumulation of motion sickness. Whereas, the orientation effects were assumed to cause ‘fast’ nauseogenic phenomenon like Coriolis effects. Thus, the latency of the two (i.e. magnitude &

orientation) effects were different (several minutes for the magnitude and tens of seconds for the orientation effects were used).

However, the practical demonstration of the extended model was limited to the simulation of combined sway and roll motions, as depicted in Figure 3.8 . It is interesting to note that the sickness levels predicted by the extended model were much higher than the expected values, which might be attributable to the way the ‘orientation’ effects were transformed into MSI i.e. using ‘fast’ path. Nevertheless, this approach could be used to account for the differences in humans’ sensitivity to become motion sick under the purely vertical and horizontal oscillations, as reported by various laboratory studies (O’Hanlon & McCauley 1974; McCauley et al. 1976; Golding & Kerguelen 1992; Golding et al. 1995; Golding & Markey 1996; Golding et al. 1997; Golding et al. 2001; Donohew & Griffin 2004).

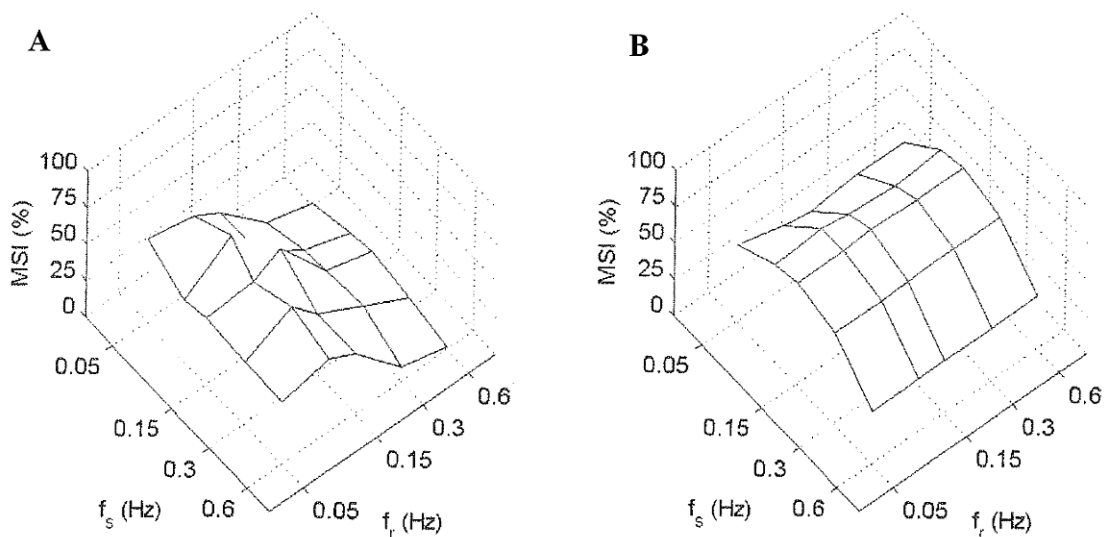


Figure 3.8. MSI for combined sway (A: 0.5 ms^{-2} , B: 1.5 ms^{-2}) and roll (A: 10° ; B: 2°) (Bos et al. 2002a)

3.7 Existing Methods & Standards of Motion Sickness Prediction for Ships

Griffin (1991a) argues that out of a large variety of theories attempting to explain why and how motion sickness occurs, none is capable of quantitatively estimating its occurrence for a given stimuli. This statement is however no longer valid, as with the

advent of “subjective vertical conflict” theory (Bles et al. 1998; Bos & Bles 1998b; Bos & Bles 1998a; Bos & Bles 2002), physiological models are now available for the quantitative prediction of motion sickness (Bos & Bles 1998b; Ververiotis 2004). The existing motion sickness prediction methods may broadly be divided into two major categories:

- Descriptive methods / models
- Physiological methods / models

The ‘descriptive’ category tries to predict incidence of motion sickness using statistical (regression) models relying on vessels’ motion (mainly vertical accelerations) covariates. A significant research has been made to identify the specific ship motions that cause people to become seasick. There have been several onboard surveys (Lawther & Griffin 1986; 1987; Turan 2006) and laboratory simulations of ship motions (Sjöberg 1970; O'Hanlon & McCauley 1974; McCauley et al. 1976; Wertheim et al. 1998), to determine the effects of various motion types (roll, pitch and heave). The second category of sickness prediction methods, with the exemption of SV-conflict model, is primarily qualitative, forecasting the elicitation of motion sickness in a given motion environment.

Needless to say, the ease of use associated with the statistical model and the difficulties linked with the realization of physiological model such as SV-conflict (which is quite recently developed anyway), have facilitated widespread use of methods falling under the descriptive category. The current (only two) standards extensively used in commercial marine industry, for seakeeping analysis of ships from human comfort / performance view point, make use of the statistical models (Lawther & Griffin 1986; 1987). In the following sub-sections, the descriptive methods widely used for motion sickness prediction aboard ships, both in literature and in practice, are presented.

3.7.1 O’Hanlon & McCauley’s (1974) MSI Method

Tyler & Bard (1949) and Sjöberg (1970) suggested that periodic vertical motions

play primary role in the etiology of motion sickness aboard conventional vessels. Influenced by these findings and the laboratory studies by Wendt (Alexander et al. 1945a; 1945c; 1945b; 1945d) at the Wesleyan University, O’Hanlon & McCauley (1974) conducted laboratory experiments involving vertical sinusoidal motions of a ship simulator. They studied the effects of motion parameters (mainly vertical acceleration amplitudes and frequencies) on the elicitation of sickness, by exposing 306 healthy, young (18-34 years) male students to simulator motions for 2 hours or lesser (if emesis occurred). The participants were subjected to simulator motions while sitting on aircraft-like seats with lap belt and headrest (to minimise head movements). They were tested in pairs; each sitting on one side of the cabin that was divided into two sub-compartments using a floor to ceiling visual barrier. The independent sample size was at least 20 subjects for each one of the fourteen combinations of average vertical sinusoidal accelerations (from 0.025 to 0.40g) and frequencies (from 0.083 to 0.5Hz). The average vertical acceleration (\bar{a}) was measured as the time integral of their absolute values for each half-wave cycle (for simple sinusoidal motions $\bar{a} = 0.637a_{max} = 0.901a_{rms}$).

O’Hanlon & McCauley (1974), quantified the severity of sickness as the percentage of subjects experiencing vomiting for a given combination of acceleration amplitude and frequency; termed as “Motion Sickness Incidence, MSI(%)”. They found that MSI(%) increased monotonically with acceleration (\bar{a}) for a given frequency as shown in Figure 3.9, and had its maxima corresponding to the oscillations of 0.167Hz. They used Equation(3.1), which effectively represents the integral of normal distribution function, to describe the relationship between MSI and logarithm of average vertical acceleration (\bar{a}).

$$MSI = \int_{-\infty}^{\log(\bar{a})} \left(\frac{100}{\sigma\sqrt{2\pi}} \right) \exp\left(-\left[\left(\frac{x - \mu}{\sigma} \right)^2 \right] \right) dx \quad (3.1)$$

Where, x is a dummy variable in terms of $\log(\bar{a})$, while σ and μ are empirically determined parameters. They found the following approximate relationship between μ and the motion frequency, f :

$$\mu = 0.654 + 3.697 \log(f) + 2.320 \{\log(f)\}^2 \quad (3.2)$$

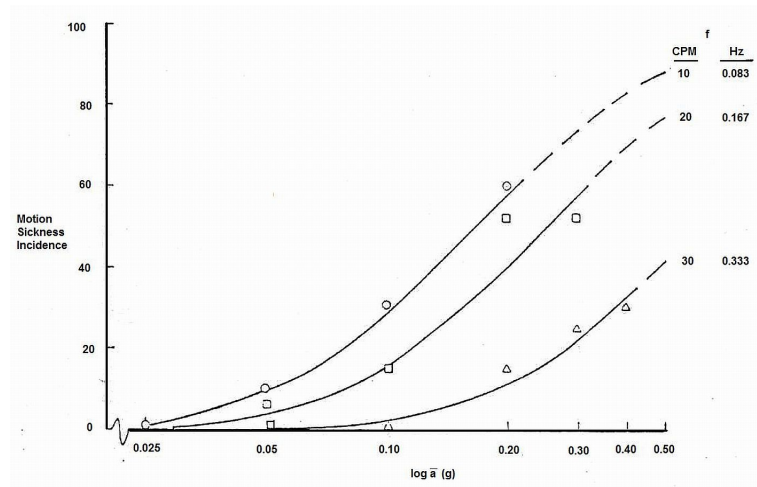


Figure 3.9. Motion Sickness Incidence (within 2 hours) as a function of log average acceleration (\bar{a}) for each wave frequency (f) [O'Hanlon & McCauley, 1974]

By substituting $\sigma = 0.40 \log(\bar{a})$ and μ from Equation(3.2) into Equation(3.1), they derived the mathematical model that links MSI (%) with acceleration magnitude (\bar{a}) and oscillation frequency (f). This model is graphically depicted in Figure 3.10.

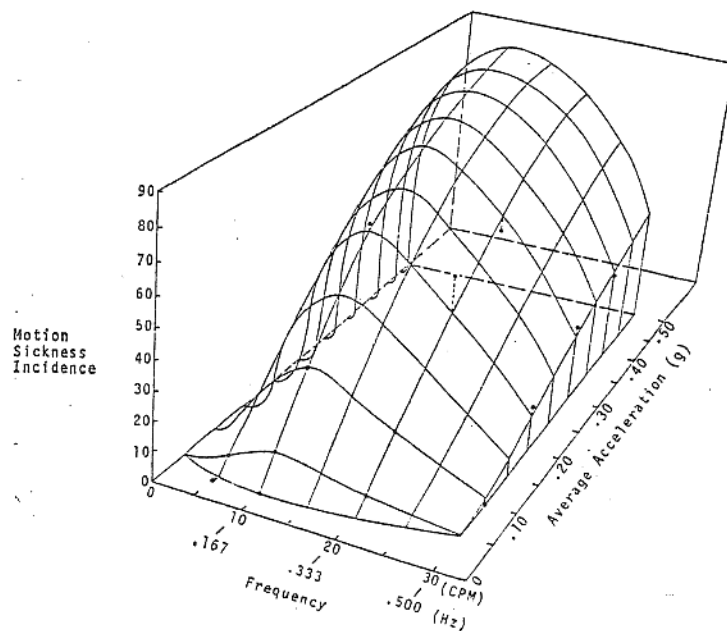


Figure 3.10. Empirically derived relationship of MSI (percent emesis within 2 hours) to wave frequency and average acceleration imparted during each half-wave cycle for vertical sinusoidal motion [O'Hanlon & McCauley, 1974]

3.7.2 McCauley et al. (1976) Method

The laboratory study undertaken by O'Hanlon & McCauley (1974) simulated vertical motions only. In order to establish the relative significance of roll, pitch, and their combinations with verticals motions on to the motion sickness and its habituation, McCauley et al. (1976) exposed 500 young male subjects to the following provoking environment of ship motion simulator:

- Pure vertical sinusoidal motions of constant peak accelerations with twenty-five combinations of ten frequencies (from 0.083 to 0.7Hz) and various (RMS) magnitudes (from 0.27 to 5.5 m/s²).
- Pure rotational sinusoidal motions (either roll or pitch) at three frequencies (0.115, 0.230 and 0.345Hz) and magnitudes up to 10 degrees.
- Combination of rotational motions (either roll or pitch) at three frequencies (0.115, 0.230 and 0.345Hz) and magnitudes up to 10 degrees with vertical oscillations at 0.25Hz and magnitude of 1.1m/s² rms.

The experiment procedure and arrangements, apart from the motion conditions, were identical to their earlier work (O'Hanlon & McCauley 1974). The participants were exposed to simulator motions for up to 2 hours (or less, in case of emesis), while seated with their heads in head rest. The findings of this study are summarised in the following:

- Observed MSIs in pitch only and roll only conditions were 9.0% and 0% respectively, which were statistically not different from zero.
- MSI for the case of heave only (0.25Hz and 1.1m/s² RMS) condition was significant at 31%.
- MSI in the pitch plus heave and roll plus heave conditions were 34% and 31%, which were not significantly different from heave only condition (i.e. 31%).

Based on these observations, McCauley et al. (1976) concluded that rotational motions (pitch or roll) either at their own or in combination with heave motions do

not contribute significantly and that the heave motion is the only significant contributor towards the elicitation of motion sickness. This conclusion was further substantiated by Lawther & Griffin (1986; 1987; 1988a), who found the vertical motions to correlate better with motion sickness, while conducting full scale trials onboard large passenger vessels. It is interesting to note that very few researchers have challenged this generally accepted premise that vertical motions are the sole cause of motion sickness. For example, Wertheim et al (1998) demonstrate that pitch and roll motions do become significantly important when combined with otherwise insignificant (from motion sickness view point) vertical motions.

The effects of magnitudes and frequencies of vertical motions on the occurrence of motion sickness found by McCauley et al.(1976) are shown in Figure 3.11. Once again the maximum sensitivity to motion sickness around 0.167Hz is quite evident.

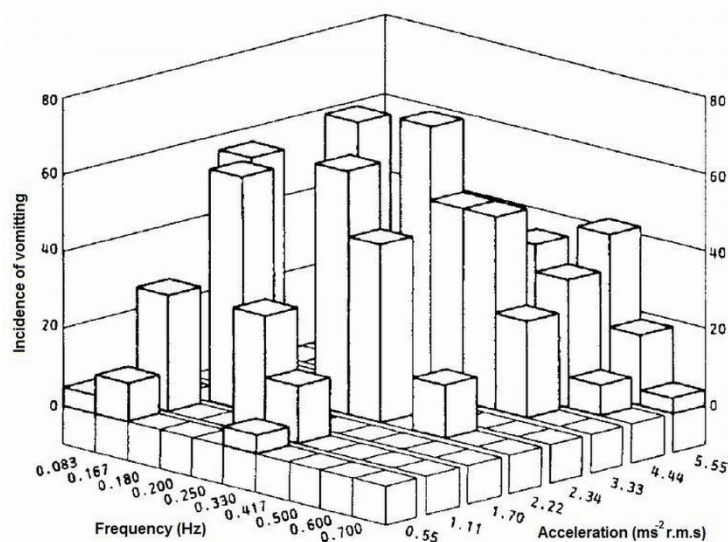


Figure 3.11. Incidence of vomiting associated with exposure to various magnitudes and frequencies of vertical oscillation [McCauley et al. (1976)]

The relationships of exposure duration with MSIs (%) and oscillation magnitudes at a given frequency are shown in Figure 3.12. It is interesting to note that initially MSI increases exponentially and subsequently becomes logarithmic function of exposure time.

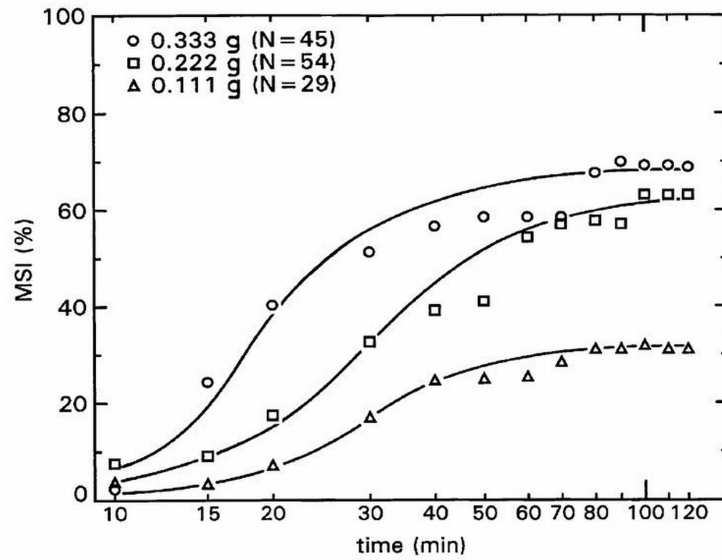


Figure 3.12. Motion sickness incidence variation with exposure time at the vertical oscillation frequency of 0.25Hz [McCauley et al. (1976)].

The mathematical model used to describe the relationship of MSI(%) with the vertical oscillation (acceleration) magnitudes, frequencies and the exposure time is given by:

$$MSI = 100\Phi(z_a)\Phi(z_t) \quad (3.3)$$

Where, $\Phi(z)$ is a cumulative distribution function of the standard normal variable z , as per:

$$\Phi(z) = \frac{1}{\sqrt{2\pi}} \int_{-\infty}^z \exp\left(-\frac{1}{2}x^2\right) dx \quad (3.4)$$

The standardized-normal-variables of Equation(3.3) are related to the vertical oscillation characteristics (magnitude, frequency and duration) by the following expressions:

$$z_t = \frac{\log(t) - 1.46}{0.76},$$

$$z'_t = \frac{z_t - \rho z_a}{\sqrt{1 - \rho^2}},$$

$$z_a = \frac{\log(a) - \mu_a(f)}{0.47\sqrt{1 - \rho^2}}$$

By using $\rho = -0.75$ and $\mu_a = 0.87 + 4.36 \log(f) + 2.73 \log^2(f)$ they estimated:

$$z_a = 2.128 \log(a) - 9.277 \log(f) - 5.809 \log^2(f) - 1.851 \quad (3.5)$$

$$z'_t = 1.13 z_a + 1.989 \log(t) - 2.904 \quad (3.6)$$

Where, a is the RMS vertical acceleration in the units of g (acceleration due to gravity); f is the oscillation frequency; and t is the exposure time in minutes. Graphical representation of Equation(3.3) and its fitness to experiment results is shown in Figure 3.13, which is identical to the previous study of O'Hanlon & McCauley (see Figure 3.10).

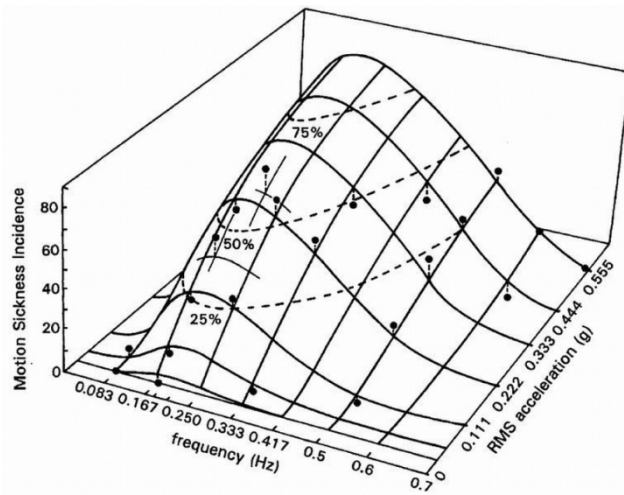


Figure 3.13. Mathematical model describing MSI(%) after 2 hours of endured motion versus frequency and acceleration [McCauley et al. (1976)].

The mathematical models proposed by O'Hanlon & McCauley (1974) [Equation(3.1)] and McCauley et al.(1976) [Equation(3.3)], being able to numerically predict the

motion sickness, provided very useful tools for the design and operation of seagoing vessels. The discovery of human's maximum sensitivity to vertical motion around 0.167Hz formed the yardstick for the seakeeping assessment of hullform during the design phases. New designs, novel or proven, were tested for the frequency response of their motions and attempts were made to avoid high magnitude vertical accelerations around this frequency.

The following shortcomings in these models render them inappropriate for predicting motion sickness incidences aboard real ships in general and High Speed Crafts (HSCs) in particular:

- HSCs exhibit horizontal (fore-and-aft and lateral) motions comparable to the vertical motions (Turan 2006). Also, the laboratory findings concerning elicitation of sickness under purely horizontal oscillations suggest almost twice nauseogenicity of such motion as compared to the purely vertical motions (Golding et al. 1995). Consequently, seasickness predicted by these models underestimate the observed value (see also §7.10 & 8.6).
- The experiments were conducted using healthy young men (18-34 years) that are not a true representative of general population found aboard ships. As explained in §3.4.2, age is one of the significant variable that affects susceptibility to motion sickness. Thus, the general population of ship passengers with a wide variation in age is expected to elicit different motion sickness characteristics than the one recorded in these studies.
- The models were derived from experiments involving vertical sinusoidal motions at one particular frequency, whereas the real ships exhibit complex random motions comprising of several sinusoids of various amplitudes and frequencies.

This last point highlighted in above was also confirmed by Guignard & McCauley (1982). In this later work, they exposed independent groups of up to 32 young men, seated with heads in head rest, to one of the five combinations of vertical motions for up to two hours (or less on vomiting). There was one control condition of 0.13g RMS

at 0.17Hz (the most nauseating frequency) and four test conditions produced by the sum to two sinusoids, the fundamental at 0.17Hz and second or third harmonic. The test conditions differed either in the phase relationships between fundamental frequency and its harmonics or in the relative acceleration levels of the harmonic components attempting to replicate real ship motions. Findings of this study (outlined below) were very interesting, as the effects of multiple motion signals (even having same fundamental frequency) become very conspicuous.

The test condition (having the highest total RMS acceleration) was supposed to represent the worst case, but it failed to produce the highest MSI. The authors expressed: “despite the apparent effects of total RMS acceleration, it is far from adequate as a sole index of the sickness-induced nature of vertical motion because it fails to account for multiple frequency effects”. In addition, not only the most nauseogenic motion signal did not have the highest total RMS acceleration but its components were also not the highest amongst all test conditions.

They could not identify any relationship between the observed and predicted MSI [using Equation(3.3)], also no correlation was found between the recorded MSI and the total RMS or peak accelerations. The natural conclusion of this study was: “An MSI model based solely on the incidences observed as a function of frequency and RMS acceleration for sinusoidal motion is not reliably predictive of MSI due to complex motion” (Guignard & McCauley 1982). Despite the aforementioned weaknesses, it is amazing to see that these methods (O'Hanlon & McCauley 1974; McCauley et al. 1976) had extensively been used and are still in use today by the maritime industry, perhaps, due to relative ease of use.

Nevertheless, it must be appreciated that no later studies on motion sickness involving laboratory experiments has ever been organised on such a large scale i.e. involving 500 or more subjects. The lab trials by McCauley and O'Hanlon may rightly be considered as the cornerstone of the modern history of experiment-based motion sickness investigations.

3.7.3 ISO 2631-3:1985

The International Standard 2631-3:1985 “*Evaluation of Human Exposure to Whole-Body Vibration Part 3: Evaluation of Exposure to Whole-Body Z-Axis Vertical Vibration in the Frequency Range 0.1 to 0.63 Hz*” (ISO 1985) was developed “...based on critical surveys and analyses of laboratory and field studies” related to motion sickness in the frequency range of 0.1 to 0.63Hz (Allen 1974). This standard provided a link between the vertical acceleration levels (RMS), the frequency of oscillations, and exposure time in a graphical format as shown in Figure 3.14. The standard acknowledges variability of general public to the effects of exposure to whole body vibration i.e. motion sickness.

As already mentioned in §3.4 & 3.5, a large variation in the susceptibility to motion sickness is observable. Some individuals with inefficient or non-functional labyrinthine apparatus do not get sick in the roughest environment, whereas, there are others readily seasick just by looking at a rocking boat. Thus, some motion sickness is inevitable for any passenger ferry operations in a provoking environment; therefore, ISO standard proposed a MSI limit of 10%. For a given frequency (or centre frequency), the limiting lines in Figure 3.14 identify the maximum vertical accelerations (RMS) that should limit the MSI to 10% (amongst sitting or standing fit young men), for a 30min, 2hours and (tentatively) an 8 hours exposure.

The acceleration magnitudes and exposure time are in an inverse-square relationship i.e. doubling the acceleration level is equivalent to four times reduction in exposure time i.e. the following relationship holds:

$$a^2 \times t = \text{Constant} \quad (3.7)$$

Where ‘ a ’ is the RMS acceleration and ‘ t ’ is the exposure duration. It can be seen from Figure 3.14 that the sensitivity to vertical accelerations is maximum from 0.1 to 0.315Hz and subsequently falls in such a way that the acceleration level required to produce 10% MSI at 0.63Hz is 3.15 times larger than the corresponding magnitude at 0.315Hz and below.

This standard became obsolete with its revision in 1997, but still some researcher refer to and make use of the acceleration limits identified in it, for example see the seakeeping study by Sariöz, K. & Narli, E. (2005).

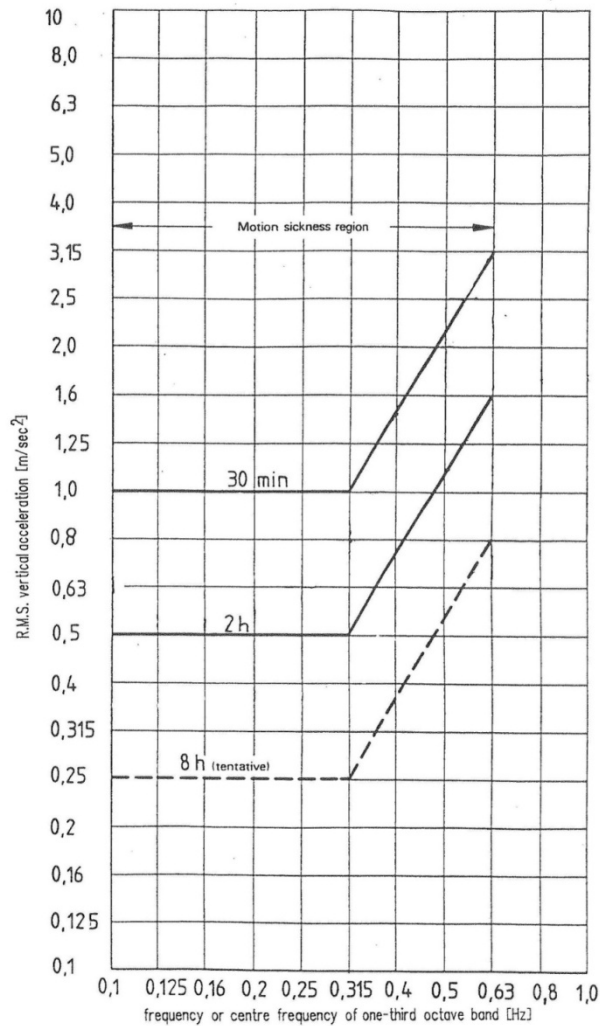


Figure 3.14. ISO 2631-3:1985 "Severe Discomfort Boundaries" [International Organisation for Standardization, 1985].

3.7.4 Lawther & Griffin (1986, 1987 and 1988) Method

Developing on the, scope-limited, past studies investigating incidence of motion sickness aboard ships (Handford et al. 1953; Nieuwenhuyzen 1958; Kennedy et al. 1965; 1968), Lawther & Griffin (1986; 1987; 1988b; 1988a) conducted full scale trials aboard six monohull, two hovercraft and one hydrofoil vessel operating around the British Isles. They recorded almost 300 hours of six degrees of freedom vessel

motions in 114 voyages ranging from half an hour to 6 hours duration. A typical set of acceleration time history for a 100sec duration of a monohull passenger ferry is shown in Figure 3.15, whereas, the corresponding spectral densities during its 4 hours of voyage are given in Figure 3.16

The representative motion time histories in Figure 3.15 and spectral densities in Figure 3.16 clearly indicate that in case of a monohull vessel, vertical motions are the highest in magnitude with dominant frequency around 0.2Hz. This frequency is believed to be the most sensitive frequency for the elicitation of motion sickness (O'Hanlon & McCauley 1974; McCauley et al. 1976), which also explains why ship motions are generally so much nauseogenic. Moreover, being coupled with each other, vertical and pitch motions as well as the lateral and roll motions have similar shapes.

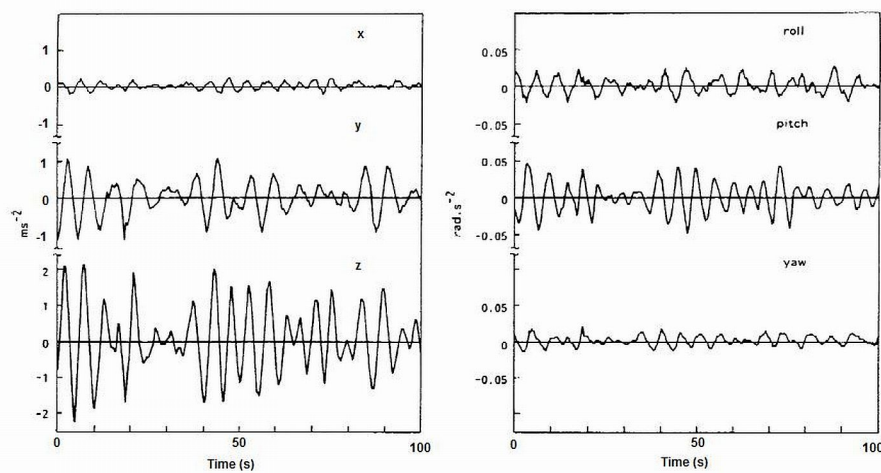


Figure 3.15. Acceleration time histories for the six degrees of freedom motion of a ship [Griffin 1990].

Lawther & Griffin (1986; 1987) recorded individual data (age, gender, regularity of travel, taking of anti-seasickness tablets and alcohol), comfort levels (using a subjective illness rating scale) and incidence of motion sickness using survey questionnaires. A total of 20,029 questionnaires were returned by the passengers that were subsequently used for an extensive statistical analysis to establish associations between individual data, comfort entities and variations of vessel motions. Their

general findings of were very similar to those of O'Hanlon & McCauley (1974) and McCauley et al. (1976), as the “vomiting incidence (VI)” (percentage of people vomited) exhibited strongest correlation with the vertical motions; both in terms of magnitude and exposure time.

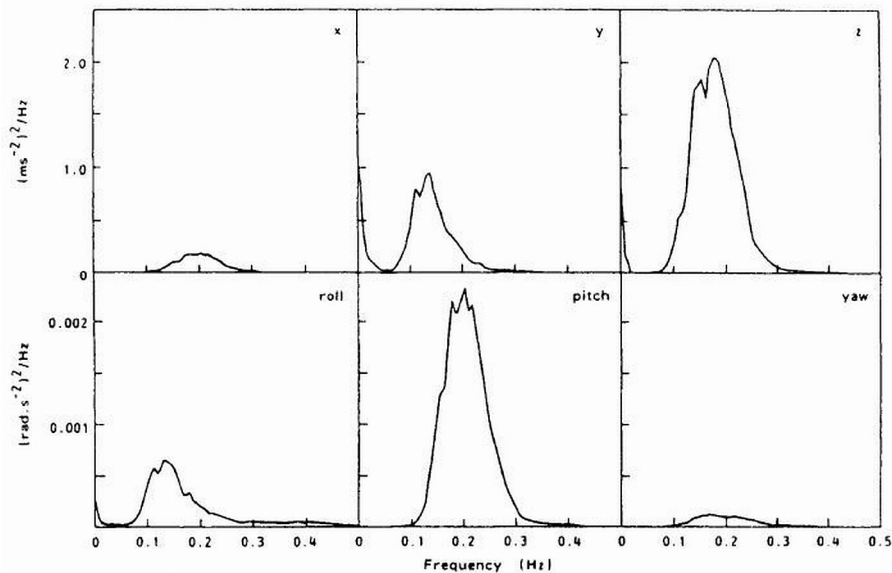


Figure 3.16. Acceleration power spectral densities for the six degrees of freedom ship motions: frequency resolution 0.01Hz; duration 4hours [Griffin 1990].

Lawther & Griffin (1987) rigorously examined the effects of vertical oscillation (acceleration) magnitudes, frequencies and exposure durations onto the elicitation of motion sickness. They used data from past experiment studies undertaken at the Wesleyan University (Alexander et al. 1945a; 1945c; 1945b; 1945d), the Human Factors Research Incorporation (O'Hanlon & McCauley 1974; McCauley et al. 1976; Guignard & McCauley 1982) and their own field trials (Lawther & Griffin 1986; 1988a). The collated results depicting effects of motion magnitudes on the occurrence of sickness are shown in Figure 3.17; wherein vomiting incidence appears to linearly increasing with RMS vertical acceleration levels for a given frequency.

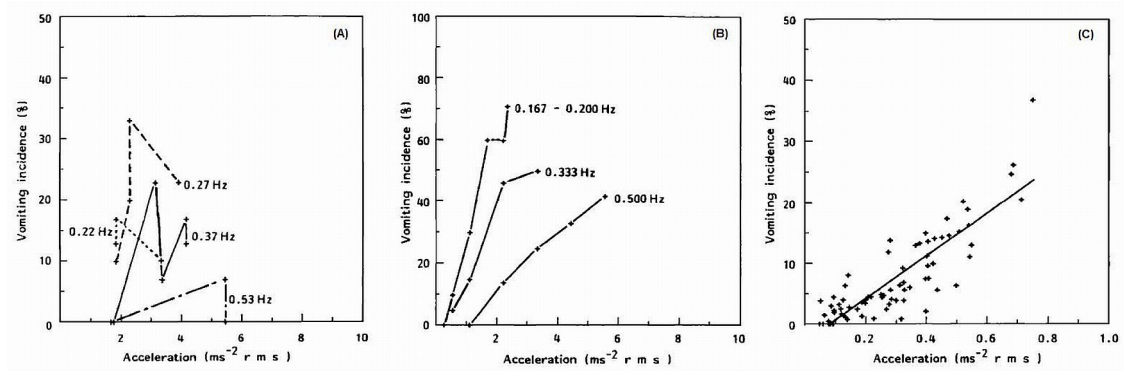


Figure 3.17. (A) Acceleration effects of 20min exposure at four frequencies [Alexander et al. 1947] (B) Acceleration effects of 2hrs exposure at three frequencies [McCauley et al. 1976] (C) Acceleration effects of 2hrs exposures on board ships with dominant frequency around 0.2Hz [Lawther & Griffin 1988b] [adopted from Lawther & Griffin 1987].

While investigating the effects of oscillation frequency on the incidence of vomiting, they assumed a linear relationship between the motion magnitude and its associated sickness. Thus, they eliminated the magnitude effects by dividing the observed VI with corresponding RMS accelerations and calculated the so called “Normalised Vomiting Score” using:

$$\text{Normalized Vomiting Score} = \frac{\text{Vomiting Incidence}}{\text{RMS acceleration}} \quad (3.8)$$

Normalised results of the past studies mentioned in above are graphically depicted in Figure 3.17. The data from Wesleyan University, based on 20min exposure, is shown in Figure 3.17(A); Human Factor Research Incorporation’s data for the 2hours exposure can be seen in Figure 3.17(B). The combined data of these studies (HFRI data re-calculated/interpolated for 25min as the original data is available for 2hours exposure) is depicted in Figure 3.17(C).

Normalised vomiting incidence exhibited a clear dependence on the frequency of (vertical) oscillation (Figure 3.17), which is more evident in the HFRI data. Lawther & Griffin (1987) noted that the relationship between oscillation frequencies and normalized VIs can be represented by a series of straight line approximations as shown in Figure 3.18. In order to take account of the frequency effects of a real

ship's vertical motions on VI, they proposed to use the aforementioned straight lines as frequency weightings.

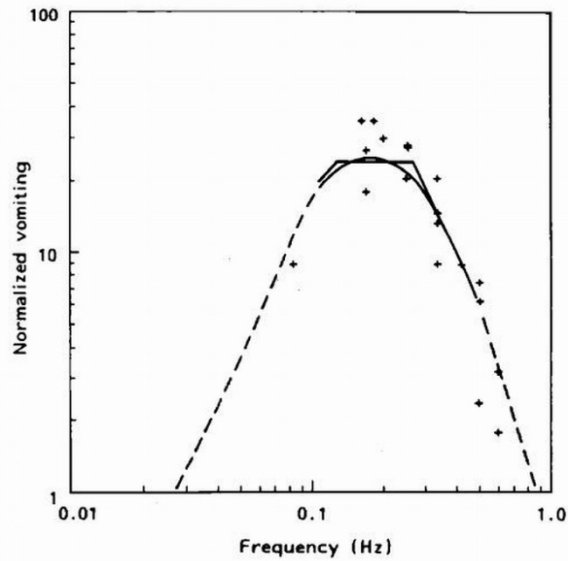


Figure 3.18. The effects of frequency on normalized vomiting incidence for 2h exposures [McCauley et al. 1976], with suggested asymptotic frequency weighting (solid lines) and approximate weightings using an analog/digital filter (dashed line) [adopted from Lawther & Griffin 1987].

These frequency weightings can be realised using an analog / digital band-pass filter that allows the acceleration signals to pass unchanged for the frequencies between 0.125 and 0.25Hz, with a 6db per octave and a 12db per octave decrease below and above this range respectively. These weightings $w(f)$, can also be estimated as functions of frequencies (f) using the following expressions (Griffin 1990):

$$\begin{aligned}
 w(f) &= \frac{f}{0.125} & \text{for } 0.1 \leq f \leq 0.125 \\
 w(f) &= 1 & \text{for } 0.125 \leq f \leq 0.25 \\
 w(f) &= \left(\frac{f}{0.125}\right)^2 & \text{for } 0.25 \leq f \leq 0.5 \\
 w(f) &= 0 & \text{otherwise}
 \end{aligned} \tag{3.9}$$

The third variable considered by Lawther & Griffin (1987) to explain variability in the motion sickness observed onboard ships was the exposure duration. They noted that the number of passengers suffering emesis continued to increase up to 6 hours of

motion exposures aboard ships, however, the accumulation rate of sickness incidences reduced with passage of time. Hence, a time-based cumulative measure of acceleration was defined as “motion dose” by the authors (Lawther & Griffin 1986) given by:

$$\text{Motion Dose} = \left[\int_0^T a^n(t) dt \right]^{\left(\frac{1}{n}\right)} \quad (3.10)$$

Where, a (m/sec^2) is the frequency-weighted vertical (z-axis) acceleration recorded during the total exposure (journey) time T (sec). They found that either $n=2$ or $n=4$ exhibit a good correlation with the full scale trial data pertaining to the accumulation of sickness incidences. If $n=2$ is used, then Equation(3.10) is equivalent to the product of (frequency weighted) RMS acceleration with the square root of exposure duration T (sec), that is:

$$\text{Motion Dose (m}/\text{sec}^{1.5}) = a_{(\text{weighted rms})} \times \sqrt{T} \quad (3.11)$$

In order to establish the link between motion dose and incidence of motion sickness, Lawther & Griffin (1987) calculated the motion dose received by the participants of past laboratory experiments at the Wesleyan University (Alexander et al. 1945a; 1945c; 1945b; 1945d) and those at the Human Factors Research Incorporation (O'Hanlon & McCauley 1974; McCauley et al. 1976; Guignard & McCauley 1982). They also calculated the motion dose administered to the passengers by the vertical motions of the ferries aboard which they had undertaken full scale trials (Lawther & Griffin 1986; 1988a). The scatter plot depicting variations of “Vomiting Incidences” for the 2hours voyages and the corresponding motion dose values are shown in Figure 3.19.

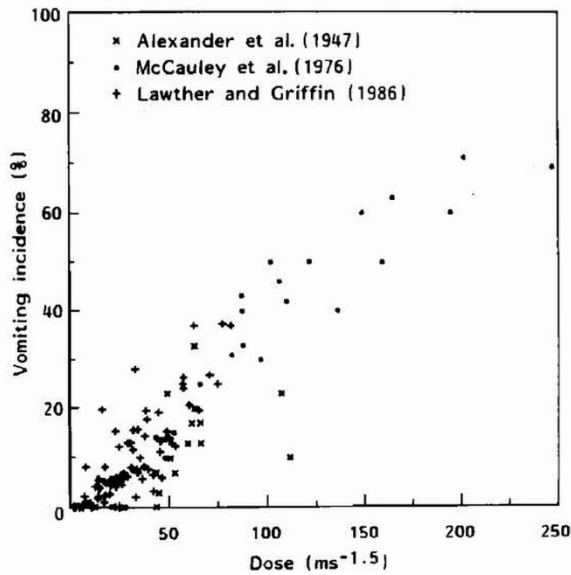


Figure 3.19. The effects of motion dose, using results from Alexander et al. (1947), McCauley et al. (1976), and Lawther & Griffin (1986) [Lawther & Griffin 1987].

They found that the slopes of regression lines attempting to explain vomiting incidences using weighted RMS accelerations for McCauley et al. (1976) and Lawther & Griffin (1988a) studies (shown in Figure 3.20), were approximately 30% / (m/sec²). These studies had exposure durations of 2-hours, which means that weighted RMS acceleration of 1 m/sec² would result into a motion dose value of 85 m/sec^{1.5}. Thus the slope of regression line linking VI with motion dose for an average mixed population should be approximately 1/3 (i.e. 30/85).

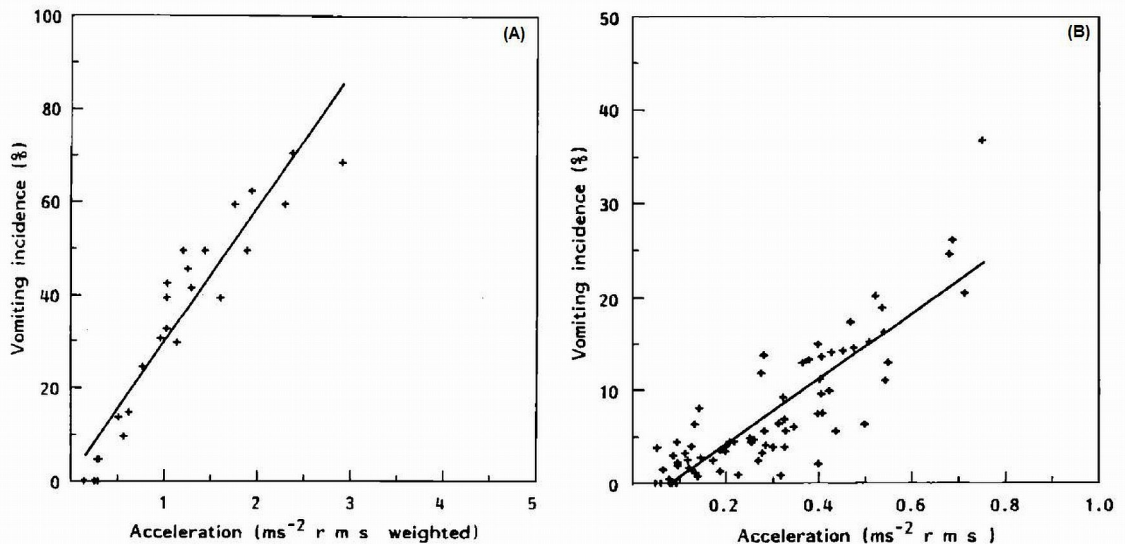


Figure 3.20. Vomiting incidence variations with weighted RMS acceleration magnitudes (A) Results from McCauley et al. (1976) (B) Results from Lawther & Griffin (1988b) [Lawther & Griffin 1987].

Lawther & Griffin (1987) proposed the following four-step method to predict the motion sickness features of a provocative environment. This method combines the effects of (vertical) acceleration magnitudes, its frequencies and exposure duration:

- **Step-I** Vertical accelerations measured at the location of interest should first be frequency weighted. Frequency weighting may either be carried out using the asymptotic weighting function [see Figure 3.18 and Equation(3.9)] or a more convenient way to accomplish this task is to use an analog / digital band-pass filter (see §3.7.5). The real world accelerations are assumed to be a sum of several sinusoids of various frequencies and amplitudes. This step, will thus, attenuate the contribution of frequencies to which human beings are less sensitive from motion sickness viewpoint. Effectively, the measured accelerations would be normalized with respect to the flat portion of weightings in the vicinity of 0.2Hz.
- **Step-II** In this step the RMS magnitudes of the weighted acceleration should be calculated by temporal integration over the whole exposure period.
- **Step-III** The weighted RMS (vertical) accelerations are multiplied with the square root of the exposure duration yielding the value of “Motion Dose”.
- **Step-IV** Finally the percentage of people likely to vomit, based on the linear regression between VI and motion dose, may be calculated by:

$$\text{Vomiting Incidence (\%)} = K \times \text{Motion Dose} \quad (3.12)$$

Where motion dose is calculated using Equation (3.11) and K is taken as 1/3.

These onboard studies by Lawther & Griffin (1986; 1988b), in principle, augmented the previous laboratory experiments of O’Hanlon & McCauley (1974) and McCauley et al. (1976). In that they primarily focused on the development of a descriptive model that could predict motion sickness, however, it cannot explain the underlying mechanism responsible for its occurrence. In addition, an implicit assumption they had in the back of their minds was about the higher significance of vertical

translational motions in the elicitation of motion sickness. Thus, in the introduction to their work they state “The prediction procedure developed in this article is intended to apply to motion sickness where the primary cause is vertical translational oscillation” (Lawther & Griffin 1986).

Interestingly, primary focus was maintained on the vertical motions despite they also observed a good correlation between sickness incidences and motions in other axes. They themselves commented that from their study it should not be concluded that motion in the axes other than vertical are unimportant. Nevertheless, due to coupling effects, the vertical acceleration dose value [Equation (3.11)], does (indirectly) include contribution from all six degrees of freedom motions; thus making their methodology more accurate than the O’Hanlon & McCauley (1974) and McCauley et al. (1976) MSI method. However, Lawther & Griffin (1987) concluded “The mathematical descriptions of the effects of the variables are not intended to reflect the underlying mechanisms that cause motion sickness, but are merely a pragmatic approach to a problem with a clearly defined scope”.

Another important shortcoming appearing in the development of this methodology is the omission of children responses, despite being ranked as highest in vomiting incidences. Lawther & Griffin (1987) report that “sickness was highest in the under-15 age group, but there may be additional factors in this age group warranting more careful study, and so people aged under-15 were excluded from further analysis”. This exclusion of children may be justified on the basis of complex factors primarily involving their onboard activities that lead to frequent head movements; thus, making them biased towards motion sickness. Exclusion of smaller biased groups such as those people who had consumed excessive alcoholic drinks and/or pills may be justifiable to improve statistical accuracy. But, exclusion of children is statistically questionable as the sample gets distorted, especially when the excluded group is exhibiting the highest ranking. Moreover, today’s children’s responses are very important as they exercise significant influence on the families’ choice to select modes of transportation. It is remarkable to see that the current standards on motion sickness like BS 6841:1987 and ISO 2631-1:1997 (see § 3.7.5) are based on Lawther

& Griffin's studies (1986; 1987; 1988b; 1988a) that deliberately excluded one of the most important group i.e. children.

3.7.5 BS 6841:1987 and ISO 2631-1:1997

BS 6841:1987 "*Guide to Measurement and Evaluation of Human Exposure to Whole-Body Mechanical Vibration and Repeated Shock*" (BSI 1987) and ISO 2631-1:1997 "*Mechanical Vibration and Shock: Evaluation of Human Exposure to Whole-Body Vibration. Part 1: General Requirements*" (ISO 1997) are the two most well known standards in the realm of motion sickness analyses. These standards provide guidelines for measurement and evaluation of human exposure to whole body vibration, which include low frequency vertical motions considered responsible for motion sickness. BS 6841:1987 directly incorporated the findings of Lawther & Griffin (1986; 1987) and renamed the "Motion Dose" as "Motion Sickness Dose Value (MSDV_z)", essentially, having the identical meanings. There are two approaches defined for the calculation of MSDV_z; first (and the preferred) option is to calculate it from motion measurements throughout the full period of exposure using:

$$MSDV_z = \sqrt{\left(\int_0^T a^2 dt\right)} \quad (3.13)$$

Where, MSDV_z is the motion sickness dose value (in m sec^{-1.5}); $a(t)$ is the frequency-weighted (using w_f shown in Figure 3.21) vertical acceleration; and T is the total period (in sec) during which the motion could occur.

Alternatively, if the motion exposure is considered to be continuous and of approximately constant magnitude, then the motion sickness dose value is allowed to be estimated from the frequency-weighted RMS vertical acceleration determined over a short period (not less than 240 sec). In such cases, MSDV_z is given by:

$$MSDV_z = \sqrt{a_w^2 \times t_0} \quad (3.14)$$

Where, $a_w(t)$ is the frequency-weighted (w_f in Figure 3.21) RMS vertical acceleration and t_0 is the total duration of motion exposure (in seconds).

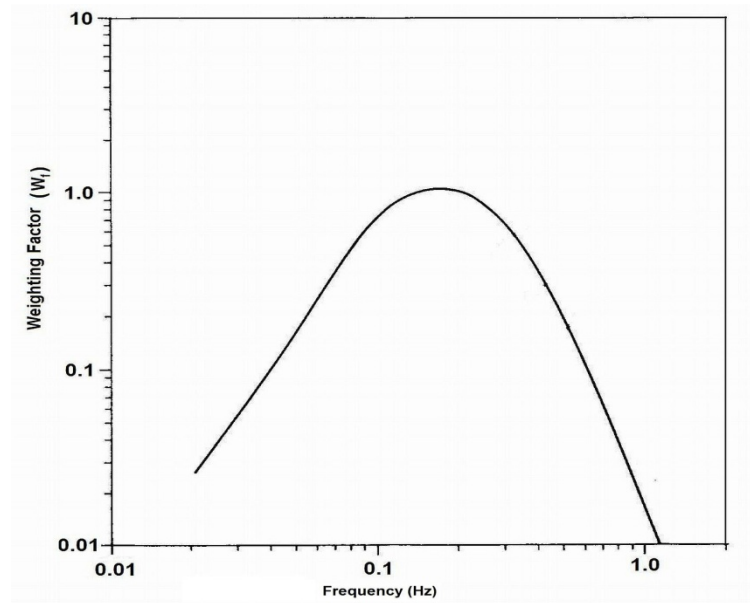


Figure 3.21. W_f frequency weightings for the prediction of vomiting incidences on passenger ferries as defined by BS 6841:1987 [Mansfield (2004)].

Once the motion sickness dose value is calculated, it can then be used to estimate the percentage of unadapted adults who are likely to vomit by multiplying it with K_m . Where, K_m is a constant which may vary depending on the exposed population and for a mixed population of unadapted male and female adults it may be approximated to 1/3. Hence:

$$\text{Percentage of persons who may vomit} = K_m \times MSDV_z \quad (3.15)$$

The standard also indicates that the procedure defined therein, is based on the laboratory and full scale data on board passenger ferries. The database comprises of motion exposures lasting from about 20min to about 6hours with vomiting incidence varying up to about 70%.

ISO 2631-1:1997 (ISO 1997), replaced its predecessor standard on motion sickness i.e. ISO 2631-3:1985 (ISO 1985), which was then withdrawn. The motion sickness

analysis procedure defined in this standard is identical to the method of Lawther & Griffin (1986; 1987; 1988b; 1988a) and BS 6841:1987 (BSI 1987). Only the weightings defined in this standard for the calculation of frequency-weighted vertical accelerations are slightly different from those given in BS. The standard gives high order s-plane equations to describe the weighting curve. However, according to Zuo & Nayfeh (2003) "...low order filter approximations are still preferred in practical applications which are very difficult to implement for practical purposes applications, especially in controller design". They proposed the following second through fifth-order continuous-time, quasi-least-square filter approximations of the frequency-weighting (W_f) for the vertical accelerations (used for motion sickness calculations):

$$\begin{aligned}
 W_f^{(2)}(s) &= \frac{0.8892s}{s^2 + 0.8263s + 1.163} \\
 W_f^{(3)}(s) &= \frac{0.0572s^3 + 3.876s}{s^3 + 4.263s^2 + 4.777s + 4.396} \\
 W_f^{(4)}(s) &= \frac{0.02633s^4 + 0.0238s^3 + 2.286s^2 + 0.2335s + 0.02902}{s^4 + 2.527s^3 + 4.584s^2 + 2.993s + 1.373} \\
 W_f^{(5)}(s) &= \frac{0.1457s^4 + 0.2331s^3 + 13.75s^2 + 1.705s + 0.3596}{s^5 + 7.757s^4 + 19.06s^3 + 28.37s^2 + 18.52s + 7.23}
 \end{aligned} \tag{3.16}$$

Where the number in the parenthesised superscript of $W_f(s)$ represents the order of filter and $s = j2\pi f$ is the complex frequency in the Laplace domain. The original frequency-weightings and its comparison with the approximations [given by Equation(3.16)] are shown in Figure 3.22.

As mentioned at the beginning of this section, these motion sickness analysis methods are fairly simple and easy to use in practice. However, in addition to the limitations arising from statistical considerations (i.e. applicability to population, motions, durations, and ship types outside the considered data), the causal factors and the underlying mechanism involved in the etiology of motion sickness, become latent and receive but very little attention by these methods.

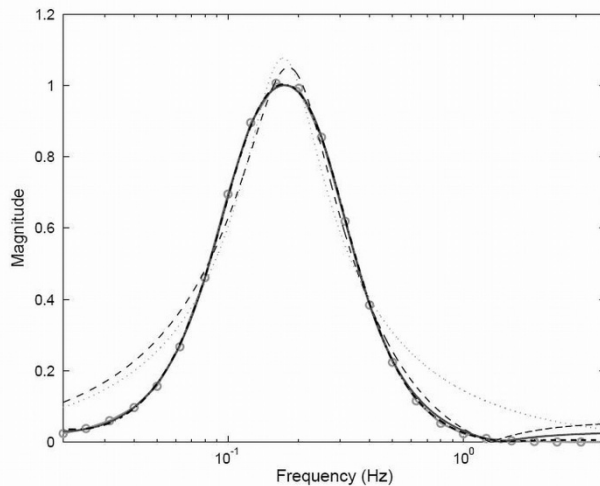


Figure 3.22. ISO 2631-1:1997 frequency weighting curve W_f (circles) and quasi-least square filter approximations: second order (dot), third order (dash), fourth order (solid), and fifth order (dash-dot) [Zuo & Nayfeh (2003)].

3.8 COMPASS Project and its Findings

The existing methodologies, identified in §3.7, for the evaluation of motion sickness characteristics of a vessel are primarily based on the typical motion responses of conventional monohull ships, which exhibit highest response energy in the vertical plane (body frame of reference attached to the centre of gravity). With the advent of advanced hullforms (e.g. catamaran, planning crafts, wave piercer catamaran, hydrofoils etc.), especially for passenger vessels, it was felt that the existing approaches may not be appropriate for the evaluation of human comfort onboard these vessels. The premise for this understanding is primarily the peculiar motion response exhibited by the contemporary vessels, which are quite different from those of the conventional monohull (Verveniotis 2004). This led to the genesis of an EU project “A Rational Approach for Reduction of Motion Sickness & Improvement of Passenger Comfort and Safety in Sea Transportation” with acronym ‘COMPASS’.

This project was funded by European Commission – DG Research and focused on the development of new methodologies and standards for the assessments of motion sickness and passenger comfort onboard contemporary and futuristic vessels. The project consortium comprised of 11 expert partners (3 ship operators , 1 shipyard, 1

fast vessel designer, 2 research/consultancy organisations, 3 educational establishments and 1 classification society) from 7 different EU countries. It commenced in September 2002 and concluded in November 2005. The primary objectives of this project were (Turan 2006):

- Development of new mathematical models for the prediction of motion sickness onboard existing and future generation passenger vessels.
- Preparation of new realistic motion sickness standards (guidelines) that would take account of the contemporary and future transportations' needs and trends.
- Development of design methodology with the aim to improve the designs of conventional and high speed crafts from passenger comfort view point.
- Development of operational guidelines and an interactive computational tool originating from the passenger comfort considerations, so as to assist captains' decision making for weather routing and speed alterations.

In overall terms:

- It was concluded that passenger comfort has very strong bearings on the ship economics.
- An extensive review of the literature revealed that existing knowledge on how the horizontal motions effect motion sickness is limited.
- A comprehensive passenger comfort survey questionnaire was developed, which has also been used in this study for the conduct of full scale field trials. The details of this questionnaire are presented at length in §8.3.1 (Chapter 8).
- Full scale field trials were carried out by the project partners, aboard several contemporary vessels to investigate the influence of ship motions, vibrations, noise, air-quality and temperature, on passenger comfort (studied through survey questionnaire).
- Laboratory experiments were also carried out / re-analysed to study the relationships between motion characteristics and resulting motion sickness.

- The ‘susceptibility’ and descriptive motion sickness models were developed. The sickness model was as an extension of the existing model employed by the current standards on motion sickness i.e. ISO 2631/BS 6841 (§3.7.5).
- The motion sickness model was successfully integrated with the ship routing system.
- The developed model was also employed for design of hypothetical vessels.

Further details on the laboratory studies and the susceptibility and motion sickness models developed by the project, having direct relevance to this work, are presented in the following sections.

3.8.1 Laboratory Tests in Motion Simulators

In a series of simulator trials by TNO, 28 subjects were exposed to the low-frequency sway, heave and their combinations with 8 different motion profiles. This study attempted to understand the effects of passively induced motions on to the cognitive, physical, provocative (requiring head movements), and eating & drinking activities of people. The salient findings were:

- Sway motions are more disturbing than the heave motions and the effects of the two motions add linearly.
- Physical activities were more affected than the cognitive tasks (which were almost immune).
- Increased motion levels result in the increased levels of perceived efforts to accomplish a task, though the performance may not be affected as much.
- Subjective ratings of comfort discriminate much more than the objective scores (actual interruptions experienced)
- Enjoyment, fatigue, motion sickness and postural balance are the significant indicators of comfort.

The Institute of Sound and Vibration Research (ISVR), investigated the link between motion sickness and pure roll, pure lateral and combined lateral and roll oscillations. Their studies involved 860 subjects and 56 motion profiles, with independent groups

of 20 participants each. The sickness levels was measured using an illness rating scale from 0 to 6 (0-No symptoms, 1-Any symptom, 2-Mild symptoms, 3-Mild nausea, 4-Mild to moderate nausea, 5-Moderate nausea but can continue, 6-Moderate nausea and want to stop). Exposure to motion continued for 30minutes or lesser if the illness rating of 6 was reached. The most significant findings of these experiments were:

- Motion sickness provoked by lateral oscillations is approximately proportional to the acceleration amplitude in the frequency range of 0.0315 to 0.25Hz.
- The displacement of lateral motions in the frequency range of 0.25 to 0.8Hz show proportionality with the motion sickness.
- Motion sickness exhibits an increase with the introduction of subtractive roll motions to the oscillatory lateral motions of constant peak velocity, in the frequency range of 0.05 to 0.315Hz. However, this increase was not statistically significant at all tested frequencies.
- Motion sickness elicited by the combined lateral and roll oscillations cannot be well-predicted by a linear function of either roll displacement (ϕ) or the corresponding lateral force component of gravity (i.e. $g \sin \phi$).

ISVR proposed frequency weightings for the horizontal (assumed to be identical for the lateral and fore-and-aft oscillations) accelerations, to explain incidence of mild nausea (normalized with the RMS accelerations). This work has been published by Donohew & Griffin (2004) and the proposed frequency weightings for the lateral oscillations (accelerations) is shown in Figure 3.23.

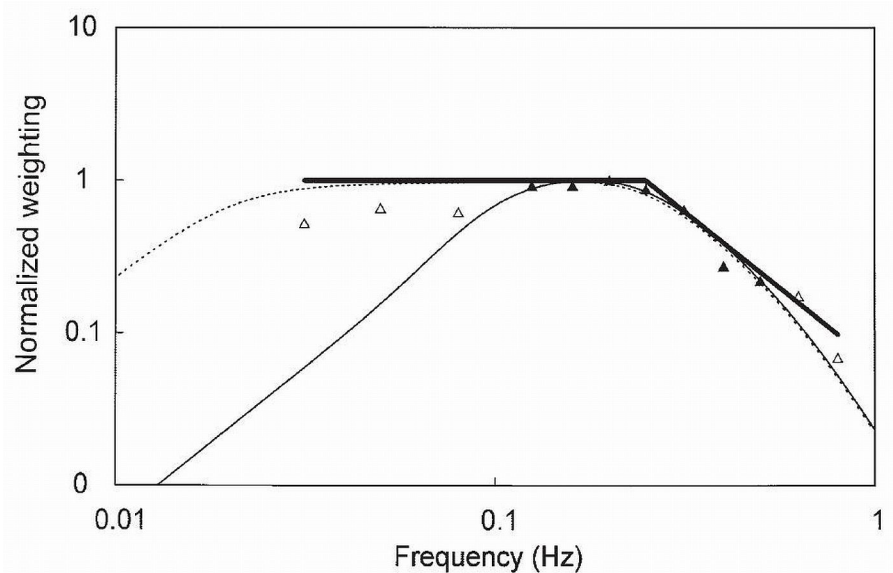


Figure 3.23. Asymptotic and realizable frequency weightings for lateral acceleration, derived from the normalized mild nausea incidence, compared with the weighting for vertical acceleration, W_f , as defined in BS 6841. All weightings are normalized such that their maximal values are 1.0. Asymptotic weighting = solid thick line; realizable weighting = dotted line; normalized mild nausea incidence: black triangles = points at which values differ significantly from static condition, open triangles = points at which values not significantly different from static condition; W_f = solid thin line [Donohew & Griffin, 2004].

3.8.2 Development of Susceptibility and Motion Sickness Models

Statistical analyses of the comfort questionnaire collected during the field trials indicated that:

- Discomfort entities like illness, unsteadiness, satisfaction, and sleep disturbance are more or less independent and might be linked to ship motions and/or other environmental factors (noise, vibration etc).
- Out of all comfort indicators considered by the project (illness, seating discomfort, unsteadiness, expectations, satisfaction, fatigue and enjoyment) only illness was found to be significantly associated with age, gender and past sickness history.
- Seasickness is the most important factor affecting the passenger comfort level onboard ships.

- The other important (dis)comfort factors, after seasickness, were unsteadiness, satisfaction and sleep disturbance.

These findings and the mathematical model of susceptibility function for the illness rating (used as a measure of motion sickness), have been published by Bos et al. (2007), which is given by:

$$S = A \left[\exp\left(-\frac{y-a}{b}\right) - \exp\left(-\frac{y-a}{c}\right) \right] \quad (3.17)$$

Where,

- $0 \leq S \leq 3$ is the susceptibility
- 'A' is the amplitude of the function
- 'y' is the age in years
- 'a' is the age below which there is no sickness
- 'b' & 'c' are the time constants describing the age dependency as observed.

Parameters of Equation(3.17) depend on the personal factors of age, gender and past history of motion sickness. The values of these parameters estimated for the illness ratings ($0 \leq IR \leq 3$) observed during the field trials are given in Table 3.2.

Table 3.2: Characteristic parameters describing the susceptibility according to Equation(3.17), based on the observed illness ratings ($0 \leq IR \leq 3$) for different groups of passengers (Bos et al. 2007).

Gender	Sick before	A (0..3)	a (years)	b (years)	c (years)
Female	no	0.36	5	40	2
	yes	0.72	5	40	2
Male	no	0.26	5	40	8
	yes	0.72	5	40	8

The department of Naval Architecture & Marine Engineering (NAME) at the University of Strathclyde established the relationships between sickness indicators of ‘Illness Rating (IR)’, ‘Motion Sickness (Vomiting) Incidence (MSI)’ and the motion records of field trials’ vessels. The mathematical model used for this purpose was, essentially, an extension of the ISO-2631-1:1997 (ISO 1997) model. The important outcomes of this venture were:

- Out of the six degrees of freedom (surge, sway, heave, roll, pitch, and yaw) motions, only the (frequency weighted) horizontal and vertical linear accelerations significantly describe the variability of motion sickness.
- The illness rating model exhibits improvement, if the effects of age, gender and sickness history are taken into account using Equation(3.17), but this would make the model much personalised than is necessary for general prediction.
- The horizontal (lateral and fore-and-aft oscillations) accelerations were frequency weighted using the weighting functions developed by ISVR (Figure 3.23), whereas vertical accelerations were weighted using the ‘ W_f ’ weighting of ISO-2631-1:1997.
- Significant difference was observed between the motion sickness characteristics (IR, MSI) for the short day-time and the long over-night journeys.
- The proposed model fitted very well to the short journeys.

The mathematical model for the illness rating (IR) is:

$$IR = dIR \times (MSDV - MSDV_{IR0}) \quad (3.18)$$

Where, dIR is the slope of illness rating equation fitted to observed data; $MSDV$ is the motion sickness dose value; and $MSDV_{IR0}$ is the pseudo-threshold level below which no illness is predicted.

Vomiting incidence i.e. Motion Sickness Incidence (MSI) is given by:

$$MSI = dMSI \times (MSDV - MSDV_{MSI0}) \quad (3.19)$$

Where, $dMSI$ is the slope of MSI equation fitted to observed data, and $MSDV_{MSI0}$ is pseudo-threshold level below which no vomiting is predicted. The motion sickness dose value (MSDV) is given by:

$$MSDV = a_v \sqrt{t} \quad (3.20)$$

With ‘ t ’, being the duration of motion exposure (in seconds) and ‘ a_v ’ is the equivalent weighted acceleration (see Figure 3.23 for the frequency weightings used) given by:

$$a_v = \sqrt{k_h^2 (a_{wx}^2 + a_{wy}^2) + a_{wz}^2} \quad (3.21)$$

Where, a_{wx} is the frequency weighted fore-and-aft acceleration; a_{wy} is the frequency weighted lateral acceleration; and a_{wz} is the frequency weighted vertical acceleration.

The parameters of Equation(3.18), (3.19), and (3.21), as shown in Table 3.3, were estimated using the full scale trials data of the COMPASS project.

Table 3.3: COMPASS seasickness model parameters (Pescetto 2006).

Journey Type	dIR	MSDV _{IR0}	dMSI	MSDV _{MSI0}	K _h
Short journeys (< 4hrs)	0.0055	0.25	0.28	6.9	0.5
Overnight journeys	0.0009	73	0.02	89	0.5

3.9 Effects of Motion Sickness on Crew Performance

Motions of vessels at sea are known to adversely influence the crew performance through seasickness (MSI), disturbance of balance (motion induced interruption, MII), and increased level of energy expenditure (motion induced fatigue, MFI) (Wertheim 1998). Haward et al. (2009), while studying the motion effects of an

FPSO vessel stationed in North sea, found a strong association of physical tasks (balancing, moving and carrying) and sleep problems with vessel motions. They also observed strong associations of cognitive task performance reduction, stomach awareness, and dizziness with vessel motion magnitude. These issues coupled with the continuous automation of systems and persistent demands on crew reduction (Lively et al. 2003; Oberman & Baker 2004; Ross 2009) may jeopardize the safety of ships in general.

Out of the three primary crew performance degraders (MSI, MII, & MFI), the motion sickness (MSI) also entails emotional issues of apathy and depression. The seasickness / nausea and the associated drowsiness / apathy are detrimental for the crew's motivation to undertake / complete the require task and duties (Stevens & Parsons 2002). According to Rolnick & Gordon (1991) a "helplessness reaction" reduces crew performance through cognitive, emotional and motivational deficit. In the aforesaid study, the decrement of performance at sea showed a significant association with the feeling of helplessness rather than the physiological signs of seasickness (Benson 2002).

Interestingly, despite a significant reduction in overall performance of seasick crew, the severely sick individuals continue to effectively carry out their tasks in emergency situation. This phenomenon is associated with "peak efficiency" that remains unaffected by all but the extreme sickness. However, the "maintenance efficiency" or the ability of the crew to execute routine work reduces significantly (Birren 1949).

In recent past the Canadian Deference Research Establishment Atlantic (DERA, now DRDC) developed a naval crew fatigue, seasickness and human Performance Assessment Questionnaires (PAQs). These check-box-type questionnaires were designed to measure a total of 41 symptoms (including a simplified Misery Scale) and performance parameters (Colwell & Heslegrave 1993). PAQs were deployed on seven frigates and destroyers in the NATO Standing Naval Forces Atlantic Fleet (STANAVFORLANT) during two weeks of winter combat exercises in the North

Atlantic in 1997 (Colwell 2000b). The analyses of these questionnaires by Colwell (2000a; 2005) revealed the following:

- There is a strong correlation between cognitive performance measures and fatigue, the latter in turn is related to the sleep quality. Incidentally, the reported severity of fatigue and sleep quality problems were the highest.
- Seasick crew members encounter significant problems with the execution of their routine tasks including sleeping. They experience three times more problems with task completions than the individuals with no motion sickness issues.
- "...one major conclusion of the associated correlation study is that low or 'background' levels of motion sickness are associated with serious performance problems on both cognitive and physical tasks."

Considering the above findings, Bos (2004) re-analysed the PAQs with emphasis on motion sickness part of the questionnaires. For the performance measures, he selected the three questions indicating completion or otherwise of a task for any reason (not completed and/or abandoned, and/or not allowed). He allocated fail-rating on individual level as 1 for the task failed or 0 for the successfully completed tasks (even with mistakes or longer duration). He plotted the task failure rates against the seasickness, averaged over all crew members of the participating naval vessels, as shown in Figure 3.24. As such, all seasickness measures (including the simplified MISC) were found to be highly correlated with subjective Misery Scale (MISC); therefore, the crew performance measures were plotted against MISC (see §3.10 for the details on MISC).

It is evident from the above figure that even in the absence of nausea (MISC = 5), motion sickness may lead to a fail rate of over 20%, which represents a significant reduction in crew performance. Given the definition used for the successful task (disregarding any mistakes and delays) by Bos (2004), this 20% reduction in crew performance is considered as an extremely important issue, especially for the critical operations.

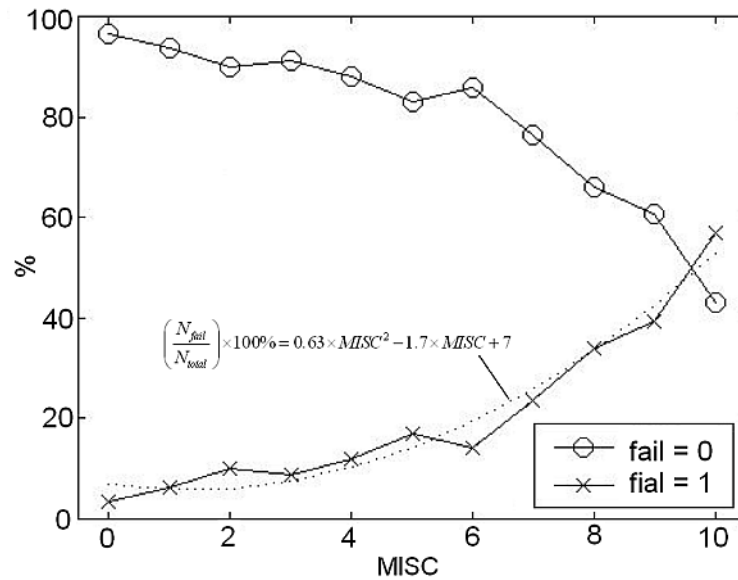


Figure 3.24. Percentage crew (all ships) with fail factor of 0 and its inverse 1 variation with MISC.

The dotted line is the best fit polynomial

Thus, it is important to realise that consideration of motion sickness is not only of paramount importance for the comfort of passengers but is equally, if not more, important for the performance of crew members; thereby the safety of ship at sea. However the model developed in this work has primarily focused on passenger comfort due to the practical limitation (data was available for the passengers only).

3.10 Subjective Measures of Motion Sickness and Wellbeing

As such, vomiting incidence is the only objective measure of motion sickness (a person vomits or not), however, it represents the extreme levels of sickness. Generally, the passengers experiencing provocative vessel motions start to feel unwell and avoid visiting the bars, restaurants and shops on board much earlier than they actually suffer emesis. Some people may not vomit even in the presence of strong retching feelings. Also, the present day laboratory experiments involving human subjects exercise restrictions on the duration (due to economics of apparatuses) and the level of sickness (avoiding emesis due to ethical reasons) that could be induced.

Consequently various subjective measures of wellbeing have been developed and used in laboratory as well as field trials. For example, Lawther & Griffin (1986)

devised and used a linearly weighted four category (0-I felt alright; 1-I felt slightly unwell; 2-I felt quite ill; and 3-I felt absolutely dreadful) scale, termed as illness rating (IR), to record the subjective feelings of the passengers' illness. They observed that a large proportion of the passengers feeling seasick to some degrees did not vomit. However, they noted a strong correlation between illness rating and vomiting incidences and identified the following relationship between the two measures of motion sickness (Lawther & Griffin 1987):

$$\text{illness rating (IR)} = 0.05 \times \text{vomiting incidence (VI\%)} \quad (3.22)$$

(The above expression is applicable for vomiting incidences more than zero but less than 30%)

Similarly, Golding et al. (1995) developed a four category subjective sickness scale (1-no symptoms; 2-mild symptoms but no nausea; 3-mild nausea and any additional symptoms; 4-moderate nausea and additional symptoms) to study the effects of motion direction, body axis, and posture on the nauseogenicity of low frequency linear oscillations. In a recent study, Golding et al. (2009) have employed a six category subjective sickness scale (1-no symptoms; 2-initial symptoms of motion sickness, but no nausea; 3-mild nausea; 4-moderate nausea; 5-severe nausea and/or retching; 6-vomiting) to evaluate the nauseogenicity of the off-vertical axis rotation of the visual field. However, no relationships between these sickness ratings and emesis have been suggested by them.

Another subjective sickness rating scale developed and validated at TNO Human Factors Research Institute (Bles et al. 1991; de Graaf et al. 1992; Wertheim et al. 1992; Wertheim et al. 1995; Wertheim et al. 1998; Bos et al. 2005) is the MISery Scale (MISC). This subjective scale explicitly acknowledges the fact that generally the sickness symptoms like dizziness, headache, (cold) sweating, and stomach awareness appear (in varying order and severity) before nausea (Reason & Brand 1975). This scale, as shown in Table 3.4, comprises of ten categories to capture the subjective sickness levels.

Table 3.4. Misery Scale (MISC) (Bos et al. 2005)

Symptom	score
No problems	0
Uneasiness (no typical symptoms)	1
Dizziness, warmth, headache, stomach awareness, sweating,...	
vague	2
slight	3
fairly	4
severe	5
Nausea	
Slight	6
Fairly	7
Severe	8
(near) retching	9
Vomiting	10

Unlike, IR [see Equation(3.22)] the relationship between MSI and MISC is non-linear, as depicted in Figure 3.25, and is given by the following expression (Wertheim et al. 2001; Bos 2004):

$$MSI = \frac{x^n}{c^n(1-x)^n + x^n} \cdot 100\% \quad (3.23)$$

with $x = \frac{MISC}{10}$, $c \approx 1.5$ and $n \approx 1.3$

The inverse of Equation(3.23) gives MISC as a function of MSI:

$$MISC = \frac{c}{y^{1/n} + c} \cdot 10 \quad (3.24)$$

with $y = \frac{(100 - MSI)}{MSI}$

It is interesting to note from Figure 3.25 that the sickness symptoms (Non-zero MISC) are likely to prevail amongst the general passenger population even if no vomiting incidence takes place. This aspect is expected to have strong bearing on the ship's economics, not only from travelling comfort point of view but also the onboard sales revenue is likely to be declined due to the low / background sickness. This observation is also evident from Figure 3.24, which is displaying the reduction in crew task performance due to the low / background seasickness (Bos 2004).

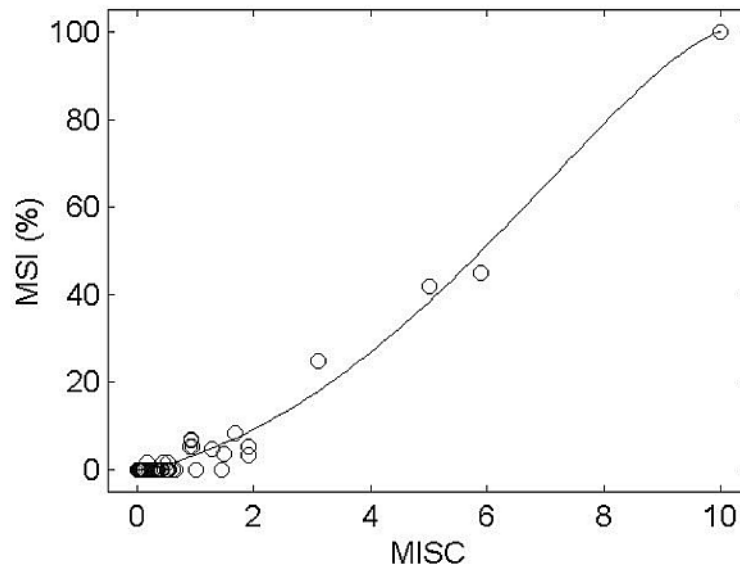


Figure 3.25. Relationship between average MSI and MISC as observed in 12 experimental studies at TNO (Bos 2004)

Based on the above, it would be prudent to pursue a motion sickness model that should capture the level of subjective wellbeing of the passengers as well as the crew members. However, this work has focused on the development of physiologic model capable of estimating MSI due to the following reasons:

- The existing marine standards (BSI 1987; ISO 1997) are based on MSI; hence it is imperative that the new model predicts MSI to facilitate tangible comparisons.
- Almost all of the existing motion sickness models (O'Hanlon & McCauley 1974; McCauley et al. 1976; Lawther & Griffin 1987; Bos & Bles 1998b; Bos et al. 2002a; Matsangas 2004; Verveniotis 2004; Turan 2006) predict

MSI. Therefore, for a legitimate comparison of the new model with the existing ones, it should be able to estimate MSI.

Nevertheless, given the fact that there is a strong association between MSI and the subjective measures of wellbeing such as illness rating (IR) (Lawther & Griffin 1986; Colwell 1994), the new MSI-based model may easily be extended in future to predict subjective well being.

3.11 Research Gap

Review of literature presented in the above has revealed that (due to the relative ease of use) the descriptive motion sickness models are widely used by the naval architects and even the marine standards on passenger comfort rely on these models. It is clear that the notion of ‘vertical motions play the key role in the elicitation of motion sickness’ has strongly influenced the existing descriptive models. Whereas, findings of the COMPASS project and other studies (e.g. Griffin & Mills 2002a; Griffin & Mills 2002b; Golding et al. 2003; Donohew & Griffin 2004; Griffin & Newman 2004; Tamura & Arima 2006; Donohew & Griffin 2007; Wyllie & Griffin 2007; Joseph 2008), indicate increasingly important role of the horizontal accelerations in the occurrence of motion sickness than perceived by such models. This very fact is also reflected in the formulation of the new descriptive model developed by the COMPASS project, which explicitly incorporates the effects of horizontal accelerations.

One way ahead would be to keep sticking with the descriptive models for the assessment of contemporary and futuristic marine vessels; however, this approach has two main disadvantages. Firstly the descriptive models (including the COMPASS model) are primarily based on the causal factors (i.e. motions) and reflect nothing of the underlying mechanism. Second, and perhaps more importantly, these models are plagued with the limitations of statistical techniques and their functional boundaries are very likely to be violated by the peculiar motions of the modern vessels.

It is evident from the above that the future motion sickness models should be physiologically driven, using the first principle approach, so that the inherited limitation of the descriptive models could be avoided. It is expected that, such models would not only reflect the underlying mechanism, but would also be suitable for the prediction of motion sickness characteristics of novel ship designs. In this regard, the literature review clearly indicates that the ‘sensory conflict’ is the most comprehensive physiologic theory of motion sickness and ‘subjective vertical (SV) conflict’ is the most pragmatic version of this theory.

However the so far, rather simplified (considering vestibular systems only), implementations of the SV-conflict theory primarily account for the vertical motions’ induced motion sickness. There has been an attempt by the originators of SV-conflict theory to extend the applicability of their models to more than one degree of freedom motions. However, the resulting model predicted excessively high level of sicknesses for the combined sway and roll motions. The model never tested for the six degrees of freedom ship motions. Although, the SV-conflict model developed at the University of Strathclyde has successfully been applied to the field trials of high speed crafts (Verveniotis 2004), however, this model also relies on the single sensory conflict between the sensed and expected gravities.

Based on the above, it is concluded that a new physiologic motion sickness model should be developed that would explicitly account for the increased level of horizontal accelerations exhibited by the modern marine vessels. It is envisaged that this could be achieved through extension of the NAME’s SV-conflict model presented in Chapter 5, by identifying a new sensory conflict between the sensed and expected horizontal accelerations.

3.12 Chapter Summary

This chapter has presented a brief overview of the motion sickness history, its symptoms, the factors rendering some people more inclined to it and the phenomenon of gradual adaption, somewhat alleviating the malaise. It then discussed at length, the existing theories of motion sickness followed by the detailed

explanation of currently used methods and standards for its evaluation aboard a marine vessel. It then skimmed through the findings of COMPASS project, while expanding a bit more on the outcomes of laboratory studies and the motion sickness models developed by the project. Finally, the chapter concluded by identifying the research gap.

The next chapter is outlining the approach adopted for this research.

Chapter 4. APPROACH ADOPTED

4.1 Overview of the Chapter

This chapter briefly describes the approach adopted to achieve the aims and objectives of this research project (Chapter 2). The mind map of the complete approach is given in §4.2, which broadly comprises of: (1) review of the vestibular apparatus and its models (§4.3); (2) development of the theoretical and mathematical framework for the new motion sickness model (§4.4); (3) calibration and validation of the new model, using the existing field trial data (§4.5); (4) conduct of a new set of field trials for the further validation of the model (§4.6); and finally (5) the detailed statistical comparisons of the physiological and descriptive motion sickness models considered in this study (§4.7).

4.2 Mind Map of the Approach Adopted

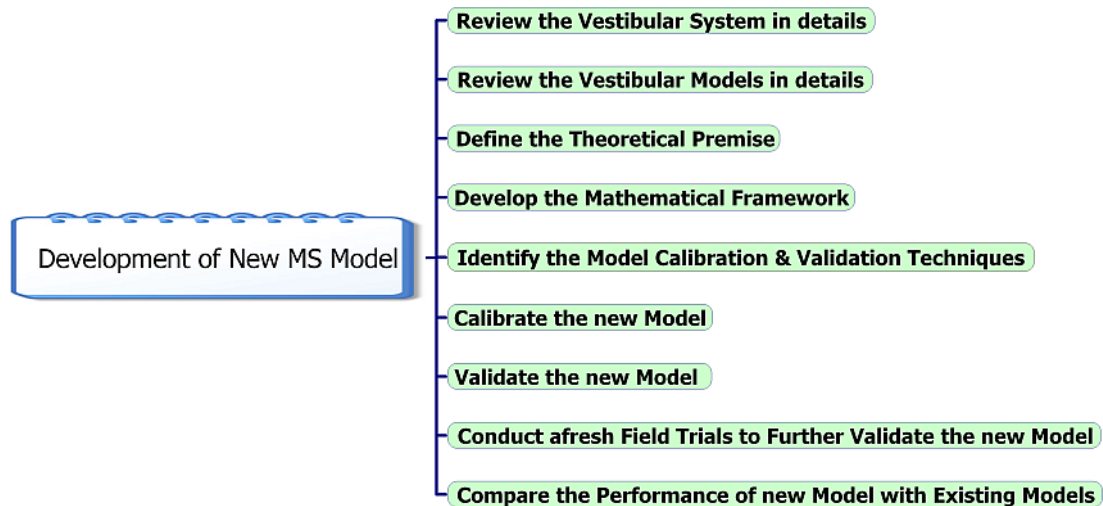


Figure 4.1. Mind map of the approach adopted

After having done a detailed review of the motion sickness literature to identify the research gaps (Chapter 3), it was imperative to establish a simple and clear strategy for achieving the aims and objective of this research project (Chapter 2). A rather

simplified mind map of the approach adopted in this work is depicted in Figure 4.1. It can be seen from the figure that the complete strategy comprised of several major phases / steps that are briefly discussed in the following sections.

4.3 Review of the Vestibular System and Its Models

Before embarking on the development of the new physiological motion sickness model, it was felt imperative to gain reasonable appreciation of human's key orientation / motion perception system i.e. the vestibular apparatus. Therefore, the system was studied at length; from the morphology to the physiology and biomechanical aspects of its constituent organs (i.e. organs, otoliths and semi circular canals). This study of the system, along with the fundamental concepts of how the nervous system is assumed to process the vestibular cues, provided important insights into the commonly observed manifestations of the system (e.g. vestibulo ocular reflex and motion perception).

The existing vestibular models were then studied in details to understand the mathematical representation of the system components as well as the physical laws, assumed to be implemented by the higher level control (nervous) systems. These models, inspired to have a slightly deeper look at the 'internal models' and 'observers'; the concepts borrowed by the vestibular scientists from optimal control engineering. Finally the existing 'qualitative' and 'quantitative' physiologic motion sickness models were studied in depth to acquire necessary conceptual foundations for the development of a new model.

4.4 Development of Theoretical & Mathematical Framework

As a theoretical premise, findings of the available (limited) laboratory studies on horizontal motions induced sickness were studied to identify the potential weaknesses of the existing SV-conflict models. It was discovered that, despite the capability of SV-conflict theory, these models were not accounting for the differences in humans' sensitivities to become motion sick under purely vertical and horizontal oscillations. The solution proposed by the originators of the SV-conflict theory to resolve the aforesaid anomalies was also studied. However, the existing

solution could not account for all shortcomings; especially the frequency response of the proposed solution was not compatible with the findings of recent laboratory experiments concerning the horizontal motions induced sickness.

Based on the above, a new solution was proposed to resolve the current anomalies of SV-conflict models. This was done by identifying a new sensory conflict and rephrasing the subjective vertical theory. The mathematical implementation of the rephrased version of SV-conflict theory was achieved by modifying the existing SV-conflict model with the following enhancements:

- Addition of a simple vectorial-process to calculate the sensed horizontal accelerations as the component of gravito-inertial acceleration normal to the sensed vertical, i.e., sensed gravity.
- Instantiation of a process identical to above in the ‘internal’ model to estimate the ‘expected’ i.e. subjective horizontal accelerations.
- Calculation of subjective horizontal (SH) conflict as the vector difference between the sensed and subjective horizontal acceleration.
- Addition of a separate fast integrating path for post processing of SH-conflict into MSI.

After being calibrated (see next section), the new (hybrid subjective vertical horizontal, SVH-conflict) model was tested to ensure that it is successfully addressing the anomalies of the existing SV-conflict models.

4.5 Calibration and Validation of the Model

Firstly, a review of the techniques employed for the calibration and subsequent validation of models simulating complex engineering / natural processes was undertaken. This was done to establish a suitable strategy for the calibration of SVH-conflict model. As a first step of calibration, the model parameters requiring calibration were identified (these were the internal observers’ feedback gain, shape parameters of hill function and the gain & time constant of the leaking integrators). Due to the non-availability of extensive laboratory experiments on horizontal motion

induced motion sickness, it was decided to calibrate the model using the field trial data archived at NAME. However, such data does not exercise control over the susceptibility characteristics of the volunteering participants. Therefore, it was decided to employ statistical inferential techniques for establishing the fitness of SVH-conflict model to the observed vomiting events from the full scale trial data.

Due to random nature of the motion sickness incidences, amongst the general passenger population, the chi-square goodness-of-fit function was employed as the objective function for the calibration of SVH-conflict model. This function was minimised so that the statistical fitness of the model, to the 15 field trials of the passenger vessel providing calibration data, is maximised. A large combination of the unknown model parameters were tested, in a full factorial design format, to identify their values resulting into minimisation of the objective function for the calibration data. However, the final values of the model parameters were determined on the basis of model fitness to 62 field trials of 8 vessels (both calibration and validation data). It may be noted that there was little difference between the optimum combinations of parameters identified for the calibration data and those of the complete archived data set.

Upon calibration of the model, it was validated using the validation field trial data of 7 passenger vessels, isolated for the purpose. Finally, the complete archived data set of past field trials was used to test the relative performance of SVH-conflict model with SV-conflict and other descriptive (ISO/BS, HFRI, and COMPASS) models. The performances of the models were measured in terms of their statistical fitness to the 62 field trials of 8 passenger vessels. It was revealed that the new model is somewhat better than the existing SV-conflict models, and is displaying much superior statistical fitness than the descriptive motion sickness models.

4.6 Field Trials for Further Validation of the Model

The statistical comparisons of the new model with the existing SV-conflict and other descriptive motion sickness models indicated its improved performance over these models. However, it was decided to carry out afresh field trials to gain a firsthand

knowledge about the involved intricacies and to further validate the SVH-conflict model. To begin the process, the considerations to be taken into account for selecting the field trial vessels and planning of the event, were identified. In total, four field trials were carried out onboard a classical monohull passenger ferry and a single full scale trial were undertaken aboard a commercial rigid hull inflatable boat (RHIB). The details of full scale motion sickness field trial procedure were established prior conducting the actual field trials.

In overall terms, the full scale trial comprised of two major activities; (1) measuring and logging of vessel motions using a motion reference unit, MRU and (2) recording of passenger comfort feelings using the passenger comfort survey questionnaire. The MRU was commercially hireable, while the survey questionnaire was identical to the one developed in COMPASS project. The motion histories of the further validation trials were used as input to the SVH-conflict model for predicting the motion sickness incidences, which were then statistically compared with the values observed through questionnaire. Thereafter, the statistical performance of the model was compared with SV-conflict and other descriptive models. However, this time the statistical fitness of the new model was similar to that of the SV-conflict. This is because the passenger vessel was a conventional monohull, while no sickness was observed during the single field trial of the RHIB. Nevertheless, the statistical fitness of the two physiological models (SV and SVH-conflict) was found to be better than the descriptive (ISO/BS, HFRI, & COMPASS) models.

The statistical analyses of the survey questionnaire were carried out in terms of summary statistics (frequency tables) and cross tabulation (searching for the significant relationships between the recorded data). A number of significant relationships were found between the recorded data of survey questionnaire collected aboard the passenger vessel. However, due to very small sample size (10 persons) of the RHIB, no significant relationships were discovered.

4.7 Comparison of the Motion Sickness Models

Lastly, detailed statistical comparisons of the physiological (SV & SVH-conflict) and descriptive (ISO/BS, HFRI, & COMPASS) models were undertaken, for all 68 field trials data of the 10 vessels. This was aimed at establishing the global performance of the two types of models in general and the physiologic SVH-conflict model in particular.

Firstly, the statistical fitnesses of the motion sickness models were checked for the individual 68 field trials of all 10 vessels. It was found that the two physiological models are statistically more accurate than the descriptive models by having maximum number of best fits and minimum number of ‘no fitness’ cases. Furthermore, the SVH-conflict model had more ‘very good fit’ and lesser ‘no fitness’ trials as compared to the SV-conflict model, which indicates somewhat better performance displayed by the former.

The two types of models were also compared on vessel-wise basis, which also indicated that the physiological models are capable of predicting statistically accurate MSIs for the multiple trials of all but one vessel. This specific vessel was a classical monohull vessel of long duration (approx 15 hours) journeys. On the other hand, descriptive models were unable to fit multiple trials of half (5) of the vessels.

Finally, the statistical fitness of all motion sickness models considered in this study, were checked for the multiple (67) field trials (Trial-7 of wave piercer-G, was discarded due to experiment error) of all 10 vessels. It was found that, only the two physiological models (SV and SVH-conflict) are able to display statistical accuracy. Moreover, SVH-conflict displayed somewhat better fitness than the SV-conflict model.

4.8 Chapter Summary

This chapter has briefly presented the approach adopted in this research work. The complete methodology has been outlined in terms of major phases / milestones of the project, beginning with the literature review, up until the statistical comparison of the

motion sickness models. This has been done to provide an overview and order of the various tasks undertaken in this work.

The next chapter is presenting the detailed account of the vestibular system and its models, which is a must to learn system from motion sickness point of view.

Chapter 5. VESTIBULAR SYSTEM AND ITS MODELS

5.1 Overview of the Chapter

This chapter aims to discuss the fundamentals of vestibular system and its mathematical representations. It begins by outlining the vital role played by the vestibular system in motion sickness etiology (§5.2) and motion perception (§5.3). Thereafter, the detailed and thorough discussions about the morphology (§5.4), physiology and biomechanics (§5.5) of the labyrinthine apparatus are given. Afterwards, §5.7 presents the mathematical models developed by various researchers to simulate the primary manifestations of the system, i.e. vestibulo-ocular reflexes (VOR) and motion perception (i.e. orientation). It then gives a brief overview of ‘internal models’ and ‘observers’ (§5.8) from physiological view point, followed by the detailed explanations of the most prominent physiologic motion sickness models (§5.9 to §5.12).

5.2 Role of Vestibular System in Motion Sickness Etiology

The crucial role of the vestibular system in the motion sickness etiology is known for more than a century (Benson 2002). It is based on the observation that people with non-functioning balance organs (Labyrinthine Defectives, LDs), such as deaf-mutes are immune to motion sickness in an otherwise highly provocative motion environment (Money 1970). It was Irwin (1881) who, probably for the first time, observed that a group of deaf-mute co-passengers did not become seasick during a rough sea voyage. Around the same era James (1882) noted similar effects in his large records of the LD patients.

Subsequent observations in a varied range of stimulations (Kennedy et al. 1968; Money 1970; Reason & Brand 1975) have further substantiated the findings that LDs do not get motion sick. Interestingly, they do not get sick even in the virtual motion

environments (Cheung et al. 1989; Cheung et al. 1991; Johnson et al. 1999). Moreover, such an immunity could be introduced in animals by labyrinthectomy e.g. Sjöber (1931) found that all four of the highly susceptible dogs he was experimenting with, could not get motion sick after the bilateral destruction of their labyrinths. Later Money & Friedberg (1964), also experimenting on dogs, reported similar findings.

Thus, the role of labyrinthine apparatus is indispensable as far as the motion sickness etiology is concerned. Resultantly, all theories on motion sickness must have a vestibular basis.

5.3 Human Inertial Guidance System–The Vestibular Apparatus

Vestibular system is one of the most important and unique proprioceptive afferent senses. It interacts with extroceptive (e.g. visual & hearing) and other somatosensory (e.g. muscular, tendon, & articular) subsystems, to perceive the relative motions between self and other objects in space. In gross terms the system facilitates perception of locomotion (own motions), self-orientation (relative to gravity), and spatial positioning and motions of the head (Purves et al. 2004). Some of the most important motor functions like gaze, head and body stabilization receive sensory inputs from vestibular apparatus. Anatomically, the system includes inner ear structure that functions like an inertial guidance system comprising of miniaturised accelerometers and angular rate sensors.

5.4 Morphology of Vestibular System

The vestibular receptor organs consist of two otoliths (utricles and saccules) and three semicircular canals (anterior, posterior, and lateral), on each side of the head behind the inner ear as shown in Figure 5.1. Collectively termed as ‘vestibular labyrinth’, these organs and cochlea (hearing sensory apparatus), are membranous ducts embedded in the temporal bone on each side of human head. It is the intricate and tortuous architecture of these ducts, depicted in Figure 5.2, that give them the title of ‘labyrinth’. These membranous ducts are filled with a fluid called endolymph, which, alike intracellular solutions, is high in K^+ and low in Na^+ ions. There is yet

another fluid surrounding the membranous labyrinth, contained inside the bony walls, called perilymph which is high in Na^+ and low in K^+ ions.

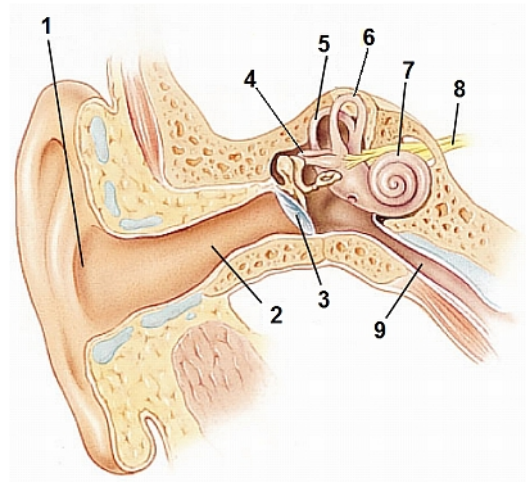


Figure 5.1. Overview of ear and vestibular system; 1 Pinna; 2 Auditory duct; 3 Ear drum; 4 Lateral canal ; 5 Posterior canal; 6 Anterior canal; 7 Cochlea; 8 Auditory nerve; 9 Eustachian tube [downloaded and adopted from www.bartleby.com].

The VIIIth cranial nerve innervates the specialised sensory hair cells of vestibular system situated in the base of otoliths and ampullae (swelled parts at the base of canals, located adjacent to utricle) of the three semicircular canals. The supporting cells of sensory epithelia form a fluid tight boundary in such a way that the apices of vestibular hair cells are dipped inside endolymph, while the basal surfaces of these cells are in contact with perilymph.

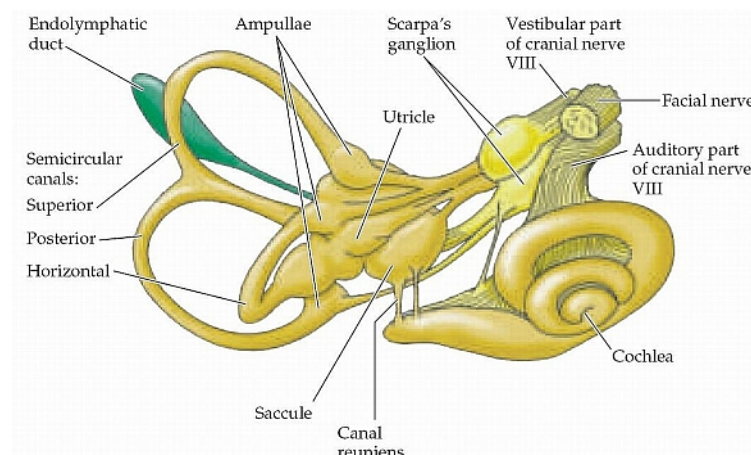


Figure 5.2. The labyrinth and its innervations [Purves et al. 2004].

5.4.1 Anatomy of Vestibular Hair Cells

Vestibular hair cells behave like mechanical to neural transducers; in that they convert their minute physical displacements into relevant sensory potential. A hair bundle is located on the top (apex) of these cells comprising of several stereocilia (a type of hairs), which taper over a small length toward a single kinocilium (another type of hairs). In the absence of any stimulation a certain spontaneous firing rate is maintained by the relevant (otoliths or canals) sensory axons. Now, as shown in Figure 5.3, if the mechanical stimulus bends the hair bundle towards kinocilium, the hair cell becomes depolarized causing an increased neural firing rate. On the other hand, deflection of hair bundle away from kinocilium hyperpolarizes the hair cell, reducing the discharge rate of sensory axons below the spontaneous value.

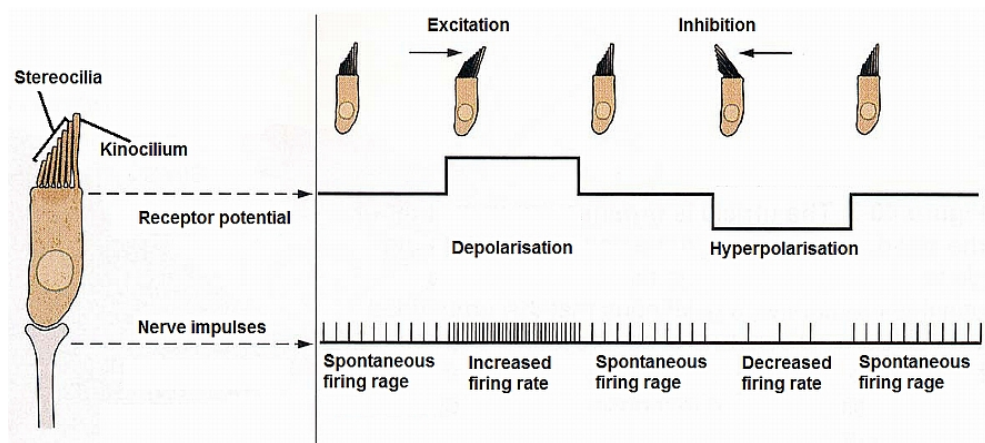


Figure 5.3. Morphological polarisation of vestibular hair cells [adopted from Perlmutter 2008].

It is very interesting to note that the hair bundles of hair cells in each vestibular organ (semicircular canals and otoliths) display specific orientations. The overall layouts of these cells are such that the vestibular receptors, as a whole, respond to mechanical stimulus in all possible directions. As shown in Figure 5.4, the sensory hair cells in the ampullae of a given semicircular canal are all oriented in the same direction, whereas, in utricle and saccule a certain area called striola divides the layout of hair cells in two oppositely polarized zones. This preferential polarization of vestibular hair cells plays a very important role for the identification of motion direction with respect to human head.

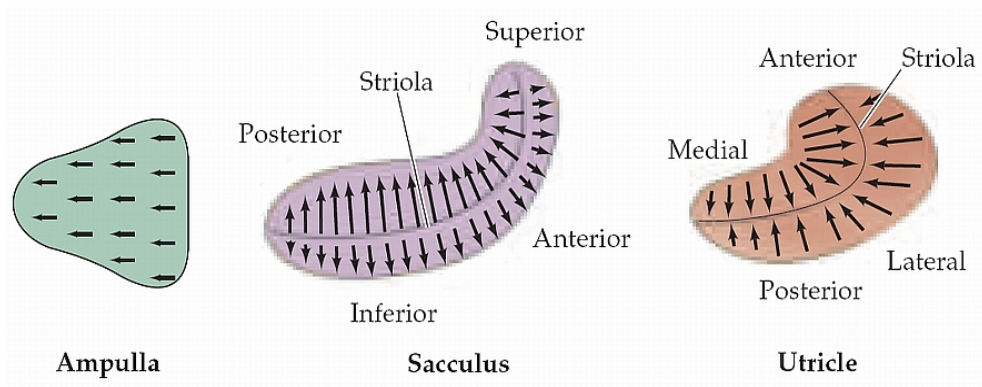


Figure 5.4. Polarization of hair cells in sensory epithelium of semicircular canal ampullae, the utricular and saccular maculae [Purves et al. 2004].

5.4.2 Anatomy of Semicircular Canals

The three, approximately orthogonal, semicircular canals detect the self-induced or passive (e.g. by vehicle) head angular accelerations. Each canal has a bulbous-like swelled zone at its base called ampulla (see Figure 5.2), which encloses a sensory epithelium called crista that contains the sensory hair cells.

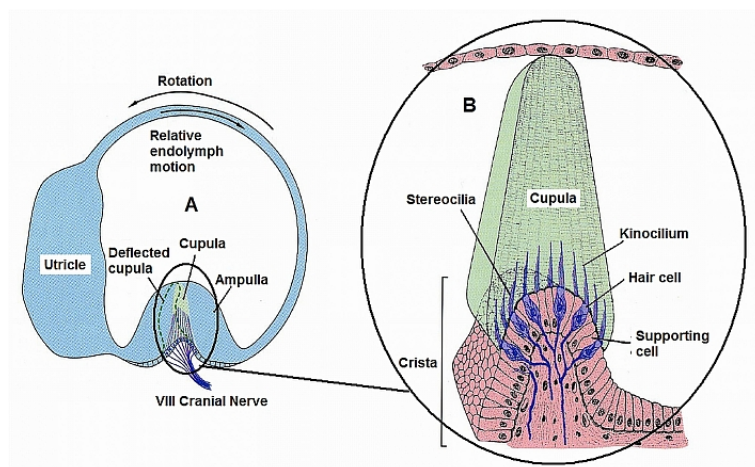


Figure 5.5. (A) Schematic representation of the semicircular canals; (B) Enlarged view of ampulla and crista [adopted from Perlmutter 2008].

As shown in Figure 5.5, the hair bundles of sensory cells extend from crista into a gelatinous mass called cupula, which bridges the gap between crista and ampullary walls. Cupula acts like a fluid-tight boundary, through which the endolymph cannot circulate. Under this peculiar arrangement the rotation of head in the plane of a canal

causes a relative motion between the walls of canals and endolymph due to inertia of the fluid. This relative motion of endolymph is transmitted to cupular diaphragm, which in turn deflects the hair cell bundles embedded inside the crista.

In contrast to rotational motions, the net relative motion between the walls of canals and endolymph is zero for the pure translational accelerations of the head. Resultantly, cupula and hair bundles are not displaced, rendering canals as insensitive to linear motions. As mentioned in §5.4.1, hair cells in the crista of each semicircular canal are polarized in the same direction. Also the six canals are arranged as coplanar pairs on the opposite sides of the head. Thus, each canal works in combination with the canal located on the other side of head with opposite polarization of hair cells. The two lateral canals work together, and the anterior canal on each side works with the posterior canal on the other side; the layout of canals is depicted in Figure 5.6.

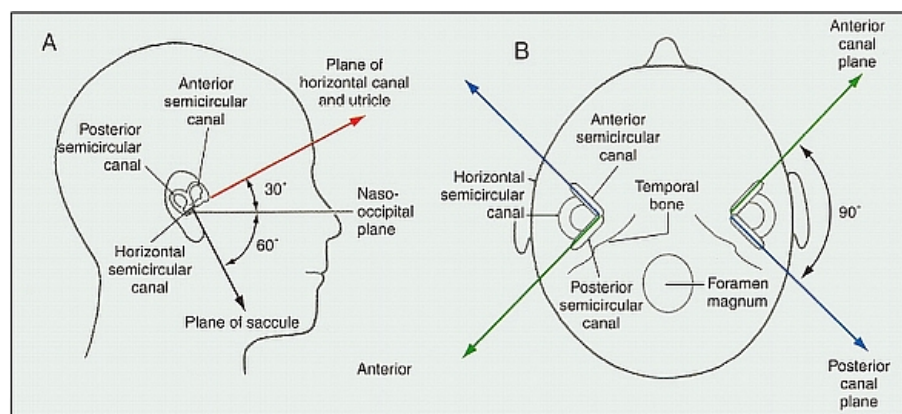


Figure 5.6. Arrangement of canals in pairs. The two horizontal canals form a pair; the right anterior canal and left posterior canal form a pair and vice versa [downloaded and adopted from scienceblogs.com].

Head rotation in the plane of a canal pair deflects their cupulae in opposing directions, leading to opposite changes in the respective hair cells firing rates. As shown in Figure 5.7, a counter-clockwise (leftward) horizontal rotation of the head causes a clockwise motion of endolymph relative to the walls of canals. This endolymphatic movement deflects the hair cells of left lateral canal to become depolarized and those of the right lateral canal to hyperpolarize, which increases and decreases the firing rates of left and right horizontal canals, respectively. This push-pull type functioning of canals coplanar pairs facilitates the brain to interpret

rotations in the plane of canal pair and in the direction of excited canal (with depolarized hair cells).

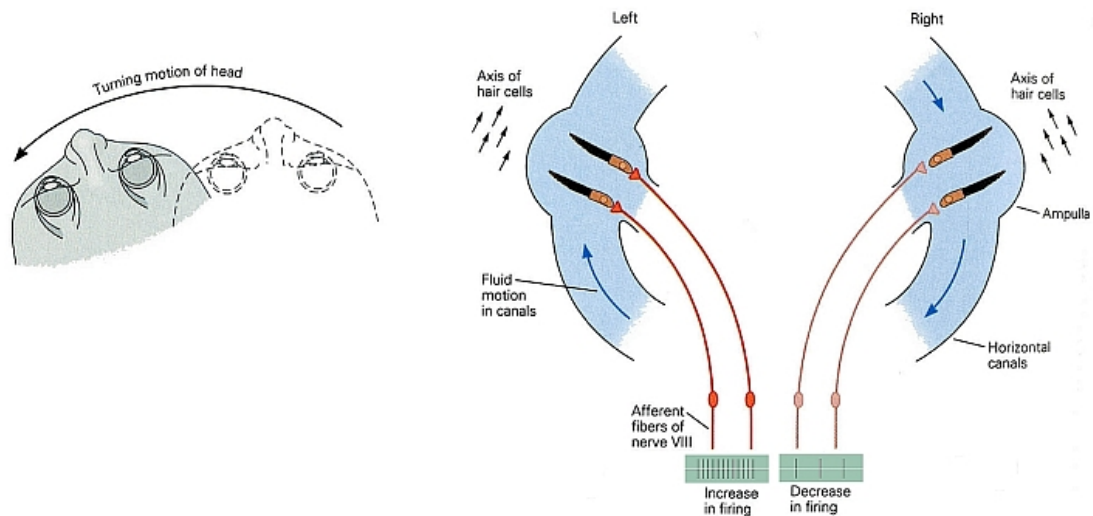


Figure 5.7. Responses of lateral canals during head rotation in horizontal plane [adopted from Perlmutter 2008].

5.4.3 Anatomy of Otolith Organs

Two otolith organs (utricle and saccule) form part of the vestibular system involved in sensing and quantifying linear accelerations or tilts (gravitational acceleration). Similar to ampullae of semicircular canals, otoliths have a sensory epithelium made up of sensory hair cells and their supporting cells, embedded at the base of macula. As shown in Figure 5.8, the hair bundles penetrate into a gelatinous sheet overlaying the sensory hair cells. The top layer of macula is a fibrous structure called ‘otolithic membrane’, which houses the crystals of calcium carbonate called ‘otoconia’. It is these crystals that give otolith organ their name; ‘otolith’ means ‘ear stones’ in Greek.

Because of otoconia, the density of otolithic membrane is considerably higher than the underlying structure and the endolymph fluid. A steady tilt of head, therefore, causes a relative shift between sensory epithelium and the membrane due to gravity, deflecting the hair bundles to change the firing rates of sensory hair cells. Similarly, due to higher inertia, a shearing motion occurs between otolithic membrane and macula base during the linear acceleration of head. Thus, it is possible to have

identical deflection of hair bundles by certain head tilts and linear acceleration, which would generate equivalent perception of the two completely different stimuli. This ambiguity is also known as ‘Equivalence Principle’ (Einstein 1907) or gravito-inertial force (GIF) resolution problem. Nevertheless, brain is able to discriminate between the two stimuli by using additional information (on head rotation) from semicircular canals (see §5.7).

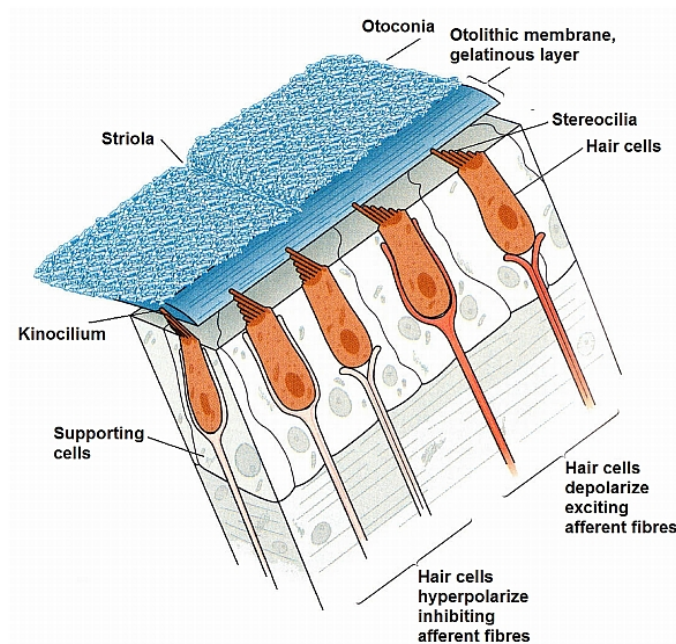


Figure 5.8. Cross section of utricular macula showing hair bundles projecting into gelatinous membrane when head is tilted [adopted from Perlmutter 2008].

Interestingly, as shown in Figure 5.9, the utricle and its macula are oriented horizontally, while the saccular macula is vertical with respect to head frame of reference in upright condition. Moreover, unlike ampullae of semicircular canals, the maculae of otoliths do not display unidirectional polarization of sensory hair cells (see also §5.4.1). The striola forms an axis of mirror symmetry in such a way that hair cells on the opposite side exhibit contrasting polarization. These variations in the morphological polarization of sensory hair cells in the maculae of otoliths facilitate detection of translational acceleration in all possible motion direction.

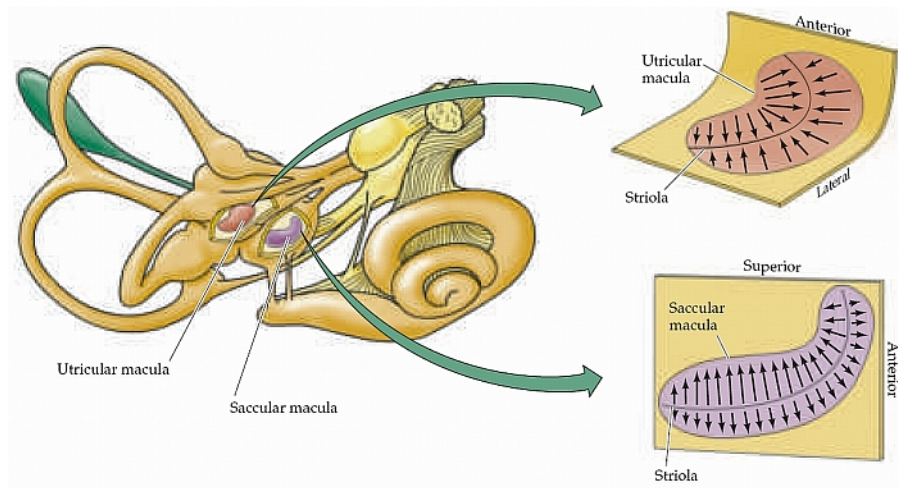


Figure 5.9. Morphological polarization of hair cells in the utricular and saccular maculae [Purves et al. 2004].

5.5 Physiology and Biomechanics of Vestibular Organs

The vestibular system continuously detects and reports about the position and movement of head and body to integrative centres of brainstem. The core part of cerebellum receiving afferents (signals from any sense organs) from this system are termed as Vestibular Nuclei (VN), which make comprehensive synaptic connections with brain stem and other cerebellar structure. According to Angelaki & Cullen (2008), “Vestibular afferents are continuously active even at rest and are strikingly sensitive for signalling motion accelerations as our head translates and rotates in space.” Dysfunction of vestibular system adversely affects the essential skills of balance, gaze stabilization, and the sense of self-orientation. The wellbeing of the individual is also severely deteriorated, resulting in vertigo, nausea and vomiting.

5.5.1 Physiology of Semicircular Canals

The nerve fibres that innervate sensory epithelium of semicircular canals display a high level of spontaneous firing rate (Purves et al. 2004). These axonal firing rates increase or decrease depending on the depolarization or hyper-polarization of sensory hair cells caused by the deflection of cupulae; thus, encoding the head rotations. Goldberg & Fernandez (1971) recorded the axonal firing rates of nerves innervating the sensory hair cells of the semicircular canals ampullae in 45 monkeys.

They exposed these primates, seated in a chair, to rotational motions in a preselected direction (clockwise or anti-clockwise) using a velocity trapezoid, similar to the one shown in Figure 5.10(A). These stimuli comprised of an initial period of rest; an acceleration period of few seconds, a period of constant rotational velocity of several seconds; a deceleration period identical to that of acceleration; and finally a period of rest. The neural activities were continuously recorded, while the animal was subjected to motion stimuli.

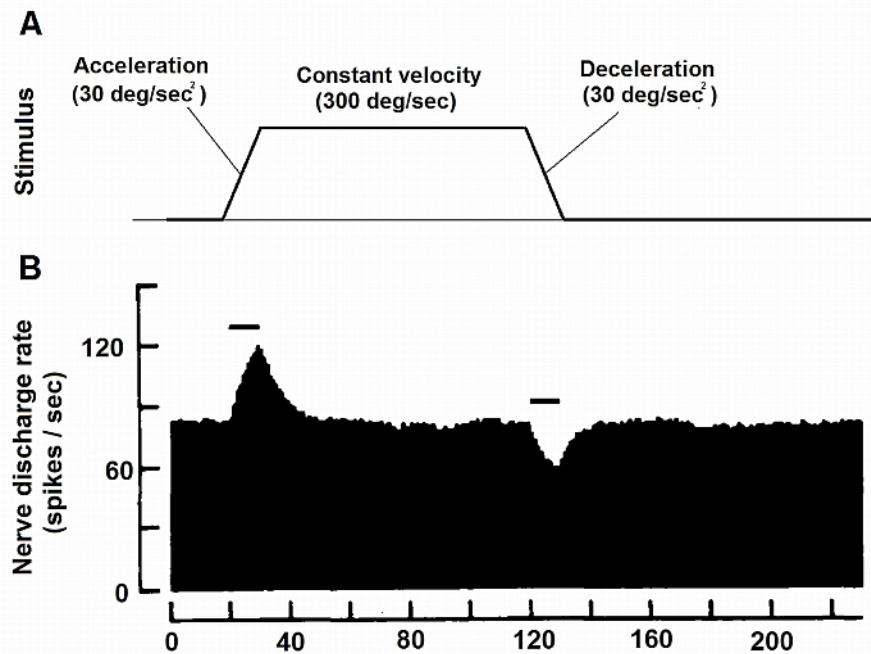


Figure 5.10. Response of axon innervated to semicircular canal; A Rotational stimulus used; B Discharge rate of vestibular nerve axon innervating anterior canal of a squirrel monkey [adopted from Goldberg & Fernandez, 1971].

They observed that maximum firing rate (excitation) of vestibular nerve corresponds to the period of acceleration, whereas, maximum reduction in firing rate (inhibition) takes place during the deceleration period. The spontaneous axonal activity is maintained during resting (no motion) period, while, the discharge rate subsides to resting level during the constant velocity phase. The neuronal activity decreases in a transient fashion to resting level after being decelerated to a stop. The rate of adaption (discharge level returning to spontaneous value) depends upon the time taken by cupula and the sensory hair cells to return to their undistorted position.

Interestingly, adoptions did occur during constant velocity rotations, as could be seen in Figure 5.10(B).

5.5.2 Biomechanics of Semicircular Canals

Rabbitt et al.(2004) assume endolymph to be an incompressible fluid and use a simple control volume approach to derive the governing expression for volume displacement (Q) of endolymph inside a semicircular canal, relative to duct's walls. Considering conservation of momentum for the elemental volume of endolymph shown in Figure 5.11, we get:

$$\rho \left(\frac{D(Au)}{Dt} + A \frac{\partial U}{\partial t} \right) = -A \frac{\partial P}{\partial s} - \tau C \quad (5.1)$$

Where, ρ is endolymph density, $P(s,t)$ is the endolymph pressure, $\tau(s,t)$ is the shear stress acting on the duct wall, $A(s)$ is the local cross-sectional area of the (relatively) rigid duct, and $C(s)$ is the local inside circumference of the duct. $U(s,t)$ is the local velocity of the duct wall in relation to the inertial frame of reference, averaged over its cross section and projected in the direction tangent to s , while $u(s,t)$ is the tangential velocity component of elemental volume relative to the duct wall.

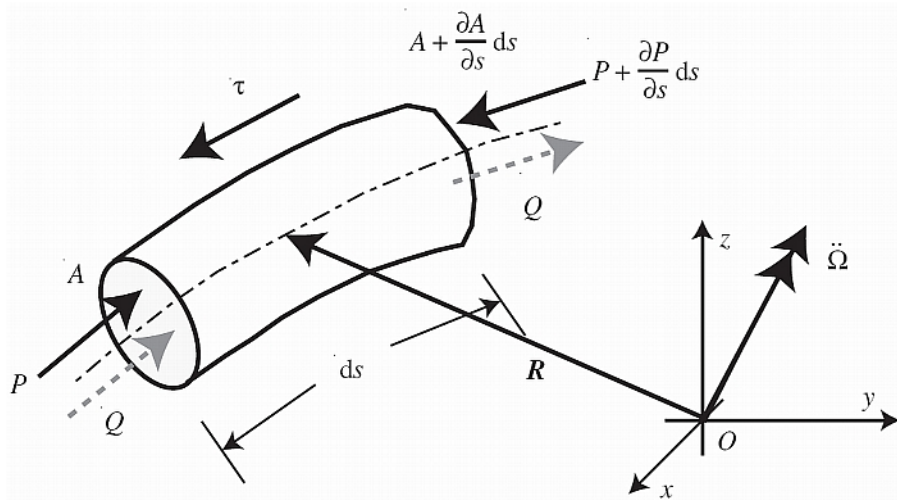


Figure 5.11. Free-body diagram of a short section of endolymph within a semicircular canal showing pressure acting within the fluid and shear stresses acting tangent to the curved centreline of the duct.

These stresses act on their respective areas to generate forces that accelerate or decelerate the endolymph in inertial space [Rabbitt et al. 2004].

Expanding the material derivative of Equation(5.1), we have:

$$\begin{aligned}\frac{D(Au)}{Dt} &= \frac{\partial(Au)}{\partial t} + (Au) \frac{\partial(Au)}{\partial s} \\ \Rightarrow \frac{D(Au)}{Dt} &= \frac{\partial(Au)}{\partial t} + Au^2 \frac{\partial A}{\partial s} + A^2 u \frac{\partial u}{\partial s}\end{aligned}$$

Damiano & Rabbitt (1996) found the convective nonlinearities, u^2 and $u(\partial u/\partial s)$ as small enough to be neglected. Thus, replacing the average fluid velocity u with $(1/A)(dQ/dt)$, Equation(5.1) may be simplified as:

$$\frac{\rho}{A} \frac{\partial^2 Q}{\partial t^2} + \frac{\tau C}{A} = -\frac{\partial P}{\partial s} - \rho \frac{\partial U}{\partial t} \quad (5.2)$$

Rabbitt et al.(2004), relate the wall shear stress τ with the kinematical variables by dividing it into two parts; one due to fluid viscosity (τ_μ) and other due to cupular shear stiffness (τ_γ) as:

$$\frac{\tau C}{A} = \frac{\tau_\mu C}{A} + \frac{\tau_\gamma C}{A} = \frac{\mu \lambda_\mu}{A^2} \frac{dQ}{dt} + \frac{\gamma \lambda_\gamma}{A^2} Q \quad (5.3)$$

Where, μ is the dynamic viscosity of endolymph (dyne sec/cm²); λ_μ is the dimensionless frequency-dependent velocity profile factor that depends on the shape of the velocity distribution over the canal cross section ($\lambda_\mu=8\pi$ for low frequency head movement with parabolic velocity profile); γ is the cupular shear stiffness (dyne/cm²); λ_γ is the dimensionless displacement profile factor that depends on the shape of the cupular displacement distribution over the ampullary cross sections ($\lambda_\gamma=8\pi$ for simple diaphragm-like displacements). Substituting shear stress terms from Equation(5.3) into(5.2), we get the key equation governing endolymph and cupular volume displacements in the semicircular canals:

$$\left(\frac{\rho}{A}\right) \frac{d^2 Q}{dt^2} + \left(\frac{\mu \lambda_\mu}{A^2}\right) \frac{dQ}{dt} + \left(\frac{\gamma \lambda_\gamma}{A^2}\right) Q = -\frac{\partial P}{\partial s} - \rho \frac{\partial U}{\partial t} \quad (5.4)$$

Due to the assumed incompressibility of endolymph and conservation of mass, the displacement volume (Q) is a function of time only (independent of the variation of canal cross-sectional areas); thereby the instantaneous volume flow of endolymph in the complete length of duct is uniform. Now, ignoring the interaction of a given canal's endolymph with the two sister canals (in vestibule), Equation(5.4) may be integrated around the toroidal loop to get:

$$m \frac{d^2 Q}{dt^2} + c \frac{dQ}{dt} + kQ = f \quad (5.5)$$

Where, the equivalent mass (m), damping (c) and stiffness (k) parameters for nearly circular cross section of endolymphatic duct are given by:

$$\begin{aligned} m &= \oint \frac{\rho}{A} ds, \\ c &= \oint \frac{\mu \lambda_{\mu}}{A^2} ds, \\ k &= \oint \frac{\gamma \lambda_{\gamma}}{A^2} ds \end{aligned} \quad (5.6)$$

While, the inertial forcing term on right hand side of Equation(5.5) is given by:

$$f = \oint \rho \left(\ddot{\vec{\Omega}} \times \vec{R}(s) \right) \cdot ds \quad (5.7)$$

Where, the vector product of angular acceleration $\ddot{\vec{\Omega}}$ and local position vector \vec{R} (see Figure 5.11) represents the local tangential acceleration ($\partial U / \partial t$). Equation(5.7) may be rewritten in a more convenient manner for rotations about a fixed axis as:

$$\begin{aligned} f &= \ddot{\Omega} g \\ \text{With} & \\ g &= \oint \rho \hat{m} \times R(s) \cdot ds \end{aligned} \quad (5.8)$$

Again, $\ddot{\Omega}$ is the magnitude of angular acceleration and \hat{m} is a unit vector in the direction of the angular acceleration.

The single canal governing expression, Equation(5.5), is similar to the work of Oman et al.(1987) and has a mathematical form identical to Steinhausen's (1931) classical torsion pendulum model given by:

$$I(\ddot{\theta}_i(t) - \ddot{\theta}_e(t)) = C\dot{\theta}_e(t) + K\theta_e(t) \quad (5.9)$$

Where, I is the moment of endolymph inertia, θ_e is the angular displacement of endolymph, θ_i is the head angular rotation, C is the moment of endolymph's viscous force per unit angular velocity and K is the moment of elastic restoring force per unit angular displacement of endolymph (and cupula).

The primary advantage of semicircular canal's macro-mechanical model developed by Rabbitt et al.(2004) [Equation(5.5)] over classical model [Equation(5.9)] is the dependency of its parameters on the morphological and physical features of canals and related fluids. This means, the model parameters are specific for a particular species.

Assuming the initial conditions to be zero (i.e. starting from rest) and taking Laplace transform of Equation(5.5), after substituting forcing function f from Equation(5.8), we get:

$$Q(s) \left(s^2 + \frac{c}{m}s + \frac{k}{m} \right) = \left(\frac{g}{m} \right) \ddot{\Omega}(s) \quad (5.10)$$

Equation(5.10) may be rearranged to establish the transfer function of semicircular canals relating endolymph/cupular volume displacement, with head accelerations as:

$$scc(s) = \frac{Q(s)}{\ddot{\Omega}(s)} = \frac{(g/m)}{(s+1/\tau_1)(s+1/\tau_2)} \quad (5.11)$$

The time constants τ_1 & τ_2 of Equation(5.11) are given by:

$$\begin{aligned}\frac{1}{\tau_1} &= \frac{c}{2m} \left(1 - \sqrt{1 - \frac{4km}{c^2}} \right) \\ \frac{1}{\tau_2} &= \frac{c}{2m} \left(1 + \sqrt{1 - \frac{4km}{c^2}} \right)\end{aligned}\tag{5.12}$$

Expanding the square root terms of Equation(5.12) using Maclaurin series, and terminating the series after two terms, we get:

$$\sqrt{1 - \frac{4km}{c^2}} \approx 1 - \frac{2km}{c^2}$$

Owing to their morphology (slenderness), the semicircular canals are highly over damped ($c^2 \gg km$), hence:

$$\frac{1}{\tau_1} \approx \frac{c}{2m} \left(1 - 1 + \frac{2km}{c^2} \right) = \frac{k}{c}\tag{5.13}$$

$$\frac{1}{\tau_2} \approx \frac{c}{2m} \left(1 + 1 - \frac{2km}{c^2} \right) \approx \frac{c}{m}\tag{5.14}$$

The canal transfer function linking cupular volume displacement with head velocity would then be:

$$scc(s) = \frac{Q(s)}{\dot{\Omega}(s)} = \frac{(g/m)s}{(s+1/\tau_1)(s+1/\tau_2)}\tag{5.15}$$

The time constants of Equation(5.15) are also be given by Equation(5.12). By using the physical and morphological data about humans' lateral semicircular canals, Rabbitt et al.(2004) calculated the approximate values of model [Equation(5.5)] parameters shown in Table 5.1.

Table 5.1. Model parameters for lateral canals in humans [Rabbitt et al.(2004)]

m (g/cm ⁴)	c (dyne s/cm ⁵)	k (dyne/cm ⁵)	g (g/cm)	τ₁ (sec)	τ₂ (sec)
1070	179000	13320	0.76	13.2	0.0060

Now, if we consider unit step change in angular velocity as input, then Equation(5.12) may be used to derive the time response of canal i.e. cupular volume displacement as:

$$Q(s) = \frac{(g/m)s}{(s+1/\tau_1)(s+1/\tau_2)} \times \frac{1}{s} = \frac{(g/m)}{(s+1/\tau_1)(s+1/\tau_2)}$$

$$\Rightarrow Q(t) = \frac{g\tau_1\tau_2}{m(\tau_1 - \tau_2)} \left(e^{-\left(\frac{t}{\tau_1}\right)} - e^{-\left(\frac{t}{\tau_2}\right)} \right) \quad (5.16)$$

Substituting the parameters given in Table 5.1, we can plot the time response of lateral canal using Equation(5.16) as shown in Figure 5.12.

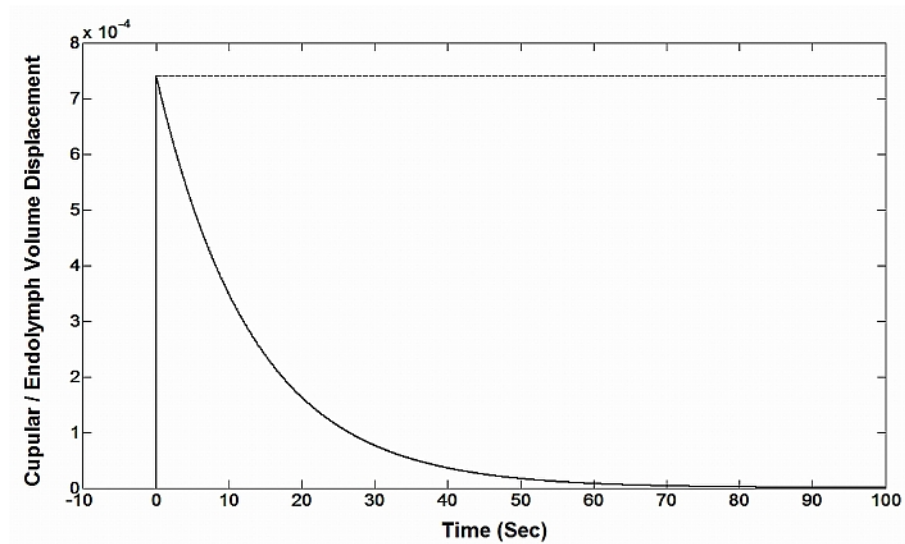


Figure 5.12. Time response of lateral semicircular canal to unit step change of angular velocity.

It can be seen from this figure that for a step change in angular velocity there would be a short impulsive inertial force at t=0, causing a rapid volumetric displacement of

cupula dominated by the long time constant (τ_1). This is followed by a relatively long period of slow recovery to zero governed by the short time constant (τ_2). Comparing Figure 5.12 with the electrophysiological recording of vestibular nerve afferent of lateral canal depicted in Figure 5.10, one can immediately spot the similarity between the hydrodynamic model proposed by Rabbitt et al.(2004) and what has been measured in laboratory by Goldberg & Fernandez (1971).

We can also investigate the frequency response of canal by substituting model parameters from Table 5.1 into Equation(5.15) and generating it's bode plot as shown in Figure 5.13. It can be observed from this figure that cupular volume displacement predicted by Equation(5.5) exhibit a bandpass filter characteristics for angular head velocity. The lower corner frequency corresponds to long (slow) time constant τ_1 ($\omega_1=1/\tau_1$, rad/sec) and upper corner frequency is related to short (fast) time constant τ_2 ($\omega_2=1/\tau_2$, rad/sec).

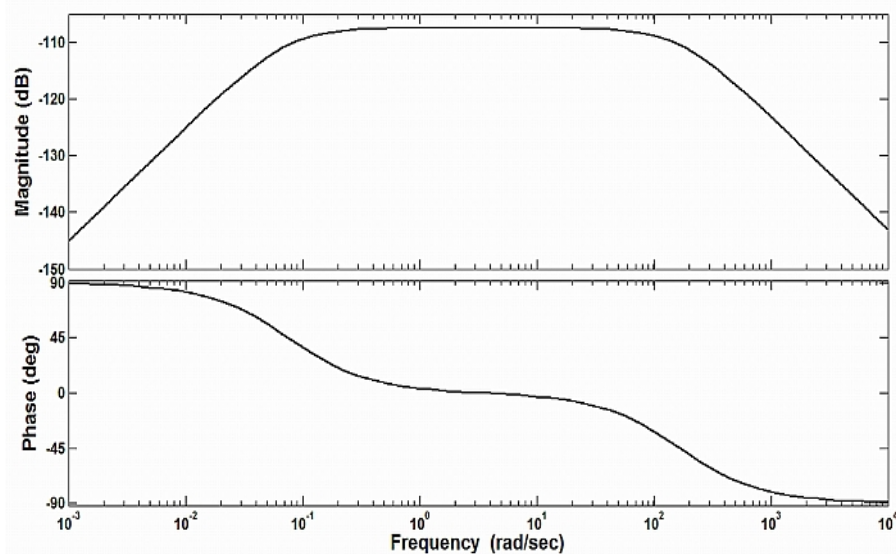


Figure 5.13. Bode diagram of lateral semicircular canal transfer function ($0.00071s/(s^2+166.7s+12.63)$) as per the hydrodynamic canal model of Rabbitt et al. 2004.

Below the lower corner frequency the response (endolymph/cupular volumetric displacement) is attenuated by the stiffness of the cupula. Whereas, above the upper corner frequency the inertia of the endolymph within the slender porting of canals decreases the response. Between these two frequencies, the model [Equation(5.10)]

predicts that the viscosity of the endolymph would dominate the response, mechanically integrating the angular acceleration of the head to produce cupular volume displacement (responsible for vestibular afferents).

On similar lines as above, we can derive the canal transfer function relating angular displacement of endolymph (θ_e) with the head rotational velocity ($\dot{\theta}_i$) using the classical torsion pendulum model of Steinhausen (1931) [Equation(5.9)] as:

$$scc(s) = \frac{\theta_e(s)}{\dot{\theta}_i(s)} = \frac{s}{(s+1/\tau_1)(s+1/\tau_2)} \quad (5.17)$$

Where, the time constants τ_1 & τ_2 are given by:

$$\frac{1}{\tau_1} = \frac{C}{2I} \left(1 - \sqrt{1 - \frac{4KI}{c^2}} \right) \approx \frac{K}{C} \quad (5.18)$$

$$\frac{1}{\tau_2} = \frac{C}{2I} \left(1 + \sqrt{1 - \frac{4KI}{c^2}} \right) \approx \frac{C}{I}$$

Mayne (1974b), also using hydrodynamic principles, estimated these time constants as 20sec(τ_1) and 0.013sec(τ_2), which would give the frequency response of canals as shown in Figure 5.14.

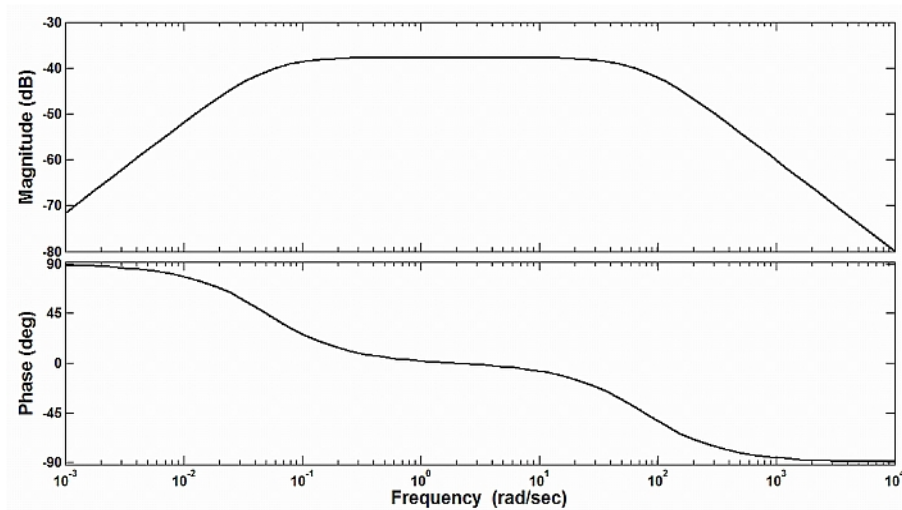


Figure 5.14. Bode diagram of semicircular canal transfer function ($s/(s^2+76.97s+3.846)$) as per the hydrodynamic model of Steinhausen 1931; time constants as estimated by Mayne 1974.

This endolymphatic angular displacement response estimated by classical model is very similar to cupular volumetric displacement response (see Figure 5.13) predicted by the macro-mechanical model of Rabbitt et al.(2004). Once again, heavy damping of canal ($C \gg KI$) is responsible for the long time constant ($\tau_1 = C/K$) as well as the short time constant ($\tau_2 = I/C$) and canals operate as velocity transducers for the frequency range $\omega_1 (=1/\tau_1 \text{ rad/s}) < \omega < \omega_2 (=1/\tau_2 \text{ rad/sec})$. The natural rotational body motions lie within the aforesaid frequency band in which the canals act like angular rate sensors with approximately zero phase lag/lead.

However, a considerable phase lead is displayed by the canals for rotations below lower cut off frequency. Consequently, the canals are inefficient in detecting low frequency angular velocities. This can also be verified by studying the time response of canals to unit step angular acceleration; where [using Equation(5.11)] cupular volume displacement (Rabbitt et al. 2004) would be given by:

$$Q(t) = \frac{g\tau_1\tau_2}{m} \left(1 - \frac{\tau_1 e^{-t/\tau_1} - \tau_2 e^{-t/\tau_2}}{\tau_1 - \tau_2} \right) \quad (5.19)$$

Likewise, endolymph displacement (Steinhausen 1931) for unit step angular acceleration would be:

$$\theta_e(t) = \tau_1\tau_2 \left(1 - \frac{\tau_1 e^{-t/\tau_1} - \tau_2 e^{-t/\tau_2}}{\tau_1 - \tau_2} \right) \quad (5.20)$$

Now, after substituting the parameter given in Table 5.1 into Equation(5.19) and employing the time constant estimated by Mayne(1974b) in Equation(5.20), we can plot the canal time responses predicted by the two model as shown in Figure 5.15. This figure is suggesting that for a unit step angular acceleration the inertial force remains constant over time, thereby, displacing cupula / endolymph as long as the stimulus persists. This also asserts our observation that canals respond to angular accelerations at low frequencies.

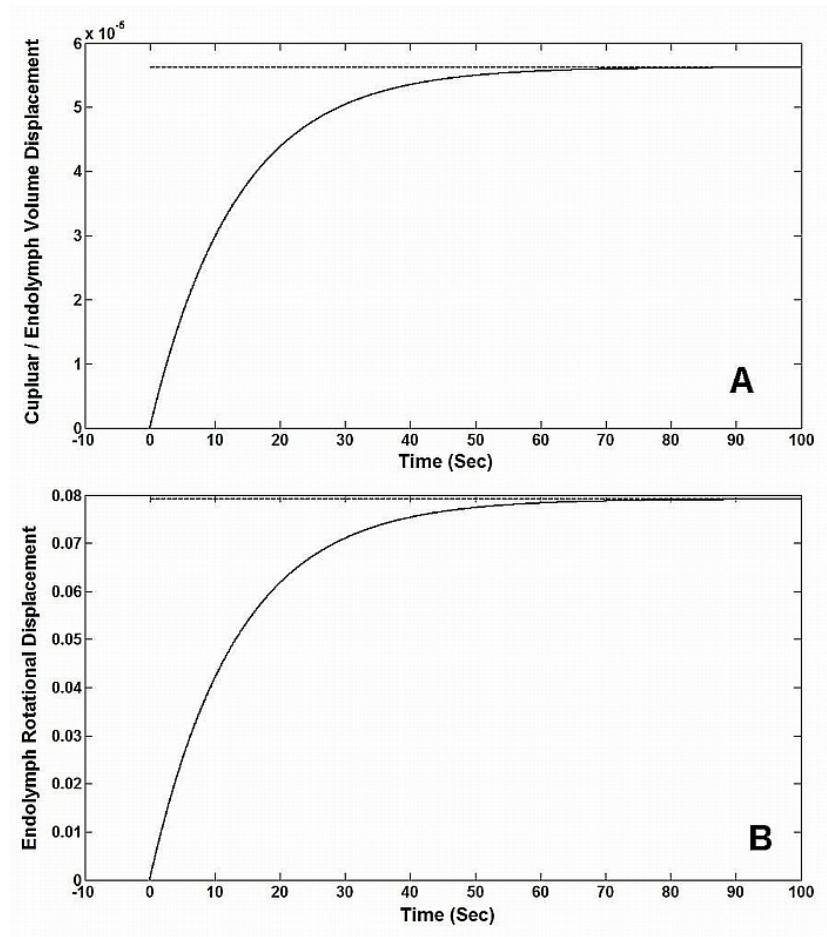


Figure 5.15. Semicircular response to unit step acceleration; A Cupular / Endolymph volumetric displacement [Rabbitt et al. 2004]; B Endolymph angular displacement [Steinhausen 1931; Mayne 1974].

According to Fernandez & Goldberg(1971), the hydrodynamic approach is suitable to estimate the short time constant (τ_2) of the model (Steinhausen 1931) governing angular displacement of endolymph (which causes angular deflection of cupula) [Equation(5.9)]. However, this time constant is (obviously) of limited use under normal (low frequency) rotational motion conditions. In contrast, the long time constant (τ_1), which is more relevant to ordinary locomotion of species, cannot be determined through hydrodynamic analysis as the elastic-restoring moment (K) has not been measured directly. Moreover, hydrodynamic approach ignores the relationship between physiological features of vestibular apparatus (sensory hair cells, axons, nuclei, etc.) and the mechanics of endolymph-cupular system.

Therefore, it is imperative to realise that cupula deflection may not assumed to be directly encoded into subjective velocity (Young 1984).

Resultantly, various studies have focused on understanding canal dynamics, usually in humans, using the subjective estimates of self rotation (Hulk & Jongkees 1948; Van Egmond et al. 1949; Hallpike & Hood 1953; Groen 1957; Niven & Hixson 1961; Ormsby & Young 1976; 1977; Young 1984). Such studies typically estimate the long time constants (τ_1) between 5 and 20 seconds, but the primary drawback of this approach is its subjective nature. Furthermore, the subjective sensation of self-rotation during and after the constant velocity rotation are likely to be influenced by the velocity storage mechanism (Raphan et al. 1977), as well as the level of an individual's adaptation (Dai et al. 2003). It is therefore not surprising to see that the magnitude of long time constant (τ_1) varied from 5 to 20 seconds when estimated using the subjective perception of the constant velocity rotations.

Ormsby & Young (1977) present a model for the perception of dynamic orientation resulting from stimuli involving the vestibular system; they propose the following transfer function for semicircular canals, capable of representing the subjective sensation while being rotated:

$$\frac{\omega(s)}{\omega_i(s)} = \frac{540s^2}{(18s+1)(30s+1)} \quad (5.21)$$

Where, $\omega(s)$ it the Laplace domain subjective perception of scalar angular velocity (rad/sec) and $\omega_i(s)$ is the stimulus angular velocity about the considered canal's sensitivity axis (rad/sec). Equation(5.21) represents a high pass filter with the frequency response depicted in Figure 5.16.

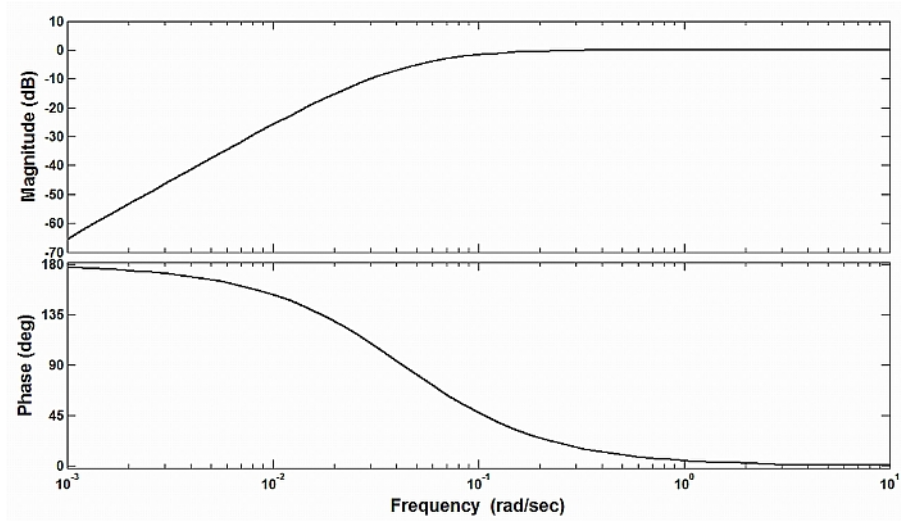


Figure 5.16. Bode diagram of semicircular canal transfer function $[540s^2/(18s+1)(30s+1)]$ as per the subjective perception model of Ormsby & Young 1977.

Borah et al.(1988) further develop the subjective transfer function [Equation(5.21)] of semicircular canals by Ormsby & Young (1977) and propose the following transfer function, relating the angular accelerations stimulus $\dot{\omega}(s)$ and firing rate of semicircular canals $\alpha_{scc}(s)$:

$$\frac{\alpha_{scc}(s)}{\dot{\omega}(s)} = \frac{0.574s(s+100)}{(s+0.1)(s+0.033)} \quad (5.22)$$

This transfer function has also been used by Elias et al.(2008) in their modelling of sensory conflict and motion sickness in artificial gravity environment; its frequency response is shown in Figure 5.17.

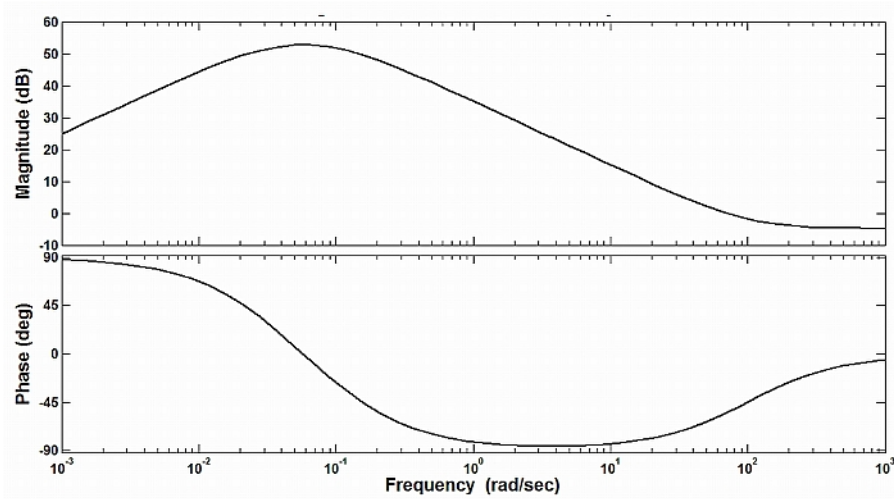


Figure 5.17. Bode diagram of semicircular canal transfer function $[(0.574s(s+100))/(s+0.1)(s+0.033)]$ as per the vestibular afferent model by Borah et al. 1988 also used by Elias et al. 2008 for modelling sensory conflict in artificial gravity.

A rather more direct approach, involving electrophysiological recording of the vestibular afferents, can also be used to measure the time constants of canal dynamics. This has been undertaken for various species (see Lysakowski & Goldberg 2004 for details) yielding the slow time constant (τ_1) in the range of 2-8sec. According to Goldberg & Fernandez(1975), “taking a value of 5 sec as typical, the computed bandwidth over which the cupula-endolymph system functions as a velocity transducer extends from 0.025-25 Hz, a range encompassing the bandwidth of physiological head movements”.

Considering the response dynamics of first-order semicircular canals afferents, Fernandez & Goldberg(1971) proposed the Laplace domain transfer function $H(s)$ of a single canal given by Equation(5.23). This transfer function relates the discharge rate of vestibular nerve innervating canals, with the stimulus rotational acceleration.

$$H(s) = \frac{\tau_A s}{(1 + \tau_A s)} \cdot \frac{1}{(1 + \tau_1 s)(1 + \tau_2 s)} \cdot (1 + \tau_L s) = H_A \cdot H_{TP} \cdot H_L \quad (5.23)$$

Where, H_A is the frequency-domain representation of adaptation operator (Young & Oman 1969); H_{TP} is the transfer function of classical canal torsion model

(Steinhausen 1931); and HL takes account of the high-frequency deviations observed in the measured data's gain and phases as compared to torsion-pendulum model.

They estimated the various time constants ($\tau_A=80\text{sec}$, $\tau_1=5.7\text{sec}$, $\tau_2=0.003\text{sec}$, and $\tau_L=0.049\text{sec}$) of Equation(5.23) by analysing electrophysiological vestibular afferents recorded from 57 (28 lateral, 19 anterior, & 10 posterior) canals of squirrel monkeys exposed to sinusoidal stimulation of different frequencies and acceleration amplitudes. The bode diagram depicting frequency response of the proposed transfer function [Equation(5.23)] is given in Figure 5.18.

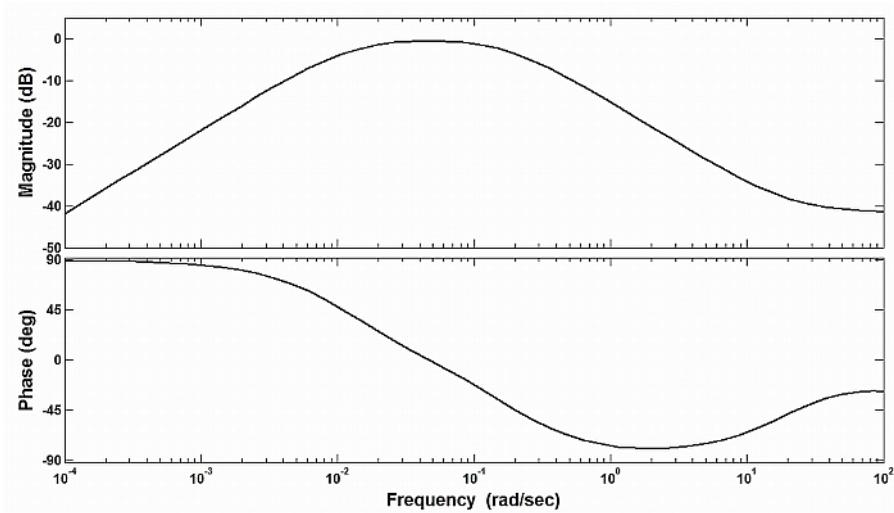


Figure 5.18. Bode diagram of semicircular canal transfer function $[(80s/(1+80s))((1+0.049s)/(1+5.7s)(1+0.03s))]$ as per the electrophysiological recordings in squirrel monkey by Fernandez & Goldberg 1971.

Merfeld et al.(1993) and later Merfeld & Zupan (2002), simplify the labyrinthine electrophysiology based transfer function [Equation(5.23)] established by Fernandez & Goldberg(1971) as:

$$\frac{\alpha_{sc}(s)}{\omega(s)} = \frac{s}{(s+1/\tau_d)} \quad (5.24)$$

Where, $\alpha_{sc}(s)$ is the scalar semicircular canal afferent; $\omega(s)$ is a scalar angular velocity along one of the three rotational axes; and $\tau_d (=5.7\text{sec})$ is the long time constant. The bode plot of this transfer function is given in Figure 5.19.

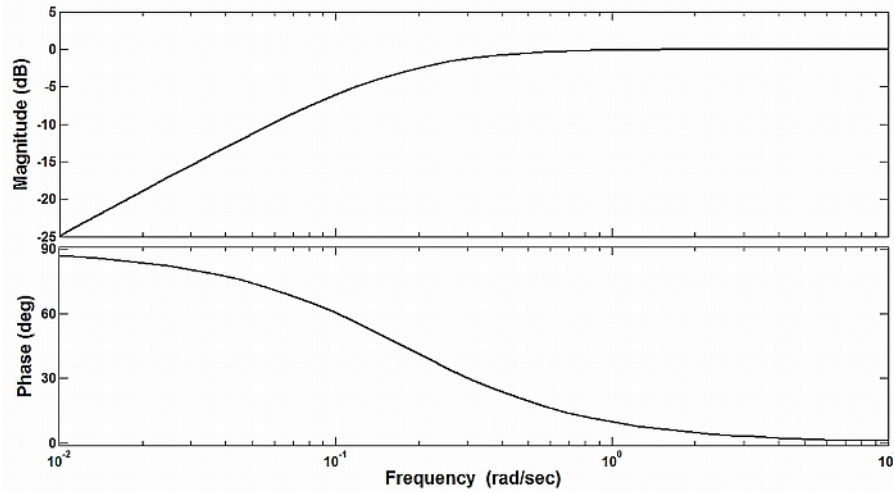


Figure 5.19. Bode diagram of afferent based semicircular canal transfer function ($s/(s+1/5.7)$) Merfeld et al. 1993 & Merfeld & Zupan 2002.

For our case, we are interested in the elicitation of motion sickness caused by the passive motions of a ship and the typical vessel motions are of low frequency ($\ll 1.0\text{Hz}$, 6.3rad/sec). Incidentally, human beings also exhibit maximum sensitivity to passive motions of very low frequency ($\ll 0.5\text{Hz}$, 3.15rad/sec) from sickness view point. Now, by comparing the bode diagrams of various canal transfer function presented in this section (Figure 5.13, Figure 5.14, Figure 5.16, Figure 5.18, Figure 5.17, & Figure 5.19), we can immediately notice that all of them display similar (high pass filter like) response for the frequencies of our interest.

Thus, it would be more logical to choose the simplest of all transfer function i.e. Equation(5.24) for mathematical modelling of semicircular canals. This transfer function has also been used by Bos & Bles (1998a; 1998b; 2002a) and later by Verveniotis & Turan (2002a; 2002b; Verveniotis 2004; Turan et al. 2009) in their physiological models for motion sickness.

5.5.3 Velocity Storage Mechanism and Adaptation

While studying the per- and post rotation angular vestibulo-ocular reflexes (VORs) of the rhesus monkeys at constant velocity, Raphan et al.(1977) observed that the dominant time constant of the nystagmus (slow phase velocity) decay was 15-30 seconds. Whereas Fernandez & Goldberg (1971) found the value of this time constant to be around 3-5 seconds while measuring the neural activities of the first order neurons innervating semicircular canals of the squirrel monkeys, under the trapezoidal velocity stimuli. Based on these observations Raphan et al. (1977) hypothesised that the CNS makes use of some form of velocity storage mechanism that elongates the decay time of the slow phase nystagmus velocity during and after the constant velocity rotations (Raphan et al. 1979). In short, the velocity storage mechanism explains the observations that the angular velocity estimates of the CNS, manifested as VOR and perceptual measures of rotation, last longer than the afferent signals from canals (MacNeilage et al. 2008).

Studies concerning habituation to motion sickness in human beings by Bos et al. (2002b), found that the nystagmus (slow) time constant under yaw rotations are significantly larger for non-adapted and highly susceptible people. This time constant has been reported to reduce as the subjects become adapted to the provocative environments. In similar studies, concerning the adaptation of human subjects to provocative roll head movements under constant velocity yaw rotations, Cohen et al. (2003) and Dai et al.(2003) observed reductions in the nystagmus time constants. These observations clearly indicate that the VOR (typical manifestation of vestibular system) rely on the central estimates of rotational velocity under low frequency / constant rotation rather than the peripheral canal afferents. The former would change depending on the habituation level while the latter remain unaltered.

As presented in §5.5.2, the estimates of slow time constant (τ_1) for canal's transfer function by the hydrodynamic considerations are in the range of 13 to 20 seconds, whereas, its value ranges from 5 to 20 seconds when estimated subjectively. On the other hand, the direct electrophysiological measurements of the first order canal afferents of squirrel monkeys yield a value of 5.7 seconds (Fernandez & Goldberg 1971). Since we are modelling the response dynamics of peripheral semicircular

canals in our motion sickness model, hence it is prudent to select the value of τ_1 on the basis of direct measures i.e. electrophysiological (5.7 second).

The reason for not selecting the value of τ_1 driven from hydrodynamic consideration, are the unreliable estimates of elastic restoring moments [K, see Equation(5.13) & (5.18)], which have not been measured directly (Fernandez & Goldberg 1971). Whereas, the values based on subjective measures are expected to be influenced by the velocity storage mechanism as well as adaptation; thereby representing the CNS estimates of velocity rather than peripheral afferents.

5.5.4 Physiology of Otoliths

The physical decoupling of otolithic membrane from the sensory base of macula (by means of an intermediate gelatinous substance, see Figure 5.8 in §5.4.3) and the surrounding endolymph, facilitates relative motion between the denser otolithic membrane and the sensory epithelium. This structural arrangement is suitable to sense the static displacement of otolithic membrane caused by the tilting of head relative to gravity as well as the transient displacement originating from linear motions of the head. Linear accelerations displace membranous utricule and saccule as a whole, but the inertia of otoconial masses forces them to lag behind the head movements; thereby deflecting the hair bundles of sensory cells. As depicted in Figure 5.20, these otoconial displacements are tonical and transient corresponding to steady tilting and translational movements of the head, respectively.

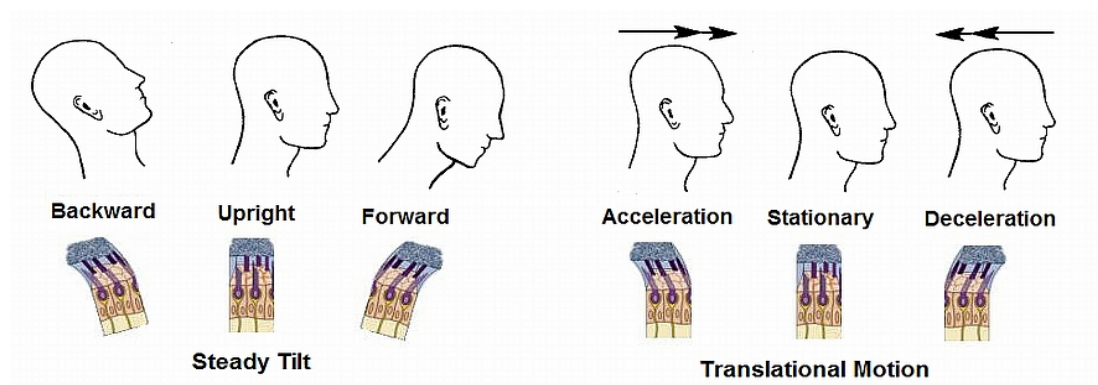


Figure 5.20. Displacement of utricular otolithic membrane during upright, tilted and under translational acceleration conditions [adopted from Purves et al. 2004].

Alike semicircular canals, the spontaneous discharge rate of the vestibular nerves innervating sensory hair cells of otoliths is relatively high when the head is in upright condition. Transient deflections of hair bundles caused by the linear accelerations transform into ephemeral changes in the axonal firing rates, while steady head tilts lead to sustained variation in the discharge rate. Fernandez & Goldberg(1976a) recorded axonal activities of the vestibular nerves connected with otolith organs in 86 squirrel monkeys. They exposed these monkeys (strapped to a purpose-built apparatus) to static tilts and centrifugal forces. The static tilt experiments aimed to identify the 'otolith-only' neurons that faithfully encoded primary otolithic afferent and did not receive any input from semicircular canals. On the other hand, the centrifugal-force experiments were used to study the physiologic response characteristics of otoliths.

The centrifugal force experiments used force-trapezoids comprising of a constant initial rotational velocity (inducing a small background centrifugal force); a short period of acceleration; a relatively large period of increased rotational velocity (i.e. increased centrifugal force); a short period of deceleration; finally a long period of rotation with velocity identical to its initial value. During these force stimuli, the primary otolithic afferents were continuously recorded and a typical axonal response of the nerve innervating utricular sensory epithelium is depicted in Figure 5.21. A relatively high spontaneous rate is visible for a small background centrifugal force (0.077g), which increases (1.23g, termed as excitation) with an increase in the rotational velocity and then declines back to steady firing rate upon reduction of the force to its initial (0.077g) level.

Reversal of force-trapezoid produces an opposite response, whereby, increased force in the opposite direction reduces the firing rate (termed as inhibition). There is some asymmetry in the variation of firing rates for oppositely directed, otherwise identical forces. These excitation and inhibition features of otolithic afferents allow the vestibular nuclei to identify the directional aspects of acceleration being experienced.

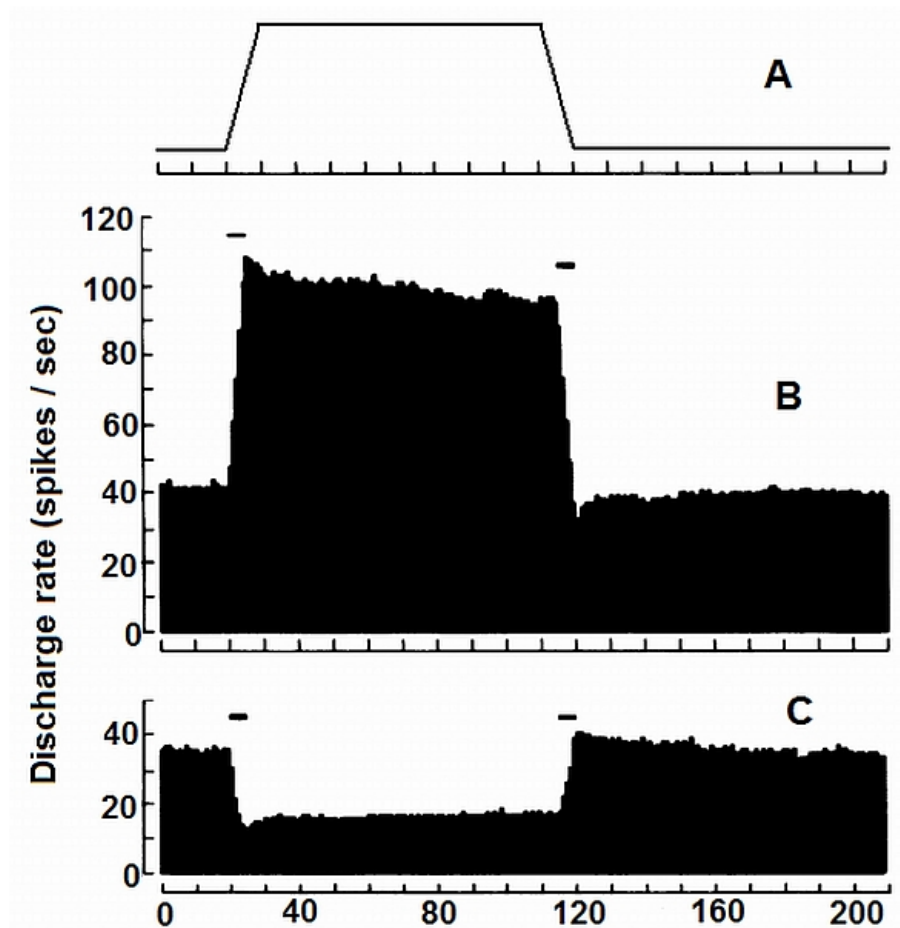


Figure 5.21. Response of vestibular nerve axon from utricular macula; A stimulating force-trapezoid; B discharge rate for excitatory force; C discharge rate for inhibitory force [after Fernandez & Goldberg 1976].

5.5.5 Biomechanics of Otoliths

The schematic diagram depicting anatomical dimensions of otoliths (Igarashi 1966; 1967; Igarashi et al. 1981) is shown in Figure 5.22; where the dense otoconial layer is approximately 20-30 μ m thick. The highly deformable middle gelatinous layer is also approximately 20-30 μ m thick, which is considered to provide most part of the viscous damping in the otolithic system. Jaeger et al.(2002; Jaeger & Haslwanter 2004) have carried out finite element simulation of otoconial layer displacements under static (head tilt) linear accelerations. Their intricate analysis of human otolith biomechanics considered the 3D orientation and geometry of the two otolith organs (utricle and saccule). Their study reinforces the importance of otoliths' anatomical

features for the excitation of multi-polarized hair cells and their subsequent contribution towards quantification and identification of the direction of linear accelerations sensed by these organs.

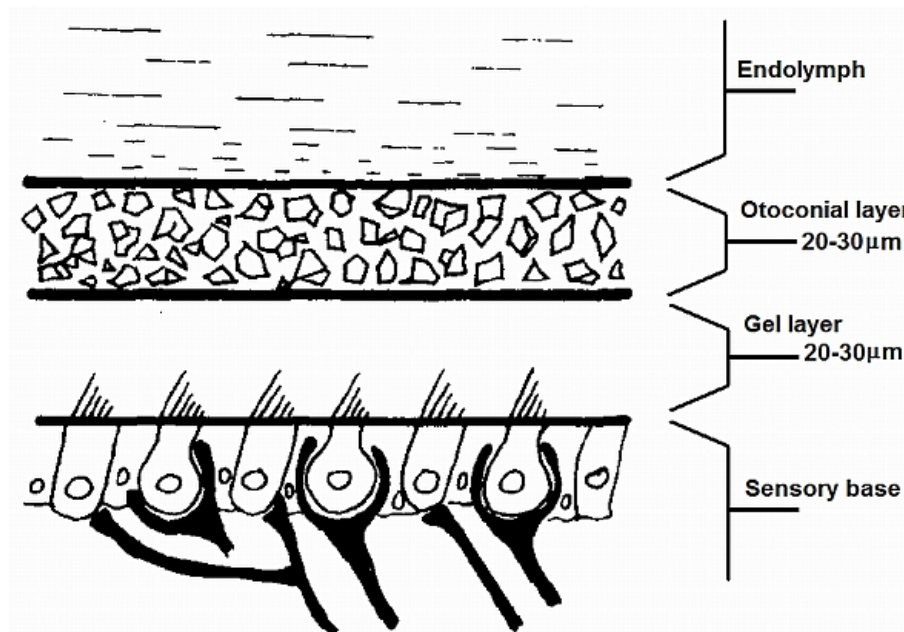


Figure 5.22. Schematic layout of otolith organs [after Igarashi 1966].

However, various researchers (Steinhausen 1935; de Vries 1950; Grant & Best 1986; Grant & Best 1987; Grant & Cotton 1990; Grant et al. 1994; Rabbitt et al. 2004) use a simple ‘lumped-parameter’ approach to model the gross behaviour of otolith organs. According to this approach, motion of the otolithic membrane relative to substrate is governed by the conservation of momentum. Rabbitt et al.(2004) treat the otolith organ as an overdamped second-order spring-mass damper system, where otoconial layer forms the solid mass, the gelatinous layer acts like isotropic viscoelastic material and the endolymph is considered as Newtonian fluid with uniform viscosity. The idealized ‘lumped-parameter’ system is shown in Figure 5.23, which also contains free-body diagrams relaying information about the various external and inter-layer forces, acting in any arbitrary direction \hat{n} (with respect to inertial frame of reference). These forces are resulting from the relative displacement (u) of otoconial layer tangential to sensory epithelium.

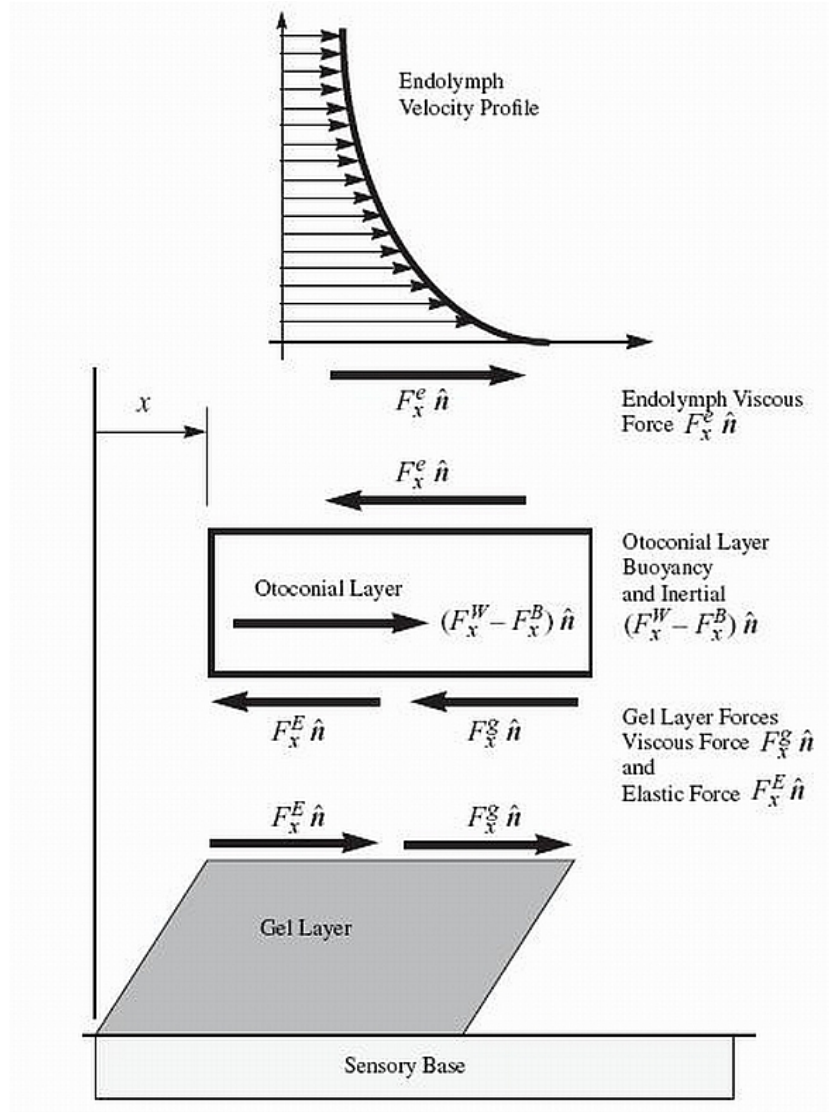


Figure 5.23. Lumped-parameter model of otolith with free-body diagram of the otoconial layer showing the various forces acting on the layer [after Rabbitt et al. 2004].

Assuming the sensory base to be rigid and firmly attached to temporal bone, the x (along the length of base) components of various forces acting on the otoconial layer would be:

$$\begin{aligned}
 F_x^W &= \rho_o V_o \hat{n} \cdot \bar{g} \\
 F_x^B &= \rho_e V_o \hat{n} \cdot (\bar{g} - \ddot{X}) \\
 F_x^D &= c_o \dot{u} \\
 F_x^E &= k_o u
 \end{aligned} \tag{5.25}$$

Where, ρ_o is the density (2.71g/cm^3) of otoconial layer; ρ_e is the density (1.0g/cm^3) of endolymph; V_o is the volume of otoconial layer; \vec{g} is the gravitational acceleration vector; $\vec{\ddot{X}}$ is the inertial acceleration of head; c_o is the effective drag coefficient (for both the endolymph as well as gel layer); \dot{u} is the relative velocity of otoconial layer (with respect to sensory base); k_o is the effective stiffness coefficient of gelatinous layer; F_x^W is the \hat{n} component of otoconial layer weight; F_x^B is the \hat{n} component of buoyancy force; F_x^D is the total viscous drag force (endolymph and gel); and F_x^E is the elastic restoration force of gelatinous layer.

Cotton & Grant (2000) report that the viscous shear stress exerted by endolymph onto the otoconial layer, is 5 to 10 times smaller in magnitude than the corresponding stress applied by the gel layer. Now considering the force balance within the plane of otoconial layer in \hat{n} direction and applying Newton's second law of motion (see Figure 5.23), we get:

$$F_x^W - F_x^B - F_x^D - F_x^E = \rho_o V_o (\ddot{u} + \hat{n} \cdot \vec{\ddot{X}}) \quad (5.26)$$

Where, $\hat{n} \cdot \vec{\ddot{X}}$ is the component of head inertial acceleration in the plane of otoconial layer and \ddot{u} is the acceleration of otoconial mass relative to sensory base. Substituting the forces given by Equation(5.25) into Equation(5.26), we obtain:

$$\begin{aligned} \rho_o V_o \hat{n} \cdot \vec{g} - \rho_e V_o \hat{n} \cdot (\vec{g} - \vec{\ddot{X}}) - c_o \dot{u} - k_o u &= \rho_o V_o \hat{n} \cdot (\ddot{u} + \hat{n} \cdot \vec{\ddot{X}}) \\ \Rightarrow m_o \ddot{u} + c_o \dot{u} + k_o u &= m_o \left(1 - \frac{\rho_e}{\rho_o}\right) \hat{n} \cdot (\vec{g} - \vec{\ddot{X}}) \end{aligned}$$

The above could be rewritten as:

$$m_o \ddot{u} + c_o \dot{u} + k_o u = g_o a \quad (5.27)$$

Where,

m_o is the mass of otoconial layer.

$g_o = m_o \left(1 - \frac{\rho_e}{\rho_o} \right)$ is the effective inertial mass of otolithic membrane.

$a = \hat{n} \cdot (\vec{g} - \ddot{\vec{X}})$ is the gravito inertial acceleration in the plane of otoconial layer in the \hat{n} direction.

It can be seen from Equation(5.27) that the inertial force causing motion of otolith layer relative to sensory base would have been zero if the density of otolithic layer were not greater than the density of surrounding endolymph. Assuming the initial conditions to be zero, the Laplace transform of this otolith governing expression would be:

$$(m_o s^2 + c_o s + k_o)u(s) = g_o a(s) \quad (5.28)$$

The above equation could be rearranged to obtain the transfer function of otolith organs, relating displacement of otoconial layer relative to sensory base and the gravito inertial acceleration in the plane of otolith as:

$$oto(s) = \frac{u(s)}{a(s)} = \frac{g_o / m_o}{(s+1/\tau_1)(s+1/\tau_2)} = \frac{(1-\rho_e/\rho_o)}{(s+1/\tau_1)(s+1/\tau_2)} \quad (5.29)$$

Where the two governing time constants are given by:

$$\begin{aligned} \frac{1}{\tau_1} &= \frac{c_o}{2m_o} \left(1 - \sqrt{1 - \frac{4k_o m_o}{c_o^2}} \right) \\ \frac{1}{\tau_2} &= \frac{c_o}{2m_o} \left(1 + \sqrt{1 - \frac{4k_o m_o}{c_o^2}} \right) \end{aligned} \quad (5.30)$$

The otolith transfer function in terms of head velocity would be:

$$oto(s) = \frac{u(s)}{a(s)} = \frac{u(s)}{sv(s)} = \frac{(g_o / m_o)s}{(s+1/\tau_1)(s+1/\tau_2)} \quad (5.31)$$

As we did for semicircular canals, expanding the square root term of Equation(5.30) using Maclaurin series and terminating the series at first derivative, we obtain:

$$\sqrt{1 - \frac{4k_o m_o}{c_o^2}} \approx 1 - \frac{2k_o m_o}{c_o^2} \quad (5.32)$$

Alike semicircular canals, otoliths organs are highly overdamped (de Vries 1950; Grant & Best 1986) i.e. ($k_o m_o \ll c_o^2$), therefore:

$$\frac{1}{\tau_1} \approx \frac{c_o}{2m_o} \left(1 - 1 + \frac{2k_o m_o}{c_o^2} \right) = \frac{k_o}{c_o} \quad (5.33)$$

$$\frac{1}{\tau_2} \approx \frac{c_o}{2m_o} \left(1 + 1 - \frac{2k_o m_o}{c_o^2} \right) \approx \frac{c_o}{m_o} \quad (5.34)$$

According to Grant & Cotton (1990; Grant et al. 1994), the value of long time constant (τ_1) has a range of 40μsec to 5.0 sec in human beings, while the short time constant (τ_2) ranges between 10msec to 4μsec. Substituting the upper limits of time constants and values of densities (otoconial & endolymph) into Equation(5.29), we can plot the frequency response of otoliths to unit sinusoids of translational accelerations shown in Figure 5.24.

The temporal response of otoliths for unit step change in linear velocity may be calculated using the transfer function given in Equation(5.31), as:

$$u(t) = \frac{g_o \tau_1 \tau_2}{m_o (\tau_1 - \tau_2)} \left(e^{(-t/\tau_1)} - e^{(-t/\tau_2)} \right) \quad (5.35)$$

Whereas, for unit step change in gravito-inertial acceleration the temporal response of otoconial displacement would be given by [using Equation(5.29)]:

$$u(t) = \frac{g_o \tau_1 \tau_2}{m_o} \left(1 - \frac{\tau_1 e^{-t/\tau_1} - \tau_2 e^{-t/\tau_2}}{\tau_1 - \tau_2} \right) \quad (5.36)$$

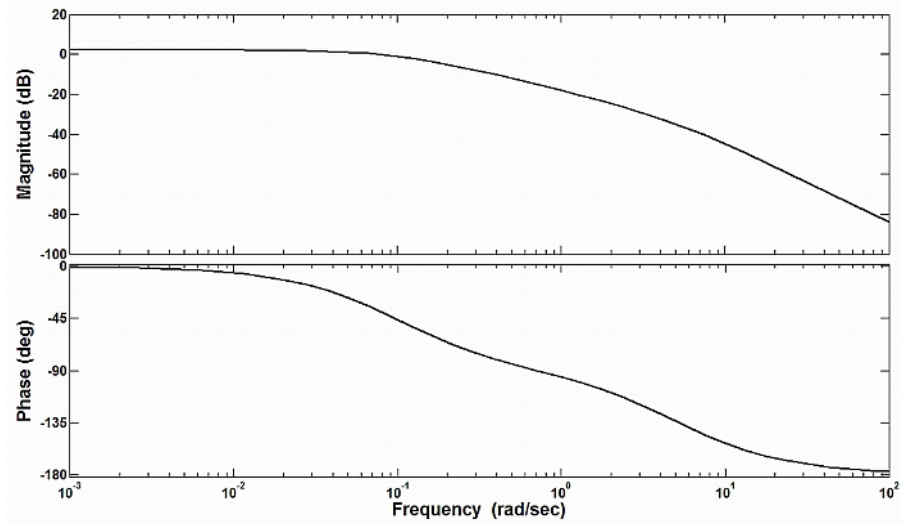


Figure 5.24. Bode diagram of otolith transfer function ($0.631/(s^2+5.1s+0.5)$) as per the hydrodynamic otolith model of Rabbitt et al. 2004.

The temporal otoconial displacements corresponding to step changes in linear velocity [Equation(5.35)] and gravito-inertial accelerations [Equation(5.36)] are shown in Figure 5.25.

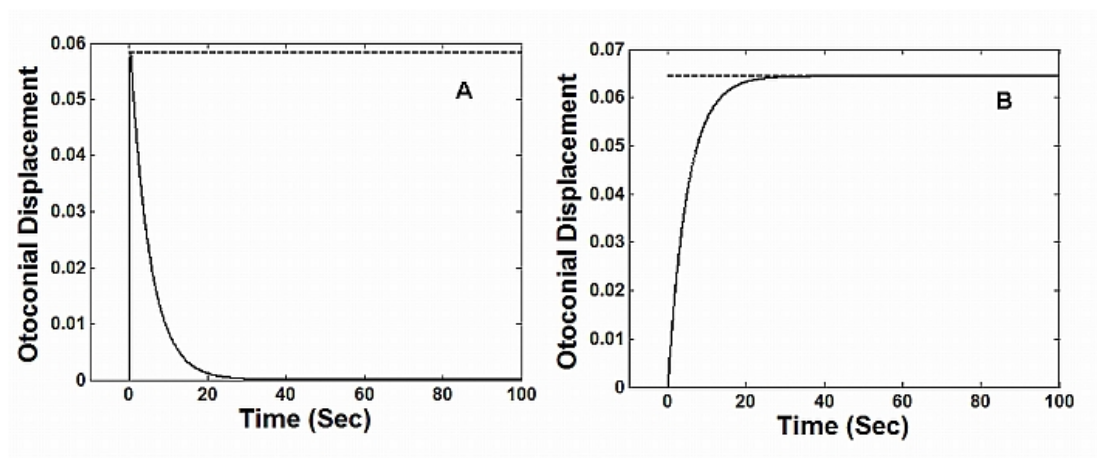


Figure 5.25. Time response of otoliths to: A unit step change of linear velocity; B unit step change of linear gravito-inertial acceleration.

It can be seen from the above figure that the otoconial layer rapidly displaces for a unit step change in velocity and then decays at a rate governed by the slow time constant (τ_I). Whereas, on completion of transient exponential decay the displacement of otoconial mass maintains itself as long as the stimulus gravito-inertial

acceleration prevails. The flat response of otoliths from DC up to first corner frequency (see Figure 5.24) renders the otolith organs as a linear accelerometer over this frequency range, which also corresponds to typical physiological motion environment experienced by humans (Rabbitt et al. 2004).

Lowenstein & Roberts(1950) recorded firing rates of axons innervating otoliths in fish preparations and were able to identify two types of receptors. The ‘static’ position receptors displayed variations in spontaneous discharge with changes in the orientation of preparations, while the ‘out-of-position’ receptors only responded when the changes in orientation were taking place. Mayne(1974b) re-analysed their data and identified three types of neurons innervating otolithic sensory hair cells, termed as ‘static’, ‘dynamic’ and ‘mixed’. He found that the ‘static’ cells respond to gravitoinertial accelerations, while the ‘dynamic’ units react to changes in the gravitoinertial accelerations applied to the sensitive axis of the cells, whereas, ‘mixed’ cells display a combined characteristics of both. He suggested to model otolith afferents as a combination of a conventional and differentiating accelerometer using the following transfer function:

$$\frac{x_o(s)}{\ddot{u}_i(s)} = k_1 - k_2 \cdot \frac{\omega_1}{(s + \omega_1)} \quad (5.37)$$

Where, x_o is the response of otolith (spikes/sec); \ddot{u}_i is the input gravitoinertial acceleration; k_1 & k_2 are constants (in sec^2); and ω_1 is the corner frequencies. When, k_2 is zero, Equation(5.37) represents a conventional accelerometer simulating response of ‘static’ cells and when $k_1=k_2$, this equation approximates the differentiating accelerometer mimicking ‘dynamic’ cells. Mayne & Belanger (1966) estimate the parameters of Equation(5.37) for ‘static’ [Equation(5.38)]and ‘dynamic’ [Equation(5.39)] units using the experimental data of Lowenstein & Roberts(1950).

$$\frac{x_o(s)}{\ddot{u}_{ix}(s)} = 20 \quad (5.38)$$

$$\frac{x_o(s)}{\ddot{u}_{ix}(s)} = 86 \frac{s}{(s+0.25)} \quad (5.39)$$

Alike their electrophysiological studies of semicircular canals (see §5.5.2), Fernandez & Goldberg (1976a; 1976b; 1976c) recorded neural activities of vestibular nerves innervating utricle and saccule in squirrel monkeys, exposed to static tilts and centrifugal forces. Depending upon the regularity of firing rates during static tilts, Fernandez et al.(1972) identified two types of axons termed as ‘regular’ and ‘irregular’ that respectively displayed characteristics similar to the ‘static’ and ‘dynamic’ cells observed by Mayne(1974b) in fish data. While studying the otolith responses, Fernandez & Goldberg (1976c) used centrifugal force sinusoids of 0.006 to 2.0Hz (super imposed onto a background force of 0.46g) generated by modulating a constant angular velocity. They carried out frequency domain analysis of excitatory (centrifugal force parallel with the unit’s polarization vector) and inhibitory (centrifugal force anti-parallel to cell’s polarization) responses recorded from 26 regular and 20 irregular units to create the averaged bode diagrams similar to the one shown in Figure 5.26.

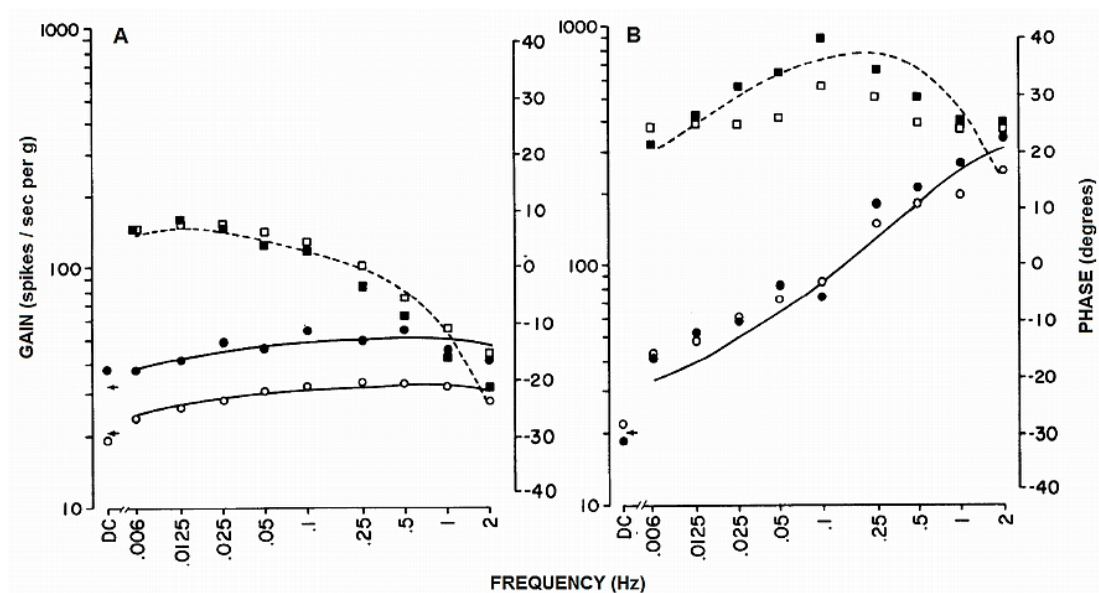


Figure 5.26. Bode diagram: A regular unit B: irregular unit. (Gains: circle and solid curves; phases: squares and dashed curves; filled symbol: excitatory; open symbol: inhibitory sinusoids; curves: as fitted to transfer function) [Fernandez & Goldberg 1976c].

It can be seen from Figure 5.26 that the response of regular nerves is primarily tonic in that the gain of the unit is nearly flat and phase is mostly zero with a minor lead and somewhat larger lag at lower and higher frequencies respectively. On the other hand, irregular unit is displaying a phasic response with a large gain enhancement and phase leads between 20 to 40 degrees. This indicates that the ‘regular’ afferents faithfully encode the gravito-inertial acceleration, while the ‘irregular’ units are sensitive to the changes in accelerations. Fernandez & Goldberg (1976c) fitted the bode-diagrams of individual unit’s experimental data to the transfer function given by Equation(5.40).

$$H(s) = (1 + k_v(\tau_v s)^{k_v}) \left(\frac{1 + k_A \tau_A s}{1 + \tau_A s} \right) \left(\frac{1}{1 + \tau_M s} \right) = H_V \cdot H_A \cdot H_M \quad (5.40)$$

Where, H_V is a velocity sensitive operator, mainly accounting for the gain enhancement and phase leads observed in the irregular units. The factor H_A is an adaptation operator primarily contributing the phase leads and gain enhancement observed from DC to 0.006Hz. H_M is a first-order lag operator representing mechanics of otolith motion; it simulates the high frequencies phase lags and reductions of phase lead observed in regular and irregular units respectively.

The median values of various parameters (k_v , k_A , τ_v , τ_A and τ_M) for the excitatory and inhibitory responses of regular as well as irregular units are given in Table 5.2.

Table 5.2. Median parameters of otolith transfer function-Fernandez & Goldberg (1976c)

Unit Type	Excitatory Sinusoids					Inhibitory Sinusoids				
	k_v	k_A	τ_v (s)	τ_A (s)	τ_M (ms)	k_v	k_A	τ_v (s)	τ_A (s)	τ_M (ms)
Regular	0.188	1.12	40	69	16	0.198	1.12	40	63	20
Irregular	0.440	1.90	40	101	9	12.3	0.415	40	1.95	74

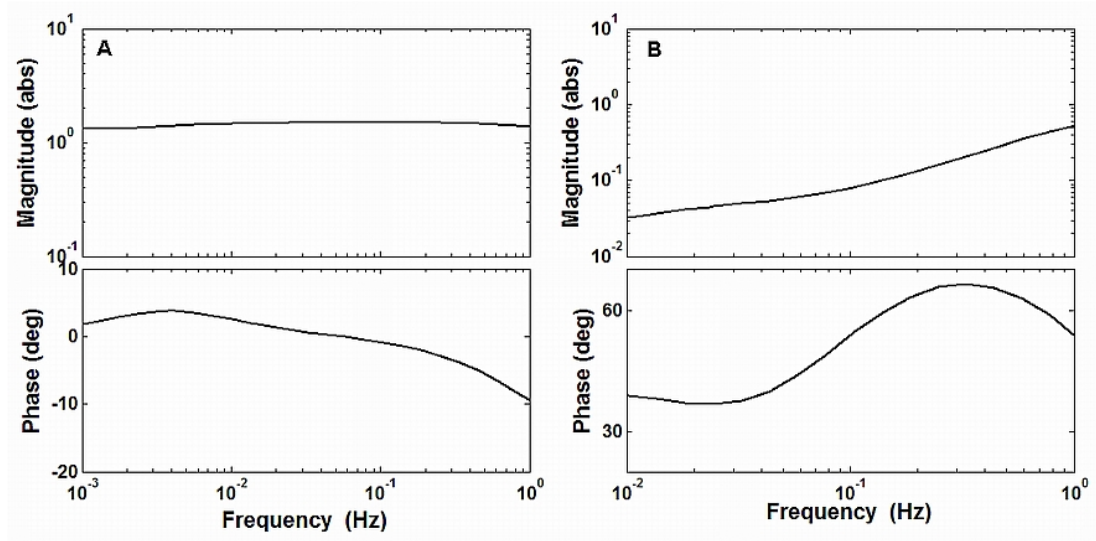


Figure 5.27. Bode diagrams of otolith transfer function as per Raphan et al. (1996); A regular afferents; B irregular afferents.

Raphan et al. (1996), using the experiment data of Fernandez & Goldberg (1976a; 1976b; 1976c), proposed a simplified transfer functions of otolith afferents. These functions are given in Equation(5.41) and (5.42) for regular and irregular axons respectively.

$$Hs(s) = \frac{(s + 0.022)(s + 0.099)(s + 15)}{(s + 0.025)(s + 0.1)(s + 10)} \quad (5.41)$$

$$Hs(s) = \frac{(s + 0.01)(s + 0.05)(s + 0.5)}{(s + 0.025)(s + 0.1)(s + 10)} \quad (5.42)$$

The bode diagrams of these simpler transfer functions [Equation(5.41) and (5.42)] are shown in Figure 5.27, which is displaying responses similar to those modelled by Fernandez & Goldberg(1976c) given in Figure 5.26.

Crane & Demer (1999) proposed, yet another simpler transfer function for the regular afferents, given by Equation(5.43). The graphical comparison of this much simpler version of otolith transfer function with the more complicated one [Equation(5.40)] is shown in Figure 5.28. They also considered a simple delay of 36ms to represent the dynamics of otolith, plotted in the same figure.

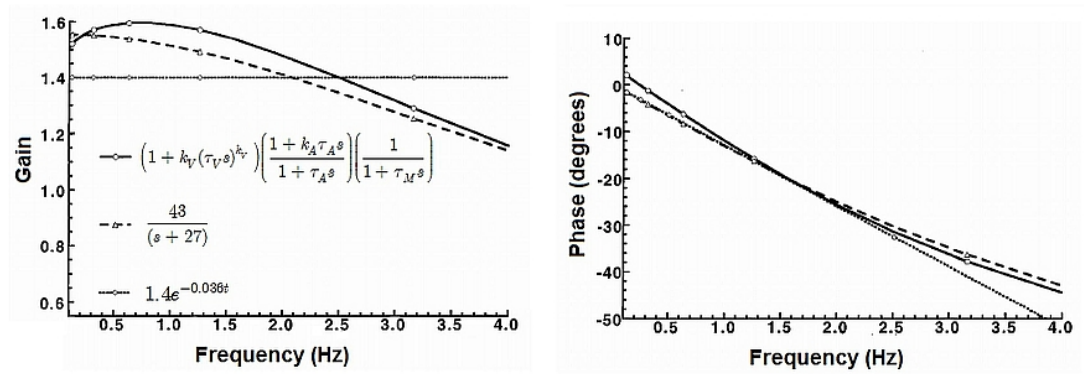


Figure 5.28. Bode diagrams comparing regular otolith afferents' transfer function suggested by Fernandez & Goldberg 1976c (solid lines), by a simpler transfer function (dashed line), and by a pure delay of 36 ms (dotted line) [Crane & Demer 1999].

It can be observed from the above figure that the simpler transfer function [Equation(5.43)] is reasonably successful in simulating the response predicted by the intricate function suggested by Fernandez & Goldberg(1976c) [Equation(5.40)].

$$H(s) = \frac{43}{(s + 27)} \quad (5.43)$$

Studies pertaining to the subjective estimates of translational motion have been carried out by several researchers in the past (Young et al. 1966; Young 1969; Ormsby & Young 1976; 1977; Young 1984). One of the transfer function suggested to relate the perceived tilt angle (or lateral acceleration) with the applied (actual) tilt angle (or lateral specific force) is given by (Young 1969):

$$\frac{\text{Perceived Tilt (Lateral Acceleration)}}{\text{Actual Tilt (Lateral Specific Force)}} = \frac{1.5(s + 0.076)}{(s + 0.19)(s + 1.5)} \quad (5.44)$$

The sinusoidal frequency response of subjective transfer function [Equation(5.44)] is depicted in the bode-diagram plot of Figure 5.29.

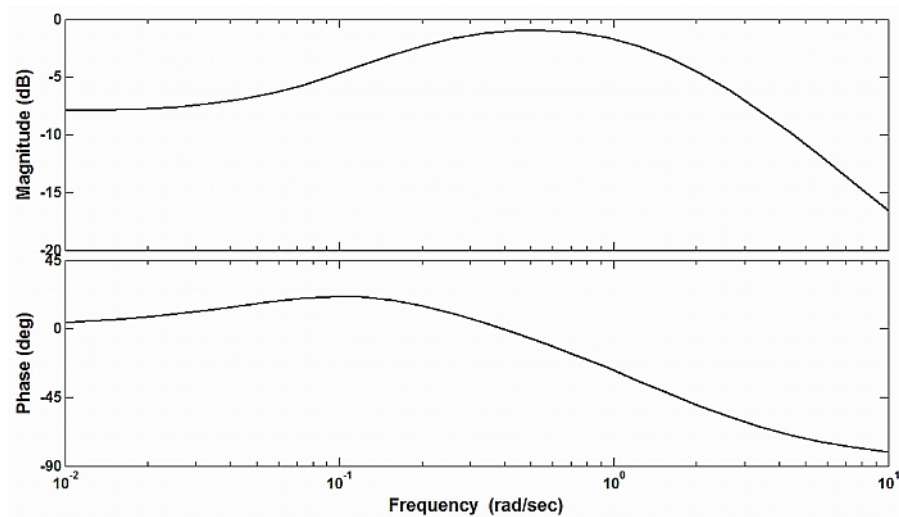


Figure 5.29. Bode diagram for subjective tilt transfer function of otoliths as per Young 1969.

Comparing the otolithic responses predicted by the hydrodynamic (Figure 5.24), electrophysiological (Figure 5.26, Figure 5.27, & Figure 5.28) and subjective perception (Figure 5.29) models, one can easily observe the similarities. All models, despite their diversities, are predicting otoliths to be faithful sensors of gravitoinertial accelerations. As such, the variations in cut off frequencies may be attributed to the neural delays, inherent to the subjective perception models, in distinguishing between tilt and translation.

According to Merfeld & Zupan(2002), modelling otolithic afferents as being directly proportional to gravitoinertial accelerations is appropriate to simulate the dynamics of regular neurons innervating maculae, but ignores the phasic response of irregular units. However, for the translational motion frequencies of interest in this study ($\ll 1.0\text{Hz}$), a transfer function of identity may be used, which has also been employed by various researchers (Glasauer 1992b; Merfeld 1995a; Merfeld & Young 1995; Merfeld 1996; Glasauer & Merfeld 1997; Merfeld et al. 1999; Bos & Bles 2002; Merfeld 2004) in their canal-otolith interaction based orientation and vestibular-ocular reflex models.

5.6 Neural Processing of Vestibular Cues

It is evident from the morphological, physiological and biomechanical details of vestibular apparatus presented in §5.3 to 5.5, that the labyrinthine peripheral acts like

an inertial guidance system (Mayne 1974b; Glasauer & Merfeld 1997). It comprises of rotational rate sensors (semicircular canals, §5.5.1) and linear accelerometers (otoliths, §5.5.4) that function independently, as one might gather from the electrophysiological recordings of vestibular nerves innervating ampullae (§5.5.2) and maculae (§5.5.5). If we assume complete isolation between the (head referenced) rotational and linear motion signals sensed by the semicircular canals and otoliths respectively, this would then lead to a fundamental issue commonly termed as ‘gravito-inertial force (FIG) resolution problem’. According to ‘Equivalence Principle’ (Einstein 1907), under complex motions the linear accelerometers (like otoliths) alone cannot distinguish between gravitational (steady tilt) and translational accelerations. This means that the otolithic signals would be identical for the static tilts (gravitational accelerations) and translational motions inducing similar inertial accelerations. This has been the case in squirrel monkeys’ primary otolithic afferents (see §5.5.5) recorded by Fernandez & Goldberg (1976a; 1976b; 1976c).

Various researchers have been investigating to identify the strategies employed by the central nervous system (CNS) to disintegrate the gravito-inertial accelerations encoded by otoliths into gravitational and translational components. The former are used by the primates to manage their attitude (i.e. orientation), while later are essentially needed to establish their motions relative to the world. There have been two significant opinions on how CNS processes the ambiguous signals from vestibular cues; these are ‘Frequency Segregation Hypothesis’ (Paige & Tomko 1991b; 1991a; Paige 1996; Wood 2002) and ‘Multisensory Integration Hypothesis’ (Mayne & Belanger 1966; Mayne 1969; Guedry 1974; Mayne 1974b; Oman 1982; 1991; Glasauer 1992b; Merfeld et al. 1993; Merfeld & Young 1995; Merfeld 1996; Glasauer & Merfeld 1997; Guedry et al. 1998; Oman 1998; Angelaki et al. 1999; Merfeld et al. 1999; Bos et al. 2001; Bos & Bles 2002; Merfeld & Zupan 2002; Bos et al. 2008).

‘Frequency Segregation Hypothesis’ suggests that CNS relies on the frequency contents of otolith signals, in that the high-frequency accelerations are interpreted as translations, while the low-frequency contents are treated as tilts. On the other hand,

according to 'Multisensory Integration Hypothesis', higher centre neurons combine signals from semicircular canals and otoliths to correctly differentiate between head motions and static tilts. It is important to understand that vestibular cues are only, though the most significant, a part of the big picture. There are several non-vestibular cues like visual, auditory and somatic at the disposal of CNS to assist sensing the self-orientation and locomotion in stationary environment like that of the Earth.

In order to test veridicality of the abovementioned hypotheses, concerning neural strategies to address GIF resolution problem, Angelaki et al.(2004; Angelaki & Cullen 2008) conceived an intelligent experiment. They recorded primary otolith afferents and higher order neural activities in vestibular nucleus (VN) of squirrel monkeys, while the primates were subjected to one of the four sinusoidal motion stimuli. The motion protocols were: Translations (sinusoidal left/right motion) only; Tilts (sinusoidal tilts toward right/left ear down without any linear displacement) only; additive and subtractive combinations of translations and tilts. In the case of combined translational and roll tilt stimuli with opposing directions, the motion magnitudes were adjusted in such a way that the gravitational and translational components of accelerations along the interaural (ear to ear) axis cancelled each other out. Thus, the head of monkeys translated in space without any net lateral linear acceleration stimulus to otolith receptors, as shown in Figure 5.30.

It can be seen from Figure 5.30(C) that the primary otolith afferents are encoding the net linear accelerations by producing similar signals for pure translational and tilting stimuli, which also substantiates the 'Equivalence Principle'. Interestingly, but not surprisingly, primary otolith afferents did not exhibit sinusoidal modulation for the combined roll tilts minus translations stimuli (with no net linear acceleration). Whereas, the amplitude of instantaneous firing rate (IFR) almost doubled for the translations plus roll tilt case. Aforesaid clearly demonstrate that the otoliths display characteristics of a classical linear accelerometer and the vestibular nerves directly innervating maculae faithfully encode the net linear acceleration applied in the polarization direction of sensory hair cells.

In contrast to primary otolith afferents, the typical IFR of many central vestibular nucleus (VN) neurons, shown in Figure 5.30(D), suggests that the responses of these neurons are somewhat immune to roll tilt stimuli and they selectively encode translational stimuli. This is obvious from the fact that the IFR of these neurons is little modulated for the tilt only condition, while their response to combined translational and tilt stimuli were identical to that of pure translation. Such order neurons were not limited to VN and are also identified in other higher order centres that not only receive sensory afferents but also distribute efferents (motor commands) for both perceptual and motor purposes (Angelaki et al. 2004).

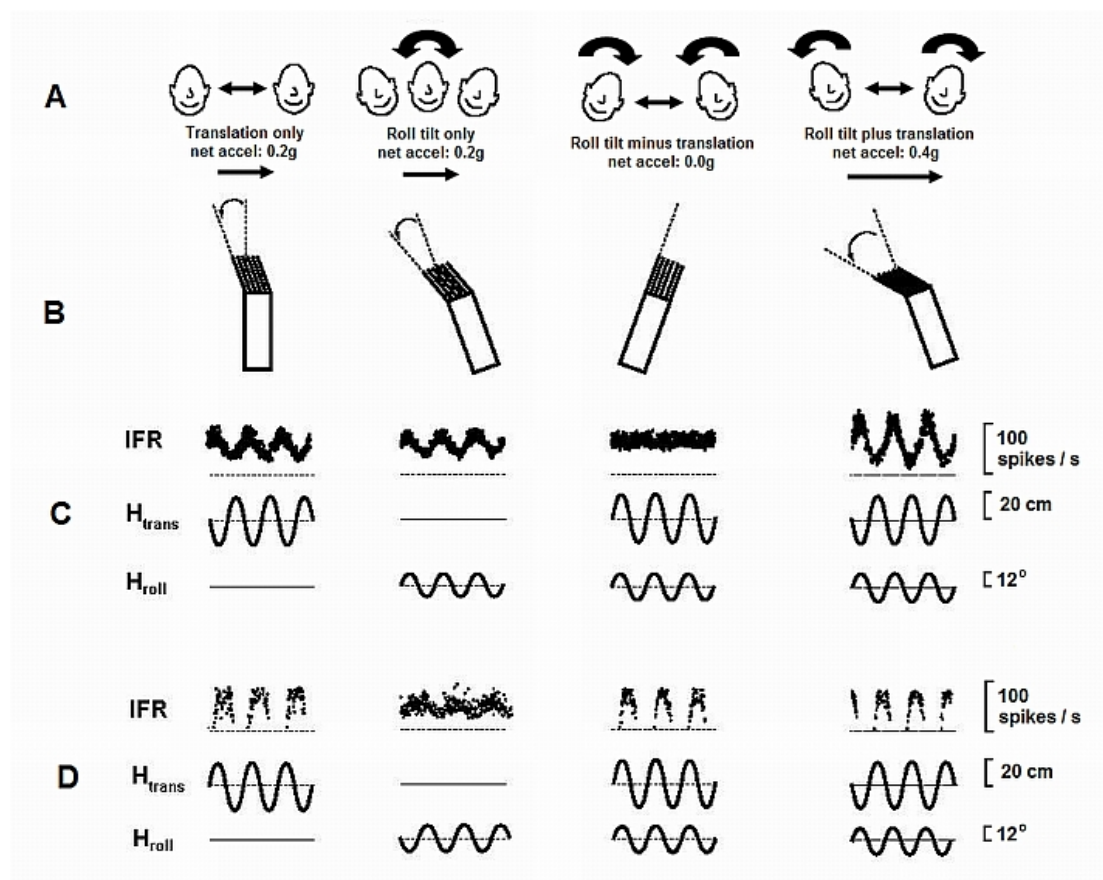


Figure 5.30. Neural processing of complex stimuli: A motion stimuli; B net polarization of otolith hair bundles during motions; C instantaneous firing rate (IFR) of primary otolith afferent; D IFR of central vestibular nucleus neuron [Angelaki & Cullen 2008].

It would be important, also interesting, to note that later studies (Shaikh et al. 2005; Yakusheva et al. 2007) have shown that inactivation of canals causes the aforesaid neurons to behave like primary otolith afferents, thereby encoding net linear

acceleration. This occurs due to the fact that these neurons also receive canal afferents and somehow combine the two to estimate the translational motions. The abovementioned experiment, as well as earlier studies by Angelaki et al.(1999) conclude “The results refute frequency segregation as the primary computational scheme used to discern movement. Rather, functional semicircular canal signals are critical for an appropriate discrimination of the source of linear acceleration and the mode of head motion”

5.7 Vestibular Response Models

It stands clear from §5.6, that ‘Multisensory Integration Hypothesis’ better explains the neural processing of vestibular cues by the central nervous system (CNS). In this section we shall, therefore, consider only those vestibular models that combine the sensory outputs of otoliths and semicircular canals. Unlike other sense modalities, vestibular cues do not display directly measureable physical characteristics. These are usually evaluated using the indirect manifestation of vestibular signals such as ‘reflexive eye movements’ and ‘perceptual correlates’ of passively induced motion stimuli. The former is termed as ‘Vestibulo Ocular Reflex’ (VOR) and is extensively studied by the vestibule scientists, especially in animals who can otherwise not provide any subjective feedback. Studies concerning ‘perceptual correlates’ rely on psychophysical methods such as; self-orientation with respect to gravity; thresholds of motion perception and perception of self-motion under passive motion stimuli (Glasauer & Merfeld 1997).

One of the primary objectives of almost all vestibular response models has been to predict spatial orientation of species as perceived by the CNS in a given (mostly) passive motion environment. Even the VOR models rely on body’s state variables (acceleration, velocities, displacement etc.) to predict complex ocular reflexes such as nystagmus. Due to the role of CNS as a control centre of myriad body functions, control engineering has established deep routes into the field of biomechanics. Therefore, all models, one way or the other, seems to be stemming from one of the control engineering techniques. The earlier vestibular models focused on CNS processing of vestibular cues to estimate self-orientation (Sperry 1950; von Holst &

Mittelstaedt 1950; von Holst 1954; Mayne & Belanger 1966; Mayne 1969; Guedry 1974; Mayne 1974b), which may be termed as ‘open loop’ models with output being an estimate of the input.

The more recent vestibular response model make use of ‘cybernetics’ and ‘estimation theory’ to optimally estimate the VOR and/or spatial orientation (Ormsby & Young 1976; 1977; Oman 1982; Borah et al. 1988; Droulez & Darlot 1989; Mittelstaedt et al. 1989; Oman 1991; Glasauer 1992b; Glasauer 1992a; Merfeld et al. 1993; Zupan et al. 1994; Merfeld 1995a; 1995b; Merfeld & Young 1995; Merfeld 1996; Glasauer & Merfeld 1997; Oman 1998; Merfeld et al. 1999; Merfeld et al. 2001; Merfeld & Zupan 2002; Reymond et al. 2002; Merfeld 2004).

5.7.1 Classical Model for Spatial Orientation

One of the earliest multisensory spatial orientation model is by Mayne(1974b), who considered the vestibular system to function like an inertial guidance system, comprising of linear (otoliths) and rotational (canals) accelerometers. He proposed a simple 2D model shown in Figure 5.32, which is able to predict the orientation of a primate with respect to gravity while undergoing translations in the sagittal-plane and rotations (pitch) about frontal-axis (see Figure 5.31 for reference axes and principal body planes).

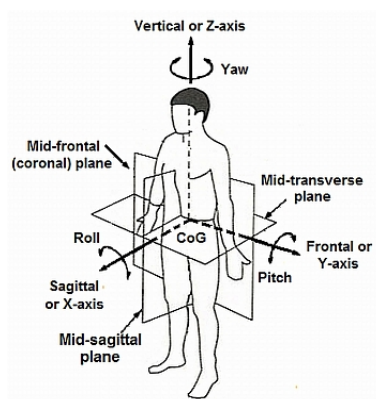


Figure 5.31. Principal planes and reference axes of human body [downloaded and adapted from <http://www.brianmac.co.uk/bodyaxis.jpg>].

The model simulates static otolith cells (block 1 & 3 of Figure 5.32), primarily sensing gravito-inertial accelerations (see §5.5.5), and semicircular canals (block 2) sensing the rotational velocities (see §5.5.2). The model (Figure 5.32) is also depicting the computational processes (presumably) taking place in the central nervous system (CNS) to estimate orientation of head with respect to Earth's vertical; these are represented by simple low and high pass filtering (block 6 & 7) and signal products (block 4 & 5). Here, the output of otoliths is fed into low-pass section, while that of semicircular canals to high-pass section of the filters.

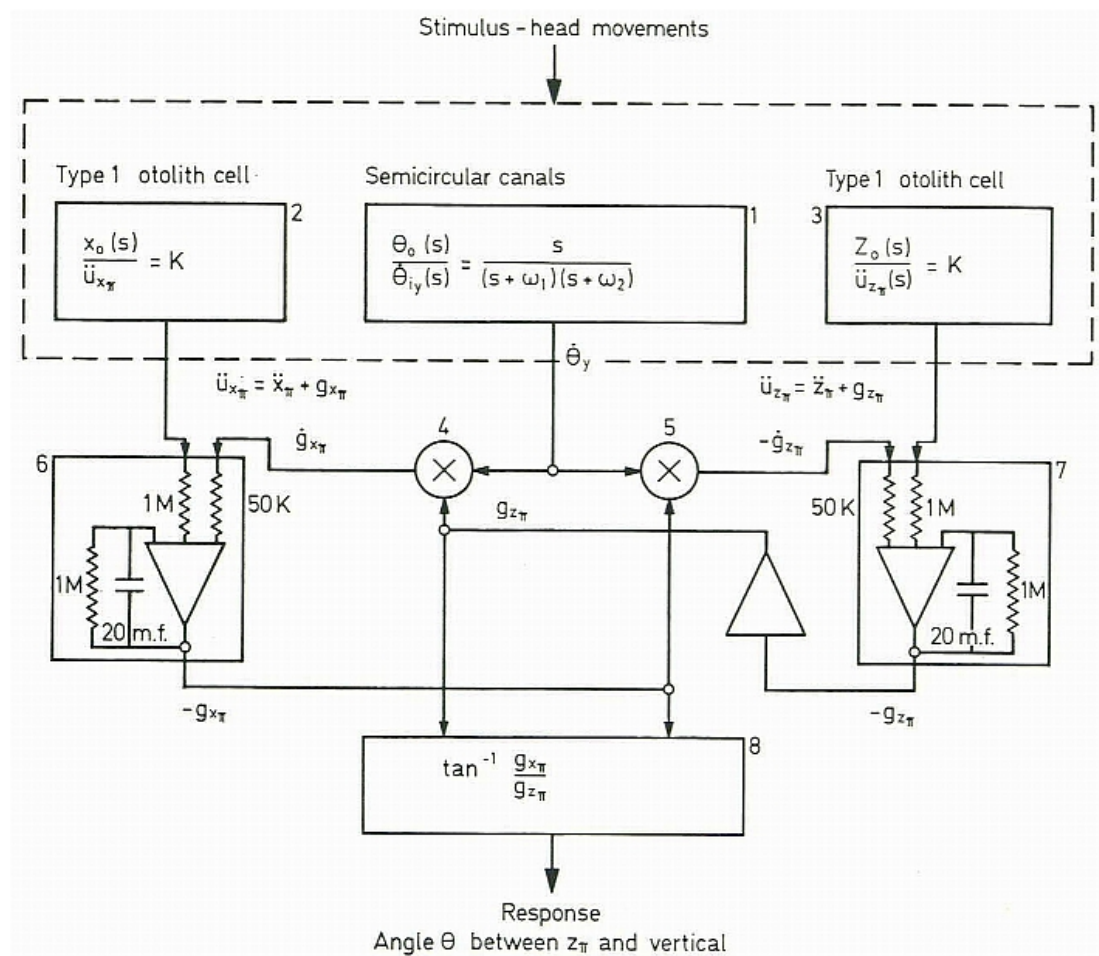


Figure 5.32. 2D spatial orientation model by Mayne 1974.

The working principle of this scheme is very simple in that the low pass filtering of otolithic signals would allow the constant magnitude of gravity to pass through unchanged, whereas the linear accelerations that are usually of high frequency during normal locomotion would be integrated to zero. Thus, for the pure translational

motions the output of this model would be true representation of the gravitational acceleration components acting along the vertical (z-axis) and sagittal (x-axis) axes. These components could be used to estimate the orientation of primate with respect to Earth's vertical (block 8), using simple trigonometric relationships. However, when the head is turned about any axis other than the vertical (z-axis) then there would be high frequency variations in the gravitational components, which will not be correctly processed by the low pass filter due to its slow response. Hence, at this point canal cues would be needed to calculate the (higher) rate of change of change of gravity due to (head) rotations, which could then be passed through high-pass filter to effect necessary fast corrections.

According to classical mechanics (Goldstein et al. 2002), the rate of change of a vector in the body frame of reference, which is otherwise constant in space frame of reference (e.g. gravity), while the body is rotating with angular velocity (ω) is given by:

$$\frac{d\vec{g}}{dt} = -\vec{\omega} \times \vec{g} \quad (5.45)$$

Careful examination of Figure 5.32 would reveal that block 4 and 5 are implementing the 2D version of Equation(5.45). Thus, in a way Mayne (1974b) gets round the high-pass characteristics of semicircular canals by using otolith signals in the low frequency range (by low pass filtering), while canal signals are being used in the high frequency region where they are better transducers of rotational velocities.

He further suggests subtracting the outputs of blocks 4 and 5 from the rate of gravitoinertial acceleration change sensed by the type-2 (dynamic) otolith cells to obtain the net rate of inertial acceleration change. Subsequent integration of later would provide information on head acceleration, velocity and displacement. However, the situation is not that straight forward in the case of 3D complex

motions. Mayne's approach, extended to 3D by Mittelstaedt et al.(1989) and later by Glasauer(1992a), is given by:

$$\frac{d\vec{g}}{dt} = \frac{\vec{f} - \vec{g}}{\tau} - \vec{\omega} \times \vec{g} \quad (5.46)$$

Where, \vec{f} is the gravito-inertial acceleration sensed by the otoliths and τ is the time constant of low pass filter.

5.7.2 Optimal Models for VOR and Spatial Orientation

Ormsby & Young(1976; 1977) proposed the pioneering optimal control theory based orientation perception models. Their first model (1976) simulates the dynamics of otoliths only to predict the illusionary effects of static tilt under different force environment. They extended their model (1977) to incorporate the sensory feedback of semicircular canals, which also included a nonlinear logic scheme to account for the dynamic interaction of canals and otoliths, estimating the perception of dynamic orientation. This later model was successful in predicting some of the well known illusionary effects, such as the dynamic elevator illusions and pitch perception in a catapult launch. However, their models could not be used to predict responses to all possible motion stimuli.

The recent vestibular models for VOR and spatial orientation are respectively by Merfeld (1990; Merfeld et al. 1993; Merfeld 1995a; 1995b; Glasauer & Merfeld 1997; Merfeld & Zupan 2002) and Glasauer (Glasauer 1992b; Glasauer 1992a; 1993; Glasauer & Merfeld 1997). Though, focusing different manifestation of vestibular responses, both the models share several common notions and process the vestibular cues in a similar fashion to estimate the state variables concerning spatial orientation. As shown in Figure 5.33, these models simulate vestibular organs and hypothesised neural processing of labyrinthine cues, using linear elements like filters, integrators and summing junctions; they also include some non-linear vector product operations.

Similar to Mayne's (1974b) approach, these models implement Equation(5.45) in both the 'physical' and 'internal' parts, relating changes in the gravitational acceleration to rotational motions. It is also assumed that otolith afferents represent the vector sum of inertial and gravitational accelerations (in accordance with 'Equivalence Principle') given by:

$$\vec{f} = \vec{a} + \vec{g} \quad (5.47)$$

Where, \vec{f} is the gravito-inertial acceleration registered by the otoliths and \vec{a} is the inertial acceleration stimuli.

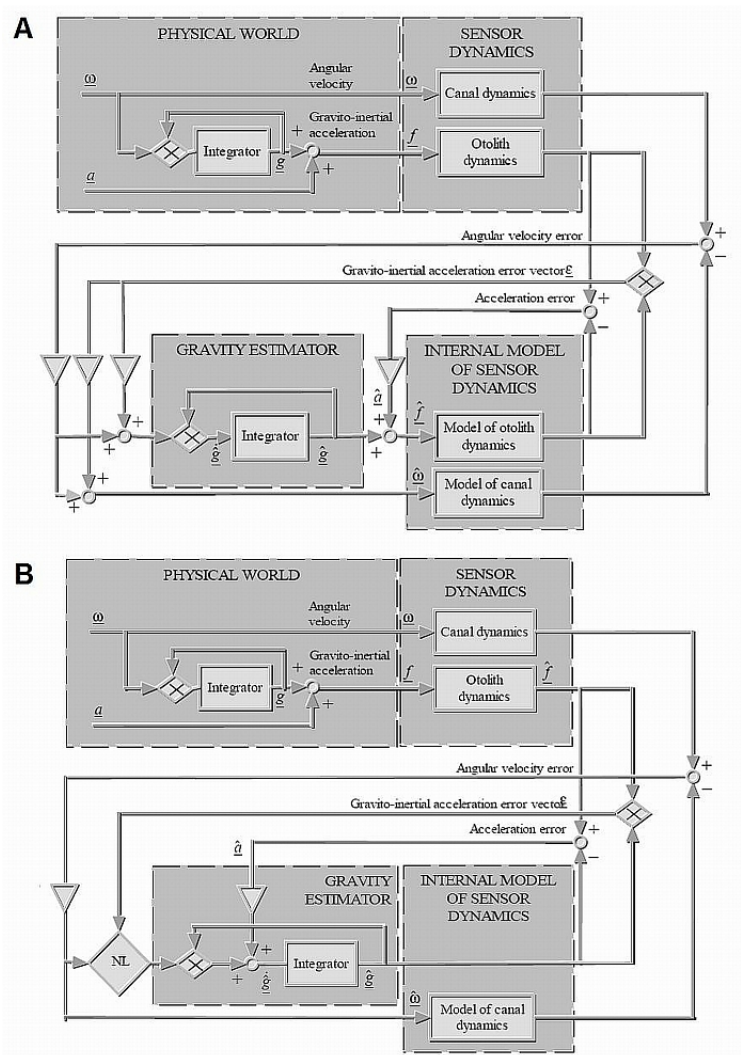


Figure 5.33. Optimal theory based vestibular response models: A schematic diagram of 3D VOR model by Merfeld; B schematic diagram of 3D orientation model by Glasauer [Glasauer & Merfeld 1997].

However, unlike Mayne's model, the processes assumed to be used by CNS, while processing vestibular cues, do not include any low-pass (of otolithic signal) or high-pass filtering (of canal afferents). Instead, it is hypothesised that CNS calculates a gravito-inertial error vector ($\vec{\epsilon}$) by implementing a cross-product of sensed and expected (calculated by an internal model, see §5.8 for further details on internal model) otolithic afferents. By assuming a unit transfer function for otoliths (see §5.5.5), Glasauer (1992a; 1993) estimates the error vector as:

$$\vec{\epsilon} = \hat{\vec{f}} \times \hat{\vec{g}} \quad (5.48)$$

Where, $\hat{\vec{f}}$ is the sensed otolith afferent (gravito-inertial acceleration, GIA) and $\hat{\vec{g}}$ is the expected magnitude of gravity estimated by the 'internal model' [see Figure 5.33 (B)]. According to Equation(5.48), the gravito-inertial error vector will only influence the internal estimates of gravity whenever the sensed GIA vector is not parallel to estimated gravity; thereby realigning the two vectors. This vector would then represent the perception of roll tilt (aligned with gravito-inertial acceleration) reported by subjects during eccentric centrifugation. Since, the magnitude of $\vec{\epsilon}$ depends on the angle between $\hat{\vec{f}}$ and $\hat{\vec{g}}$, directed perpendicular to the plane containing them; hence it may be interpreted as angular velocity vector attempting to realign the two.

Effectively, these models (Figure 5.33) employ otolithic afferents to modulate the internal estimates of state variables during DC (e.g. static tilt) to low frequency (lower cut off frequency of high-pass canals, see §5.5.2) rotational motions, where the canals are relatively ineffective. Whereas, canal cues mainly influence the internal estimate of gravity during the high-frequency rotational motions. Hence, the overall philosophy of these models is not very different from that of Mayne(1974b), with the added features of optimal control theory. Both, Glasauer and Merfeld have used their vestibular models to simulate the subjective vertical (Glasauer 1992a) and VOR (Merfeld & Young 1995) for pure lateral roll tilts and eccentric rotation about Earth's vertical stimuli. In addition, they have successfully simulated much more complicated stimuli such as spatial orientation perception in a pivoting centrifuge, tilt

perception during catapult launch, and eye movements during off-vertical axis rotations (OVAR).

5.7.3 Vestibular-Visual Interaction Models

Robinson (1977) took into account the visual-vestibular interaction while modelling the optokinetic nystagmus (OKN, the slow involuntary eye oscillations that take away the eye from gaze target) and vestibulo-ocular reflex (VOR, the stabilization of retinal images during head movement, achieved by counter-rotation of eyes at the same speed as that of head but in opposite direction). He successfully simulated various eyes related responses such as circularvection, sustained nystagmus, after nystagmus and prevention of later two in the presence of light; however, he used his model to simulate rotational motions only.

Since then, several researchers have proposed a variety of vestibular-visual interaction models (Raphan et al. 1977; Lau et al. 1978; Henn et al. 1980; Schmid et al. 1980; Buizza & Schmid 1982; 1983; Schmid & Buizza 1983; Henriksson et al. 1984; Kotaka et al. 1984; Borah et al. 1988; Oman 1990; 1991; Salami et al. 1996; Das et al. 1998; Mergner & Rosemeier 1998; Oman 1998; Das & Leigh 2000; Mergner et al. 2001; Oman et al. 2001; Brandt et al. 2002; Matsangas 2004; Prsa & Galiana 2007; Bos et al. 2008; Salami et al. 2008). However, in the context of seasickness aboard real ships the visual feedback primarily carries information about the body-fixed visual environment that remains stationary with respect to the eyes. This is supported by the observation that passengers confine their visual activities to inside of the cabin, especially when they are not feeling well. Consequently, for simplicity reasons, the vestibular visual interactions are not considered in this study and their models are not discussed in any further details.

5.8 Internal Models and Observer Theory from Physiologic Perspectives

Physiological studies make extensive use of 'Internal models' and 'observer theory' to simulate reconstruction of world's state by the nervous system (Oman 1982;

Merfeld et al. 1993; Merfeld 1995b; Bos & Bles 1998b; Bos & Bles 1998a; Bos & Bles 2002). In control engineering, ‘Internal models’ are the mathematical replication of plants and their sensors, usually represented in terms of transfer functions that relates the output (controlled variable) to the input (e.g. controlling signal). On the other hand, the ‘observer theory’ is an estimation technique, frequently used in control engineering to optimise the performance of a controller (Kailath 1974; Chen 2003). These two fundamental tools are briefly discussed in the following subsections from physiological perspectives (see MacNeilage et al. 2008 for an extensive review of the subject).

5.8.1 Physiologic ‘Internal Models’

In physiologic applications, the ‘Internal models’ are hypothesised to represent the dynamic characteristic of and relationships between sensors, motors and relevant physical laws. These models are assumed to exist ‘internally’, i.e. they reside inside the CNS, and essentially required by the nervous system to accurately manage the sensorimotor functionalities. Before discussing any further about the internal models, it is important to understand why the CNS makes use of these models instead of employing simple servomechanisms? To this end let us consider a simple servo equivalent, shown in Figure 5.34, of the classical physiologic body motion control observer (Figure 5.37) discussed in the next subsection.

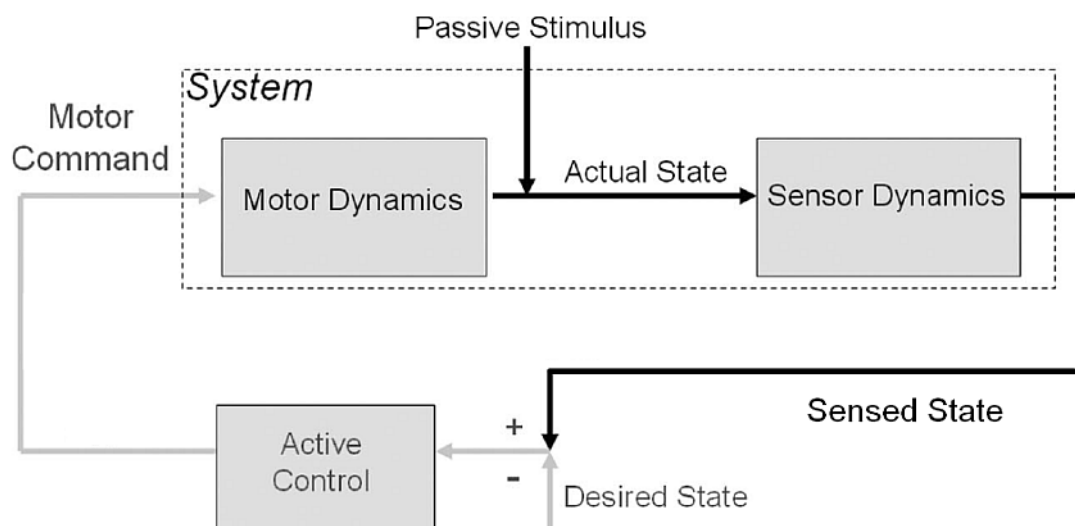


Figure 5.34. A simple servomechanism to control body motions

Here the desired body state is compared with the sensed body state to generate the corrective motor commands. This system would work fault free only if the sensed state is perfect i.e. exact replica of the actual body state and the afferents processing delays are insignificant relative to the temporal features of the body motions to be controlled. This could only be possible if the sensors are perfect and very little neural processing of the afferents is needed to establish the sensed states. However, as discussed in §5.5 the vestibular organs are not perfect sensors (e.g. high pass nature of semicircular canals). Furthermore the CNS is required to resolve the GIF resolution problem (§5.7) to distinguish between the tilt and translation. This involves central neural processing of the sensory afferents leading to delays of several milliseconds that may easily lead to instabilities (Bos et al. 2002b). Thus, it is very unlikely that the CNS uses a simple servo scheme to control the body motions.

The alternate and perhaps the most tangible option is the prevalence of emulation theory of representation, which accounts for the feedback delays and sensor imperfections. According to Grush (2004) "...in addition to simply engaging with the body and environment, the brain constructs neural circuits that act as (internal) models of the body and environment". Furthermore, "...During overt sensorimotor engagement, these (internal) models are driven by efference copies in parallel with the body and environment, in order to provide expectations of the sensory feedback, and to enhance and process sensory information." Thus, internal models not only facilitate overcoming the potential issues of neural delays but also eliminate the effects of imperfect sensors under optimal conditions. In addition, the habituation process is assumed to modify the internal models so that the provocative environment / impairment of vestibular function due to a disease could be dealt with (Bos et al. 2002b).

Internal models may be divided into 'sensor dynamics', 'motor dynamics' and 'physical laws' models. The first two categories may further be sub-divided into 'inverse' and 'forward' models as shown in Figure 5.35. The 'forward motor dynamics' models are laid out to predict the state of a muscle given the efference

copy of motor command is known. While, the ‘inverse motor dynamics’ models estimate the required motor command for acquiring the desired state of the body muscles; these models are also treated as controllers in simulating motor learning processes (Wolpert & Kawato 1998).

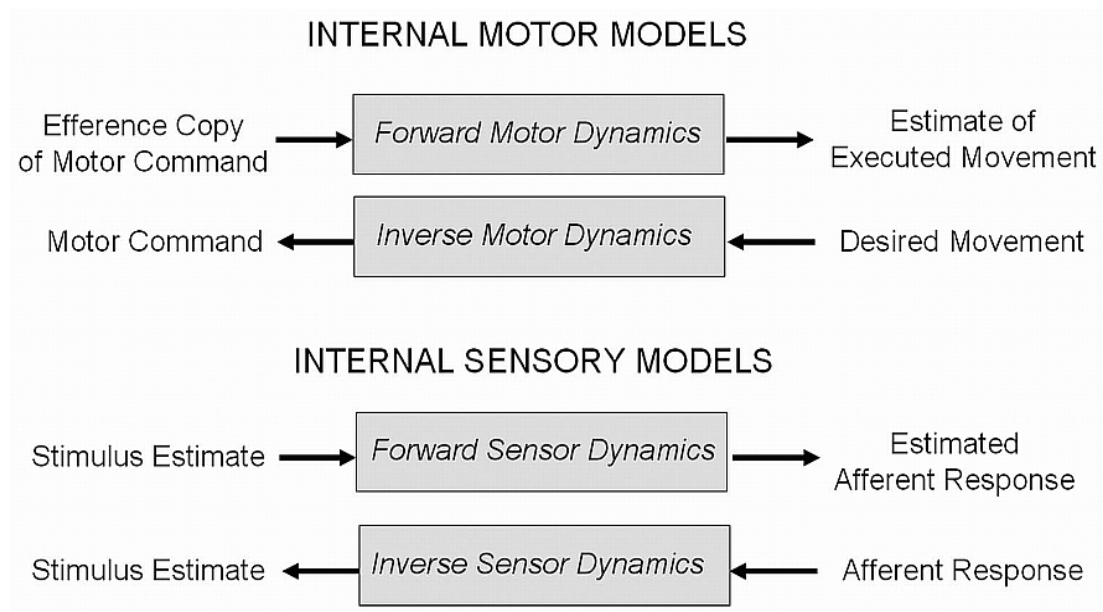


Figure 5.35. Sub-division of internal models for sensory and motor processing [MacNeilage et al. 2008].

The internal models of ‘forward sensor dynamics’ comprise of mathematical representation of sensors (e.g. transfer functions of vestibular organs, see §5.5) to estimate the ‘expected’ sensory afferent signals for the known sensory stimuli. For example, these models may be used to predict the average activities of vestibular nerves innervating otolithic sensory epithelium while the head experiences gravito-inertial accelerations. Such models are postulated to be employed by CNS to mimic the sensory dynamics in the ‘physical world’ (see Figure 5.33 in §5.7.2). In contrast, the ‘inverse sensory dynamics’ models translate the observed sensory afferents into relevant sensory stimuli, again via some mathematical linkage between the two. As an example, CNS is assumed to estimate angular velocity from the canal afferent signal using canal’s sensor model presented in §5.5.2. These models are employed by the ‘observers’ (see §5.8.2) to reconstruct the ‘expected’ physical stimuli from the known afferents.

On the other hand, the internal models of ‘physical laws’ represent the physical relationships and governing laws of various physical variables used as inputs or predicted by the ‘motor dynamics’ and ‘sensor dynamics’ model. Typical examples of this type of models would include the ‘equivalence principle’ discussed in §5.7.2 [see Equation(5.47)]. Other common example would be the rate of change of gravity as experienced by head undergoing some rotational motion [Equation(5.45)]. This research mainly uses the internal models of ‘sensor dynamics’ and ‘physical laws’.

5.8.2 Physiologic Observers

Ellis(2002) defines observer as, “... a mathematical structure that combines sensor output and plant excitation signals with models of the plant and sensor” to provide “... feedback signals that are superior to the sensor output alone”. Observers are used in control engineering when either the sensor feedback is inaccurate, noisy, or when the desired physical quantity is simply immeasurable e.g. trying to measure the temperature of a motor’s rotor. In such cases, the observers, which are mere algorithms, combine the noisy / limited sensed signals with the knowledge of plant and sensor to estimate the desired ‘observed’ or ‘expected’ signals. Under such arrangements, due to higher accuracy and greater reliability, the observed signals are used to close the control loop instead of sensors’ signals (see Figure 5.36).

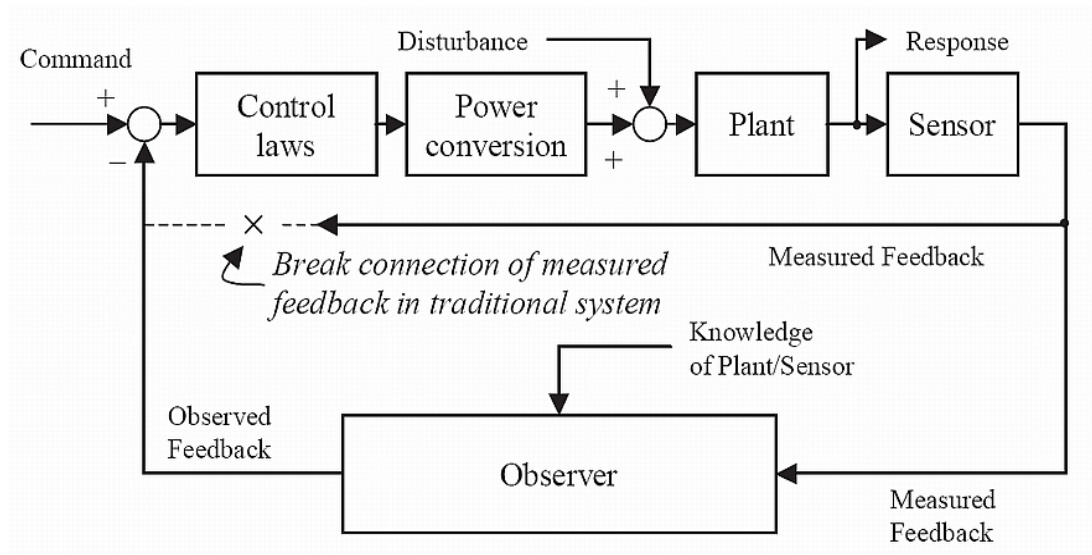


Figure 5.36. Role of observer in a control system [Ellis 2002].

The role of ‘observers’ in physiology is similar to their counterparts in control engineering. They provide the means to extract the internal (inside CNS) states of the physical world that cannot be directly measured as sensory or motor outputs. The most significant role of physiologic observers is to simulate the complex simultaneous interactions of several dynamic (afferents and state) variables in a coordinated overarching manner. A typical sensorimotor observer model (similar to the ones presented in §5.7.2) is shown in Figure 5.37. It comprises of two distinctive parts; the ‘system’ part (upper half) that represents the body and sensor dynamics in physical world, while the ‘observer’ part (lower half) models the internal (CNS) representation of these body and sensory dynamics.

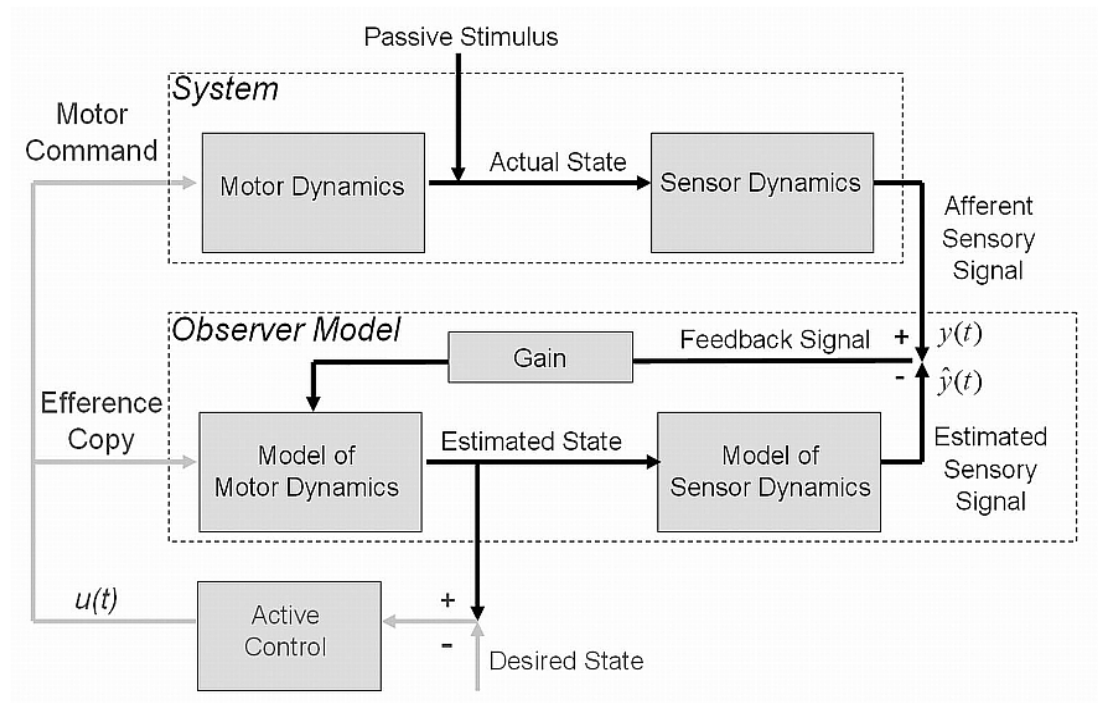


Figure 5.37. Traditional physiological observer model [MacNeilage et al. 2008].

Functionally, the outputs of ‘system’ model i.e. physiological sensory cues (e.g. vestibular and visual afferents) are compared with the ‘expected’ sensory cues estimated by the ‘observer model’. The difference of the two is used as feedback by the internal models of body and sensors through a suitable gain, to drive the observed sensory cues towards the reality. While this being done, the state estimates that could otherwise not be measured directly become available for comparison with the desired

state (see lower half of Figure 5.37). The difference between desired and estimated states produces the error signal, which is translated, through a control strategy, into efference (motor command) and its copy to effect necessary muscular activities achieving the required orientation.

However, for passively moving individuals (the case of interest in most physiological studies as well as this research) the input command vector $[\mathbf{u}(t)]$ is set to zero. In such cases, the motor dynamics are also irrelevant and replaced with the unity transfer functions. Also, there is no comparison of estimated states with the desired states to generate the control signal (i.e. the grey signal routes of Figure 5.37 become redundant). Resultantly, the body state variables are primarily modified by the passive perturbation such as motions of a vessel / vehicle. The motion sickness models discussed in the subsequent sections of this chapter, including the one developed as part of this research, consider the passive stimuli as primary source of sickness. These models, therefore, treat the difference between the sensed (by system part) and ‘expected’ (by observer part) sensory afferents / physical variables as ‘sensory conflict’ responsible for the elicitation of motion sickness.

How the ‘sensory conflict’ signal is weighted before being fed back to the internal models determines the nature of the ‘observer’. The traditional physiologic-observers models (Merfeld 1990; Glasauer 1992b; Glasauer 1992a; 1993; Merfeld et al. 1993; Merfeld 1995a; 1995b; Glasauer & Merfeld 1997; Bos & Bles 1998b; Bos & Bles 1998a; Bos & Bles 2002; Bos et al. 2002a; Merfeld & Zupan 2002; Turan et al. 2003; Turan et al. 2009) treat the gains as free parameters and their values are adjusted to ensure that the system dynamics match the empirical observations. Consequently, the measurement noise, which is an inherent feature of most if not all physical systems and real world signals, is ignored. The other class of observer-based physiologic models (Young 1970; Borah et al. 1988; Wolpert & Ghahramani 2000; Todorov 2004) employs Kalman-filtering (Kalman 1960; 1961; Kalman & Bucy 1961) approach to combine the strengths of observer and Bayesian theories. In such models, the gain applied to the ‘sensory-conflict’ feedback is not arbitrarily chosen. Rather, the relevant gains are calculated in a statistically optimal manner that

depends on the noise or probability distributions associated with the sensor and motor signals. In short, these models are effectively Bayes-optimal observer models for noisy dynamic systems.

It is not feasible to measure Motion sickness as objectively as other physiological manifestations of vestibular systems, like VOR or motion perceptions. Moreover as identified in §3.4, there are several sources of sickness susceptibility variations that cannot be controlled for general passenger population (people we are interested in). Hence, it is rather important to keep the vestibular modelling as simple as possible till the time enough database become available to ensure adequate statistical fittings of more complex, and perhaps more realistic, models. This is the reason that the research presented here makes use of simpler physiologic-observer models to simulate the orientation/motion perception features.

5.9 Oman's Sensory Conflict Model for Motion Sickness

As already identified in §3.6.5, sensory conflict theory of motion sickness (§3.6.2) is highly successful in identifying the sickness provoking (real/virtual) motion environments, but cannot quantify the malaise. This principle weakness of the theory has been criticised by various researchers (see §3.6.5). Nevertheless, by combining the neural mismatch model of Reason (1978b) [see Figure 3.5 in §3.6.4] with the optimal spatial orientation models such as those by Young(1973) and Borah et al.(1988); Oman (1978; 1982; 1990; 1991) proposed the 'heuristic model' for sensory conflict theory. He defined and modelled two distinctive but interrelated functionalities/regions of CNS dealing with the etiology of motion sickness, termed as 'orientation' and 'emetic' brains. These hypothetical operational divisions are respectively responsible for managing self-orientation/motion and post-processing of any observed 'sensory-conflict' into sickness susceptibility.

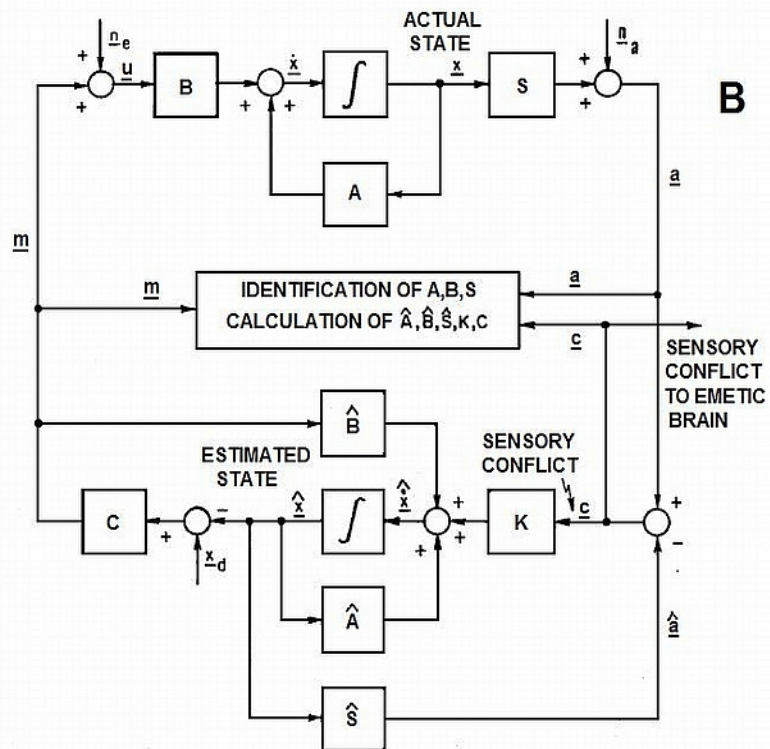
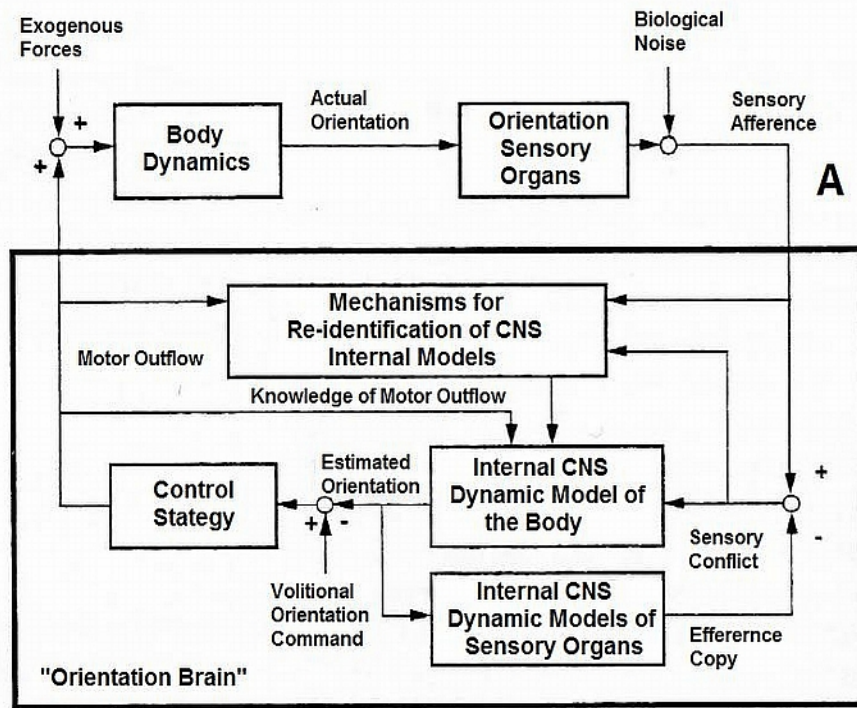


Figure 5.38. Orientation brain model: A schematic diagram [Oman 1990]; B mathematical realization [Oman 1982].

The schematic and mathematical block diagrams depicting the processes assumed to be executed by ‘orientation brain’ are shown in Figure 5.38. One can easily spot from the figure that, alike recent vestibular models for spatial orientation described in §5.7.2, the ‘orientation brain’ simulates differential equations governing body and sensor dynamics in both the ‘physical world’ (upper half) and ‘internal models’ (lower half). When in operation, the internal model of body dynamics estimates the resulting orientation by using the information about current muscle command being executed, which is then compared with the desired orientation to generate new motor command, if necessary.

Provided the internal models appropriately represent sensorimotor activities of physical world and there are no external disturbances (e.g. passive motions), the ‘efference copy’ generated by internal model of sensor dynamics would be equal to that of polysensory (visual, vestibular & proprioceptive) sensed afference. Therefore, the two (efference-copy and afferents) would cancel each other out (this implements the reafference principle, see §3.6.3) and no ‘sensory conflict’ would be generated. In otherwise case, the difference would lead to ‘sensory conflict’ vector, which is employed by the internal model (as per optimal observer theory) to steer the model estimations toward reality. It is also used to initiate corrective motor commands and, if the conflict prevails long enough, to re-identify governing expression and steering factors of internal models (mimicking adaptation process).

As depicted graphically in Figure 5.38(B), the following state-space expressions implement the body and sensor dynamics (upper part):

$$\begin{aligned}
 \dot{\mathbf{x}} &= \mathbf{A}\mathbf{x} + \mathbf{B}\mathbf{u} \\
 \mathbf{a} &= \mathbf{S}\mathbf{x} + \mathbf{n}_a \\
 \mathbf{u} &= \mathbf{m} + \mathbf{n}_e
 \end{aligned}
 \tag{5.49}$$

Where, \mathbf{x} is combined body and sensory organs’ state vector; matrices \mathbf{A} & \mathbf{B} contain coefficients of differential equations governing states of body; matrix \mathbf{S} contains coefficients of expressions governing sensor dynamics; \mathbf{u} is exogenous noise added

motor command vector; \mathbf{a} is noise added sensed afferent vector; \mathbf{n}_a is biological sensor noise vector; \mathbf{n}_e is external (passive motion or sensory rearrangement) noise vector; \mathbf{m} is the motor command vector resulting from the comparison of desired state vector \mathbf{x}_d with the expected state vector $\hat{\mathbf{x}}$.

The state-space expressions implemented by the ‘internal models’ [lower part of Figure 5.38(B)] are analogous to Equation(5.49) using hatted variables with an additional feedback from sensory conflict vector. This part of the ‘orientation model’ corresponds to the neural store of Reason (1978b) (§3.6.4) and predicts the expected sensory afferents $\hat{\mathbf{a}} = \hat{\mathbf{S}}\hat{\mathbf{x}}$, which are then compared with sensed afferents \mathbf{a} to calculate the sensory conflict vector \mathbf{c} . This conflict is fed back to the internal model after multiplication with a Kalman-type (Kalman & Bucy 1961) gain matrix \mathbf{K} to steer expected state towards the sensed ones. It is interesting to note that sensory conflict would only exist in the presence of exogenous (passively induced) motion or sensory rearrangement cues \mathbf{n}_e and/or sensor noise \mathbf{n}_a .

The second element of Oman’s sensory conflict model (revised in Oman 1987; Oman 1990) i.e. ‘emetic brain’, assumed to translate sensory conflict vector \mathbf{c} into discomfort and nausea, is shown in Figure 5.39. The components of multimodal (visual, vestibular and proprioceptive) sensory conflict are first rectified and weighted (vestibular anomalies get maximally weighted as LD subjects seldom get motion sick) before being processed through two parallel interacting paths. Oman identified the nausea paths based on the laboratory studies concerning elicitation of motion sickness using various types of stimuli. These include off vertical axis rotations with ‘Coriolis’ head movements and provoking head movements while wearing left-right vision reversing prim goggles (Bock & Oman 1982; Oman & Cook 1983; Oman 1987; Eagon 1988). The fast path is assumed to represent ‘neurally mediated’ nausea, while slow path mimics the humoral mediation; the combined effect of the two path leads to incremental stimulation observed in long-duration sickness.

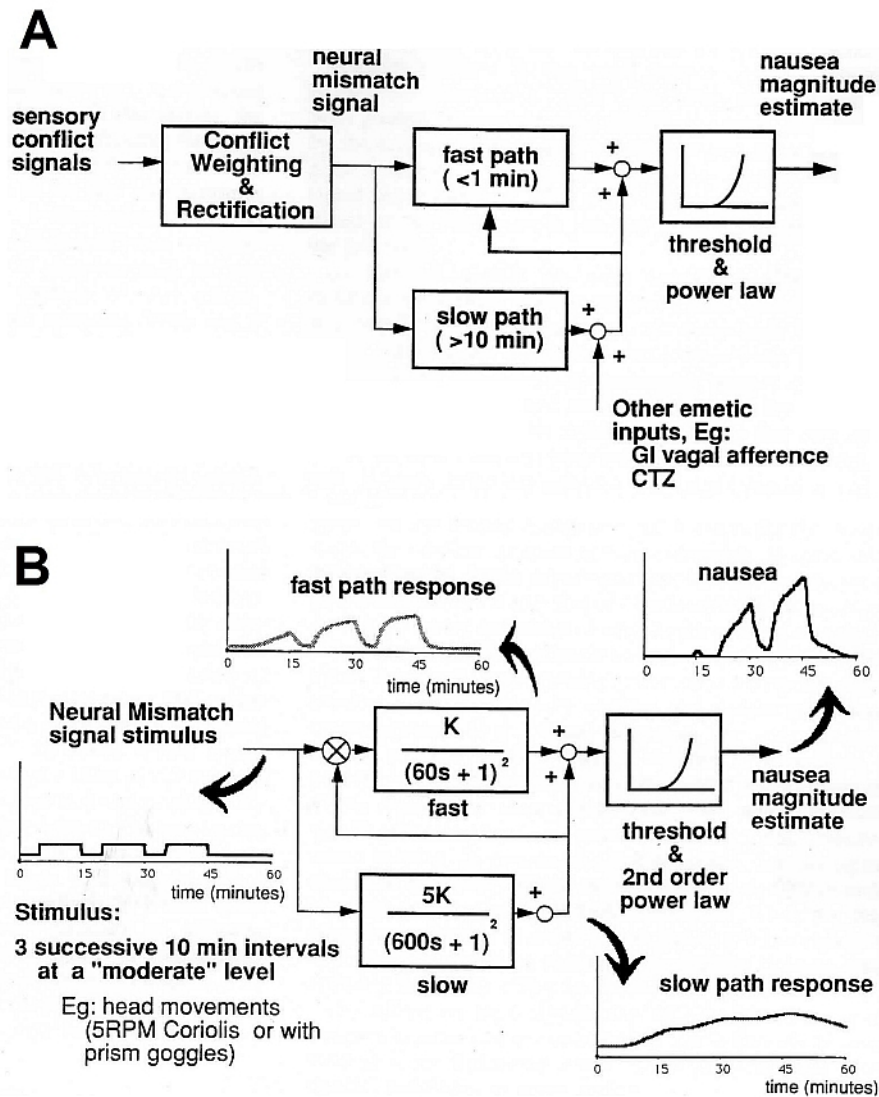


Figure 5.39. Emetic brain model: A schematic diagram; B mathematical realization [Oman 1990].

As shown in Figure 5.39, both nausea paths include second order low-pass filters behaving like ‘leaky’ integrators; accumulating the weighted and rectified conflict signals. The accumulated conflict is then passed through a threshold block before being translated into nausea magnitude using a 2 order power law relationship suggested by Stevens(1957). The threshold represents Oman’s (1982) notion that during normal daily activities some sensory conflicts prevails that is averaged at ‘subliminal’ level and might be a key determining factor for various nausea dynamics like latency, avalanching tendency, recovery time etc.

The ‘heuristic model’ of Oman proved to be a vital step forward in the history of sensory conflict theory for motion sickness. However, alike the theory, the model is mainly qualitative and no details about the ‘orientation brain’ state Equation(5.49) were provided. Moreover, the multimodal nature of the model renders it intricate and difficult to implement practically due to myriad of multisensory conflict possibilities. These issues have been elegantly addressed by ‘subjective vertical’ theory of motion sickness described in §3.6.7. The next sections of this chapter present the models implementing this revised and condensed version of sensory conflict theory.

5.10 TNO’s Subjective Vertical Model for Motion Sickness

Bles et al.(1998) at TNO, reduced the plethora of explanations suggested by sensory conflict theory of motion sickness into a single sensory conflict between the sensed and subjective (expected) verticals (see §3.6.7). The mathematical realization of subjective vertical theory by Bos and co-workers (Bos & Bles 1998a; Bos & Bles 1998b; Bos et al. 2001; Bos & Bles 2002; Bos et al. 2002a; Bos et al. 2002c; Bos et al. 2008) is clearly inspired by the ‘heuristic model’ of Oman (1982). They implement the processes of sensory conflict estimations and sickness prediction that are similar to the ‘orientation’ and ‘emetic’ brains (see §5.9), respectively. Their observer theory based elaborative ‘spatial orientation and motion sickness’ model (Bos et al. 2008) is depicted in Figure 5.40. The model is multisensory and takes account of visual, vestibular and somatosensory (non-vestibular) sense modalities. Being a predominantly ‘orientation’ model, it simulates regulation of sensorimotor functions of the body motion and attitude, undertaken by CNS.

In Figure 5.40, the matrices **P**, **C**, and **B** (also **B’**) contain coefficients of differential equations governing states of preparatory, controller and body functionalities, respectively. The preparatory phase is a sort of cognitive stage where a person (e.g. driver of a car) prepares him/her self for some future motion environment (e.g. anticipating a distant turn). The controller implements psychomotor control laws, whereas, body functionalities include physical activation of body muscles to achieve the desired orientation.

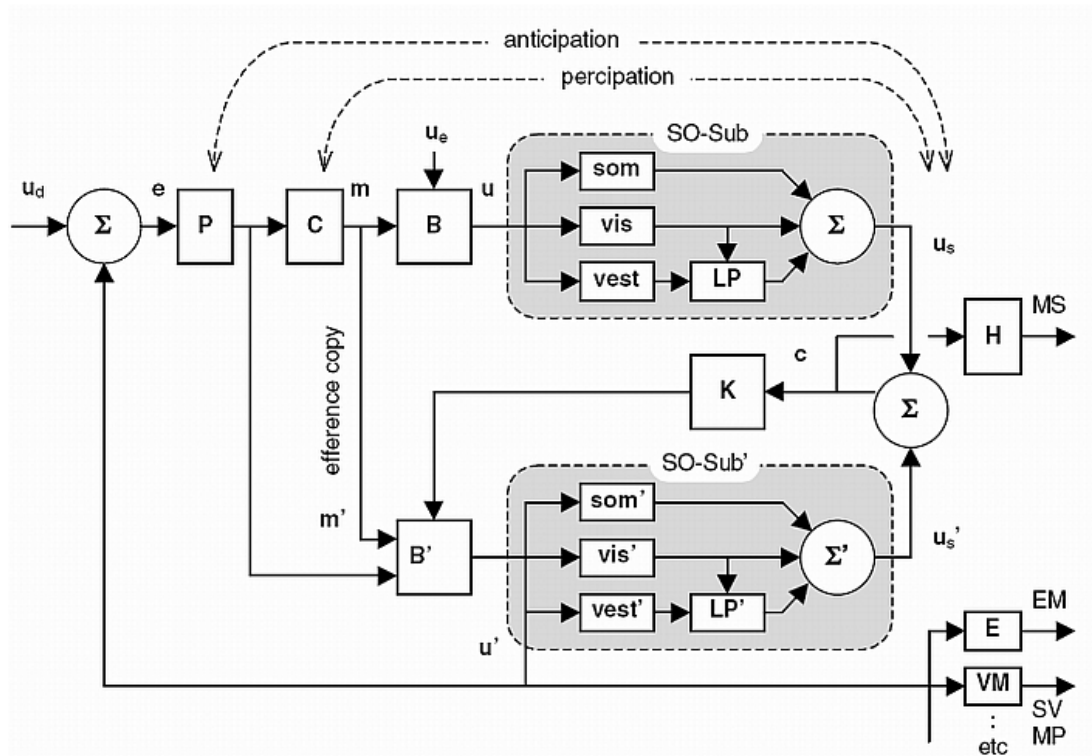


Figure 5.40. Spatial orientation and motion sickness model [Bos et al. 2008].

Operationally, the desired body state vector \mathbf{u}_d (comprising of positional states) is processed by some preparatory stage \mathbf{P} , which in turn directs the controller \mathbf{C} to translate it into motor command \mathbf{m} vector. The latter initiates body muscles \mathbf{B} activities, attempting to achieve the target states. At this point, exogenous disturbances \mathbf{u}_e (e.g. passive motions of vehicle) add up with the actively pursued motions resulting into the actual state vector \mathbf{u} . This state vector is sensed by the multisensory (visual, vestibular and somatosensory) system and processed by CNS, using laws of physics, into sensed state vector \mathbf{u}_s .

The expectation part of SV-conflict theory (see §3.6.7) is realized using an ‘internal model’ (lower part of Figure 5.40) that, as per observer theory (§5.8), implements dynamic models of motor (body), sensory and physical laws utilised by CNS (dashed vectors, matrices and transfer functions). Alike Oman’s(1982) heuristic model the ‘internal model’ mimics Reason’s (1978b) ‘neural store’ (see Figure 3.5 in §3.6.4), in that the ‘efference copy’ of muscle command vector \mathbf{m}' is processed by body function model \mathbf{B}' to generate the ‘expected’ state vector \mathbf{u}' . Given the sensorimotor

models implemented ‘internally’ are correct representation of reality, the expected state vector would be better estimate of body state as compared to the sensed state vector \mathbf{u}_s . Thus, \mathbf{u}' is compared with \mathbf{u}_d to generate the error signal \mathbf{e} that further controls the body muscular activities; this expected state vector is also simultaneously processed by the sensory and physical law models to predict the ‘expected’ sensory output \mathbf{u}'_s .

In absence of any exogenous perturbation, the \mathbf{u}'_s should be equal to \mathbf{u}_s , however, if external noise (e.g. passive motions of the vehicle) is present then the difference of the two would lead to sensory conflict $\mathbf{c} (= \mathbf{u}_s - \mathbf{u}'_s)$. This conflict vector, comprising of multi-dimensional signals (encoding body kinetics), is fed back to body model \mathbf{B}' after being weighted by \mathbf{K} to drive \mathbf{u}'_s towards \mathbf{u}_s and hence the ‘expected’ body state towards reality. According to Bos et al. (2008), the part of \mathbf{c} representing the difference between sensed and expected gravitational acceleration correlates with motion sickness (MS). The later is calculated using the transfer function \mathbf{H} that also takes account of the temporal responses of motion sickness i.e. the malaise builds up gradually if the conflict persists.

Unlike Oman’s (1978; 1982; 1990; 1991) approach, the model shown in Figure 5.40 also simulates certain psycho-physical and physiological responses like subjective vertical (SV), motion perception (MP) and eye movement (EM) etc. It also caters for the pseudo-sensory modality of ‘control’ (Mansfield 2004), in that the preparatory phase \mathbf{P} creates an ‘anticipatory’ signal for the future interaction with the spatial environment. This is assumed to be used by the drivers, pilots, etc., rendering them less sensitive to the (controlled) motions of the vehicle that may otherwise be highly provocative for the passengers (also see §3.6.2). One more, and perhaps the vital, difference between Oman and Bos’ models, is the absence of inter-modality (e.g. canal and otoliths) conflicts in latter’s work.

5.11 NAME’s Subjective Vertical Model for Motion Sickness

Inspired by the work of Bos & Bles (1998a; 1998b; Bos et al. 2002a), Verveniotis & Turan (2002a; 2002b; Turan et al. 2003; Verveniotis 2004; Turan et al. 2009) at

NAME developed their six degrees of freedom motion sickness SV-conflict model shown in Figure 5.41. Comparing it with the latest version of SV-conflict model by Bos et al.(2008) shown in Figure 5.40, one can easily spot some important similarities and differences. In terms of similarities, both models calculate only one sensory conflict, which is the vector difference between the sensed and subjective ('expected') vertical (gravity) using observer theory approach.

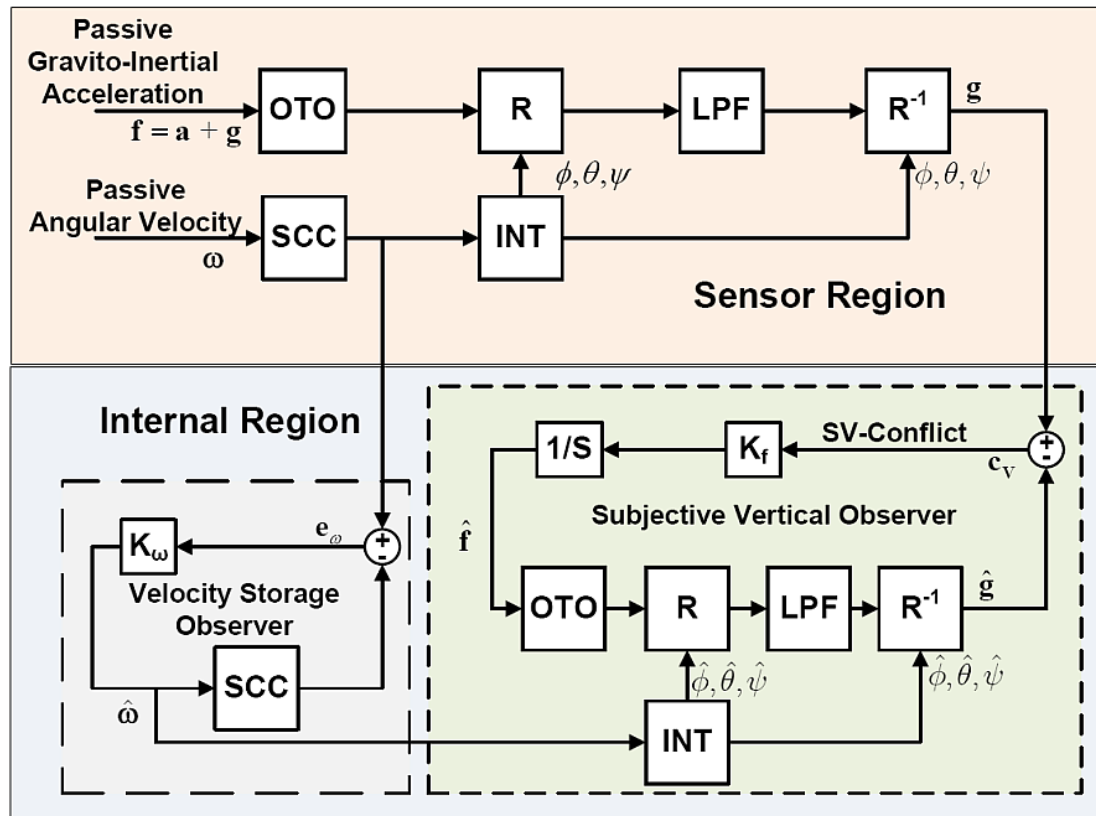


Figure 5.41. Subjective vertical conflict model for six degrees of freedom ship motions [Verveniotis 2004].

However, unlike earlier implementation of SV-conflict theory by Bos & Bles (1998a; 1998b; Bos & Bles 2000), this model utilises only one sense modality i.e. vestibular cues, under passive motions with the desired input u_d set to zero. Moreover, an identity matrix is used for the body function **B** (compare Figure 5.41 with Figure 5.40). As such, the exteroceptive (visual, hearing, smell, skin), non-vestibular proprioceptive (somatosensory) and even the cognitive senses play important role in the perception of orientation as well as motion sickness. However, the indispensable

role of vestibular system in motion sickness etiology is well established for over 100 years (Irwin 1881). It is also evident from the fact that blind people with functioning vestibular system do get motion sick under provocative environment (Graybiel 1970). In contrast, the LDs with functioning visual and somatic cues are immune to sickness even in the visually provocative environments (Cheung et al. 1991).

The NAME motion sickness model is not only attractive from simplicity point of view, but the well established knowledge about the transfer functions of the otoliths and canals (§5.5) as well as the reasonable estimates of the processing of vestibular cues by the CNS, makes it a pragmatic model. It is especially valuable for seasickness prediction as the visual environments of the passengers move with the vessel; therefore, exclusion of stationary visual cues from the model should not be an issue.

In this model (Figure 5.41), the labyrinthine organs are assumed to be aligned with the head frame of reference depicted in Figure 5.42. Since, passengers are assumed to be passively moving with ship and active head movements are ignored, the body and head-fixed coordinate systems would be identical.

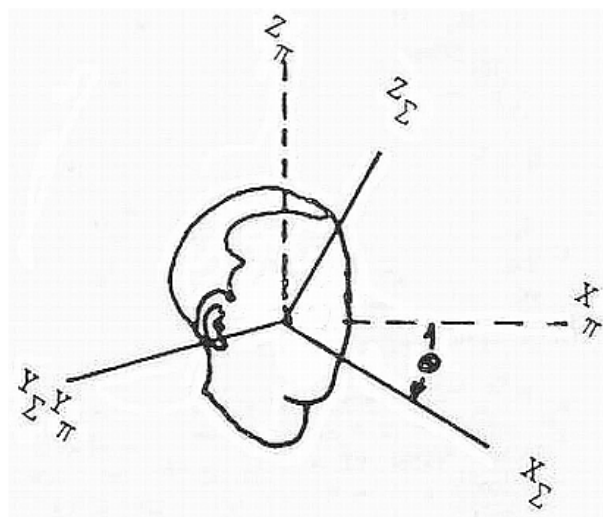


Figure 5.42. Reference axes with respect to head (Π) & space (Σ) [Mayne 1969].

Functionally, as depicted in the upper half of Figure 5.41, the gravito-inertial accelerations sensed by otoliths (OTO block, see also §5.5.5) are low pass filtered

(LPF block) to isolate the otherwise constant gravity vector i.e. the sensed vertical (\mathbf{V}_{sense}). However, gravity is only constant in the inertial frame of reference. Therefore gravitoinertial vector is first transformed into such a reference frame (block T); low pass filtered, and then transformed back (block T^{-1}) to head referenced axes. The rotational matrices (T & T^{-1}) needed for transformation between the two frames of reference are calculated by integrating (INT block) the rotational velocities sensed by the semicircular canals (SCC block, see also §5.5.2).

Ignoring any rotational motions for a moment, the low pass filtering of head referenced specific gravitoinertial force \mathbf{f}_h (i.e. gravitoinertial acceleration) to obtain sensed vertical (gravity \mathbf{g}_h) vector \mathbf{V}_{sense} shall be given by:

$$\mathbf{V}_{sense} = \mathbf{g}_h = \frac{\mathbf{f}_h}{(\tau s + 1)} \quad (5.50)$$

Where, τ is time constant of low pass filter and s is the frequency domain Laplace variable. Now assuming the initial conditions to be zero, the Equation(5.50) may be rearranged and written in time domain as:

$$\begin{aligned} \mathbf{g}_h(\tau s + 1) &= \mathbf{f}_h \\ \Rightarrow s\mathbf{g}_h &= \frac{(\mathbf{f}_h - \mathbf{g}_h)}{\tau} \\ \Rightarrow \frac{d\mathbf{g}_h}{dt} &= \frac{(\mathbf{f}_h - \mathbf{g}_h)}{\tau} \end{aligned} \quad (5.51)$$

In absence of rotational motions, Equation(5.51) may be used to isolate gravity (\mathbf{g}_h) from gravitoinertial accelerations (\mathbf{f}_h). However, if the earlier prevail, as is the case of a ship's complex motions, we would need to transform these vectors into inertial frame of reference before low pass filtering. For this purpose we can use the following rotation matrix \mathbf{R} (used inside T block):

$$\mathbf{R} = \begin{pmatrix} \cos \psi \cos \theta & \cos \psi \sin \theta \sin \phi - \sin \psi \cos \phi & \cos \psi \sin \theta \cos \phi + \sin \psi \sin \phi \\ \sin \psi \cos \theta & \sin \psi \sin \theta \sin \phi + \cos \psi \cos \phi & \sin \psi \sin \theta \cos \phi - \cos \psi \sin \phi \\ -\sin \theta & \cos \theta \sin \phi & \cos \theta \cos \phi \end{pmatrix} \quad (5.52)$$

Where, ϕ , θ , and ψ are the Euler angles and for a passively moving (seated) passenger, represent the roll, pitch and yaw respectively, of the body about the local inertial frame of reference (usually fixed to ship's centre of gravity). These angles are assumed to be calculated by CNS through integration (INT block) of rotational velocities sensed by canals. Nevertheless, as shown shortly, calculation of \mathbf{R} and its inverse $\mathbf{R}^{-1}(= \mathbf{R}^T)$ is not essential and can easily be avoided by CNS. The relationship between our quantities of interest (gravitoinertial and gravitational accelerations) in the head (h) and space (s) i.e. inertial frames of reference shall be:

$$\begin{aligned} \mathbf{f}_s &= \mathbf{R}\mathbf{f}_h \\ \Rightarrow \mathbf{f}_h &= \mathbf{R}^{-1}\mathbf{f}_s \\ &\& \\ \mathbf{g}_s &= \mathbf{R}\mathbf{g}_h \\ \Rightarrow \mathbf{g}_h &= \mathbf{R}^{-1}\mathbf{g}_s \end{aligned} \quad (5.53)$$

As mentioned in above, the gravity is only constant in the inertial (space) frame of reference, hence in the presence of rotational motion, Equation(5.51) may be rewritten as:

$$\frac{d\mathbf{g}_s}{dt} = \frac{(\mathbf{f}_s - \mathbf{g}_s)}{\tau} \quad (5.54)$$

However, all species reference kinematics to their head frame of reference, hence combining Equation(5.53) & (5.54), we obtain:

$$\begin{aligned} \frac{d\mathbf{R}\mathbf{g}_h}{dt} &= \frac{(\mathbf{R}\mathbf{f}_h - \mathbf{R}\mathbf{g}_h)}{\tau} \\ \Rightarrow \frac{d\mathbf{R}\mathbf{g}_h}{dt} &= \frac{\mathbf{R}(\mathbf{f}_h - \mathbf{g}_h)}{\tau} \end{aligned} \quad (5.55)$$

Expanding the right hand side of Equation(5.55) using product rule of differentiation, we get:

$$\frac{d\mathbf{R}}{dt}\mathbf{g}_h + \mathbf{R}\frac{d\mathbf{g}_h}{dt} = \frac{\mathbf{R}(\mathbf{f}_h - \mathbf{g}_h)}{\tau} \quad (5.56)$$

Now applying the inverse transformation (\mathbf{R}^{-1}) on both sides, Equation(5.56) becomes:

$$\begin{aligned} \mathbf{R}^{-1}\mathbf{R}\frac{d\mathbf{g}_h}{dt} &= \frac{\mathbf{R}^{-1}\mathbf{R}(\mathbf{f}_h - \mathbf{g}_h)}{\tau} - \mathbf{R}^{-1}\frac{d\mathbf{R}}{dt}\mathbf{g}_h \\ \Rightarrow \frac{d\mathbf{g}_h}{dt} &= \frac{(\mathbf{f}_h - \mathbf{g}_h)}{\tau} - \mathbf{R}^{-1}\frac{d\mathbf{R}}{dt}\mathbf{g}_h \end{aligned} \quad (5.57)$$

According to Bos & Bles (2002) $\frac{d\mathbf{R}}{dt}\mathbf{g}_h = \mathbf{R}(\boldsymbol{\omega} \times \mathbf{g}_h)$, therefore Equation(5.57) gives:

$$\frac{d\mathbf{g}_h}{dt} = \frac{(\mathbf{f}_h - \mathbf{g}_h)}{\tau} - \boldsymbol{\omega} \times \mathbf{g}_h \quad (5.58)$$

Where, $\boldsymbol{\omega}$ is the rotational velocity vector of head, sensed by the semicircular canals. Effectively speaking, the overall processing of gravito-inertial accelerations to obtain gravity does not require CNS to explicitly calculate the rotational matrices [Equation(5.52)]. Also by comparing Equations (5.58) and (5.46) (§5.7.1), one can easily see that it represents an extension of Mayne's (1974b) 2D approach to 3D by Mittelstaedt et al.(1989) and Glasauer (1992a).

The first half of Equation(5.58), on right hand side, is the low pass filtering of net inertial acceleration to isolate the low frequency gravitational acceleration variations. The second term accounts for high frequency rate of gravitational acceleration changes attributable to head (body) rotations. Thus, the low frequency changes of gravitational accelerations (sensed vertical) are primarily processed using otoliths

signals. Whereas, canal cues are used during the high frequency rotations during which they behave as effective transducers of rotational velocities.

A process identical to the one outlined in above takes place inside the ‘internal model’ or ‘neural store’ (lower half of Figure 5.41) to estimate the ‘expected’ gravity vector i.e. the subjective vertical (gravity $\hat{\mathbf{g}}_h$) vector \mathbf{V}_{subj} . Under extraneous perturbations, e.g. motions of a ship, the two verticals shall not be identical and their difference ($\mathbf{c} = \mathbf{V}_{\text{sense}} - \mathbf{V}_{\text{subj}} = \mathbf{g}_h - \hat{\mathbf{g}}_h$) is the subjective vertical (SV) conflict. It is the magnitude of this sensory conflict vector i.e. $|\mathbf{c}|$, which is processed into motion sickness incidences (MSI) using an ‘emetic’ brain type approach.

As far as the simulated orientation and emetic behaviours are concerned, there are two transfer functions of critical interest in the SV-conflict model (Figure 5.41). The first is the transfer function of estimated and input gravitoinertial accelerations [i.e. $\hat{f}(s)/f(s)$], which should be equal to 1 under optimal conditions. While the second is the transfer function of conflict vector to the input gravitoinertial accelerations [i.e. $c(s)/f(s)$], which should capture the frequency response of the MSI observed in laboratory experiments (O'Hanlon & McCauley 1974; McCauley & Kennedy 1976). For simplicity, let us assume that the only external perturbations are the linear motions i.e. rotations are absent (e.g. laboratory experiments on vertical motion induced sickness). In such case the ratios of our interest can easily be driven for the model by inspection, as per the following:

$$\frac{\hat{f}(s)}{f(s)} = \frac{\frac{K_f}{s} \text{oto}(s) \text{LPF}(s)}{1 + \frac{K_f}{s} \text{oto}(s) \text{LPF}(s)} = \frac{\left(\frac{K_f}{s}\right) (1) \left(\frac{1}{\tau s + 1}\right)}{1 + \left(\frac{K_f}{s}\right) (1) \left(\frac{1}{\tau s + 1}\right)} = \frac{K_f}{\tau s^2 + s + K_f} \quad (5.59)$$

$$\frac{c(s)}{f(s)} = \frac{\text{oto}(s) \text{LPF}(s)}{1 + \frac{K_f}{s} \text{oto}(s) \text{LPF}(s)} = \frac{1 \cdot \left(\frac{1}{\tau s + 1}\right)}{1 + \left(\frac{K_f}{s}\right) \left(1 \cdot \left(\frac{1}{\tau s + 1}\right)\right)} = \frac{s}{\tau s^2 + s + K_f} \quad (5.60)$$

The transfer functions of the otoliths [$oto(s)$] and low pass filter [$LPF(s)$] used in the above expressions are summarised later in Table 5.3. As mentioned earlier, under optimal conditions the transfer function of the estimated and actual gravito-inertial accelerations [i.e. $\hat{f}(s)/f(s)$] should be unity. Here Equation(5.59), representing a low pass filter, is suggesting that this would indeed be the case, however, within the observer bandwidth (Ellis 2002). Furthermore, the transfer function of conflict vector to the input gravito-inertial accelerations [i.e. $c(s)/f(s)$] [Equation(5.60)] is representing a band-pass filter, which appropriately mimics the observed behaviour of MSI (O'Hanlon & McCauley 1974; McCauley & Kennedy 1976).

By substituting the values of low pass filter time constant (τ) as well as the compensator feedback gain (K_f) from Table 5.3 into Equation(5.59), we can get:

$$\frac{\hat{f}(s)}{f(s)} = \frac{K_f}{\tau s^2 + s + K_f} = \frac{5}{5s^2 + s + 5} \quad (5.61)$$

The bode diagram of the above transfer function is shown in Figure 5.43 below, which is also depicting the response of the transfer function for a feedback gain (K_f) of 100. It can be seen from the figure that the magnitude of the feedback gain K_f plays a crucial role in converging the estimated GIA (and vertical) to the actual GIA (and vertical).

As such the compensator gain should be obtained using the classical techniques for observer tuning. However, according to Merfeld et al.(1993) the “Linear optimal observer theory (Kalman filtering) provides one method to optimally design this feedback for a linear system, but the nonlinear nature of the model and the time-varying nature of the feedback for a nonlinear model make this theory inappropriate for this application.” Consequently, the value of compensator gain was manually adjusted, while ensuring the sensory conflict peaks around 0.17 Hz (1 rad/s).

Now substituting the values of low pass filter time constant (τ) and compensator gain (K_f) into Equation(5.60), we obtain:

$$\frac{c(s)}{f(s)} = \frac{s}{\tau s^2 + s + K_f} = \frac{s}{5s^2 + s + 5} \quad (5.62)$$

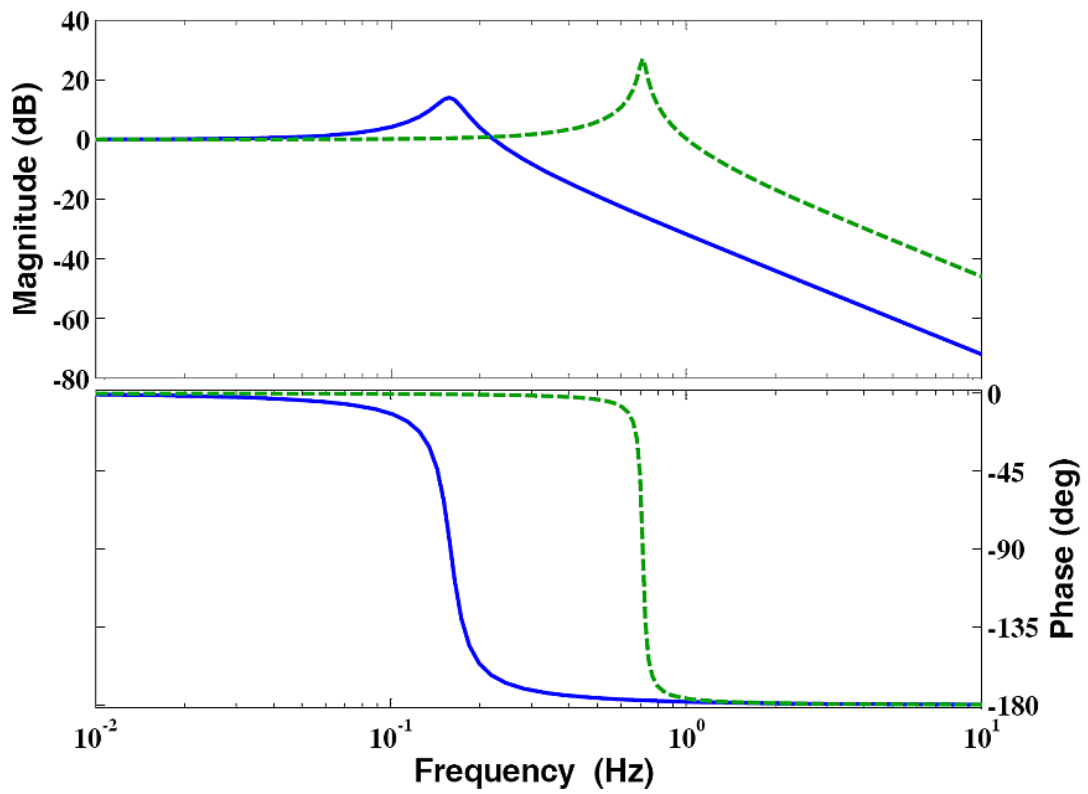


Figure 5.43. Bode plot of estimated to actual GIA transfer function with $K_f = 5$ (solid line) and $K_f = 100$ (dashed line).

The bode plot of the above transfer function is shown in Figure 5.44, which is also depicting the same transfer function for $K_f = 100$. It is evident from this figure that for the selected value of feedback gain ($K_f = 5 \text{ s}^{-1}$) and time constant of low pass filter ($\tau = 5 \text{ sec}$) the SV-conflict peaks around 0.17 Hz (1 rad/sec). The increased compensator gain pushes the peak to a higher frequency (0.7 Hz), which is incompatible with the laboratory results. Thus, the chosen magnitude of the feedback gain is primarily driven by the requirement to ensure that the frequency behaviour of the SV-conflict model is in line with the MSI response under purely vertical oscillation.

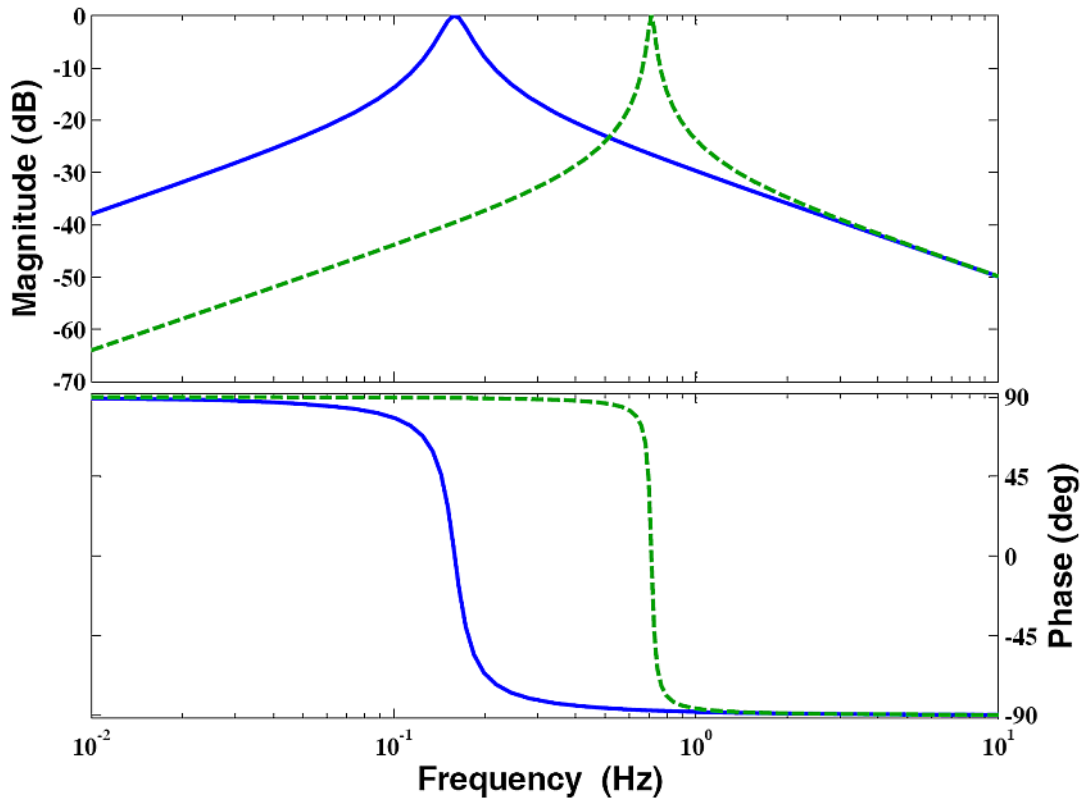


Figure 5.44. Bode plot of SV-conflict transfer function with $K_f = 5$ (solid line) and $K_f = 100$ (dashed line).

It is important to realise that without the use of an integrator (or other sample-and-hold function) in the feedback path, the model would become unstable (oscillate) under zero conflict conditions (expected vertical being equal to sensed vertical). Furthermore, the Equation(5.60) would then represent a high pass filter, contradicting the observed behaviour of MSI.

Briefly, the fundamental error signal in the SV-conflict model is the difference between the expected and sensed verticals, which is sufficient for use in the internal model to converge the two verticals as well as the expected and actual gravito inertial accelerations. Thereby, eliminating the need to directly compare the otolithic afferents as used in similar models (Merfeld et al. 1993). Thus, only the gravity storage is used by the model to estimate the gravity and the linear acceleration i.e. gravito inertial acceleration.

As discussed in §5.5.2, semicircular canals behave like high pass filters of head rotational velocities, hence, accounting for the abatement of angular VOR and rotational perception during long duration constant velocity/low frequency rotations. However, during the constant velocity / low frequency rotations, the time constant of diminishing angular VOR (approx. 15sec) is much longer than the time constant of decaying canal primary afferents (approx. 5sec) (Wong 2008). This phenomenon is commonly termed as ‘velocity storage’ (Cohen et al. 1977; Raphan et al. 1979) and plays an important role in the spatial orientation problem during normal locomotion (see §5.5.3).

In NAME’s model, the sensed canal afferents (α_ω) are compared with the ‘expected’ afferents ($\hat{\alpha}_\omega$) estimated by the ‘internal model’ to generate the canal afferent error $\mathbf{e}_\omega (= \alpha_\omega - \hat{\alpha}_\omega)$. This error is then weighted by a scalar observer gain K_ω and fed back to the internal model, driving the expected afferent towards reality and consequently the estimate of angular velocity ($\hat{\omega}$) to the sensed value (ω). This whole process implements the ‘velocity storage’ mechanism, similar to the Merfeld et al.’s (1993) spatial orientation model. Thus, the expected head kinematics are estimated by CNS, using the ‘internal model’ observers that embeds the following governing expression that is the internal version of Equation(5.58):

$$\frac{d\hat{\mathbf{g}}_h}{dt} = \frac{(\mathbf{f}_h - \hat{\mathbf{g}}_h)}{\tau} - \hat{\omega} \times \hat{\mathbf{g}}_h \quad (5.63)$$

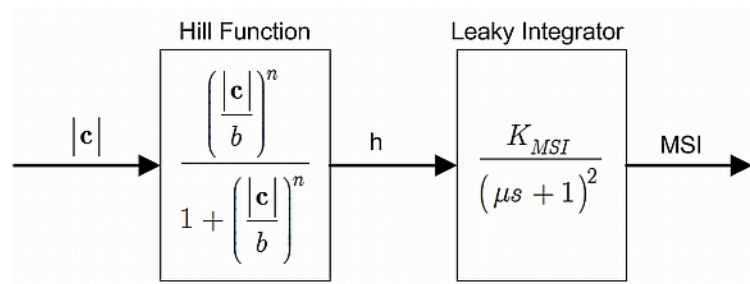


Figure 5.45. Post processing of subjective vertical conflict into motion sickness incidence [Verveniotis 2004].

Once calculated, the subjective vertical conflict (c) is processed into motion sickness incidence using the ‘emetic-brain’ type approach suggested by Bos & Bles(1998a; 1998b), as depicted in Figure 5.45. It comprises of two sequential stages; in the first stage the magnitude of conflict vector ($|c|$) is processed using a hill function given by Equation(5.64) that normalizes it and ensures that small conflicts are transformed exponentially while larger conflicts are translated logarithmically into MSI. This processing of conflict mimics the stimuli (vertical acceleration magnitude) response characteristics of MSI data recorded by O’Hanlon & McCauley(1974) and McCauley et al.(1976) [also see §3.7.2].

$$h = \frac{(|c|/b)^n}{1 + (|c|/b)^n} \quad (5.64)$$

Where, ‘b’ and ‘n’ are the parameters that determine the shape of hill function ‘h’, as depicted in Figure 5.46.

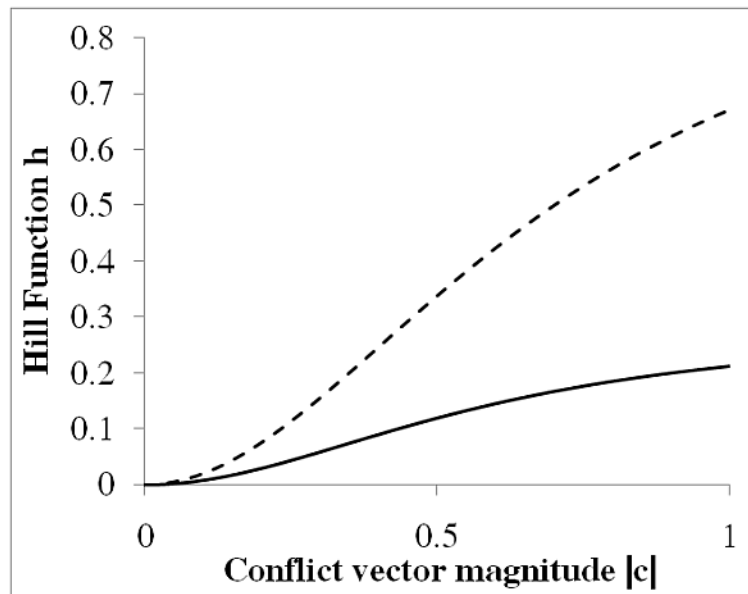


Figure 5.46. Hill function plot (solid line: $b = 2.5, n = 1$; dotted line: $b = 0.7, n = 2$).

In the second stage of conflict processing, similar to Oman’s (1987; 1990) model, the normalized conflict (h) is accumulated into motion sickness incidences (MSI%) using ‘leaky integrator’ given by:

$$MSI(\%) = \frac{K_{MSI}(\%)}{(\mu s + 1)^2} \cdot h \quad (5.65)$$

Where, $K_{MSI}(\%)$ is the maximum percentage of people likely to get motion sick, μ is the time constant of the second order low pass filter. The ‘leaky integrator’ simulates the cumulative nature of motion sickness, whereby individuals (usually) do not become instantaneously sick on exposure to provoking environment. Also the symptoms do not abate immediately on removal / reduction of stimuli and an overshoot of malaise is common. The time constant used by Verveniotis & Turan (2002a; 2002b) for the low pass filter is 12minutes (i.e. $\mu = 720s$) as their model primarily focuses on the slow response of sensory conflict i.e. motion sickness and fast nauseogenic symptoms like vertigo were not considered.

The transfer functions of vestibular organs and values of other parameters used in NAME’s subjective vertical conflict model (Figure 5.41) are summarised in Table 5.3.

Table 5.3: Transfer functions and other parameters of NAME’s SV-conflict model

Description	Transfer Function / Magnitude	Remarks
Transfer functions of otoliths.	$oto(s) = \frac{\alpha_f}{f(s)} = \widehat{oto}(s) = \frac{\hat{\alpha}_f}{\hat{f}(s)} = 1$	This is in accordance with the conclusion arrived at in §5.5.5.
Transfer functions of semicircular canals.	$scc(s) = \frac{\alpha_\omega(s)}{\omega(s)} = \widehat{scc}(s) = \frac{\hat{\alpha}_\omega(s)}{\hat{\omega}(s)} = \frac{\tau_{scc}s}{(\tau_{scc}s + 1)}$	Same as Equation(5.24)
Time constant of semicircular canals	$\tau_{scc} = 5.7 \text{ sec}$	As per Merfeld et al.(1993) and Merfeld & Zupan (2002), also see §5.5.2.

Low Pass Filter processing gravito-inertial acc.	$\frac{1}{\tau s + 1}$	Standard single pole first order low pass filter.
Time constant of LPF	$\tau = 5.0 \text{ sec}$	Suggested by Bos & Bles (1998a; 1998b) as determined by de Graaf et al. (1998).
SV-conflict feedback gain.	$K_f = 5.0 \text{ sec}^{-1}$	Obtained empirically by Bos & Bles (1998a; 1998b).
Velocity storage feed-back gain.	$K_\omega = 3.0 \text{ deg/sec / deg/sec}$	As per Merfeld et al.(1993) and Merfeld & Zupan (2002).
Hill function parameters.	$b = 0.7 \text{ m / sec}^2$ $n = 2.0$	As per Bos & Bles (1998a; 1998b).
Time constant of leaky integrator	$\mu = 12 \text{ minutes} = 720 \text{ sec}$	Also as per Bos & Bles (1998a; 1998b).

5.12 Other Physiological Models for Orientation / Motion Sickness

In addition to the ‘orientation / motion sickness’ models discussed so far, Droulez & Darlot (1989) came up with ‘coherence constraints’ model that has successfully been used in simulating VOR under 3D motion stimuli in darkness as well as in light (Zupan et al. 1994; Zupan 1995). Reymond et al. (2002) used this model to simulate the complex sensory interactions, while driving a (physical or virtual) automobile. The approach adopted by Droulez & Darlot (1989) is different from the ‘internal model’ paradigm; they argue that CNS must use simpler and more robust method

than the ‘internal model’ (Kalman filter) to estimate spatial orientation and related vestibular responses.

For each variable of interest (e.g. angular velocity), they model a corresponding central representation as well as related captor (e.g. semicircular canals) dedicated to provide the most reliable information about the considered variable. In addition to aforesaid, a secondary set of information is deemed to originate from the ‘coherent copy’ of the same variable calculated using other centrally coded, but related variables (e.g. gaze and eye angular velocity). It is the interaction between these central representations of the same variable that initiates the corrective measures rather than the interactions between sensory cues.

On similar lines to the ‘sensory conflict’ (of sensed and expected sensory afferents) considered by Oman and others, Denise & Darlot(1993) considered ‘internal incoherence’ as the sickness provoking factor. It is defined as the error between coherent copy and its central representation. They computed ‘incoherence’ using rotational velocity and tilt angle during off vertical axis rotation (OVAR) to define a quantitative model for motion sickness prediction. In a later study Denise et al. (1996), used ‘coherence model’ to quantify the latency of motion sickness under various rotational speeds at constant tilt angle (OVAR).

However, to the knowledge of the author, there is no known application of ‘coherence model’ for the prediction of motion sickness under complex motions of a real vessel / vehicle. Furthermore, the abovementioned applications of ‘coherence model’ model for the prediction of motion sickness characteristics have not been very encouraging. Therefore, ‘coherence model’ has not been pursued in this study to simulate motion sickness.

5.13 Chapter Summary

This chapter has attempted to illuminate the necessary theoretical and mathematical details of human inertial guidance system i.e. the vestibular system, which is indispensable for the physiological explanation of motion sickness. It was found that

current, but simpler, models simulating vestibular manifestations, make extensive use of ‘internal models’ and ‘observer theory’. All ‘sensory conflict’ models simulate motion sickness by dividing the relevant CNS functionalities into ‘orientation/motion perception’ and ‘emetic’ brain parts. The former employs optimal control theory to identify the postulated conflicts, while the latter is used to translate these conflicts into the malaise.

The next chapter presents the new physiologic model developed as part of this research, by identifying and employing a new sensory conflict that is readily predictable using SV-conflict theory (§3.6.7).

Chapter 6. THEORETICAL AND MATHEMATICAL FRAMEWORK

6.1 Overview of the Chapter

This chapter seeks to explicate the theoretical and mathematical basis of the physiologic motion sickness model developed in this project. Firstly, the findings of very limited laboratory studies concerning elicitation of kinetosis under horizontal oscillations are discussed in the next section. Based on the aforesaid, §6.3 identifies the anomalies of existing SV-conflict models, while §6.4 discusses the available solution and its shortcomings. Thereafter, §6.5 briefly outlines a new solution providing foundations for the development of a new physiologic model presented in §6.6. Finally, §6.7 verifies that the proposed approach and the developed model are able to address the limitations of existing solution (§6.4).

6.2 Laboratory Studies – Pure Horizontal Oscillations’ Induced Sickness

The known literature on motion sickness elicited by the pure horizontal (fore-and-aft and/or lateral) oscillations is rather limited, and none could parallel the work of O’Hanlon & McCauley (1974) and McCauley (1976). This becomes even peculiar when seen from the mass mode of transportation’s perspectives, as horizontal motions are believed to be the primary contenders for the causation of car and train-sicknesses (Griffin & Mills 2002b; Griffin & Newman 2004). Nonetheless, the following sections are summarising findings of the limited laboratory studies, concerning initiation of motion sickness under fore-and-aft as well as lateral motions.

6.2.1 Studies on Fore-and-Aft Oscillations

Golding & co-workers (Golding & Kerguelen 1992; Golding et al. 1995; Golding & Markey 1996; Golding et al. 1997; Golding et al. 2001) conducted a series of laboratory experiments (though with small sample size, usually twelve) to compare

the nauseogenicity of fore-and-aft sinusoidal oscillations with vertical motions. They studied the effects of posture and oscillation frequency onto the occurrence of sickness, in addition to the direction of motions. Their findings were:

- Oscillations along the human's mid-body (Z-axis, from feet to head) are more provocative for the sitting upright (motions were vertical along body's Z-axis) than the supine position (motions were horizontal, again along body's Z-axis) (Golding & Kerguelen 1992). Horizontal motions (fore-and-aft) are twice as nauseogenic than the vertical motions in the sitting upright position. Furthermore, there is little difference between supine and sitting upright positions for the motion sickness elicited by vertical motion (Golding et al. 1995).
- The effects of motion frequencies are less steeper for the horizontal motions as compared to the vertical oscillations suggested by the O'Hanlon & McCauley (1974) and McCauley et al.'s (1976) models (Golding & Markey 1996).
- Percentage of people experiencing motion sickness decreases with increasing frequency (0.35, 0.50, 0.70, and 1.00 Hz were tested) (Golding et al. 1997).
- Maximum motion sickness was observed at 0.2Hz horizontal (fore-and-aft) sinusoidal motions with a decrease at lower (0.1Hz) and higher (0.3Hz) frequencies (Golding et al. 2001).

Griffin & Mills (2002a; 2002b) also carried out laboratory experiments to study the motion sickness characteristics of fore-and-aft horizontal oscillations. The primary differences between the works of Golding & co-workers and that of Griffin were:

- Golding selected the same 12 (motion sickness) susceptible subjects for his studies, whereas Griffin did not ensemble his 192 participants into susceptible or otherwise groups.
- Golding exposed the subjects to constant peak accelerations, while constant peak velocity oscillations were used by Griffin.

One disadvantage of using constant peak velocity is the difficulty in separating the effects of varying accelerations from those caused by the difference of frequencies. Griffin & Mills (2002a) assume a linear relationship (works well for vertical oscillations, see §3.7.4) between the incidence of sickness rating and magnitude of acceleration; they normalized their results with corresponding peak accelerations.

In the following, Figure 6.1 is depicting the relationship between frequencies of oscillation and the normalized incidence of motion sickness, as reported by Golding & co-workers and Griffin & Mills for the fore-and-aft sinusoidal motions. A discrepancy may be observed at 0.25Hz frequency in the data reported by Griffin & Mills (2002a), as the observed value is much less than the expected value, otherwise the two studies are displaying similar trends.

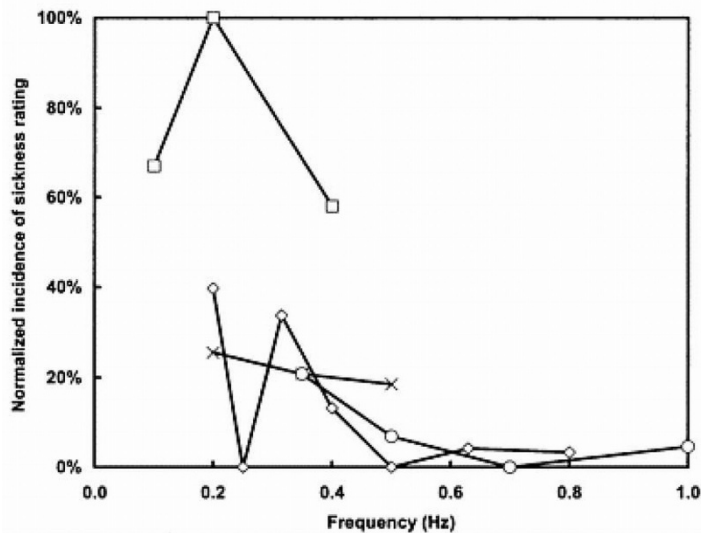


Figure 6.1. Effect of frequency of fore-and-aft sinusoidal oscillation on motion sickness incidence for a 30-min exposure. Results are normalized by division of the raw incidence data by the peak acceleration. Data are from Golding and Markey, 1996 (3.6 m/s² peak acceleration, moderate nausea, -x-); Golding et al., 1997 (3.6 m/s² peak acceleration, moderate nausea, -O-); Golding et al., 2001 (1 m/s² peak acceleration, moderate nausea, -□-) and from Griffin and Mills, 2002 (0.5 m/s peak velocity, moderate nausea, —◇—) [Mansfield 2004]

6.2.2 Studies on Lateral Oscillations

Lobb (2001) and later on Griffin & co-workers (Griffin & Mills 2002a; 2002b; Donohew & Griffin 2004) carried out (limited) laboratory experiments to establish relationships between motion sickness and purely lateral oscillations. All of these studies used constant peak velocity motions to explore the relationships of motion sickness incidence with the oscillation frequencies, amplitudes, and durations of exposure.

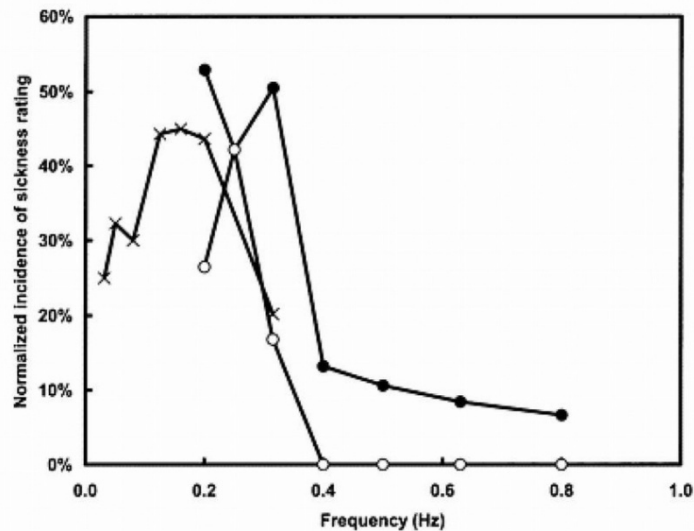


Figure 6.2. Effect of frequency of lateral sinusoidal oscillation on motion sickness incidence for a 30-min exposure. Results are normalized by division of the raw incidence data by the peak acceleration. Data are from Lobb, 2001 (1 m/s peak velocity at frequencies below 0.315 Hz, 0.5 m/s peak velocity at 0.315 Hz, mild nausea, -x-) and from Griffin and Mills, 2002a (0.5 m/s peak velocity, mild nausea - •-; moderate nausea, -O-) [Mansfield, 2004]

Figure 6.2 is depicting the sickness ratings, normalized by the lateral peak accelerations, as reported by Lobb (2001) and Griffin & Mills(2002a). Their findings were:

- A positive association exists between the amplitude (and exposure duration) and motion sickness rating.
- Lobb (2001) observed a peak in the normalized motion sickness ratings around 0.16Hz with a decrease in sickness level above and below this frequency.

- Griffin & Mills (2002a), report maximum sickness around 0.25Hz with a decrease at frequencies above 0.25Hz up to 0.8Hz.

More recently, Donohew & Griffin (2004) carried out laboratory experiments to study the effects of lateral oscillations onto the elicitation of motion sickness. In their study, they divided 120 participants into 6 independent groups of 20 subjects each. The groups were organised in such a way that there were no significant differences in age, illness and vomiting susceptibilities (measured through pre-test questionnaire) amongst the groups. They exposed their subjects to sinusoidal lateral oscillations with a constant peak velocity of 1.0 m/sec at one of the six oscillation frequencies (0.0315, 0.05, 0.08, 0.125, 0.16 and 0.20Hz) for up to 30min or less if moderate nausea was reached.

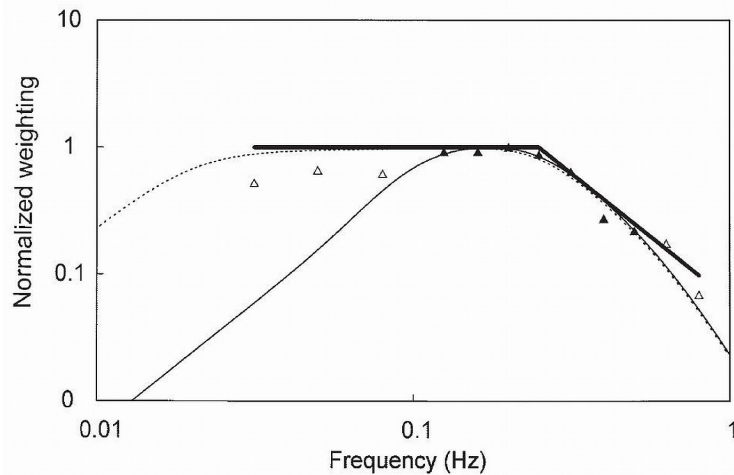


Figure 6.3. Asymptotic and realizable frequency weightings for lateral acceleration, derived from the normalized mild nausea incidence, compared with the weighting for vertical acceleration, W_f , as defined in BS 6841. All weightings are normalized such that their maximal values are 1.0. Asymptotic weighting = solid thick line; realizable weighting = dotted line; normalized mild nausea incidence: black triangles = points at which values differ significantly from static condition, open triangles = points at which values not significantly different from static condition; W_f = solid thin line [Donohew & Griffin, 2004].

Donohew & Griffin (2004) have proposed the frequency weightings for lateral accelerations shown in Figure 6.3 that, in agreement with previous studies (Lobb 2001; Griffin & Mills 2002a; 2002b), depict a decline in sickness at 12dB per octave,

from 0.20 to 0.8Hz. However, contrary to the pure vertical motions, the sickness is independent of the oscillation frequencies below 0.20Hz.

It is important to note that Golding et al.(1997) assumed that the lateral horizontal oscillations would exhibit similar nauseogenic characteristics as those of the fore-and-aft motions. This has been confirmed by Griffin & Mills (2002a; 2002b) as they found no significant difference between the motion sickness ratings reported by their participants, when exposed to either direction (fore-and-aft or lateral) horizontal motions. Thus, the nauseogenic frequency weightings shown in Figure 6.3 for the lateral motions are equally valid under pure fore-and-aft oscillations.

6.3 Anomalies of Existing SV-Conflict Models

Based on the contents of §6.2.1 & 6.2.2 above, we may now summarize the studies pertaining to the elicitation of motion sickness provoked by the horizontal oscillations, as:

- Pure horizontal (fore-and-aft or lateral) oscillations do lead to motion sickness.
- Amplitudes of horizontal and vertical oscillations (assumed to) exhibit similar effects on the incidence of motion sickness i.e. a linear relationship holds between MSI and magnitudes of horizontal / vertical accelerations.
- Oscillation frequency plays a significant role in the occurrence of motion sickness for the horizontal as well as vertical motions.
- There is no significant difference in the incidence of motion sicknesses for the fore-and-aft and lateral horizontal oscillations.
- The time required to elicit moderate nausea is half or lesser in the case of horizontal motions, as compared to vertical oscillations of identical frequency and amplitude.
- MSI caused by the pure horizontal oscillations attains its maximum around 0.2 Hz with a decline at higher frequencies and, unlike pure vertical oscillations, exhibits independence at lower frequencies.

The above outlined points raise some important concerns about the existing SV-conflict models (§5.11), when viewed in the context of motion sickness provoked by the pure horizontal oscillations.

- First of all, the vestibular system oriented SV-conflict models by Bos & Bles (1998a; 1998b) and later by Ververiotis (2004) do not distinguish between the sensory-conflict resulting from pure vertical and pure horizontal oscillations. This means that, despite being more nauseogenic, these models would estimate identical sickness for pure horizontal oscillations as for the pure vertical motions. One may argue that visual system may become handy at this point, but it is imperative to understand that aboard real ships – visual feedback of moving environment is mostly very limited or even missing. This is due to the fact that, in general, passengers confine their visual activities to inside of the cabin, especially when they are not feeling well.
- Second issue pertains to the time response of these models; since the abovementioned SV-conflict models post process a single conflict (between the sensed and expected gravities), hence these do not take account of the lower latency exhibited by pure horizontal oscillations' induced sickness. The real ship motions comprise of six degrees of freedom and this shortcoming may have its bearings on the predicted sickness level. This would be especially true for contemporary ships that exhibit high levels of horizontal accelerations.
- Final point in the row is about frequency response of SV-conflict models. While simulating the laboratory experiments of McCauley et al. (1976), Bos & Bles (1998a; 1998b) selected and adjusted the parameters of 'internal' observer to ensure a peak around 0.2Hz with decline of sickness on either side. Though, this frequency response is very much valid for pure vertical motions but, as identified by Donohew & Griffin (2004), is not suitable for pure horizontal motions below 0.2Hz.

6.4 Existing Solution of the (SV-Conflict) Model Anomalies

One solution of the anomalies highlighted in §6.3, was suggested by Bos et al. (2002a). They proposed to independently translate the magnitude and orientation effects of the SV-conflict vector into MSIs. The concept is very simple; if the only perturbations from the vessel/vehicle motions are vertical then the sensed and expected gravity vectors would remain aligned. In such cases, their orientation differences would be zero and only the magnitude differences would exist. While in all other motion combinations, both effects (magnitude and orientation) would prevail.

Bos et al. (2002a) assume that the orientation differences lead to fast effects, such as cross-coupled Coriolis effects (Bles 1998). Hence, the orientation differences were accumulated over time using a fast integrator with a time constants of some tens of seconds. On the other hand, a slow accumulator with time constants of several minutes was suggested to be used for the magnitude effects. It is worth mentioning that this approach (i.e. having a slow and a fast integrating path) follows similar suggestions by Oman (1990; 1991) for translating sensory conflicts into motion sickness. However, the practical demonstration of this approach by Bos et al. (2002a), has been limited to the combined sway and roll motions only, with the predicted sickness being much larger than the expected values. Also, the proposed methodology has not been validated for predicting the motion sickness aboard real vessels, executing the six degrees of freedom motions.

In addition, the independent processing of the orientation and magnitude effects of the SV-conflict, only addresses the first two of the anomalies discussed in above (i.e. the ability to distinguish between the conflicts arising from pure horizontal or pure vertical motions as well as having different latency for pure horizontal oscillations). As such, the frequency responses of the orientation effects are expected to follow the frequency response of the magnitude differences under pure vertical or horizontal motions. Thus the overall frequency response of the SV-conflict model (MSI) under pure sway motions would remain identical to its frequency response under pure

heave oscillations. Hence, the anomaly concerning frequency behaviour of the model would still prevail.

The normalized ‘orientation’ (for sway motions) and ‘magnitude’ (for heave motions) differences of the sensory conflict predicted by the SV-conflict model (Verveniotis 2004), are shown in Figure 6.4. In both the cases, the simulated sinusoidal oscillations have unit RMS amplitude and varying frequencies (0.01 to 0.5Hz).

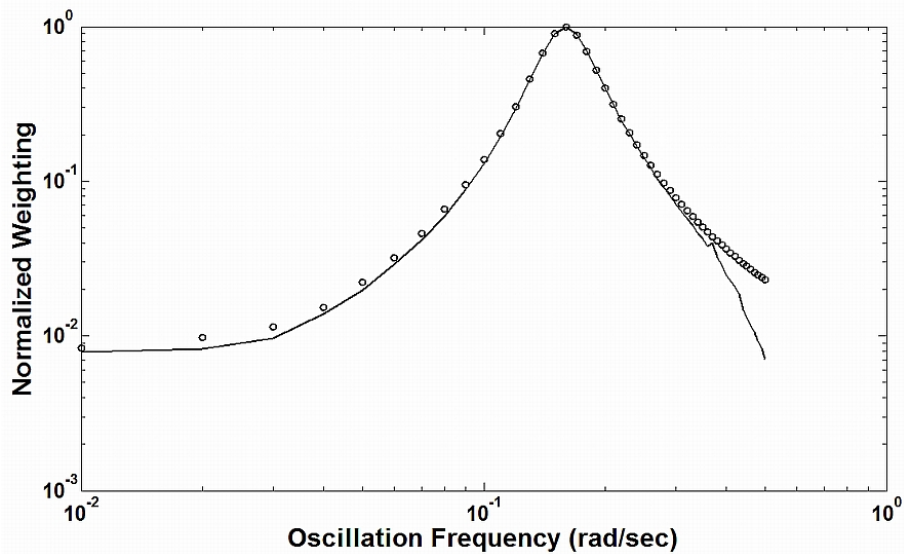


Figure 6.4. Normalized orientation (dotted line) and magnitude (circles) differences of the subjective vertical conflict under the sinusoidal sway and heave oscillations, respectively

It can be seen from the figure that the frequency response of the normalized ‘orientation differences’ under the pure horizontal oscillations (sway) is similar to the frequency behaviour of the ‘magnitude differences’ under the pure vertical (heave) motions. Thus, the output (MSI) frequency response of SV-conflict model would be identical for the pure horizontal or pure vertical oscillations. Splitting the SV-conflict into magnitude and orientation effects, therefore, may not work well for predicting sickness under predominantly horizontal oscillations and their combinations with other degrees of freedom motions.

6.5 Proposed Solution of the (SV-Conflict) Model Anomalies

In order to address the model anomalies discussed in §6.3, we presently identify another sensory conflict that is readily predictable by the SV-conflict theory. It is the conflict between the sensed and ‘expected’ horizontal accelerations, which we shall refer to as the subjective horizontal (SH) conflict. The aforesaid accelerations are, respectively defined as the components of gravito-inertial accelerations normal to the sensed and subjective verticals. We postulate that the SH-conflict in combination with SV-conflict may improve the motion sickness prediction-ability of the SV-conflict theory under the six degrees of freedom motions. We, therefore, rephrase the theory as; “All situations producing a variance between the vertical (gravity) sensed through human’s sense modalities and the subjective vertical ‘expected’ (by the nervous system) from past exposure to spatial environment causes motion sickness. In addition, the difference between horizontal accelerations (normal to gravity) sensed through the integrated sensory system and those ‘expected’ from previous experience (i.e. subjective horizontal accelerations) add up to elicit motion sickness.”

We refer to the new model, driven by the above statement of SV-conflict theory, as subjective vertical-horizontal (SVH) conflict model. This work limits the human motion sensing systems to vestibular apparatus, which is also indispensable for motion sickness etiology and has well defined mathematical models (see Chapter 5). Thus, SVH-conflict model is identical to SV-conflict models shown in Figure 5.41 (Bos et al. 2001; 2002; Bos et al. 2002c; Ververiotis & Turan 2002a; 2002b; Turan et al. 2003; Ververiotis 2004; Bos et al. 2008; Turan et al. 2009), with the following enhancements:

- Addition of a simple vectorial-process to calculate sensed horizontal accelerations as the component of gravito-inertial acceleration normal to the sensed vertical, i.e., sensed gravity.
- Instantiation of a process identical to above in the ‘internal’ model to estimate the ‘expected’ i.e. subjective horizontal accelerations.

- Calculation of subjective horizontal (SH) conflict as the vector difference between the sensed and subjective horizontal acceleration.
- Addition of a separate fast (twice as quick as the SV conflict) integrating path for post processing of SH-conflict into MSI. It should be noted that faster nauseogenic responses like Coriolis effects and vertigo have not been considered in this work.

Overall MSI for a given motion environment would then be a simple combination of sickness proportions attributable to SV and SH conflicts. It is important to note that in the SVH-conflict model, major part of motion sickness elicitation variability is still explained by the SV-conflict, while the remaining is estimated by the SH-conflict.

6.6 Hybrid Subjective Vertical Horizontal Conflict Model for Motion Sickness

The functional block diagrams of the SVH-conflict model are depicted in Figure 6.5 and Figure 6.10. This model is an extended version of NAME's SV-conflict model (Verveniotis & Turan 2002a; 2002b; Turan et al. 2003; Verveniotis 2004; Turan et al. 2009). As such, the SVH-conflict model is laid out to simulate the vestibular system discussed in Chapter 5. Similar to Oman's (1978; 1982; 1990; 1991) (see Figure 5.38 & Figure 5.39) and SV-conflict models (see Figure 5.41 & Figure 5.45), the SVH-conflict model simulates two major functionalities of CNS related to the etiology of motion sickness, namely 'orientation' and 'emetic' brains. The details of mathematical models simulating these two related, but unique functionalities are presented in the following.

6.6.1 Orientation / Motion Perception Part

The 'orientation / motion perception' part of the SVH-conflict model is based on the 'Luenberger observer theory' (Luenberger 1964; 1966; 1971) and comprises of two similar but distinctive regions shown in Figure 6.5. The 'sensor region' simulates

labyrinthine receptors (canals and otoliths) and the physical laws assumed to be implemented by the vestibular nuclei, to extract information about self orientation and motions. On the other hand the ‘internal region’, presumably located somewhere in medulla, is responsible for the estimation of ‘expected’ orientation and motions (see Chapter 5 for further details on vestibular system and its models).

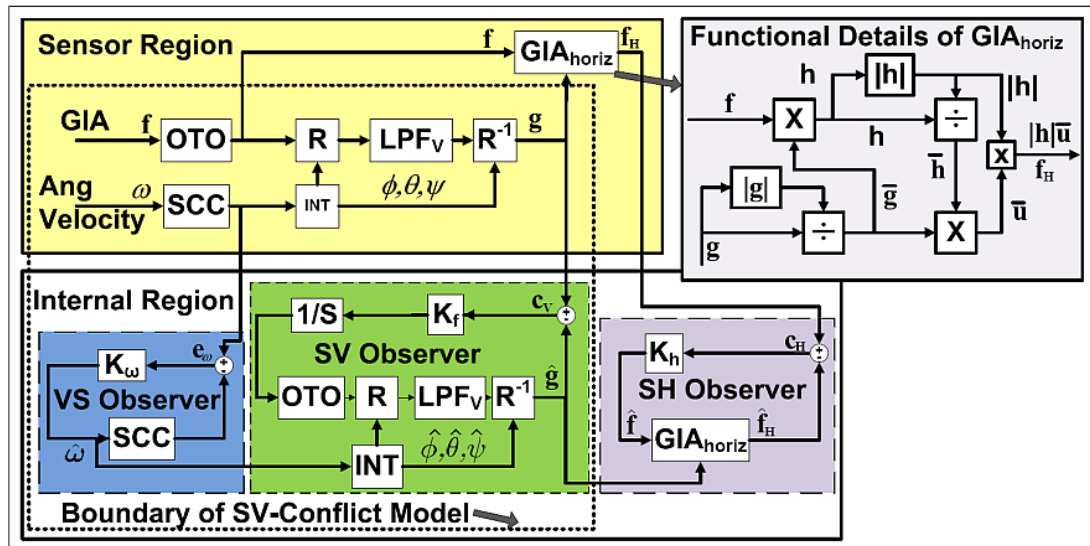


Figure 6.5. Schematic diagram of 'orientation / motion perception' part of the hybrid subjective vertical horizontal (SVH) conflict model of motion sickness.

It is assumed that central nervous system (CNS) carries imprints of all human sensory systems and, being aware of their functioning, is able to predict their typical outputs. Thus, (large and long enough) variances between the sensed and ‘expected’ outputs of vestibular system alarm the CNS of a possible hallucination (usually caused by toxins). The natural consequence of which is the initiation of nauseogenic malaise (see Treisman 1977).

6.6.1.1 Estimation of Vertical in the Sensor Region

Due to their anatomical characteristics (§5.4.3), the otoliths (OTO block) act like linear accelerometers. A consequence of this is the prevalence of the ‘equivalence principle’ (Einstein 1907). Thus, the otoliths at their own, cannot distinguish between the tilt (gravitational, $g \sin\theta$) and translational accelerations. It is, therefore, imperative to establish information about self rotation. This functionality is provided

by the semi-circular canals. The question which now needs to be addressed is how vestibular nuclei isolate gravity from gravito-inertial accelerations (GIA, \mathbf{f}) (bold face letters are used for vectors) registered by the vestibular system, under passive motions. The answer to this question was first given by Mayne (1969; 1974a) for 2D motions. He suggested to low pass filter the GIA to separate the (constant) gravity from it (see §5.7.1 for further details).

The sensor region of the SVH-conflict model is laid out to estimate the magnitude and direction of gravity using Mayne's principle, generalised to 3D (Glasauer 1992a; Glasauer & Merfeld 1997; Bos & Bles 2002). Since, gravity is only constant in an Earth fixed frame of reference. Hence, the human head-referenced GIAs (measured by the otoliths) are first transformed onto an Earth fixed frame of reference (see Figure 5.42) using the rotational transformation matrix (R-block of Figure 6.5) given by:

$$\mathbf{R} = \begin{pmatrix} \cos \psi \cos \theta & \cos \psi \sin \theta \sin \phi - \sin \psi \cos \phi & \cos \psi \sin \theta \cos \phi + \sin \psi \sin \phi \\ \sin \psi \cos \theta & \sin \psi \sin \theta \sin \phi + \cos \psi \cos \phi & \sin \psi \sin \theta \cos \phi - \cos \psi \sin \phi \\ -\sin \theta & \cos \theta \sin \phi & \cos \theta \cos \phi \end{pmatrix} \quad (6.1)$$

Where, ϕ , θ , and ψ are the Euler angles (roll, pitch and yaw respectively) that, for a passively moving i.e. seated passenger, describe rotation of body about a local (i.e. body / head fixed) frame of reference (see Figure 5.42). The rotation matrix \mathbf{R} may be obtained from the semicircular canals' signals (SCC block).

After being rotated, the Earth referenced GIAs are low pass filtered (LPF_v block) and transformed back to head frame of reference (\mathbf{R}^{-1} block) using inverse (a transpose i.e. \mathbf{R}^T) of the rotational matrix given by Equation(6.1). Mathematically, this process is identical to the SV-conflict models (note the SV-conflict model boundary in Figure 6.5) by TNO (see §5.10) (Bos et al. 2001; 2002; 2002c; 2008) and NAME (see §5.11) (Verveniotis & Turan 2002a; 2002b; Turan et al. 2003; Verveniotis 2004; Turan et al. 2009). As derived in §5.11 for the SV-conflict model, the Equation(6.2)

below, represent the complete process of estimating gravity (\mathbf{g}) from GIA (\mathbf{f}) in the sensor region of SVH-conflict model:

$$\dot{\mathbf{g}} = \left(\frac{\mathbf{f} - \mathbf{g}}{\tau} \right) - \boldsymbol{\omega} \times \mathbf{g} \quad (6.2)$$

In the above equation \mathbf{f} & \mathbf{g} are the sensed GIA and gravity vectors in the body (head, Π) frame of reference (see Figure 5.42). While, $\boldsymbol{\omega}$ is the angular velocity vector sensed by the canals and τ is the time constant of low pass filter. It can easily be inferred from Equation(6.2), that explicit calculation of rotational matrices [Equation(6.1)] is not needed for the estimation of sensed vertical (gravity). The angular velocity vector sensed by the semicircular canals would be able to account for the rotational effects (see e.g. Bos & Bles 2002 for further details). Based on the human sleds and centrifuge experiments Bos & Bles (1998b), suggest a value of 5s for τ i.e.:

$$\tau = 5(sec) \quad (6.3)$$

As presented in §5.5, semicircular canals act like mechanical integrators and have a frequency response similar to a band pass filter (see Figure 5.13, Figure 5.14, & Figure 5.18). However, laboratory experiments by O’Hanlon & McCauley (1974), McCauley et al. (1976) and Donohew & Griffin (2004) suggest a rapid decline in (motion sickness) sensitivity above 0.2Hz. Moreover, the peak frequencies of typical rigid body motions of most real vessels lie within the decade of 0.1 to 1.0Hz (Guignard & McCauley 1990). Thus, for the frequencies of our interest (i.e. <0.5Hz), canals may be treated as high pass filters with the following transfer function, suggested by Merfeld et al (1993) (also see Figure 5.19):

$$\frac{\alpha_{\omega}(s)}{\omega(s)} = \frac{5.7s}{5.7s + 1} \quad (6.4)$$

Where, α_ω is the canal afferent response and ω is the angular velocity in Laplace Domain (in any one of the three axis). As far as the otoliths (OTO block) are concerned, their afferents (α_f) faithfully follow the sensed GIA (\mathbf{f}) in the frequency range up to 5Hz (Bos & Bles 2002). Since, the frequency contents of a real vessel's rigid body motions are far below this range (Guignard & McCauley 1990), therefore, a transfer function of unity can be used for simplicity without any significant loss of accuracy. Based on foregoing, the transfer functions used for the representation of vestibular system in the SVH-conflict model (Figure 6.5), including that of the low pass filter, are summarized by the Equation(6.5) below:

$$\begin{aligned}\frac{\alpha_f(s)}{f(s)} &= oto(s) = 1 \\ \frac{\alpha_\omega(s)}{\omega(s)} &= scc(s) = \frac{\tau s}{\tau s + 1} = \frac{5.7s}{5.7s + 1} \\ LPF_v(s) &= \frac{1}{\tau s + 1} = \frac{1}{5s + 1}\end{aligned}\tag{6.5}$$

The 'orientation / motion perception part' of the SVH-conflict model, simulates the vestibular system and its associated processing for the six degrees of freedom motions. Therefore, similar to Merfeld et al.'(1993) spatial orientation model, the transfer functions of otoliths and canals would be given by Equation(6.6) in the following.

$$\begin{aligned}\frac{\alpha_f(s)}{f(s)} &= OTO(s) = \begin{pmatrix} oto(s) & 0 & 0 \\ 0 & oto(s) & 0 \\ 0 & 0 & oto(s) \end{pmatrix} = \begin{pmatrix} 1 & 0 & 0 \\ 0 & 1 & 0 \\ 0 & 0 & 1 \end{pmatrix} \\ \frac{\alpha_\omega(s)}{\omega(s)} &= SCC(s) = \begin{pmatrix} scc(s) & 0 & 0 \\ 0 & scc(s) & 0 \\ 0 & 0 & scc(s) \end{pmatrix}\end{aligned}\tag{6.6}$$

6.6.1.2 Estimation of Horizontal in the Sensor Region

As discussed in §6.5, we define ‘sensed horizontal accelerations’ as the component of GIA (\mathbf{f}) exactly normal to sensed gravity (in the body frame of reference). The sensed vertical (gravity) readily carries the effects of (low frequency) translational accelerations parallel to it. Thus, this definition of sensed horizontal, establishes the component of GIA not accounted by the SV-conflict. The hypothetical process used by the nervous system, to estimate the sensed horizontal accelerations, is fairly simple and comprises of a few vector manipulations. The details of this process are encapsulated inside the $\text{GIA}_{\text{horiz}}$ block, which is expended in the inset of Figure 6.5.

Firstly, a vector product of the sensed GIA (\mathbf{f}) with a unit vector in the direction of sensed gravity ($\bar{\mathbf{g}}$) (bold letters with a bar on top represent unit vectors) results into a vector \mathbf{h} . This resultant vector has its magnitude equal to the component of GIA normal to sensed gravity but is directed out of the plane containing them i.e.:

$$\mathbf{h} = \mathbf{f} \times \bar{\mathbf{g}} = \{|\mathbf{f}| \cdot |\bar{\mathbf{g}}| \cdot \sin(\gamma)\} \bar{\mathbf{n}} = |\mathbf{f}| \cdot \sin(\gamma) \cdot \bar{\mathbf{n}} \quad (6.7)$$

Where, γ is the angle between sensed GIA (\mathbf{f}) and gravity ($\bar{\mathbf{g}}$), while $\bar{\mathbf{n}}$ is a unit vector normal to the plane containing them. We can find out magnitude of the vector of our interest i.e. $|\mathbf{h}|$ but its direction is incorrect. Now, a cross product of the unit vectors in the direction of gravity ($\bar{\mathbf{g}}$) and \mathbf{h} ($\bar{\mathbf{h}}$) results into a unit vector $\bar{\mathbf{u}}$, which being their coplanar, is normal to the sensed gravity ($\bar{\mathbf{g}}$) and directed towards GIA (\mathbf{f}) i.e.:

$$\bar{\mathbf{u}} = \bar{\mathbf{g}} \times \bar{\mathbf{h}} \quad (6.8)$$

Now, a simple multiplication of $\bar{\mathbf{u}}$ with $|\mathbf{h}|$, would gives us the vector of our interest:

$$\mathbf{f}_H = |\mathbf{h}| \cdot \bar{\mathbf{u}} \quad (6.9)$$

6.6.1.3 Estimation of Vertical in the Internal Region

As shown in Figure 6.5, the segment of internal region responsible to estimate ‘expected’ gravity (the subjective vertical) comprises of two observers. A ‘velocity storage (VS)’ and a ‘subjective vertical (SV)’ observer; the former replicates velocity storage mechanism (Raphan et al. 1977) needed for the prediction of low frequency rotational oscillations (remember canals act like high pass filters for the frequencies of our interest, see §6.6.1.1).

The afferents predicted by VS-observer are compared with sensed afferents of canals and difference of the two results into an error signal (e_{ω}). This error signal is weighted (K_{ω}) and fed to the internal model of canals by the compensator, steering the estimates to sensed afferents (see Figure 6.5). Merfeld et al. (1993) have recommended a value of 3.0 (deg/sec per deg/sec) for the feedback gain K_{ω} i.e.:

$$K_{\omega} = 3.0(\text{deg/ sec/ deg/ sec}) \quad (6.10)$$

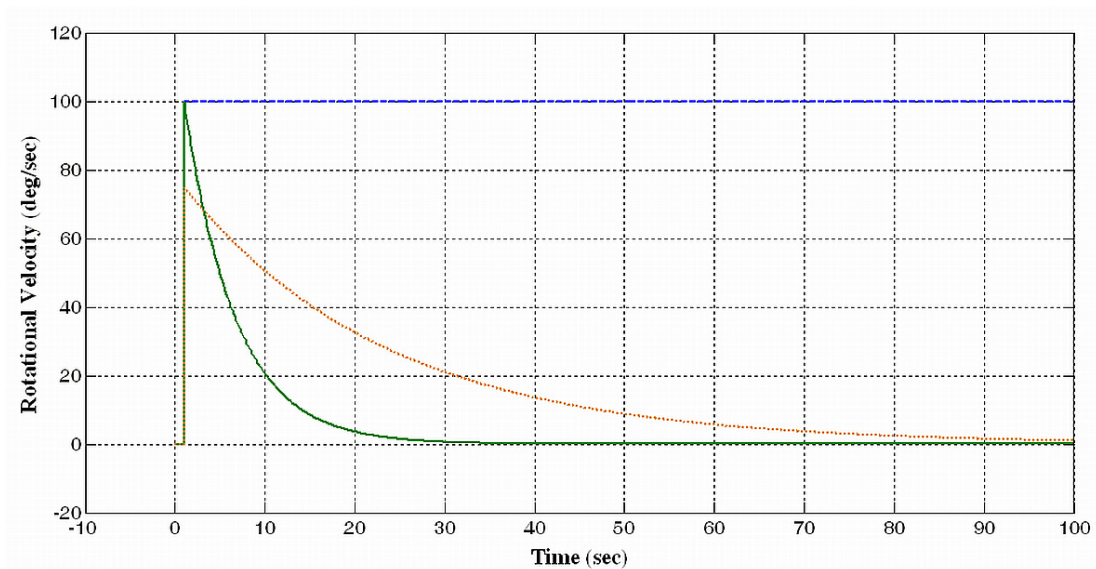


Figure 6.6. Time responses of first order SCC neurons (solid green line) and VS-observer (dotted orange line) to a step angular velocity (dashed blue line).

As depicted in Figure 6.6, in the case of a step input to canals, the VS-observer retains impression of the canal afferents for a period longer than what would

otherwise be exhibited by the first order neurons innervating the canals (this is the core function of velocity storage mechanism).

It is important to note that Bos et al. (2002b) observed that the velocity storage mechanism primarily works for the horizontal (lateral) canal afferents only. However, this should not be an issue in the present context (being applied to all three canal afferents), as the rotational motions of real ships are rarely of frequencies below the cut off frequencies [0.028Hz as per Equation(6.5)] of the canals. Thus, VS-observer is merely there to facilitate calculation of internal estimates of angular velocities, in line with the orientation model by Merfeld et al. (1993).

The outputs of the VS-observer i.e. estimated rotational velocities ($\hat{\boldsymbol{\omega}}$) (hatted bold face letter represent internal/subjective vectors) are fed into the SV-observer for the calculation of rotational transformation matrices. The physical laws embedded inside subjective vertical (SV) observer for the estimation of ‘expected’ gravity $\hat{\mathbf{g}}$ i.e. the subjective vertical, are identical to those employed by vestibular nuclei in the sensor region. Thus, Equation(6.11) in the following is assumed to be implemented by the nervous system to estimate the ‘expected’ vertical ($\hat{\mathbf{g}}$).

$$\hat{\mathbf{g}} = \left(\frac{\hat{\mathbf{f}} - \hat{\mathbf{g}}}{\tau} \right) - \hat{\boldsymbol{\omega}} \times \hat{\mathbf{g}} \quad (6.11)$$

The difference between sensed and subjective verticals results into the SV-conflict vector i.e.:

$$\mathbf{c}_v = \hat{\mathbf{g}} - \mathbf{g} \quad (6.12)$$

This conflict (\mathbf{c}_v) is used by the compensator of SV-observer through a proportional gain (K_f) and an integrator (1/s), to steer internal estimates of gravity $\hat{\mathbf{g}}$ towards the sensed gravity \mathbf{g} . The frequency response of SV-observer depends on the magnitude of weighting K_f . While detailing the SV-conflict for vertical motions, Bos & Bles(1998b) suggest a value of 5 (s^{-1}) for K_f i.e.:

$$K_f = 5(\text{sec}^{-1}) \quad (6.13)$$

This causes the conflict to have its maxima around 1.0rad/sec (0.16Hz), which is the frequency at which human beings exhibit maximum sensitivity to vertical oscillations from motion sickness point of view (see Figure 3.10. and Figure 3.13).

6.6.1.4 Estimation of Horizontal in the Internal Region

Analogous to SV-observer, the processes implemented by the subjective horizontal (SH) observer are exact copies of those being carried out in sensor region. It is hypothesised that the SH-observer compares the estimates of subjective horizontal accelerations ($\hat{\mathbf{f}}_H$) with the sensed values (\mathbf{f}_H), to calculate the subjective horizontal (SH) conflict i.e.:

$$\mathbf{c}_H = \hat{\mathbf{f}}_H - \mathbf{f}_H \quad (6.14)$$

This conflict (\mathbf{c}_H) is then weighted (K_h) and fed back to the SH-observer through a compensator, to minimise the difference between the sensed and subjective horizontal accelerations. As presented in Chapter 7 (calibration and validation of the model), the magnitude of K_h has been estimated to be equal to 1 (ms^{-2} per ms^{-2}), by statistically fitting the SVH-conflict model to the 15 full scale trials of a high speed wave piercing catamaran vessel ($p=0.134$; $\chi^2=21.09$; $dof=15$) (see §7.8.4) i.e.:

$$K_h = 1.0(\text{m}\cdot\text{sec}^{-2} / \text{m}\cdot\text{sec}^{-2}) \quad (6.15)$$

6.6.2 Emetic Part

Before we discuss how exactly the ‘emetic brain’ of SVH-conflict model is laid out, it is important to realise that the ‘orientation \ motion perception’ part of this model does not predict SH-conflict for pure vertical oscillations. For such cases, it is equivalent to SV-conflict model (§5.11); hence, it makes sense to split the emetic part into two segments, each independently transforming the individual sensory

conflict (\mathbf{c}_V or \mathbf{c}_H) into MSI (the percentage of passenger likely to vomit under a given motion environment). Thereafter, the two predicted MSIs should be combined together to estimate the overall MSI. This is exactly how the ‘emetic’ part of SVH-conflict model is arranged, as presented in §6.6.2.2.

It is pertinent to highlight that, similar to SV-conflict model, the SVH-conflict model only considers the slow responses of the sensory conflicts leading to emesis and disregards any fast nauseogenic responses like vertigo. This assumption is valid as long as the passengers are seated and passively moving with the vessel without executing excessive volitional head movements. Details of the way SVH-conflict model translates the sensory conflicts predicted by the ‘orientation / motion perception part’ are given in the following sections.

6.6.2.1 Transformation of Sensory Conflicts into MSI

There are two important features of MSI that should be taken into account while transforming the conflicts (\mathbf{c}_V & \mathbf{c}_H) into MSIs; these are (1) nonlinearity and (2) accumulation. Based on McCauley et al.’s (1976) laboratory data, Bos & Bles (1998a; 1998b) proposed to rectify the SV-conflict using the hill function ‘ h_V ’ given by Equation(6.16), which accounts for the nonlinearity characteristics of MSI. Here, ‘ h_V ’ will increase exponentially for small conflicts and would be logarithmically increasing for the large values.

$$h_V = \frac{|\mathbf{c}_V|^{n_V}}{b_V^{n_V} + |\mathbf{c}_V|^{n_V}} \quad (6.16)$$

$$h_H = \frac{|\mathbf{c}_H|^{n_H}}{b_H^{n_H} + |\mathbf{c}_H|^{n_H}}$$

b_V and n_V are the shape parameters for the SV-conflict (\mathbf{c}_V) hill function h_V , while b_H and n_H are the shape parameters for the SH-conflict (\mathbf{c}_H) hill function h_H .

We know that (generally) people do not get motion sick instantly on exposure to provoking environment and do recover from it on removal / reduction of the causal

motions. Furthermore, MSI can attain a maximum value of 100% and does not cumulate infinitely. The mathematical function that can take account of these accumulation features, is a second order low pass filter termed as ‘leaking integrator’(Bos & Bles 1998a). Thus, MSI may be linked to the rectified sensory conflicts i.e. h_V and h_H by:

$$MSI_V = \frac{K_{MSI_V}}{(\mu_V s + 1)^2} \cdot h_V \quad (6.17)$$

$$MSI_H = \frac{K_{MSI_H}}{(\mu_H s + 1)^2} \cdot h_H$$

Where, K_{MSI} is the maximum value of the output i.e. maximum proportion of people likely to get motion sick, while μ_V & μ_H are the time constants of the ‘leaking integrators’ for the vertical and horizontal conflicts, respectively. As discussed in §6.2, all laboratory experiments concerning elicitation of motion sickness under pure horizontal oscillations (e.g. Golding et al. 2001; Lobb 2001; Griffin & Mills 2002a; Donohew & Griffin 2004) suggest a decrease in sickness sensitivity to the motions with frequencies above 0.2Hz.

However, under the proposed arrangement of model’s ‘orientation / motion perception part’ (Figure 6.5), the frequency response of SH-conflict (c_H) is like a high pass filter (Figure 6.7), which should be adjusted before being translated into MSI. This has been achieved by filtering the SH-conflict using a single pole low-pass filter with corner frequency of 0.2Hz (1.26rad/sec), given by:

$$LPF_H(s) = \frac{1.26}{s + 1.26} = \frac{1}{0.79s + 1} \quad (6.18)$$

The pre and post filtered magnitudes of SH-conflicts for the pure lateral (sway) motions of varying frequencies are depicted in Figure 6.7. The low pass filtering of horizontal conflict proposed here, is primarily meant to simulate the ‘subjective sickness sensitivity’ to pure horizontal oscillations.

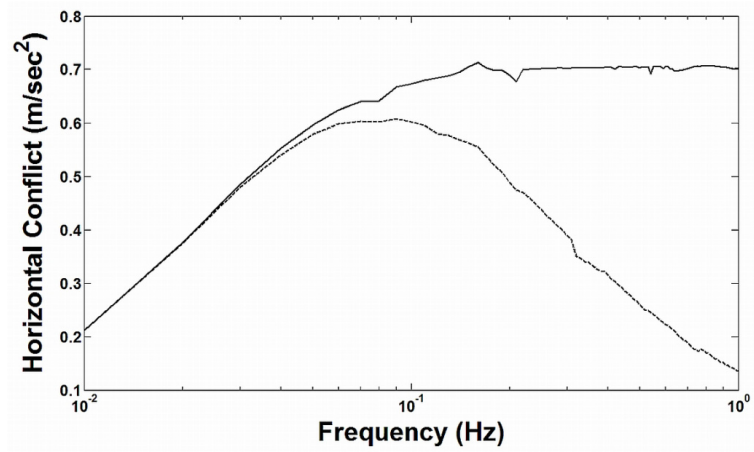


Figure 6.7. Frequency response of SH-conflict before (solid line) and after (dotted line) low pass filtering.

It may be noted that the reduction in nauseogeny of horizontal motions above 0.2 Hz may be attributed to the human beings' habituation to the high frequency (0.5 to 10 Hz) linear accelerations, experienced during the normal locomotion (walking, running, jumping, etc.) (Benson 2002). The magnitudes of the two conflicts, before being passed through the hill functions, for the unit RMS horizontal accelerations of various frequencies are depicted in the following figure:

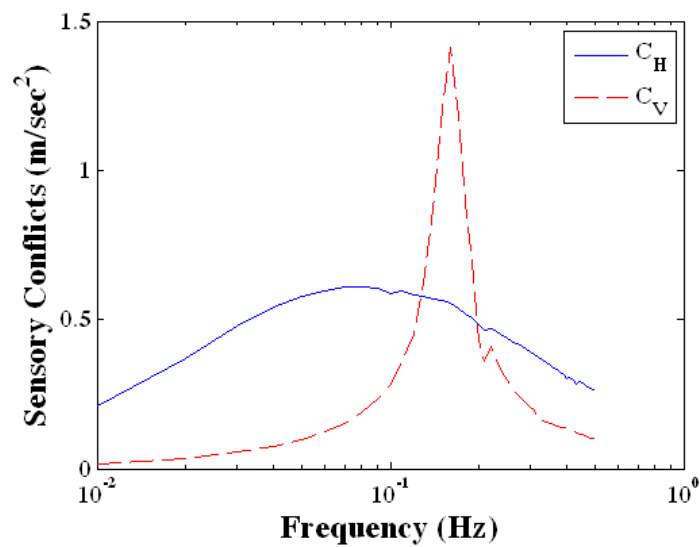


Figure 6.8. Magnitudes of sensory conflicts for unit RMS accelerations (before the hill functions): SV-conflict (dashed line); SH-conflict (solid line)

The following figure is depicting the magnitudes of the two conflicts after being passed through the hill functions:

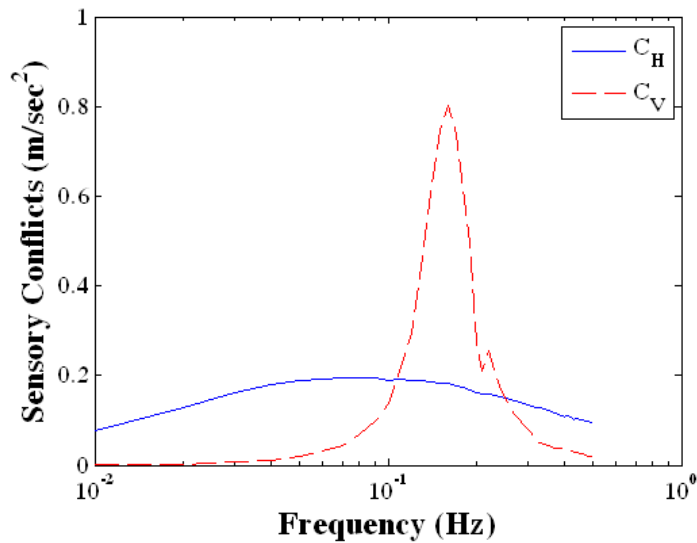


Figure 6.9. Magnitudes of sensory conflicts for unit RMS accelerations (after the hill functions): SV-conflict (dashed line); SH-conflict (solid line)

It can easily be gathered from Figure 6.8 and Figure 6.9 that the two types of sensory conflicts (c_V and c_H) estimated by the SVH-conflict model show different responses. These frequency responses are respectively compatible with the laboratory studies concerning elicitation of sickness under purely vertical (O'Hanlon & McCauley 1974; McCauley et al. 1976) and horizontal oscillations (Donohew & Griffin 2004).

6.6.2.2 Layout of Emetic Brain

It is important to realise that the conflict rectifier [Equation(6.16)] and its accumulator [Equation(6.18)] for the post-processing of SV-conflict (c_V), are originally based on the laboratory results for pure vertical oscillations. However, in the absence of as abundant data, it has been assumed that the aforesaid relationships hold true for the SH-conflicts and resulting MSIs under the pure horizontal oscillations. Thus, as mentioned at the beginning of §6.6.2, we estimate MSIs corresponding to each sensory conflict i.e. SV & SH separately and then combine them to calculate the overall MSI. It is intuitive that the shape parameters of hill

function and time constant of leaking integrator would be unique for the two (fundamentally different) conflicts.

It is not known how exactly the CNS combines the sickness effects of SV and SH conflicts. Therefore, out of numerous possibilities, we considered two: (1) simple linear addition and (2) Pythagoras-type addition by treating MSI_V (due to SV-conflict) & MSI_H (due to SH-conflict) as sides of a right-angled triangle. However as shown later in §7.8.4, calibration of the SVH-conflict model reveals that the Pythagoras approach (depicted in Figure 6.10 below) is more promising than the simple addition.

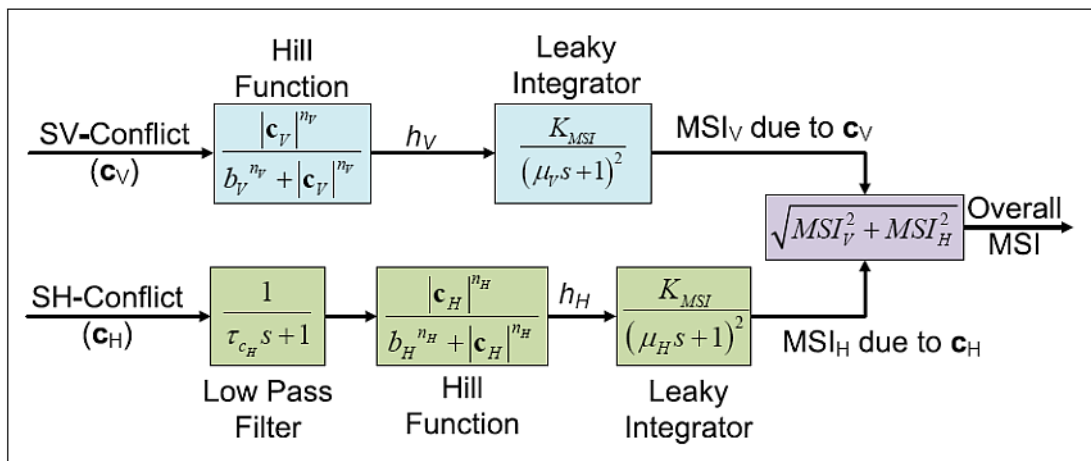


Figure 6.10. Schematic diagram of 'emetic brain' part of the hybrid subjective vertical horizontal (SVH) conflict model of motion sickness.

It is important to note that the COMPASS motion sickness model (§3.8.2), being the only descriptive mode accounting for the vertical as well as horizontal accelerations, does not contain any interaction term for the two types of accelerations. Based on the aforesaid and for simplicity reasons, this work did not consider any interaction between the two types of sensory conflict (SV and SH) used by the SVH model.

Thus, once the MSIs corresponding to SV and SH conflicts are calculated, these can then be combined together to estimate the overall MSI using Equation(6.19).

$$MSI_{Overall} = \sqrt{MSI_V^2 + MSI_H^2} \quad (6.19)$$

Parameters of the hill functions [Equation(6.16)] and the leaking integrators [Equation(6.18)], summarised in Table 6.1 were found to be optimum (see §7.8.4).

Table 6.1. Hill function and leaking integrator parameters.

Parameter	SV-Conflict	SH-Conflict
b	0.7	2.5
n	2	1.0
K_{MSI}	85(%)	85(%)
μ	12 minutes	6 minutes

It is important to reiterate that the parameter values for the post processing of SV-conflict are exactly the same as proposed by Bos & Bles (1998a; 1998b) to replicate laboratory experiments by McCauley et al. (1976). The time constant of the ‘leaking integrator’ used for processing the SH-conflict is set as half of the one used for SV-conflict. This is done to take account of lower (almost half) latency of motion sickness for pure horizontal oscillations (see §6.2). While, other parameters of the hill function for SH-conflict post processing were established by statistically fitting the model to 15 field trials of a high speed passenger ferry (see §7.8)

6.7 Calculation of Frequency Weightings

It could easily be gathered from §6.6 that the new (SVH-conflict) model is able to distinguish between the sensory conflicts arising from purely vertical (c_H would be zero) and horizontal oscillations. Furthermore, the individualised emetic paths (Figure 6.10) allow us to choose different latency for the two different, but related, conflicts. Based on foregoing, first two of the three anomalies (of the existing SV-conflict models) highlighted in §6.3, stand resolved. However, we need to verify that the SVH-conflict model displays different frequency responses for the purely vertical and horizontal motions, so that the third anomaly may be verified as addressed. Thus,

this section aims to establish the frequency responses of the model by calculating normalised MSIs for the unit (RMS) heave / sway oscillations of varied frequencies (i.e. frequency weightings).

The SVH-conflict model has been implemented in SIMULINK[®], the companion software of MATLAB[®] from MathWorks[™]. Now, by running the model for unit RMS lateral (sway) accelerations and a range of frequencies (0.01 to 1.0Hz), we can estimate the normalized MSIs caused by the pure horizontal oscillations. If we further normalize these MSIs such that the maximum value of MSI is 1.0 then the resulting graph, as shown in Figure 6.11, would represent the frequency weightings for purely horizontal oscillations.

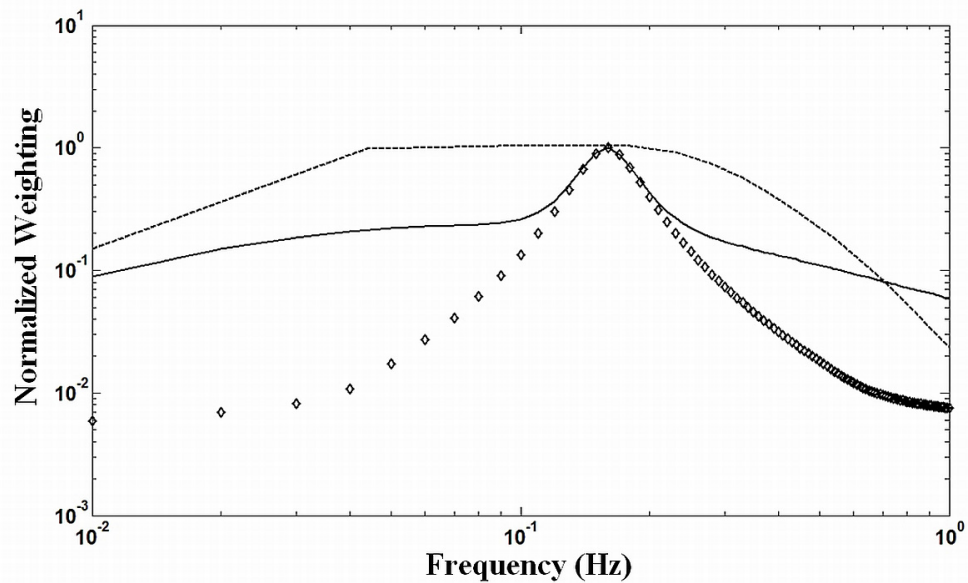


Figure 6.11. Normalized frequency weighting for pure horizontal (lateral) oscillations (unit RMS accelerations); SVH-conflict model (solid line); SV-conflict model (diamonds); Donohew & Griffin [2004] (dotted line).

The figure is also displaying normalized frequency weightings calculated using SV-conflict model and those suggested by Donohew and Griffin(2004). Frequency weightings predicted by SVH-conflict and those by laboratory experiments are displaying similar trends, whereas, SV-conflict model is showing reduction in sickness levels below and above 0.16Hz, substantiating the reservation mentioned in §6.3.

Similar to above, we can calculate the frequency weightings shown in Figure 6.12, for the pure vertical accelerations by running the SVH and SV-conflict models for unit RMS vertical (heave) accelerations of varying frequencies. This time SVH and SV-conflict models are predicting identical weightings that are displaying features similar to the frequency weightings derived by Lawther & Griffin(1987) for pure vertical oscillations.

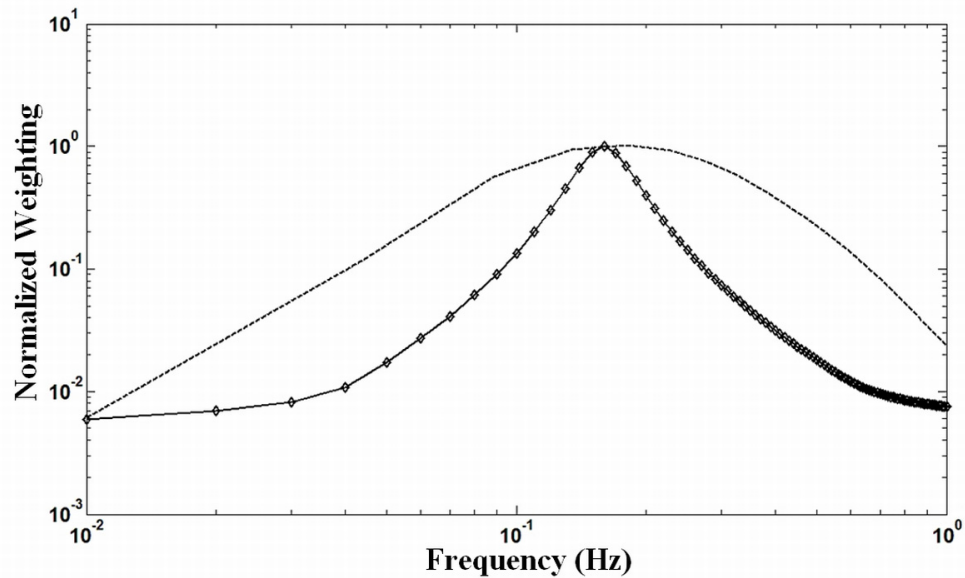


Figure 6.12. Normalized frequency weighting for pure vertical (heave) oscillations (unit RMS acceleration); SVH-conflict model (solid line); SV-conflict model (diamonds); Lawther & Griffin [1987] (dotted line)

It can be seen that the SVH-conflict model, unlike SV-conflict, is displaying different frequency responses for the pure horizontal and vertical oscillations. The model is, therefore, expected to perform better when large horizontal motions are exhibited by any vessel and would be similar to SV-conflict in the otherwise situations.

6.8 Chapter Summary

This chapter has briefly presented the theoretical and mathematical details of the new physiological motion sickness model developed in this research project. The ability of SVH-conflict model to predict two sensory conflicts with dedicated emetic paths, allows addressing the anomalies of existing SV-conflict models. The frequency response of the new model is compatible with the laboratory studies for the purely

vertical and horizontal oscillations' induced motion sickness. It is expected that SVH-conflict would exhibit better performance for the contemporary high speed vessels with high level of lateral accelerations, and would be equivalent to SV-conflict model in the cases of classical monohull vessels.

The next chapter is dedicated to elucidate the calibration procedure of SVH-conflict model. It also presents validation of the new model by applying it to the full scale trials of various ships archived at NAME.

Chapter 7. CALIBRATION AND VALIDATION OF THE MODEL

7.1 Overview of the Chapter

The chapter begins with an introduction to the general model calibration and validation techniques (§7.2). This is followed by the overview of the methodology adopted for the calibration of SVH-Conflict model (§7.3). The parameters selected for the model calibration process are discussed in §7.4. Selections of the objective function and calibration data are respectively discussed in §7.5 and §7.7. The detailed procedure employed for the estimation of selected model parameters is given §7.8. After being calibrated, the SVH-Conflict model has been validated using the available full scale trials data in §7.9. Finally in §7.10, the archived field trials data are used to test the performance of SVH-Conflict model in relation to other physiological and descriptive motion sickness models. The chapter concludes with a summary in §7.11.

7.2 Model Calibration and Validation Techniques

This section briefly presents the techniques used for the calibration and subsequent validations of the mathematical models simulating complex engineering / natural processes.

7.2.1 Typical Model Types

Depending on the development methodology, all mathematical models of real world processes/phenomenon may be attributed to one of the three main categories. On one end we have the so called ‘black box’ or ‘empirical’ models that are mainly built from the measured data while using the model parameters and/or structure estimation techniques (e.g. see Ljung 1987; Walter et al. 1997). On the other end of the spectrum, we have the ‘white-box’ models that are developed using the first engineering principles comprising of well-defined and duly solvable mathematical

expressions (Sjoberg et al. 1995). The third and most commonly found/used category of the models are the ‘Grey-box’ models that are usually built using the first engineering principles, but part of the model parameters and/or structure is unknown (Bohlin 1991).

A simple examination of SVH-conflict model would reveal its ‘greyish’ nature, as it has been developed using the physiological knowledge of the vestibular system duly taking account of the simple physical laws (§6.6). However, the validity of some assumptions and the values of its matching parameters are unknown.

7.2.2 Calibration and Validation of Models for Engineering Processes

According to Hangos & Cameron (2001), the process of estimating missing model parameters and/or structure using experimental data from real world is called ‘model calibration’. Whereas, comparison of values predicted by the calibrated model with field data, other than the one used for calibration, is termed as ‘model validation’. They identify the following main ingredients needed to calibrate a model developed for the process system engineering:

- The ‘grey-box’ model of the process being simulated.
- Availability of measured data from the real system called calibration data.
- Identification of a measure of fit/loss function/objective function that could be used to measure the quality of the ‘process model’ for the estimated parameters / structural elements.

Hangos & Cameron (2001) suggest the following ‘conceptual steps’, to be carried out during a model calibration exercise:

- **Analysis of model specification:** In this step the constituents of grey-box process model are evaluated to identify the parameters and/or structural elements that would render them solvable.
- **Sampling of continuous time dynamic models:** Since majority of the engineering processes are continuous in time domain, while most of the

statistical procedures employed for the parameter estimation are discrete in nature. Hence, it is important to discretise the engineering process being modelled.

- **Data analysis and pre-processing:** This step concerns the measured data of a real process system that would generally be of varying quality. It is important to identify data biasness and outliers, if any.
- **Model parameter and structure estimation:** This represents the core phase of model calibration that involves estimation of model parameter and structure (if required) using some optimisation approach that seeks to minimise the loss function.
- **Evaluation of the quality of the estimate:** The final step in the calibration procedure of a grey-box process model is to verify the quality of parameter estimated. It is either carried out empirically using graphical methods or (preferably) by exact hypothesis testing provided the relevant statistical properties of the estimates are available.

Once calibrated the model is validated to decide on its quality. This phase of grey-box model development is similar to its calibration process in the sense that the data used for model validation is still a measured data, but from another independently measured set called the validation data.

7.2.3 Calibration and Validation of Models for Natural Processes

Based on the non-linear regression approaches, Hill & Tiedeman (2007) present the typical steps (Figure 7.1) considered for the calibration and subsequent validation of the models mimicking natural systems, e.g. groundwater flow system. According to their approach, there are four major issues that need to be addressed to accomplish an effective calibration and validation venture. These are: (1) parameter definition or parameterisation; (2) selection of an appropriate objective function; (3) estimation of parameters; (4) quantitatively connecting parameters, observations, and predictions using the model.

Parameterisation is concerned with the identification of parameters most relevant to the overall objectives of the model. Generally, the numbers of possible parameters are enormous, as the natural systems are usually temporal as well as spatial in nature. However, the observations (measured data) are often very limited, therefore, it is essential to establish the minimum number of parameters that could satisfactorily define model inputs throughout the spatial and time domains.

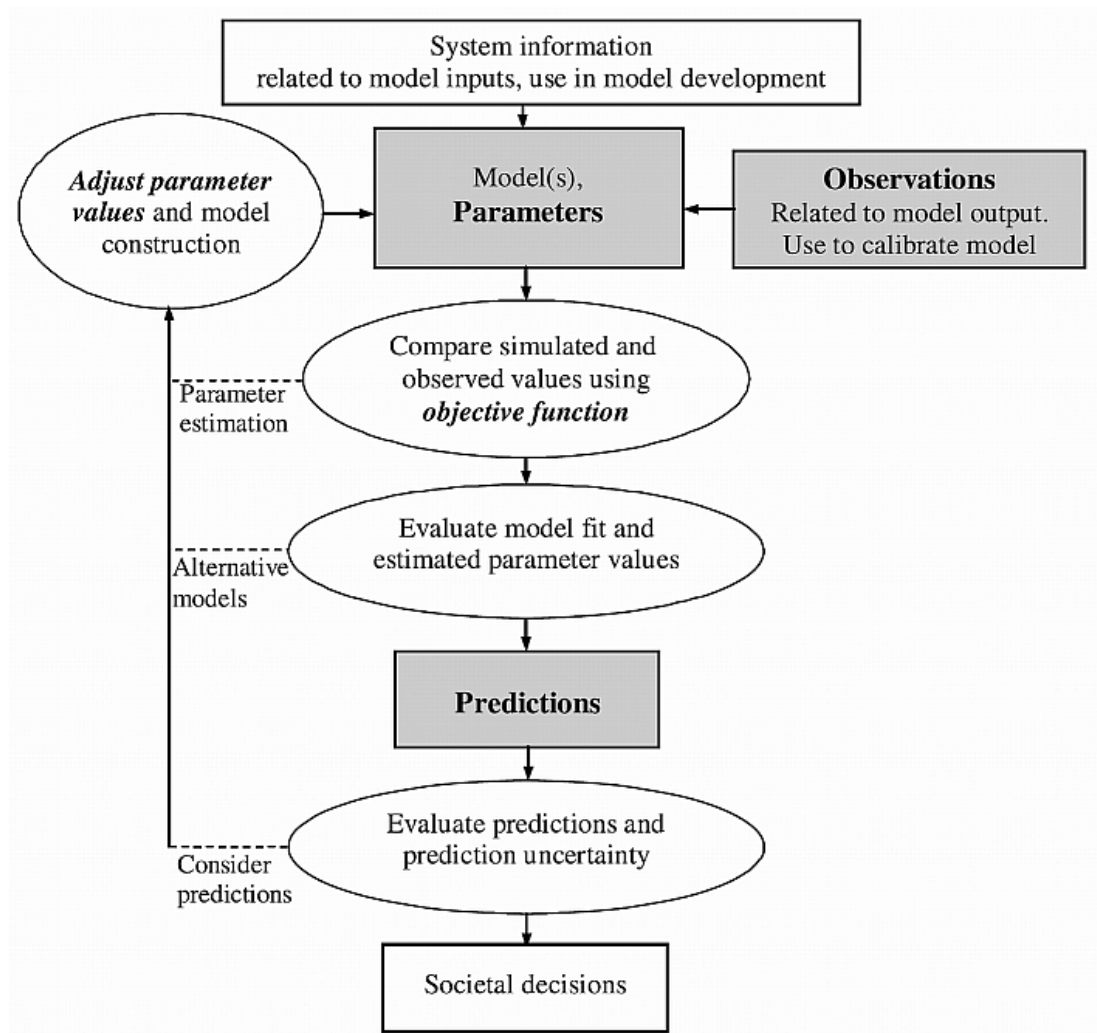


Figure 7.1. Flowchart showing the major steps of calibrating a model and using it to make predictions [Hill & Tiedeman 2007].

Objective functions, sometimes also called loss functions, are needed to compare the simulated and observed values in a quantitative manner. Most importantly, the combinations of parameter values producing the smallest value of the objective function are reckoned as the ‘best fit’. Typical objective functions include least

square (Rawlings et al. 1998), maximum-likelihood (Burnham & Anderson 2002), and L_1 norms (Menke 1989). The least square and its related functions are probably the most commonly used objective functions for regression and other optimisation analyses.

Parameter estimation may also be considered as an ‘optimisation problem’, wherein the parameter values are identified in a way that (usually) minimises the selected objective function. In general, there are several combinatorial values of the parameters that would produce similar small values of the objective function and it is necessary to identify those values that would produce the global minimum. This could be achieved using various optimisation techniques like the modified Gauss-Newton (Hartley 1961), simulated annealing (Laarhoven & Aarts 1987), genetic algorithms (Goldberg 1989), tabu search (Glover & Laguna 1997; Glover & Marti 2006), or shuffled complex evolution methods (Duan et al. 1992; Duan et al. 2006).

The model itself provides a **quantitative linkage** between the simulated system, measured field data and prediction. As a final step of calibration, it is important to evaluate overall fitness of the model to observed data using some statistical measures to compare the later with the predicted values. The typical statistical evaluations consider the magnitudes of residuals, correlation coefficients, objective function value, error variance, and standard error. Other methods graphically evaluate the fitness of the model such as weighted residual plots against weighted/un-weighted simulated values, minimum, maximum and average weighted residuals.

7.3 Calibration Procedure for SVH-Conflict Model

The discussions presented in §7.2, reveal insightful commonalities of the procedures used for the calibration of otherwise much diversified models of (relatively well established) engineering processes and (highly random) natural systems. In short, the typical steps for the calibration of a ‘grey-model’ should include:

- Establishing the model parameters required to be estimated.
- Selecting an appropriate objective function.

- Identifying the field data to be used for calibration purpose i.e. calibration data.
- Estimating the ‘best fit’ parameters using the calibration data that would minimise the objective function.
- Validating the calibrated model using the field data retained for the validation purpose.

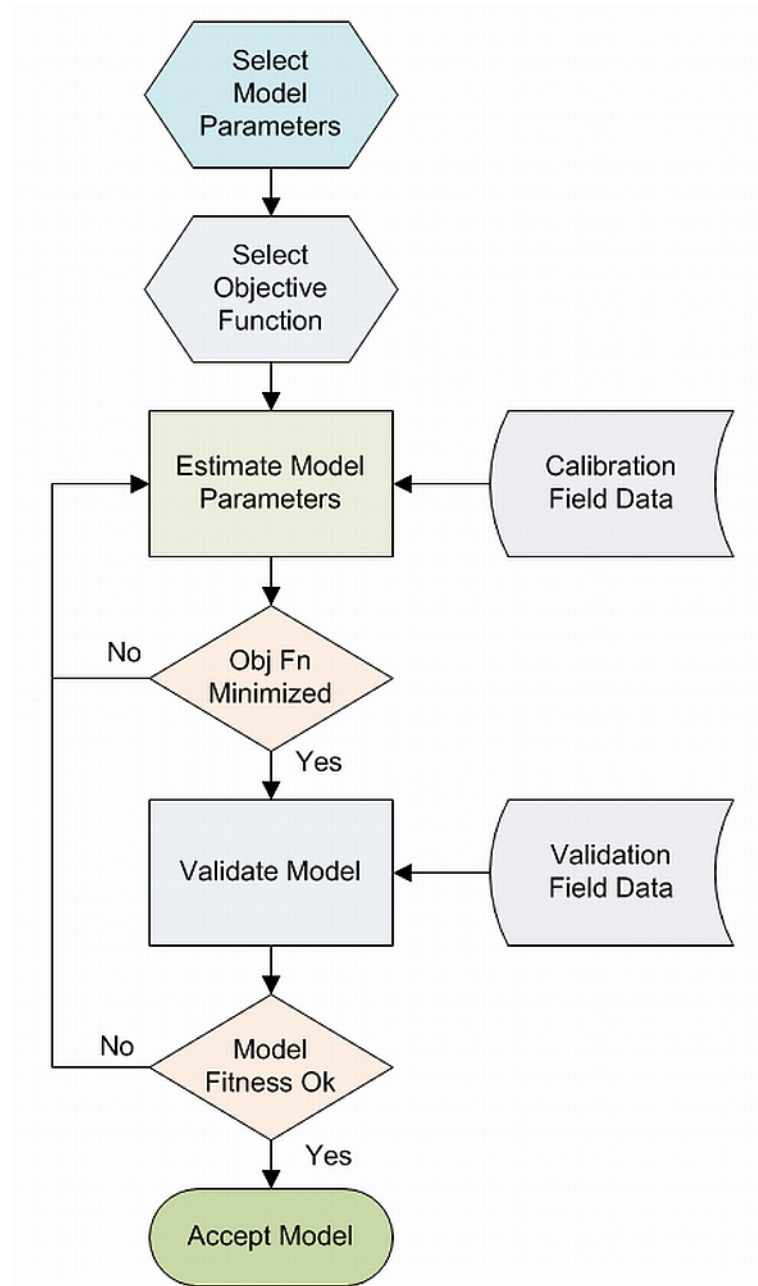


Figure 7.2. Schematic diagram of calibration procedure adopted for SVH-conflict model.

The procedure adopted for the calibration of SVH-conflict model is schematically depicted in Figure 7.2. Details of the calibration steps are presented in the following sections (§7.4 to §7.8), whereas, validation part of the procedure is covered in §7.9.

7.4 Selection of Model Parameters

As presented in §6.6, the SVH-conflict model comprises of two primary parts i.e. the ‘orientation or motion perception’ part (Figure 6.5) and the ‘emetic or sickness prediction’ part (Figure 6.10). The former simulates the vestibular system, its internal model and the relevant processing of sensory cues (implementation of physical laws) by the nervous system. The variable parameters of this part include: (1) time constants of the semicircular canals (τ_{sc}) and the low-pass filters (τ_{LPF}); (2) feedback gains for the canal afferent errors (K_{ω}), the SV-conflict (K_f) and the SH-conflict (K_h). Thus, in total there are five unknown parameters in the ‘orientation’ part that could be varied to optimise the performance of SVH-conflict model. However, as highlighted in §6.6, being an extended version of NAME’s SV-conflict model (§5.11), values of the parameters concerning SV-segment of the SVH-model are maintained as per Table 5.3. Thereby there is only one parameter, namely the feedback gain of SH-conflict (K_h), which requires estimation.

The ‘emetic or sickness prediction’ part is responsible for translating the sensory conflict, detected by the ‘orientation’ part, into percent vomiting incidences i.e. MSI (see §6.6.2). There are ten variable parameters in this part that could be adjusted to optimise the performance of SVH-conflict model. These are:(1) four shape parameters of the hill functions (n_v , b_v , n_h , & b_h) [see Equation(6.16)]; (2) two peak values of MSIs (K_{MSIv} & K_{MSIh}) (3) two time constants of the ‘leaky integrators’ (μ_v & μ_h); (4) a time constant of the low pass filter for SH-conflict (τ_{CH}).

The values of various parameters in the SV-conflict post-processing (emetic) path (n_v , b_v , K_{MSIv} , & μ_v) are retained in accordance with the SV-conflict model (see Table 5.3) to preserve the essential / proven features of this model. Hence, there is a need to identify the following parameters of various components dwelling in the emetic path of SH-conflict:

- The time constant of the low pass filter for SH-conflict i.e. τ_{CH} .
- The peak value of MSIs i.e. K_{MSIh} .
- The time constant of the ‘leaky integrator’ i.e. μ_H .
- The shape parameters of the hill function i.e. n_H , & b_H .

As mentioned earlier (§3.8.1 & §6.2), all laboratory experiments concerning elicitation of motion sickness due to the pure horizontal oscillations (Golding et al. 2001; Lobb 2001; Griffin & Mills 2002a; Donohew & Griffin 2004) suggest a decrease in sickness sensitivity to the motions for frequencies above 0.2Hz (1.26rad/sec). Therefore, the time constant of the SH-conflict LPF may be set equal to 0.79sec ($\tau_{CH}= 1/1.26 = 0.79$).

In order to keep the model simple, it was decided to use identical value of the peak MSI for the SH-conflict path as that of the SV-conflict path i.e. $K_{MSIv} = K_{MSIh} = 85\%$. The time constant of ‘leaky integrator’ μ_H was set as half the value of μ_V (i.e. 6min). This is in accordance with the findings of Golding et al.(1995) as they observed that the vertical oscillations, with frequency and magnitude identical to horizontal motions, require almost twice as exposure duration to reach similar sickness levels (see §6.2. Hence, there are only two parameters of the ‘emetic’ part that remain to be estimated and these are the shape parameters of the hill function (n_H , & b_H) [Equation(6.16)] of SH-conflict path.

Based on the above, appropriate values of the following three parameters of SVH-conflict model require estimation:

- The scalar feedback gain ‘ K_h ’ of the ‘orientation / motion perception’ part.
- Shape parameters ‘ b_{CH} ’ and ‘ n_{CH} ’ of the ‘emetic’ part.

7.5 Statistical Testing of Model Fitness

It is important to understand that passive motions induced by the movements of a ship (or as a matter of fact any means of transport e.g. cars, busses, aeroplanes etc.) are not enough to fully define the variability of motion sickness. We are dealing with

a sort of socio-physical scenario, where the personal characteristics of individuals play significant roles; the relevant factors have already been discussed at length in §3.4. The real passenger population aboard any vessel is expected to exhibit significant variations in these factors. Therefore, it would not be wise to directly compare the magnitude of MSI predicted by the SVH-conflict model with those observed onboard during the field trials. This comparison should be made using a statistical inferential technique, as presented in the following.

The SVH-conflict model predicts occurrence of motion sickness, which is dichotomous on an individual level (i.e. a person may or may not vomit). Although, this measure of motion sickness discounts other, perhaps equally important, feelings of malaise that precede this extreme event, but vomiting incidence is the only parameter that can be measured objectively. Besides, Lawther & Griffin (1986) and later Colwell (1994) report strong correlations between MSI (motion sickness incidence) and other subjective measures of motion sickness, such as illness ratings (IRs). Thus, with the assumption of independence of the individual emesis events, we may represent our variable of interest, i.e. MSI, using discrete binomial distribution. We, therefore, define the following two hypotheses for the statistical testing of the fitness of predicted values to the observed vomiting incidences:

H_0 : The proportion of passengers vomiting, observed during the field trial is not different from the value predicted by the SVH-conflict model.

H_1 : The proportion of passengers vomiting, observed during the field trial is different from the value predicted by the SVH-conflict model.

Since under moderate sea states we expect a small number of passengers to vomit, hence it is important to use the method of small *p-values* (SISA 2010) for estimating the significance level of two-tailed exact binomial test (McDonald 2008). However, before presenting the formulation used for testing the hypothesis outlined in above, it is imperative to understand how the exact binomial test of significance works as discussed in the next section.

7.5.1 Exact Binomial Test of Significance

As such the exact binomial test of significance is a nonparametric (no test statistics is needed to estimate the significance levels) exact probability test, based on the rules of probability (Garson 2008a). This test is used if the nominal variable in question is dichotomous in nature (e.g. MSI). The observed data (number of passengers actually vomiting) is compared with the expected (number of passengers likely to vomit, as estimated by the MSI model in question). In this test, the null hypothesis (H_0) is that the number of observations (from field trials) in each category (vomit and not-vomit) is equal to that predicted by a theory / model (e.g. MSI model). Consequently, the alternative hypothesis (H_1) suggests that the observed data (field trial) is different from the expected (MSI model) values.

In a binomial test, the exact binomial probability of getting 'r' observation in one category of dichotomy and '(n-r)' observations in other category with a sample size 'n' is calculated using the following expression:

$$p(r)_{binomial} = \frac{n! p^r (1-p)^{(n-r)}}{r!(n-r)!} \quad (7.1)$$

For example if the predicted MSI (using a model) is 10% and we find that 15 passengers out of the 100 returning questionnaire report emesis, then the probability of observing such a number of vomiting-passengers would be:

$$p(15)_{binomial} = \frac{100!(0.1)^{15} (0.9)^{85}}{15!85!} = 0.03268$$

For a single-sided exact test we will be interested in establishing the probability of observing all deviations from the null expectations (here 10) as large as, or larger, than the observed vomiting incidences (i.e. 15 or more). This is obtained by adding $p(15)_{binomial} + p(16)_{binomial} + \dots + p(100)_{binomial}$, resulting in a total of 0.07257. This

result at a 5% significance level, represents a non-significant observation i.e. the observed vomiting incidences are higher than the expected value by chance only.

However, according to the alternative hypothesis H_1 (the observed vomiting incidences are not equal to the predicted vomiting incidences) there could be as too few emesis events as too many (above the expected number). Therefore, we should employ the two-tailed test, which considers the probability of having a particular effect size (observed deviation from the expected value) either above or below the expectation. Here, the effect size is 5 (15-10) i.e. the number of emesis events more than the expected incidences. Thus, for a two-tailed exact binomial test we also need to calculate the probability of observing vomiting incidences of 4 or below, which is given by adding $p(4)_{binomial} + p(3)_{binomial} + \dots + p(0)_{binomial}$, giving a total of 0.02368 [It should be noted that $p(5)_{binomial}$ has not been considered here as its value (0.03387) is larger than $p(15)_{binomial}$, which represents a more likely or less extreme event]. Thus, the probability of observing 15 passengers getting motion sick in a sample of 100 participants returning questionnaire, with an (model) estimated MSI of 10% shall be $0.07257 + 0.02368 = 0.09625$ (9.6%), which is also not significant at 5% level.

According to the method of small p-values: “If the *p-value* of an individual alternative is smaller than the original *p-value* [corresponding to the observed event], this alternative is more different from the null hypothesis than the observed situation. To obtain the cumulative double-sided probability according to the method of small *p-values*, all *p-values* of alternative outcomes more different compared with the observed situation are accumulated and the sum gives you the result, the sum (cumulative probability!) of *p-value's* of all alternative outcomes the same or more different as the situation observed.” (SISA 2010)

7.5.2 Calculation of the Exact Binomial Test Significances (*p-values*)

Based on the above, the two-sided exact binomial test significance (*p-values*) in a sea trial where ‘*n*’ passengers reporting to have vomited out of the ‘*N*’ returning questionnaires, with a model estimates of ‘*p_{VI}*’ (proportion of people likely to vomit), shall be given by:

$$p = \sum_{k=0}^N B(k, N, p_{VI}) \quad \forall B(k, N, p_{VI}) \leq B(n, N, p_{VI}) \quad (7.2)$$

Where, $B(k, N, p_{VI})$ is the binomial probability mass function with ‘ k ’ success (vomiting incidences) in ‘ N ’ trials (peoples returning questionnaire) of a binomial distribution with theoretical proportion of p_{VI} . It is given by:

$$B(k, N, p_{VI}) = \frac{p_{VI}^k (1 - p_{VI})^{(N-k)} N!}{k!(N-k)!} \quad (7.3)$$

It should be noted that p -value given by Equation(7.2) is the probability of observing the recorded MSI, given the predicted value is statistically correct (i.e. erroneously rejecting H_0 for a given field trial). Therefore, assuming $p < 0.05$ as significant enough to support alternate hypothesis (H_1), Equation(7.2) may be used to decide whether the model statistically fits a given field trial or not. That is, if $p > 0.05$, then there is not enough evidence to reject H_0 and the difference between observed MSI and model prediction is attributable to variations of the susceptibility factors highlighted in §3.4. Thus, the larger the magnitude of p -value the better would be the statistical fitness of the model.

7.5.3 Accounting for the ‘Multiple Hypotheses Testing’

It is important to note that multiple full scale trials were undertaken aboard several vessels considered in this work. This would require testing of the null hypothesis (H_0) for several individual trials, leading to ‘multiple hypothesis testing’ scenario (Farcomeni 2008). Thus, it is not sufficient to verify validity of the model for the individual field trials only and a test must be carried out to check its suitability for the multiple trials of all considered vessels. This can be done using the Chi-square goodness-of-fitness test, where the test statistics suggested by Prof. McKenzie (2008), are:

$$\chi^2 = \sum_{i=1}^{N_{trials}} -2 \ln(p_i) \quad (7.4)$$

Where, p_i is the p -value of each field trial calculated using Equation(7.2) and N_{trials} is the total number of trials of the considered vessels. As such, p_i is the likelihood value calculated using Equation(7.2) for the i^{th} field trial. Therefore, the right hand side of Equation(7.4) represents the ‘log-likelihood’ (Kleinbaum et al. 2002) of observing the vomiting incidences during the multiple field trials.

Given the assumption that the ‘ideal’ model (100% accurate for all sea trials) will have a log-likelihood value of zero, the difference between the log-likelihood values of the ideal and actual (MSI model) represent the log-likelihood ratio statistics. The latter is an approximate chi-square statistics, which may be used to estimate the one-tailed probability of a chi-distribution with N_{trials} degrees of freedom. The resulting probability represents the model’s overall fitness p -value for the multiple trials of the considered vessels. Assuming $p_{overall} < 0.05$ to be significant, we may establish the goodness-of fit of the model to multiple field trials. Again, larger overall p -values would indicate better overall fitness of the model.

7.6 Selection of Objective Function

As discussed in §7.5, the output variable of our interest i.e. vomiting or motion sickness incidence is random and dichotomous in nature, which may be represented using discrete binomial distribution. Hence, one of the options would be to use the ‘Pearson chi-square’ or ‘G’ statistics of the calibration field trials as objective function and try minimising these to optimise model fitness. However, in most of the full scale trials, the expected (model estimate) proportion and the number of passengers vomiting are small (<5) and it would be inappropriate to use ‘Pearson chi-square’ or ‘G’ statistics as objective function.

Due to small values of the expected proportions of passengers likely to vomit, it is necessary that the ‘exact binomial’ test [Equation(7.2)] should be carried out to evaluate the statistical fitness of the model to the individual field trial (the relevant hypotheses are defined in 7.5). Once the p -values of individual field trials become known, the chi-square goodness-of-fit statistics for all full scale trials of the considered vessel(s) may be estimated using Equation(7.4). These statistics, in

conjunction with the chi-square distribution, would reveal the overall fitness of the model to multiple field trials of the given vessel(s).

Thus a rationale way of optimising the SVH-conflict model, while using the full scale trials' data of the selected vessel(s), would be to minimise the abovementioned chi-square statistics [Equation(7.4)]. Hence, the objective function $S(b)$ selected for the calibration of SVH-conflict model is:

$$S(b) = \sum_{i=1}^{N_{trials}} -2 \ln(p_i) \quad (7.5)$$

Where, p_i is the *p-value* of exact binomial test of each field trial [Equation(7.2)] and N_{trials} is the total number of full scale trials of the given vessel(s).

Minimising $S(b)$ shall increase the one-tailed probability of chi-square distribution with ' N_{trials} ' degrees of freedom i.e. the evidence against H_0 will become weaker; thereby promising a better fitness of model to the field trials. Since, the available field trials data are limited (see next section), hence, we had to be cautious to avoid indulging into 'over-fitness' issues. This is attempted by choosing coarse values for the parameters identified in §7.4 for model calibration.

7.7 Selection of Calibration Data

Considering the 'extra-motion' sources of MSI variability i.e. susceptibility (§3.4), an extensive series of laboratory experiments about the elicitation of sickness under pure horizontal oscillations would have provided a good set of calibration data for the SVH-Conflict model. This is because such experiments do exercise good control over some of the motion sickness susceptibility features like age, gender, past sickness history, activities, etc., that are otherwise impractical to control in the full scale trials of a real ship. However, there are some shortcomings associated with laboratory experiments; in that the controlled environments remain artificial and do not stimulate the psychological panic/fear experienced by a real passenger. Also the participants usually represent a somewhat biased sample as the susceptible

individuals seldom volunteer for such studies, while they would travel aboard a ship in the absence of otherwise choice. Moreover the recent laboratory experiments get enticed by the findings of past experiments and, sometimes, miss out the global picture.

One must realise that there are no strict professing of using either the laboratory experiment or the field trial data for the calibration / validation of a motion sickness model like ours. The latter are excellent source of revealing global behaviours, while the former are inevitable for identifying specific trends. Here, we are primarily interested in the global behaviour of general passenger population, so that the proposed model (SVH-conflict) may confidently be used for operational as well as vessel design purposes. It is important to realise that the inclination of a given passenger to become motion sick might be partly accounted for, by using the susceptibility functions such as the one proposed by Bos et al.(2007) [see Equation(3.17)]. However, such an adjustment would render the model much personalised and it may not be able to reflect the general population behaviour, which is of prime interest; especially during the design phases.

The rather limited series of laboratory experiments studying pure horizontal oscillations (Golding & Kerguelen 1992; Golding et al. 1995; Golding & Markey 1996; Golding et al. 1997; Golding et al. 2001; Lobb 2001; Griffin & Mills 2002a; 2002b; Donohew & Griffin 2004) induced sickness, have been extremely valuable for identifying the specific trends like the effects of magnitude and frequencies of oscillation [see Figure 3.23]. In the case of SVH-conflict model, the results of laboratory experiments have been integrated into the SH-segment by ensuring that the frequency response of SH-conflict mimics the laboratory findings (see Figure 6.7). Whereas, the full scale field trials' data has been used for the model calibration by estimating appropriate values of the unknown parameters identified in §7.4.

The full scale trials of the passenger ferries carried out by NAME at its own and being part of COMPASS project (§3.8) consortium, as well as other project partners, are summarised in Table 7.1. Due to the commercial sensitivities, the hullforms of

these vessels are not reproduced in this thesis, while their principal particulars presented in the table are approximate values. In all field trials the six degrees of freedom vessels' motion histories were logged. Survey questionnaire were distributed amongst the passengers enquiring about the comfort levels including the incidences of motion sickness. Further details of trials procedure are covered in §8.3.

Table 7.1: Summary of field trials used for the model calibration and subsequent validation.

Characteristics	Vessels							
	A	B	C	D	E	F	G	H
Hull form ¹	Cat	DV	MH	MH	Cat	Cat	WP	WP
L _{BP} (m)	120	130	160	163	33	37	90	90
Beam (m)	40	20	29	27	10	10	25	25
Draught (m)	4.5	3.5	7.0	6.5	2.0	2.0	3.5	3.5
Speed (Knots)	40	40	20	22	35	38	40	40
Passengers	800	1700	2500	2000	270	380	850	850
Cars	200	400	400	3600	Nil	Nil	200	200
Journey time (Hrs)	1.5- 2.0	2.0- 3.0	10.0- 16.0	14.75- 15	0.75- 3.50	1.5- 1.75	2.75- 3.75	3.0- 3.8
Operation Area ²	UK	GR	FI	IT	NO	GR	UK	UK
Total trips	2	4	3	6	24	4	16	4
Abbreviation used in the text	Cat- A	DV- B	MH- C	MH- D	Cat- E	Cat- F	WP- G	WP- H

¹ MH: Monohull, Cat: Catamaran, DV: Deep-V Monohull, WP: Wave Piercer;

² FI: Finland, GR: Greece, IT: Italy, NO: Norway, UK: United Kingdom)

It can be seen from the above table that the high speed catamaran vessel-E (Cat-E) has the largest number of field trials. However, little sickness (only one trip) was reported during the field study of this vessel; hence, its results were not considered for the calibration of SVH-conflict model. The other vessel with large number of trips is the wave piercer-G (WP-G). In this case, as summarised in Table 7.2, the vomiting incidences were reported in 13 out of the 16 trips; hence, the results of WP-G were employed to calibrate the SVH-conflict model.

Table 7.2: Summary of full scale field trials for WP-G

Trip	Total Replies	Vomiting Incidence	MSI%	Duration of Trial (HH:MM:SS)
1	58	1	1.72%	03:13:48
2	140	5	3.57%	02:43:44
3	48	3	6.25%	02:41:45
4	137	5	3.65%	03:14:08
5	38	2	5.26%	02:58:11
6	68	0	0.00%	02:46:03
7	114	0	0.00%	03:05:58
8.	109	3	2.75%	02:53:45
9	38	2	5.26%	03:33:12
10	64	6	9.38%	02:53:28
11	64	7	10.94%	02:49:00
12	64	2	3.13%	02:47:57
13	37	9	24.32%	03:45:56
14	45	5	11.11%	01:56:14
15	51	0	0.00%	03:03:10
16	100	1	1.00%	03:04:33

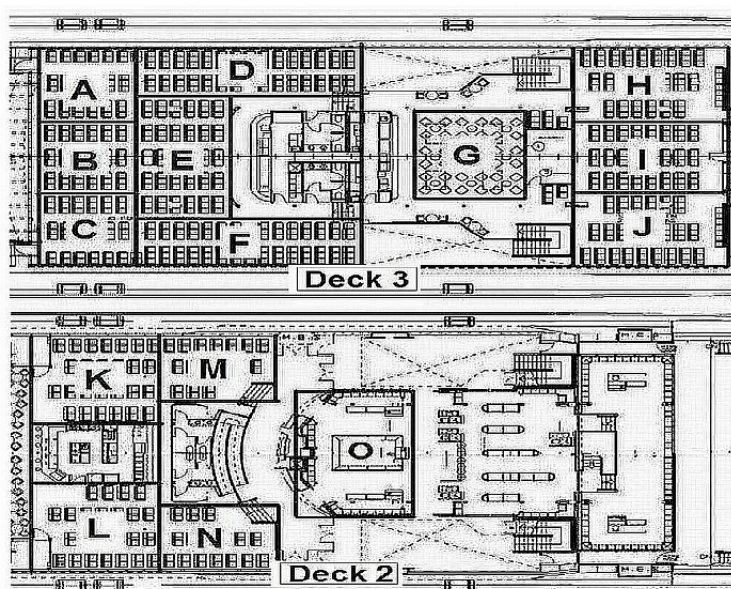


Figure 7.3. Passenger zones of WP-G.

As shown in Figure 7.3, the passenger areas aboard WP-G were divided into 14 zones to account for the lever-arm effects of the rotations (roll, pitch & yaw) onto the absolute (longitudinal, lateral and vertical) motions. The numbers of passengers reporting emesis in each zone were, however, quite low. Therefore, the overall incidences of motion sickness during a particular voyage has been calculated as a ratio of the total number of people reporting sick to the total number of passengers returning the questionnaires.

According to McDonald (2008) a sample size of at least 1000 is necessary for Pearson chi-square or G-test to produce *p-values* closer to exact binomial test. It can be seen from Table 7.2 that in all sea trials, the number of replies are far below this number (i.e. 1000). Hence, as already mentioned in §7.5, it is imperative to carry out exact binomial test to verify the fitness of SVH-conflict model to the observed results.

7.8 Estimation of Model Parameters

This section presents the methodology adopted for the estimation of the unknown model parameters identified in §7.4. Firstly, the motion and survey data available from the field trials of the WP-G are presented. Thereafter, the procedure used for estimating the optimized values of the parameters is discussed.

7.8.1 Available Field Trial Data

Field trial procedures of all the vessels tabulated in Table 7.1 had been similar, which has also been adopted for the further validation trials carried out solely for this study (see Chapter 8). Briefly, in all full scale trials of WP-G, the motion histories of the vessel were recorded using a motion reference unit (MRU). While, the survey questionnaire similar to the one developed in COMPASS project (§3.8) were employed to collect comfort related information from the passengers, including the vomiting incidences.

7.8.1.1 Motion Histories

The motion histories comprise of the following being measured at the installation location of MRU, at a sampling frequency of 10Hz. The detailed specifications of MRU are presented in Appendix D:

- Linear inertial acceleration in the longitudinal (G-x), lateral (G-y) and vertical (G-z) directions with respect to body frame of reference (assumed to be fixed at the ship's centre of gravity) shown in Figure 7.4. The software interface of MRU duly compensates the measured linear accelerations for parasitic gravity components (equivalence principle) resulting from the attitude changes.
- Angular (roll, pitch, and yaw) accelerations and velocities about the body frame of reference.

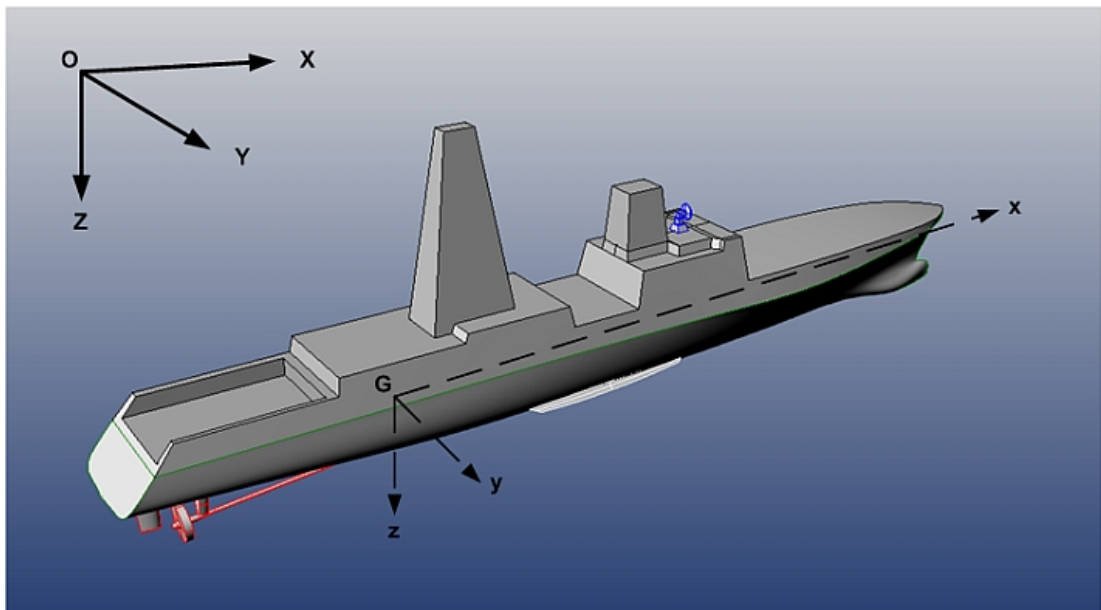


Figure 7.4. Inertial (OXYZ) and body (Gxyz) frame of references for the vessel motions.

MRU measures the rotational velocities using the three, orthogonally arranged, Coriolis-force based angular rate sensors. While, the linear accelerations are sensed using the three pendulum-type accelerometers (also orthogonal to each other). The unit is capable of measuring absolute angular velocities and dynamic (relative) linear accelerations of the vessel. All other kinematics of interest are numerically derived

by integrating or differentiating these six variables, (physically) measured in the appropriate frame of reference.

By assuming the ship to be a rigid body, i.e. ignoring any flexural deformations, and knowing the vessel kinematics at MRU location, the linear accelerations at any position of interest (e.g. passenger-zone centres) may be calculated using (Huston & Liu 2001):

$$\mathbf{a}_p = \mathbf{a}_{\text{mru}} + \boldsymbol{\alpha} \times \mathbf{r} + \boldsymbol{\omega} \times (\boldsymbol{\omega} \times \mathbf{r}) \quad (7.6)$$

Where, \mathbf{a}_p is the linear accelerations vector (in m/sec^2) for position P; \mathbf{a}_{mru} is the linear acceleration vector (in m/sec^2) for MRU installation location; $\boldsymbol{\alpha}$ is the angular acceleration vector (in rad/sec^2); $\boldsymbol{\omega}$ is the angular velocity vector (in rad/sec) and \mathbf{r} is the relative position vector (in m) directed from MRU to the remote location of interest.

The SVH-conflict model (see Figure 6.5) only uses the three orthogonal linear accelerations and rotational velocities as input. However, the angular accelerations were also recorded, so as to be able to calculate the vessel motions (in particular the linear accelerations as the rotational velocities do not change with position) at the positions of interest by using Equation(7.6). In all the cases, the unit was installed away from the passenger area to avoid any unnecessary tempering.

The motion histories of all voyages are available for a single point (the MRU installation point) aboard WP-G and Equation(7.6) could easily be used to estimate these for, virtually, any point aboard WP-G. However, following the standard procedure of seakeeping analyses, the passenger areas were grouped into zones (Figure 7.3). It was then assumed that the passive motions experienced by the (presumably) seated passengers are those of their corresponding zone-centres. Thus, the linear accelerations were calculated for the zone-centres during each voyage.

7.8.1.2 Passenger Replies

Details of the survey questionnaire enquiring (dis)comfort experience of the passenger are given in §8.3.1. In short, the questionnaire comprises of various ‘tick-box’ type questions, aiming to collect the following information about the personal characteristics (from susceptibility view point) and voyage (sickness) experience of the passengers:

- Age and gender.
- Onboard location.
- Activities undertaken during the journey.
- Use of alcohol.
- Feelings of motion sickness.
- Illness ratings.
- Time aspects of sickness.
- Use of anti-sickness medications.
- Regularity of travel.
- Sickness history.
- Sitting comfort (other than sickness).
- Steadiness while standing or walking.
- Discomfort in executing various mundane tasks.
- Most significant sources of discomfort.
- Comfort expectations.
- Comfort satisfaction.
- Fatigue.
- Enjoyment.

The question related to the feelings of motion sickness is in line with the misery scale, MISC, developed at TNO (Bles et al. 1991; de Graaf et al. 1992; Wertheim et al. 1992; Wertheim et al. 1995; Colwell 2004; Colwell et al. 2008). However, for the calibration purposes, only the part of this question related to emesis has been used in

this work. The statistical analyses of other comfort entities have already been covered in COMPASS project (Turan 2006).

Though, the dispersion of passengers returning the questionnaire may be established to some extent (not all passengers indicated their onboard position). However, this distribution may not be appropriate for the larger passenger population onboard. Being a voluntary participation, it is not feasible to get the feedback from every individual. In addition, such a scattering of passenger would not be known during the design stages; hence, one way round this issue is to assume equal number of passengers in all zones. This means the sickness predicted for each zone, using its motion history, should then be averaged to estimate the overall sickness level of a given voyage.

7.8.2 Selection of Parameter Values

SVH-conflict model is an attempt to simulate a highly random phenomenon, which is known to be influenced by many factors (§3.4 & §3.8.2) other than the vessel motions. These factors themselves display significant variation amongst the general passenger population. Hence, a large field trial database accompanied by extensive laboratory experiments would be needed to identify and modulate the physiological model by incorporating the effects of these factors. Nevertheless, it is still possible to estimate the unknown parameters identified in §7.4, that would allow the model (§6.6) to predicted vomiting incidences with reasonable statistical accuracy for a general population of ferry commuters.

However, due to the availability of limited field trial data, we have to carefully avoid any over-fitting of the model. For this reason, a range of pilot searches were carried out wherein various values of the unknown parameters were considered and corresponding model fitness to the calibration as well validation field trial data were tested. The results of aforesaid pilot searches are not reproduced here to control the volume of this work. Moreover, the model itself has evolved through a large number of generations, hence not all pilot searches are applicable to the version presented in this work.

In short, the coarse values of the unknown parameters given in Table 7.3 were considered for the full factorial optimization searches.

Table 7.3: Values of unknown parameters considered for searches.

S.No.	Mode Part	Description	Values Considered
1.	Orientation/ Motion Perception	Scalar feedback gain ' K_h '	1/12, 1/11, 1/10, 1/9, 1/8, 1/7, 1/6, 1/5, 1/4, 1/3, 1/2, 1, 2, 3, 4, 5, 6, 7, 8, 9, 10, 11, 12
2.	Emetic	Shape parameter of hill function ' b_{CH} '	0.5, 1.0, 1.5, 2.0, 2.5, 3.0, 3.5
3.	Emetic	Shape parameter of hill function ' n_{CH} '	0.5, 1.0, 1.5, 2.0, 2.5, 3.0, 3.5

It is worth noting that:

For K_h : Since K_h is the scalar feedback gain of the SH compensator. Traditionally, integral values are selected for this gain in control engineering. Therefore, integers and their reciprocals were considered here.

For b & n : The values for SV hill function parameters are already known and it was assumed that the parameters of SH hill function would be in close proximity of the former. Therefore, the values chosen for these parameters are primarily influenced by the SV-hill function parameters.

The reason for using equidistant values was to avoid over-fitting to WP-G trials as the exact behaviour of SH-conflict is not known. A possible alternative would have been to use some sort of genetic algorithms for optimising the parameters. However, this option was not chosen due to the time consuming calculations involved in predicting motion sickness events for the sixteen trials of WP-G.

7.8.3 Procedure used for the Parameter Estimation

The methodology adopted to search for the optimized values of the unknown model parameters (§7.4) may be divided into the sequence of following steps/phases.

7.8.3.1 Step-1: Filtering of Motion History

As discussed in §3.7 (for vertical motions) and §6.2 (for horizontal motions), human beings exhibit a decline in the (sickness) sensitivity to linear accelerations with frequencies above 0.2Hz. However, despite all measures (e.g. careful selection of onboard location, installation arrangements, analog filtering by MRU), it is not practically feasible to eliminate registering of high frequency vibrations by the MRU. The primary sources of such vibrations include but not limited to the, (1) main machinery, (2) auxiliary machinery, (3) wave slamming, (4) wave impacts on side hulls, (5) wave impacts on box structure etc. In addition, as depicted in Figure 7.5, it was observed that the unit displays some DC and/or low frequency shifts in the raw motion histories recorded at MRU position (probably due to the errors in physical installation).

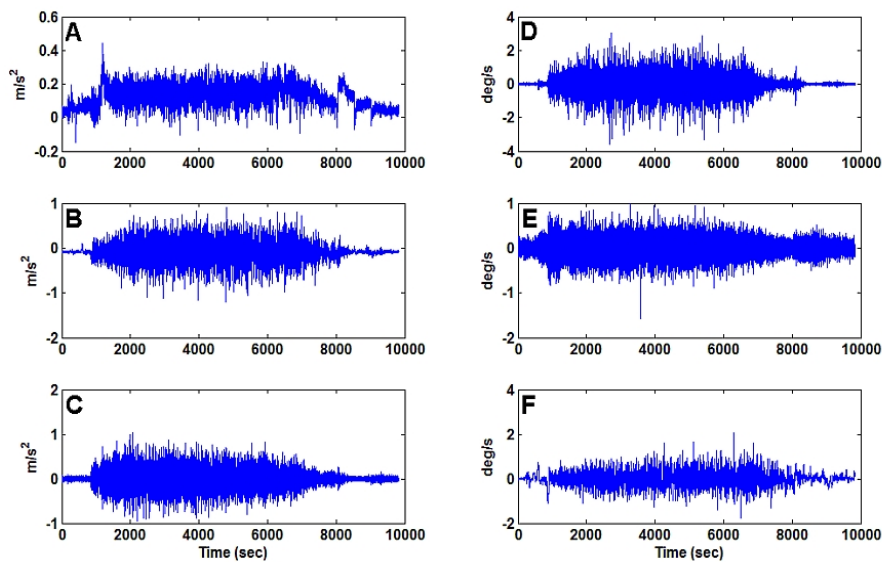


Figure 7.5. Raw motion history of WP-G at MRU position during Trip-1; linear accelerations (A) longitudinal (B) lateral (C) vertical; angular velocities (D) roll (E) pitch (F) yaw.

It was, therefore, decided to filter the raw motion histories before being used to estimate the motions of the individual zones (Figure 7.3).

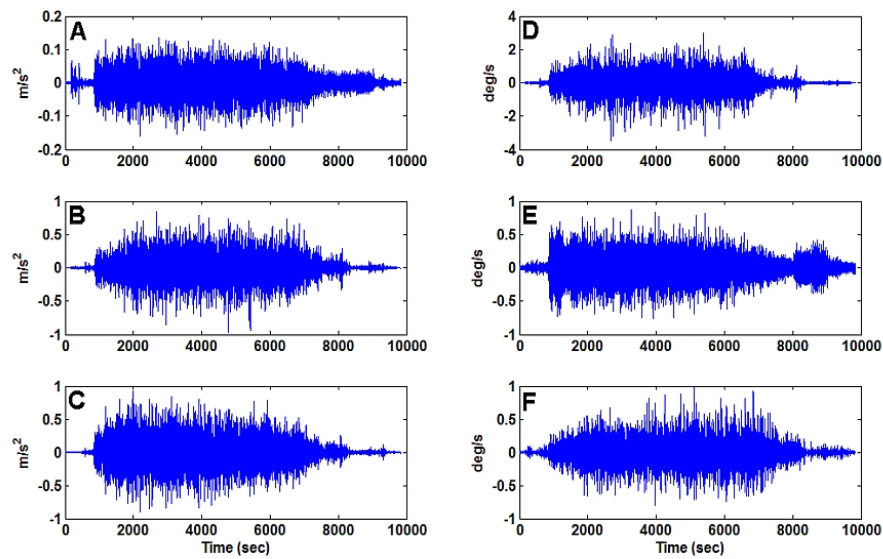


Figure 7.6. Filtered motion history of WP-G at MRU position during Trip-1; linear accelerations (A) longitudinal (B) lateral (C) vertical; angular velocities (D) roll (E) pitch (F) yaw.

Firstly, the recorded raw data was digitally filtered using a third order Butterworth high pass filter (Smith 2003) with a corner frequency of 0.05Hz. Thereafter, the motion histories were filtered using a third order Chebyshev low pass filter (Karris 2008) with a cut off frequency of 1.0Hz. It is worth highlighting that the peak frequencies of typical rigid body motions of real vessels lie within the decade 0.1 to 1.0Hz (Guignard & McCauley 1990). These digital filtering processes were implemented in MATLAB[®] by using the ‘**butter**’ and ‘**cheby1**’ functions. The filtered motion histories corresponding to the raw data plotted in Figure 7.5 are shown in Figure 7.6

It should be noted that the high pass filtering eliminates the gravitational accelerations from the raw data. These components are, therefore, added to the raw data before being used by the model using:

$$\begin{aligned}
\mathbf{f}_b &= \mathbf{a}_b + \mathbf{R}^T \mathbf{g}_G \\
\begin{bmatrix} f_x \\ f_y \\ f_z \end{bmatrix} &= \begin{bmatrix} a_x \\ a_y \\ a_z \end{bmatrix} + \begin{bmatrix} \cos \psi \cos \theta & \sin \psi \cos \theta & -\sin \theta \\ \cos \psi \sin \theta \sin \phi - \sin \psi \cos \phi & \sin \psi \sin \theta \sin \phi + \cos \psi \cos \phi & \cos \theta \sin \phi \\ \cos \psi \sin \theta \cos \phi + \sin \psi \sin \phi & \sin \psi \sin \theta \cos \phi - \cos \psi \sin \phi & \cos \theta \cos \phi \end{bmatrix} \begin{bmatrix} 0 \\ 0 \\ g \end{bmatrix} \\
\begin{bmatrix} f_x \\ f_y \\ f_z \end{bmatrix} &= \begin{bmatrix} a_x \\ a_y \\ a_z \end{bmatrix} + \begin{bmatrix} -g \sin \theta \\ g \cos \theta \sin \phi \\ g \cos \theta \cos \phi \end{bmatrix} \tag{7.7} \\
\begin{bmatrix} f_x \\ f_y \\ f_z \end{bmatrix} &= \begin{bmatrix} a_x - g \sin \theta \\ a_y + g \cos \theta \sin \phi \\ a_z + g \cos \theta \cos \phi \end{bmatrix}
\end{aligned}$$

Where, \mathbf{f}_b and \mathbf{a}_b are respectively the gravitoinertial and inertial accelerations in body frame of reference. While, \mathbf{g}_G is the gravitational accelerations in the Earth-fixed frame of reference and \mathbf{R}^T is the inverse of rotational transformation matrix with ϕ , θ , and ψ being the Euler roll and pitch angles (also recorded using MRU).

A clear difference can be seen between the raw and filtered motion histories in terms of signal mean values and high frequency components. The graphs depicting raw and (corresponding) filtered motion histories' for the remaining fifteen trips of the WP-G are given in Figure A.1.1 to Figure A.1.15 of Appendix A.

7.8.3.2 Step-2: Calculation of Passenger Zone Motions

The filtered motion histories of MRU were used to estimate the linear accelerations at the centres of passenger zones (Figure 7.3) by using Equation(7.6). The relative position vectors of these passenger zones, originating from the unit's installation location are given in Table 7.4. The sign conventions used for the calculation of these vectors are as per the body reference axes shown in Figure 7.4

The sample linear acceleration histories for zone A, during the first field trial of the WP-G are depicted in Figure 7.7(G to I). This figure (A to F) is also showing the corresponding motion records of the MRU position for comparison purposes. A significant influence of pitch motions (E) is visible on the linear longitudinal (G) and vertical (I) accelerations at zone A. Furthermore, the lateral accelerations (H) at zone A are also displaying the effects of roll (D) and yaw (F) motions.

Table 7.4: Relative position vectors \mathbf{r} (meters) of WP-G's passenger zones.

Zone	r_x	r_y	r_z
A	-36.2	-8.0	-6.2
B	-36.2	0.0	-6.2
C	-36.2	8.0	-6.2
D	-25.2	-9.0	-6.2
E	-28.2	0.0	-6.2
F	-25.2	9.0	-6.2
G	-11.2	0.0	-5.2
H	0.0	-8.0	-5.2
I	0.0	0.0	-5.2
J	0.0	8.0	-5.2
K	-36.2	-8.0	-3.2
L	-36.2	8.0	-3.2
M	-26.2	-9.0	-3.2
N	-26.2	9.0	-3.2
O	-20.2	0.0	-3.2

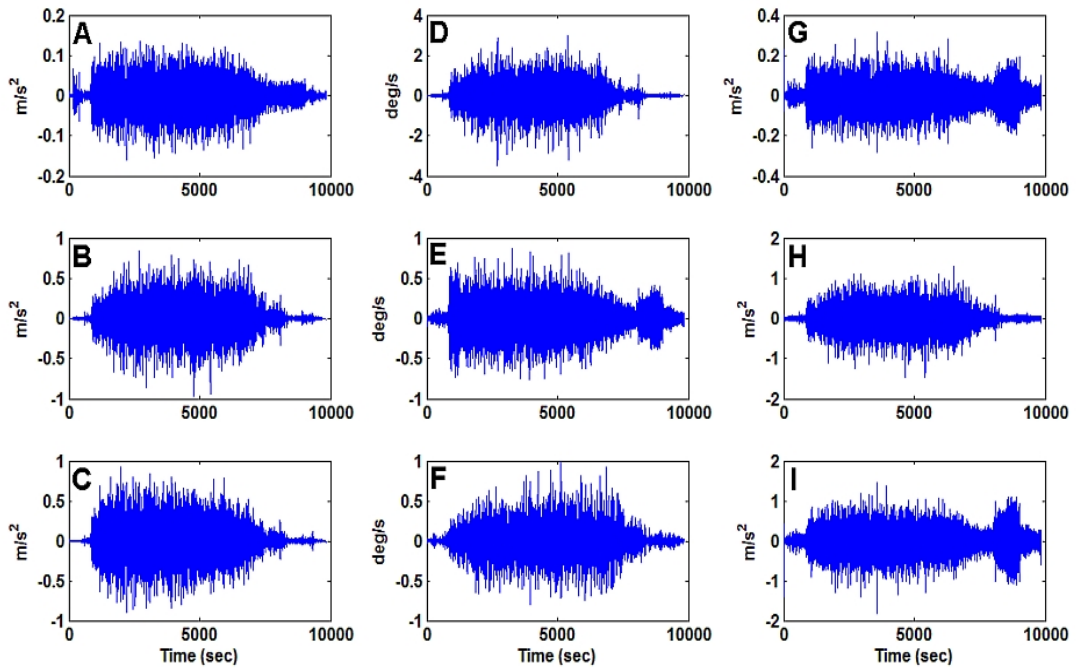


Figure 7.7. Motion history of WP-G during Trip-1 at MRU; linear accelerations (A) longitudinal (B) lateral (C) vertical; angular velocities (D) roll (E) pitch (F) yaw; and Zone-A; linear accelerations (G) longitudinal (H) lateral (I) vertical.

The calculated motion histories of other zones and trips of WP-G are not reproduced in this work to save on space.

7.8.3.3 Step-3: Calculation of Motion Sickness Incidences

The SVH-conflict model has been developed in SIMULINK[®]; which is the companion software of MATLAB[®] by The MathWorks[™] USA. This software is very convenient for the time domain realisation of dynamic systems/models. In this step, for each combination of the parameter values given in Table 7.3, the SVH-conflict model was run to estimate MSIs for all zones (Figure 7.3). This was done for all sixteen field trials of the WP-G (Table 7.1). The motion histories of each zone (§7.8.3.2) were fed into SIMULINK[®] that numerically solves the SVH-conflict model using the ‘variable-step’, ‘Dormand and Prince’ (Dormand & Prince 1980; 1986; Dormand et al. 1987) ODE solver.

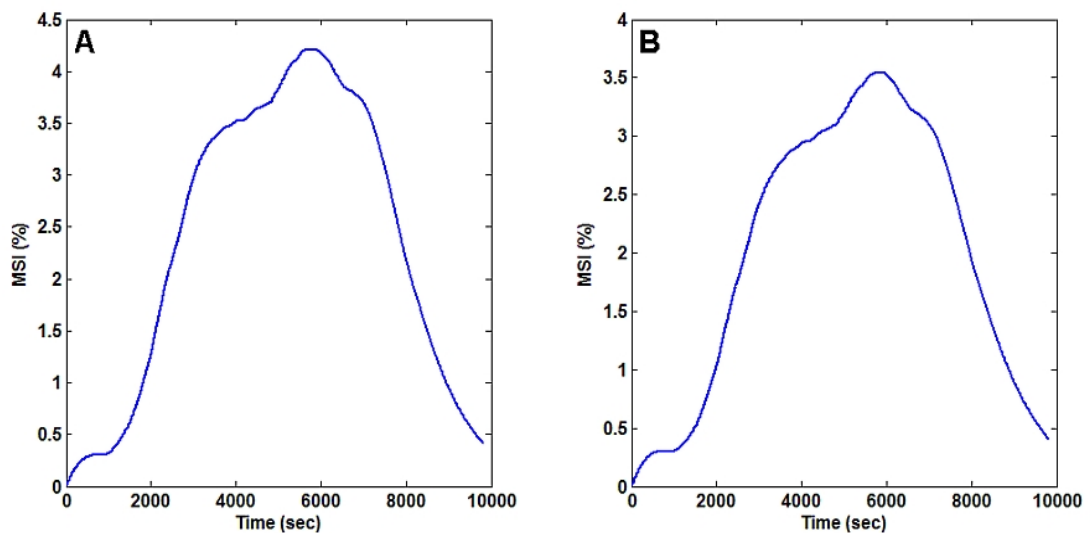


Figure 7.8. Predict MSI for zone A during the WP-G Trip-1 ($K_h = 1/2$, $b_{CH} = 1.5$, $n_{CH} = 2.0$); (A) simple sum (B) Pythagoras approach.

It is important to note that the MSI components, related to SV and SH-conflicts, were combined together in two different ways (see §6.6.2): (1) direct addition of MSI_V and MSI_H ; (2) Pythagoras-type approach i.e. using Equation(6.19). Depending on the severity of vessel motions, the output of SVH-conflict model varies with time as depicted in Figure 7.8. The maximum value of the predicted (total) MSI was taken as

the cumulative sickness level of a given passenger zone. Whereas, the overall incidences of motion sickness for a specific field trial were calculated by averaging out the zone-values (see also §7.8.1.2).

Table 7.5: Overall MSI (simple sum), for the various combinations of hill function shape parameters and $K_h = 1$, during the WP-G Trip-1.

b_{CH}	n_{CH}						
	0.5	1	1.5	2	2.5	3	3.5
0.5	28.63%	17.15%	11.42%	8.59%	7.14%	6.37%	5.95%
1.0	23.35%	11.82%	7.64%	6.17%	5.63%	5.43%	5.35%
1.5	20.68%	9.80%	6.59%	5.68%	5.42%	5.33%	5.30%
2.0	18.97%	8.73%	6.14%	5.51%	5.35%	5.31%	5.30%
2.5	17.77%	8.07%	5.90%	5.43%	5.33%	5.30%	5.29%
3.0	16.84%	7.62%	5.76%	5.39%	5.32%	5.30%	5.29%
3.5	16.09%	7.30%	5.66%	5.36%	5.31%	5.29%	5.29%

Table 7.6: Overall MSI (Pythagoras-type approach), for the various combinations of hill function shape parameters and $K_h = 1$, during the WP-G Trip-1.

b_{CH}	n_{CH}						
	0.5	1	1.5	2	2.5	3	3.5
0.5	24.11%	13.07%	8.14%	6.25%	5.61%	5.40%	5.33%
1.0	18.92%	8.44%	5.79%	5.37%	5.30%	5.29%	5.29%
1.5	16.35%	6.97%	5.45%	5.31%	5.29%	5.29%	5.29%
2.0	14.73%	6.32%	5.36%	5.30%	5.29%	5.29%	5.29%
2.5	13.59%	5.98%	5.33%	5.29%	5.29%	5.29%	5.29%
3.0	12.73%	5.79%	5.31%	5.29%	5.29%	5.30%	5.29%
3.5	12.06%	5.66%	5.31%	5.29%	5.30%	5.29%	5.29%

Table 7.5 is presenting a sample of the predicted overall MSIs (averaged over 14 zones) for the first trip of WP-G, wherein zone (MSI) values have been calculated by the simple addition of MSI components. Table 7.6, on the other hand, is depicting corresponding results for the Pythagoras-type approach [Equation(6.19)]. In both the

cases, the scalar feedback gain (K_h) has a value of 1 with various combinations of hill function shape parameters. Similar tables, are given in Appendix A as Table A.2.1 to Table A.2.30 for all combinations of the unknown parameters (Table 7.3) and remaining (15) field trials of WP-G.

7.8.3.4 Step-4: Calculation of Statistical Fitness for the Individual Trials

As discussed in §7.5, MSI may be treated as dichotomous random variable and represented using the binomial distribution. The observed proportions of passengers reporting emesis during the full scale trials of WP-G (see Table 7.2) are mostly small. Thus, as explained in §7.5, for small proportions the two-tailed exact binomial test (McDonald 2008) should be carried out to check the fitness of model predictions to the actual values. In this step, Equation(7.2) has been used to calculate the *p-values* of exact binomial tests.

For example, the MSI% observed during the first filed trial of WP-G is 1.72% (see Table 7.2). Now, considering the predicted magnitudes of overall MSIs given in Table 7.5, the *p-values* for these MSI estimates would be as given in Table 7.7. Likewise, Table 7.8 is depicting the corresponding *p-values* for the model predictions presented in Table 7.6.

Table 7.7: Exact binomial test *p-values* for the predicted overall MSIs (simple sum), under various combinations of hill function shape parameters and $K_h = 1$, for the WP-G Trip-1.

b_{CH}	n_{CH}						
	0.5	1.0	1.5	2.0	2.5	3.0	3.5
0.5	0.000	0.000	0.012	0.060	0.127	0.183	0.263
1.0	0.000	0.013	0.131	0.266	0.382	0.376	0.374
1.5	0.000	0.042	0.184	0.262	0.376	0.374	0.373
2.0	0.000	0.060	0.266	0.378	0.374	0.374	0.373
2.5	0.000	0.088	0.262	0.376	0.374	0.373	0.373
3.0	0.001	0.130	0.262	0.375	0.374	0.373	0.373
3.5	0.001	0.128	0.262	0.374	0.373	0.373	0.373

Table 7.8: Exact binomial test *p-values* for the predicted overall MSIs (Pythagoras-type approach), under various combinations of hill function shape parameters and $K_h = 1$, for the WP-G Trip-1.

b_{CH}	n_{CH}						
	0.5	1.0	1.5	2.0	2.5	3.0	3.5
0.5	0.000	0.005	0.089	0.268	0.381	0.375	0.374
1.0	0.000	0.091	0.262	0.375	0.373	0.373	0.373
1.5	0.001	0.188	0.376	0.373	0.373	0.373	0.373
2.0	0.002	0.270	0.375	0.373	0.373	0.373	0.373
2.5	0.004	0.263	0.374	0.373	0.373	0.373	0.373
3.0	0.005	0.262	0.374	0.373	0.373	0.373	0.373
3.5	0.008	0.262	0.373	0.373	0.373	0.373	0.373

It can be seen from above tables that certain combinations of the hill function shape parameters render the model predictions as significant; while others are favourable towards H_0 . Briefly, once the predicted values of MSIs become known (§7.8.3.3) for all combinations of parameters (Table 7.3), these are then used to calculate exact binomial test *p-values*. The latter are as summarized in

Table A.3.1 to Table A.3.30 of Appendix A for the remaining (15) field trials of WP-G. It can be seen from Table A.3.13 & Table A.3.14 that the *p-values* of full scale trial No.7 remain highly significant ($\ll 0.05$) for all combinations of hill function shape parameters. It is interesting to note that none of the other sickness prediction models (§7.10) considered for comparison with the SVH-conflict model, is fitting this specific trial of WP-G.

A closer look at trial No.7 reveals that 21.05% passengers did report ‘nausea’ but none reported emesis. A possible reason for this could be an early completion of questionnaire i.e. before the actual vomiting incidence occurred. Moreover, the eye account of the trip by the researcher engaged in carrying out this particular field trial also suggested otherwise, as they did observe signs of vomiting in the toilets. This could mean that the passengers who did vomit may not have participated in the

survey in the first place, due to the melancholy they suffered. Thus, the results of field trial No.7 of WP-G have not been used for the calibration of SVH-conflict model.

7.8.3.5 Step-5: Calculation of Objective Function

In this phase, the *p-values* of exact binomial test calculated in the previous step (§7.8.3.4) were used to determine the magnitudes of objective function [Equation(7.5)] discussed in §7.5. It is important to note that the *p-values* are calculated on individual trial basis for all combinations of the unknown parameters. Whereas, the objective function is estimated using the *p-values* for the fifteen trials of the WP-G (trial No.7 excluded, see §7.8.3.4). All combinations of the unknown parameters specified in Table 7.3, and the two approaches of estimating total MSIs (i.e. simple sum or Pythagoras-type approach, §7.8.3.3), have been taken into account for calculating the magnitudes of objective function.

A sample table presenting the magnitudes of the objective function [Equation(7.5)] for $K_h=1$ and the various combinations of hill function shape parameters (b_{CH} and n_{CH}), while the total MSI is a simple sum of its components, is given below:

Table 7.9: Magnitude of the objective function for $K_h=1$, while the total MSI being calculated as simple sum (minimum value in bold).

b_{CH}	n_{CH}						
	0.5	1.0	1.5	2.0	2.5	3.0	3.5
0.5	447.182	197.580	95.381	55.860	37.857	30.386	25.872
1.0	320.218	94.179	34.713	25.204	22.912	23.187	23.358
1.5	256.710	60.713	25.333	24.733	22.770	24.306	24.430
2.0	224.276	44.958	23.099	23.566	24.255	24.431	24.487
2.5	199.384	35.588	22.733	23.212	24.371	24.476	24.500
3.0	180.212	31.861	24.312	23.400	24.427	24.489	24.510
3.5	166.106	27.449	23.868	24.248	24.458	24.501	24.511

Similarly, the values of objective function for $K_h=1$ and the various combinations of hill function shape parameters (Table 7.3), while the total MSI is being calculated

using the Pythagoras-type approach [Equation(6.19)], are given in Table 7.10. Additional tables presenting the magnitudes of the objective function for all considered values of the parameters (Table 7.3) are tabulated in Table A.4.1 to Table A.4.44 of Appendix A.

Table 7.10: Magnitude of the objective function for $K_h=1$, while the total MSI being calculated using Pythagoras-type approach (minimum value in bold).

b_{CH}	n_{CH}						
	0.5	1.0	1.5	2.0	2.5	3.0	3.5
0.5	346.559	123.969	45.991	26.404	23.330	23.441	23.658
1.0	232.566	46.780	22.020	23.291	24.423	24.490	24.509
1.5	181.875	27.726	23.187	24.426	24.501	24.514	24.514
2.0	152.070	23.753	23.645	24.487	24.513	24.514	24.517
2.5	130.431	21.090	24.292	24.503	24.512	24.518	24.514
3.0	115.439	22.776	24.397	24.509	24.514	24.513	24.517
3.5	104.683	22.708	24.440	24.513	24.516	24.516	24.515

7.8.4 Identification of the Optimised Parameter Values

As discussed in §7.5, the optimised values of the parameters should result into minimisation of the selected objective function [Equation(7.5)]. The calculated values of this function may be seen in Table A.4.1 to Table A.4.44 of Appendix A. Table 7.11 in the following is summarising the minimum values of the objective functions for all (considered) values of the feedback gain (K_h) and the appropriate (leading to minimisation) combinations of the hill function shape parameters (n_{CH} and b_{CH}).

This table is also depicting the overall P-value of the chi-square goodness-of-fit test for the 15 filed trials of WP-G. The graphical representation of the contents of Table 7.11 is shown in Figure 7.9.

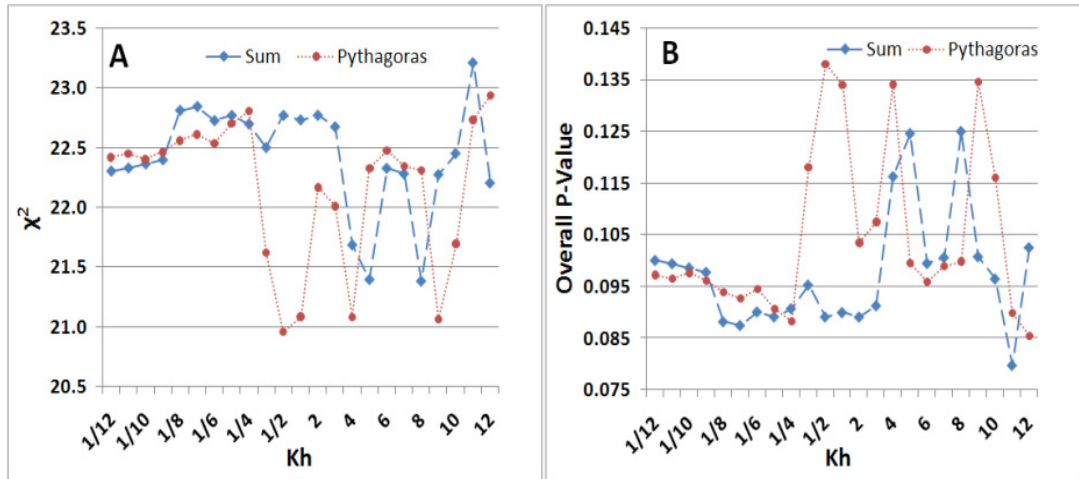


Figure 7.9. (A) Minimum χ^2 and (B) maximum overall P-value variations with K_h for WP-G.

Table 7.11: Minimum values of the objective function for the various considered values of feedback gain (K_h) and the associated magnitudes of the hill function shape parameters.

K_h	Simple Sum Approach				Pythagoras-Type Approach			
	χ^2	Overall P-value	b_{CH}	n_{CH}	χ^2	Overall P-value	b_{CH}	n_{CH}
1/12	22.305	0.100	1.5	3.0	22.423	0.097	2.0	1.5
1/11	22.331	0.099	1.5	3.0	22.451	0.097	2.0	1.5
1/10	22.364	0.099	1.5	3.0	22.405	0.098	1.5	1.5
1/9	22.400	0.098	1.5	3.0	22.467	0.096	1.5	1.5
1/8	22.813	0.088	2.0	3.0	22.562	0.094	2.0	1.5
1/7	22.844	0.087	2.0	3.0	22.613	0.093	2.0	1.5
1/6	22.727	0.090	2.5	2.5	22.538	0.094	2.0	1.5
1/5	22.770	0.089	2.5	2.5	22.705	0.091	1.0	2.0
1/4	22.699	0.091	3.5	1.5	22.809	0.088	4.0	1.0
1/3	22.502	0.095	1.5	3.5	21.626	0.118	3.5	1.0
1/2	22.771	0.089	2.0	2.5	20.965	0.138	3.5	1.0
1	22.733	0.090	2.5	1.5	21.090	0.134	2.5	1.0
2	22.771	0.089	1.0	2.5	22.170	0.103	1.5	1.0
3	22.675	0.091	3.5	1.0	22.013	0.107	0.5	1.5
4	21.689	0.116	3.5	1.0	21.089	0.134	1.0	1.0

5	21.400	0.125	3.0	1.0	22.329	0.099	1.5	1.0
6	22.329	0.099	2.5	1.0	22.476	0.096	1.5	1.0
7	22.283	0.101	2.5	1.0	22.350	0.099	1.0	1.0
8	21.387	0.125	2.0	1.0	22.316	0.100	1.0	1.0
9	22.276	0.101	2.0	1.0	21.071	0.135	0.5	1.0
10	22.453	0.096	2.0	1.0	21.698	0.116	1.0	1.0
11	23.210	0.080	1.5	1.0	22.737	0.090	0.5	1.0
12	22.206	0.103	1.5	1.0	22.939	0.085	1.0	1.0

The following may be observed from Table 7.11 and Figure 7.9:

- The Pythagoras-type approach of combining the MSI components [Equation(6.19)] is displaying relatively smaller values of χ^2 and larger overall P-values than the simple sum approach ($MSI_{total} = MSI_V + MSI_H$).
- The following four combinations of the SVH-conflict model parameters are leading to similar (minimum) chi-statistics for the Pythagoras-type approach:

Table 7.12: Optimised combinations of SVH-conflict model parameters for the Pythagoras-type approach.

Combination	K_h	Pythagoras-Type Approach			
		b_{CH}	n_{CH}	χ^2	Overall P-value
C1	1/2	3.5	1.0	20.965	0.138
C2	1	2.5	1.0	21.090	0.134
C3	4	1.0	1.0	21.089	0.134
C4	9	0.5	1.0	21.071	0.135

In order to identify the most suitable combination(s) of parameters from the above table, the SVH-conflict model was applied to the 62 field trials (trip-7 of WP-G was excluded, see §7.8.3.4) of all vessels tabulated in Table 7.1. The overall chi-statistics and P-values calculated to assess the statistical fitness of SVH-conflict model for the aforesaid parameter combinations are given in Table 7.13.

Table 7.13: Overall Chi-statistics and P-values for the optimum combinations of model parameters (see Table 7.12).

Combination	K_h	Pythagoras-Type Approach			
		b_{CH}	n_{CH}	χ^2	Overall P-value
C1	1/2	3.5	1.0	74.151	0.139
C2	1	2.5	1.0	73.484	0.151
C3	4	1.0	1.0	73.478	0.151
C4	9	0.5	1.0	73.535	0.150

It is evident from the above table that combinations ‘C2’ and ‘C3’ are producing almost identical fitness and are little better than the combinations ‘C1’ and ‘C4’. In order to keep the model simpler, it was decided to choose the parameter combination with feedback gain K_h being equal to unity i.e. ‘C2’.

It may be noted that details of the abovementioned application of SVH-conflict model to the 62 field trials of all vessels is not reproduced in this thesis. However, the procedure used for this purpose has been identical to the methodology adopted for the validation of SVH-conflict model presented in §7.9.

7.9 Validation of SVH-Conflict Model

The onboard field trials carried out by NAME at its own and as part of the COMPASS project (§3.8) are summarized in Table 7.1. Considering the number of sea trials and relatively higher observed sickness (vomiting incidences), the data pertaining to WP-G has been used for the calibration of SVH-conflict model (see §7.3 to §7.8). This leaves us with the field trial data of 7 passenger vessels (Cat-A, DV-B, MH-C, MH-D, Cat-E, Cat-F, & WP-H) summarised in Table 7.1, which may be used for the validation of SVH-conflict model.

It is important to note the field trials of Cat-A and DV-B were carried out as part of the academic research projects (Dimitrios 2002; Verveniotis 2004). Hence, the passenger survey data of aforesaid vessels was collected using a somewhat different questionnaire (see Verveniotis 2004) than the one used for the remaining ferries (see

§8.3.1 for the questionnaire details). Nevertheless, the two types of questionnaire do explicitly enquire about the incidence of emesis, which is of main concern for this validation section. The detailed steps of the validation procedure are discussed in the following.

7.9.1 Step-1: Filtering of Motion Histories

Motion histories of all the vessels enlisted in Table 7.1, with the exception of Cat-F, were collected using motion reference units (MRU). While, an in-house motion measuring system was used by the COMPASS consortium partner for logging the motion histories of Cat-F. Nonetheless, in all cases the recorded motions included (at least) the three linear accelerations (longitudinal, lateral, & vertical) and the six rotational accelerations & velocities (roll, pitch, & yaw) at the installation location of MRU/motion measuring system.

For reasons similar to the ones highlighted in §7.8.3.1, the raw motion histories of all vessels were first digitally high-pass filtered using 3-pole Butterworth filter (Smith 2003) with a corner frequency of 0.05Hz. Afterwards, the recorded motions were (digitally) low-pass filtered by employing the 3-pole Chebyshev filter (Karris 2008) with a cut off frequency of 1.0Hz. Finally, the gravity components were added to the signal using Equation(7.7).

The sample graphs depicting the raw and filtered motion histories (pertaining to installation location of MRU/ measuring system) of the full scale trials of all vessels providing validation data (Cat-A, DV-B, MH-C, MH-D, Cat-E, Cat-F, & WP-H) are presented in Figure B.1.1 to Figure B.1.47 of Appendix B.

7.9.2 Step-2: Calculation of Passenger Zone Motions

The passenger areas aboard the vessels providing validation data (Cat-A, DV-B, MH-C, MH-D, Cat-E, Cat-F, & WP-H, see Table 7.1) were divided into various zones to account for the differences in the absolute linear accelerations attributable to the rotational motions. The passenger zone layouts of these vessels are shown in Figure B.2.1 to Figure B.2.7 of Appendix B. The relative position vectors of these

zones, with respect to the installation position of MRU/motion measuring system, are summarized in Table B.3.1 to Table B.3.7 of the same appendix.

Alike step-2 of calibration procedure, Equation(7.6) was used to calculate the linear acceleration histories of all passenger zones for a given field trial of a particular vessel. The filtered motion data from the previous step (§7.9.1) was used for this purpose. For the brevity reasons, the calculated passenger zone motion histories are not reproduced in this work, however, the remote location (away from the motion measuring point) display characteristics similar to the ones visible in Figure 7.7 (see §7.8.3.2).

7.9.3 Step-3: Calculation of Motion Sickness Incidences

In this phase, the calculated (linear accelerations) and the recorded (angular accelerations and velocities) motion histories were fed into the SVH-conflict model implemented in SIMULINK[®]. The proportions of passengers likely to vomit were estimated for each individual zones of a specific ship for the considered full scale trial. Similar to the procedure used for WP-G in the calibration part (7.8.3.3), the overall sickness level of a specific field trial of the given ship was calculated by averaging out the predicted MSI values of all passenger zones.

Explicitly speaking, equal distribution of passengers in all zones has been assumed, which is considered to be an appropriate choice in the absence of detailed information about the passenger dispersion. The numeric values of the observed and model predicted percent vomiting incidences (i.e. MSI) are given in Table 7.14.

7.9.4 Step-4: Statistical Testing of Model Fitness to Individual Trial

Following the premise presented in §7.5 and §7.8.3.4, the two-tailed exact binomial test [Equation(7.2)] was conducted to test the fitness of model predictions to the observed proportion of passengers reporting to have vomited. This test has been carried out considering the observed and overall predicted MSI for each (validation) trip of all ships. The observed MSIs and the corresponding exact binomial test results of the considered vessels are given in Table 7.14.

Table 7.14: Observed and predicted MSIs along with the exact binomial test *p-values*.

Trip	Observed			SVH-Conflict	
	N ¹	VI ²	MSI	MSI	P-value
Vessel Cat-A					
1	248	14	5.65%	6.11%	0.894
2	229	18	7.86%	8.00%	1.000
Vessel DV-B					
1	340	7	2.06%	3.13%	0.347
2	335	53	15.82%	16.24%	0.882
3	187	12	6.42%	6.18%	0.879
4	475	29	6.11%	4.53%	0.098
Vessel MH-C					
1	262	4	1.53%	1.59%	1.000
2	388	8	2.06%	2.95%	0.368
3	221	4	1.81%	3.01%	0.427
Vessel MH-D					
1	22	0	0.00%	4.15%	1.000
2	43	1	2.33%	10.39%	0.126
3	24	1	4.17%	10.02%	0.507
4	50	1	2.00%	9.43%	0.086
5	27	0	0.00%	14.36%	0.026
6	51	1	1.96%	5.03%	0.520
Vessel Cat-E					
1	54	0	0.00%	2.29%	0.638
2	38	0	0.00%	0.68%	1.000
3	28	0	0.00%	2.18%	1.000
4	52	0	0.00%	2.29%	0.635
5	43	0	0.00%	1.13%	1.000
6	24	0	0.00%	1.13%	1.000
7	19	0	0.00%	3.45%	1.000
8	5	0	0.00%	1.25%	1.000

Trip	Observed			SVH-Conflict	
	N ¹	VI ²	MSI	MSI	P-value
9	7	0	0.00%	1.25%	1.000
10	63	0	0.00%	1.25%	1.000
11	15	0	0.00%	0.67%	1.000
12	8	0	0.00%	0.84%	1.000
13	26	0	0.00%	1.14%	1.000
14	4	1	25.00%	1.67%	0.065
15	52	0	0.00%	1.67%	1.000
16	15	0	0.00%	0.74%	1.000
17	14	0	0.00%	0.94%	1.000
18	20	0	0.00%	1.66%	1.000
19	137	0	0.00%	1.46%	0.275
20	38	0	0.00%	1.52%	1.000
21	30	0	0.00%	1.42%	1.000
22	55	0	0.00%	1.49%	1.000
23	37	0	0.00%	0.86%	1.000
24	114	0	0.00%	1.05%	0.637
Vessel Cat-F					
1	93	6	6.45%	7.79%	0.846
2	50	4	8.00%	7.90%	1.000
3	66	0	0.00%	3.90%	0.187
4	172	7	4.07%	7.18%	0.138
Vessel WP-H					
1	67	0	0.00%	2.38%	0.413
2	76	2	2.63%	2.11%	0.676
3	37	1	2.70%	2.09%	0.542
4	45	1	2.22%	2.39%	1.000

(¹N: total replies; ²VI: people reported to have vomited)

Assuming $p < 0.05$ to be statistically significant, it can be seen from the above table that except for a single field trial of MH-D (trip-5), the SVH-conflict model is

capable of predicting statistically accurate MSIs for all validation field trials. The journey time of this specific trial of MH-D is approximately 15 hours, therefore, the difference between the predicted and observed MSI may be attributed to ‘habituation effects’ (see § 3.5). Also, a single passenger out of four, vomited during the trip-14 of Cat-E that resulted into very high level of MSI (25%). This high value of MSI is not statistically significant due to very small sample size, which is also reflected by the *p-value* (=0.065) of exact binomial test.

7.9.5 Step-5: Statistical Testing of Model Fitness to all Validation Field Trials

The step-4 (§7.9.4) evaluates statistical fitness of the SVH-conflict model to the individual trials of all passenger ferries considered for model validation. In this final validation step, model’s fitness to multiple trials of all ferries is tested. The chi-square goodness-of-fit test statistics given by Equation(7.4) has been calculated for all trials of all ships. Here, the exact binomial test *p-values* of the individual trials (Table 7.14) were used as input to Equation(7.4). The statistics so obtained, were subsequently used to compute the one-tailed probability of chi-distribution with its degrees of freedom being equal to the total number of trials of the considered vessel. This one-tailed probability represents the overall *p-value*, indicating statistical fitness of the model to multiple trials of all vessels. The following table is summarising the chi-square goodness-of-fit test for all trials of the passenger ships providing validation data:

Table 7.15: Chi-square goodness-of-fit test result for SVH-conflict model

DoF	χ^2	<i>Overall p-value</i>
47	52.394	0.273

Again *assuming overall $p < 0.05$* to be significant, it is evident from above table that the SVH-conflict model is able to predict statistically accurate MSIs for all validation field trails.

7.10 Comparison with Other Models

The validation exercise presented in §7.9 supports the usefulness of SVH-conflict model for predicting motion sickness aboard contemporary ships. However, it is equally important to compare model's performance with other prominent physiological and statistical motion sickness models. For this work, NAME's SV-conflict model by Verveniotis & Turan (2002a; 2002b; Turan et al. 2003; Verveniotis 2004; Turan et al. 2009) has been considered under the first category (i.e. physiological model). While, the models considered under statistical category are:

- The descriptive model developed at Human Factors Research Incorporation (HFRI) by O'Hanlon & McCauley (1974) and McCauley et al. (1976), see §3.7.1 & 3.7.2. Here onward, this model shall be referred to as the HFRI model.
- The statistical model (by Lawther & Griffin 1986; 1987) that has been implemented by the sole maritime standards (ISO 2631-1:1997 & BS 6841:1987) on motion sickness (see §3.7.5). It shall be referred to as ISO/BS model.
- The descriptive model developed in the COMPASS project (see §3.8), hereafter called COMPASS model.

Procedurally speaking, each model (SVH, SV, HFRI, ISO/BS, and COMPASS) has been used to predict the motion sickness (proportions of passengers vomiting) for the full scale trials of all ferries enlisted in Table 7.1. Thereafter, the statistical fitness of each model to the individual field trials of each ferry is tested [using Equation(7.2)]. This is then followed by the chi-square goodness-of-fit test [using Equation(7.4)]; evaluating individual model's fitness to all field trials of all ferries.

Thus, instead of comparing the magnitudes of the predicted sickness incidences, the overall fitness (chi-square statistics and the associated overall P-value) of each model to all field trials of the considered ferries has been compared. The details of the procedure used for the inter-model comparison is given in the following.

7.10.1 Time Domain Calculation of Motion Sickness Incidences

The SVH, SV and ISO/BS are time domain models (ISO/BS also has a frequency domain option). This means the appropriate motion histories of the vessels may directly be used by these models to estimate the vomiting incidences. The details of SVH and SV models are, respectively, covered in §6.6 and §5.11. Whereas, the schematic diagram depicting the time domain implementation of ISO/BS model (§3.7.5) is shown in Figure 7.10. Firstly, the vertical acceleration history of the concerned location (passenger zone centre) is filtered using the fifth-order continuous-time quasi-least-square filter that approximates the vertical acceleration frequency-weighting (W_f) [Equation(3.16)] of ISO 2631-1:1997. The squared-magnitude of weighted vertical acceleration (a_v) is then integrated ($1/s$) before calculating its square-root. The latter is then multiplied with a constant $1/3$ ($= K_m$, see §3.7.5) to obtain the percent motion sickness incidences (MSI %).

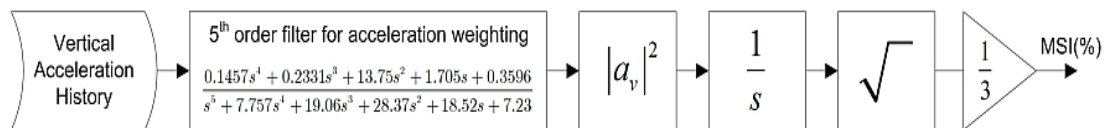


Figure 7.10. Schematic diagram of ISO 2631-1:1997/BS 6841:1987 time domain implementation.

In this work, all of the abovementioned time domain models (SVH, SV, and ISO/BS) have been developed in SIMULINK[®]. The filtered, ‘zone-based’ motion histories (see §7.8.3.2 and §7.9.2) were fed to these models as input, which in turn predicted the time varying percent incidences of the sickness. The maximum sickness level estimated by each model for a given motion record of a particular zone, of a specific ship, is taken as zone-value of MSI. These zone-values were then averaged over all zones of the considered vessel, to estimate the overall MSI of that particular voyage of the ferry. This procedure, is identical to what has been adopted for the calibration (§7.8.3.3) as well as validation (§7.9.3) of the SVH-conflict model.

7.10.2 Frequency Domain Calculation of Motion Sickness Incidences

In addition to the time domain implementation of ISO/BS (BSI 1987; ISO 1997) motion sickness models (Figure 7.10), the frequency domain approach suggested by

the aforementioned standards was also used. Firstly, the power spectral densities (PSDs) of the vessel's measured (MRU) / calculated (passenger zone) and filtered linear motion (acceleration) records were estimated using Welch's (1967) averaged modified periodogram method of spectral estimation. The 'pwelch' function of MATLAB™'s Signal Processing Toolbox™ with the following arguments was used for this purpose:

- Length of Hamming window 1024.
- Number of the overlap signal points 256.
- Number of signal points for Fast Fourier Transform (FFT) 1024.
- Sampling frequency F_s actual F_s .

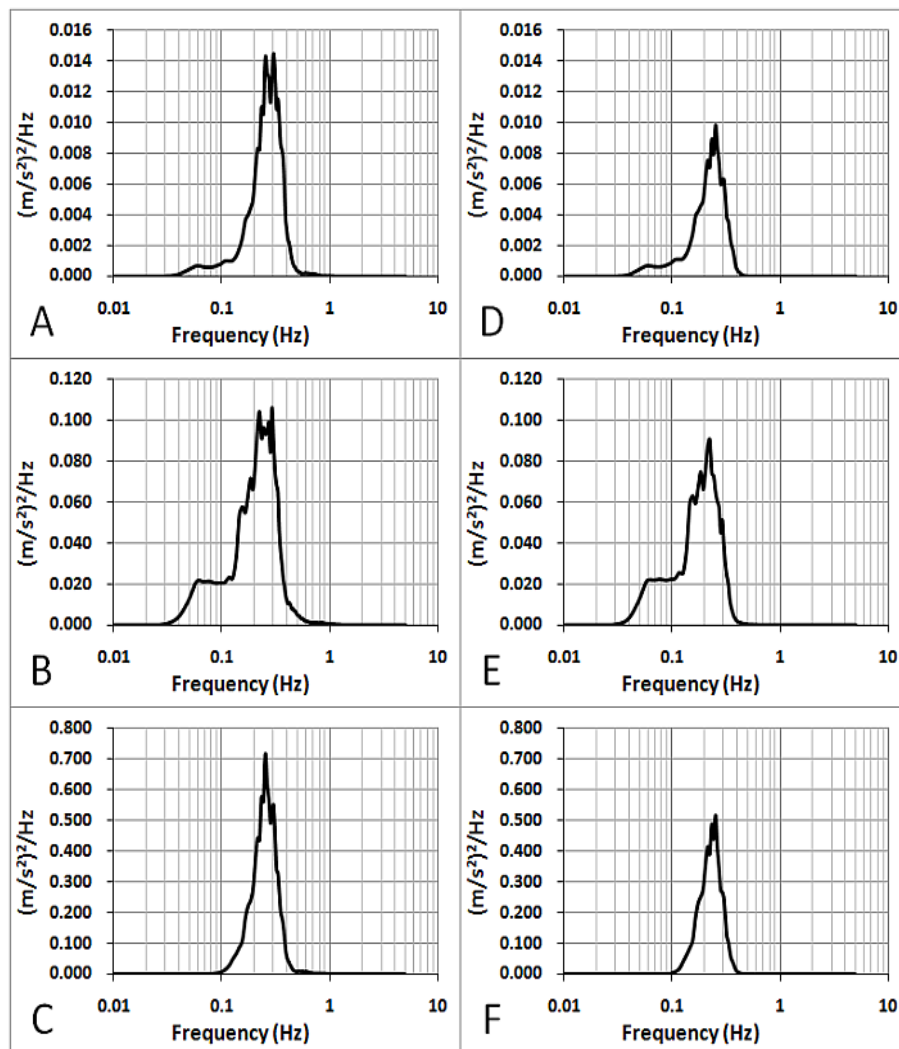


Figure 7.11. Linear acceleration PSDs of WP-G at MRU position during Trip-1; non-weighted (A) longitudinal (B) lateral (C) vertical; weighted (D) longitudinal (E) lateral (F) vertical;.

The sample PSDs of WP-G's linear accelerations during her first field trial, at the MRU location, are shown in Figure 7.11 (The time histories of these motions may be seen in Figure 7.6). The figure is also depicting the frequency-weighted PSDs that have been weighted with the appropriate weightings depicted in Figure 3.23. Once the frequency-weighted vertical accelerations PSDs (e.g. Figure 7.11F) were calculated, the weighted RMS (vertical) accelerations (a_w) at the considered location of the vessel were estimated by:

$$a_w = \sqrt{\int_0^{F_s} S_w(f) df} \quad (7.8)$$

Where, $S_w(f)$ is the frequency-weighted PSD. Afterwards Equations (3.14) and (3.15) were used to predict the percentage of commuters likely to become motion sick i.e. MSI% in the given zone of the vessel. The procedure was repeated for all passenger zones of the vessel and the resulting zone values were averaged to estimate the overall MSI of a specific field trial.

As far as the HFRI statistical model (O'Hanlon & McCauley 1974; McCauley et al. 1976) is concerned; here the non-weighted, zone-based vertical PSDs (e.g. Figure 7.11C) were calculated. These PSDs were then used to establish the corresponding RMS vertical acceleration amplitudes and modal frequencies. The aforesaid along with the voyage durations were used to estimate the MSI% by employing Equations(3.3) to (3.6). Once again, the zone-MSI values were averaged over all zones of a particular ferry to establish the overall MSI of a certain field trial.

In the case of COMPASS model, the frequency-weighted linear acceleration PSDs (e.g. Figure 7.11D to F) were used to estimate weighted RMS (longitudinal, lateral and vertical) accelerations. Thereafter, Equations (3.19) to (3.21) were employed for the prediction of zonal-MSI%, which were then averaged for all considered zones of the vessel to estimate the voyage MSI%. The proportions of vomiting incidences predicted by all four models (SVH, SV, ISO/BS, and O'Hanlon & McCauley) along with the observed sickness levels are presented in Table 7.16.

7.10.3 Testing Statistical Fitness to Individual Trials

Alike §7.8.3.4 and §7.9.4, the statistical fitness of each model's (SVH, SV, HFRI, ISO/BS, and COMPASS) prediction to the observed vomiting incidences is tested by using the two-tailed exact binomial test [Equation(7.2)]. Wherein, the underlying assumptions about the variable of our interest i.e. MSI are same as those discussed in §7.5 and §7.8.3.4. The predicted and observed proportions of vomiting incidences along with the *p-values* of the exact binomial tests for the individual field trials of the considered vessels (Table 7.1) are summarized in Table 7.16. Assuming *p-value* < 0.05 as significant, the following may be observed from the table:

- The SVH-conflict model is able to predict statistically accurate MSIs for all but the 2 (3.2%) field trials.
- SV-conflict model is also able to predict statistically correct values of MSIs for all but the 4 (6.3%) full scale trials.
- The ISO/BS time and frequency domain implementations are estimating similar MSIs. However, this descriptive model is statistically inaccurate for the 9 (14.3%) field trials.
- HFRI model is displaying the worst performance by not being able to correctly estimate the MSIs for the 21 (33.3%) full scale trials of the considered vessels.
- COMPASS model is somewhat better than HFRI model but still less accurate than the ISO/BS and the physiological (SVH & SV) models. This model was unable to predict correct MSIs for the 11 (17.5%) field trials.

It is important to note that none of the motion sickness model is able to correctly predict the MSI for trial No.7 of WP-G. As already mentioned in §7.8.3.4, during this specific trial 21.05% passengers did report 'nausea' but none reported to have vomited. Also the eye account of the researchers conducting this trial was otherwise i.e. they did see symptoms of vomiting in the toilets of this vessel. Therefore, the results of this specific field trial have been discarded. Further discussions on the results summarised in Table 7.16 above, are given in Appendix E.

Table 7.16: Predicted and observed MSI along with the exact binomial test *p-values*

Trip	Observed			SVH-Conflict		SV-Conflict		ISO/BS (TD ⁴)		ISO/BS (FD ⁵)		HFRI		COMPASS	
	N ¹	VI ²	MSI	MSI	P ³	MSI	P	MSI	P	MSI	P	MSI	P	MSI	P
Vessel Cat-A															
1	248	14	5.65%	6.11%	0.894	5.51%	0.889	3.75%	0.128	3.81%	0.133	0.54%	0.000	2.01%	0.001
2	229	18	7.86%	8.00%	1.000	7.50%	0.802	4.67%	0.028	4.70%	0.040	1.12%	0.000	2.68%	0.000
Vessel DV-B															
1	340	7	2.06%	3.13%	0.347	2.69%	0.614	4.92%	0.011	4.98%	0.009	0.75%	0.015	2.50%	0.729
2	335	53	15.82%	16.24%	0.882	15.63%	0.940	11.35%	0.012	11.32%	0.012	5.44%	0.000	8.56%	0.000
3	187	12	6.42%	6.18%	0.879	5.62%	0.632	5.52%	0.523	5.58%	0.631	0.70%	0.000	3.22%	0.021
4	475	29	6.11%	4.53%	0.098	3.95%	0.024	5.59%	0.617	5.59%	0.617	1.07%	0.000	3.03%	0.000
Vessel MH-C															
1	262	4	1.53%	1.59%	1.000	1.05%	0.359	4.80%	0.009	4.84%	0.009	0.15%	0.001	2.39%	0.540
2	388	8	2.06%	2.95%	0.368	2.66%	0.634	5.44%	0.002	5.51%	0.001	0.38%	0.000	3.12%	0.304
3	221	4	1.81%	3.01%	0.427	2.74%	0.536	5.69%	0.008	5.77%	0.008	0.28%	0.004	3.29%	0.340
Vessel MH-D															
1	22	0	0.00%	4.15%	1.000	3.82%	1.000	9.18%	0.258	9.30%	0.259	6.21%	0.397	6.32%	0.397
2	43	1	2.33%	10.39%	0.126	10.16%	0.124	10.86%	0.083	11.05%	0.084	6.71%	0.366	7.80%	0.256
3	24	1	4.17%	10.02%	0.507	9.80%	0.726	16.24%	0.162	16.37%	0.162	8.34%	0.717	12.40%	0.352
4	50	1	2.00%	9.43%	0.086	9.22%	0.086	13.89%	0.012	14.17%	0.008	7.23%	0.265	10.37%	0.059
5	27	0	0.00%	14.36%	0.026	13.90%	0.026	22.12%	0.002	22.45%	0.002	11.94%	0.068	17.85%	0.009

Trip	Observed			SVH-Conflict		SV-Conflict		ISO/BS (TD ⁴)		ISO/BS (FD ⁵)		HFRI		COMPASS	
	N ¹	VI ²	MSI	MSI	P ³	MSI	P	MSI	P	MSI	P	MSI	P	MSI	P
6	51	1	1.96%	5.03%	0.520	4.81%	0.519	10.22%	0.060	10.43%	0.061	6.08%	0.372	7.23%	0.181
Vessel Cat-E															
1	54	0	0.00%	2.29%	0.638	1.27%	1.000	2.38%	0.641	2.48%	0.646	0.03%	1.000	0.52%	1.000
2	38	0	0.00%	0.68%	1.000	0.30%	1.000	0.22%	1.000	0.24%	1.000	0.00%	1.000	0.00%	1.000
3	28	0	0.00%	2.18%	1.000	1.32%	1.000	3.66%	0.626	3.69%	0.626	0.04%	1.000	1.36%	1.000
4	52	0	0.00%	2.29%	0.635	1.27%	1.000	2.42%	0.639	2.53%	0.644	0.03%	1.000	0.60%	1.000
5	43	0	0.00%	1.13%	1.000	0.30%	1.000	0.41%	1.000	0.39%	1.000	0.00%	1.000	0.00%	1.000
6	24	0	0.00%	1.13%	1.000	0.30%	1.000	0.49%	1.000	0.45%	1.000	0.00%	1.000	0.00%	1.000
7	19	0	0.00%	3.45%	1.000	2.34%	1.000	4.29%	1.000	4.23%	1.000	0.18%	1.000	1.97%	1.000
8	5	0	0.00%	1.25%	1.000	0.53%	1.000	1.04%	1.000	1.05%	1.000	0.00%	1.000	0.00%	1.000
9	7	0	0.00%	1.25%	1.000	0.53%	1.000	1.08%	1.000	1.08%	1.000	0.00%	1.000	0.00%	1.000
10	63	0	0.00%	1.25%	1.000	0.53%	1.000	1.09%	1.000	1.10%	1.000	0.00%	1.000	0.00%	1.000
11	15	0	0.00%	0.67%	1.000	0.30%	1.000	0.17%	1.000	0.17%	1.000	0.00%	1.000	0.00%	1.000
12	8	0	0.00%	0.84%	1.000	0.30%	1.000	0.49%	1.000	0.48%	1.000	0.00%	1.000	0.00%	1.000
13	26	0	0.00%	1.14%	1.000	0.36%	1.000	2.27%	1.000	2.26%	1.000	0.01%	1.000	0.25%	1.000
14	4	1	25.00%	1.67%	0.065	0.63%	0.025	1.54%	0.060	1.56%	0.061	0.00%	0.000	0.10%	0.004
15	52	0	0.00%	1.67%	1.000	0.61%	1.000	1.64%	1.000	1.65%	1.000	0.00%	1.000	0.03%	1.000
16	15	0	0.00%	0.74%	1.000	0.31%	1.000	0.36%	1.000	0.41%	1.000	0.00%	1.000	0.00%	1.000
17	14	0	0.00%	0.94%	1.000	0.31%	1.000	0.54%	1.000	0.46%	1.000	0.00%	1.000	0.00%	1.000

Trip	Observed			SVH-Conflict		SV-Conflict		ISO/BS (TD ⁴)		ISO/BS (FD ⁵)		HFRI		COMPASS	
	N ¹	VI ²	MSI	MSI	P ³	MSI	P	MSI	P	MSI	P	MSI	P	MSI	P
18	20	0	0.00%	1.66%	1.000	0.79%	1.000	2.79%	1.000	2.83%	1.000	0.02%	1.000	0.71%	1.000
19	137	0	0.00%	1.46%	0.275	0.61%	1.000	1.83%	0.188	1.86%	0.190	0.00%	1.000	0.11%	1.000
20	38	0	0.00%	1.52%	1.000	0.73%	1.000	3.18%	0.635	3.26%	0.637	0.06%	1.000	1.02%	1.000
21	30	0	0.00%	1.42%	1.000	0.47%	1.000	1.21%	1.000	1.24%	1.000	0.00%	1.000	0.00%	1.000
22	55	0	0.00%	1.49%	1.000	0.33%	1.000	1.88%	0.629	1.91%	0.629	0.01%	1.000	0.19%	1.000
23	37	0	0.00%	0.86%	1.000	0.30%	1.000	0.82%	1.000	0.81%	1.000	0.00%	1.000	0.00%	1.000
24	114	0	0.00%	1.05%	0.637	0.30%	1.000	1.02%	0.635	0.99%	0.633	0.00%	1.000	0.00%	1.000
Vessel Cat-F															
1	93	6	6.45%	7.79%	0.846	7.08%	1.000	5.31%	0.639	5.54%	0.648	1.63%	0.004	3.32%	0.133
2	50	4	8.00%	7.90%	1.000	6.96%	0.777	6.01%	0.543	6.19%	0.551	1.71%	0.011	3.81%	0.123
3	66	0	0.00%	3.90%	0.187	2.92%	0.269	3.36%	0.176	3.34%	0.176	0.35%	1.000	1.35%	1.000
4	172	7	4.07%	7.18%	0.138	6.26%	0.273	5.33%	0.609	5.38%	0.610	1.31%	0.008	3.07%	0.377
Vessel WP-G															
1	58	1	1.72%	5.98%	0.263	5.29%	0.373	8.24%	0.089	8.29%	0.090	2.01%	1.000	5.54%	0.379
2	140	5	3.57%	4.43%	0.836	3.45%	0.817	5.13%	0.563	5.25%	0.566	0.31%	0.000	3.27%	0.810
3	48	3	6.25%	6.60%	1.000	5.80%	0.757	8.62%	0.797	8.79%	0.797	2.84%	0.155	6.04%	0.766
4	137	5	3.65%	3.37%	0.810	2.46%	0.396	3.84%	1.000	3.89%	1.000	0.13%	0.000	2.01%	0.205
5	38	2	5.26%	5.21%	1.000	4.32%	0.679	7.18%	1.000	7.23%	1.000	1.37%	0.096	4.65%	0.696
6	68	0	0.00%	4.46%	0.077	3.39%	0.177	4.59%	0.077	4.72%	0.078	0.58%	1.000	2.95%	0.272

Trip	Observed			SVH-Conflict		SV-Conflict		ISO/BS (TD ⁴)		ISO/BS (FD ⁵)		HFRI		COMPASS	
	N ¹	VI ²	MSI	MSI	P ³	MSI	P	MSI	P	MSI	P	MSI	P	MSI	P
7	114	0	0.00%	10.38%	0.000	9.47%	0.000	11.35%	0.000	11.46%	0.000	5.36%	0.003	8.56%	0.000
8	109	3	2.75%	6.53%	0.122	5.41%	0.290	6.35%	0.165	6.44%	0.167	1.24%	0.154	4.56%	0.493
9	38	2	5.26%	8.21%	0.767	7.30%	1.000	9.93%	0.583	10.13%	0.428	2.84%	0.294	7.23%	1.000
10	64	6	9.38%	6.19%	0.291	5.05%	0.140	5.39%	0.159	5.42%	0.161	0.49%	0.000	3.83%	0.036
11	64	7	10.94%	11.48%	1.000	10.52%	0.839	12.85%	0.851	13.24%	0.714	7.46%	0.334	10.16%	0.835
12	64	2	3.13%	8.51%	0.174	7.42%	0.238	6.85%	0.324	6.95%	0.325	1.88%	0.340	5.31%	0.776
13	37	9	24.32%	21.00%	0.686	20.11%	0.538	22.09%	0.695	22.66%	0.844	18.26%	0.392	18.17%	0.391
14	45	5	11.11%	8.76%	0.593	7.44%	0.384	5.93%	0.190	6.03%	0.194	1.20%	0.000	4.44%	0.049
15	51	0	0.00%	1.92%	1.000	1.44%	1.000	3.43%	0.423	3.51%	0.265	0.06%	1.000	1.22%	1.000
16	100	1	1.00%	1.04%	1.000	0.30%	0.260	1.74%	1.000	1.77%	1.000	0.00%	0.001	0.00%	0.001
Vessel WP-H															
1	67	0	0.00%	2.38%	0.413	1.37%	1.000	3.54%	0.178	3.63%	0.180	0.09%	1.000	1.74%	0.634
2	76	2	2.63%	2.11%	0.676	1.20%	0.231	4.27%	0.774	4.27%	0.774	0.17%	0.007	2.12%	0.677
3	37	1	2.70%	2.09%	0.542	1.12%	0.340	2.98%	1.000	2.98%	1.000	0.05%	0.017	1.11%	0.338
4	45	1	2.22%	2.39%	1.000	1.18%	0.414	4.84%	0.725	4.90%	0.726	0.41%	0.171	2.68%	1.000

(¹N: total replies; ²VI: people reported to have vomited; ³P: exact binomial test p-value; ⁴TD: time domain; ⁵FD: frequency domain)

7.10.4 Testing Statistical Fitness to all Trials of the Considered Vessels

Similar to §7.9.5, here the aim is to evaluate the overall goodness-of-fit of the model under question (SVH, SV, HFRI, ISO/BS, and COMPASS) to all field trials of the considered vessels (Table 7.1). The chi-square test statistics were calculated using Equation(7.4), wherein the exact binomial test *p-values*, estimated in §7.10.3, were used as input to the equation. Once calculated, the chi-square statistics were used to determine the one-tailed probability of chi-distribution (degrees of freedom being equal to the total number of full scale trials minus the trail 7 of WP-G i.e. 62). The probability so calculated represents the overall *p-value* of a given model for the multiple trials of all vessels. The overall statistical fitness of the models (SVH, SV, HFRI, ISO/BS, and COMPASS) is summarized in the following table.

Table 7.17: Model-wise chi-square goodness-of-fit results – validation vessels (including WP-G)

Model	DOF	χ^2	Overall P-value
SVH-Conflict	62	73.484	0.151
SV-Conflict	62	77.163	0.093
ISO/BS (TD)	62	155.527	5.415E-10
ISO/BS (FD)	62	157.574	2.859E-10
HFRI	62	503.403	2.213E-70
COMPASS	62	175.946	7.551E-13

It is evident from above table that the SVH-Conflict model, with minimum value of chi-square statistic and the highest overall P-value, is significantly superior to the descriptive models and is better than the SV-Conflict model.

7.11 Chapter Summary

This chapter has presented the procedure used for the calibration of SVH-Conflict model. Statistically speaking, the model is capable of predicting correct percentage of passengers likely to vomit, for all except a single field trial of the passenger ferries

(Table 7.1) considered for the model calibration and validation (Table 7.16) purpose. This specific trial (No.5 of MH-D) is of long duration (≈ 15 hours) and, as discussed in §7.9.4, ‘habituation’ may have caused this disparity. In overall terms, the SVH-Conflict model is displaying performance superior to the existing physiological (SV-Conflict) and descriptive (HFRI, ISO/BS, and COMPASS) motion sickness models (Table 7.17).

The next chapter is laid out to present the dedicated sea trials carried out as part of this thesis for the further validation of SVH-Conflict model.

Chapter 8. **FIELD TRIALS FOR THE FURTHER VALIDATION**

8.1 Overview of the Chapter

This chapter begins with an introduction to vessel features considered for the full scale motion sickness trials (§8.2), carried out to further validate the SVH-conflict model. It describes the procedure (§8.3) adopted for these field trials; wherein the survey questionnaire is also discussed at length. Simulations of the field trials by SVH-conflict model are outlined in §8.5, before comparing its performance with other physiologic and descriptive motion sickness models in §8.6. Thereafter, the chapter is presenting the statistical analyses of comfort data, collected during the field trials of a monohull ferry (§8.7) and a rigid hull inflatable boat (§8.8). Finally, the salient observations of the comfort questionnaires' statistical analyses are in §8.9.

8.2 Full Scale Trials for the Further Validation of SVH-Conflict Model

Validation (§7.9) and subsequent comparison (§7.10) of the SVH-conflict model with other motion sickness models in Chapter 7, provides good evidence in favour of the new model. However, it was considered imperative to carry out afresh field trials to further validate the model. Thus, primary objective of the full scale trials undertaken as part of this research project was to further substantiate model's ability to predict incidences of motion sickness aboard real vessels.

The model has been calibrated using field trials data of a high speed passenger ferry with relatively short commuting time (up to 3.75 hours, see Table 7.2 in §7.7). For such journeys, Crossland (1998) suggests little or no habituation. It was, therefore, decided to conduct the new set of sea trials aboard a passenger ferry with short journey time. A total of four full scale trials were carried out aboard a monohull ferry

operating around the Scotland. In addition a single field trial was carried out onboard a small, but commonly used, Rigid Hull Inflatable Boat (RHIB).

8.2.1 Vessel Features Considered for the Field Trials

Apart from personal characteristics of the passengers, i.e. susceptibility (§3.4) and habituation (§3.5), the following factors are known to influence seakeeping and hence the motion sickness characteristics of a vessel:

Vessel Size: The size of vessel plays a crucial role in its seakeeping behaviour, which influences the motion and consequently the seasickness felt by the passengers. For example, large cruise liners experience much smaller motions (amplitudes) as compared to the typical short journey Ropax ferries. Consequently, considerations of ergonomics and luxurious facilities aboard cruise vessels, take priority over factors like motion sickness. Moreover, passengers of such vessels are primarily holiday makers rather than the daily commuters with completely different moods (psychology comes into play).

Hullform: The hullform primarily influences magnitudes and modal frequencies of the six degrees of freedom vessel motions. For example, attributable to the two separate hulls and larger beams, the roll natural periods of catamaran vessels are generally shorter than the monohulls of similar displacements (Bonafoux et al. 2001). Resultantly, the roll motions as well as lateral accelerations exhibited by a catamaran are significantly higher than the equivalent displacement monohull, which leads to increased level of seasickness.

Service Speed: Service speed is yet another important parameter that not only alters the seakeeping characteristics of similar displacement vessels, but also influences the design considerations of hullform (e.g. planning monohull or catamaran) as well as the journey time. High speed crafts (vessels with speeds in excess of 30Knots) are known to exhibit peculiar responses; in that the lateral accelerations are of the order of or even higher than the vertical accelerations (Verveniotis 2004). In contrast, the

classical medium and slow speed ships predominantly display large vertical motions (Lawther & Griffin 1986; 1987).

Onboard Passenger Areas: Intuitively enough, onboard locations affect the way rotational motions alter absolute translational motions experienced by the passengers. In general the centre of gravity (the usually assumed pivot point for rotations) of a ship is close to amidships. Therefore, the passenger areas located near bow or stern and high above the waterline (points of interest for most of the passengers) experience higher level of absolute linear accelerations and hence the motion sickness.

Journey Time: Role of the journey time is highly significant in the adaptation of passengers to vessel motions. Long duration exposures to provoking motions of a vessel, lead to the reductions in seasickness (see Figure 3.1). Therefore it is important that the routes and voyage durations of selected vessels should be of appropriate duration.

Area of Operation / Weather Condition: The area of vessel operation is another important consideration, as the weather conditions and sea severities directly contribute to the vessel motions and hence the sickness levels. It is highly desirable to avoid both extremes i.e. (1) a rough weather situation where all passengers get motion sick and (2) a calm weather scenario where no passenger feels seasick.

Internal Environmental Variables and Ergonomics: Finally, the inside environmental variables like ambient temperature, air-quality, noise, and illumination levels, etc. display profound psychological effects, so does the ergonomics i.e. layout and type of seating arrangements. Factors like odours act catalytically for the initiation and aggravation of seasickness. However, a significant research has already been directed into these aspects (Card et al. 2005; Baker et al. 2007). Moreover, classification societies provide very good guidelines (e.g. ABS 2001) on these aspects. Resultantly, a remarkable consistency of these factors have been reported to

prevail across the variety of passenger ships, displaying no significant relationships with onboard comfort levels (Pescetto 2006).

It can easily be gathered from the above that, with the exception of internal environment / ergonomics and journey time, all features of a vessel altering its seasickness characteristics directly / indirectly influence the passive motions experienced by the passengers. Therefore, despite variations of such factors (displacement, hullform, speed, etc.), the motion histories of any vessel should provide enough information to predict statistically accurate seasickness. This means the selection of a ship for the motion sickness field trials should mainly be based on the journey time and environmental conditions of the operation area. The latter is important to offset the 'all/no-sick' situations.

It is important to understand that the real life considerations for selecting a particular vessel for the full scale trials go much beyond of what has been mentioned in the above. The most significant, if not alone, is the willingness of vessel operators. In general, they would consider such an expedition as hostile and an attempt to expose the weaknesses of their prestige ship(s). The choice of passenger ferry that became available for the field trials of this work was primarily driven by this very factor and the valuable willingness of the anonymous (to the readers) ship operator is much appreciated.

As far as the selection of RHIB is concerned, the seakeeping trials of this boat were primarily aimed at the identification of the design considerations affecting vertical accelerations and its operability (Lonsdale 2009). However, a single field trial of the boat was carried out as part of this project to study its motion sickness characteristics, wherein, 10 volunteer students including the author participated.

8.2.2 Brief Descriptions of the Vessels and Operation Area

Due to commercial sensitivities, hullforms of the vessels are not reproduced in this work, whereas, their approximate particulars are given in Table 8.1.

Table 8.1: Approximate particulars of the vessels used for further validation field trials

Description	Monohull Ferry	RHIB
Length (m)	91	10
Beam (m)	16	2.8
Draught (m)	3.0	Variable
Max speed (Knots)	16	52
Passengers	600	10
Cars	100	Nil
Abbreviation used in the text	MH-I	RHIB-J

Onboard facilities of the monohull ferry include cafeteria, children’s play area, observation lounge, pet area, rest lounge, and the external (open deck) seating. At the time of full scale trials, the ferry was operating around Scotland with typical voyage duration of 2 hours. This journey time was considered to be long enough to allow manifestation of motion sickness. Only small parts of the vessel routes (10-15minutes of journey time) were protected from winds by the surrounding land masses. However as a whole, the operation area of the vessel was of ‘fetch-limited’ type, with short-crested sea conditions.

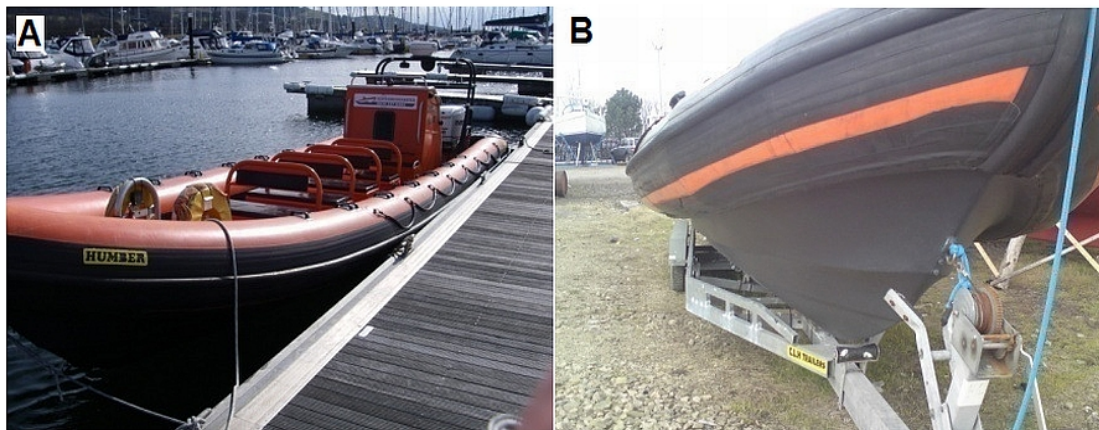


Figure 8.1. Rigid Hull Inflatable Boat: (A) layout (B) hullform.

On the other hand, the commercial RHIB had been modified by Quinquari Marine for seating a total of 10 passengers. The boat was hired along with the professional

drivers to fulfil the health and safety requirements concerning sea trials involving human subjects. As shown in Figure 8.1, the inflatable part of the boat was of Humber design, while, the rigid part had a deep ‘V’ hullform with variable deadrise angles and three knuckles.



Figure 8.2. Field trial area of RHIB [map downloaded from <http://maps.google.com/maps>].

The single full scale trial of the boat was undertaken in a stretch of water on east side of the Isle of Arran, in the lower Firth of Clyde (see Figure 8.2). This specific area is considered as open water by the MCA (Maritime & Coastguard Agency) UK and was in an easy access of the available RHIB. The idea was to have an increased probability of rough sea condition, conducive for eliciting seasickness. However, contrary to the forecast, the weather turned out to be very calm with a maximum wind speed of 5.3 knots and significant wave height of less than a meter.

8.3 Field Trial Procedure

Procedures adopted for the full scale trials of passenger ferry MH-I and boat RHIB-J were identical to the methodology used at NAME in the past, to investigate motion sickness aboard various types of passenger vessel (Table 7.1). The approach has been developed on the basis of past studies concerning field trials with similar objectives (Lawther & Griffin 1986; 1987; 1988b; 1988a). The technique presented here, was

adopted by the COMPASS project (§3.8) for the sea trials of passenger ferries to investigate onboard comfort levels.

Briefly, the whole process comprises of two major activities: (1) measuring and recording vessel motions; (2) enquiring comfort experience of the passengers. The motions were measured and recorded using the commercially hireable motion reference unit (Seatex MRU5), developed by Kongsberg Maritime. While, survey questionnaire were used to collect salient information about the personal characteristics (related to susceptibility, see §3.4) of passengers and their experience of voyage comfort (including seasickness). This meticulous questionnaire was also developed in the COMPASS project (§3.8).

Prior discussing any further the actual activities undertaken during full scale trials (§8.3.2 & §8.3.3), the passenger comfort survey questionnaire employed during the trials is described in the next section. The technical and configuration details of MRU utilized for measuring and logging of vessel motions, are given in Appendix D.

8.3.1 Description of Survey Questionnaire

The survey questionnaire used in this study is identical to the one developed and employed in COMPASS project (§3.8); it is shown in Figure 8.3. This rigorous questionnaire is based on the field studies by (Lawther & Griffin 1988b; Turner & Griffin 1999; Haward et al. 2000; Turner et al. 2000). It aims to establish the frequencies and/or extents of following features relevant to motion sickness and/or general onboard comfort:

- Personal characteristics of the passengers (age, gender, and past sickness history).
- Seasickness indicators (sickness symptoms experienced, subjective feelings, and sources of discomfort).

- Motion related discomforts other than seasickness (sitting comfort, unsteadiness while standing or walking, interruptions in mundane activities and fatigue).
- Confounding factors for seasickness (onboard activities, use of alcohol, anti-seasickness drugs).
- Psychological measures of discomfort (travel experience, expectations, satisfaction, and enjoyment)
- Motion exposure factors (onboard location and time to experience discomfort).

In addition to the above, the last question (Q20) provides the volunteering passengers with the opportunity to express themselves on matters that are not explicitly covered by the questionnaire. There is one question regarding the port of journey commencement (Q2), which is primarily there from questionnaire management view point and has little or no bearing on the sickness / discomfort study. Further details of the above identified questionnaire scopes are presented in the following.

8.3.1.1 Personal Characteristics of the Passengers

As discussed in §3.4, various studies concerning susceptibility to motion sickness suggest significant role of age, gender, and previous history of sickness in the similar or different modes of transportation (see Bos et al. 2007 for a comprehensive review). Therefore, Q1 (question No.1) enquires about the gender and age of the subjects. Q11 seeks to establish participant's past history of kinetosis. It encompasses all common modes of transportation like ships/boats, coaches/busses, cars, aircrafts and trains. Since, the focus of this research concerns the physical motions; hence, any sickness experiences of virtual environment like 3D games, Cinerama, simulators, etc. were excluded.

8.3.1.2 Seasickness Indicators

There are three questions (Q6, Q7, & Q15) that aim to identify the different, but related motion sickness indicators. Q6 is focusing on the direct symptoms that could be felt or observed by the sickness sufferers themselves.

Passenger Survey (Student Research Project) [Please fill in towards the end of your journey]

This survey is part of a PhD research project investigating the effects of ship motion on passenger comfort. We would be grateful if you could spare the time to fill in the following questionnaire, which will be collected from you. Please answer the following questions about your own impressions of your journey by ticking the relevant boxes (e.g. $\sqrt{\quad}$ or X) or entering the requested information in the spaces provided. It would further improve our analysis if you could fill one questionnaire each for the accompanied children, if any.

<p>1. Your age and gender</p> <p>Gender: (please tick one box) <input type="checkbox"/> Male <input type="checkbox"/> Female</p> <p>Enter your age in years: _____</p> <p>2. At which port did you board this ship?</p> <p style="text-align: center;"><input type="checkbox"/> _____ <input type="checkbox"/> _____</p> <p>3. Where in the ship have you spent most time?</p> <p>Please enter a zone according to the plan on the back of this sheet <input style="width: 50px;" type="text"/></p> <p>4. Did you do any of the following activities on this voyage? (please tick all appropriate boxes)</p> <p style="text-align: right;">Reading <input type="checkbox"/></p> <p style="text-align: right;">Operating computer or game <input type="checkbox"/></p> <p style="text-align: right;">Listening to music etc. <input type="checkbox"/></p> <p style="text-align: right;">Talking <input type="checkbox"/></p> <p style="text-align: right;">No particular activity <input type="checkbox"/></p> <p style="text-align: right;">Resting or sleeping <input type="checkbox"/></p> <p style="text-align: right;">In restaurant, bar or shop <input type="checkbox"/></p> <p style="text-align: right;">Looking outside vessel <input type="checkbox"/></p> <p style="text-align: right;">Other (specify): _____ <input type="checkbox"/></p> <p>5. Have you had more than two alcoholic drinks?</p> <p style="text-align: right;">During the voyage <input type="checkbox"/> No <input type="checkbox"/> Yes</p> <p style="text-align: right;">Up to 12h before the voyage <input type="checkbox"/> <input type="checkbox"/></p> <p>6. Have you felt any of the following on this voyage? (please tick all the appropriate boxes)</p> <p style="text-align: right;">Feeling hot or sweating <input type="checkbox"/></p> <p style="text-align: right;">Headache <input type="checkbox"/></p> <p style="text-align: right;">Change in skin colour <input type="checkbox"/></p> <p style="text-align: right;">Mouth watering <input type="checkbox"/></p> <p style="text-align: right;">Cold sweating <input type="checkbox"/></p> <p style="text-align: right;">Drowsiness <input type="checkbox"/></p> <p style="text-align: right;">Dizziness <input type="checkbox"/></p> <p style="text-align: right;">Stomach awareness <input type="checkbox"/></p> <p style="text-align: right;">Nausea (feeling sick) <input type="checkbox"/></p> <p style="text-align: right;">Vomiting <input type="checkbox"/></p>	<p>7. Which of the following corresponds most closely with the worst you felt on this voyage? (please tick one box only)</p> <p style="text-align: right;">I felt all right <input type="checkbox"/></p> <p style="text-align: right;">I felt slightly unwell <input type="checkbox"/></p> <p style="text-align: right;">I felt quite ill <input type="checkbox"/></p> <p style="text-align: right;">I felt absolutely dreadful <input type="checkbox"/></p> <p>8. If you did feel unwell or vomited, how long after the start of the voyage did each occur?</p> <p style="text-align: right;">Hours:Minutes</p> <p style="text-align: right;">Felt unwell _____ : _____</p> <p style="text-align: right;">Vomited _____ : _____</p> <p>9. Have you taken any anti-seasickness tablets?</p> <p style="text-align: right;">Please tick one box <input type="checkbox"/> No <input type="checkbox"/> Yes</p> <p>10. Do you travel regularly by sea? (please tick one box in each column)</p> <table style="width: 100%; border: none;"> <tr> <td style="text-align: center;">All vessels</td> <td style="text-align: center;">This type of vessel</td> </tr> <tr> <td style="text-align: right;">Rarely or never before <input type="checkbox"/></td> <td style="text-align: right;"><input type="checkbox"/></td> </tr> <tr> <td style="text-align: right;">Twice a year or less <input type="checkbox"/></td> <td style="text-align: right;"><input type="checkbox"/></td> </tr> <tr> <td style="text-align: right;">Up to 6 times a year <input type="checkbox"/></td> <td style="text-align: right;"><input type="checkbox"/></td> </tr> <tr> <td style="text-align: right;">More than 6 times a year <input type="checkbox"/></td> <td style="text-align: right;"><input type="checkbox"/></td> </tr> </table> <p>11. Have you ever suffered from sickness in the following? (please tick all appropriate boxes)</p> <p style="text-align: right;">Ships or boats <input type="checkbox"/></p> <p style="text-align: right;">Coaches or buses <input type="checkbox"/></p> <p style="text-align: right;">Cars <input type="checkbox"/></p> <p style="text-align: right;">Aircraft <input type="checkbox"/></p> <p style="text-align: right;">Trains <input type="checkbox"/></p> <p>12. Please indicate how uncomfortable the vessel motions on this voyage made you feel while sitting (other than through seasickness)? (tick one box)</p> <p style="text-align: right;">Extremely uncomfortable <input type="checkbox"/></p> <p style="text-align: right;">Very uncomfortable <input type="checkbox"/></p> <p style="text-align: right;">Uncomfortable <input type="checkbox"/></p> <p style="text-align: right;">Fairly uncomfortable <input type="checkbox"/></p> <p style="text-align: right;">A little uncomfortable <input type="checkbox"/></p> <p style="text-align: right;">Not uncomfortable <input type="checkbox"/></p>	All vessels	This type of vessel	Rarely or never before <input type="checkbox"/>	<input type="checkbox"/>	Twice a year or less <input type="checkbox"/>	<input type="checkbox"/>	Up to 6 times a year <input type="checkbox"/>	<input type="checkbox"/>	More than 6 times a year <input type="checkbox"/>	<input type="checkbox"/>	<p>13. Please indicate how much the vessel motions made you unsteady or caused loss-of-balance while standing or walking? (please tick one box)</p> <p style="text-align: right;">Extremely unsteady <input type="checkbox"/></p> <p style="text-align: right;">Very unsteady <input type="checkbox"/></p> <p style="text-align: right;">Unsteady <input type="checkbox"/></p> <p style="text-align: right;">Fairly unsteady <input type="checkbox"/></p> <p style="text-align: right;">A little unsteady <input type="checkbox"/></p> <p style="text-align: right;">Not unsteady <input type="checkbox"/></p> <p>14. Please indicate how difficult the vessel motions made any of the following tasks or activities, other than through sea sickness? (please tick one box in each column)</p> <table style="width: 100%; border: none;"> <tr> <td style="text-align: center;">Eating & drinking</td> <td style="text-align: center;">Reading</td> <td style="text-align: center;">Writing</td> <td style="text-align: center;">Other (specify)</td> </tr> <tr> <td style="text-align: right;">I did not do this <input type="checkbox"/></td> <td style="text-align: right;"><input type="checkbox"/></td> <td style="text-align: right;"><input type="checkbox"/></td> <td style="text-align: right;"><input type="checkbox"/></td> </tr> <tr> <td style="text-align: right;">Extremely difficult <input type="checkbox"/></td> <td style="text-align: right;"><input type="checkbox"/></td> <td style="text-align: right;"><input type="checkbox"/></td> <td style="text-align: right;"><input type="checkbox"/></td> </tr> <tr> <td style="text-align: right;">Very difficult <input type="checkbox"/></td> <td style="text-align: right;"><input type="checkbox"/></td> <td style="text-align: right;"><input type="checkbox"/></td> <td style="text-align: right;"><input type="checkbox"/></td> </tr> <tr> <td style="text-align: right;">Difficult <input type="checkbox"/></td> <td style="text-align: right;"><input type="checkbox"/></td> <td style="text-align: right;"><input type="checkbox"/></td> <td style="text-align: right;"><input type="checkbox"/></td> </tr> <tr> <td style="text-align: right;">Fairly difficult <input type="checkbox"/></td> <td style="text-align: right;"><input type="checkbox"/></td> <td style="text-align: right;"><input type="checkbox"/></td> <td style="text-align: right;"><input type="checkbox"/></td> </tr> <tr> <td style="text-align: right;">A little difficult <input type="checkbox"/></td> <td style="text-align: right;"><input type="checkbox"/></td> <td style="text-align: right;"><input type="checkbox"/></td> <td style="text-align: right;"><input type="checkbox"/></td> </tr> <tr> <td style="text-align: right;">Not difficult <input type="checkbox"/></td> <td style="text-align: right;"><input type="checkbox"/></td> <td style="text-align: right;"><input type="checkbox"/></td> <td style="text-align: right;"><input type="checkbox"/></td> </tr> </table> <p>15. Which of the following have caused you the most discomfort during this voyage? (please tick one box in each column)</p> <table style="width: 100%; border: none;"> <tr> <td style="text-align: center;"></td> <td style="text-align: center;">Most discomfort</td> <td style="text-align: center;">2nd most discomfort</td> </tr> <tr> <td style="text-align: right;">Sea Sickness <input type="checkbox"/></td> <td style="text-align: right;"><input type="checkbox"/></td> <td style="text-align: right;"><input type="checkbox"/></td> </tr> <tr> <td style="text-align: right;">Discomfort while sitting <input type="checkbox"/></td> <td style="text-align: right;"><input type="checkbox"/></td> <td style="text-align: right;"><input type="checkbox"/></td> </tr> <tr> <td style="text-align: right;">Unsteadiness/loss-of-balance while standing <input type="checkbox"/></td> <td style="text-align: right;"><input type="checkbox"/></td> <td style="text-align: right;"><input type="checkbox"/></td> </tr> <tr> <td style="text-align: right;">Difficulties with tasks or activities <input type="checkbox"/></td> <td style="text-align: right;"><input type="checkbox"/></td> <td style="text-align: right;"><input type="checkbox"/></td> </tr> <tr> <td style="text-align: right;">Noise <input type="checkbox"/></td> <td style="text-align: right;"><input type="checkbox"/></td> <td style="text-align: right;"><input type="checkbox"/></td> </tr> <tr> <td style="text-align: right;">Vibration <input type="checkbox"/></td> <td style="text-align: right;"><input type="checkbox"/></td> <td style="text-align: right;"><input type="checkbox"/></td> </tr> <tr> <td style="text-align: right;">Air quality <input type="checkbox"/></td> <td style="text-align: right;"><input type="checkbox"/></td> <td style="text-align: right;"><input type="checkbox"/></td> </tr> <tr> <td style="text-align: right;">Other (specify): _____ <input type="checkbox"/></td> <td style="text-align: right;"><input type="checkbox"/></td> <td style="text-align: right;"><input type="checkbox"/></td> </tr> <tr> <td style="text-align: right;">No discomfort experienced <input type="checkbox"/></td> <td style="text-align: right;"><input type="checkbox"/></td> <td style="text-align: right;"><input type="checkbox"/></td> </tr> </table> <p>16. How did the comfort of the voyage compare with your expectations?</p> <p style="text-align: right;">Less comfortable than expected <input type="checkbox"/></p> <p style="text-align: right;">Same as expected <input type="checkbox"/></p> <p style="text-align: right;">More comfortable than expected <input type="checkbox"/></p>	Eating & drinking	Reading	Writing	Other (specify)	I did not do this <input type="checkbox"/>	<input type="checkbox"/>	<input type="checkbox"/>	<input type="checkbox"/>	Extremely difficult <input type="checkbox"/>	<input type="checkbox"/>	<input type="checkbox"/>	<input type="checkbox"/>	Very difficult <input type="checkbox"/>	<input type="checkbox"/>	<input type="checkbox"/>	<input type="checkbox"/>	Difficult <input type="checkbox"/>	<input type="checkbox"/>	<input type="checkbox"/>	<input type="checkbox"/>	Fairly difficult <input type="checkbox"/>	<input type="checkbox"/>	<input type="checkbox"/>	<input type="checkbox"/>	A little difficult <input type="checkbox"/>	<input type="checkbox"/>	<input type="checkbox"/>	<input type="checkbox"/>	Not difficult <input type="checkbox"/>	<input type="checkbox"/>	<input type="checkbox"/>	<input type="checkbox"/>		Most discomfort	2nd most discomfort	Sea Sickness <input type="checkbox"/>	<input type="checkbox"/>	<input type="checkbox"/>	Discomfort while sitting <input type="checkbox"/>	<input type="checkbox"/>	<input type="checkbox"/>	Unsteadiness/loss-of-balance while standing <input type="checkbox"/>	<input type="checkbox"/>	<input type="checkbox"/>	Difficulties with tasks or activities <input type="checkbox"/>	<input type="checkbox"/>	<input type="checkbox"/>	Noise <input type="checkbox"/>	<input type="checkbox"/>	<input type="checkbox"/>	Vibration <input type="checkbox"/>	<input type="checkbox"/>	<input type="checkbox"/>	Air quality <input type="checkbox"/>	<input type="checkbox"/>	<input type="checkbox"/>	Other (specify): _____ <input type="checkbox"/>	<input type="checkbox"/>	<input type="checkbox"/>	No discomfort experienced <input type="checkbox"/>	<input type="checkbox"/>	<input type="checkbox"/>	<p>17. Please indicate your satisfaction with the comfort of this voyage (please tick one box)</p> <p style="text-align: right;">Extremely satisfied <input type="checkbox"/></p> <p style="text-align: right;">Very satisfied <input type="checkbox"/></p> <p style="text-align: right;">Satisfied <input type="checkbox"/></p> <p style="text-align: right;">Fairly satisfied <input type="checkbox"/></p> <p style="text-align: right;">A little satisfied <input type="checkbox"/></p> <p style="text-align: right;">Not satisfied, may return <input type="checkbox"/></p> <p style="text-align: right;">Not satisfied, will not return <input type="checkbox"/></p> <p>18. Please indicate how fatiguing (tiring) you have found this voyage (please tick one box)</p> <p style="text-align: right;">Extremely tiring <input type="checkbox"/></p> <p style="text-align: right;">Very tiring <input type="checkbox"/></p> <p style="text-align: right;">Fairly tiring <input type="checkbox"/></p> <p style="text-align: right;">Tiring <input type="checkbox"/></p> <p style="text-align: right;">A little tiring <input type="checkbox"/></p> <p style="text-align: right;">Not tiring <input type="checkbox"/></p> <p>19. Please indicate your enjoyment of this voyage (please tick one box)</p> <p style="text-align: right;">Extremely enjoyable <input type="checkbox"/></p> <p style="text-align: right;">Very enjoyable <input type="checkbox"/></p> <p style="text-align: right;">Enjoyable <input type="checkbox"/></p> <p style="text-align: right;">Fairly enjoyable <input type="checkbox"/></p> <p style="text-align: right;">A little enjoyable <input type="checkbox"/></p> <p style="text-align: right;">Not enjoyable <input type="checkbox"/></p> <p>20. If there is any other information you would like to add, please use the space provided on the back of this sheet.</p>
All vessels	This type of vessel																																																																										
Rarely or never before <input type="checkbox"/>	<input type="checkbox"/>																																																																										
Twice a year or less <input type="checkbox"/>	<input type="checkbox"/>																																																																										
Up to 6 times a year <input type="checkbox"/>	<input type="checkbox"/>																																																																										
More than 6 times a year <input type="checkbox"/>	<input type="checkbox"/>																																																																										
Eating & drinking	Reading	Writing	Other (specify)																																																																								
I did not do this <input type="checkbox"/>	<input type="checkbox"/>	<input type="checkbox"/>	<input type="checkbox"/>																																																																								
Extremely difficult <input type="checkbox"/>	<input type="checkbox"/>	<input type="checkbox"/>	<input type="checkbox"/>																																																																								
Very difficult <input type="checkbox"/>	<input type="checkbox"/>	<input type="checkbox"/>	<input type="checkbox"/>																																																																								
Difficult <input type="checkbox"/>	<input type="checkbox"/>	<input type="checkbox"/>	<input type="checkbox"/>																																																																								
Fairly difficult <input type="checkbox"/>	<input type="checkbox"/>	<input type="checkbox"/>	<input type="checkbox"/>																																																																								
A little difficult <input type="checkbox"/>	<input type="checkbox"/>	<input type="checkbox"/>	<input type="checkbox"/>																																																																								
Not difficult <input type="checkbox"/>	<input type="checkbox"/>	<input type="checkbox"/>	<input type="checkbox"/>																																																																								
	Most discomfort	2nd most discomfort																																																																									
Sea Sickness <input type="checkbox"/>	<input type="checkbox"/>	<input type="checkbox"/>																																																																									
Discomfort while sitting <input type="checkbox"/>	<input type="checkbox"/>	<input type="checkbox"/>																																																																									
Unsteadiness/loss-of-balance while standing <input type="checkbox"/>	<input type="checkbox"/>	<input type="checkbox"/>																																																																									
Difficulties with tasks or activities <input type="checkbox"/>	<input type="checkbox"/>	<input type="checkbox"/>																																																																									
Noise <input type="checkbox"/>	<input type="checkbox"/>	<input type="checkbox"/>																																																																									
Vibration <input type="checkbox"/>	<input type="checkbox"/>	<input type="checkbox"/>																																																																									
Air quality <input type="checkbox"/>	<input type="checkbox"/>	<input type="checkbox"/>																																																																									
Other (specify): _____ <input type="checkbox"/>	<input type="checkbox"/>	<input type="checkbox"/>																																																																									
No discomfort experienced <input type="checkbox"/>	<input type="checkbox"/>	<input type="checkbox"/>																																																																									



Figure 8.3. Passenger comfort survey questionnaire.

These are: increased bodily warmth or sweating; headache; pallor, increased salivation, cold sweating, drowsiness (feeling sleepy), dizziness (whirling sensation with a tendency to fall), stomach awareness, nausea and vomiting (emesis). The passengers may choose one or more of the aforementioned symptoms that best represent their kinetosis feelings. Only the last part of Q6 (i.e. vomited or not) represents an objective measure of seasickness, while all other features are more or less subjective and may prevail due to reasons other than the motion sickness.

Q7 relies on the subjective measures of seasickness, as proposed by Lawther & Griffin (1987) to calculate the 'illness rating (IR)'. The passengers were allowed to pick only one of the four possible choices in the aggravated sickness order as: 'I felt all right'; 'I felt slightly unwell'; 'I felt quite ill'; 'I felt absolutely dreadful'.

Q15 asks the participants to choose the 'most' and the '2nd most' discomfort (only one in each category) from the following:

- Seasickness.
- Discomfort while sitting.
- Unsteadiness/loss-of-balance while standing.
- Difficulties with tasks or activities.
- Noise.
- Vibration.
- Air quality.
- Others (passengers are asked to specify).
- No discomfort experienced.

It can be seen from the above choices that Q15 rather aims to establish the sources of overall discomfort than to merely inquire about motion sickness. Nevertheless, it indirectly serves the purpose.

8.3.1.3 Motion Related Discomforts Other than Seasickness

Vessel motions are known to cause annoyance other than the seasickness, the most important of which are the ‘Motion Induced Interruptions (MII)’ and the ‘Motion Induced Fatigue (MIF)’. MII is defined as an event where ship motions become large enough to cause the passenger/crew to momentarily abandon their (non-seated) task to maintain their upright posture. MIF are the feelings of ‘tiredness’ resulting from the subconscious spontaneous strain setup in the body in response to passive motions of the vehicle. MII and MIF have extensively been studied from human performance view point, in particular for the naval vessels (Baitis et al. 1984; Graham 1990; Lloyd 1998; Crossland & Rich 2000; Pattison et al. 2004; Riola & de Arboleya 2006).

The extra-kinetosis discomfort features are targeted by four questions (Q12, Q13, Q14, & Q18). Q12 is about the ‘sitting discomfort’, which may be a result of inappropriate deck layout or simply due to the bad seat-ergonomics. Here the passengers were allowed to pick one of the six choices: ‘extremely uncomfortable’; ‘very uncomfortable’; ‘uncomfortable’; ‘fairly uncomfortable’; ‘a little uncomfortable’ and ‘not uncomfortable’.

Q13 is a qualitative query regarding the MIIs experienced by the commuters while standing or walking due to ship’s motions. Passengers could select one of the six options in an increased unsteadiness order as: ‘extremely unsteady’; ‘very unsteady’; ‘unsteady’; ‘fairly unsteady’; ‘a little unsteady’; and ‘not unsteady’.

Q14 aims to interrogate MIIs while carrying out ordinary passenger tasks of ‘eating & drinking’, ‘reading’, ‘writing’ and any ‘other activity’ (to be specified by the participants). Passengers were required to pick one of the seven possibilities for each of the aforementioned activities. These are: ‘I did not do this’; ‘extremely difficult’; ‘very difficult’; ‘difficult’; ‘fairly difficult’; ‘a little difficult’; and ‘not difficult’.

Q18 concerns the fatigue experienced by the passengers during their journey. The passenger were allowed to pick only one of the six answers: ‘extremely tiring’; ‘very tiring’; ‘fairly tiring’; ‘tiring’; ‘a little tiring’; and ‘not tiring’.

8.3.1.4 Confounding Factors for Seasickness

As discussed at length in §3.4, there are several permanent as well as temporal aspects that predispose people to become seasick. The most pertinent of which include their onboard activities, consumption of alcohol and anti-seasickness drugs. These aspects are the subject of three questions (Q4, Q5, & Q9), wherein, Q4 allowed the passengers to pick all relevant activities from a carefully established list. The typical activities included in this list are: ‘reading’; ‘operating computer or video game’; ‘listening to music etc.’; ‘talking’; ‘no particular activity’; ‘resting or sleeping’; ‘in restaurant, bar or shop’; ‘ looking outside the vessel’; and ‘any other activity’ (to be specified by the participant).

Q5 enquires about the consumption of alcohol (two or more drinks) by the passengers, during as well as up to 12 hours before the commencement of their voyage. On the other hand, Q9 is about the usage of anti-seasickness medication. In the aforesaid questions, the passengers were required to tick either a yes or a no to confirm the use of these confounding entities.

8.3.1.5 Psychological Measures of Discomfort

Apart from the queries concerning discomforts originating from vessel’s motions (§8.3.1.3), there are three questions (Q16, Q17, & Q19) pertaining to psychological measures of discomfort. These are about the expectation, satisfaction, and overall enjoyment of the voyage. Q16 enquires fulfilment of passengers’ expectation of the voyage comfort, wherein, they could choose one of the options from: ‘less comfortable than expected’; ‘same as expected’; and ‘more comfortable than expected’.

Q17 is related to passengers’ satisfaction about the voyage comfort; they were allowed to pick one of the seven choices: ‘extremely satisfied’; ‘very satisfied’;

‘satisfied’; ‘fairly satisfied’; ‘a little satisfied’; ‘not satisfied, may return’; and ‘not satisfied, will not return’. Q19, in contrast, concerns with the overall enjoyment experience of the passengers. Here, the participants had the option to select one reply from: ‘extremely enjoyable’; ‘very enjoyable’; ‘enjoyable’; ‘fairly enjoyable’; ‘a little enjoyable’; and ‘not enjoyable’.

8.3.1.6 Motion Exposure Factors

Past studies and existing standards (see §3.7.1 to §3.7.5) suggest that the motion sickness is directly proportional to the magnitude and duration of exposure to provoking environment. Moreover, the lever-arm effects of rotational motions lead to increased level of absolute linear motions (see Lloyd 1998).

Q3 inquires the passengers about their onboard locations where they spent most of the time during the voyage. The individuals participating in the survey were asked to identify their onboard position using the passenger zones marked on the vessel’s representative general arrangements, plotted at the back of the questionnaire. Once the onboard position of a person is known, the corresponding kinetics (linear accelerations) of that zone and hence that of the passenger may be calculated using Equation(7.6).

Q8 aims to establish the motion exposure time of the passenger before any discomfort is felt and the time when vomiting took place, if any. Here, the passengers were requested to indicate the time in hours and minutes, before they ‘felt unwell’ and/or ‘vomited’.

8.3.2 Details of Ferry MH-I Trial Procedure

A total of four full scale trials were carried out onboard MH-I on the same day at the beginning of April 2009. The major activities carried out prior and during the actual field trials are briefly discussed in the following.

8.3.2.1 Identifying Suitable Weather Window

One of the most important considerations, while carrying out field studies pertaining to motion sickness, is the prevailing sea state in the operation area of the vessel. It is desirable to avoid a completely calm sea that would lead to no seasickness, as well as extremely rough weather that might cause the majority of passengers to become seasick. Given the cooperation of the ship operator, this could be achieved to some extent by identifying the weather window likely to have reasonably rough sea state. Based on the past sea trials carried out by NAME, Beaufort (Beer 1997) sea states 5 or 6 with 2.0 to 3.0 meters significant wave heights are considered rough enough to elicit moderate seasickness.

Despite the maturity of weather predictions by numerical methods, emerged with the pioneering work of Lewis Fry Richardson in 1920s (Richardson 2007), the typical weather predictions available in the public domain are still very fragile. Nevertheless, efforts were made to identify the day with the most suitable weather conditions by gathering forecasts from the various online (relatively reliable) resources enlisted in Table 8.2. The forecast up until the afternoon of the day before sea trials were very promising with the expected wind speeds to be in excess of 22 knots; possibly resulting into significant wave heights greater than 3.0m. However, on the actual day of field trial, the weather changed dramatically and the significant wave heights were smaller than 2.0m for most part of the day.

Table 8.2: Online weather forecast resources.

Web Address	Forecasted Quantities
http://www.windguru.cz/	Wind speed. Significant wave height.
http://magicseaweed.com/	Wind speed. Significant wave height.
http://www.metoffice.gov.uk/	Wind speed.
http://www.grib.us/	Wind speed.

8.3.2.2 Passenger Statistics

In order to ensure that adequate quantities of printed questionnaire and other stationary items (pens/pencils to fill) are available for the sea trials, it is imperative to estimate the number of passenger expected to travel on the D-day. In this regard, the vessel operator played the key role by providing the passenger statistics in terms of the total number of commuters travelling on the selected date in the last five years. On average 1261.6 passengers were transported by the ferry with standard deviation of 301.99 people. However, probably due to the economic slump of the year 2008/2009, a total of 361 people actually travelled on the day of field trial.

8.3.2.3 Measuring and Recording Vessel Motions

The six degrees of freedom vessel motions were measured and recorded using Seatex MRU5 (see Appendix D for the detailed description of the unit). The motion reference unit was installed in the damage control room of the vessel. This room was in the close proximity of vessel's centre of gravity and had an easy access from the passenger deck. This allowed frequent visual inspection of the unit by the author to ensure that it was not malfunctioning during entire duration of the field trials. As depicted in Figure 8.4 the MRU, housed inside a purpose built mounting bracket, was bolted to an 18mm thick steel plate. The latter was then rigidly bolted to a 6mm thick supporting column of a vertical cable tray.

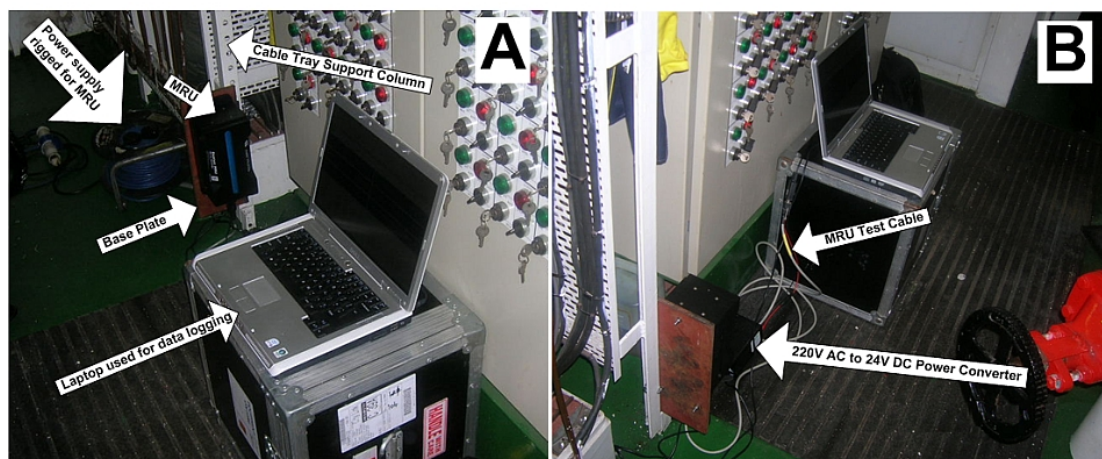


Figure 8.4. MRU installation arrangement aboard Ferry-I: (A) installation details (B) powering & connection details.

A dedicated 220VAC to 24VDC power converter was shipped with the MRU by the OEM (Kongsberg Maritime Limited). The power converter was empowered with a 220VAC supply, especially rigged for the purpose (see Figure 8.4A). For a temporary installation of the unit, like in our case, the OEM recommends using the MRU (RS-232 compliant) test cable provided by them (see Figure 8.4B) for establishing the communication between the unit and the data logging computer. The length of this test cable is relatively short ($\approx 3.0\text{m}$); hence, the ‘Dell Inspiron6400’ laptop used for interacting with MRU and recording of the measured motions (see Table D.1.5 in Appendix D), was kept in the close proximity of the unit.

The information about ship’s centre of gravity (with respect to aft perpendicular and centre line at keel level) was obtained from the captain of the ship who estimated it using the ‘onboard-NAPA’ stability analysis software. The installation location of MRU was estimated by using the general arrangement drawings of the vessel. After the installation, the details about the aforesaid parameters were downloaded to MRU using MRC (the configuration software, see §D.1.2) and the unit remained empowered throughout the day. Only the logging of measured motions was started at every port on commencement of voyage and stopped on reaching the destination port.

8.3.2.4 Distribution and Collection of Survey Questionnaire

Past field trials (Verveniotis 2004; Turan 2006) observed that in general, contrary to the clearly printed advice, the participating passengers prefer to fill the questionnaire as soon as they get. However, it is necessary that the passenger should have received enough ‘motion dose’ to initiate the sickness feelings before they fill out such a survey. Hence, all questionnaires were distributed to the passengers towards the end of their journeys and collected within 10 to 15 minutes of distribution i.e. just before the ship berthed.

In this regard, announcements were made on the PA (Public Address) system by one of the ship’s officer; explaining the purpose of this study to the passengers. Thereafter, the author assisted by two other colleagues distributed the questionnaire

to the passenger and later on collected them. The queries raised by the passengers about the purpose of this study were immediately answered by the team members. In addition, visual surveillance of the general comfort features of the ferry was maintained by the team for cross validation of the passenger replies, if needed.

8.3.3 Details of RHIB-J Trial Procedure

The procedure adopted for the single field trial of RHIB-J was very similar to the one used for the ferry MH-I. As a pre-experiment step the likely weather states at the trial area were gathered using the resources summarized in Table 8.2. However, unlike field trials of MH-I, the actual weather conditions were far from what was forecasted a day before. The wind speed observed during the field trial did not exceed 5.3 knots resulting into a sea state of 2 or below on Beaufort scale.

For the motion sickness trial of the RHIB-J, 10 student volunteers, including the author, were selected. With an average age of 22.4 (standard deviation of 4.4), these volunteers consisted of 7 males and 3 females with some prior experience of RHIBs. Before going to sea, all participants were briefed by the boat's crew about the safety procedures and the usage of personal protective equipment (life jackets and waterproof thermal clothing) provided to them.

In addition to the motion and comfort measurements explained in the following, the speed and absolute heading of the boat was recorded at a five minute interval. Ideally, the boat would have followed a southward course (Figure 8.2) towards the open sea to expose the participants to the 'expected' rough weather. However, in absence of the same (i.e. rough weather), several manoeuvres of the RHIB were carried out in an attempt to mimic the motions typically experienced during a rough sea state.

8.3.3.1 Measuring and Recording of Motion

Alike MH-I, the six degrees of freedom motions of the RHIB-J were measured and recorded using a Seatex MRU5. Since, it was not allowed to drill holes in the limited panels of the boat; the mounting bracket of MRU was bolted to a 24mm thick wooden board. As depicted in Figure 8.5, the supporting board was then fastened at the back of seat number 7 and 8 with the help of clamping ropes. This installation layout exposed the unit to a high frequency vibration, arising from the relatively floppy fastening as well as being in a close proximity of the boat's engines. However, no alternate arrangement was feasible without drilling a hole in boat's structure, which was not allowed due to safety reasons.

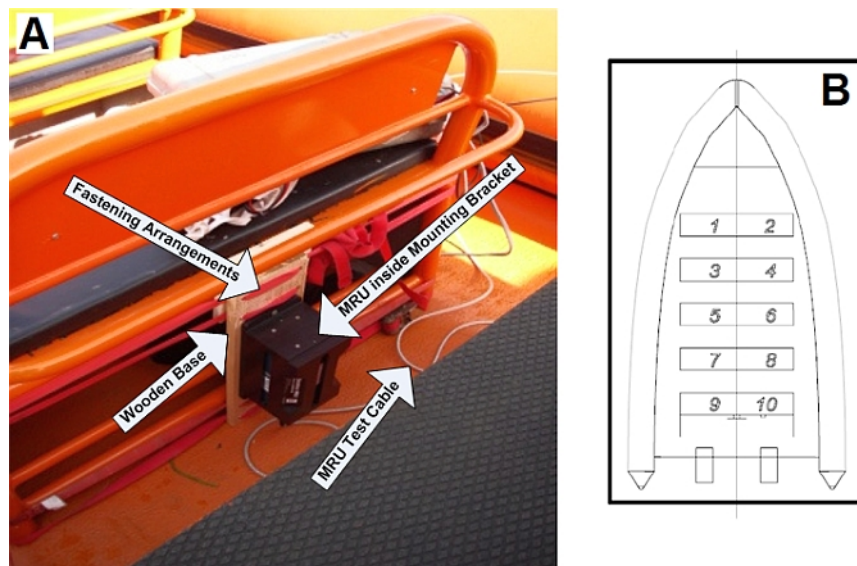


Figure 8.5. MRU installation arrangement aboard RHIB: (A) installation details; (B) seating arrangements.

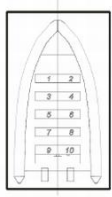
MRU was directly powered from the 24VDC batteries of the boat, whereas, a DC to AC inverter was used to energize the 'Sony Vaio VGN-FS215Z' laptop for logging the motion records. Once again, the MRU test cable (RS-232) was used for configuring and communicating with the unit. Here too, the histories of the kinematic variables enlisted in Table D.1.5 of Appendix D, were recorded during the field trial of RHIB-J.

8.3.3.2 Survey Questionnaire and Comfort Feedback

The survey questionnaire used for the field trial of RHIB was a modified version of the one explained in §8.3.1. This questionnaire, as shown in Figure 8.6, comprised of two main parts. The first part aimed at establishing the time course of discomfort development. This part had three questions respectively enquiring about the onboard sitting location (Q1), sickness symptoms (Q2, as per §8.3.1.2) and the fatigue (Q3, as per 8.3.1.3) experienced by the participants.

A

1 Please indicate where in the RHIB you were sitting



10 Have you felt any of the following on this trip?
(Please tick all appropriate boxes at each of the following intervals during the trip)

	At the start	After 30 mins	After 1 hour	After 1 hour 30 mins	After 2 hours	6 hours after coming ashore
Hot or sweating						
Headache						
Change in skin colour						
Mouth Watering						
Cold Sweats						
Drowsiness						
Dizziness						
Stomach Awareness						
Nausea						
Vomiting						

11 How fatigued have the boats motions made you feel?
(Please tick one box at each of the following intervals during the trip)

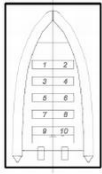
	At the start	After 30 mins	After 1 hour	After 1 hour 30 mins	After 2 hours	6 hours after coming ashore
Extremely tired						
Very tired						
A little tired						
Not tired						

12 If you do suffer any ill feeling please indicate how long you have been onboard for.

Please fill in this part of the questionnaire Before, During and After the trip.

B

1 Please indicate where in the RHIB you were sitting



2 What is your age?

3 What is your gender?
(Please tick)

Male	<input type="checkbox"/>
Female	<input type="checkbox"/>

4 Have you ever been ill due to the motions of the following?
(Please tick all appropriate boxes)

Ships or boats	<input type="checkbox"/>
Coaches or buses	<input type="checkbox"/>
Cars	<input type="checkbox"/>
Aircraft	<input type="checkbox"/>
Trains	<input type="checkbox"/>

5 Have you had more than 2 alcoholic drinks in the past 12 hours?
(Please tick)

Yes

No

If so roughly what drinks?
(Please indicate the number of each)

Pint of lager	<input type="text"/>
Small glass of wine	<input type="text"/>
Large glass of wine	<input type="text"/>
Rum	<input type="text"/>
Vodka	<input type="text"/>
Other (Please Specify)	<input type="text"/>

6 Which of the following corresponds the worst you felt during the trip?
(Please tick only 1 box)

I felt alright	<input type="checkbox"/>
I felt slightly unwell	<input type="checkbox"/>
I felt quite ill	<input type="checkbox"/>
I felt very ill	<input type="checkbox"/>

If you wish to add any more information please do so on the back of this sheet.

7 Please indicate how comfortable (or otherwise) you felt due to the boats motions.

Extremely uncomfortable	<input type="checkbox"/>
Very uncomfortable	<input type="checkbox"/>
Fairly uncomfortable	<input type="checkbox"/>
Slightly uncomfortable	<input type="checkbox"/>
Comfortable	<input type="checkbox"/>

8 Did you experience any of the following during the trip?
(Please tick all appropriate boxes)

Upper back pain	<input type="checkbox"/>
Lower back pain	<input type="checkbox"/>
Tail bone pain	<input type="checkbox"/>
Neck pain	<input type="checkbox"/>
Other pain (Please Specify)	<input type="text"/>

Leg & Ankle

9 Which of the following caused you the most discomfort during the trip?
(Please tick 1 box in each column)

	Most discomfort	2nd Most discomfort
Sea sickness	<input type="checkbox"/>	<input type="checkbox"/>
Discomfort due to vertical jerking	<input type="checkbox"/>	<input type="checkbox"/>
Discomfort due to lateral jerking	<input type="checkbox"/>	<input type="checkbox"/>
Lack of feeling of security	<input type="checkbox"/>	<input type="checkbox"/>
Noise	<input type="checkbox"/>	<input type="checkbox"/>
Vibration	<input type="checkbox"/>	<input type="checkbox"/>
Spray	<input type="checkbox"/>	<input type="checkbox"/>
Cold	<input type="checkbox"/>	<input type="checkbox"/>
Other (Please Specify)	<input type="text"/>	<input type="text"/>

Figure 8.6. Questionnaire used onboard RHIB: (A) during and (B) after the trial.

The second part focused on establishing the personal characteristics (Q2 & Q3), past motion sickness history (Q4, as per §8.3.1.1), use of alcohol (Q5, as per §8.3.1.4), sickness symptoms (Q6 & Q9, as per §8.3.1.2), and discomfort (Q7, as per §8.3.1.3).

There was one additional question (Q8) about the back pain caused by the motions of the boat. The participants could choose from: ‘upper back pain’; ‘lower back pain’; ‘tail bone pain’; ‘neck pain’; ‘other (to be specified)’. The first part of the questionnaire (Figure 8.6A) was plastic laminated and filled by the participants every 30minutes during the hour and half long trip, while, the second part (Figure 8.6B) was completed just after the culmination of field trial.

8.4 Summary of the Passenger Participation / Weather Condition / Vessel Motions

A total of 361 commuters used passenger ferry MH-I during the four field trials, while 10 volunteers participated in the single field trial of RHIB-J. Summary of the prevailing weather conditions and the passengers voluntarily participating in the aforesaid field trials is given in Table 8.3. The information on wind speed, wave height and wave period was provided by the bridge staff for MH-I. They collected this information using onboard navigation aid systems and logged it after every 15 minutes during the journeys.

Table 8.3: Summary of the field trial weather conditions and reply rates.

Trip	Total Passengers Travelled	Passengers Replied	Rate of Reply	Average Wind Speed (Knots)	Average Significant Wave Height (m)	Average Peak Period (sec)
MH-I						
1	66	46	69.7%	26.50	2.500	5.00
2	120	81	67.5%	24.60	2.100	3.80
3	119	78	65.5%	20.00	1.875	3.25
4	63	36	57.1%	19.75	1.950	3.00
RHIB-J						
1	10	10	100%	3.5	0.5	1

The average rate of questionnaire returned by the ferry passenger was 65% (S.D=5.5%), which is relatively high and implies conducive weather conditions for sea travel (nauseating people are normally reluctant to participate in such studies). The wind speed ranged from 5 to 6 on Beaufort Scale (Huler 2005), resulting into sea state of 4 (as per World Meteorological Organization, WMO Code Table 1555). Thus, the sea severity on the day of MH-I field trials was mostly ‘moderate’ or lower, while the weather was ‘very calm’ during the full scale trial of RHIB-J.

The RMS motions (translational acceleration and rotational velocities) of the two vessels, averaged over the passenger zones of MH-I (Figure 8.9) / seating position of RHIB-J (Figure 8.5B), are summarised in Table 8.4. Once again, small amplitudes of the translational accelerations and rotational velocities are indicative of relatively ‘calm’ weather conditions on the day of MH-I field trials. However, RMS motions of RHIB-J were relatively large as compared to the prevailing sea state; this is because of the small size of the boat.

Table 8.4: Summary of the RMS translational accelerations and rotational velocities (averaged over passenger zone / seating position) of MH-I and RHIB-J.

Motions	Units	MH-I				RHIB-J
		Trip-1	Trip-2	Trip-3	Trip-4	Trip-1
Surge Acceleration	m/sec ²	0.0924	0.0450	0.0213	0.0398	0.1823
Sway Acceleration	m/sec ²	0.1501	0.1288	0.0659	0.0720	0.2093
Heave Acceleration	m/sec ²	0.2955	0.1918	0.0648	0.1056	0.7685
Roll Velocity	deg/sec	0.0018	0.0024	0.0018	0.0018	0.1178
Pitch Velocity	deg/sec	0.0048	0.0030	0.0015	0.0019	0.1488
Yaw Velocity	deg/sec	0.0019	0.0023	0.0015	0.0009	0.0601

8.5 Analysis of the Field Trial Results Using SVH-Conflict Model

Analyses of further validation field trials presented in the following, pertain to the simulation of motion sicknesses observed during the field trials of ferry MH-I and RHIB-J. Whereas, statistical analyses of other comfort entities collected through survey questionnaires are respectively given in §8.7 and §8.8. As detailed below, the

procedure used for simulations is identical to the methodology adopted for the calibration (§7.8.3) and subsequently validation (§7.9) of SVH-conflict model.

8.5.1 Step-1: Filtering of Motion Histories

Due to the reasons elaborated in §7.8.3.1, the motion records of MH-I as well as RHIB-J (see Table D.1.5 for the list of recorded motions) were firstly high-pass filtered using a three pole Butterworth filter (Smith 2003) with a cut off frequency of 0.05Hz. Thereafter, a three pole Chebyshev filter (Karris 2008) with a corner frequency of 1.0Hz, was employed to low-pass filter the raw motion data.

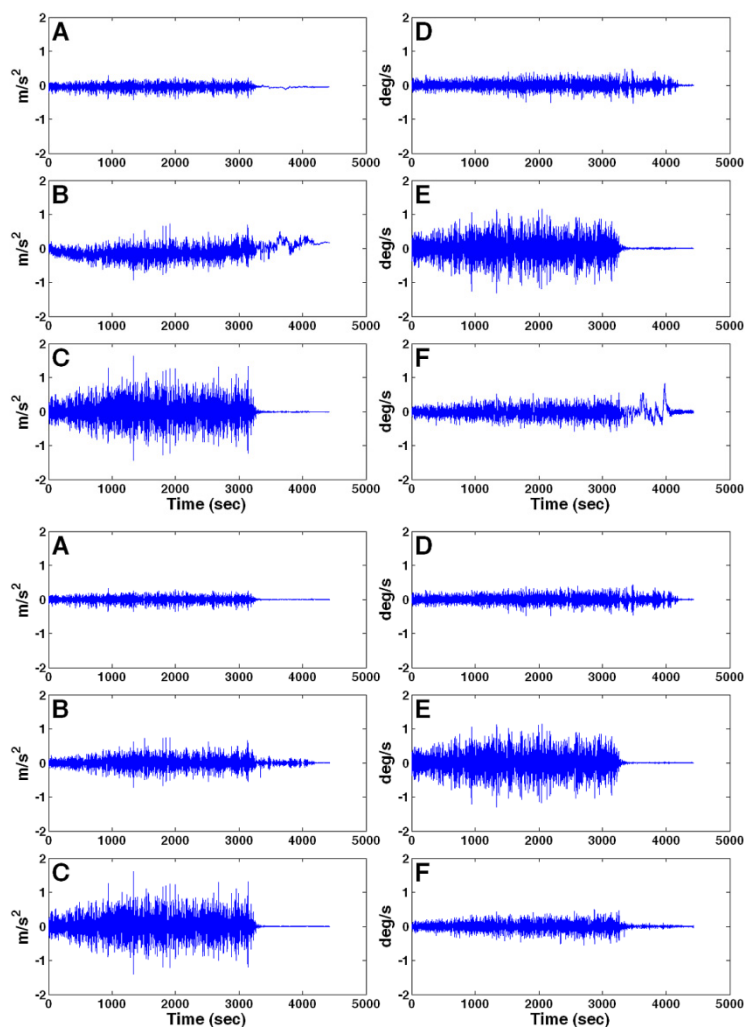


Figure 8.7. Motion history (upper-row; lower-filtered) of MH-I at MRU position during Trip-1; linear accelerations (A) longitudinal (B) lateral (C) vertical; angular velocities (D) roll (E) pitch (F) yaw

The raw and filtered motion histories of MH-I, at the MRU installation location, during the first trip are shown in Figure 8.7, whereas, similar plots for the remaining (three) trips are shown in Figure C.1.1 to Figure C.1.3 of Appendix C. It is interesting to note that the predominant angular motion of this classical monohull is pitch, while heave is the dominant translational motion.

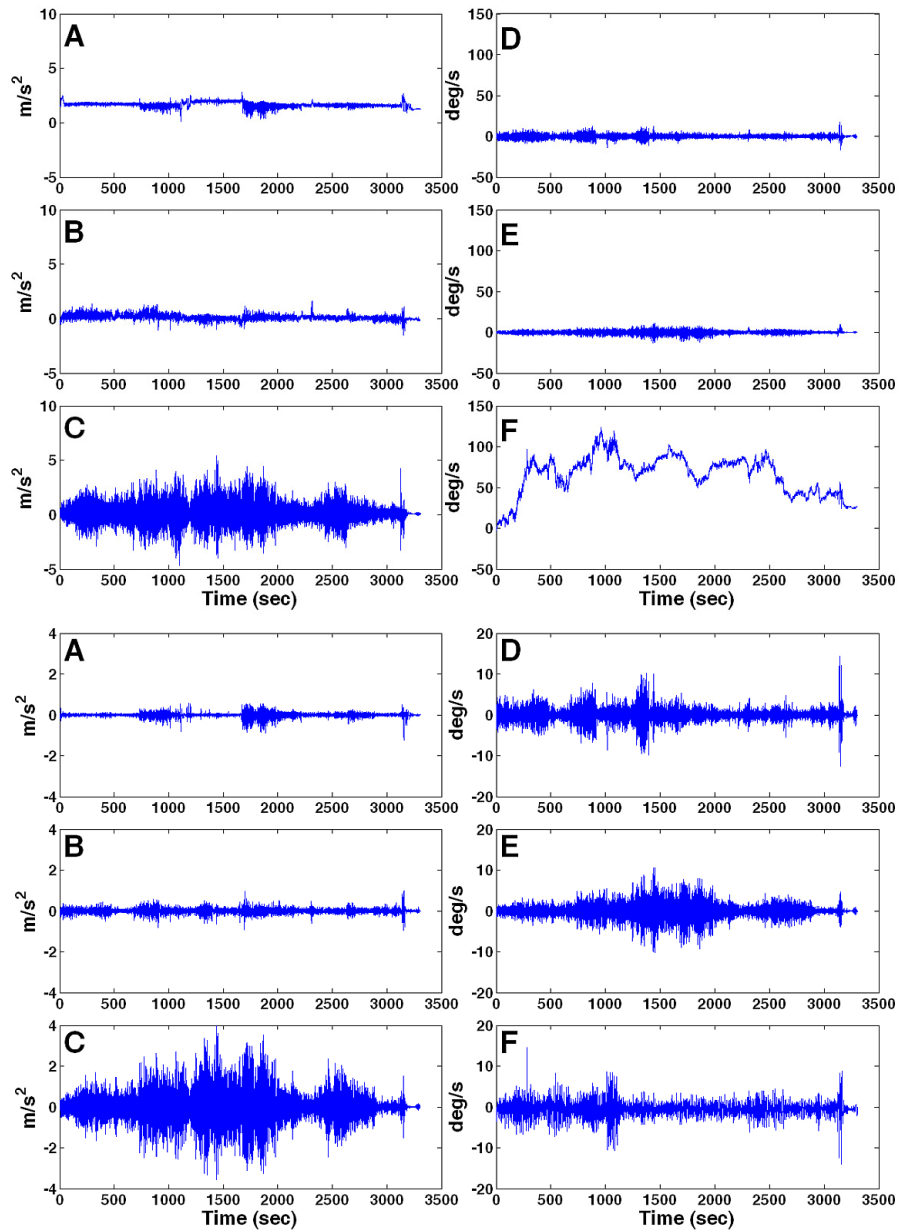


Figure 8.8. Motion history (upper-row; lower-filtered) of RHIB-J at MRU position during Trip-1; linear accelerations (A) longitudinal (B) lateral (C) vertical; angular velocities (D) roll (E) pitch (F) yaw

The raw and filtered motion histories for the single field trial of RHIB-J are depicted in Figure 8.8 above. This time, both roll and pitch motions are of similar amplitudes, while, alike monohull, heave is the dominant translational motion.

8.5.2 Step-2: Calculation of Passenger Zone / Sitting Position Motions

In order to account for the lever-arm effects of rotational motions, the passenger areas of MH-I were divided into fourteen passenger zones shown in Figure 8.9 below, whereas, the sitting arrangement of RHIB is depicted in Figure 8.5B.

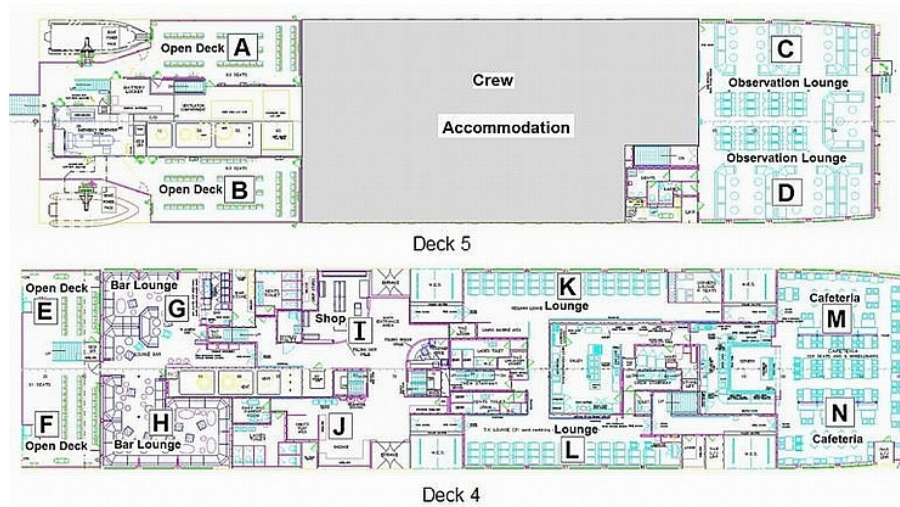


Figure 8.9. Passenger zones layout of MH-I

The relative position vectors of the abovementioned zones / sitting positions, with respect to the installation position of MRU, are summarized in Table 8.5.

Table 8.5: Relative position vectors \mathbf{r} (meters) of passenger zones (aboard Ferry-I) and sitting positions (aboard RHIB-J).

MH-I				RHIB-J			
Zone	r_x	r_y	r_z	Seat	r_x	r_y	r_z
A	-19.58	-5	-4.825	1	2.565	-0.25	-0.75
B	-19.58	6	-4.825	2	2.565	0.25	-0.75
C	23.32	-5	-4.825	3	1.785	-0.25	-0.75
D	23.32	6	-4.825	4	1.785	0.25	-0.75
E	-34.38	-4	-2.2	5	1.005	-0.25	-0.75

MH-I				RHIB-J			
Zone	r_x	r_y	r_z	Seat	r_x	r_y	r_z
F	-34.38	3.9	-2.2	6	1.005	0.25	-0.75
G	-29.78	-4.5	-2.2	7	0.225	-0.25	-0.75
H	-28.68	5.1	-2.2	8	0.225	0.25	-0.75
I	-13.68	-3.5	-2.2	9	-0.35	-0.25	-0.75
J	-16.68	5.1	-2.2	10	-0.35	0.25	-0.75
K	3.62	-6.2	-2.2				
L	3.62	7.2	-2.2				
M	24.32	-3.8	-2.2				
N	24.32	4.8	-2.2				

The band-pass filtered motion records of MRU were combined with the position vectors (Table 8.5) using Equation(7.6) to calculate the motion histories for the passenger zones / sitting positions. These histories are not reproduced here to save on the volume of this work, however, they exhibit features similar to the ones visible in Figure 7.7 (see §7.8.3.2).

8.5.3 Step-3: Calculation of Motion Sickness Incidences

Similar to §7.8.3.3, and §7.9.3, the motion histories of MRU and passenger zones / sitting positions were fed into the SVH-conflict model implemented in SIMULINK®. The proportions of people predicted to become seasick i.e. vomit, were averaged over all zones (MH-I) / sitting positions (RHIB-J) to estimate the overall sickness level (MSI) for a given field trial. The magnitudes of predicted and observed vomiting incidences are summarized in Table 8.6.

8.5.4 Steop-4: Statistical Fitness Testing

Based on the reasoning explained in §7.5 and §7.8.3.4, the two-tailed exact binomial tests [using Equation(7.2)] were carried out for verifying the statistical fitness of SVH-conflict model predictions to the MSIs observed aboard MH-I and RHIB-J. The trip-wise predicted and observed MSI (calculated by dividing the total reported

vomiting events with the number of questionnaire returned by the volunteering passengers) for all field trials of MH-I and RHIB-J are summarised in Table 8.6.

Table 8.6: Observed MSI and the exact binomial test *p-values* for MH-I and RHIB-J

Trip	Observed			SVH-Conflict	
	N ¹	VI ²	MSI	MSI	P-value
Vessel MH-I					
1	46	0	0.00%	6.31%	0.118
2	81	4	4.94%	5.52%	1.000
3	78	0	0.00%	1.09%	1.000
4	36	0	0.00%	1.18%	1.000
Vessel RHIB-J					
1	10	0	0.00%	1.76%	1.000

(¹N: total replies; ²VI: people reported to have vomited)

The above table is also depicting the *p-values* of exact binomial tests and it can be seen that the model predictions are not significant (assuming $p < 0.05$ to be significant) for any field trial. Thus, the SVH-conflict is statistically accurate in predicting the MSI% for the individual trials of MH-I and RHIB-J. However, we should check the statistical fitness of SVH-conflict model to the multiple field trials by carrying out the chi-square goodness of fit test. The test statistics and resulting one-tailed chi-distribution probability i.e. overall *p-value* are given in Table 8.7. The overall *p-value* is highly insignificant, indicating very good fitness of the model.

Table 8.7: Chi-square goodness-of-fit test result for SVH-conflict model

DoF	χ^2	Overall <i>p-value</i>
5	4.277	0.510

8.6 Comparison with Other Models

In this section, the statistical performance of SVH-conflict model has been compared with other physiological and statistical motion sickness models. The procedure

summarized in the following is identical to the one explained in §7.10 for model validation.

8.6.1 Calculation of Motion Sickness Incidences

The motion sickness incidences (MSIs) for the four field trials of MH-I and the single trial of RHIB-J were calculated using the time / frequency domain physiological / statistical models / methods summarised in Table 8.8.

Table 8.8: Motion sickness calculation models/methods used for comparison with SVH-conflict model

Model / Method	Calculation Domain	Type	Remarks
NAME's SV-conflict model. (see §5.11)	Time	Physiologic	Implemented in SIMULINK®
ISO/BS (Time Domain). (see §7.10.1 and Figure 7.10)	Time	Descriptive	Implemented in SIMULINK®
ISO/BS (Frequency Domain). (see §7.10.2)	Frequency	Descriptive	Calculated using Equations(3.14) and (3.15)
HFRI (Human Factor Research Institute). (see §7.10.2)	Frequency	Descriptive	Calculated using Equations(3.3) to (3.6)
COMPASS (see §7.10.2)	Frequency	Descriptive	Calculated using Equation(3.19) to (3.21)

Relevant filtered motion histories of the passenger zones / sitting positions (Table 8.5) were used as input to the time domain models (SV & ISO/BS). On the other hand, relevant spectral densities of the weighted (for ISO/BS and COMPASS) and non-weighted (for HFRI) accelerations calculated for each zone / sitting positions were employed for the frequency domain methods. The proportions of vomiting events predicted by the aforementioned models / methods are given in Table 8.9.

8.6.2 Statistical Fitness Testing

In this step, firstly, the two-tailed exact binomial tests [Equation(7.2)] were carried out to establish the statistical fitness of each model (Table 8.8) to the observed vomiting incidences aboard MH-I and RHIB-J. The predicted and observed MSIs, as well as the *p-values* of the exact binomial test are given in Table 8.9. Assuming $p < 0.05$ as significant, it can be seen from the table that all motion sickness models are able to predict statistically accurate proportions of sickness incidences. The only exception are the estimates of HFRI model for the 2nd field trial of MH-I, wherein the model predictions are much lower than the observed value.

Table 8.9: Predicted and observed MSI along with the exact binomial test *p-values*

Ship		MH-I				RHIB-J
Trip		1	2	3	4	1
Observed	N¹	46	81	78	36	10
	VI²	0	4	0	0	0
	MSI	0.00%	4.94%	0.00%	0.00%	0.00%
SVH	MSI	6.31%	5.52%	1.09%	1.18%	1.76%
	P³	0.118	1.000	1.000	1.000	1.000
SV	MSI	5.96%	5.18%	0.59%	0.83%	0.92%
	P	0.114	1.000	1.000	1.000	1.000
ISO 2631 (TD⁴)	MSI	6.01%	4.30%	1.47%	2.30%	1.30%
	P	0.114	0.780	0.633	1.000	1.000
ISO 2631 (FD⁵)	MSI	6.18%	4.45%	1.49%	2.36%	1.31%
	P	0.116	0.784	0.634	1.000	1.000
HFRI	MSI	1.51%	0.51%	0.01%	0.07%	0.00%
	P	1.000	0.001	1.000	1.000	1.000
COMPASS	MSI	3.49%	2.04%	0.00%	0.33%	0.00%
	P	0.411	0.084	1.000	1.000	1.000

(¹N: total replies; ²VI: people reported to have vomited; ³P: exact binomial test p-value; ⁴TD: time domain; ⁵FD: frequency domain)

In order to verify statistical fitness of the considered models (Table 8.8) to the multiple field trials of MH-I and RHIB-J, the chi-square goodness of fit statistics were calculated by using Equation(7.4). Model-wise summary of these test statistics as well as the one-tailed probability of chi-distribution is given in Table 8.10.

Table 8.10: Model-wise chi-square goodness-of-fit results – vessels enlisted in Table 8.1

Model	DOF	χ^2	Overall P-value
SVH-Conflict	5	4.277	0.510
SV-Conflict	5	4.350	0.500
ISO/BS (TD)	5	5.753	0.331
ISO/BS (FD)	5	5.707	0.336
HFRI	5	14.223	0.014
COMPASS	5	6.724	0.242

Since, most of the verification trials (4/5) were carried out aboard medium speed classical monohull ferry (MH-I); hence, it can be seen from the above table that there is little difference between the statistical fitness of SVH and SV-Conflict models. The two physiological models are somewhat superior to ISO/BS and COMPASS descriptive models, while, the HFRI model is unable to predict statistically correct MSIs. Further deliberations on the results of verification trials are presented in Appendix E.

8.7 Statistical Analyses of MH-I Questionnaires

The primary objective of the statistical analyses presented here is to identify the significant relationships (if any) between the various qualitative and quantitative comfort data, collected (using survey questionnaires) during the four field trials of MH-I. This has been done without having regards to the vessel motions, so that the ‘extra-motion-factors’ likely to influence the comfort entities may be established. However, due to time constraints and relatively small database (241 replies), the venture to establish MSI susceptibility function (similar the one proposed by Bos et al. 2007 for IR) has been avoided. As the statistical analyses given in the subsequent sections discount vessel’s motions, hence the data collected during the four full scale trials of MH-I are grouped together.

It can be seen from the questionnaire depicted in Figure 8.3 that the survey data comprises of several ‘quantitative’ as well as ‘qualitative information. In general, such statistical variables may be assigned one of the four categories (Urdan 2005) enlisted in Table 8.11.

Table 8.11: Type and categories of statistical data.

Data Type	Category	Description	Examples
Quantitative (Qty)	Continuous / Interval / Ratio / Parametric	A variable scored in such a way that the numbers, or values, indicate some sort of amount.	Age. Height.
Qualitative (Qual.)	Dichotomous	A variable that has only two possible / considered categories.	Gender. Yes/No type questions.
	Nominal	A variable with two or more labels that are used to identify the different types. Such variables do not have weight, or numeric values.	Colours. Onboard location.
	Ordinal	A variable with more than two categories, which could be placed	Ranking of top 10 rich

Data Type	Category	Description	Examples
		into an order and assigned meaningful numerical values. However, the distance between these scores is meaningless.	persons. Exam grades.

The type, category and values of the queries used in the survey questionnaire are summarized in Table C.2.1 of Appendix C. It may be noted that the various parts of the same questions are appended with small alphabets e.g. Q6c refers to third part of question 6 i.e. pertaining to pallor (change in skin colour). Similarly, Q1b is related to second part of Q1, i.e. passenger's age. Furthermore, the ordinal data has been assigned numerical values from '0' upwards in such a way that zero represents the least discomfort / effects while the higher numbers correspond to increased level of discomfort / effects. It may be noted that all questions except Q1b (age) and Q8 (time) are qualitative in nature. The aforesaid variables were, therefore, binned as per Table 8.12 to produce comparable statistics.

Table 8.12: Binning of continuous variables

Query	Description	Bins
Q1	Age	≤ 18; 19-30; 31-50; 51-65 and >65 years
Q8	a. Time to felt unwell b. Time to vomit	≤ 30min; 31-60min

The statistical analyses of MH-I questionnaire data have been limited to the following:

- Summarising of the data as frequency tables (in the form of column graphs).
- Cross tabulation of all variables with the aim to establish significant dependencies.

8.7.1 Summary Statistics – Frequency Tables

The summary statistics of Q1 (age and gender) are shown in Figure 8.10. It can be seen from the figure that almost 55% of participants were male. Approximately, 60% were aged 50 years or less with majority (32%) in their middle age (31-50 years).

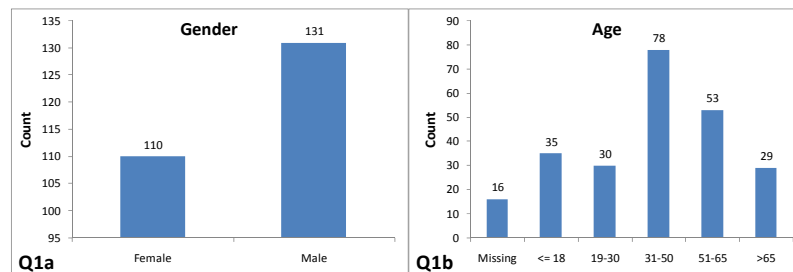


Figure 8.10: Frequency statistics of Q1

Frequency statistics of Q2 (port of embarkation) is shown in Figure 8.11. Since, the vessel visited port-A twice, therefore most participants (52%) boarded the vessel at this port.

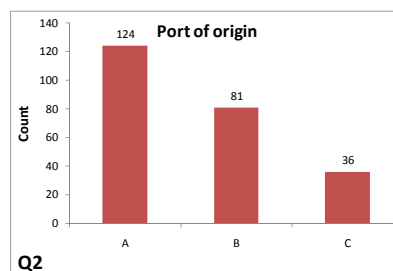


Figure 8.11: Frequency statistics of Q2

Frequency table of Q3 (passenger zone) is given in Figure 8.12. Ferry MH-I was operating on a short journey (approximately 2 hours) route, resultantly most commuters spent their time in restaurant / bars (34%) and sitting area (24%).

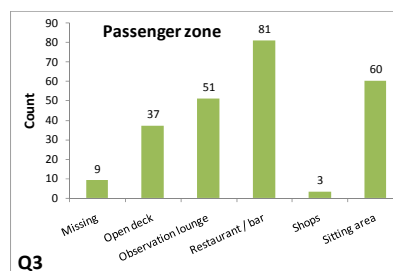


Figure 8.12: Frequency statistics of Q3

Figure 8.13 is showing the summary statistics of Q4 (primary activities). Reading (44%), talking (65%), visiting restaurant / bar / shops (59%) and looking outside (52%) were amongst the popular activities. ‘Other activities’ comprised of knitting (1 person), makeup (1), mobile phone (2), photography(1), watching TV (5), playing domino (2), writing (1) and smoking (2).

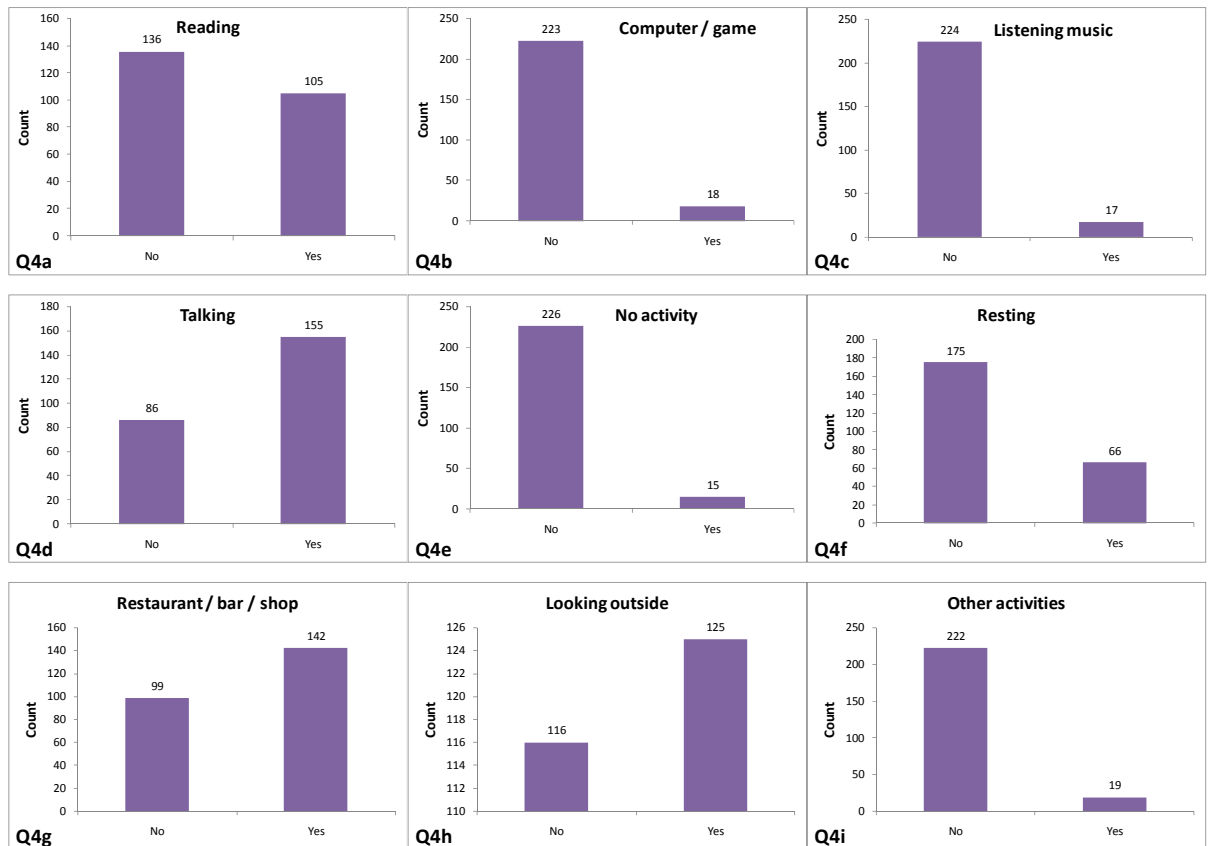


Figure 8.13: Frequency statistics of Q4

Frequency statistics of Q5 (use of alcohol) is given in Figure 8.14. Very few passenger had consumed more than two alcoholic drinks before (4%) and during (2.5%) the voyages.

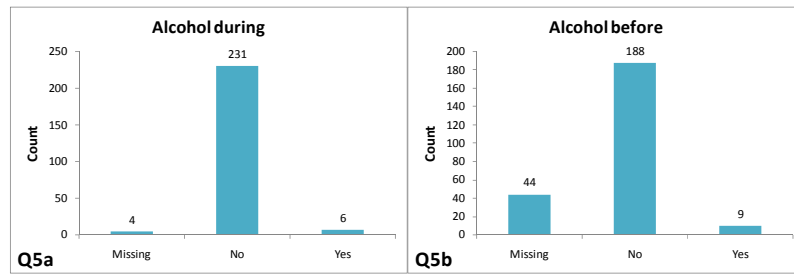


Figure 8.14: Frequency statistics of Q5

The summary statistics of Q6 (sickness symptoms) are shown in Figure 8.15. Hot / sweating (13.3%), headache (8.3%), stomach awareness (9.1%), and nausea (13.7%) were amongst the commonly reported symptoms of seasickness. While, less than 2% passengers reported to have vomited.

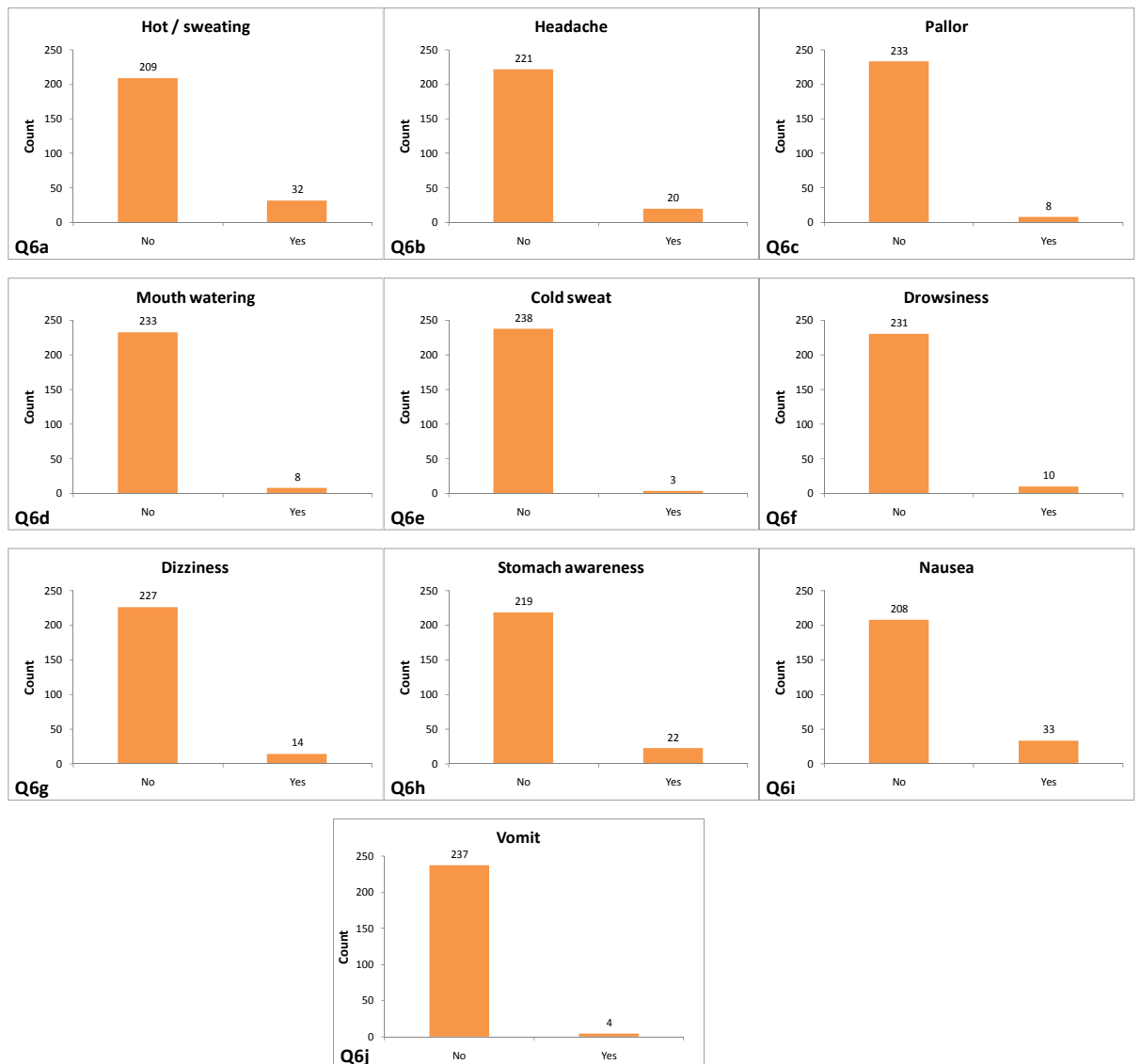


Figure 8.15: Frequency statistics of Q6

Figure 8.16 below, is depicting the frequency statistics of Q7 (sickness feelings). Almost 79% commuters felt 'alright' while 19.9% felt otherwise, which is in line with the prevailing weather conditions and the outcome of Q6 above.

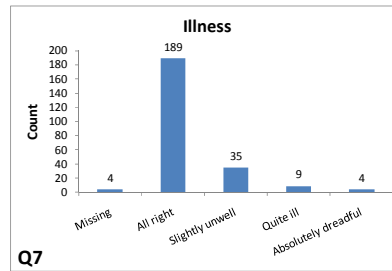


Figure 8.16: Frequency statistics of Q7

The frequency data pertaining to Q8 (time to felt unwell and vomit) is shown in Figure 8.17. In both the cases, most people did not mention the time by which they felt unwell (77%) or vomited (84%).

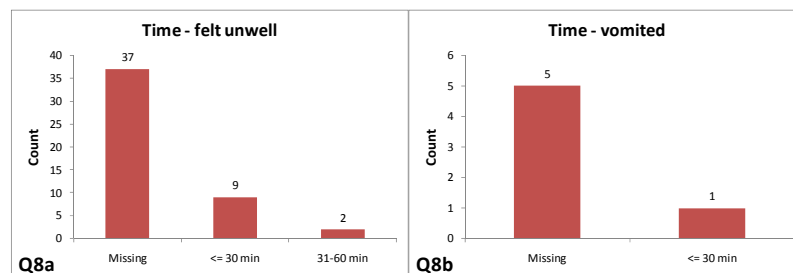


Figure 8.17: Frequency statistics of Q8

Frequency statistics of Q9 (use of anti-sickness medication) is given in Figure 8.18. Perhaps due to good weather, very few people (2.9%) resolved to use anti-sickness medications.

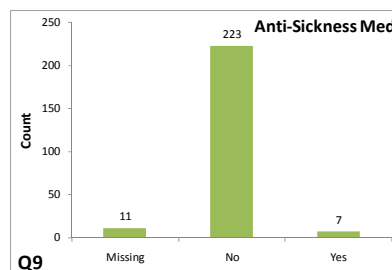


Figure 8.18: Frequency statistics of Q9

As shown in Figure 8.19, most people (58.5%) were frequent travellers on various types of ships, as well as a majority (58.1%) used ferry MH-I on regular basis.

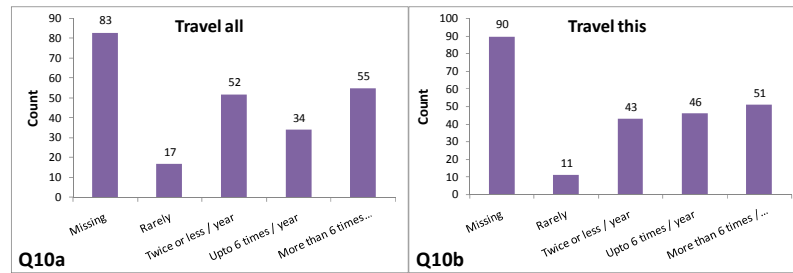


Figure 8.19: Frequency statistics of Q10

The summary statistics of Q11 (sickness history) is depicted in Figure 8.20. Most participants had experienced motion sickness aboard ships (44%), cars (27.8%), and busses (20.7%). While, aircraft (12.4%) and train sickness (6.6%) histories were not very common, as these modes of transportation are not very popular in the area of vessel operation.

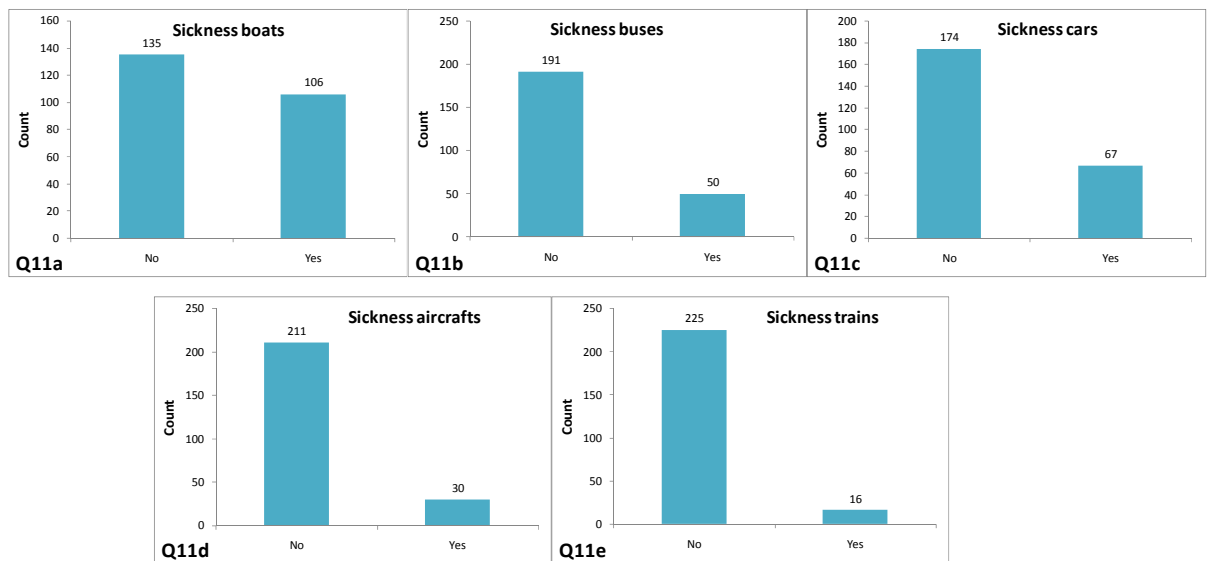


Figure 8.20: Frequency statistics of Q11

As depicted in Figure 8.21, almost 35% participants found the vessel motions interfering with sitting and 61.4% experienced some form of difficulties in standing.

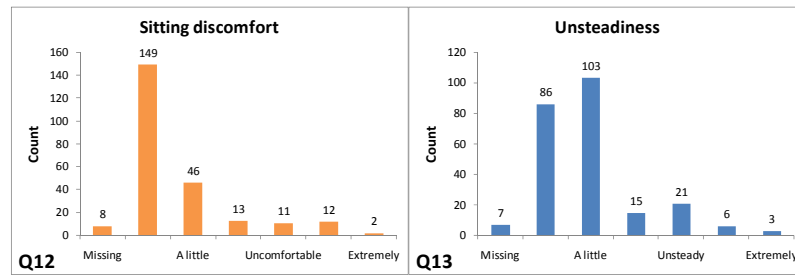


Figure 8.21: Frequency statistics of Q12 and 13

Frequency statistics of Q14 (difficulties in mundane activities due to vessel motions) are shown in Figure 8.22. Vessel motions were considered to interfere with eating & drinking (14.1%), reading (10.8%), writing (12.4%), and other activities (5.4%).

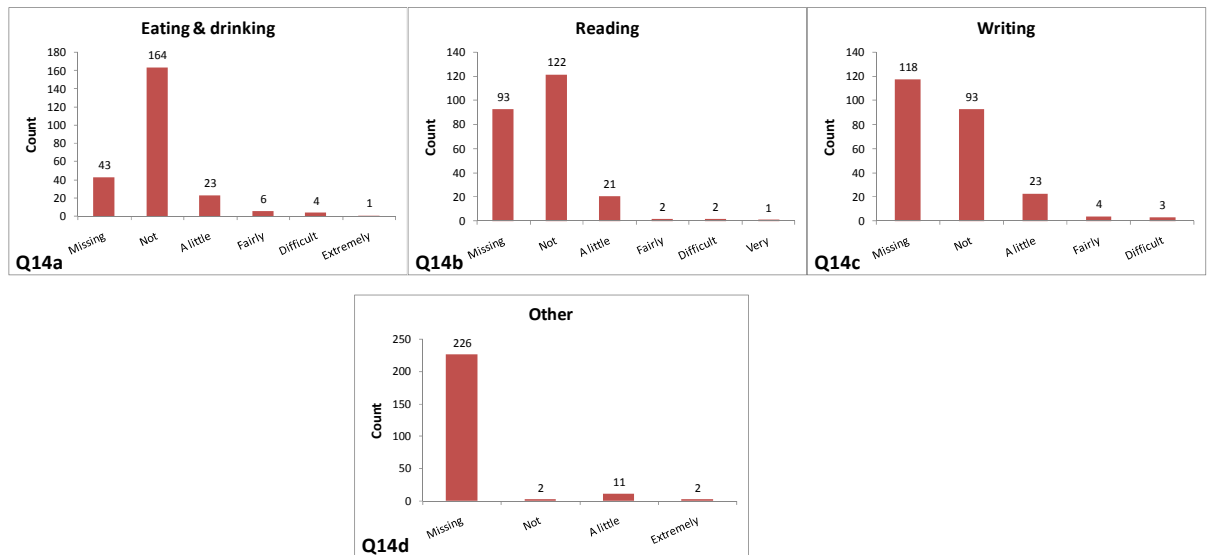


Figure 8.22: Frequency statistics of Q14

Summary statistics for Q15 (most discomforting factors) are shown in Figure 8.23. 11% considered seasickness as the most discomforting factor, followed by unsteadiness (10.8%), vibration (7.9%), and noise (5.0%). For the second most discomforting factor the order was vibration (10%), unsteadiness (4.1%) and noise (3.7%).

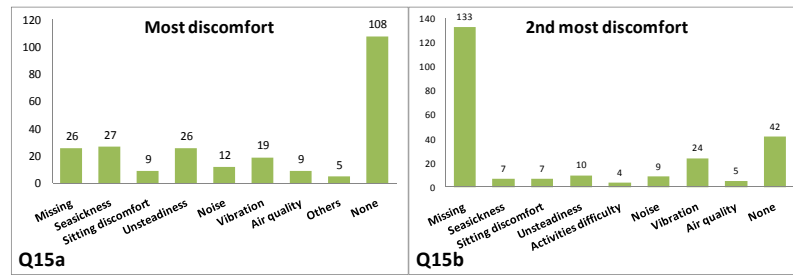


Figure 8.23: Frequency statistics of Q15

The frequency statistics of Q16 to 19 are given in Figure 8.24 below. Majority of the participants (96%) found their expectations to be met or exceeded. 98.8% were satisfied with the comfort levels, however, 31.1% did feel fatigue. Lastly, 94.2% respondents enjoyed their travel aboard ferry MH-I.

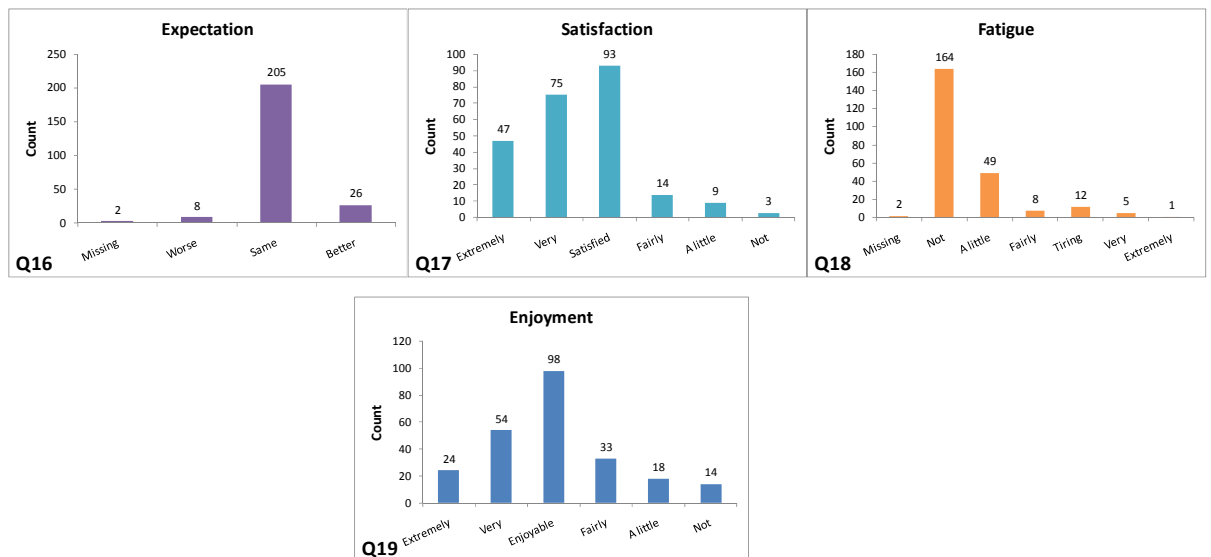


Figure 8.24: Frequency statistics of Q16 to Q19

8.7.2 Cross Tabulations - Significant Dependencies

All questionnaire replies were fed into SPSS¹ software, to produce cross tables of all answers in various categories of the first nineteen questions of the survey questionnaire (Figure 8.3), used aboard MH-I. The last i.e. 20th question was an open query for which a total of four replies were received: two of which praised the vessel environment and remaining two expressed their dislike for sea travel.

¹ Statistical Package for Social Science (SPSS) is a trademark of “SPSS: An IBM Company”

In order to establish significant dependencies amongst the recorded data, the χ^2 statistics were calculated, using Pearson's method, by comparing the observed frequencies in a cell with the expected ones if no relationship existed. These χ^2 statistics were then employed to estimate the probability (*p-value*) of observing the recorded frequencies if the null hypothesis were true (H_0 : there are no dependencies; H_1 : there are significant dependencies amongst the row and column variables). This is a typically procedure of cross tabulations for establishing the relationships between the considered variable. It is well covered in most standard texts on statistical analysis, therefore, further details of the method are not discussed here (see, e.g. Croarkin et al. 2003; DeCoursey 2003; Gibilisco 2004; Field 2005; Ryan 2007; Sá 2007; McDonald 2008 for further details).

One important condition imposed by the Pearson-Chi statistics is that the expected count of a cross table cell should not be less than 5. Since the data comprised of relatively small size (241 replies in total), hence this requirement was violated by several categories of different variables. In all such cases, the Fisher's Exact Test was employed to estimate the *p-value*. These probabilities (*p-values*) of committing type-I error (i.e. erroneously rejecting H_0) for all cross tabulations are summarised in Table C.2.2 of Appendix C. It is intuitive to guess that the smaller the *p-value* is, the larger the chances are that a significant relationship exists between the row and column variables in a cross table.

In general a $p < 0.05$ is considered to be significant enough to reject H_0 ; however, this only holds true if we are to conduct a single hypothesis test i.e. while comparing only one feature of two samples. In our case, each variable (e.g. Q1a) was cross tabulated with remaining 47 variable i.e. 47 null hypotheses were tested simultaneously. Such a situation is referred to as 'multiple hypothesis testing' and is one of the active area of research in statistics (see Farcomeni 2008 for a recent review). A *p-value* of 0.05 implies that there are 5% chances of observing the recorded data given the null hypothesis is true. Now, if we were to carry out 100 statistical tests for which H_0 is actually true; we would still expect 5 tests to be significant at $p < 0.05$ level, just by chance. There are several approaches to tackle this situation, however, the two most

popular ones are (1) family-wise error rate (FWER) and (2) false discovery rate (FDR) control.

The family wise error rate (FWER), controls the probability (α_{Family}) of observing at least one significant result in a series (family) of statistical tests while the H_0 is true (Abdi 2007). Given the m statistical tests are independent; a threshold p -value for each test ($\alpha_{PerTest}$) is calculated using the Šidák-Bonferonni correction [Equation(8.1)]. A statistical test in a series (family) would be considered significant if $p < \alpha_{PerTest}$. (i.e. p -value of that test is less than $\alpha_{PerTest}$). However, FWER is very conservative in controlling type-I error (rejecting H_0 when it is true) in ‘multiple-hypothesis testing’ and is known to possess relatively small statistical power, which may easily lead to type-II errors (not rejecting false H_0). Moreover, FWER control is considered to be appropriate when a single false-positive (type-I error) in a set of tests may affect the conclusions drawn by the whole family (McDonald 2008).

$$\alpha_{PerTest} = 1 - (1 - \alpha_{Family})^{1/m} \quad (8.1)$$

The false discovery rate (FDR), on the other hand, controls the proportion of discoveries (significant results) that are actually false positives (Benjamini & Hochberg 1995; Benjamini & Yekutieli 2001). In this case the allowable percentage of false discoveries (q) is decided prior conducting the multiple-tests. Afterwards, the p -values of each independent test in a series of m tests are arranged in an ascending order, with the smallest p -value having a rank $k=1$ and the largest $k=m$. These p -values of individual tests are then compared with ‘ $(k/m)q$ ’ values and all test up to and including the one with largest p -value $\leq (k/m)q$ are considered to be significant. FDR has higher statistical power than FWER, which increases with the increasing number of hypothesis being tested. If the individual tests are not independent then the largest k is established such that:

acceptable i.e. allowing 5% false discoveries, the significant relationships of each variable has been established using FDR approach. The resulting significant dependencies are summarized in

Table 8.13, which by virtue of cross-tabulation procedure is symmetrical about its diagonal e.g. relationship between Q1b and Q4a is same as Q4a and Q1b.

8.7.3 Cross Tabulation – Measures of Association

As such,

Table 8.13 is only indicating the significant dependencies amongst various recorded variables and provides no information about the strength and direction of these relationships. There are several measures of associations that represent the strength and direction of relationship between the categorical variables of a cross table. The specific measure of association to be used depends on the type of data (dichotomous, nominal, ordinal or interval/continuous) as well as the size of cross table (2-by-2 or r-by-c; r: row; c: columns). Garson (2008b) has discussed some of the commonly used measures of association for cross tabulation, given in Table 8.14.

Table 8.14: Measures of association for cross tabulation (Garson 2008b)

Data Type	Table Size	Measures of Association
Dichotomous	2-by-2 / any	1. Percent difference (%d) 2. Yule's Q 3. Yule's Y 4. Relative Risk Coefficient, RR 5. Relative Risk Reduction, RRR 6. Odds Ratio, OR
Nominal	2-by-2	1. Phi
	any	2. The Contingency Coefficient, Pearson's C 3. Sakoda's adjusted Pearson's C, C* 4. Tshuprow's T 5. Cramer's V

Data Type	Table Size	Measures of Association
		6. Goodman-Kruskal's Lambda 7. The Uncertainty Coefficient, UC 8. Goodman-Kruskal's Tau
Ordinal	any	1. Goodman-Kruskal's Gamma 2. Kendall's Tau-b 3. Kendall's Tau-c 4. Somers' D

Being outside the scope of this work, the detailed account of the measures of associations enlisted in above table are not presented here (see Darlington 1996 and; Garson 2008b for further details). However considering simplicity and, especially, the ease of interpretation, the measures of associations given in Table 8.15 have been chosen to assess the strength and direction of significant cross tabulation dependencies identified in §8.7.2.

Table 8.15: Measures of association selected for assessing the strength and direction of significant dependencies of survey questionnaires

Data Type	Survey Questions	Measure of Association	Remarks
Dichotomous	Q1a Q4a to Q4i Q5a & Q5b Q6a to Q6j Q9 Q11a to Q11e	Percent difference (%d)	It is the simplest of all measures of association. It provides the influence of column (independent variable) dichotomy on row variable. The survey question being considered at a given instant (e.g. Q1a or Q4a, etc.) were treated as independent (column) variables.
Nominal	Q3 Q15a & Q15b	Goodman- Kruskal Tau	Tau is a PRE (proportionate reduction in error) measure. Its value indicates how much error (in percentage) would be reduced in predicting the dependent

			variable if the independent variable is known. Thus, a large value of Tau would indicate a greater probability of predicting row variable given the knowledge of column variable i.e. a strong association between the two.
Ordinal	Q1b Q7 Q10a & Q10b Q12 Q13 Q14a to Q14c Q16 to Q19	Goodman- Kruskal Gamma	Gamma may also be interpreted as a PRE measure. However, it represents the percentage reduction of error in predicting the rank (not value) of dependent variable given the knowledge of independent variable. Also a large (positive or negative) gamma represents strong association.

It is important to note that, for the cases of mixed data levels (e.g. dichotomous-by-nominal, nominal-by-ordinal etc.), Garson(2008b) suggests to use the measure of association appropriate for the lower data level. This means, if we cross tabulate dichotomous with nominal (or ordinal) and vice versa, then measure of association appropriate for dichotomous should be used. Consequently, the following subsections presenting the strength of significant dependencies are arranged on the basis of lower level data type. Thus, though there is no difference in terms of dependencies between dichotomous Q1a and ordinal Q7 as well as between Q7 and Q1a, the discussions are limited to the first case (i.e. Q1a-by-Q7) and dichotomous measure of association (percent difference) is given. Similarly for the cross tabulation of ordinal Q7 and nominal Q15a, the discussions only refer to Q15a-by-Q7 relationship using measure of association appropriate for nominal data (i.e. Tau).

8.7.4 Measures of Association / Effects for the Dichotomous Variables

As shown in Table 8.15, the percent difference has been selected as the measure of association for the interactions of dichotomous variables with dichotomous and

higher level (nominal and ordinal) variables. These measures are summarised in Table 8.16 for all dichotomous variables of survey questionnaires, displaying significant relationships with other variables (as established in §8.7.2).

Since the

Table 8.13 depicting significant dependencies is symmetric about its diagonal, the measures of association for the dichotomous variables are not discussed for both variables. For example, the percent differences are discussed for Q1a-by-Q6i and not for the Q6i-by-Q1a cross tabulation. Also for the dichotomous-by-higher level data (nominal or ordinal) interactions, the discussions are limited to the dichotomous variable only. Thus, for the interactions between variable Q1a and Q7 the percent differences are discussed for Q1a-by-Q7 tabulation only.

Due to space limitations, the complete set of cross tables are not reproduced in the thesis, however, sample tables for each dichotomous variable displaying significant dependency are given in Table C.2.3 to Table C.2.26 of Appendix C. The measures of these associations (Table 8.16)/effects of the aforesaid variables are briefly discussed in the following (for the lower triangle of Table 8.13):

8.7.4.1 Effects of Q1a (Gender)

- Males experienced lesser nausea (18.3%) [Q6i].
- Males reported lesser illness levels than females [Q7].
- Males had more travelling experience aboard ships [Q10a].
- Males reported reduced history of motion sickness on boats, busses, cars, aircrafts and trains [Q11a to Q11e].
- Males experienced lesser sitting discomfort [Q12] and unsteadiness [Q13].
- In terms of primary issues, males considered noise and air quality to be more disturbing, while seasickness, sitting discomfort, unsteadiness, and activities to be less discomforting than did consider the females [Q15a].
- For secondary discomforts, only seasickness was rated more by males than females.

8.7.4.2 Effects of Q4a (Reading Activity)

- There was an increase in reading activity with aging [Q1b].
- Readers experienced lesser (14.1%) nausea [Q6i].
- Readers also reported reduced illness feelings [Q7].
- Passenger engaged in reading felt lesser sitting discomfort [Q12].
- People involved in reading also felt lesser unsteadiness [Q13].
- Only vibration was considered as the primary discomforting factor by the people involved in reading (perhaps due to vibration induced visual disturbances) [Q15a].

8.7.4.3 Effects of Q4c (Listening to Music)

- There was a decrease in music listening activity with aging [Q1b].
- Music listeners experienced more (22.7%) headache [Q6b]. It appears that age is playing the role of confounding variable in this case, as the younger people tend to listen to music more and complain about headache (see the relationship of Q6b with age in §8.7.4.11).
- The sickness history of music listeners was higher for aircrafts and trains [Q11d & Q11e].

8.7.4.4 Effects of Q4d (Talking)

- Onboard location of the passenger had a bearing on talking activity [Q3].
- People engaged in talking also visited restaurant / bar / shops more frequently [Q4g].
- Talking passengers also had an increased tendency of looking outside [Q4h].
- Talkers complained more (10.4%) about nausea [Q6i].
- The commuters spending their time talking reported higher history of bus and air sickness [Q11b & Q11d].

8.7.4.5 Effects of Q4e (No Activity)

- Passengers not engaged in any specific activity felt more (17.8%) pallor [Q6c] and (25.8%) stomach awareness [Q6h].

Table 8.16: Measures of association (percent differences) for dichotomous variables (red cells: %d > +1%; blue: %d < -1%; green: -1% < %d < +1%)

Questions		Categories	Gender	Reading	Music	Talk	Nothing	Resting	Restaurant/bar/shop	Looking out	Alcohol before	Hot/sweating	Headache	Pallor	Mouth watering	Cold sweat	Drowsiness	Dizziness	Stomach awareness	Nausea	Vomit	Anti-Sickness Medicine	Sickness boats	Sickness buses	Sickness cars	Sickness aircrafts	
			Q1a	Q4a	Q4c	Q4d	Q4e	Q4f	Q4g	Q4h	Q5a	Q6a	Q6b	Q6c	Q6d	Q6e	Q6f	Q6g	Q6h	Q6i	Q6j	Q9	Q11a	Q11b	Q11c	Q11d	
Q1a	Gender	Male																									
Q1b	Age	<18		-14.2	30.4				4.0				19.3								-38.4	26.9	25.0				
		18-30		-8.5	19.3				16.9				21.7									7.0	47.7				
		31-50		3.8	-17.1				-8.2				-13.5									-6.5	-35.5				
		51-65		10.2	-18.6				-6.6				-25.6									-19.8	-24.1				
		>65		8.7	-13.9				-6.0				-1.9									-7.5	-13.2				
Q3	Passenger zone	Open deck				-1.4																					
		Obs lounge				4.0																					
		Restaurant/bar				17.9																					
		Shops				-3.5																					
		Sitting area				-8.3																					
Q4a	Reading	Yes																		-29.4							
Q4b	Computer	Yes																		20.3							
Q4c	Music	Yes										19.6													14.8		
Q4d	Talk	Yes						21.7	19.3															19.8	25.5		
Q4e	Nothing	Yes											32.3						18.2								
Q4f	Resting	Yes																46.8	34.9	20.9							
Q4g	Rest/bar/shop	Yes				22.9			28.8																		
Q4h	Looking out	Yes				21.0		29.7																	21.2		
Q4i	Other	Yes																									
Q6a	Hot/sweating	Yes												50.9		87.8	38.3			23.2							
Q6b	Headache	Yes			22.7															18.5				12.2			
Q6c	Pallor	Yes					17.8				14.2				48.3	64.1	48.7	26.8	21.4	20.7	37.5					11.4	
Q6d	Mouth water	Yes																		13.7	37.5		7.5				
Q6e	Cold sweat	Yes									9.4			24.6						9.1							
Q6f	Drowsiness	Yes									13.2			60.4					20.4	9.2							
Q6g	Dizziness	Yes						12.9						45.7						21.4							
Q6h	Stomach aware	Yes					25.8	14.6						55.2			42.6			24.5						20.0	
Q6i	Nausea	Yes	-18.3	-14.1		10.4		12.4				23.8	28.7	76.3	50.5	87.4	27.4	46.1	35.0		88.1		14.0	13.7	18.2	33.9	
Q6j	Vomit	Yes												23.7	23.7					15.2						9.1	
Q7	Illness	All right	18.9	21.8				-25.1				-34.4	-46.6	-69.6	-43.7	-80.8			-54.4	-67.9	-85.6	-81.5		-27.7	-25.0	-20.2	-37.9
		SI unwell	-13.7	-17.3				19.9				15.4	29.7	23.5	10.6	18.8			14.7	53.9	49.7	-15.1		20.2	24.4	11.0	25.1
		Quite ill	-4.9	-1.5				3.2				13.7	13.0	21.9	9.0	63.7			26.3	10.8	27.3	37.0		3.6	0.3	9.4	10.9
		Abs dreadful	-0.3	-3.0				1.9				5.3	3.9	24.1	24.1	-1.7			13.4	3.2	8.6	59.6		3.9	0.4	-0.2	1.9

Questions		Categories	Gender	Reading	Music	Talk	Nothing	Resting	Restaurant/br r/shop	Looking out	Alcohol before	Hot / sweating	Headache	Pallor	Mouth watering	Cold sweat	Drowsiness	Dizziness	Stomach awareness	Nausea	Vomit	Anti-Sickness Medicine	Sickness boats	Sickness buses	Sickness cars	Sickness aircrafts	
			Q1a	Q4a	Q4c	Q4d	Q4e	Q4f	Q4g	Q4h	Q5a	Q6a	Q6b	Q6c	Q6d	Q6e	Q6f	Q6g	Q6h	Q6i	Q6j	Q9	Q11a	Q11b	Q11c	Q11d	
			Male	Yes	Yes	Yes	Yes	Yes	Yes	Yes	Yes	Yes	Yes	Yes	Yes	Yes	Yes	Yes	Yes	Yes	Yes	Yes	Yes	Yes	Yes	Yes	Yes
Q15a	Most discomfort	Seasickness	-16.0	-10.8				10.3				16.4	24.7	38.9	38.9			19.4	21.5	71.1	69.0		19.3	21.4		33.3	
		Sitting discom	-3.5	-1.7				1.1				6.8	0.9	-4.3	-4.3			11.9	0.4	2.2	-4.3		1.4	2.7		7.1	
		Unsteadiness	-0.1	-8.0				13.3				1.4	-2.3	0.4	-12.6			19.9	16.9	-3.5	-12.4		-0.4	5.9		-2.0	
		Noise	2.9	-4.2				1.5				-2.6	-0.6	-5.8	-5.8			-5.9	-6.2	-6.6	-5.7		-4.9	-4.5		-6.5	
		Vibration	-0.5	1.5				-5.3				5.2	6.8	16.8	16.8			-1.2	10.4	0.3	11.4		5.7	-0.6		-6.2	
		Air quality	2.1	-3.6				1.1				18.4	0.9	8.6	8.6			-4.5	-4.7	-4.9	-4.3		-2.3	2.7		3.1	
		Others	0.6	-0.3				3.7				1.2	2.9	-2.4	-2.4			5.7	-2.6	-2.7	-2.4		-0.7	-3.0		-2.7	
None	14.5	27.1				-25.8				-46.8	-33.3	-52.2	-39.2			-45.3	-35.7	-55.8	-51.4		-18.2	-24.4		-26.2			
Q15b	2nd most discomfort	Seasickness	2.0					4.9			3.9							16.8	10.7	37.9		6.6					
		Sitting discom	-1.3					-0.2			3.9							-3.2	7.2	37.9		-0.1					
		Unsteadiness	-0.7					3.6			-1.2							10.4	12.7	-4.2		4.4					
		Act difficulty	-0.3					2.8			-1.9								-1.8	1.6	-1.7		0.4				
		Noise	-1.5					-7.4			-4.3								0.9	-0.8	-3.8		3.4				
		Vibration	-3.4					3.2			24.6								4.0	2.5	10.3		-0.9				
		Air quality	-2.9					-1.6			4.8								2.7	-2.4	-2.1		3.0				
None	20.4								-16.5								-19.2	-20.2	-17.8		-5.8						
Q16	Expectation	Worse																16.3	10.2	37.4							
		Same																-14.4	-1.1	-26.3							
		Better																-2.0	-9.1	-11.1							
Q17	Satisfaction	Extremely									-22.5	-10.4	-20.2					-20.7	-16.5	-15.6	-19.9						
		Very									-7.1	-12.1	-32.2					-17.9	-19.2	-11.5	-31.8						
		Satisfied									13.2	-9.4	24.7					-10.6	7.6	0.9	1.4						
		Fairly									4.1	15.5	-6.0					9.0	13.6	3.8	-5.9						
		A little									10.1	12.3	22.0					26.4	10.9	16.7	37.0						
Not									2.2	4.1	11.6					13.8	3.6	5.6	19.2								
Q18	Fatigue	Not					-32.0			-43.1	-36.7	-58.1	-45.1				-29.9	-50.1	-25.5	-40.9					-23.6	-32.7	
		A little					15.6			8.8	10.4	-8.3	-8.3				-11.0	16.2	-2.6	14.9					15.6	18.5	
		Fairly					-0.4			10.6	7.3	9.5	22.4				-3.5	11.6	1.3	10.2					1.7	0.0	
		Tiring					14.0			15.9	10.9	46.5	20.7					36.5	17.4	24.5	15.3					3.5	9.5
		Very					1.3			8.4	8.6	10.8	10.8					8.3	5.4	2.7	1.1					3.4	5.2
		Extremely					1.5			-0.5	-0.5	-0.4	-0.4					-0.4	-0.4	-0.5	-0.5					-0.6	-0.5
Q19	Enjoyment	Extremely									-7.9	-5.4	-10.3	-10.3	-10.1			-10.6	-6.0	-8.0	-10.2						
		Very									-18.6	-19.0	-23.2	2.7	-22.7			-16.2	-24.7	-11.9	-2.5						
		Enjoyable									3.6	-17.1	-29.1	-29.1	-41.2			-12.8	-9.7	-22.5	-21.1						
		Fairly									-5.0	17.8	-14.2	-14.2	-13.9			0.6	9.9	1.7	-14.0						
		A little									23.8	8.2	56.9	31.1	93.7			22.4	21.8	26.5	-7.6						
		Not									4.1	15.5	19.8	19.8	-5.9			16.6	8.6	14.3	55.3						

8.7.4.6 Effects of Q4f (Resting / Sleeping)

- The commuters trying to rest / sleep during the voyage felt more dizziness, stomach awareness and nausea [Q6g, Q6h, & Q6i].
- Passengers resting / sleeping reported increased level of illness [Q7].
- The passengers resting / sleeping felt elevated levels of unsteadiness, which may be due to the illness they experienced.
- Seasickness, sitting discomfort, unsteadiness, noise, and air quality were the primary sources of discomfort for passengers trying to rest / sleep [Q15a].
- Passengers trying to rest / sleep also felt increased level of fatigue [Q18].

8.7.4.7 Effects of Q4g (Visiting Restaurant / Bar / Shops)

- There was a decrease in visiting of restaurant / bar / shops with aging [Q1b].
- The passengers visiting restaurant / bar / shop looked outside the ship [Q4h] more often. Such commuters found seasickness, unsteadiness, activity difficulties and vibration as the second most important sources of discomfort [Q15b].

8.7.4.8 Effects of Q4h (Looking Outside)

- The passengers looking outside reported higher history of carsickness [Q11c].

8.7.4.9 Effects of Q5a (Consuming Alcohol before Travelling)

- The passengers consuming more than two alcoholic drinks prior to their voyage experienced increased level of sitting discomfort [Q12].

8.7.4.10 Effects of Q6a (Feeling Hot / Sweating)

- Passengers feeling hot / sweating also reported more (14.2%) pallor [Q6c], (9.4%) cold sweating [Q6e], (13.2%) drowsiness [Q6f] and (23.8%) nausea [Q6i] than those not feeling hot / sweating.
- Illness level of passengers feeling hot / sweating was higher than those not feeling hot / sweating [Q7].
- The Passengers feeling hot / sweating experienced more sitting discomfort [Q12]. Such commuters also reported increased level of unsteadiness [Q13]. They

considered seasickness, sitting discomfort, unsteadiness, vibration, and air quality as the primary sources of discomfort, more often [Q15a]. Seasickness, sitting discomfort, vibration and air quality were also their second most important sources of discomfort [Q15b]. They had lower level of satisfaction [Q17], felt more fatigued [Q18] and did not enjoy their trip much [Q19].

8.7.4.11 Effects of Q6b (Feeling Headache)

- Younger passengers felt headaches more often and there was a decrease with aging [Q1b].
- Passengers experiencing headache complained more (28.7%) about nausea [Q6i].
- Passengers feeling headache also felt higher levels of illness [Q7]. They (perhaps the younger ones) had lesser experience of sea travel [Q10a]. Such passengers had more history of bus [Q11b] and train [Q11e] sickness. They felt more sitting discomfort [Q12]. The primary discomforting sources of such commuters included seasickness and vibrations [Q15a].
- The passengers feeling headache were not very satisfied with their travel [Q17], got more fatigued [Q18] and did not enjoy their trip as much [Q19].

8.7.4.12 Effects of Q6c (Experiencing Pallor)

- Passengers experiencing pallor, complained more about (48.3%) mouth watering [Q6d], (24.6%) cold sweating [Q6e], (60.4%) drowsiness [Q6f], (45.7%) dizziness [Q6g], (55.2%) stomach awareness [Q6f], (76.3%) nausea [Q6i], and (23.7%) vomiting [Q6j].
- Illness levels of the passenger experiencing pallor were also elevated [Q7]. They had higher history of air [Q11d] and train [Q11e] sickness. Such commuters felt more sitting discomfort [Q12], unsteadiness [Q13]. They observed more difficulties in eating & drinking [Q14a].
- The passengers feeling pallor found seasickness, vibration and air quality as the primary sources of discomfort, more often [Q15a]. The satisfaction level [Q17] of such people was lower, they felt more fatigued [Q18] and did not enjoy [Q19] the voyages much.

8.7.4.13 Effects of Q6d (Feeling Mouth Watering)

- Passengers noting mouth watering, complained more about (50.5%) nausea [Q6i], and (23.7%) vomiting [Q6j].
- The commuters feeling mouth watering also felt more illness [Q7]. They had higher history of boat [Q11a] and train [Q11e] sickness. These passengers felt sitting discomfort [Q12] and unsteadiness [Q13] more often. Their primary sources of discomfort included seasickness, vibration and air quality more often. Such commuters felt more fatigued [Q18] and did not enjoy their sea travel much [Q19].

8.7.4.14 Effects of Q6e (Experiencing Cold Sweating)

- Passengers reporting cold sweating also experienced more (87.4%) nausea [Q6i].
- Illness level of the passengers feeling cold sweating was higher [Q7]. They felt sitting discomfort [Q12] and unsteadiness [Q13] more often. Such commuters also found it more difficult to eat and drink [Q14a] and could not enjoy their voyage much [Q19].

8.7.4.15 Effects of Q6f (Drowsiness)

- Passengers experiencing drowsiness also experienced more (42.6%) stomach awareness [Q6h] and (27.4%) and nausea [Q6i].
- The passengers feeling drowsiness got fatigued [Q18] more often.

8.7.4.16 Effects of Q6g (Dizziness)

- Passengers reporting dizziness also experienced nausea [Q6i] more often (46.1%).
- Commuters feeling dizziness also felt increased levels of illness [Q7] and unsteadiness [Q13]. Their primary sources of discomfort included seasickness, sitting discomfort, and unsteadiness more often. They were less satisfied [Q17] with the voyage comfort, felt more fatigued [Q18] and did not enjoy [Q19] their travelling aboard the ship much.

8.7.4.17 Effects of Q6h [Stomach Awareness]

- Passengers experiencing stomach awareness also felt nausea [Q6i] more often (35%).
- Illness levels of the stomach aware passengers were higher [Q7]. Such passengers reported to have increased history of boats [Q11a], busses [Q11b], aircraft [Q11d] and train [Q11e] sickness. They experienced unsteadiness [Q13] more often and had more difficulty in eating and drinking [Q14a]. The primary sources of discomforts of such passengers included seasickness, unsteadiness, and vibration [Q15a]. While, the second most important discomfort comprised of seasickness, unsteadiness, vibration and air quality [Q15b].
- The commuters experiencing stomach awareness found the voyage to be less comfortable than their expectations [Q17], less satisfying [Q17], more fatiguing [Q18] and less enjoyable [Q19].

8.7.4.18 Effects of Q6i (Nausea)

- Feelings of nausea decreased with aging [Q1b].
- Passengers feelings nausea vomited [Q6j] more often (15.2%).
- The commuters feeling nausea also felt increased level of illness [Q7]. Such people had higher history of motion sickness on boats [Q11a], busses [Q11b], cars [Q11c], aircrafts [Q11d] and trains [Q11e]. They reported sitting discomfort [Q12], higher unsteadiness in standing [Q13], more difficulties in eating & drinking [Q14a], reading [Q14b], and writing [Q14c] more often. Their primary sources of discomforts included seasickness and sitting discomforts [Q15b]. While the second most important discomforts comprised of seasickness, sitting discomforts, unsteadiness, activity difficulties, and vibrations [Q15b].
- Comfort expectations of passengers feeling nausea were not met [Q16], they were less satisfied [Q17], got more fatigued [Q18] and did not enjoy their voyage [Q19].

8.7.4.19 Effects of Q6j (Vomiting)

- Interestingly, gender did not show any significant relationship with vomiting (perhaps due to good weather conditions, as not many people vomited).

- The passengers experiencing emesis felt more illness [Q7]. They had higher history of boat [Q11a] and aircraft [Q11d] sickness. Such commuters experienced increased level of sitting discomforts [Q12], unsteadiness in standing [Q13] and difficulties in eating & drinking [Q14a]. The primary discomforts of such people comprised of seasickness and vibration [Q15a]. Whereas, for the second most important discomfort, they considered seasickness, sitting discomfort, and vibration more often [Q15b]. Due to understandable reasons, their expectations of voyage comfort were not met [Q16], they were less satisfied [Q17] and did not enjoy [Q19] their travel.

8.7.4.20 Effects of Q9 (Usage of Anti-Sickness Medication)

- The passengers using anti-sickness medicines prior to their travel had difficulties in eating and drinking [Q14a] more often.

8.7.4.21 Effects of Q11a (Past History of Motion Sickness in Boats)

- The passengers with past history of seasickness felt increased level of illness [Q7]. They also had higher history of bus [Q11b], car [Q11c], aircraft [Q11d] and train [Q11e] sickness. Such commuters felt sitting discomfort [Q12] and unsteadiness in standing [Q13] more often.
- The primary discomforts of passengers with past history of seasickness included seasickness, sitting discomfort, and vibration [Q15a]. While for the second most important discomforts, they considered seasickness, unsteadiness, noise, and air quality more often.

8.7.4.22 Effects of Q11b (Past History of Motion Sickness in Busses)

- The commuters with past history of motion sickness in busses experienced higher level of illness during the voyage [Q7]. Such people also had higher history of cars [Q11c], aircraft [Q11d] and train [Q11e] sickness.
- The passengers with bus-sickness history felt it more difficult to do writing work [Q14c]. Their primary sources of discomfort comprised on seasickness, sitting discomfort, unsteadiness and air quality [Q15a].

8.7.4.23 Effects of Q11c (Past History of Motion Sickness in Cars)

- The commuters with carsickness history felt elevated level of illness [Q7]. These passengers also had past history of air-sickness [Q11d] and train-sickness [Q11e] more often. Such people got more fatigued during the voyage [Q18].

8.7.4.24 Effects of Q11d (Past History of Motion Sickness in Aircrafts)

- The passengers with air-sickness histories, also felt more ill [Q7]. Such people also had past history of train-sickness [Q11e]. They also felt more sitting discomforts [Q12], increased level of standing unsteadiness [Q13] and more difficulties in eating & drinking [Q14a]. Their primary discomforts comprised of seasickness, sitting discomfort and air quality [Q15a]. These commuters also felt more fatigued [Q18].

8.7.4.25 Effects of Q11e (Past History of Motion Sickness in Trains)

- The passengers with past history of train-sickness reported higher illness levels [Q7]. Such commuters also felt sitting discomfort more often. These people considered, seasickness, sitting discomfort and air quality as their primary sources of discomfort [Q15a], whereas, the second most important discomforts of such passengers included seasickness, unsteadiness, noise, vibration and air quality.
- The passengers with past history of train-sickness also felt more fatigued [Q18].

8.7.5 Measures of Association for the Nominal Variables

There were three nominal queries (Q3, Q15a and Q15b) in the passenger comfort survey questionnaires that displayed significant interactions with each other and higher level (ordinal) variables (

Table 8.13). As shown in Table 8.15, the Goodman-Kruskal Tau has been selected to measure the associations of such variable. Tau is an asymmetric measure, therefore, Table 8.17 in the following is summarising it for both way interactions of nominal variables (e.g. Q3-by-Q15a and vice versa). However, considering the suggestions of Garson(2008b) (to use the measure of association applicable to the lower data level),

the Tau values have only been presented for the nominal-by-ordinal (e.g. Q15a-by-Q7) dependencies and not for the vice versa.

Alike dichotomous variables, only sample cross tables of the nominal variables are reproduced as Table C.2.27 to Table C.2.29 in Appendix C. It may be noted that Goodman-Kruskal Tau varies from 0 to 1, where a 0 value indicates there is no improvement in guessing the dependent variable given the independent variable is known. While, a Tau equal to 1 suggests 100% improvement in predicting the dependent variable for a known independent variable. Keeping the aforesaid in view, the measures of associations for the nominal variables of survey questionnaire are briefly discussed in the following sections.

Table 8.17: Measures of association (Goodman-Kruskal Tau) for the nominal variables

		Description	Independent Variables		
			Q3	Q15a	Q15b
Dependent Variables	Q3	Passenger zone		5.1%	
	Q7	Illness		34.4%	12.6%
	Q10a	Travel all		7.7%	
	Q10b	Travel this		10.2%	
	Q12	Sitting discomfort		19.4%	10.7%
	Q13	Unsteadiness		16.9%	10.1%
	Q14a	Eating & drinking		18.1%	11.0%
	Q14b	Reading		13.0%	24.8%
	Q14c	Writing		25.2%	23.5%
	Q15a	Most discomfort	5.6%		
	Q15b	2nd most discomfort		16.3%	
	Q16	Expectation		5.9%	
	Q17	Satisfaction		7.4%	4.7%
	Q18	Fatigue		14.2%	
	Q19	Enjoyment		5.4%	3.6%

8.7.5.1 Measures of Association for Q3 (Passenger Zone)

- 5.6% improvement could be achieved in predicting the most discomforting factor [Q15a], by knowing the onboard location where the passengers spent their time. Thus, there is significant but relatively weak relationship between Q3 and Q15a.

8.7.5.2 Measures of Association for Q15a (Primary Discomforting Factors)

- The knowledge of primary discomforting factors contribute relatively small improvements in the predictability of:
 - the onboard location of the passengers (5.6%) [Q3]
 - the general frequency of travel at sea (7.7%) [Q10a].
 - the frequency of travelling aboard the vessel being surveyed (10%) [Q10b].
 - meeting passengers' comfort expectations (5.9%) [Q16].
 - the passengers' satisfaction level (7.4%) [Q17].
 - the passengers' enjoyment level (5.4%) [Q19].
- By knowing the primary discomforting factors, somewhat large improvements could be made in the predictability of:
 - the illness level (34.4%) [Q7].
 - the sitting discomfort experienced by the passengers (19.4%) [Q12].
 - the unsteadiness in standing (16.9%) [Q13].
 - the difficulties in eating & drinking (18.1%) [Q14a], reading (13.0%) [Q14b], and writing (25.2%) [Q14c].
 - the second most discomforting factor (16.3%) [Q15b].
 - the fatiguing characteristics of the voyage (14.2%) [Q18].

8.7.5.3 Measures of Association for Q15b (Second Most Discomforting Factors)

- Given the second most discomforting factors are known, relatively small improvements could be made in predicting the following:
 - the satisfaction level of the passengers (4.7%) [Q17].
 - the enjoy-ability of the voyage (3.6%) [Q19].

- Whereas, comparatively large improvements could be gained in the predictability of the following, provided the second most discomforting factors are known:
 - the illness level of the passengers (12.6%) [Q7].
 - the sitting discomfort experienced by them (10.7%) [Q12].
 - the unsteadiness in standing (10.1%) [Q13].
 - the difficulties in eating & drinking (11.0%) [Q14a], reading (24.8%) [Q14b], and writing (23.5%) [Q14c].

8.7.6 Measures of Association for the Ordinal Variables

As shown in

Table 8.13, there are thirteen ordinal queries displaying significant relationships with each other (Q1b, Q7, Q10a, Q10b, Q12, Q13, Q14a to Q14c, and Q16 to Q19). The measure of association selected for these variables is the Goodman-Kruskal's gamma. Gamma varies from -1 (100% negative association, perfect inversion) to +1 (100% positive association, perfect agreement), with a zero value indicating 'no association'. It is a symmetrical measure, therefore, the Table 8.18 summarising gamma values is symmetric about its diagonal i.e. Q1b-by-Q7 has measure of association identical to Q7-by-Q1b.

Table 8.18: Measures of association (Goodman-Kruskal Gamma) for the ordinal variables

		Description	Independent Variables															
			Q1b	Q7	Q10a	Q10b	Q12	Q13	Q14a	Q14b	Q14c	Q16	Q17	Q18	Q19			
Dependent Variables	Q1b	Age		-47.9%	11.3%													-19.5%
	Q7	Illness	-47.9%				78.9%	83.8%	83.4%	63.1%	53.2%	-55.9%	55.9%	71.2%	61.7%			
	Q10a	Travel all	11.3%			80.2%		-32.7%		-65.6%							-34.4%	
	Q10b	Travel this			80.2%													
	Q12	Sitting discomfort		78.9%				58.4%	61.6%	55.7%	42.1%	-45.7%	41.0%	50.3%	39.3%			
	Q13	Unsteadiness		83.8%	-32.7%		58.4%		84.0%	52.8%	59.7%	-46.7%	53.2%	57.3%	46.1%			
	Q14a	Eating & drinking		83.4%			61.6%	84.0%		79.4%	51.0%		58.5%	56.7%	58.6%			
	Q14b	Reading		63.1%	-65.6%		55.7%	52.8%	79.4%		92.0%			71.1%				
	Q14c	Writing		53.2%			42.1%	59.7%	51.0%	92.0%								
	Q16	Expectation		-55.9%			-45.7%	-46.7%						-56.5%				-54.2%
	Q17	Satisfaction		55.9%			41.0%	53.2%	58.5%					-56.5%		50.8%		77.5%
	Q18	Fatigue		71.2%	-34.4%		50.3%	57.3%	56.7%	71.1%				50.8%				52.7%
	Q19	Enjoyment		-19.5%	61.7%		39.3%	46.1%	58.6%					-54.2%	77.5%	52.7%		

As such, only sample cross tables for each ordinal variable are given as Table C.2.30 to Table C.2.42 in Appendix C. Whereas, considering the symmetry of Table 8.18, the measures of associations for the upper half of this table are briefly discussed in the following section.

8.7.6.1 Measures of Association for Q3 (Passenger Zone)

- Knowledge of passengers age may improve the predictability of:
 - Illness; increasing age is leading to decrease in feelings of illness (-47.9%) [Q7].
 - travelling experience; it had a positive association with age (11.3%) [Q10a].
 - enjoyment level; this showed negative association with age (-19.5%) [Q19].

8.7.6.2 Measures of Association for Q7 (Illness)

- If illness levels of the passengers are known then improvements may be made in the predictability of:
 - the passengers' sitting discomfort; increasing with illness (78.9%) [Q12].
 - the unsteadiness in standing; increasing with illness (83.8%) [Q13].
 - the increasing difficulties in eating & drinking (83.4%) [Q14a], reading (63.1%) [Q14b], and writing (53.2%) [Q14c] with illness.
 - meeting of the passengers' expectation of voyage comfort; decreasing with illness (-55.9%) [Q16].
 - satisfaction level of the passengers; decreasing with illness (55.9%) [Q17].
 - fatiguing of passengers; increasing with illness (71.2%) [Q18].
 - passengers' enjoyment level; decreasing with illness (61.7%) [Q19].

8.7.6.3 Measures of Association for Q10a (Travel Experience – All Ships)

- Knowledge about the passengers travel experience aboard all types of ships could lead to improvements in the predictability of:
 - their travelling frequency aboard survey ship; positive association (80.2%) [Q10b].
 - the unsteadiness in standing; decreasing with experience (-32.7%) [Q13].
 - the difficulties in reading; reducing with more experience (-65.6%) [Q14b].

- fatiguing level of the passenger; decreasing with experience (-34.4%) [Q18].

8.7.6.4 Measures of Association for Q12 (Sitting Discomfort)

- If the level of sitting comfort is known then the predictability of following may be improved:
 - the unsteadiness in standing; increasing with sitting discomfort (58.4%) [Q13].
 - the difficulties in eating & drinking (61.6%) [Q14a], reading (55.7%) [Q14b], and writing (42.1%) [Q14c]; all increasing with rise in sitting discomfort.
 - the decrease in expectation level (-45.7%) [Q16].
 - the satisfaction level of the passenger; decreasing with sitting discomfort (41.0%) [Q17].
 - fatiguing experience of the voyage; increasing with sitting discomfort (50.3%) [Q18].
 - reducing enjoy-ability of the travel (39.3%) [Q19].

8.7.6.5 Measures of Association for Q13 (Unsteadiness in Standing)

- Given the unsteadiness in standing experienced by the passengers are known, the predictability of following could largely be improved:
 - the rising difficulties in eating & drinking (84.0%) [Q14a], reading (52.8%) [Q14b], and writing (59.7%) [Q14c] with increased unsteadiness in standing.
 - the meeting of voyage comfort expectations; reducing with increasing unsteadiness (-46.7%) [Q16].
 - the reduction in satisfaction level of the passengers (53.2%) [Q17].
 - the decrease in travel enjoyment (46.1%) [Q19].

8.7.6.6 Measures of Association for Q14a (Difficulties in Eating & Drinking)

- The knowledge about difficulties in eating & drinking, improves the predictability of:

- the difficulties in reading (79.4%) [Q14b] and writing (51.0%) [Q14c]; rising with increase in eating & drinking difficulties.
- the satisfaction level of passengers for the voyage comfort; reducing with increased eating & drinking difficulties (58.5%) [Q17].
- the increase in passenger fatigue (56.7%) [Q18] and reduction in the enjoyment level (58.6%) [Q19].

8.7.6.7 Measures of Association for Q14b (Difficulties in Reading)

- If the difficulties experienced by the passengers in reading are known, then these may improve the predictability of:
 - the difficulties in writing (92.0%) [Q14c].
 - the rising fatigue level (71.1%) [Q18].

8.7.6.8 Measures of Association for Q16 (Meeting of Comfort Expectation)

- If we know how much the comfort expectations of the passengers are met, then these would assist in improving the predictability of:
 - the decrease in passenger satisfaction (-56.5%) [Q17].
 - the reduction in their enjoyment of the voyage (-54.2%) [Q19].

8.7.6.9 Measures of Association for Q17 (Satisfaction)

- The knowledge about the passengers' satisfaction levels for the voyage comfort could lead to improvements in the predictability of:
 - the increase in passengers' fatigue (50.8%) [Q18].
 - the decrease in the voyage enjoy-ability (77.5%) [Q19].

8.7.6.10 Measures of Association for Q18 (Fatigue)

- The increase in fatigue is leading to reduction in the enjoyment levels of the passengers (52.7%) [Q19].

8.8 Statistical Analyses of RHIB-J Questionnaires

Alike MH-I, the comfort survey questionnaire used for the field trial of RHIB-J (Figure 8.6) comprises of various 'quantitative' as well as 'qualitative' queries.

These queries may be attributed to one of the four data categories enlisted in Table 8.11, as summarised in Table C.3.1 of Appendix C. Similar to MH-I survey data, various parts of the same questions were appended with small alphabets and the ordinal variables were assigned numerical values from ‘0’ upwards in an increasing order of discomfort. As mentioned in §8.3.3, a single field trial was carried aboard the RHIB-J with 10 volunteer students (including the author).

The following statistical analyses of the RHIB-J questionnaire data have been carried out and presented in the subsequent sections:

- Frequency tables; in the form of column graphs.
- Cross tabulation of all variables to check for significant dependencies.

8.8.1 Summary Statistics – Frequency Tables

The summary statistics of Q2 (age) and Q3 (gender) are depicted in Figure 8.25. The average age of the participants was 22.4 years (S.D = 4.52 years), with 30% participants being females.

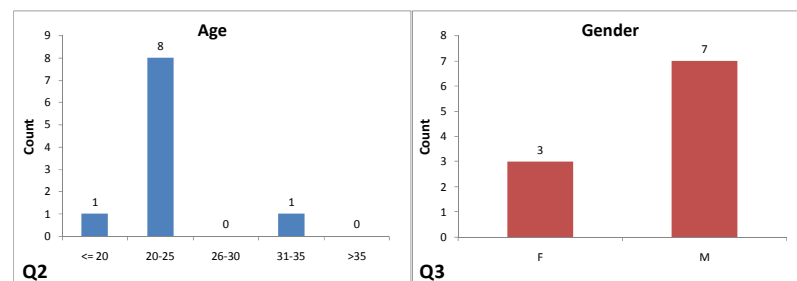


Figure 8.25: Frequency statistics of Q2 and Q3

The frequency statistics pertaining to Q4 (past history of motion sickness) are shown in Figure 8.26. It can be seen from the figure that 50% participants had experienced motion sickness on ships, 20% on busses, 40% in cars, and 20% aboard aircrafts. None of the participant had experienced train-sickness.

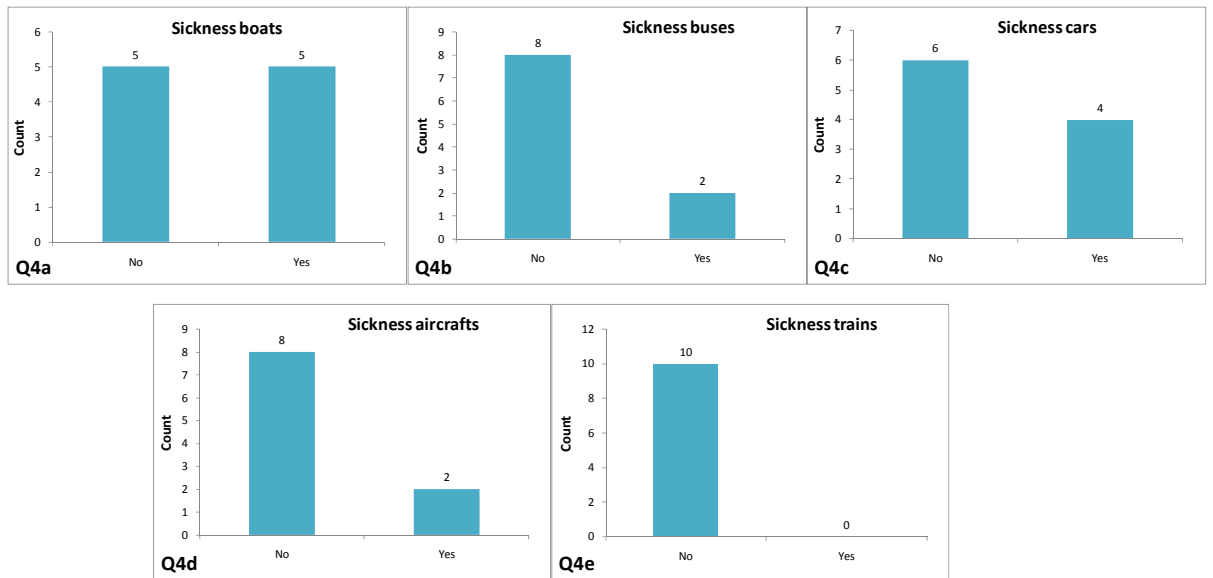


Figure 8.26: Frequency statistics of Q4

As shown in Figure 8.27, none of the student participants consumed alcohol 12 hours before the field trial.

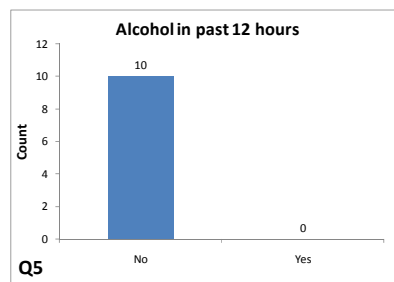


Figure 8.27: Frequency statistics of Q5

The frequency data of Q6 (illness level) and Q7 (sitting discomfort) are shown in Figure 8.28 below. During the field trial of RHIB-J, only 20% participants felt ‘slightly unwell’, while 80% felt ‘alright’. As expected (due to calm weather conditions), illness level of the trip was quite low. On the other hand, 60% participants experienced sitting discomfort, which may primarily be attributed to the non-ergonomic seats of the boat (made up of wooden planks with a hard and rather shallow back support).

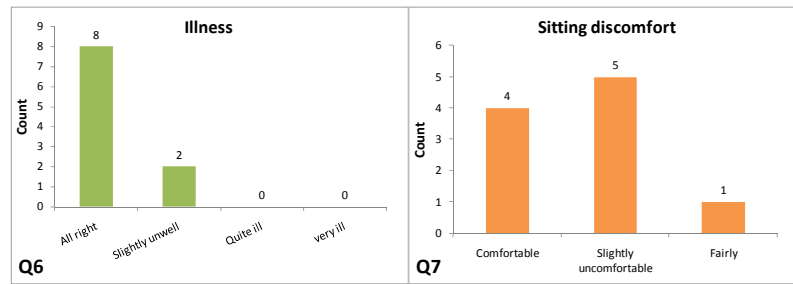


Figure 8.28: Frequency statistics of Q6 & Q7

The summary statistics of Q8 (motion induced pain) are given in Figure 8.29. It is evident from this figure that the most commonly experienced form of pain was the neck pain (40%), followed by upper back (20%) and lower back (10%) pain. 20% participants also experienced ‘leg & ankle’ pain.

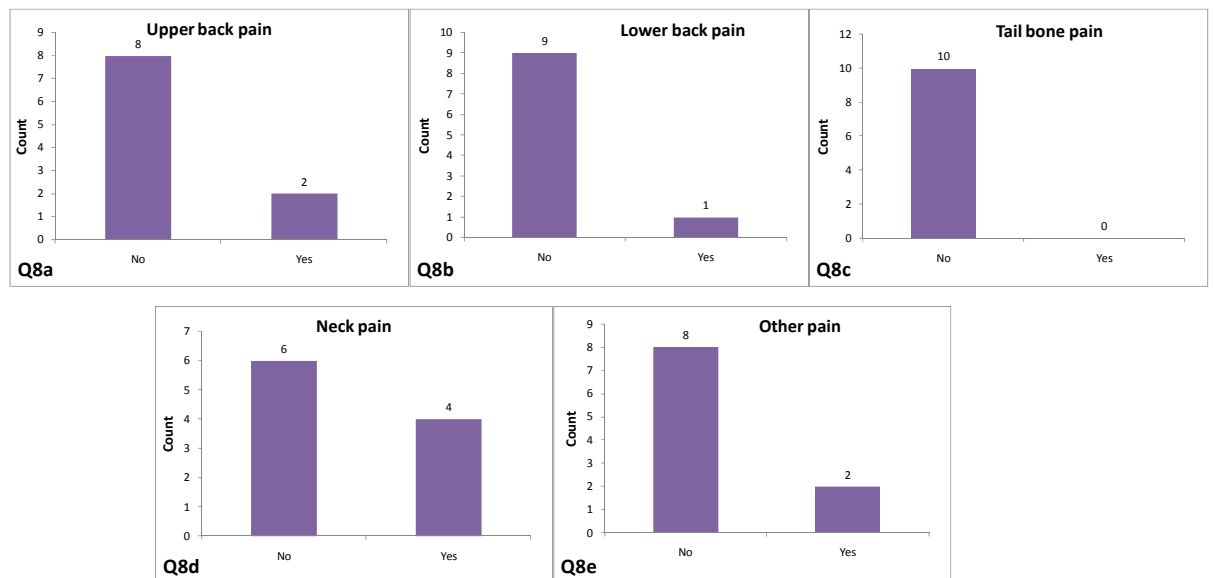


Figure 8.29: Frequency statistics of Q8

As depicted in Figure 8.30, ‘cold’ was the primary discomforting factor felt by most (80%) participants, this was despite the fact that ambient temperature on the day of trial was around 14°C, with little breeze. The second most discomforting factors included vibration (30%), noise (20%), spray (20%), and vertical jerking (10%). None of the participants considered seasickness as a discomforting element.

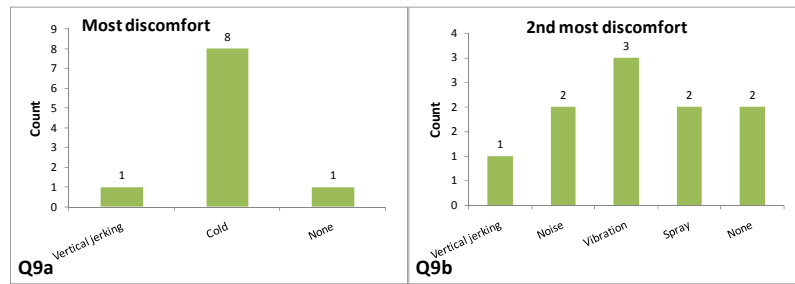


Figure 8.30: Frequency statistics of Q9

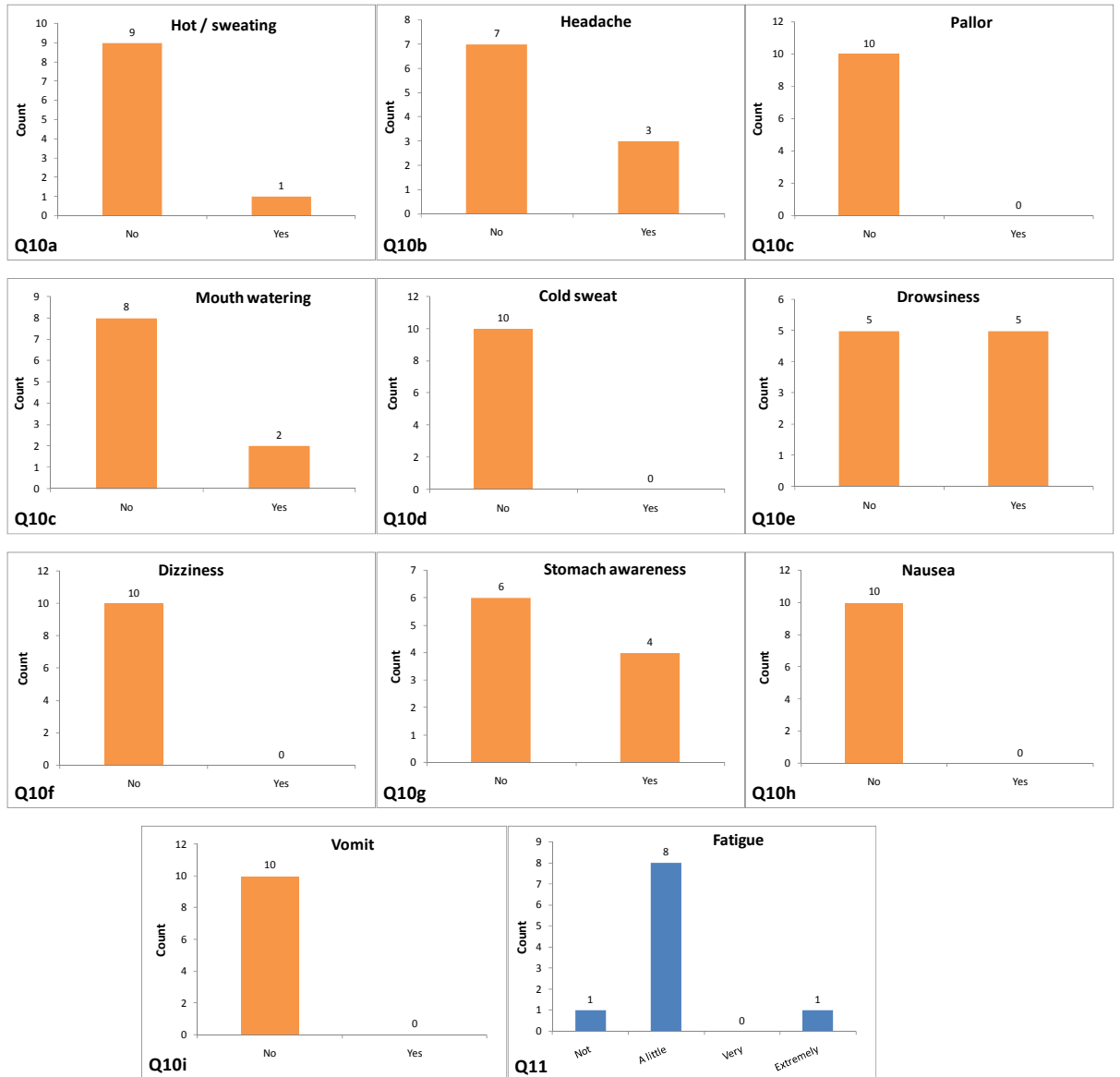


Figure 8.31: Frequency statistics of Q10 & Q11

Participants of the RHIB-J full scale trial, filled in Q10 (sickness indicators) and Q11 (fatigue) of the survey questionnaire (Figure 8.6A) every half an hour (for an hour

and half). However, for the purpose of statistical analyses (i.e. frequency tables and cross tabulation), only the worst response given by each participants has been considered. Summary statistics of the aforesaid variables are depicted in Figure 8.31. It is evident from the figure that ‘drowsiness’ was the most common sickness symptom as 50% participants experienced it. The order of remaining sickness indicators felt by the participants was ‘stomach awareness’ (40%), ‘headache’ (30%), ‘mouth watering’ (20%), and ‘hot/sweating’ (10%). While, ‘pallor’, ‘dizziness’, ‘nausea’ and ‘emesis’ was reported by none. As far as the fatigue is concerned, almost all (90%) participants got fatigued by the motions of the RHIB.

8.8.2 Cross Tabulations - Significant Dependencies

Replies of all questionnaires were fed into SPSS for the production of cross tables of all answers in various categories of the 10 questions (Q1 pertains to seating position, while no reply was received for Q12). However, the sample size for the full scale trial of RHIB-J was very small (only 10 reply). Consequently, most categories of the various questions were void and as such no significant relationships (at $\alpha=0.05$ level) emerged from the aforementioned cross tabulations. The detailed results of these cross tabulations are, therefore, not presented here to save space. The *p-values* of the ‘Exact Fisher’s Test’ for all dependencies are summarised in Table C.3.2 of Appendix C.

8.9 Salient Observations of Statistical Analyses

The statistical analyses of MH-I (§8.7) and RHIB-J (§8.8) comfort questionnaire presented in above, primarily aim to identify the important trends and significant relationships between (dis)comfort (especially illness) and other objective and subjective covariates. It is important to note that out of the 20 survey questions, only gender (Q1a), age (Q1b), use of alcohol (Q5) / anti-sickness medicines (Q9), travel frequency (Q10) and past history (Q11) of motion sickness are the objective measures. These variables may be established prior commencement of the voyage to determine the susceptibility of a person to get seasick. In the case of MH-I comfort analyses, only gender, age, and past history of motion sickness have shown

significant relationship with illness (Q7), which is in line with the findings of Bos et al. (2007) who regressed on these variables to develop their susceptibility model.

However, in contrast with the past findings (Nieuwenhuyzen 1958; Lawther & Griffin 1988a), use of alcohol / anti-sickness medicine did not display any relationship with illness or vomiting. This may be due to the fact that very small number of passengers used alcohol (4%) / anti-sickness medicine (2.9%) before and during (alcohol 2.5%) the voyage. Alike illness, vomiting (Q6j) also displayed significant interactions with age and past history, however, contrary to past studies (Turner & Griffin 1995) it did not show dependencies on gender. This is perhaps due to the fact that sample size of people vomiting (only 4) was extremely small due to conducive (to travel) weather conditions.

It is interesting to note that gender, use of alcohol (before travel) and past history of motion sickness displayed significant relationships with sitting discomfort, while gender, travel frequency and past history were significantly related with unsteadiness. Thus, if one were to develop comfort model then the above mentioned objective covariates should be regressed upon to begin with.

8.10 Chapter Summary

This chapter has primarily dwelled on explaining the methodology used for the further validation of SVH-conflict model through dedicated field trials. The procedure explained herein has been adopted from past experiments with similar objectives. Simulation of the full scale trials' using SVH-conflict model has displayed very good statistical fitness (Table 8.7). Statistical comparison with other physiological and descriptive motion sickness models indicates that SVH and SV-conflict models have almost identical fitness for the multiple field trials of MH-I and RHIB-J (Table 8.10). This makes sense, as the passenger ferry is a medium speed classical monohull vessel. Nevertheless, the two physiological models (SVH and SV) are displaying statistical fitness superior to the descriptive (ISO/BS, HFRI, & COMPASS) models. As expected, the old vintage HFRI model did not show considerable performance.

The chapter has summarized (as frequency tables) the ‘subjective-comfort’ data collected through survey questionnaires aboard ferry MH-I and the boat RHIB-J. It has also outlined the endeavours made to establish significant relationships between the survey variables of ferry MH-I, through cross tabulation. A number of significant dependencies have been identified between the comfort questions and their appropriate measures of associations have also been presented. However, attributable to small sample size, no significant relationships emerged between the queries of survey questionnaires deployed for RHIB-J. Finally, the chapter has summarised the salient findings of the comfort questionnaires’ statistical analyses.

The next chapter is presenting detailed comparison between the SVH-conflict and other physiological (SV-conflict) as well as descriptive (ISO/BS, HFRI, and COMPASS) motion sickness models, while utilising the field trial data of Chapter 7 as well as this chapter.

Chapter 9. **DISCUSSIONS & RECOMMENDATIONS FOR FUTURE RESEARCH**

9.1 Overview of the Chapter

The chapter begins by briefly recapping the thesis, while highlighting its novelties (§9.2). It then presents the contributions and research achievements (§9.3), followed by the identification of underlying simplifications / limitations of the developed model (§9.4). Thereafter, it outlines some recommendations for future research in §9.5 to guide future endeavours. It finally concludes with a chapter summary in §9.6.

9.2 A Brief Recap of the Thesis and Its Novelties

The advent of advanced hullform to reduce commuting time have, rather exacerbated the onboard comfort (seasickness) situations. This is because of the reason that comfort evaluations of these vessels, during their design stages, were carried out using the descriptive motion sickness models (which did prove their worth for classical monohulls). However, seakeeping behaviour of the novel hullform are significantly different from those of the typical monohull vessels, therefore, the statistical models are unable to correctly predict the seasickness characteristics of such vessels.

This is where the development of physiological motion sickness models, based on human sensors of motion, has become even imperative. The timely availability of the subjective-vertical-conflict theory of motion sickness provides the necessary platform for the development of such models that could be used ‘outside-the-statistical-limitations’ of descriptive methods. Being based on the human sense modalities of self orientation, the theory (Bles et al. 1998) has proven its practical worth in predicting motion sickness aboard high speed crafts (Verveniotis 2004) and other classical vessels (Dallinga et al. 2002).

Due to simplicity reasons, the existing physiological (SV-conflict) motion sickness models make use of a single sensory conflict (between expected and observed gravity). However, this warrants a revisit considering the prevalence of significant horizontal (longitudinal & lateral) accelerations aboard contemporary vessels. In this regard, the originators of SV-conflict theory also attempted to extend the capabilities of their models by splitting the SV-conflict into magnitude and orientation effects (Bos et al. 2002a). However, their extended model overestimated the motion sickness incidences when applied to laboratory simulations and was never tested for the real vessels. In addition, frequency response of the model is identical for pure vertical as well as pure horizontal oscillations, which is incompatible with the laboratory findings (see Chapter 5).

In this research project a new physiological motion sickness model based on the subjective vertical theory has been developed. The new model, termed as subjective vertical-horizontal conflict (SVH) model, uses an additional sensory conflict between the expected and sensed horizontal accelerations that explicitly accounts for the peculiar nauseating effects of the horizontal motions. The most important feature / novelty of the SVH-conflict model is the ability to display distinctively different frequency responses for the pure vertical and pure horizontal motions (§6.6.2). These responses of the model are compatible with the findings of past and recent laboratory investigations, concerning elicitation of motion sickness under purely vertical and horizontal oscillations.

The second most important eminence of the new model is its ability to estimate statistically accurate proportions of passengers likely to get seasick. In that the model is able to estimate statistically correct values of the observed motion sickness incidences ($p=0.1734$; $\chi^2=77.761$; $d.o.f=67$), when applied to multiple field trials (67) of several ships (10) (see Appendix E). Thus, the SVH-conflict model is one of the most advanced and validated motion sickness model of its time. The model, within the limitations of ‘habituation’ (see §9.4.6 later), can be used to predict statistically accurate motion sickness incidences for all types of vessels during their

design stages. However, in all such analyses it would be imperative to represent the estimates of the random vessel motions in time domain.

It is well-known that large differences are exhibited by the individuals in their motion sickness susceptibilities. In this respect, this work has borrowed the well-established and proven techniques from statistics, which indirectly cater for the variations in population parameters (susceptibility factors) while assessing the differences between hypothesised and observed outcomes. Therefore, another unique feature of this work is the usage of statistical comparison techniques to indirectly (partly) account for the variations exhibited by the general passenger population in becoming seasick. In this respect, the objective function used for the estimation of new model's parameters is a variant of chi-square statistic, which ensures that the model prediction represent 'average' response of the passenger population.

Moreover, while assessing the performance of different motion sickness models for comparative (Appendix E) analyses, the chi-square goodness-of-fit approach has been used. This is another innovative feature of this project, which (to the knowledge of the author) is not traceable in the literature concerning full scale motion sickness trials of real vessels. The statistical comparisons of the models also aim to acknowledge the fact that real passenger populations are very likely to display significant variations in their susceptibility characteristics. Thus, instead of comparing absolute estimates of the different models, their statistical fitness are compared, which provides a more justifiable basis for establishing their relative effectiveness.

Another important deliverable of this research project is the full scale trials carried out aboard a monohull passenger ferry and a rigid hull inflatable boat (RHIB). These trials not only provided the necessary data for the further validation of the new model but also extended the knowledge and experience of the author concerning the intricacies involved in materialising such experiments. The importance of weather and passenger statistics became immediately evident, so did the role of ships staff on

the D-day. These trials have also extended the field trial database of the department (NAME), which would be very handy for further research on similar lines.

9.3 Contributions & Achievement of Research Objectives

The contributions of this work in the field of naval architecture in general and motion sickness research in particular as well as details of the objectives achieved are summarised in the following.

9.3.1 Main Contributions

The first main contribution of this research is the development of a physiologic motion sickness model using a rephrased version of the subjective vertical conflict theory. Originality of the work lies in the fact that the new model, in addition to SV-conflict, estimates and uses another sensory conflict between the sensed and expected passive horizontal accelerations. Although, this new conflict is readily predicable by the theory; however, it has not been employed in any of the existing models of the theory. Practical application of the developed model to the field trials of contemporary vessels (see §E.4 in Appendix E) also reveals a worthwhile improvement in motion sickness predictability over the existing SV-conflict models.

The second main and novel contributions of this work in the field of applied motion sickness, is the use of statistical hypothesis testing scheme as objective function for the optimisation of model parameters. Verveniotis (2004) estimated the unknown parameters of SV-conflict motion sickness model in a way that minimises the difference between the model estimated and MSIs observed aboard real vessels. Though this approach is acceptable, however, it does not reflect the prevalence of susceptibility-variations of real passenger population. Moreover, such an approach does not account for the significance of sample size (statistically, large and randomly selected sample sizes are more representative of the population). Thus, by devising an objective function based on a variant of chi-statistics, an attempt has been made to indirectly cater for the susceptibility-variations of the general passenger population.

9.3.2 Further Contribution to Existing Knowledge

The third significant contribution of this work is the validation of the new model and its comparison with the existing prominent motion sickness models. The following has been revealed through this exercise:

- In overall terms, the physiological models (SVH & SV conflict) perform much better than the descriptive models in predicting observed proportions of passengers becoming seasick i.e. MSIs, see §E.4 (Appendix E).
- In relative terms, the new model (i.e. SVH-conflict) is somewhat better than the SV-conflict model ($\cong 5\%$ improvement), see §E.4 (Appendix E).
- The descriptive motion sickness models employed by the current maritime comfort analysis standards (BSI 1987; ISO 1997) are reasonably accurate. However, they may err under peculiar vessel motions (e.g. presence of large lateral accelerations), motion environment (e.g. initially mild but later severe weather), and/or journey durations (e.g. due to habituation effects).
- The old vintage HFRI model is highly inaccurate in predicting motion sickness, even that of the typical monohull vessels. This point has also been concluded by the past studies (Verveniotis 2004).

Another considerable contribution of this research is the adaptation of statistical inferential techniques for the comparison of physiologic (SVH & SV) and descriptive (ISO/BS, HFRI & COMPASS) kinetosis models. The underlying idea of employing statistical comparison techniques is to account for the fact that real passenger population exhibits significant variations in their susceptibilities to become seasick.

The last, but not least, key contribution of this work are the four motion sickness field trials of a passenger ferry and one full scale trial of a RHIB. These trials have further validated the new model and are an important addition to the existing database on the subject.

9.3.3 Research Objectives Achieved

As discussed in the following; the aims and objectives of this research project outlined in Chapter 2 have broadly been achieved:

- This venture began with an extensive review of scientific literature pertaining to the (initially daunting but later on) very ‘exciting’ field of ‘motion sickness’. In this phase, a deeper understanding of the subject was developed starting from the historical accounts of the malaise. The reasons, ‘why some mates never get seasick’ while the author struggles to survive a moderate sea state became obvious through detailed accounts of ‘susceptibility’. This was followed by a critical review of existing motion sickness theories. An in-depth study of the prevailing ‘black box’ type descriptive sea-sickness prediction models revealed that the understanding of underlying physiology is indispensable for any ‘successful’ seasickness prediction model. Review of literature, concerning the physiological theories of motion sickness, conspicuously demonstrated that the subjective vertical theory of motion sickness is the way ahead.
- Using the knowledge gained through literature review, an alternative model of subjective vertical theory has been developed in this work. This new implementation of the theory relies on two sensory conflicts, namely, the differences between sensed and expected (1) vertical and (2) passive horizontal accelerations. The model is co-founded on several diversified fields such as physiology, estimation theory, control engineering, digital signal processing and ship hydrodynamics. It is a six-degrees-of-freedom spatial orientation model that may be used to predict seasickness characteristics of any vessel during the design and operation stages, with a due concession for ‘habituation’ effects.
- As set forth in the research objectives (§2.3), the developed model has been calibrated using statistical fitness techniques to account for the variations in susceptibility factors exhibited by the general passenger populations. In total 15 full scale trials of a wave piercer vessel were used for this purpose. Subsequent to this calibration, 48 field trials of 7 different types of vessels

were employed for the validation of the model in statistical terms. In addition to the aforesaid validation of the model, 4 full scale trials were carried out onboard a monohull passenger ferry to further validate the developed model. Also a single field trial of a rigid hull inflatable boat contributed towards the very objective of successful model validation.

- Finally, a detailed comparison has been made between the physiologic (SV & SVH) and the prominent descriptive (ISO/BS, HFRI, & COMPASS) motion sickness models. This comparison clearly indicates superiority of the physiologic models over the descriptive models (obviously, discounted for the habituation effects that are similar in both the cases).

9.4 Underlying Simplifications /Limitations of the Model

Alike any mathematical model simulating real life phenomenon, the motion sickness model developed in this study has some underlying simplifications / limitations. Those considered as significant are discussed in the following to establish recommendations for future research (§9.5).

9.4.1 Modelling of the Limited Sense Modalities

The orientation estimation part of SVH-conflict model only simulates the sense modalities of somewhat imperfect labyrinthine apparatus and its processing by the nervous system. In reality, visual and other somatic afferents do play significant compensatory / complimentary roles in this regard. However, the following points support the way SVH-conflict model has been developed:

- First and most importantly, the vestibular organs are indispensable for the elicitation of motion sickness (see §3.6 and 5.2). Furthermore their transfer functions as well as processing of vestibular cues by the central nervous system are well established (see Chapter 5). Abundant research has been carried out on this specific apparatus (from overall labyrinthine arrangement to the detailed sensory hair cell structure and functioning), which provides significant insight into its morphology and physiology.

- Although somatosensory subsystems do help in establishing the orientation of human body, however, they play no role in motion sickness etiology. This is evident from the fact that LDs are able to maintain their postures in the provocative motion environments without getting sick.
- Most, if not all, passengers limit their visual activities to inside of the vessels e.g. eating, drinking, reading, watching TV etc. Therefore, the visual environment is body-fixed and appears stationary to them. Resultantly, the simplified model simulating vestibular system only should be acceptable from pragmatic point of view. Nevertheless, it would be interesting and important to incorporate the visual cues in the orientation part of the model.

9.4.2 Model being Partly Statistical

During the design stages of a vessel, the sensory conflicts (SV and SH) estimated by the SVH-conflict model may directly be used to compare relative seasickness characteristics of the available candidates. However, in order to be of practical use, these conflicts are transformed into tangible quantities like percent incidences of motion sickness (MSI). In this respect, the SVH-conflict model, alike other descriptive motion sickness models, makes use of the statistical estimation techniques to link the SV and SH conflicts with MSI.

Development of such a physiological model that ultimately relies on statistical fitness approaches might be questioned. However, answer lies in the physiologic nature of the model, wherein, the knowledge about human sense modalities and their processing by the CNS are employed to estimate the sensory conflicts. These conflicts are in turn deemed responsible for the elicitation of motion sickness. Thus, the SVH-conflict model, unlike all descriptive models, clearly reflects the underlying mechanism of motion sickness and is not like a 'black box'.

Furthermore, being based on the human sense modalities of motions rather than statistical data collected aboard specific ship types, the model is not expected to be limited by the type as well as the era of vessel. This very point can easily be

observed from the discussions presented in Appendix E, wherein the model is able to estimate statistically accurate MSIs for an otherwise varied types of vessel.

9.4.3 Usage of Observers

In its current configuration, the SVH-conflict model makes use of widely accepted hypothesis that CNS employs ‘observers (internal models)’ to compute self orientation by implementing physical laws on to the vestibular cues (Merfeld et al. 1999; Angelaki et al. 2004; Merfeld 2004; Zupan et al. 2004; Poon & Merfeld 2005; Tin & Poon 2005). Although, ‘observer theory’ successfully predicts the labyrinthine apparatus originated ‘Vestibulo Ocular Reflex’ (VOR) and perception of self-orientations, however, it assumes linearity and at best, represents mean response of a single neuron. In reality, a significant amount of noise prevails in the typical activities of neural population, which maybe better captured through more intricate techniques like ‘Kalman’ or ‘Particle’ filtering (MacNeilage et al. 2008).

Nevertheless, this research preferred simplicity over complexity as the aim was to provide the naval architectural community with a tool that may (relatively) easily be understood and successfully employed at the earliest design stages of the novel / proven vessels. The model developed in this work may also be made part of a multi-objective decision support system that can assist skippers to plan and modify the vessel routes, thereby improving onboard comfort levels of the passengers.

9.4.4 Consideration of Passive Motions Only

The SVH-conflict model assumes that the passengers are passively moving with the vessel without executing any volitional head movements. The former part of this assumption is more or less valid for a typical vessel type; whereas, active body (especially the head) movements are unavoidable. In this regard the reafference principle by von Holst & Mittelstaedt (1950) may be invoked and the differential processing of active head movement may assumed to prevail, as displayed by the second order ‘vestibular only (VO)’ neurons (Angelaki & Cullen 2008). From aforesaid, it might appear that none of the volitional head movements directly contribute towards the onset or aggravation of motion sickness, which could be true

for a ‘rotational-motion-free’ environment. However, the real ship motions comprise of significant rotational motions that would give rise to Coriolis-accelerations in the presence of active head movements, leading to fast nauseogenic effects.

Nonetheless, a real adult passenger population executes infrequent head movements, especially when they are suffering from strong nausea. Probably, this is the reason that minors display increased tendency to get seasick as they would seldom sit at one place with no head moments (unless they are asleep). However, it is important to note that some studies suggest head movements to have exacerbating effects (Johnson et al. 1951; Johnson & Mayne 1953; Jones et al. 1980; Lackner & Graybiel 1986) on motion sickness, while others report them to be neutral or even ameliorating (Morton et al. 1947; Keist et al. 1956; McCauley & Kennedy 1976; Lawther & Griffin 1986; 1988a; Griffin 1990). Therefore, certain head movements may reduce while other may increase the nauseogenic potential of a passively moving (ship) environment. Thus the overall sporadic head movements of the passengers may cancel out these effects and may therefore be ignored.

9.4.5 Layout of Emetic Brain

This work does present the ‘orientation’ brain neurophysiology to a reasonable depth, however, the details on ‘emetic’ neurophysiology like vomiting centres and their neural linkages with vestibular organs are not considered in details. Therefore, the transformation of sensory conflicts (SV & SH) into motion sickness (MSI) is primarily treated as a ‘black box’ with little information about its contents. It might be interesting to establish relationships between the neural activities of the labyrinthine apparatus and the parts of cerebellar cortex assumed to be responsible for the elicitation of motion sickness. However, this aspect is beyond the scope of this research.

9.4.6 Consideration of Habituation

Habituation does play a significant role in the mitigation of motion sickness, as is obvious from the field trial results of MH-D (see §E3.4 in Appendix E). However, the current implementation of SVH-conflict model does not account for the

habituation effects. Originally, the plan was to introduce some sort of habituation function in the emetic part of the model to be able to use it for the seasoned crew of a naval ships or vessels with long duration exposure to the provoking sea environments. In this regard relevant data was expected from the ‘ABCD Working Group on Human Performance at Sea’ (ABCD 2010), which could not become available. Therefore, the model is unable to capture the ameliorative features of habituation; also it does not take into account the nausea relieving effects of emesis.

9.4.7 Limited Representation of Comfort

SVH-conflict model only estimates the proportion of passengers likely to vomit under a given motion environment, which is the sole parameter that can objectively be measured. However, this measure of motion sickness discounts other, and perhaps equally important, feelings of malaise that precede this extreme event. This is even more relevant for the high speed crossings of short distances that may not allow enough accumulation time for emesis to occur. In such cases, other (though somewhat subjective) measures of motion sickness such as illness ratings (IRs) should be simulated. However, this work has focused on the development of physiologic MSI model due to the following reasons:

- The existing marine standards (BSI 1987; ISO 1997) are based on MSI; hence it is imperative that the new model predicts MSI to facilitate tangible comparisons.
- Almost all of the existing motion sickness models (O’Hanlon & McCauley 1974; McCauley et al. 1976; Lawther & Griffin 1987; Bos & Bles 1998b; Bos et al. 2002a; Matsangas 2004; Verveniotis 2004; Turan 2006) predict MSI. Therefore, for a legitimate comparison of the new model with the existing ones, it should be able to estimate MSI.

Nevertheless, given the fact that there is a strong correlation between MSI and the subjective measures of wellbeing such as illness rating (IR) (Lawther & Griffin 1986; Colwell 1994) [see also §3.10], the new MSI-based model may easily be extended in future to predict subjective well being.

9.4.8 Frequency Response for Pure Horizontal Motions

The feedback path of the orientation brain, estimating expected horizontal accelerations and thereby the SH-conflict, is designed in a way that the frequency response of SVH-conflict model replicates the findings of laboratory experiments (Donohew & Griffin 2004). However, it is important to realise that these experiments, unlike the ones carried out at HFRI (O'Hanlon & McCauley 1974; McCauley et al. 1976) for pure vertical motions, make use of subjective motion sickness rather than the actual emesis. Although, the two measures of sickness strongly correlate, yet there could be subtle differences that may influence human's sensitivity to different frequencies of horizontal oscillations if the actual vomiting had been considered. Furthermore, due to apparatus limitation, the levels of accelerations used in horizontal motion studies were of relatively smaller amplitudes (as compared to the vertical oscillation experiments). Though, the good statistical accuracy of the model supports the current frequency-domain response of the model, however, it may be necessary to revisit the layout and parameters of the SH-conflict part of the model once more laboratory data becomes available.

9.4.9 Limited Improvement over the SV-Conflict Models

As such the SVH model is displaying marginal improvement over SV model (5%) [see §E.4 in Appendix E]. However, this may be attributable to the facts that more than 60% (42) field trials were either carried out aboard monohull vessels (14 trials, 20%) or the weather conditions were so calm that no emesis event took place aboard High Speed Craft (28 trials, 40%). In the former case the SVH model is expected to display characteristics identical to SV model as the predominant motions of the classical monohull vessels are in the vertical directions. On the other hand, little difference is likely to prevail between the two types of physiologic models for small motions of HSC.

Furthermore, it is important to remember that the self-orientation state vector comprises of several linear and rotational motion characteristics (displacement, velocities, and accelerations). This research has tapped only two of those (gravity and passive horizontal accelerations), leading to a reasonable improvement over the

existing SV-models that employ a single conflict (gravity). There is still room for further improvements, which may be achieved by considering additional sensory conflicts. However, due to the time limitation, this research has focused on adding only one more conflict in the emetic link, further sensory conflicts may be considered on a step-wise fashion to enhance the performance of the physiologic models.

9.5 Recommendations for Future Research

Based on the underlying simplifications / limitations (§9.4) of the physiologic seasickness model developed in this work, the following improvements / extensions of the model are recommended to be sought in the future researches:

- Inclusion of additional motion sense modalities, in particular the visual, within the orientation estimation part of the model. In this regard, it would be interesting to investigate ameliorating as well as exacerbating combinations of the visual sense for motion sickness. Resultantly, a visual display system, similar to the work of Houben & Bos (2010), may be developed to provide Earth-fixed reference of the visual vertical. Thereby, improving the comfort levels aboard passenger ships, leading to improved ferry economics.
- Considering the part statistical nature of the model, its calibration should be revisited when a larger database of full scale trials aboard varied type of vessels become available.
- The orientation part should be remodelled using the more intricate (and perhaps better representations of the CNS' processing of vestibular cues) computational approaches of spatial orientation, such as 'Kalman' or 'Particle' filtering.
- The emetic part of the sickness model should be modified to simulate the neurophysiologic processing of sensory conflict signals, once such a model becomes available in future.
- Subject to the availability of motion sickness data, either for the crew of commercial ships or personnel of naval vessels, a habituation function should be implemented in the emetic part of the model. This would extend model's

applicability to the long journeys as well as the seasoned seafarers, thereby improving prediction of human comfort and performance. Alternatively, the parameters of the 'internal model' may be modified to reflect habituation. For example the feedback coefficient of the velocity storage may be reduced to unity using a time-driven function to replicate the typical motion sickness habituation reflected by the decrease of nystagmus decay time constant (Bos et al. 2002b; Cohen et al. 2003; Dai et al. 2003).

- The model should be extended to estimate other comfort features in addition to the vomiting incidences. Such as illness ratings, motion induced interruptions, and fatigue experienced by the personnel working / passengers travelling onboard ships.
- The feedback path of 'subjective-horizontal' conflict should be revisited in terms of its frequency response by adjusting the type and parameters of the SH-compensator. Furthermore the parameters of hill function and leaky integrator may also be refined in the SH-emetic path. This should be done once more data become available from the laboratory experiments concerning the elicitation of motion sickness under purely horizontal oscillations.
- Effects of introducing additional sensory conflicts between the expected and sensed state vectors of self-orientation, in the emetic part of the physiological model, should be investigated on gradual basis. However, this would necessitate availability of a large database of laboratory experiments as well as full scale trails.

In addition to the above, it is recommended that a multi-objective decision support system should be developed that makes use of the physiological comfort model to assist the passenger vessel skippers in planning / modifying the vessel routes. Furthermore, and perhaps most importantly, future standards on motion induced (dis)comfort should be based on physiologic models rather than the descriptive methods / approaches.

9.6 Chapter Summary

This chapter has presented the novelty of this research project, while identifying its contributions. The primary contribution of the work is the development of a new tool for the comfort evaluation of ships during their design and operation phases. Validation of the new model through dedicated full scale trials as well as the existing database of past field trials, is another important contribution of the project. The shortcomings of the developed models are discussed in details towards the culmination of the chapter, before proposing the course of action for future research.

The next chapter is summarising the conclusions of this thesis.

Chapter 10. CONCLUSIONS

10.1 Overview of the Chapter

This chapter is summarising the conclusions of the thesis.

10.2 Concluding Statements

This research work has defined an alternate statement of the Subjective Vertical (SV)-conflict theory that allows improving its ability to predict motion sickness. Using this alternate version of the physiologic theory, a new six degrees of freedom motion sickness model, termed as ‘Subjective Vertical Horizontal (SVH)-conflict model’, has successfully been developed and validated. This model, in addition to the SV-conflict, explicitly takes account of the horizontal motions by implementing an alternative component in the existing SV-conflict models.

In overall terms, the concluding statements of this research work are as follows:

- This research proves that the role of horizontal accelerations is significant for the prediction of seasickness, especially, aboard contemporary high speed vessel with unconventional hullforms. In that the new model (SVH-conflict) is displaying better statistical fitness than the SV-conflict models for the high speed deep-V monohull [DV-B ($p_{SVH}=0.123$; $p_{SV}=0.050$; $dof=4$)] and catamarans [Cat-A ($p_{SVH}=0.894$; $p_{SV}=0.713$; $dof=2$), WP-G ($p_{SVH}=0.134$; $p_{SV}=0.057$; $dof=15$), & WP-H ($p_{SVH}=0.437$; $p_{SV}=0.144$; $dof=4$)] hullforms.
- The field trials carried out for this project, also clearly indicate that the new (SVH-conflict) and existing (SV-conflict) physiologic models display similar performance ($p_{SVH}=0.370$; $p_{SV}=0.361$; $dof=4$) for the monohull vessel. This is because of the predominantly vertical motions exhibited by such vessels. Hence, the new model shows improvement in the presence of horizontal

accelerations, which also implies increasingly important contribution of horizontal motions for the seasickness etiology.

- It is practically demonstrated that the statistical inferential techniques can successfully be employed to indirectly (partly) account for the variations in susceptibility characteristics of general passenger population. It is, therefore, possible to develop and validate motion sickness models without personalising them by the usage of susceptibility functions.
- The physiologic (SV & SVH-conflict) as well as descriptive (ISO/BS, HFRI, & COMPASS) motion sickness models have been applied to the 68 field trials of 10 vessels. The overarching statistical fitness testes clearly indicate that the new physiologic model (SVH-conflict) is much superior to the descriptive models and is showing reasonable improvements over the SV-conflict models.
- In response to the research question of this project, it may be concluded that the statistical accuracy of SV-conflict models for predicting the motion sickness incidences aboard contemporary vessels is improved. This is achieved by defining and implementing an additional sensory conflict between the sensed and subjective horizontal accelerations.
- In relative terms, the statistical fitness of the ISO/BS descriptive motion sickness models is better than the HFRI model, which fails to fit almost 1/3 of the full scale trials. This, once again confirms the unsuitability of HFRI model for analysing motion sickness characteristics of contemporary vessels.
- Age, gender, and past history of motion sickness are the most significant covariates of illness. Therefore, these should be taken into account for the development of any illness / vomiting likelihood prediction models.
- Future motion sickness prediction models / standards should be developed on physiological basis to not only reflect the underlying mechanism but also to ensure relatively more realistic evaluations of futuristic, especially the novel, designs.

REFERENCES

- (2004). Directive 2004/58/Ec: On the Right of Citizens of the Union and Their Family Members to Move and Reside Freely within the Territory of the Member States. EC, available at <http://eur-lex.europa.eu/> as for 21 Feb 2010.
- ABCD. (2010). "Abcd Working Group on Human Performance at Sea." from <http://www.abcd-wg.org/>.
- Abdi, H. (2007). "The Bonferonni and Šidák Corrections for Multiple Comparisons." Encyclopedia of measurement and statistics.
- American Bureau of Shipping (2001). Guide for Passenger Comfort on Ships American Bureau of Shipping, Houston, Texas
- Alexander, S. J., Cotzin, M., Hill, C. J., Ricciuti, E. A. and Wendt, G. R. (1945a). "Wesleyan University Studies on Motion Sickness: 1. The Effects of Variation of Time Intervals between Accelerations Upon Sickness Rates." *Journal of Psychology* **19**: 49-62.
- Alexander, S. J., Cotzin, M., Hill, C. J., Ricciuti, E. A. and Wendt, G. R. (1945b). "Wesleyan University Studies on Motion Sickness: 2. A Second Approach to the Problem of the Effects of Variation of Time Intervals between Accelerations Upon Sickness Rates." *Journal of Psychology* **19**: 63-68.
- Alexander, S. J., Cotzin, M., Hill, C. J., Ricciuti, E. A. and Wendt, G. R. (1945c). "Wesleyan University Studies on Motion Sickness: 3. The Effects of Various Accelerations Upon Sickness Rates." *Journal of Psychology* **20**: 3-8.
- Alexander, S. J., Cotzin, M., Hill, C. J., Ricciuti, E. A. and Wendt, G. R. (1945d). "Wesleyan University Studies on Motion Sickness: 4. The Effects of Waves Containing Two Acceleration Levels Upon Motion Sickness." *Journal of Psychology* **20**: 9-18.
- Allen, G. R. (1974). Proposed Limits for Exposure to Whole-Body Vertical Vibration, 0.1 to 1.0 Hz. AGARD (Advisory Group for Aerospace Research and Development) Conference Proceedings No. 145: Vibration and Combined Stresses in Advanced Systems, Paper B-26, Neuilly-sur-Seine.
- Angelaki, D. E. and Cullen, K. E. (2008). "Vestibular System: The Many Facets of a Multimodal Sense." *Annu Rev Neurosci* **31**: 125-50.
- Angelaki, D. E., McHenry, M. Q., Dickman, J. D., Newlands, S. D. and Hess, B. J. (1999). "Computation of Inertial Motion: Neural Strategies to Resolve Ambiguous Otolith Information." *J Neurosci* **19**(1): 316-27.
- Angelaki, D. E., Shaikh, A. G., Green, A. M. and Dickman, J. D. (2004). "Neurons Compute Internal Models of the Physical Laws of Motion." *Nature* **430**(6999): 560-564.
- Apostolyuk, V. (2006). "Theory and Design of Micromechanical Vibratory Gyroscopes." *MEMS/NEMS Handbook*, Springer **1**: 173-195.
- Arribas, F. L. P. and Pineiro, A. L. (2007). "Seasickness Prediction in Passenger Ships at the Design Stage." *Ocean Engineering* **34**(14-15): 2086-2092.
- Attias, J., Gordon, C., Ribak, J., Binah, O. and Rolnick, A. (1987). "Efficacy of Transdermal Scopolamine against Seasickness: A 3-Day Study at Sea." *Aviation, Space and Environmental Medicine* **58**(1): 60-62.
- Baitis, A. E., Applebee, T. R. and McNamara, T. M. (1984). "Human Factor Considerations Applied to Operations of the Ffg-8 and Lamps Mk Iii." *Naval Engineers Journal* **97**(4).

- Baker, C., McSweeney, K. and McCafferty, D. (2007). "Habitability: Setting Criteria Fit for Humans."
- Beer, T. (1997). Environmental Oceanography, CRC.
- Benjamini, Y. and Hochberg, Y. (1995). "Controlling the False Discovery Rate: A Practical and Powerful Approach to Multiple Testing." *Journal of the Royal Statistical Society. Series B (Methodological)* **57**(1): 289-300.
- Benjamini, Y. and Yekutieli, D. (2001). "The Control of the False Discovery Rate in Multiple Testing under Dependency." *The Annals of Statistics* **29**(4): 1165-1188.
- Benson, A. (1988). "Motion Sickness & Spatial Disorientation." In J. Ernesting & P. King(Eds.), *Aviation Medicine*. London: Butterworth: 318-493.
- Benson, A. and Brand, J. (1968). "Some Effects of L-Hyoscine Hydrobromide on Post-Rotatory Sensation and Nystagmus in Man." *Experimental Physiology* **53**(3): 296-311.
- Benson, A. J. (1999). Motion Sickness. In J. Ernesting, A. Nicholson and D. Rainford (Ed.), *Aviation Medicine*. Oxford, Butterworth & Heinmann.
- Benson, A. J. (2002). Motion Sickness. In K. Pandolf and R. Burr (Ed.), *Medical Aspects of Harsh Environments. Volume 2*, Walter Reed Army Medical Center, Washington DC, USA.
- Birren, J. (1949). "Motion Sickness: Its Psychophysiological Aspects." A Survey Report on Human Factors in Undersea Warfare: 375-397.
- Bles, W. (1981). Stepping Around: Circular Vection and Coriolis Effects. In J. Long and A. Baddeley (Ed.), *Attention and Performance IX*. Hillsdale NJ, Lawrence Erlbaum.
- Bles, W. (1998). "Coriolis Effects and Motion Sickness Modelling." *Brain Research Bulletin* **47**(5): 543-549.
- Bles, W., Bos, J. E., de Graaf, B., Groen, E. and Wertheim, A. H. (1998). "Motion Sickness: Only One Provocative Conflict?" *Brain Research Bulletin* **47**(5): 481-487.
- Bles, W., Bos, J. E. and Kruit, H. (2000). "Motion Sickness." *Current Opinion in Neurology* **13**(1): 19-25.
- Bles, W., De Graaf, B., Keuning, J., Ooms, J., De Vries, J. and Wientjes, C. (1991). Experiments on Motion Sickness Aboard the Mv "Zeefakkel". Report IZF-1991-A-34, TNO Human Factors Research Institute. Soesterberg, The Netherlands.
- Bles, W., de Graaf, B. and Krol, J. (1995). Space Adaptation Syndrome and Sickness Induced by Centrifugation-Vestibular Consequences of Earth Anomalous Gravity. Report TNO-TM 1995 B-12. TNO Human Factors Research Institute, Soesterberg, the Netherlands.
- Bock, O. L. and Oman, C. M. (1982). "Dynamics of Subjective Discomfort in Motion Sickness as Measured with a Magnitude Estimation Method." *Aviation Space and Environmental Medicine* **53**(8): 773-777.
- Bohlin, T. (1991). *Interactive System Identification: Prospects and Pitfalls*. Berlin, Heidelberg, New York, London, Springer-Verlag, Inc.
- Bonafoux, J., Dudson, E. and Sherwood, D. (2001). An Evaluation of the Effect of Hull Form Choice on the Operability of Fast Ferries. FAST.

- Bonnet, C. T., Faugloire, E., Riley, M. A., Bardy, B. G. and Stoffregen, T. A. (2006). "Motion Sickness Preceded by Unstable Displacements of the Center of Pressure." *Human Movement Science* **25**(6): 800-820.
- Bonnet, C. T., Faugloire, E., Riley, M. A., Bardy, B. G. and Stoffregen, T. A. (2008). "Self-Induced Motion Sickness and Body Movement During Passive Restraint." *Ecological Psychology* **20**(2): 121-145.
- Borah, J., Young, L. R. and Curry, R. E. (1988). "Optimal Estimator Model for Human Spatial Orientation." *Annals of the New York Academy of Sciences* **545**(Representation of Three-Dimensional Space in the Vestibular, Oculomotor, and Visual Systems): 51-73.
- Bos, J. E. (2004). How Motions Make People Sick Such That They Perform Less: A Model Based Approach NATO RTO/AVT-110 Symp. Habitability of Combat and Transport Vehicles: Noise, Vibration and Motion. Prague, Czech Republic, 4-7 October, 2004.
- Bos, J. E. and Bles, W. (1998a). Modelling Motion Sickness. Models for Aircrew Safety Assessment: Uses, Limitations and Requirements, 26-28 Oct 1998. Ohio (USA), RTO MP-20.
- Bos, J. E. and Bles, W. (1998b). "Modelling Motion Sickness and Subjective Vertical Mismatch Detailed for Vertical Motions." *Brain Research Bulletin* **47**(5): 537-542.
- Bos, J. E. and Bles, W. (2000). Performance and Sickness at Sea. RINA International Conference, Human Factors in Ship Design and Operation. London, UK.
- Bos, J. E. and Bles, W. (2002). "Theoretical Considerations on Canal-Otolith Interaction and an Observer Model." *Biological Cybernetics* **86**(3): 191-207.
- Bos, J. E. and Bles, W. (2004). "Motion Sickness Induced by Optokinetic Drums." *Aviat Space Environ Med* **75**: 172-174.
- Bos, J. E. and Bles, W. (2006). "Rotation Direction Change Hastens Motion Sickness Onset in an Optokinetic Drum." *Aviat Space Environ Med* **77**: 464-464.
- Bos, J. E., Bles, W. and Dallinga, R. (2002a). Prediction of Seasickness with More Than One Degree of Freedom. Human Factors in Ship Design & Operation II, RINA, London, Royal Institute of Naval Architects.
- Bos, J. E., Bles, W. and de Graaf, B. (2002b). "Eye Movements to Yaw, Pitch, and Roll About Vertical and Horizontal Axes: Adaptation and Motion Sickness." *Aviation Space and Environmental Medicine* **73**(5): 436-444.
- Bos, J. E., Bles, W. and Groen, E. L. (2008). "A Theory on Visually Induced Motion Sickness." *Displays* **29**(2): 47-57.
- Bos, J. E., Bles, W. and Hosman, R. J. A. W. (2001). Modelling Human Spatial Orientation and Motion Perception. AIAA Modelling and Simulation Technologies Conference Proceedings 2001, AIAA.
- Bos, J. E., Damala, D., Lewis, C., Ganguly, A. and Turan, O. (2007). "Susceptibility to Seasickness." *Ergonomics* **50**(6): 890-901.
- Bos, J. E., Hosman, R. J. and Bles, W. (2002c). Visual-Vestibular Interactions and Spatial (Dis)Orientation in Flight and Flight Simulation. TNO Report TM-02-C009. TNO Human Factors. Soesterberg, The Netherlands.
- Bos, J. E., MacKinnon, S. N. and Patterson, A. (2005). "Motion Sickness Symptoms in a Ship Motion Simulator: Effects of inside, Outside, and No View." *Aviat Space Environ Med* **76**: 1111-1118.

- Brandt, T., Glasauer, S., Stephan, T., Bense, S., Yousry, T. A., Deutschlander, A. and Dieterich, M. (2002). "Visual-Vestibular and Visuovisual Cortical Interaction: New Insights from Fmri and Pet." *Ann N Y Acad Sci* **956**: 230-41.
- Brooks, M. (1939). "The Etiology of Seasickness." *Med. Rec* **150**: 23-26.
- Bruner, J. M. (1955). "Seasickness in a Destroyer Escort Squadron." *U S Armed Forces Med J* **6**(4): 469-90.
- The British Standards Institution (1987). *Guide to Measurement and Evaluation of Human Exposure to Whole-Body Mechanical Vibration and Repeated Shock. BS 6841:1987*, The British Standards Institution, London, United Kingdom.
- Buizza, A. and Schmid, R. (1982). "Visual-Vestibular Interaction in the Control of Eye Movement: Mathematical Modelling and Computer Simulation." *Biol Cybern* **43**(3): 209-23.
- Buizza, A. and Schmid, R. (1983). "Model Interpretation of Visual-Vestibular Interaction in Patients with Labyrinthine and Cerebellar Pathologies." *Biol Cybern* **47**(3): 203-11.
- Burnham, K. and Anderson, D. (2002). *Model Selection and Multimodel Inference: A Practical Information-Theoretic Approach*. New York, USA, Springer Verlag.
- Card, J., Baker, C., McSweeney, K. and McCafferty, D. (2005). "Human Factors in Classification and Certification." *Transactions, Society of Naval Architects and Marine Engineers*: 129.
- Chen, Z. (2003). *Bayesian Filtering: From Kalman Filters to Particle Filters, and Beyond*. Technical Report, Adaptive System Laboratory McMaster University. Hamilton, ON, Canada.
- Cheung, B., Howard, I., Nedzelski, J. and Landolt, J. (1989). "Circularvection About Earth-Horizontal Axes in Bilateral Labyrinthine-Defective Subjects." *Acta Oto-Laryngologica* **108**(5): 336-344.
- Cheung, B. S., Howard, I. P. and Money, K. E. (1991). "Visually-Induced Sickness in Normal and Bilaterally Labyrinthine-Defective Subjects." *Aviat Space Environ Med* **62**(6): 527-31.
- Chinn, H. (1951). "Motion Sickness in the Military Service." *Milit Surg*, **108**(1): 20-29.
- Claremont, C. A. (1931). "The Psychology of Seasickness." *Psyche* **11**: 86-90.
- Clark, B. and Stewart, J. D. (1968). "Comparison of Sensitivity for the Perception of Bodily Rotation and the Oculogyral Illusion(Human Angular Acceleration Sensitivity Compared Using Perception of Bodily Rotation and Oculogyral Illusion as Indicators, Discussing Nature of Illusion)." *Perception and Psychophysics* **3**(4): 253-256.
- Cohen, B., Dai, M. and Raphan, T. (2003). "The Critical Role of Velocity Storage in Production of Motion Sickness." *Ann N Y Acad Sci* **1004**: 359-76.
- Cohen, B., Maruta, J. and Raphan, T. (2001). "Plenary Lecture: Orientation of the Eyes to Gravito-inertial Acceleration." *Annals of the New York Academy of Sciences* **942**(The Vestibular Labyrinth in Health and Disease): 241-258.
- Cohen, B., Matsuo, V. and Raphan, T. (1977). "Quantitative Analysis of the Velocity Characteristics of Optokinetic Nystagmus and Optokinetic after-Nystagmus." *J Physiol* **270**(2): 321-44.

- Collins, W. and Lentz, J. (1976). Some Psychological Correlates of Motion Sickness Susceptibility. THREE STUDIES OF MOTION SICKNESS SUSCEPTIBILITY.
- Colwell, J. (1989). Human Factors in the Naval Environment: A Review of Motion Sickness and Biodynamic Problems. DREA Technical Memorandum 89/220, Canadian National Defence Research Establishment Atlantic, Dartmouth.
- Colwell, J. (1994). Motion Sickness Habituation in the Naval Environment. DREA Technical Memorandum 94/211. Defence Research Establishment Atlantic.
- Colwell, J. (2009). Empirical Models Relating Ship Motions, Sleep, Fatigue, Motion Sickness and Task Performance in the Naval Environment. Human Factors in Ship Design and Operation. London, UK, Royal Institution of Naval Architects: 9-18.
- Colwell, J., Allen, N., Bos, J., Bridger, R., Duncan, C., Elischer, P., Grech, M., Green, A., Hogervorst, M. and MacKinnon, S. (2008). "Human Performance Sea Trial Quest Q-303." Proceedings of Pacific.
- Colwell, J. L. (2000a). Nato: Questionnaire: Correlation between Ship Motion, Fatigue, Sea Sickness and Naval Task Performance. RINA Conference Proceedings, Human Factors in Ship Design and Operation, 27-29 September 2000, London.
- Colwell, J. L. (2000b). Performance Assessment Questionnaire (Paq): Paq Project, Questionnaire Design and Reliability of Responses. Technical Memorandum DREA TM 2000-141. Defence Research Establishment Atlantic (DREA). Dartmouth, Canada.
- Colwell, J. L. (2004). Protocol for an Experiment on Controlling Motion Sickness Severity in a Ship Motion Simulator. Defence Research and Development Canada, TM 2004-282. Atlantic, Canada.
- Colwell, J. L. (2005). "Modeling Ship Motion Effects on Human Performance for Real Time Simulation." Naval Engineers Journal **117**(1): 77-90.
- Colwell, J. L. and Heslegrave, R. (1993). Sea Sickness, Fatigue and Performance Assessment Questionnaire. DREA Report 93/105. Defence Research Establishment Atlantic (DREA). Dartmouth, Canada.
- Cotton, J. R. and Grant, J. W. (2000). "A Finite Element Method for Mechanical Response of Hair Cell Ciliary Bundles." Journal of Biomechanical Engineering **122**(1): 44-50.
- Crampton, G. (1990). Motion and Space Sickness, CRC Press.
- Crane, B. T. and Demer, J. L. (1999). "A Linear Canal-Otolith Interaction Model to Describe the Human Vestibulo-Ocular Reflex." Biological Cybernetics **81**(2): 109-118.
- Croarkin, C., Tobias, P., Filliben, J., Hembree, B., Guthrie, W., Prins, J., Zey, C., Heckert, N. and Trutna, L. (2003). Nist/Sematech E-Handbook of Statistical Methods, NIST Handbook.
- Crossland, P. (1998). A Rational Approach to Specifying Seakeeping Performance in the Ship Design Process. Paper presented at RINA International Symposium, Warship '98.
- Crossland, P. and Rich, K. (2000). A Method for Deriving Mii Criteria. Human Factors in Ship Design and Operation, London, UK, RINA.

- Dai, M., Kunin, M., Raphan, T. and Cohen, B. (2003). "The Relation of Motion Sickness to the Spatial-Temporal Properties of Velocity Storage." *Exp Brain Res* **151**(2): 173-89.
- Dallinga, R., Pinkster, D. and Bos, J. (2002). Human Factors in the Operational Performance of Ferries. Proc. of Human Factors in Ship Design and Operation Conference, RINA: 89-97.
- Damiano, E. and Rabbitt, R. (1996). "A Singular Perturbation Model of Fluid Dynamics in the Vestibular Semicircular Canal and Ampulla." *Journal of Fluid Mechanics Digital Archive* **307**: 333-372.
- Darlington, R. B. (1996). Measures of Association in Crosstab Tables. Statnotes: Some Works of Richard B. Darlington. Retrieved Apr 2010 from <http://www.psych.cornell.edu/Darlington/crosstab/TABLE0.HTM>, Cornell University: Department of Psychology.
- Das, V. E., DiScenna, A. O., Feltz, A., Yaniglos, S. and Leigh, R. J. (1998). "Tests of a Linear Model of Visual-Vestibular Interaction Using the Technique of Parameter Estimation." *Biol Cybern* **78**(3): 183-95.
- Das, V. E. and Leigh, R. J. (2000). "Visual-Vestibular Interaction in Progressive Supranuclear Palsy." *Vision Res* **40**(15): 2077-81.
- de Graaf, B., Bles, W. and Bos, J. E. (1998). "Roll Motion Stimuli: Sensory Conflict, Perceptual Weighting and Motion Sickness." *Brain Research Bulletin* **47**(5): 489-495.
- de Graaf, B., Bles, W., Ooms, J. and Douwes, E. (1992). Exploratory Study with a Seasickness Questionnaire on Hr. Ms. Frigate Tromp. TNO Report IZF1992 A-1, TNO Human Factors Research Institute. Soesterberg, The Netherlands.
- de Vries, H. (1950). "Mechanics of the Labyrinth Organs." *Acta Otolaryngol* **38**: 262-273.
- de Wit, G. (1953). "Seasickness; (Motion Sickness) a Labyrinthological Study." *Acta Otolaryngol Suppl* **108**: 7-56.
- DeCoursey, W. (2003). *Statistics and Probability for Engineering Applications*, Newnes.
- Denise, P. and Darlot, C. (1993). "The Cerebellum as a Predictor of Neural Messages--Ii. Role in Motor Control and Motion Sickness." *Neuroscience* **56**(3): 647-55.
- Denise, P., Etard, O., Zupan, L. and Darlot, C. (1996). "Motion Sickness During Off-Vertical Axis Rotation: Prediction by a Model of Sensory Interactions and Correlation with Other Forms of Motion Sickness." *Neuroscience Letters* **203**(3): 183-186.
- Dft (2010). *Transport Statistics Bulletin; Sea Passenger Statistics: 2009*. Department for Transport, UK.
- Dimitrios, A. (2002). Motion Sickness and Its Effect on Passengers' Comfort in High Speed Vessels. Naval Architecture and Marine Engineering. Glasgow , Scotland, Glasgow and Strathclyde. **MSc**: 171.
- Dobie, T. (1974). *Airsickness in Aircrew*. Advisory Group for Aerospace Research and Development (AGARD) Report No.177. Technical Editing and Reproduction Ltd., London.
- Dobie, T. (2000). The Importance of the Human Element in Ship Design. Presented at the Ship Structure Symposium, Arlington VA, June 13 (<http://www.shipstructure.org/pdf/2000symp06.pdf>).

- Dodge, R. (1923). "Habituation to Rotation." *Journal of Experimental Psychology* **6**: 1-35.
- Donohew, B. E. and Griffin, M. J. (2004). "Motion Sickness: Effect of the Frequency of Lateral Oscillation." *Aviation, Space, and Environmental Medicine* **75**(8): 649-656.
- Donohew, B. E. and Griffin, M. J. (2007). "Low Frequency Motions and Motion Sickness on a Tilting Train." *Proceedings of the Institution of Mechanical Engineers, Part F: Journal of Rail and Rapid Transit* **221**(1): 125-133.
- Dormand, J., El-Mikkawy, M. and Prince, P. (1987). "Families of Runge-Kutta-Nystrom Formulae." *IMA Journal of Numerical Analysis* **7**(2): 235.
- Dormand, J. and Prince, P. (1980). "A Family of Embedded Runge-Kutta Formulae." *Journal of Computational and Applied Mathematics* **6**(1): 19-26.
- Dormand, J. and Prince, P. (1986). "A Reconsideration of Some Embedded Runge-Kutta Formulae." *Journal of Computational and Applied Mathematics* **15**(2): 203-211.
- Dowd, P. (1974). "Sleep Deprivation Effects on the Vestibular Habituation Process." *Journal of Applied Psychology* **56**: 748-752.
- Droulez, J. and Darlot, C. (1989). "The Geometric and Dynamic Implications of the Coherence Constraints in Three-Dimensional Sensorimotor Interactions." *Attention and Performance XIII*: 495-526.
- Duan, Q., Schaake, J., Andréassian, V., Franks, S., Goteti, G., Gupta, H. V., Gusev, Y. M., Habets, F., Hall, A., Hay, L., Hogue, T., Huang, M., Leavesley, G., Liang, X., Nasonova, O. N., Noilhan, J., Oudin, L., Sorooshian, S., Wagener, T. and Wood, E. F. (2006). "Model Parameter Estimation Experiment (Mopex): An Overview of Science Strategy and Major Results from the Second and Third Workshops." *Journal of Hydrology* **320**(1-2): 3-17.
- Duan, Q., Sorooshian, S. and Gupta, V. (1992). "Effective and Efficient Global Optimization for Conceptual Rainfall-Runoff Models." *Water Resour. Res.* **28**.
- Eagon, J. C. (1988). *Quantitative Frequency Analysis of the Electrogastrogram During Prolonged Motion Sickness*. M.D Thesis, Harvard-MIT Div. of Health Science and Technology. Cambridge, Massachusetts Institute of Technology.
- Einstein, A. (1907). "On the Relativity Principle and the Conclusions Drawn from It." *Jahrbuch der Radioaktivitat und Elektronik* **4**: 411-462.
- Elias, P. Z., Jarchow, T. and Young, L. R. (2008). "Modeling Sensory Conflict and Motion Sickness in Artificial Gravity." *Acta Astronautica* **62**(2-3): 224-231.
- Ellis, G. (2002). *Observers in Control Systems - a Practical Guide*. London, United Kingdom, Elsevier Science.
- Farcomeni, A. (2008). "A Review of Modern Multiple Hypothesis Testing, with Particular Attention to the False Discovery Proportion." *Statistical Methods in Medical Research* **17**(4): 347-388.
- Faugloire, E., Bonnet, C. T., Riley, M. A., Bardy, B. G. and Stoffregen, T. A. (2007). "Motion Sickness, Body Movement, and Claustrophobia During Passive Restraint." *Experimental Brain Research* **177**(4): 520-532.
- Fernandez, C. and Goldberg, J. M. (1971). "Physiology of Peripheral Neurons Innervating Semicircular Canals of the Squirrel Monkey. Ii. Response to

- Sinusoidal Stimulation and Dynamics of Peripheral Vestibular System." *Journal of Neurophysiology* **34**(4): 661-675.
- Fernandez, C. and Goldberg, J. M. (1976a). "Physiology of Peripheral Neurons Innervating Otolith Organs of the Squirrel Monkey. I. Response to Static Tilts and to Long-Duration Centrifugal Force." *Journal of Neurophysiology* **39**(5): 970-984.
- Fernandez, C. and Goldberg, J. M. (1976b). "Physiology of Peripheral Neurons Innervating Otolith Organs of the Squirrel Monkey. Ii. Directional Selectivity and Force-Response Relations." *Journal of Neurophysiology* **39**(5): 985-995.
- Fernandez, C. and Goldberg, J. M. (1976c). "Physiology of Peripheral Neurons Innervating Otolith Organs of the Squirrel Monkey. Iii. Response Dynamics." *Journal of Neurophysiology* **39**(5): 996-1008.
- Fernandez, C., Goldberg, J. M. and Abend, W. K. (1972). "Response to Static Tilts of Peripheral Neurons Innervating Otolith Organs of the Squirrel Monkey." *J Neurophysiol* **35**(6): 978-87.
- Field, A. (2005). *Discovering Statistics Using Spss*, Sage Publications Inc.
- Fraser, A. and Manning, G. (1950). "Effect of Variation in Swing Radius and Arc on Incidence of Swing Sickness." *J Appl Physiol* **2**(10): 580-584.
- Garson, G. D. (2008a). Binomial Test of Significance. *Statnotes: Advanced Quantitative Research in Public Administration*. Retrieved Sep 2010 from <http://faculty.chass.ncsu.edu/garson/PA765/binomial.htm>, North Carolina State University.
- Garson, G. D. (2008b). Measures of Association. *Statnotes: Topics in Multivariate Analysis*. Retrieved Apr 2010 from <http://faculty.chass.ncsu.edu/garson/pa765/statnote.htm>, North Carolina State University.
- Gibilisco, S. (2004). *Statistics Demystified*, McGraw-Hill Professional.
- Gillingham, K. K. (1966). *A Primer of Vestibular Function, Spatial Disorientation, and Motion Sickness (Review of Vestibular Function, Spatial Disorientation, and Motion Sickness)*
- USAF School of Aerospace Medicine, Brooks Air Force Base, Texas.
- Gizzi, M., Raphan, T., Rudolph, S. and Cohen, B. (1994). "Orientation of Human Optokinetic Nystagmus to Gravity: A Model-Based Approach." *Experimental Brain Research* **99**(2): 347-360.
- Glasauer, S. (1992a). *Das Zusammenspiel Von Otolithen Und Bogengängen Im Wirkungsgefüge Der Subjektiven Vertikale*, Doctoral Thesis, TU München.
- Glasauer, S. (1992b). "Interaction of Semicircular Canals and Otoliths in the Processing Structure of the Subjective Zenith." *Ann N Y Acad Sci* **656**: 847-9.
- Glasauer, S. (1993). Human Spatial Orientation During Centrifuge Experiments: Non-Linear Interaction of Semicircular Canals and Otoliths. In H. Krejčova and J. Jerábek(Eds.), *Proceedings of XVIIth Barany Society Meeting, Prague, Czech Republic*.
- Glasauer, S. and Merfeld, D. M. (1997). "Modelling Three Dimensional Vestibular Responses During Complex Motion Stimulation." *Three-Dimensional Kinematics of Eye, Head and Limb Movements*: 387-98.
- Glover, F. and Laguna, M. (1997). *Tabu Search*, Springer.

- Glover, F. and Marti, R. (2006). Tabu Search. (Ed.), Metaheuristic Procedures for Training Neural Networks: 53-69.
- Goldberg, D. E. (1989). Genetic Algorithms in Search, Optimization and Machine Learning. Boston, MA, USA, Addison-Wesley Longman Publishing Co.
- Goldberg, J. M. and Fernandez, C. (1971). "Physiology of Peripheral Neurons Innervating Semicircular Canals of the Squirrel Monkey. I. Resting Discharge and Response to Constant Angular Accelerations." *Journal of Neurophysiology* **34**(4): 635-660.
- Goldberg, J. M. and Fernandez, C. (1975). "Vestibular Mechanisms." *Annu Rev Physiol* **37**: 129-62.
- Golding, J. F., Arun, S., Wortley, E., Wotton-Hamrioui, K., Cousins, S. and Gresty, M. A. (2009). "Off-Vertical Axis Rotation of the Visual Field and Nauseogenicity." *Aviat Space Environ Med* **80**(6): 516-21.
- Golding, J. F., Bles, W., Bos, J. E., Haynes, T. and Gresty, M. A. (2003). "Motion Sickness and Tilts of the Inertial Force Environment: Active Suspension Systems Vs. Active Passengers." *Aviation Space and Environmental Medicine* **74**(3): 220-227.
- Golding, J. F., Finch, M. I. and Stott, J. R. R. (1997). "Frequency Effect of 0.35-1.0 Hz Horizontal Translational Oscillation on Motion Sickness and the Somatogravic Illusion." *Aviation Space and Environmental Medicine* **68**(5): 396-402.
- Golding, J. F. and Kerguelen, M. (1992). "A Comparison of the Nauseogenic Potential of Low-Frequency Vertical Versus Horizontal Linear Oscillation." *Aviation Space and Environmental Medicine* **63**(6): 491-497.
- Golding, J. F. and Markey, H. M. (1996). "Effect of Frequency of Horizontal Linear Oscillation on Motion Sickness and Somatogravic Illusion." *Aviation Space and Environmental Medicine* **67**(2): 121-126.
- Golding, J. F., Markey, H. M. and Stott, J. R. R. (1995). "The Effects of Motion Direction, Body Axis, and Posture on Motion Sickness Induced by Low-Frequency Linear Oscillation." *Aviation Space and Environmental Medicine* **66**(11): 1046-1051.
- Golding, J. F., Mueller, A. G. and Gresty, M. A. (2001). "A Motion Sickness Maximum around the 0.2 Hz Frequency Range of Horizontal Translational Oscillation." *Aviation Space and Environmental Medicine* **72**(3): 188-192.
- Goldstein, H., Poole, C., Safko, J. and Addison, S. (2002). *Classical Mechanics* 3rd Ed., Addison-Wesley, Reading, Massachusetts, USA, ISBN 0-321-18897-7.
- Graham, R. (1990). "Motion-Induced Interruptions as Ship Operability Criteria." *Naval Engineers Journal* **102**(2): 65-71.
- Grant, J. W. and Best, W. A. (1986). "Mechanics of the Otolith Organ-Dynamic Response." *Ann Biomed Eng* **14**(3): 241-56.
- Grant, J. W. and Cotton, J. R. (1990). "A Model for Otolith Dynamic Response with a Viscoelastic Gel Layer." *J Vestib Res* **1**(2): 139-51.
- Grant, J. W., Huang, C. C. and Cotton, J. R. (1994). "Theoretical Mechanical Frequency Response of the Otolithic Organs." *J Vestib Res* **4**(2): 137-51.
- Grant, W. and Best, W. (1987). "Otolith-Organ Mechanics: Lumped Parameter Model and Dynamic Response." *Aviat Space Environ Med* **58**(10): 970-6.
- Graybiel, A. (1970). "Susceptibility to Acute Motion Sickness in Blind Persons." *Aerosp Med* **41**(6): 650-3.

- Griffin, M. (1991a). Physical Characteristics of Stimuli Provoking Motion Sickness. AGARD (Advisory Group for Aerospace Research and Development) Lecture series 175: Motion Sickness: Significance in Aerospace Operations and Prophylaxis.
- Griffin, M. (1991b). Sea Sickness. AGARD (Advisory Group for Aerospace Research and Development) Lecture Series 175: Motion Sickness: Significance in Aerospace Operations and Prophylaxis.
- Griffin, M. J. (1990). Handbook of Human Vibration. London, United Kingdom, Academic Press.
- Griffin, M. J. and Mills, K. L. (2002a). "Effect of Frequency and Direction of Horizontal Oscillation on Motion Sickness." *Aviation Space and Environmental Medicine* **73**(6): 537-543.
- Griffin, M. J. and Mills, K. L. (2002b). "Effect of Magnitude and Direction of Horizontal Oscillation on Motion Sickness." *Aviation Space and Environmental Medicine* **73**(7): 640-646.
- Griffin, M. J. and Newman, M. M. (2004). "An Experimental Study of Low-Frequency Motion in Cars." *Proceedings of the Institution of Mechanical Engineers, Part D: Journal of Automobile Engineering* **218**(11): 1231-1238.
- Groen, J. J. (1957). "Cupulometry." *Laryngoscope* **67**(9): 894-905.
- Grush, R. (2004). "The Emulation Theory of Representation: Motor Control, Imagery, and Perception." *Behavioral and Brain Sciences* **27**(03): 377-422.
- Guedry, F. E. (1964). "Visual Control of Habituation to Complex Vestibular Stimulation in Man." *Acta Otolaryngol* **58**: 377-389.
- Guedry, F. E. (1968). Conflicting Sensory Orientation Cues as a Factor in Motion Sickness 4th symposium on the role of the vestibular organs in space exploration. Washington, DC, Office of Technology Utilization, NASA. **NASA SP-187: 45-2.**
- Guedry, F. E. (1974). Psychophysics of Vestibular Sensation. In H. H. Kornhuber (Ed.), *Handbook of Sensory Physiology*. Vol. VI/2: The Vestibular System Part 2, Psychophysics, Applied Aspects and General Interpretations. New York, Springer-Verlag. **VI**: 1-154.
- Guedry, F. E. (1991a). "Factors Influencing Susceptibility: Individual Differences and Human Factors." 1991. 18.
- Guedry, F. E. (1991b). Motion Sickness and Its Relation to Some Forms of Spatial Orientation: Mechanisms and Theory. AGARD (Advisory Group for Aerospace Research and Development) Lecture Series 175: Motion Sickness: Significance in Aerospace Operations and Prophylaxis.
- Guedry, F. E., Rupert, A. R. and Reschke, M. F. (1998). "Motion Sickness and Development of Synergy within the Spatial Orientation System. A Hypothetical Unifying Concept." *Brain Research Bulletin* **47**(5): 475-480.
- Guignard, J. and McCauley, M. (1990). The Accelerative Stimulus for Motion Sickness. In G. H. Crampton (Ed.), *Motion and Space Sickness*. Florida, USA, CRC Press: 123-152.
- Guignard, J. C. and McCauley, M. E. (1982). "Motion Sickness Incidence Induced by Complex Periodic Waveforms." *Aviat Space Environ Med* **53**(6): 554-63.
- Hallpike, C. S. and Hood, J. D. (1953). "The Speed of the Slow Component of Ocular Nystagmus Induced by Angular Acceleration of the Head: Its

- Experimental Determination and Application to the Physical Theory of the Cupular Mechanism." *Proc R Soc Lond B Biol Sci* **141**(903): 216-30.
- Handford, S. W., Cone, T. E., Jr. and Gover, S. C. (1953). "A Ship's Motion and the Incidence of Seasickness." *Mil Surg* **113**(3): 157-67.
- Hangos, K. and Cameron, I. (2001). *Process Modelling and Model Analysis*, Academic Press.
- Hartley, H. O. (1961). "The Modified Gauss-Newton Method for the Fitting of Non-Linear Regression Functions by Least Squares." *Technometrics* **3**(2): 269-280.
- Haward, B., Lewis, C. and Griffin, M. (2000). *Crew Response to Motions of an Offshore Oil Production and Storage Vessel. Human Factors in Ship Design and Operation*. London, UK, RINA.
- Haward, B. M., Lewis, C. H. and Griffin, M. J. (2009). "Motions and Crew Responses on an Offshore Oil Production and Storage Vessel." *Applied Ergonomics* **40**(5): 904-914.
- Held, R. (1961). "Exposure-History as a Factor in Maintaining Stability of Perception and Co-Ordination." *Journal of Nervous and Mental Disease* **132**: 26-32.
- Henn, V., Cohen, B. and Young, L. R. (1980). "Visual-Vestibular Interaction in Motion Perception and the Generation of Nystagmus." *Neurosci Res Program Bull* **18**(4): 457-651.
- Henriksson, N. G., Wennmo, C., Pyykko, I. and Schalen, L. (1984). "A Model of Visual-Vestibular Interaction in Cerebellar Disorders." *ORL J Otorhinolaryngol Relat Spec* **46**(6): 302-9.
- Highstein, M. S., Fay, R. R. and Popper, N. A. (2004). *Springer Handbook of Auditory Research: The Vestibular System*. New York, Springer.
- Hill, J. (1936). "The Care of the Sea-Sick." *British Medical Journal* **2**(3955): 802-807.
- Hill, M. C. and Tiedeman, C. R. (2007). *Effective Groundwater Model Calibration: With Analysis of Data, Sensitivities, Predictions, and Uncertainty*, Wiley-Interscience.
- Houben, M. M. J. and Bos, J. E. (2010). *Reduced Seasickness by an Artificial 3d Earth-Fixed Visual Reference. Human Performance at Sea, HPAS 16-18 June 2010*. Glasgow, UK.
- Huler, S. (2005). *Defining the Wind: The Beaufort Scale, and How a 19th-Century Admiral Turned Science into Poetry*, Three Rivers Pr.
- Hulk, J. and Jongkees, L. B. (1948). "The Turning Test with Small Regulable Stimuli; the Normal Cupulogram." *J Laryngol Otol* **62**(2): 70-5.
- Huston, R. L. and Liu, C. Q. (2001). *Formulas for Dynamic Analysis*. New York, USA, Marcel Dekker Incorporation.
- Igarashi, M. (1966). *Dimensional Study of the Vestibular End Organ Apparatus. Second Symposium on the Role of the Vestibular Organs in Space Exploration. NASA SP-115, Moffett Field, CA NASA Ames Research Center, Washington, DC.*
- Igarashi, M. (1967). "Dimensional Study of the Vestibular Apparatus." *The Laryngoscope* **77**(10): 1806-1817.
- Igarashi, M. and Nagaba, M. (1962). "Vestibular End-Organ Damage in Squirrel Monkeys after Exposure to Intensive Linear Acceleration." *NASA SP*.

- Igarashi, M., O-Uchi, T. and Alford, B. R. (1981). "Volumetric and Dimensional Measurements of Vestibular Structures in the Squirrel Monkey." *Acta Oto-Laryngologica* **91**(1): 437 - 444.
- Imai, T., Moore, S. T., Raphan, T. and Cohen, B. (2001). "Interaction of the Body, Head, and Eyes During Walking and Turning." *Experimental Brain Research* **136**(1): 1-18.
- Irwin, J. A. (1881). "The Pathology of Seasickness." *Lancet* **2**(907-909).
- International Organisation for Standardization (1985). *Evaluation of Human Exposure to Whole-Body Vibration Part 3: Evaluation of Exposure to Whole-Body Z-Axis Vertical Vibration in the Frequency Range 0,1 to 0,63 Hz. ISO 2631-3:1985*, International Organisation for Standardization, Geneva, Switzerland.
- International Organisation for Standardization (1997). *Mechanical Vibration and Shock: Evaluation of Human Exposure to Whole-Body Vibration. Part 1: General Requirements. ISO 2631-1*, International Organisation for Standardization, Geneva, Switzerland.
- Jaeger, R. and Haslwanter, T. (2004). "Otolith Responses to Dynamical Stimuli: Results of a Numerical Investigation." *Biological Cybernetics* **90**(3): 165-175.
- Jaeger, R., Takagi, A. and Haslwanter, T. (2002). "Modeling the Relation between Head Orientations and Otolith Responses in Humans." *Hearing Research* **173**(1-2): 29-42.
- James, W. (1882). "The Sense of Dizziness in Deaf-Mutes." *Am. J. Otology* **4**: 239-254.
- Janelle, D. and Beuthe, M. (2002). "Globalization and Transportation." *Social change and sustainable transport*: 49.
- Johnson, W. H. and Mayne, J. W. (1953). "Stimulus Required to Produce Motion Sickness; Restriction of Head Movement as a Preventive of Airsickness; Field Studies on Airborne Troops." *J Aviat Med* **24**(5): 400-11; *passim*.
- Johnson, W. H., Stubbs, R. A., Kelk, G. F. and Franks, W. R. (1951). "Stimulus Required to Produce Motion Sickness. I. Preliminary Report Dealing with Importance of Head Movements." *J Aviat Med* **22**(5): 365-74.
- Johnson, W. H., Sunahara, F. A. and Landolt, J. P. (1999). "Importance of the Vestibular System in Visually Induced Nausea and Self-Vection." *J Vestib Res* **9**(2): 83-7.
- Jones, G. M., Rolph, R. and Downing, G. H. (1980). "Comparison of Human Subjective and Oculomotor Responses to Sinusoidal Vertical Linear Acceleration." *Acta Otolaryngol* **90**(5-6): 431-40.
- Joseph, J. A. (2008). *Motion Sickness with Earth-Horizontal Translational and Rotational Oscillation Presented in Isolation and in Combination*. Institute of Sound and Vibration Research. Southampton, University of Southampton. **PhD**: 200.
- Kailath, T. (1974). "A View of Three Decades of Linear Filtering Theory." *Information Theory, IEEE Transactions on* **20**(2): 146-181.
- Kalman, R. E. (1960). "A New Approach to Linear Filtering and Prediction Problems." *Journal of basic Engineering* **82**(1): 35-45.

- Kalman, R. E. (1961). New Methods in Wiener Filtering Theory. Proc. of the Symposium on Engineering Applications of Random Function Theory and Probability: 270-288.
- Kalman, R. E. and Bucy, R. S. (1961). "New Results in Linear Filtering and Prediction Theory." *J. Basic Eng., Trans ASME* **83**: 95-108.
- Karris, S. (2008). *Signals and Systems: With Matlab Computing and Simulink Modeling*. USA, Orchard Publications.
- Keist, B. F., Sheeley, W. F., Byers, J. M. and Chinn, H. I. (1956). "Effect of Head Immobilization on Incidence of Airsickness." *J Appl Physiol* **8**(4): 369-70.
- Kennedy, R. S., Graybiel, A., McDonough, R. C. and Beckwith, F. D. (1965). "Symptomatology under Storm Conditions in the North Atlantic in Control Subjects and in Persons with Bilateral Labyrinthine Defects. Nsam-928." *Res Rep U S Nav Sch Aviat Med*: 1-10.
- Kennedy, R. S., Graybiel, A., McDonough, R. C. and Beckwith, F. D. (1968). "Symptomatology under Storm Conditions in the North Atlantic in Control Subjects and in Persons with Bilateral Labyrinthine Defects." *Acta Otolaryngol* **66**(6): 533-40.
- Kirkner, F. J. (1949). "Psychophysiological Studies of Motion Sickness and Airsickness." *J Comp Physiol Psychol* **42**(4): 273-85.
- Kleinbaum, D., Klein, M. and Pryor, E. (2002). *Logistic Regression a Self-Learning Text Statistics for Biology and Health*, Springer.
- Kotaka, S., Watanabe, I. and Bles, W. (1984). "[Somatosensory-Visual-Vestibular Interaction in a Case of Vermis Agenesis]." *No To Shinkei* **36**(11): 1083-8.
- Kottenhoff, H. and Lindahl, L. (1960). "Laboratory Studies on the Psychology of Motion-Sickness." *Acta Psychologica* **17**: 89-91.
- Laarhoven, P. J. M. and Aarts, E. H. L. (1987). *Simulated Annealing: Theory and Applications*. Reidel, Dordrecht, The Netherlands, Springer.
- Lackner, J. R. and Graybiel, A. (1986). "Head Movements in Non-Terrestrial Force Environments Elicit Motion Sickness: Implications for the Etiology of Space Motion Sickness." *Aviat Space Environ Med* **57**(5): 443-8.
- Lansberg, M. (1960). *A Primer of Space Medicine*. New York, Elsevier Publishing Co.
- Lau, C. G., Honrubia, V., Jenkins, H. A., Baloh, R. W. and Yee, R. D. (1978). "Linear Model for Visual-Vestibular Interaction." *Aviat Space Environ Med* **49**(7): 880-5.
- Lawther, A. and Griffin, M. J. (1986). "The Motion of a Ship at Sea and the Consequent Motion Sickness Amongst Passengers." *Ergonomics* **29**(4): 535-552.
- Lawther, A. and Griffin, M. J. (1987). "Prediction of the Incidence of Motion Sickness from the Magnitude, Frequency, and Duration of Vertical Oscillation." *J Acoust Soc Am* **82**(3): 957-66.
- Lawther, A. and Griffin, M. J. (1988a). "Motion Sickness and Motion Characteristics of Vessels at Sea." *Ergonomics* **31**(10): 1373-1394.
- Lawther, A. and Griffin, M. J. (1988b). "A Survey of the Occurrence of Motion Sickness Amongst Passengers at Sea." *Aviat Space Environ Med* **59**(5): 399-406.
- Lishman, J. and Lee, D. (1973). "The Autonomy of Visual Kinesthesia." *Perception* **2**: 287-294.

- Lively, K. A., Seman, A. J. and Kirkpatrick, M. (2003). "Human Systems Integration and Advanced Technology in Engineering Department Workload and Manpower Reduction." *Naval Engineers Journal* **115**(1): 57-65.
- Ljung, L. (1987). *System Identification: Theory for the User*. Englewood Cliffs, New Jersey, USA, Prentice Hall.
- Lloyd, A. R. M. J. (1998). *Seakeeping: Ship Behavior in Rough Weather*. Gosport, UK.
- Lobb, B. (2001). A Frequency Weighting for Motion Sickness Susceptibility in the Lateral Axis. 36th UK Group Conference on Human Response to Vibration, 12-14 Sep 2001. Farnborough, UK: 386-398.
- Lonsdale, K. (2009). Design Considerations Affecting Vertical Accelerations & Operability in Rigid Hulled Inflatable Boats. *Naval Architecture & Marine Engineering*. Glasgow, University of Strathclyde. **M.Eng**: 108.
- Lowenstein, O. and Roberts, T. D. (1950). "The Equilibrium Function of the Otolith Organs of the Thornback Ray (*Raja Clavata*)." *J Physiol* **110**(3-4): 392-415.
- Luenberger, D. (1966). "Observers for Multivariable Systems." *IEEE Transactions on Automatic Control* **11**(2): 190-197.
- Luenberger, D. (1971). "An Introduction to Observers." *Automatic Control, IEEE Transactions on* **16**(6): 596-602.
- Luenberger, D. G. (1964). "Observing the State of a Linear System." *Military Electronics, IEEE Transactions on* **8**(2): 74-80.
- Lysakowski, A. and Goldberg, J. (2004). Morphophysiology of the Vestibular Periphery. In M. S. Highstein, R. R. Fay and N. A. Popper (Ed.), *Springer Handbook of Auditory Research: The Vestibular System*. New York, USA, Springer: 57-152.
- Mach, E. (1875). *Grundlinien Der Lehre Von Den Bewegungsempfindungen*. Engelmann, Leipzig Reprint Bonset, Amsterdam (1967). Young Lr, Henn V, Scherberger H (Trans)(2001) *Fundamentals of the Theory of Movement Perception*, Kluwer/Plenum, Dordrecht, London.
- MacNeilage, P. R., Ganesan, N. and Angelaki, D. E. (2008). "Computational Approaches to Spatial Orientation: From Transfer Functions to Dynamic Bayesian Inference." *Journal of Neurophysiology* **100**(6): 2981-2996.
- Maluf, N. and Williams, K. (2004). *An Introduction to Microelectromechanical System Engineering*, 2nd Ed. London, UK, Artech House, Inc.
- Manning, G. and Stewart, W. (1949). "Effect of Body Position on Incidence of Motion Sickness." *J Appl Physiol* **1**(9): 619-628.
- Mansfield, N. J. (2004). *Human Response to Vibration*, CRC PRESS.
- Matsangas, P. (2004). A Linear Physiological Visual-Vestibular Interaction Model for the Prediction of Motion Sickness Incidence. Monterey, California, Naval Postgraduate School. **MSc**: 186.
- Mayne, R. (1969). The Analogy of the Vestibular Organs to an Inertial Guidance System. 9th In't. Conf. Oto-Rhino-Laryngology, Mexico City, Amsterdam: Excerpta Medica.
- Mayne, R., Ed. (1974a). *Handbook of Sensory Physiology*. Berlin Heidelberg, New York, Springer.
- Mayne, R. (1974b). A Systems Concept of the Vestibular Organs. In H. H. Kornhuber (Ed.), *Handbook of Sensory Physiology: Vestibular System Part*

- 2- Psychophysics, Applied Aspects, and General Interpretations Berlin, Springer-Verlag. **6**: 493-580.
- Mayne, R. and Belanger, F. (1966). The Functions and Operating Principles of the Otolith Organs. Part 111. The Interpretation of "Single Fiber" or "Few Fiber" Recordings. GERA-1113. Goodyear Aerospace. Litchfield Park, Arizona.
- McCauley, M. and Kennedy, R. (1976). Recommended Human Exposure Limits for Very-Low-Frequency Vibration. Technical Publication TP-76-36. Pacific Missile Test Center. Point Mugu, California.
- McCauley, M., Royal, J., Wylie, C., O'Hanlon, J. and Mackie, R. (1976). Motion Sickness Incidence: Exploratory Studies of Habituation, Pitch and Roll, and the Refinement of a Mathematical Model. Technical Report No.1733-2. Office of Naval Research (Human Factors Research).
- McCauley, M. E., Pierce, E. C. and Matsagas, P. (2007). "The High-Speed Navy: Vessel Motion Influences on Human Performance." *Naval Engineers Journal* **119**(1): 35-44.
- McDonald, J. (2008). Handbook of Biological Statistics, University of Delaware (<http://udel.edu/~mcdonald/statexactbin.html>).
- McKenzie, E. (2008). Personal Discussion Regarding Goodness-of-Fit Test for Field Trials on Motion Sickness. Department of Statistics and Modelling Science University of Strathclyde, Glasgow, UK.
- Menke, W. (1989). Geophysical Data Analysis: Discrete Inverse Theory. San Diego, California, USA, Academic Press.
- Merfeld, D. (1990). Spatial Orientation in the Squirrel Monkey: An Experimental and Theoretical Investigation. Cambridge, Massachusetts, Massachusetts Institute of Technology. **PhD**.
- Merfeld, D. M. (1995a). "Modeling Human Vestibular Responses During Eccentric Rotation and Off Vertical Axis Rotation." *Acta Otolaryngol Suppl* **520**: 354-359.
- Merfeld, D. M. (1995b). "Modeling the Vestibulo-Ocular Reflex of the Squirrel Monkey During Eccentric Rotation and Roll Tilt." *Exp Brain Res* **106**(1): 123-34.
- Merfeld, D. M. (1996). "Vestibulo-Ocular Reflex of the Squirrel Monkey During Eccentric Rotation with Centripetal Acceleration Along the Naso-Occipital Axis." *Brain Research Bulletin* **40**(5-6): 303-309.
- Merfeld, D. M. (2004). "Internal Models and Spatial Orientation." *Behavioral and Brain Sciences* **27**(3): 410-410.
- Merfeld, D. M. and Young, L. R. (1995). "The Vestibulo-Ocular Reflex of the Squirrel Monkey During Eccentric Rotation and Roll Tilt." *Experimental Brain Research* **106**(1): 111-122.
- Merfeld, D. M., Young, L. R., Oman, C. M. and Shelhamer, M. J. (1993). "A Multidimensional Model of the Effect of Gravity on the Spatial Orientation of the Monkey." *J Vestib Res* **3**(2): 141-61.
- Merfeld, D. M., Zupan, L. and Peterka, R. J. (1999). "Humans Use Internal Models to Estimate Gravity and Linear Acceleration." *Nature* **398**(6728): 615-618.
- Merfeld, D. M. and Zupan, L. H. (2002). "Neural Processing of Gravitoinertial Cues in Humans. Iii. Modeling Tilt and Translation Responses." *J Neurophysiol* **87**(2): 819-33.

- Merfeld, D. M., Zupan, L. H. and Gifford, C. A. (2001). "Neural Processing of Gravito-Inertial Cues in Humans. Ii. Influence of the Semicircular Canals During Eccentric Rotation." *J Neurophysiol* **85**(4): 1648-60.
- Mergner, T., Nasios, G., Maurer, C. and Becker, W. (2001). "Visual Object Localisation in Space. Interaction of Retinal, Eye Position, Vestibular and Neck Proprioceptive Information." *Exp Brain Res* **141**(1): 33-51.
- Mergner, T. and Rosemeier, T. (1998). "Interaction of Vestibular, Somatosensory and Visual Signals for Postural Control and Motion Perception under Terrestrial and Microgravity Conditions--a Conceptual Model." *Brain Res Brain Res Rev* **28**(1-2): 118-35.
- Mittelstaedt, H. (1983). "A New Solution to the Problem of the Subjective Vertical." *Naturwissenschaften* **70**(6): 272-281.
- Mittelstaedt, H., Glasauer, S., Gralla, G. and Mittelstaedt, M. L. (1989). "How to Explain a Constant Subjective Vertical at Constant High Speed Rotation About an Earth-Horizontal Axis." *Acta Oto-Laryngologica* **108**(5 supp 468): 295-299.
- Money, K. E. (1970). Motion Sickness, *Am Physiological Soc.* **50**: 1-39.
- Money, K. E. and Friedberg, J. (1964). "The Role of the Semicircular Canals in Causation of Motion Sickness and Nystagmus in the Dog." *Can J Physiol Pharmacol* **42**: 793-801.
- Moore, S. T., Hirasaki, E., Raphan, T. and Cohen, B. (2001). "The Human Vestibulo-Ocular Reflex During Linear Locomotion." *Annals of the New York Academy of Sciences* **942**(1): 139-147.
- Morales, M. (1946). "Asynchrony of Labyrinthine Receptors as a Physical Factor in Motion Sickness." *Bulletin of Mathematical Biology* **8**(4): 147-157.
- Morales, M. F. (1949). "Motion Sickness: Physical Considerations Regarding Its Etiology." A Survey Report on Human Factors in Undersea Warfare.
- Morton, G., Cipriani, A. and McEachern, D. (1947). "Mechanism of Motion Sickness." *Arch Neurol Psychiatry* **57**(1): 58-70.
- Nieuwenhuyzen, J. H. (1958). Experimental Investigations on Seasickness., University of Utrech. **PhD Thesis**.
- Niven, J. and Hixson, W. (1961). Frequency Response of the Human Semicircular Canals, US Naval School of Aviation Medicine; US Naval Aviation Medical Center.
- Nyquist, H. (1928). "Certain Factors Affecting Telegraph Speed. At&T, 1924 and Certain Topics in Telegraph Transmission Theory." *Trans. American Institute of Elect. Eng* **47**: 617-644.
- O'Hanlon, J. F. and McCauley, M. E. (1974). "Motion Sickness Incidence as a Function of the Frequency and Acceleration of Vertical Sinusoidal Motion." *Aerospace Medicine* **45**: 366-369.
- Oberman, F. and Baker, C. (2004). "A Hybrid Approach to Optimizing Workload, Manpower, and Ship Sizing." *Naval Engineers Journal* **116**(1): 43-53.
- OECD/ITF (2009). Trends in the Transport Sector 1970-2007. Organisation for Economic Co-operation and Development/International Transport Forum.
- Oman, C. M. (1978). A Sensory Motor Conflict Model for Motion Sickness Workshop III. Space Motion Sickness Symposium, Nov 16, 1978. NASA Johnson Space Center, Houston, TX.

- Oman, C. M. (1982). "A Heuristic Mathematical Model for the Dynamics of Sensory Conflict and Motion Sickness." *Acta Otolaryngol Suppl* **392**: 1-44.
- Oman, C. M. (1987). "Spacelab Experiments on Space Motion Sickness." *Acta Astronautica* **15**(1): 55-66.
- Oman, C. M. (1990). "Motion Sickness - a Synthesis and Evaluation of the Sensory Conflict Theory." *Canadian Journal of Physiology and Pharmacology* **68**(2): 294-303.
- Oman, C. M. (1991). *Sensory Conflict in Motion Sickness: An Observer Theory Approach*. In R. E. Stephen, K. K. Mary and C. G. Arthur (Ed.), *Pictorial Communication in Virtual and Real Environments*. London, Taylor & Francis: 362-376.
- Oman, C. M. (1998). "Sensory Conflict Theory and Space Sickness: Our Changing Perspective." *Journal of Vestibular Research-Equilibrium & Orientation* **8**(1): 51-56.
- Oman, C. M. and Cook, W. J. C. (1983). *Dynamics of Skin Pallor in Motion Sickness as Measured Using an Infrared Reflectance Technique*. Paper presented at the 54th Annual Aerospace Medical Association Meeting, May 1983, Houston, TX.
- Oman, C. M., Howard, I. P., Shebilske, W. L. and Taube, J. S. (2001). "Visual Orientation in Unfamiliar Gravito-Inertial Environments." *Neurophysiology Platform Presentation* **186**.
- Oman, C. M., Marcus, E. N. and Curthoys, I. S. (1987). "The Influence of Semicircular Canal Morphology on Endolymph Flow Dynamics. An Anatomically Descriptive Mathematical Model." *Acta Otolaryngol* **103**(1-2): 1-13.
- Ormsby, C. and Young, L. (1976). "Perception of Static Orientation in a Constant Gravito-inertial Environment." *Aviat Space Environ Med* **47**: 159-164.
- Ormsby, C. and Young, L. (1977). "Integration of Semicircular Canal and Otolith Information for Multisensory Orientation Stimuli." *Mathematical Biosciences* **34**: 1-21.
- Paige, G. (1996). *How Does the Linear Vestibulo-Ocular Reflex Compare with the Angular Vestibulo-Ocular Reflex*. In R. W. Baloh and G. M. Halmagyi (Ed.), *Disorders of the Vestibular System*, Oxford University Press, New York: 93-104.
- Paige, G. D. and Tomko, D. L. (1991a). "Eye Movement Responses to Linear Head Motion in the Squirrel Monkey. I. Basic Characteristics." *J Neurophysiol* **65**(5): 1170-82.
- Paige, G. D. and Tomko, D. L. (1991b). "Eye Movement Responses to Linear Head Motion in the Squirrel Monkey. II. Visual-Vestibular Interactions and Kinematic Considerations." *J Neurophysiol* **65**(5): 1183-96.
- Pattison, J., Sheridan, D. and VA, N. (2004). *Human Performance Factors and Measures in Hull Form Selection. Habitability of Combat and Transport Vehicles: Noise, Vibration and Motion*. Prague, Czech Republic, RTO AVT Symposium.
- Pescetto, A. (2006). *A Rational Approach for Reduction of Motion Sickness & Improvement of Passenger Comfort and Safety in Sea Transportation*. COMPASS Final Technical Report No. PRO/90/012/012/39

- Pethybridge, R. (1982). Sea Sickness Incidence in Royal Navy Ships. INM Report 37/82. Institute of Naval Medicine. Gosport, England.
- Pethybridge, R., Davies, J. and Walters, J. (1978). A Pilot Study on the Incidence of Sea Sickness in Rn Personnel on 2 Ships. INM Report 55/78. Institute of Naval Medicine Alverstoke, Hampshire, England.
- Poon, C.-S. and Merfeld, D. M. (2005). "Internal Models: The State of the Art." *Journal of Neural Engineering* **2**(3): S147-S151.
- Prsa, M. and Galiana, H. L. (2007). "Visual-Vestibular Interaction Hypothesis for the Control of Orienting Gaze Shifts by Brain Stem Omnipause Neurons." *J Neurophysiol* **97**(2): 1149-62.
- Purves, D., Augustine, G. J., Fitzpatrick, D., Hall, W. C., Lamantia, A.-S., Mcnamara, J. O. and Williams, S. M. (2004). *Neuroscience*, 3rd Edn. Sunderland, Massachusetts U.S.A., Sinauer Associates, Inc.
- Quix, F. H. (1922). "Le Mal De Mer Et Le Mal Des Aviateur." *Monograph Oto Rhion Laryngol Intern* **8**: 828-987.
- Rabbitt, R. D., Damiano, E. R. and Grant, J. W. (2004). Biomechanics of the Semicircular Canals and Otolith Organs. In M. S. Highstein, R. R. Fay and N. A. Popper (Ed.), *Springer Handbook of Auditory Research: The Vestibular System*. New York, USA, Springer.
- Raphan, T., Cohen, B. and Matsuo, V. (1977). "A Velocity Storage Mechanism Responsible for Optokinetic Nystagmus (Okn), Optokinetic after-Nystagmus (Okn) and Vestibular Nystagmus." *Control of Gaze by Brain Stem Neurons* **1**: 37—47.
- Raphan, T., Matsuo, V. and Cohen, B. (1979). "Velocity Storage in the Vestibulo-Ocular Reflex Arc (Vor)." *Experimental Brain Research* **35**(2): 229-248.
- Raphan, T., Wearne, S. and Cohen, B. (1996). "Modeling the Organization of the Linear and Angular Vestibulo-Ocular Reflexes." *Ann N Y Acad Sci* **781**: 348-63.
- Rawlings, J., Pantula, S. and Dickey, D. (1998). *Applied Regression Analysis: A Research Tool*. New York, USA, Springer
- Reason, J. (1968). *An Investigation of Some Factors Contributing to Individual Variation in Motion Sickness Susceptibility*, Ministry of Defence, Air Force Dept.
- Reason, J. (1978a). "Motion Sickness: Some Theoretical and Practical Considerations." *Applied Ergonomics* **9**(3): 163-167.
- Reason, J. and Graybiel, A. (1969). *Adaptation to Coriolis Accelerations: Its Transfer to the Opposite Direction of Rotation as a Function of Intervening Activity at Zero Velocity*. NASA Order R-93. Naval Aerospace Medical Institute (NAMI-1086), Pensacola Fla. Naval Aerospace Medical Institute.
- Reason, J. and Graybiel, A. (1972). *Factors Contributing to Motion Sickness Susceptibility: Adaptability and Receptivity*. AGARD (Advisory Group for Aerospace Research and Development) Conference Proceedings No. 109.
- Reason, J. T. (1969). "Motion Sickness-Some Theoretical Considerations." *International Journal of Man-Machine Studies* **1**(1): 21-38.
- Reason, J. T. (1970). "Motion Sickness: A Special Case of Sensory Rearrangement." *Adv Sci* **26**(130): 386-93.
- Reason, J. T. (1978b). "Motion Sickness Adaptation: A Neural Mismatch Model." *Journal of the Royal Society of Medicine* **71**(11): 819-29.

- Reason, J. T. and Brand, J. J. (1975). *Motion Sickness*, Academic Press Inc.
- Reymond, G., Droulez, J. and Kemeny, A. (2002). "Visuovestibular Perception of Self-Motion Modeled as a Dynamic Optimization Process." *Biological Cybernetics* **87**(4): 301-314.
- Reynolds, T. (1884). "On the Nature and Treatment of Seasickness." *Lancet* **i**: 1161-1162.
- Riccio, G. E. and Stoffregen, T. A. (1991). "An Ecological Theory of Motion Sickness and Postural Instability." *Ecological Psychology* **3**(3): 195 - 240.
- Richardson, L. F. (2007). *Weather Prediction by Numerical Process*, 2nd Ed. Cambridge, UK, Cambridge University Press.
- Riola, J. and de Arboleya, M. (2006). "Habitability and Personal Space in Seakeeping Behaviour." *Journal of Maritime Research* **3**(1): 41-54.
- RITA/BTS (2009). *Transportation Services Index (December 2009)*. available at <http://www.bts.dot.gov/> as of 20 Feb 2010. Research and Innovative Technology Administration (RITA) and Bureau of Transport Statistics (BTS). USA.
- Robinson, D. (1977). *Vestibular and Optokinetic Symbiosis: An Example of Explaining by Modelling*. In R. Baker and A. Berthoz (Ed.), *Control of Gaze by Brain Stem Neurons, Developments in Neuroscience*, Elsevier/North-Holland Biomedical Press: 49-58.
- Rolnick, A. and Gordon, C. (1991). *The Effects of Motion Induced Sickness on Military Performance*. In R. Gal and A. D. Mangelsdorff (Ed.), *Handbook of Military Psychology*. Chichester, England, John Wiley & Sons: 279-293.
- Ross, J. M. (2009). *Human Factors Considerations for Marine Vehicle Design*. RINA, Royal Institution of Naval Architects International Conference - Human Factors in Ship Design, Safety and Operation, February 25, 2009 - February 26, 2009, London, United kingdom, Royal Institution of Naval Architects.
- Ryan, T. (2007). *Modern Engineering Statistics*, Wiley-Interscience.
- Sá, J. P. M. d. (2007). *Applied Statistics Using Spss, Statistica, Matlab and R*, Springer.
- Salami, A., Dellepiane, M., Crippa, B., Baretini, L. and Mora, R. (2008). "Visual-Vestibular Interaction Test in the Diagnosis of Vertigo in Children." *Int J Pediatr Otorhinolaryngol* **72**(1): 1-7.
- Salami, A., Medicina, M. C., Dellepiane, M., Mora, R. and Guglielmetti, G. (1996). "[Optokinetic Nystagmus and Visual-Vestibular Interaction in Subjects with "Whiplash Injuries"]." *Acta Otorhinolaryngol Ital* **16**(2): 91-8.
- Sariöz, K. and Narli, E. (2005). "Effect of Criteria on Seakeeping Performance Assessment." *Ocean Engineering* **32**(10): 1161-1173.
- Sariöz, K. and Sariöz, E. (2005). "Habitability Assessment of Passenger Vessels Based on Iso Criteria." *Marine Technology* **42**(1): 43-51.
- Schmid, R. and Buizza, A. (1983). "Visual-Vestibular Interaction in Oculomotor Control: A Model Interpretation of Pathological Situations." *Adv Otorhinolaryngol* **30**: 217-21.
- Schmid, R., Buizza, A. and Zambarbieri, D. (1980). "A Non-Linear Model for Visual-Vestibular Interaction During Body Rotation in Man." *Biol Cybern* **36**(3): 143-51.

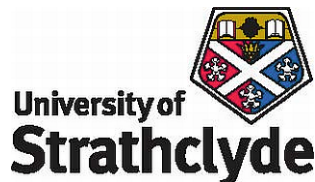
- Shaikh, A., Green, A., Ghasia, F., Newlands, S., Dickman, J. and Angelaki, D. (2005). "Sensory Convergence Solves a Motion Ambiguity Problem." *Current Biology* **15**(18): 1657-1662.
- Shannon, C. (1949). "Communication in the Presence of Noise." *Proceedings of the IRE* **37**(1): 10-21.
- SISA (2010). Method of Small P-Values (<http://www.quantitativeskills.com/sisa/papers/paper5.htm>) retrieved on 06 Sep 2010.
- Sjöberg, A. (1931). "Experimental Studies of the Eliciting Mechanism of Seasickness." *Acta Otolaryngol Suppl.* **14**: 1-136.
- Sjöberg, A. (1970). *Experimental Studies of the Eliciting Mechanism of Motion Sickness. Fourth Symposium on The Role of the Vestibular Organs in Space Exploration.* NASA SP-187, Washington, DC.
- Sjöberg, J., Zhang, Q., Ljung, L., Benveniste, A., Delyon, B., Glorennec, P., Hjalmarsson, H. and Juditsky, A. (1995). "Nonlinear Black-Box Modeling in System Identification: A Unified Overview." *Automatica* **31**(12): 1691-1724.
- Smith, S. (2003). *Digital Signal Processing: A Practical Guide for Engineers and Scientists.* London, UK, Newnes.
- Sperry, R. W. (1950). "Neural Basis of the Spontaneous Optokinetic Response Produced by Visual Inversion." *J Comp Physiol Psychol* **43**(6): 482-9.
- Steele, J. E. and Major, U. (1961). *Motion Sickness and Spatial Perception.* ASD Technical Report 61-530, Wright-Patterson Air Force Base, Ohio.
- Steinhausen, W. (1931). "On the Proof of the Movement of the Cupula in the Complete Arcade-Ampulla of the Labyrinth under Rotary and Caloric Stimulation." *Pflüers Arch. Ges. Physiol* **22**: 322-328.
- Steinhausen, W. (1935). "Über Die Durch Die Otolithen Ausgelösten Kräfte." *Pflügers Archiv European Journal of Physiology* **235**(1): 538-544.
- Stevens, S. C. and Parsons, M. G. (2002). "Effects of Motion at Sea on Crew Performance: A Survey." *Marine Technology* **39**(1): 29-47.
- Stevens, S. S. (1957). "On the Psychophysical Law." *Psychol Rev* **64**(3): 153-81.
- Stoffregen, T. A. (1985). "Flow Structure Versus Retinal Location in the Optical Control of Stance." *Journal of experimental psychology. Human perception and performance* **11**(5): 554-565.
- Stoffregen, T. A., Hettinger, L. J., Haas, M. W., Roe, M. M. and Smart, L. J. (2000). "Postural Instability and Motion Sickness in a Fixed-Base Flight Simulator." *Human Factors* **42**(3): 458-469.
- Stoffregen, T. A. and Riccio, G. E. (1991). "An Ecological Critique of the Sensory Conflict Theory of Motion Sickness." *Ecological Psychology* **3**(3): 159 - 194.
- Stoffregen, T. A., Smart, L. J., Bardy, B. G. and Pagulayan, R. J. (1999). "Postural Stabilization of Looking." *Journal of experimental psychology. Human perception and performance* **25**(6): 1641-1658.
- Stoffregen, T. A. and Smart Jr, L. J. (1998). "Postural Instability Precedes Motion Sickness." *Brain Research Bulletin* **47**(5): 437-448.
- Stott, J. (1986). "Mechanisms and Treatment of Motion Illness." *Nausea and vomiting-mechanisms and treatment.* Berlin, Heidelberg, New York, Tokyo: Springer Verlag: 110-29.

- Tamura, Y. and Arima, M. (2006). Measurement and Analysis of Ship Motion of a High-Speed Passenger Craft. Cupertino, International Society Offshore & Polar Engineers.
- Tin, C. and Poon, C.-S. (2005). "Internal Models in Sensorimotor Integration: Perspectives from Adaptive Control Theory." *Journal of Neural Engineering* **2**(3): S147-S163.
- Todorov, E. (2004). "Optimality Principles in Sensorimotor Control." *Nature Neuroscience* **7**(9): 907-915.
- Torggrimson, B. N. and Minson, C. T. (2005). "Sex and Gender: What Is the Difference?" *J Appl Physiol* **99**(3): 785.
- Treisman, M. (1977). "Motion Sickness: An Evolutionary Hypothesis." *Science* **197**(4302): 493-495.
- Trumbull, R., Chinn, H., Maag, C., Milch, L., Handford, S., Seibert, R., Sperling, P. and Smith, P. (1960). "Effect of Certain Drugs on the Incidence of Seasickness." *Clinical Pharmacology and Therapeutics* **1**(3): 280-283.
- Turan, O. (2006). A Rational Approach for Reduction of Motion Sickness & Improvement of Passenger Comfort and Safety in Sea Transportation (Compass). COMPASS Project Technical Report. Universities of Glasgow & Strathclyde. Glasgow.
- Turan, O., Ganguly, A., Aksu, S. and Verveniotis, C. (2003). Human Comfort and Motion Sickness Onboard High Speed Craft. FAST. Ischia (Italy), Comitato Organizzatore FAST 2003.
- Turan, O., Sebastiani, L., Ganguly, A., BOS, J. and Lewis, C. H. (2005). Compass Project: New Findings Regarding Effects of Ship Motions on Human Comfort and the Way Forward. Human Factors Impact on Ship Design International Workshop. Genova, Italy.
- Turan, O., Verveniotis, C. and Khalid, H. (2009). "Motion Sickness Onboard Ships- Subjective Vertical Theory and Its Application to Full Scale Trials." *Journal of Marine Science and Technology* **14**(4): 1-8.
- Turner, M. and Griffin, M. J. (1995). "Motion Sickness Incidence During a Round-the-World Yacht Race." *Aviat Space Environ Med* **66**(9): 849-56.
- Turner, M. and Griffin, M. J. (1999). "Motion Sickness in Public Road Transport: Passenger Behaviour and Susceptibility." *Ergonomics* **42**(3): 444-461.
- Turner, M., Griffin, M. J. and Holland, I. (2000). "Airsickness and Aircraft Motion During Short-Haul Flights." *Aviation Space and Environmental Medicine* **71**(12): 1181-1189.
- Tyler, D. B. and Bard, P. (1949). "Motion Sickness." *Physiol Rev* **29**(4): 311-69.
- Ujike, H., Yokoi, T. and Saida, S. (2004). Effects of Virtual Body Motion on Visually-Induced Motion Sickness. Piscataway, NJ 08855-1331, United States, Institute of Electrical and Electronics Engineers Inc.
- Urdan, T. (2005). *Statistics in Plain English*, 2nd Ed. London, UK, Lawrence Erlbaum Associates, Inc.
- Van Egmond, A. A., Groen, J. J. and Jongkees, L. B. (1949). "The Mechanics of the Semicircular Canal." *J Physiol* **110**(1-2): 1-17.
- Varjú, D. (1990). "A Note on the Reafference Principle." *Biological Cybernetics* **63**(4): 315-323.

- Verveniotis, C. S. (2004). Prediction of Motion Sickness on High-Speed Passenger Vessels : A Human-Oriented Approach. Naval Architecture & Marine Engineering. Glasgow, United Kingdom, University of Strathclyde. **PhD**.
- Verveniotis, C. S. and Turan, O. (2002a). Motion Sickness Prediction Model: A Human Oriented Approach. I.M.A.M. Crete, Hellas.
- Verveniotis, C. S. and Turan, O. (2002b). Prediction of Motion Sickness in High Speed Craft. RINA High Speed Craft Conference London, UK.
- Villard, S. J., Flanagan, M. B., Albanese, G. M. and Stoffregen, T. A. (2008). "Postural Instability and Motion Sickness in a Virtual Moving Room." *Human Factors* **50**(2): 332-345.
- von Holst, E. (1954). "Relations between the Central Nervous System and the Peripheral Organs." *Brit J. Anim. Behav* **2**: 89-94.
- von Holst, E. and Mittelstaedt, H. (1950). "The Reafference Principle. Interaction between the Central Nervous System and the Periphery." *The behavioral physiology of animals and man: selected papers of E. von Holst*.
- Walter, E., Pronzato, L. and Norton, J. (1997). Identification of Parametric Models from Experimental Data. London, UK, Springer Verlag.
- Warwick-Evans, L. and Beaumont, S. (1995). "An Experimental Evaluation of Sensory Conflict Versus Postural Control Theories of Motion Sickness." *Ecological Psychology* **7**(3): 163 - 179.
- Warwick-Evans, L. A., Symons, N., Fitch, T. and Burrows, L. (1998). "Evaluating Sensory Conflict and Postural Instability. Theories of Motion Sickness." *Brain Research Bulletin* **47**(5): 465-469.
- Watson, W. S. (2006). Improved Vibratory Gyro Pick-Off and Driver Geometry. Symposium Gyro Technology, Stuttgart, Germany.
- Welch, P. D. (1967). "The Use of Fast Fourier Transform for the Estimation of Power Spectra: A Method Based on Time Averaging over Short, Modified Periodograms." *IEEE Transactions on Audio and Electroacoustics* **15**(2): 70-73.
- Wertheim, A., De Groene, G. and Ooms, J. (1995). Seasickness and Performance Measures Aboard the Hr. Ms. Tydeman. Report TNO-TM 1995-A48, TNO Human Factors Research Institute. Soesterberg, The Netherlands.
- Wertheim, A., Ooms, J., De Regt, G. and Wientjes, C. (1992). Incidence and Severeness of Sea Sickness: Validation of a Rating Scale. Report IZF-1992-A-41, TNO Human Factors Research Institute. Soesterberg, Netherlands.
- Wertheim, A. H. (1998). "Working in a Moving Environment." *Ergonomics* **41**(12): 1845-1858.
- Wertheim, A. H., Bos, J. E. and Bles, W. (1998). "Contributions of Roll and Pitch to Sea Sickness." *Brain Research Bulletin* **47**(5): 517-524.
- Wertheim, A. H., Bos, J. E. and Krul, A. J. (2001). Predicting Motion Induced Vomiting from Subjective Misery (Misc) Ratings Obtained in 12 Experimental Studies. Report TNO-TM-01-A066, TNO Human Factors Research Institute. Soesterberg, The Netherlands.
- Wiker, S., Kennedy, R., McCauley, M. and Pepper, R. (1979). Reliability, Validity and Application of an Improved Scale for Assessment of Motion Sickness Severity. Coast Guard Office of Research Development. Washington DC, USA.

- Wizemann, T. and Pardue, M. (2001). Exploring the Biological Contributions to Human Health: Does Sex Matter?, National Academies Press.
- Wolpert, D. M. and Ghahramani, Z. (2000). "Computational Principles of Movement Neuroscience." *Nature Neuroscience* **3**(Supplement): 1212-1217.
- Wolpert, D. M. and Kawato, M. (1998). "Multiple Paired Forward and Inverse Models for Motor Control." *Neural Networks* **11**(7-8): 1317-1329.
- Wong, A. (2008). Eye Movement Disorders, Oxford University Press, USA.
- Wood, S. J. (2002). "Human Otolith-Ocular Reflexes During Off-Vertical Axis Rotation: Effect of Frequency on Tilt-Translation Ambiguity and Motion Sickness." *Neuroscience Letters* **323**(1): 41-44.
- Wyllie, I. H. and Griffin, M. J. (2007). "Discomfort from Sinusoidal Oscillation in the Roll and Lateral Axes at Frequencies between 0.2 and 1.6 Hz." *Journal of the Acoustical Society of America* **121**(5): 2644-2654.
- Yakusheva, T. A., Shaikh, A. G., Green, A. M., Blazquez, P. M., Dickman, J. D. and Angelaki, Dora E. (2007). "Purkinje Cells in Posterior Cerebellar Vermis Encode Motion in an Inertial Reference Frame." *Neuron* **54**(6): 973-985.
- Young, L. (1970). On Visual-Vestibular Interaction. Proceedings of the 5th Symposium on Role of the Vestibular Organs in Space Exploration. NASA SP 314, Washington: 205-210.
- Young, L. (1973). On Visual-Vestibular Interaction. Proceedings of the 5th Symposium on Role of the Vestibular Organs in Space Exploration, NASA SP 314, Washington.
- Young, L., Meiry, J. and Li, Y. (1966). Control Engineering Approaches to Human Dynamic Space Orientation.
- Young, L. R. (1969). "The Current Status of Vestibular System Models." *Automatica* **5**(3): 369-383.
- Young, L. R. (1984). Perception of the Body in Space. (Ed.), Handbook of Physiology, Section 1: The Nervous System. **3: Sensory Processes:** 1023-1066.
- Young, L. R. and Oman, C. M. (1969). "Model for Vestibular Adaptation to Horizontal Rotation." *Aerosp Med* **40**(10): 1076-80.
- Zuo, L. and Nayfeh, S. A. (2003). "Low Order Continuous-Time Filters for Approximation of the Iso 2631-1 Human Vibration Sensitivity Weightings." *Journal of Sound and Vibration* **265**(2): 459-465.
- Zupan, L. (1995). Modelisation Du Reflexe Vestibulo-Oculaire Et Prediction Des Cinetoses. Ecole Nationale Superieure des Telecommunications. Paris, France. **PhD**.
- Zupan, L., Droulez, J., Darlot, C., Denise, P. and Maruani, A. (1994). Modelization of Vestibulo-Ocular Reflex (Vor) and Motion Sickness Prediction. In M. M and M. P. G(Eds.), Proceedings of the International Congress on Application of Neural Networks, Sorrento, Italy, Springer-Verlag.
- Zupan, L. H., Park, S. and Merfeld, D. M. (2004). The Nervous System Uses Internal Models to Achieve Sensory Integration. Annual International Conference of the IEEE Engineering in Medicine and Biology - Proceedings, San Francisco, CA, United States, Institute of Electrical and Electronics Engineers Inc., Piscataway, NJ 08855-1331, United States.

University of Strathclyde
Department of Naval Architecture & Marine
Engineering



Development of Physiological Motion Sickness Model
for the Contemporary Marine Vessels

Appendices

by

Hassan Khalid

A thesis presented in fulfilment of the requirements for the degree of
Doctor of Philosophy

2010

Appendix A. Data Pertaining to Calibration of SVH-Conflict Model

A.1 Raw and Filtered Motion Histories of WP-G

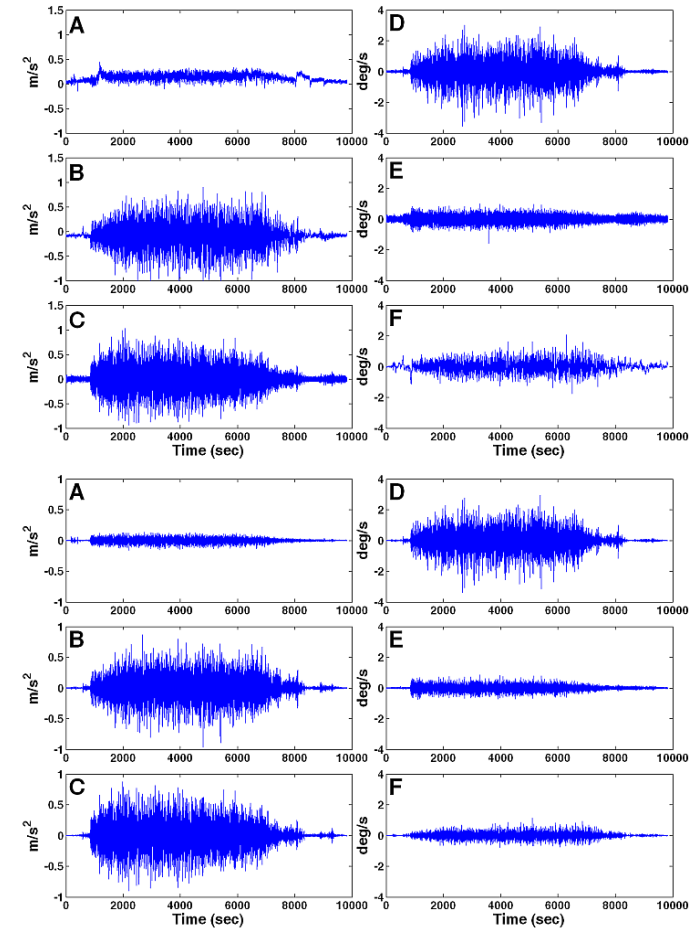


Figure A.1.1. Motion history (upper-row; lower-filtered) of WP-G at MRU position during Trip-2; linear accelerations (A) longitudinal (B) lateral (C) vertical; angular velocities (D) roll (E) pitch (F) yaw.

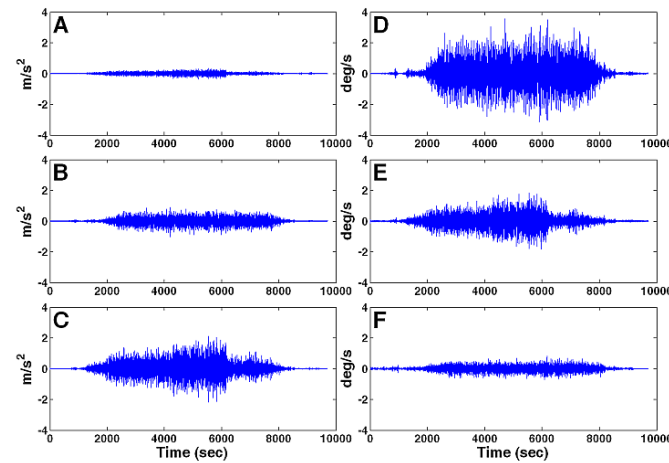
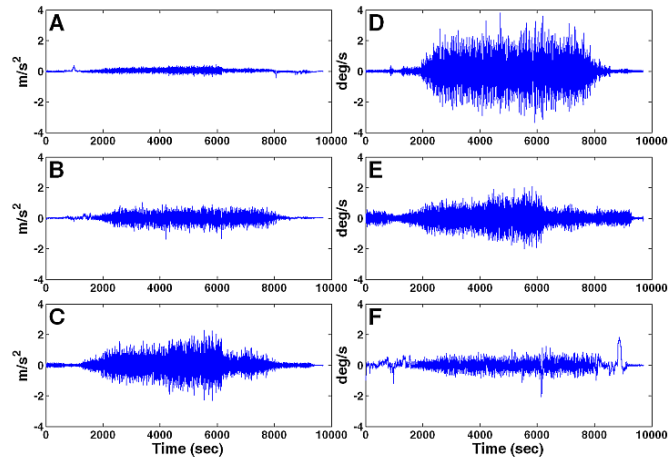


Figure A.1.2. Motion history (upper-row; lower-filtered) of WP-G at MRU position during Trip-3; linear accelerations (A) longitudinal (B) lateral (C) vertical; angular velocities (D) roll (E) pitch (F) yaw.

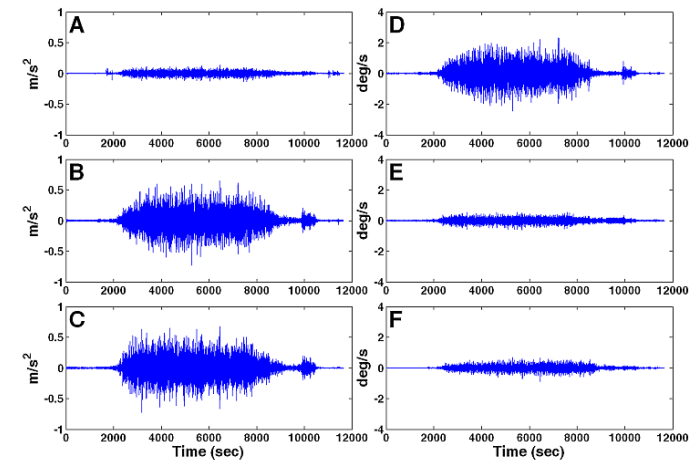
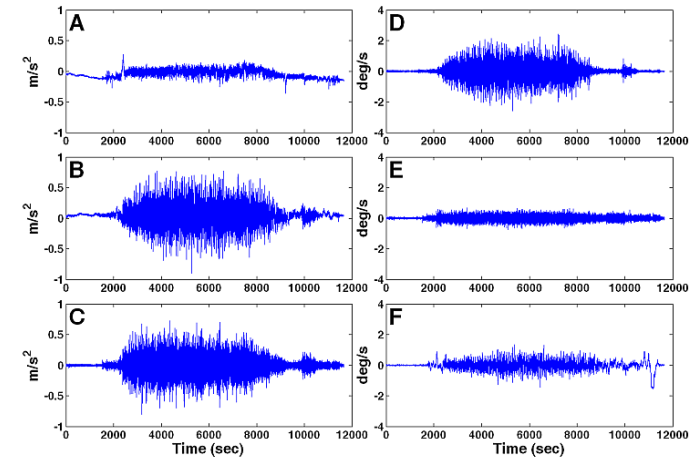


Figure A.1.3. Motion history (upper-row; lower-filtered) of WP-G at MRU position during Trip-4; linear accelerations (A) longitudinal (B) lateral (C) vertical; angular velocities (D) roll (E) pitch (F) yaw.

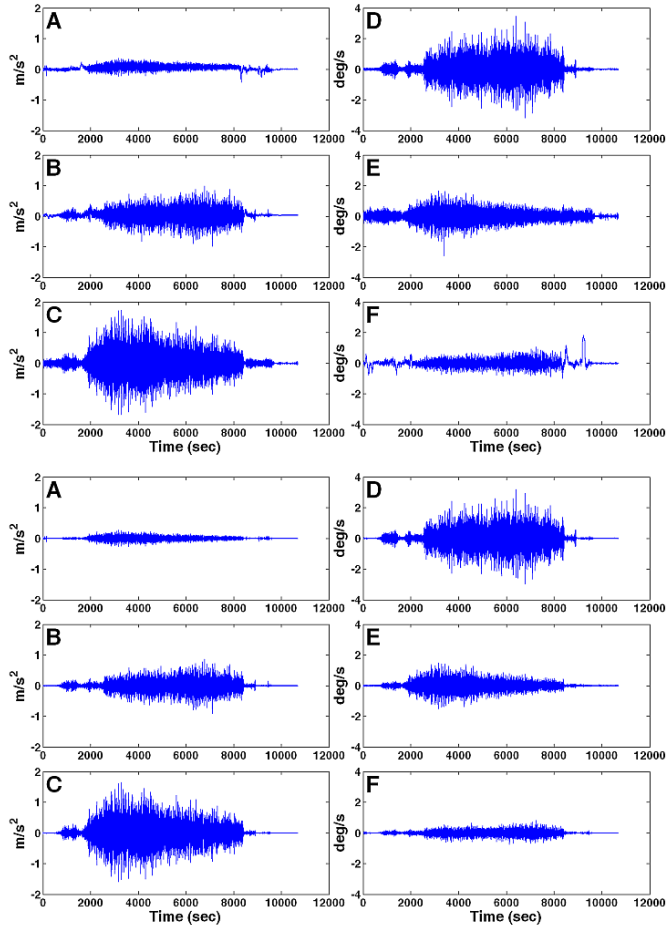


Figure A.1.4. Motion history (upper-row; lower-filtered) of WP-G at MRU position during Trip-5; linear accelerations (A) longitudinal (B) lateral (C) vertical; angular velocities (D) roll (E) pitch (F) yaw.

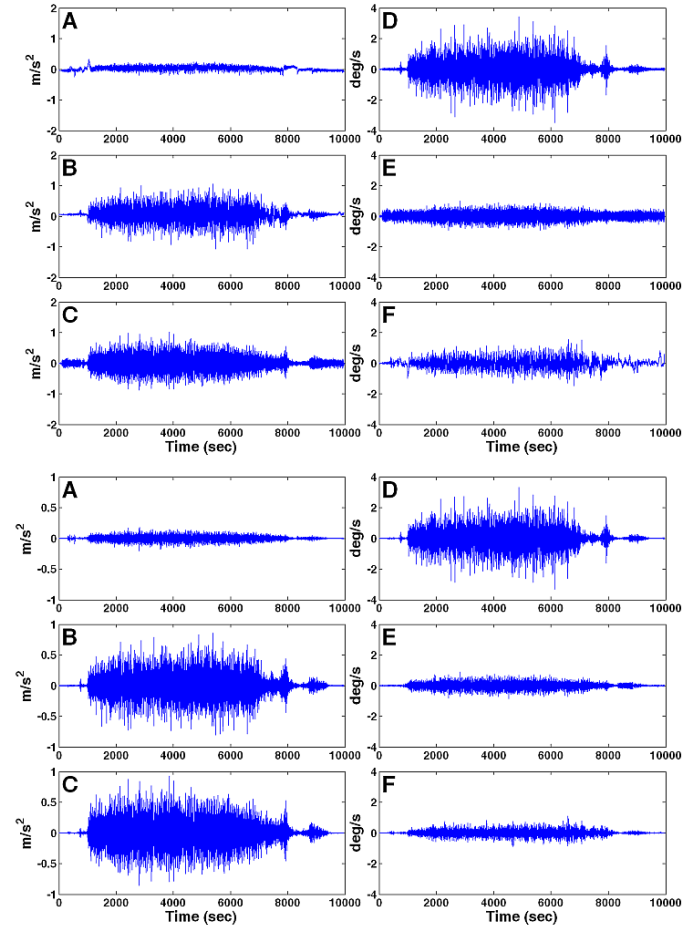


Figure A.1.5. Motion history (upper-row; lower-filtered) of WP-G at MRU position during Trip-6; linear accelerations (A) longitudinal (B) lateral (C) vertical; angular velocities (D) roll (E) pitch (F) yaw.

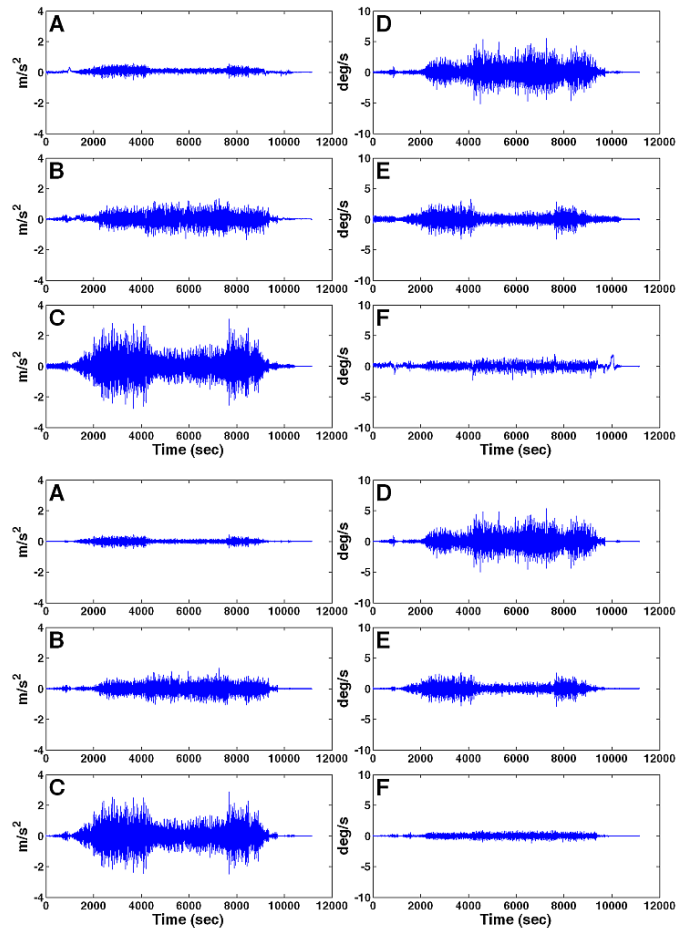


Figure A.1.6. Motion history (upper-row; lower-filtered) of WP-G at MRU position during Trip-7; linear accelerations (A) longitudinal (B) lateral (C) vertical; angular velocities (D) roll (E) pitch (F) yaw.

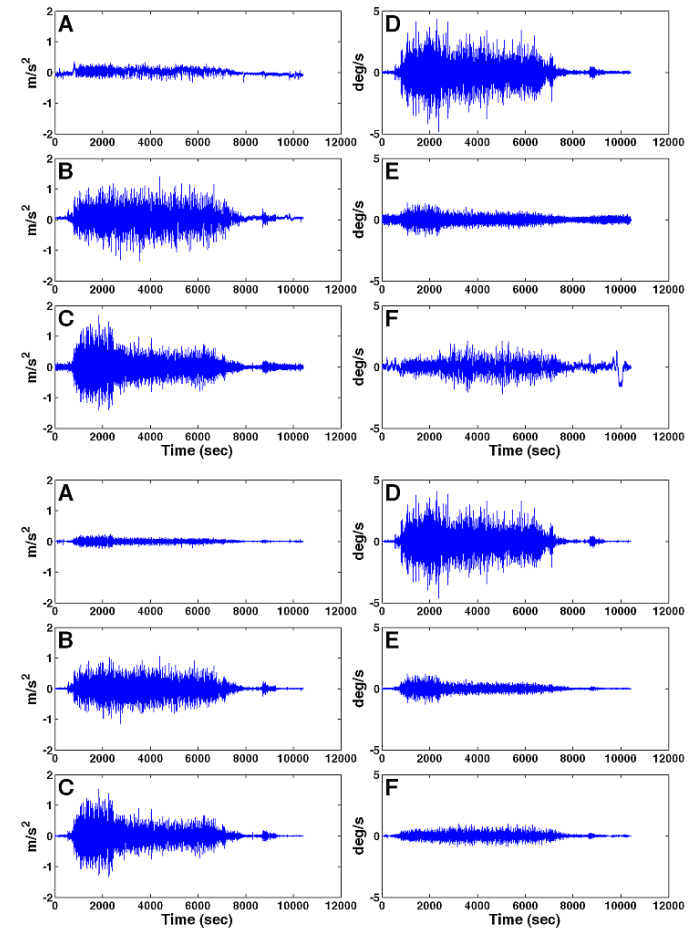


Figure A.1.7. Motion history (upper-row; lower-filtered) of WP-G at MRU position during Trip-8; linear accelerations (A) longitudinal (B) lateral (C) vertical; angular velocities (D) roll (E) pitch (F) yaw.

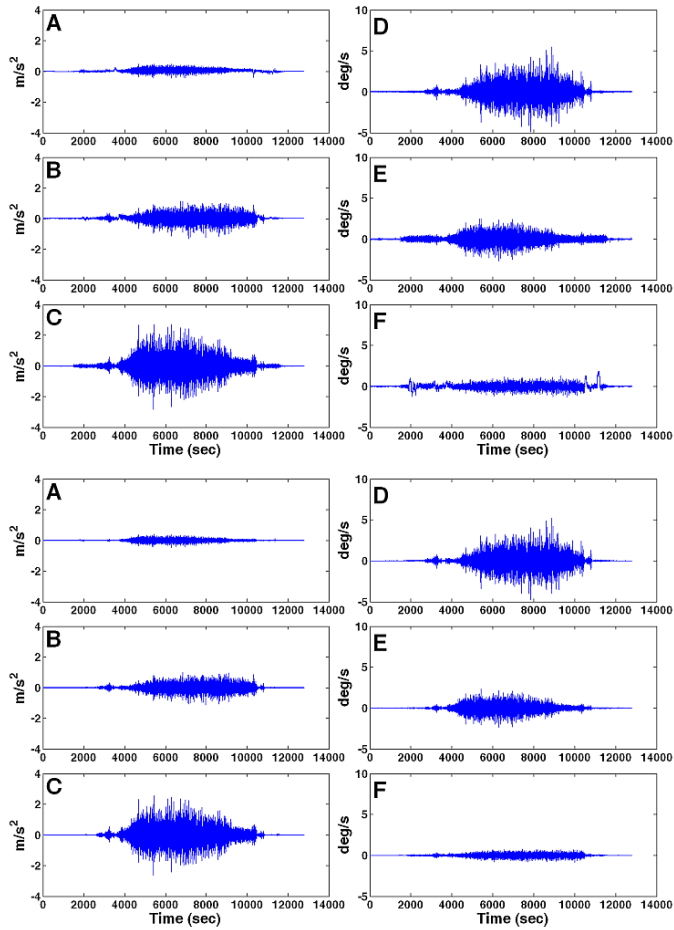


Figure A.1.8. Motion history (upper-row; lower-filtered) of WP-G at MRU position during Trip-9; linear accelerations (A) longitudinal (B) lateral (C) vertical; angular velocities (D) roll (E) pitch (F) yaw.

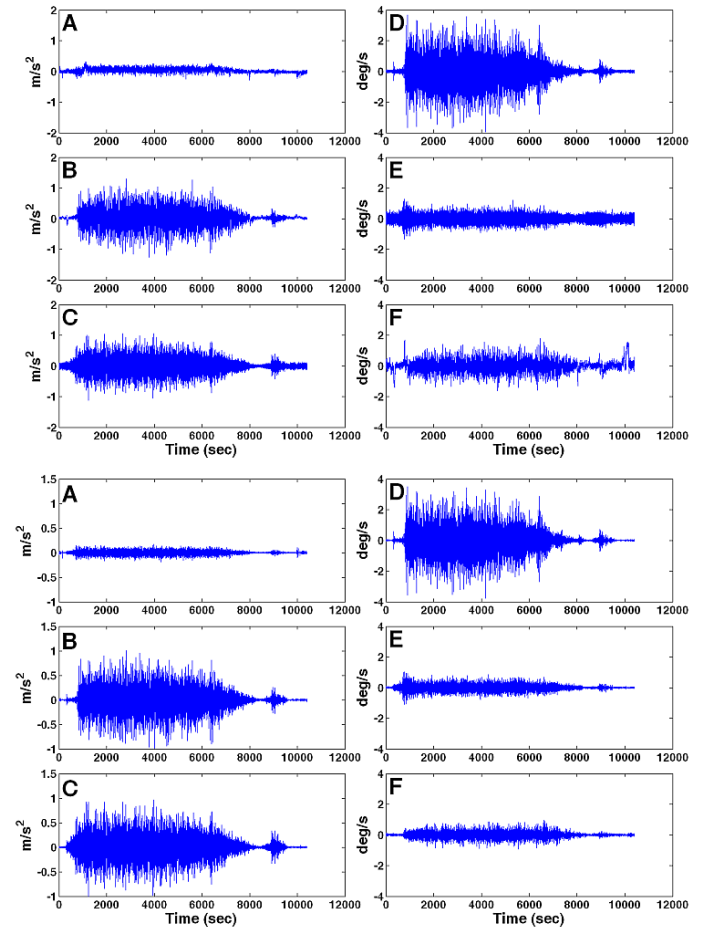


Figure A.1.9. Motion history (upper-row; lower-filtered) of WP-G at MRU position during Trip-10; linear accelerations (A) longitudinal (B) lateral (C) vertical; angular velocities (D) roll (E) pitch (F) yaw.

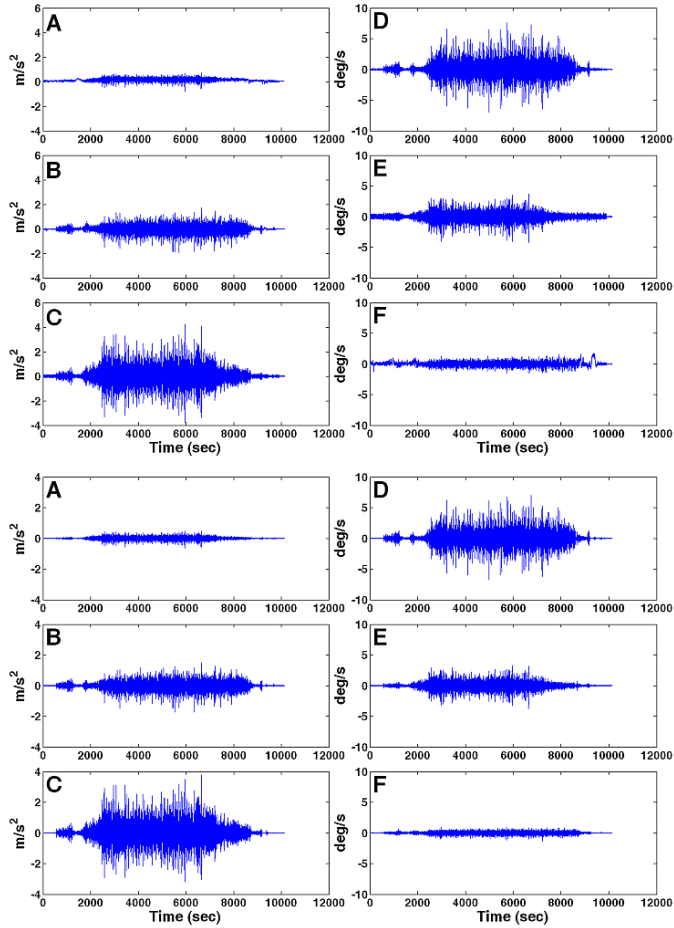


Figure A.1.10. Motion history (upper-row; lower-filtered) of WP-G at MRU position during Trip-11; linear accelerations (A) longitudinal (B) lateral (C) vertical; angular velocities (D) roll (E) pitch (F) yaw.

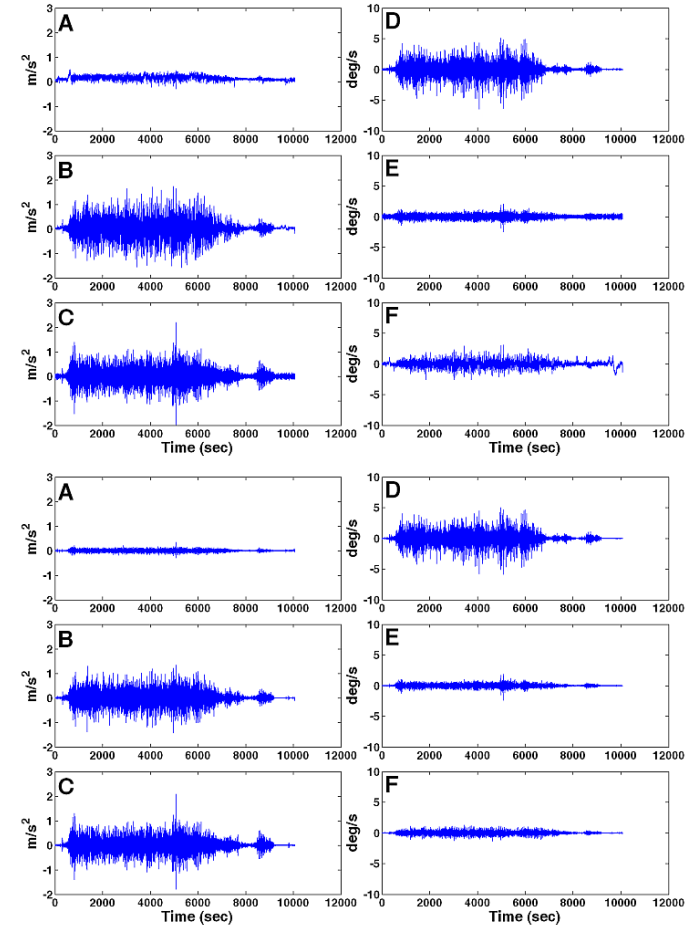


Figure A.1.11. Motion history (upper-row; lower-filtered) of WP-G at MRU position during Trip-12; linear accelerations (A) longitudinal (B) lateral (C) vertical; angular velocities (D) roll (E) pitch (F) yaw.

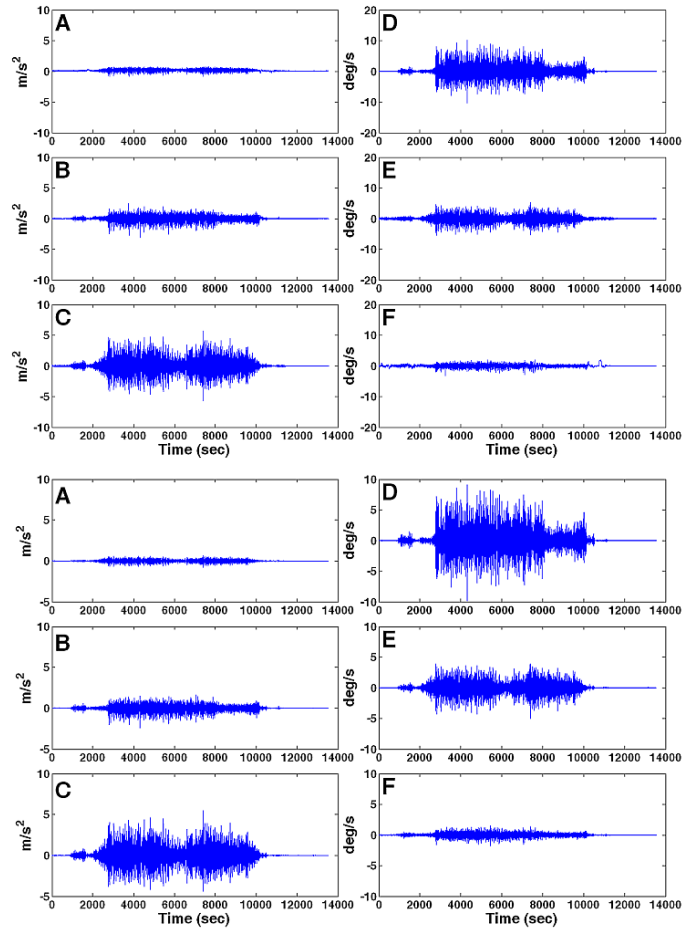


Figure A.1.12. Motion history (upper-row; lower-filtered) of WP-G at MRU position during Trip-13; linear accelerations (A) longitudinal (B) lateral (C) vertical; angular velocities (D) roll (E) pitch (F) yaw.

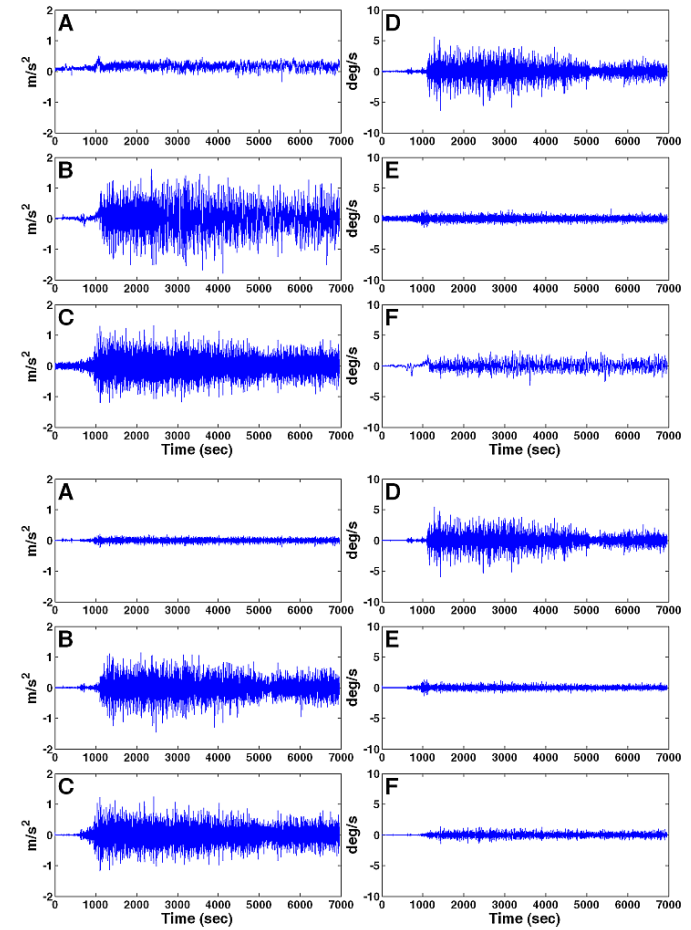


Figure A.1.13. Motion history (upper-row; lower-filtered) of WP-G at MRU position during Trip-14; linear accelerations (A) longitudinal (B) lateral (C) vertical; angular velocities (D) roll (E) pitch (F) yaw.

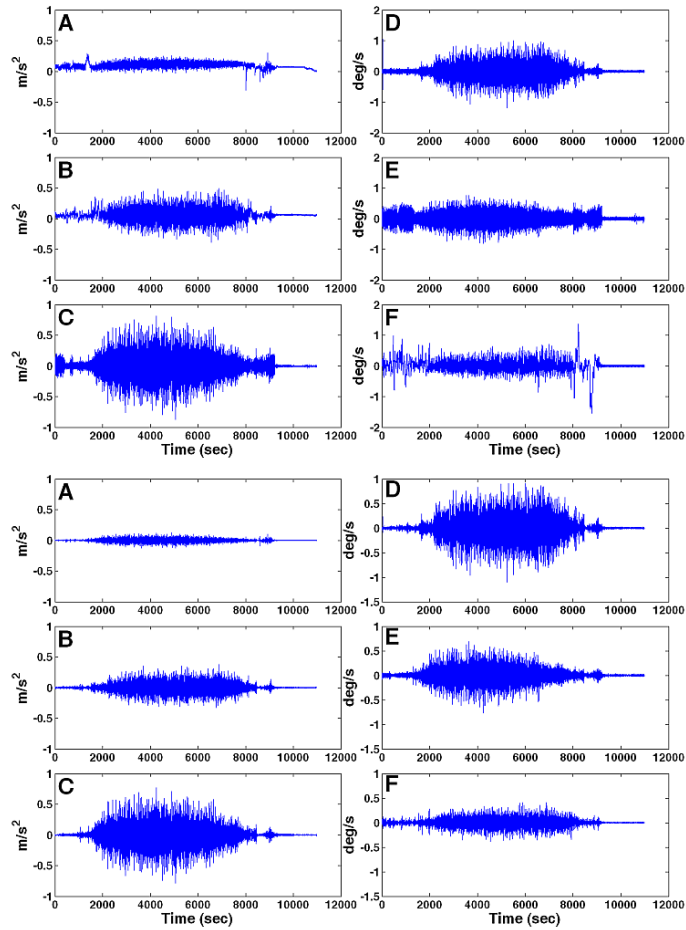


Figure A.1.14. Motion history (upper-row; lower-filtered) of WP-G at MRU position during Trip-15; linear accelerations (A) longitudinal (B) lateral (C) vertical; angular velocities (D) roll (E) pitch (F) yaw.

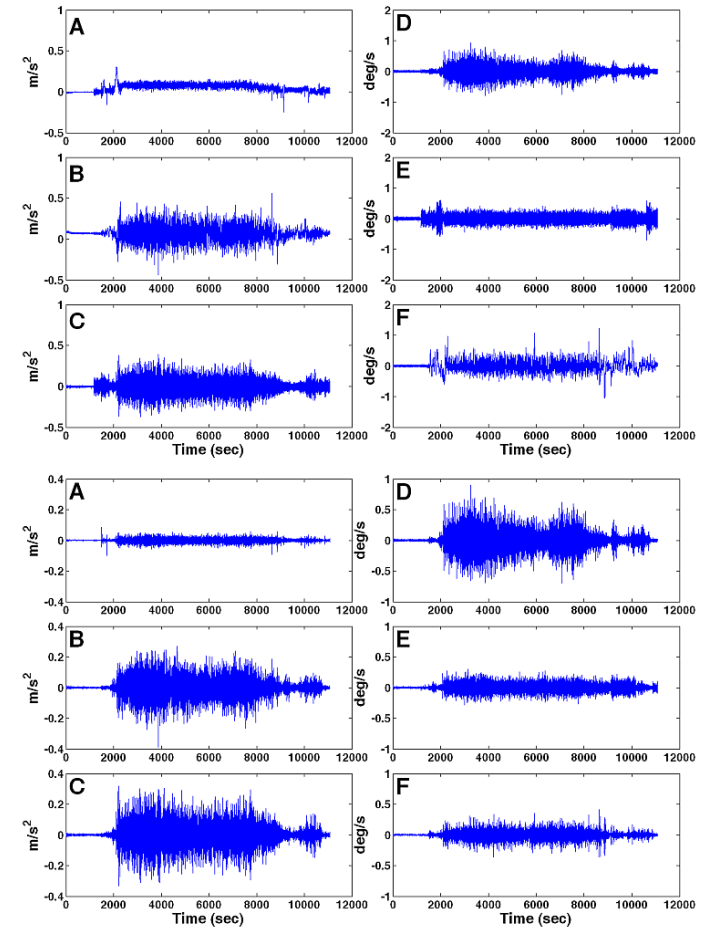


Figure A.1.15. Motion history (upper-row; lower-filtered) of WP-G at MRU position during Trip-16; linear accelerations (A) longitudinal (B) lateral (C) vertical; angular velocities (D) roll (E) pitch (F) yaw.

A.2 Trip-Wise Predicted Overall MSI for WP-G

Table A.2.1. Overall MSI (simple sum), for the various combinations of hill function shape parameters and $K_h = 1$, during the WP-G Trip-2.

b_{CH}	n_{CH}						
	0.5	1	1.5	2	2.5	3	3.5
0.5	26.56%	15.22%	9.64%	6.88%	5.44%	4.66%	4.22%
1.0	21.33%	9.95%	5.85%	4.37%	3.83%	3.61%	3.52%
1.5	18.69%	7.95%	4.78%	3.86%	3.59%	3.50%	3.47%
2.0	17.00%	6.88%	4.32%	3.69%	3.52%	3.47%	3.46%
2.5	15.80%	6.23%	4.08%	3.60%	3.49%	3.47%	3.46%
3.0	14.88%	5.78%	3.93%	3.56%	3.48%	3.46%	3.46%
3.5	14.15%	5.46%	3.83%	3.53%	3.47%	3.46%	3.46%

Table A.2.2. Overall MSI (Pythagoras-type approach), for the various combinations of hill function shape parameters and $K_h = 1$, during the WP-G Trip-2.

b_{CH}	n_{CH}						
	0.5	1	1.5	2	2.5	3	3.5
0.5	23.39%	12.29%	7.10%	4.87%	3.98%	3.65%	3.53%
1.0	18.24%	7.38%	4.20%	3.57%	3.48%	3.46%	3.46%
1.5	15.65%	5.68%	3.70%	3.48%	3.46%	3.45%	3.45%
2.0	14.00%	4.87%	3.56%	3.47%	3.46%	3.45%	3.45%
2.5	12.84%	4.43%	3.51%	3.46%	3.46%	3.46%	3.46%
3.0	11.96%	4.16%	3.49%	3.46%	3.45%	3.45%	3.46%
3.5	11.27%	3.99%	3.47%	3.46%	3.46%	3.45%	3.46%

Table A.2.3. Overall MSI (simple sum), for the various combinations of hill function shape parameters and $K_h = 1$, during the WP-G Trip-3.

b_{CH}	n_{CH}						
	0.5	1	1.5	2	2.5	3	3.5
0.5	30.43%	19.05%	12.98%	9.84%	8.17%	7.25%	6.72%

b_{CH}	n_{CH}						
	0.5	1	1.5	2	2.5	3	3.5
1.0	24.93%	13.14%	8.58%	6.89%	6.25%	5.99%	5.88%
1.5	22.12%	10.87%	7.35%	6.29%	5.96%	5.85%	5.81%
2.0	20.33%	9.68%	6.82%	6.07%	5.87%	5.82%	5.80%
2.5	19.05%	8.93%	6.53%	5.98%	5.84%	5.81%	5.80%
3.0	18.07%	8.44%	6.36%	5.92%	5.82%	5.80%	5.80%
3.5	17.29%	8.07%	6.24%	5.89%	5.82%	5.80%	5.79%

Table A.2.4. Overall MSI (Pythagoras-type approach), for the various combinations of hill function shape parameters and $K_h = 1$, during the WP-G Trip-3.

b_{CH}	n_{CH}						
	0.5	1	1.5	2	2.5	3	3.5
0.5	25.40%	14.54%	9.27%	7.08%	6.27%	5.98%	5.87%
1.0	20.07%	9.39%	6.44%	5.90%	5.81%	5.80%	5.79%
1.5	17.40%	7.72%	6.00%	5.81%	5.80%	5.79%	5.79%
2.0	15.71%	6.98%	5.89%	5.80%	5.79%	5.79%	5.79%
2.5	14.52%	6.60%	5.84%	5.80%	5.80%	5.79%	5.79%
3.0	13.63%	6.38%	5.82%	5.80%	5.79%	5.80%	5.79%
3.5	12.92%	6.23%	5.82%	5.80%	5.79%	5.79%	5.79%

Table A.2.5. Overall MSI (simple sum), for the various combinations of hill function shape parameters and $K_h = 1$, during the WP-G Trip-4.

b_{CH}	n_{CH}						
	0.5	1	1.5	2	2.5	3	3.5
0.5	23.99%	12.45%	7.20%	4.81%	3.68%	3.12%	2.83%
1.0	19.00%	7.89%	4.26%	3.08%	2.69%	2.55%	2.49%
1.5	16.52%	6.20%	3.46%	2.74%	2.54%	2.49%	2.47%
2.0	14.94%	5.31%	3.11%	2.62%	2.50%	2.47%	2.46%
2.5	13.82%	4.76%	2.93%	2.56%	2.48%	2.47%	2.46%
3.0	12.96%	4.39%	2.82%	2.53%	2.47%	2.46%	2.46%
3.5	12.28%	4.12%	2.75%	2.51%	2.47%	2.46%	2.46%

Table A.2.6. Overall MSI (Pythagoras-type approach), for the various combinations of hill function shape parameters and $K_h = 1$, during the WP-G Trip-4.

b_{CH}	n_{CH}						
	0.5	1	1.5	2	2.5	3	3.5
0.5	21.76%	10.34%	5.36%	3.41%	2.75%	2.55%	2.49%
1.0	16.80%	5.98%	3.05%	2.54%	2.47%	2.46%	2.46%
1.5	14.34%	4.48%	2.66%	2.48%	2.46%	2.46%	2.46%
2.0	12.77%	3.77%	2.55%	2.47%	2.46%	2.46%	2.46%
2.5	11.67%	3.37%	2.51%	2.46%	2.46%	2.46%	2.46%
3.0	10.82%	3.13%	2.49%	2.46%	2.46%	2.46%	2.46%
3.5	10.16%	2.97%	2.48%	2.46%	2.46%	2.46%	2.46%

Table A.2.7. Overall MSI (simple sum), for the various combinations of hill function shape parameters and $K_h = 1$, during the WP-G Trip-5.

b_{CH}	n_{CH}						
	0.5	1	1.5	2	2.5	3	3.5
0.5	27.77%	16.49%	10.85%	8.00%	6.52%	5.69%	5.20%
1.0	22.49%	11.07%	6.86%	5.32%	4.73%	4.50%	4.40%
1.5	19.81%	8.99%	5.73%	4.77%	4.47%	4.37%	4.33%
2.0	18.10%	7.89%	5.25%	4.57%	4.39%	4.34%	4.32%
2.5	16.88%	7.21%	4.98%	4.48%	4.36%	4.33%	4.32%
3.0	15.95%	6.75%	4.83%	4.43%	4.34%	4.32%	4.32%
3.5	15.21%	6.41%	4.72%	4.40%	4.33%	4.32%	4.32%

Table A.2.8. Overall MSI (Pythagoras-type approach), for the various combinations of hill function shape parameters and $K_h = 1$, during the WP-G Trip-5.

b_{CH}	n_{CH}						
	0.5	1	1.5	2	2.5	3	3.5
0.5	23.87%	12.94%	7.86%	5.70%	4.86%	4.54%	4.41%
1.0	18.70%	8.04%	5.02%	4.43%	4.34%	4.32%	4.31%
1.5	16.11%	6.38%	4.55%	4.34%	4.32%	4.32%	4.31%
2.0	14.47%	5.62%	4.42%	4.32%	4.31%	4.32%	4.32%

b_{CH}	n_{CH}						
	0.5	1	1.5	2	2.5	3	3.5
2.5	13.31%	5.21%	4.37%	4.32%	4.32%	4.31%	4.31%
3.0	12.44%	4.96%	4.35%	4.32%	4.32%	4.32%	4.32%
3.5	11.74%	4.80%	4.34%	4.32%	4.31%	4.32%	4.32%

Table A.2.9. Overall MSI (simple sum), for the various combinations of hill function shape parameters and $K_h = 1$, during the WP-G Trip-6.

b_{CH}	n_{CH}						
	0.5	1	1.5	2	2.5	3	3.5
0.5	26.98%	15.72%	10.04%	7.16%	5.62%	4.77%	4.28%
1.0	21.66%	10.22%	5.96%	4.39%	3.80%	3.57%	3.47%
1.5	18.98%	8.10%	4.81%	3.84%	3.54%	3.45%	3.41%
2.0	17.25%	6.99%	4.31%	3.64%	3.47%	3.42%	3.40%
2.5	16.03%	6.29%	4.05%	3.55%	3.43%	3.41%	3.39%
3.0	15.09%	5.82%	3.90%	3.51%	3.42%	3.40%	3.39%
3.5	14.34%	5.48%	3.80%	3.48%	3.41%	3.40%	3.39%

Table A.2.10. Overall MSI (Pythagoras-type approach), for the various combinations of hill function shape parameters and $K_h = 1$, during the WP-G Trip-6.

b_{CH}	n_{CH}						
	0.5	1	1.5	2	2.5	3	3.5
0.5	23.90%	12.86%	7.51%	5.08%	4.05%	3.65%	3.50%
1.0	18.65%	7.66%	4.25%	3.53%	3.42%	3.40%	3.39%
1.5	16.01%	5.83%	3.67%	3.42%	3.39%	3.39%	3.39%
2.0	14.33%	4.95%	3.52%	3.40%	3.39%	3.39%	3.39%
2.5	13.14%	4.46%	3.46%	3.39%	3.39%	3.39%	3.39%
3.0	12.24%	4.17%	3.43%	3.40%	3.39%	3.39%	3.39%
3.5	11.52%	3.98%	3.42%	3.39%	3.39%	3.39%	3.39%

Table A.2.11. Overall MSI (simple sum), for the various combinations of hill function shape parameters and $K_h = 1$, during the WP-G Trip-7.

b_{CH}	n_{CH}						
	0.5	1	1.5	2	2.5	3	3.5
0.5	36.51%	26.18%	20.14%	16.60%	14.47%	13.11%	12.21%
1.0	30.70%	19.06%	13.86%	11.57%	10.52%	10.02%	9.76%
1.5	27.72%	16.20%	11.97%	10.43%	9.85%	9.64%	9.55%
2.0	25.77%	14.67%	11.13%	10.02%	9.66%	9.54%	9.50%
2.5	24.39%	13.70%	10.67%	9.82%	9.59%	9.51%	9.49%
3.0	23.32%	13.04%	10.39%	9.71%	9.54%	9.49%	9.48%
3.5	22.46%	12.56%	10.20%	9.66%	9.52%	9.48%	9.47%

Table A.2.12. Overall MSI (Pythagoras-type approach), for the various combinations of hill function shape parameters and $K_h = 1$, during the WP-G Trip-7.

b_{CH}	n_{CH}						
	0.5	1	1.5	2	2.5	3	3.5
0.5	28.67%	19.24%	14.30%	11.89%	10.73%	10.16%	9.87%
1.0	23.28%	13.51%	10.45%	9.71%	9.53%	9.49%	9.47%
1.5	20.59%	11.64%	9.80%	9.52%	9.47%	9.47%	9.48%
2.0	18.88%	10.82%	9.62%	9.49%	9.47%	9.47%	9.47%
2.5	17.70%	10.38%	9.55%	9.48%	9.48%	9.47%	9.47%
3.0	16.81%	10.13%	9.52%	9.47%	9.47%	9.47%	9.47%
3.5	16.10%	9.97%	9.50%	9.48%	9.47%	9.47%	9.47%

Table A.2.13. Overall MSI (simple sum), for the various combinations of hill function shape parameters and $K_h = 1$, during the WP-G Trip-8.

b_{CH}	n_{CH}						
	0.5	1	1.5	2	2.5	3	3.5
0.5	30.93%	20.23%	14.31%	11.02%	9.13%	7.99%	7.27%
1.0	25.34%	13.79%	8.99%	7.01%	6.16%	5.78%	5.60%
1.5	22.48%	11.26%	7.42%	6.14%	5.69%	5.53%	5.46%
2.0	20.64%	9.90%	6.74%	5.82%	5.55%	5.46%	5.43%

b_{CH}	n_{CH}						
	0.5	1	1.5	2	2.5	3	3.5
2.5	19.32%	9.06%	6.37%	5.68%	5.49%	5.44%	5.42%
3.0	18.31%	8.48%	6.14%	5.60%	5.46%	5.42%	5.42%
3.5	17.50%	8.06%	5.99%	5.55%	5.45%	5.42%	5.41%

Table A.2.14. Overall MSI (Pythagoras-type approach), for the various combinations of hill function shape parameters and $K_h = 1$, during the WP-G Trip-8.

b_{CH}	n_{CH}						
	0.5	1	1.5	2	2.5	3	3.5
0.5	26.14%	15.83%	10.45%	7.81%	6.57%	6.00%	5.72%
1.0	20.71%	10.00%	6.49%	5.64%	5.46%	5.42%	5.41%
1.5	17.95%	7.98%	5.77%	5.46%	5.42%	5.42%	5.41%
2.0	16.20%	7.03%	5.57%	5.43%	5.41%	5.41%	5.41%
2.5	14.96%	6.53%	5.49%	5.42%	5.41%	5.41%	5.41%
3.0	14.02%	6.22%	5.46%	5.42%	5.41%	5.41%	5.41%
3.5	13.27%	6.02%	5.44%	5.41%	5.41%	5.41%	5.41%

Table A.2.15. Overall MSI (simple sum), for the various combinations of hill function shape parameters and $K_h = 1$, during the WP-G Trip-9.

b_{CH}	n_{CH}						
	0.5	1	1.5	2	2.5	3	3.5
0.5	33.20%	22.39%	16.33%	12.96%	11.03%	9.88%	9.15%
1.0	27.55%	15.85%	10.95%	8.93%	8.06%	7.68%	7.50%
1.5	24.66%	13.28%	9.37%	8.05%	7.59%	7.42%	7.35%
2.0	22.80%	11.89%	8.67%	7.73%	7.44%	7.35%	7.32%
2.5	21.44%	11.04%	8.29%	7.58%	7.39%	7.34%	7.31%
3.0	20.43%	10.45%	8.06%	7.50%	7.36%	7.32%	7.31%
3.5	19.60%	10.02%	7.90%	7.45%	7.34%	7.32%	7.31%

Table A.2.16. Overall MSI (Pythagoras-type approach), for the various combinations of hill function shape parameters and $K_h = 1$, during the WP-G Trip-9.

b_{CH}	n_{CH}						
	0.5	1	1.5	2	2.5	3	3.5
0.5	26.96%	16.78%	11.63%	9.27%	8.22%	7.76%	7.55%
1.0	21.55%	11.26%	8.18%	7.49%	7.35%	7.32%	7.31%
1.5	18.84%	9.46%	7.60%	7.34%	7.31%	7.31%	7.31%
2.0	17.14%	8.64%	7.43%	7.32%	7.30%	7.31%	7.31%
2.5	15.93%	8.21%	7.38%	7.31%	7.31%	7.31%	7.31%
3.0	15.04%	7.96%	7.35%	7.31%	7.31%	7.31%	7.31%
3.5	14.32%	7.80%	7.33%	7.31%	7.31%	7.31%	7.31%

Table A.2.17. Overall MSI (simple sum), for the various combinations of hill function shape parameters and $K_h = 1$, during the WP-G Trip-10.

b_{CH}	n_{CH}						
	0.5	1	1.5	2	2.5	3	3.5
0.5	30.33%	19.54%	13.69%	10.47%	8.62%	7.51%	6.82%
1.0	24.80%	13.25%	8.53%	6.60%	5.77%	5.40%	5.23%
1.5	21.96%	10.78%	7.01%	5.75%	5.32%	5.15%	5.09%
2.0	20.12%	9.46%	6.34%	5.45%	5.18%	5.09%	5.06%
2.5	18.82%	8.63%	5.99%	5.30%	5.12%	5.06%	5.05%
3.0	17.82%	8.06%	5.76%	5.23%	5.10%	5.06%	5.05%
3.5	17.02%	7.65%	5.62%	5.18%	5.08%	5.05%	5.05%

Table A.2.18. Overall MSI (Pythagoras-type approach), for the various combinations of hill function shape parameters and $K_h = 1$, during the WP-G Trip-10.

b_{CH}	n_{CH}						
	0.5	1	1.5	2	2.5	3	3.5
0.5	25.79%	15.35%	10.01%	7.42%	6.19%	5.62%	5.35%
1.0	20.39%	9.64%	6.14%	5.28%	5.10%	5.06%	5.05%
1.5	17.65%	7.64%	5.42%	5.10%	5.05%	5.04%	5.05%
2.0	15.90%	6.71%	5.21%	5.06%	5.05%	5.05%	5.04%

b_{CH}	n_{CH}						
	0.5	1	1.5	2	2.5	3	3.5
2.5	14.67%	6.19%	5.14%	5.05%	5.05%	5.04%	5.05%
3.0	13.74%	5.88%	5.10%	5.05%	5.05%	5.05%	5.04%
3.5	13.00%	5.68%	5.08%	5.05%	5.04%	5.04%	5.04%

Table A.2.19. Overall MSI (simple sum), for the various combinations of hill function shape parameters and $K_h = 1$, during the WP-G Trip-11.

b_{CH}	n_{CH}						
	0.5	1	1.5	2	2.5	3	3.5
0.5	38.50%	28.38%	22.25%	18.60%	16.36%	14.94%	14.00%
1.0	32.57%	20.85%	15.42%	12.95%	11.80%	11.23%	10.93%
1.5	29.47%	17.80%	13.32%	11.65%	11.00%	10.73%	10.62%
2.0	27.48%	16.14%	12.37%	11.16%	10.76%	10.60%	10.56%
2.5	26.05%	15.10%	11.86%	10.93%	10.65%	10.56%	10.54%
3.0	24.93%	14.38%	11.55%	10.81%	10.61%	10.55%	10.53%
3.5	24.05%	13.86%	11.34%	10.73%	10.58%	10.54%	10.53%

Table A.2.20. Overall MSI (Pythagoras-type approach), for the various combinations of hill function shape parameters and $K_h = 1$, during the WP-G Trip-11.

b_{CH}	n_{CH}						
	0.5	1	1.5	2	2.5	3	3.5
0.5	29.92%	20.77%	15.80%	13.30%	12.07%	11.44%	11.10%
1.0	24.45%	14.77%	11.61%	10.80%	10.60%	10.55%	10.52%
1.5	21.70%	12.81%	10.89%	10.58%	10.53%	10.52%	10.52%
2.0	19.99%	11.94%	10.68%	10.54%	10.52%	10.51%	10.52%
2.5	18.78%	11.48%	10.60%	10.53%	10.52%	10.52%	10.52%
3.0	17.87%	11.21%	10.57%	10.52%	10.52%	10.52%	10.52%
3.5	17.17%	11.04%	10.55%	10.52%	10.52%	10.52%	10.52%

Table A.2.21. Overall MSI (simple sum), for the various combinations of hill function shape parameters and $K_h = 1$, during the WP-G Trip-12.

b_{CH}	n_{CH}						
	0.5	1	1.5	2	2.5	3	3.5
0.5	34.24%	24.12%	18.26%	14.83%	12.73%	11.39%	10.51%
1.0	28.43%	16.93%	11.81%	9.57%	8.53%	8.02%	7.76%
1.5	25.44%	14.06%	9.92%	8.41%	7.84%	7.60%	7.50%
2.0	23.51%	12.54%	9.08%	7.99%	7.63%	7.50%	7.45%
2.5	22.12%	11.58%	8.62%	7.78%	7.54%	7.46%	7.44%
3.0	21.06%	10.94%	8.34%	7.67%	7.50%	7.45%	7.43%
3.5	20.21%	10.46%	8.15%	7.61%	7.47%	7.44%	7.42%

Table A.2. 22. Overall MSI (Pythagoras-type approach), for the various combinations of hill function shape parameters and $K_h = 1$, during the WP-G Trip-12.

b_{CH}	n_{CH}						
	0.5	1	1.5	2	2.5	3	3.5
0.5	28.12%	18.50%	13.26%	10.51%	9.09%	8.38%	8.01%
1.0	22.54%	12.14%	8.62%	7.72%	7.51%	7.44%	7.43%
1.5	19.71%	9.97%	7.83%	7.48%	7.43%	7.42%	7.42%
2.0	17.91%	9.02%	7.60%	7.44%	7.43%	7.42%	7.42%
2.5	16.63%	8.51%	7.52%	7.43%	7.42%	7.42%	7.42%
3.0	15.66%	8.21%	7.48%	7.42%	7.43%	7.42%	7.42%
3.5	14.90%	8.02%	7.45%	7.42%	7.42%	7.42%	7.42%

Table A.2.23. Overall MSI (simple sum), for the various combinations of hill function shape parameters and $K_h = 1$, during the WP-G Trip-13.

b_{CH}	n_{CH}						
	0.5	1	1.5	2	2.5	3	3.5
0.5	50.77%	42.15%	36.51%	32.89%	30.50%	28.88%	27.75%
1.0	44.51%	33.28%	27.38%	24.33%	22.69%	21.75%	21.22%
1.5	41.23%	29.51%	24.36%	22.12%	21.12%	20.63%	20.39%
2.0	39.06%	27.43%	22.96%	21.27%	20.61%	20.33%	20.22%

b_{CH}	n_{CH}						
	0.5	1	1.5	2	2.5	3	3.5
2.5	37.50%	26.12%	22.18%	20.87%	20.39%	20.22%	20.15%
3.0	36.29%	25.20%	21.71%	20.63%	20.29%	20.18%	20.13%
3.5	35.32%	24.52%	21.38%	20.50%	20.23%	20.15%	20.13%

Table A.2.24. Overall MSI (Pythagoras-type approach), for the various combinations of hill function shape parameters and $K_h = 1$, during the WP-G Trip-13.

b_{CH}	n_{CH}						
	0.5	1	1.5	2	2.5	3	3.5
0.5	36.74%	29.89%	25.99%	23.85%	22.66%	21.96%	21.53%
1.0	31.67%	24.05%	21.39%	20.55%	20.28%	20.17%	20.15%
1.5	29.20%	22.20%	20.56%	20.22%	20.14%	20.12%	20.11%
2.0	27.67%	21.40%	20.31%	20.14%	20.12%	20.11%	20.11%
2.5	26.61%	21.00%	20.21%	20.13%	20.11%	20.11%	20.10%
3.0	25.84%	20.75%	20.18%	20.11%	20.11%	20.11%	20.10%
3.5	25.23%	20.59%	20.15%	20.11%	20.11%	20.11%	20.12%

Table A.2.25. Overall MSI (simple sum), for the various combinations of hill function shape parameters and $K_h = 1$, during the WP-G Trip-14.

b_{CH}	n_{CH}						
	0.5	1	1.5	2	2.5	3	3.5
0.5	35.04%	25.31%	19.59%	16.16%	13.98%	12.54%	11.55%
1.0	29.19%	17.84%	12.57%	10.09%	8.87%	8.24%	7.91%
1.5	26.16%	14.79%	10.37%	8.67%	7.98%	7.68%	7.56%
2.0	24.20%	13.12%	9.39%	8.14%	7.71%	7.54%	7.48%
2.5	22.78%	12.07%	8.86%	7.89%	7.60%	7.49%	7.46%
3.0	21.69%	11.35%	8.52%	7.76%	7.54%	7.47%	7.45%
3.5	20.81%	10.82%	8.31%	7.67%	7.50%	7.46%	7.45%

Table A.2.26. Overall MSI (Pythagoras-type approach), for the various combinations of hill function shape parameters and $K_h = 1$, during the WP-G Trip-14.

b_{CH}	n_{CH}						
	0.5	1	1.5	2	2.5	3	3.5
0.5	28.65%	19.44%	14.30%	11.49%	9.91%	9.02%	8.49%
1.0	23.05%	12.81%	9.04%	7.90%	7.57%	7.48%	7.45%
1.5	20.19%	10.46%	8.00%	7.54%	7.46%	7.44%	7.44%
2.0	18.37%	9.36%	7.69%	7.47%	7.45%	7.44%	7.44%
2.5	17.08%	8.76%	7.57%	7.45%	7.45%	7.44%	7.44%
3.0	16.10%	8.40%	7.52%	7.45%	7.44%	7.44%	7.44%
3.5	15.33%	8.17%	7.49%	7.44%	7.44%	7.44%	7.44%

Table A.2.27. Overall MSI (simple sum), for the various combinations of hill function shape parameters and $K_h = 1$, during the WP-G Trip-15.

b_{CH}	n_{CH}						
	0.5	1	1.5	2	2.5	3	3.5
0.5	18.78%	7.26%	3.36%	2.09%	1.67%	1.53%	1.48%
1.0	14.54%	4.49%	2.14%	1.61%	1.49%	1.46%	1.45%
1.5	12.47%	3.51%	1.82%	1.52%	1.46%	1.45%	1.44%
2.0	11.18%	3.00%	1.69%	1.49%	1.45%	1.45%	1.45%
2.5	10.26%	2.70%	1.62%	1.47%	1.45%	1.45%	1.44%
3.0	9.57%	2.49%	1.58%	1.46%	1.45%	1.44%	1.44%
3.5	9.03%	2.34%	1.55%	1.46%	1.45%	1.45%	1.44%

Table A.2.28. Overall MSI (Pythagoras-type approach), for the various combinations of hill function shape parameters and $K_h = 1$, during the WP-G Trip-15.

b_{CH}	n_{CH}						
	0.5	1	1.5	2	2.5	3	3.5
0.5	17.41%	6.00%	2.41%	1.59%	1.46%	1.45%	1.45%
1.0	13.18%	3.38%	1.61%	1.45%	1.45%	1.45%	1.44%
1.5	11.13%	2.53%	1.50%	1.45%	1.45%	1.44%	1.44%
2.0	9.84%	2.13%	1.47%	1.45%	1.44%	1.45%	1.45%

b_{CH}	n_{CH}						
	0.5	1	1.5	2	2.5	3	3.5
2.5	8.94%	1.92%	1.46%	1.44%	1.44%	1.45%	1.44%
3.0	8.26%	1.79%	1.45%	1.44%	1.44%	1.44%	1.44%
3.5	7.73%	1.71%	1.45%	1.45%	1.44%	1.44%	1.44%

Table A.2.29. Overall MSI (simple sum), for the various combinations of hill function shape parameters and $K_h = 1$, during the WP-G Trip-16.

b_{CH}	n_{CH}						
	0.5	1	1.5	2	2.5	3	3.5
0.5	15.79%	4.95%	1.69%	0.72%	0.42%	0.33%	0.31%
1.0	11.93%	2.71%	0.79%	0.39%	0.31%	0.30%	0.30%
1.5	10.06%	1.92%	0.56%	0.33%	0.30%	0.30%	0.30%
2.0	8.90%	1.52%	0.46%	0.31%	0.30%	0.30%	0.30%
2.5	8.08%	1.27%	0.41%	0.31%	0.30%	0.30%	0.30%
3.0	7.47%	1.11%	0.38%	0.30%	0.30%	0.30%	0.30%
3.5	6.98%	0.99%	0.36%	0.30%	0.30%	0.30%	0.30%

Table A.2.30. Overall MSI (Pythagoras-type approach), for the various combinations of hill function shape parameters and $K_h = 1$, during the WP-G Trip-16.

b_{CH}	n_{CH}						
	0.5	1	1.5	2	2.5	3	3.5
0.5	15.52%	4.68%	1.44%	0.52%	0.32%	0.30%	0.30%
1.0	11.66%	2.45%	0.58%	0.31%	0.30%	0.30%	0.30%
1.5	9.79%	1.67%	0.39%	0.30%	0.30%	0.30%	0.30%
2.0	8.63%	1.27%	0.33%	0.30%	0.30%	0.30%	0.30%
2.5	7.81%	1.04%	0.31%	0.30%	0.30%	0.30%	0.30%
3.0	7.20%	0.88%	0.31%	0.30%	0.30%	0.30%	0.30%
3.5	6.71%	0.77%	0.30%	0.30%	0.30%	0.30%	0.30%

A.3 Trip-Wise Exact Binomial Test P-Values for WP-G

Table A.3.1. Exact binomial test *p-values* for the predicted overall MSIs (simple sum), under various combinations of hill function shape parameters and $K_h = 1$, for the WP-G Trip-2.

b_{CH}	n_{CH}						
	0.5	1.0	1.5	2.0	2.5	3.0	3.5
0.5	0.000	0.000	0.010	0.134	0.454	0.689	1.000
1.0	0.000	0.007	0.364	0.836	1.000	1.000	0.820
1.5	0.000	0.059	0.690	1.000	1.000	0.819	0.818
2.0	0.000	0.134	0.836	1.000	0.820	0.818	0.817
2.5	0.000	0.290	1.000	1.000	0.819	0.817	0.817
3.0	0.000	0.362	1.000	1.000	0.818	0.817	0.817
3.5	0.000	0.454	1.000	0.821	0.818	0.817	0.817

Table A.3.2. Exact binomial test *p-values* for the predicted overall MSIs (Pythagoras-type approach), under various combinations of hill function shape parameters and $K_h = 1$, for the WP-G Trip-2.

b_{CH}	n_{CH}						
	0.5	1.0	1.5	2.0	2.5	3.0	3.5
0.5	0.000	0.001	0.135	0.692	1.000	1.000	0.821
1.0	0.000	0.103	1.000	1.000	0.818	0.817	0.817
1.5	0.000	0.361	1.000	0.818	0.817	0.817	0.817
2.0	0.000	0.692	1.000	0.817	0.817	0.817	0.817
2.5	0.000	0.836	0.820	0.817	0.817	0.817	0.817
3.0	0.001	1.000	0.818	0.817	0.817	0.817	0.817
3.5	0.002	1.000	0.818	0.817	0.817	0.817	0.817

Table A.3.3. Exact binomial test p -values for the predicted overall MSIs (simple sum), under various combinations of hill function shape parameters and $K_h = 1$, for the WP-G Trip-3.

b_{CH}	n_{CH}						
	0.5	1.0	1.5	2.0	2.5	3.0	3.5
0.5	0.000	0.025	0.200	0.625	0.796	1.000	1.000
1.0	0.001	0.200	0.796	1.000	1.000	0.764	0.760
1.5	0.005	0.483	1.000	1.000	0.763	0.759	0.758
2.0	0.011	0.624	1.000	0.767	0.760	0.758	0.757
2.5	0.025	0.798	1.000	0.763	0.759	0.757	0.757
3.0	0.037	0.796	1.000	0.761	0.758	0.757	0.757
3.5	0.053	1.000	1.000	0.760	0.758	0.757	0.757

Table A.3.4. Exact binomial test p -values for the predicted overall MSIs (Pythagoras-type approach), under various combinations of hill function shape parameters and $K_h = 1$, for the WP-G Trip-3.

b_{CH}	n_{CH}						
	0.5	1.0	1.5	2.0	2.5	3.0	3.5
0.5	0.001	0.148	0.622	1.000	1.000	0.764	0.760
1.0	0.017	0.622	1.000	0.761	0.758	0.757	0.757
1.5	0.037	1.000	0.764	0.758	0.757	0.757	0.757
2.0	0.075	1.000	0.760	0.757	0.757	0.757	0.757
2.5	0.148	1.000	0.758	0.757	0.757	0.757	0.757
3.0	0.203	1.000	0.758	0.757	0.757	0.757	0.757
3.5	0.201	1.000	0.758	0.757	0.757	0.757	0.757

Table A.3.5. Exact binomial test p -values for the predicted overall MSIs (simple sum), under various combinations of hill function shape parameters and $K_h = 1$, for the WP-G Trip-4.

b_{CH}	n_{CH}						
	0.5	1.0	1.5	2.0	2.5	3.0	3.5
0.5	0.000	0.001	0.134	0.689	1.000	0.621	0.444
1.0	0.000	0.079	1.000	0.618	0.423	0.405	0.399
1.5	0.000	0.286	0.814	0.431	0.404	0.398	0.397

b_{CH}	n_{CH}						
	0.5	1.0	1.5	2.0	2.5	3.0	3.5
2.0	0.000	0.564	0.621	0.414	0.400	0.397	0.396
2.5	0.000	0.689	0.606	0.407	0.398	0.396	0.396
3.0	0.000	0.836	0.443	0.403	0.397	0.396	0.396
3.5	0.001	1.000	0.431	0.401	0.397	0.396	0.396

Table A.3.6. Exact binomial test *p-values* for the predicted overall MSIs (Pythagoras-type approach), under various combinations of hill function shape parameters and $K_h = 1$, for the WP-G Trip-4.

b_{CH}	n_{CH}						
	0.5	1.0	1.5	2.0	2.5	3.0	3.5
0.5	0.000	0.007	0.566	0.812	0.432	0.405	0.399
1.0	0.000	0.364	0.615	0.404	0.397	0.396	0.396
1.5	0.000	0.836	0.419	0.397	0.396	0.396	0.396
2.0	0.000	1.000	0.405	0.396	0.396	0.396	0.396
2.5	0.002	0.810	0.400	0.396	0.396	0.396	0.396
3.0	0.004	0.622	0.398	0.396	0.396	0.396	0.396
3.5	0.007	0.609	0.397	0.396	0.396	0.396	0.396

Table A.3.7. Exact binomial test *p-values* for the predicted overall MSIs (simple sum), under various combinations of hill function shape parameters and $K_h = 1$, for the WP-G Trip-5.

b_{CH}	n_{CH}						
	0.5	1.0	1.5	2.0	2.5	3.0	3.5
0.5	0.001	0.077	0.430	0.767	1.000	1.000	1.000
1.0	0.010	0.432	1.000	1.000	0.701	0.689	0.683
1.5	0.023	0.577	1.000	0.703	0.687	0.682	0.680
2.0	0.035	0.767	1.000	0.692	0.683	0.681	0.680
2.5	0.053	1.000	0.714	0.688	0.682	0.680	0.680
3.0	0.077	1.000	0.706	0.685	0.681	0.680	0.680
3.5	0.111	1.000	0.700	0.684	0.680	0.680	0.679

Table A.3.8. Exact binomial test *p-values* for the predicted overall MSIs (Pythagoras-type approach), under various combinations of hill function shape parameters and $K_h = 1$, for the WP-G Trip-5.

b_{CH}	n_{CH}						
	0.5	1.0	1.5	2.0	2.5	3.0	3.5
0.5	0.004	0.225	0.767	1.000	0.708	0.691	0.684
1.0	0.035	0.767	0.716	0.685	0.680	0.680	0.679
1.5	0.077	1.000	0.691	0.681	0.680	0.679	0.679
2.0	0.161	1.000	0.684	0.680	0.679	0.679	0.679
2.5	0.227	1.000	0.682	0.680	0.680	0.679	0.679
3.0	0.225	0.713	0.681	0.679	0.679	0.679	0.679
3.5	0.312	0.705	0.680	0.679	0.679	0.679	0.679

Table A.3.9. Exact binomial test *p-values* for the predicted overall MSIs (simple sum), under various combinations of hill function shape parameters and $K_h = 1$, for the WP-G Trip-6.

b_{CH}	n_{CH}						
	0.5	1.0	1.5	2.0	2.5	3.0	3.5
0.5	0.000	0.000	0.002	0.015	0.033	0.079	0.122
1.0	0.000	0.001	0.035	0.077	0.116	0.180	0.178
1.5	0.000	0.006	0.080	0.116	0.179	0.177	0.177
2.0	0.000	0.015	0.123	0.182	0.178	0.177	0.177
2.5	0.000	0.022	0.117	0.180	0.177	0.177	0.177
3.0	0.000	0.034	0.116	0.179	0.177	0.177	0.177
3.5	0.000	0.054	0.188	0.178	0.177	0.177	0.177

Table A.3.10. Exact binomial test *p-values* for the predicted overall MSIs (Pythagoras-type approach), under various combinations of hill function shape parameters and $K_h = 1$, for the WP-G Trip-6.

b_{CH}	n_{CH}						
	0.5	1.0	1.5	2.0	2.5	3.0	3.5
0.5	0.000	0.000	0.009	0.051	0.117	0.182	0.178
1.0	0.000	0.010	0.121	0.179	0.177	0.177	0.177
1.5	0.000	0.034	0.183	0.177	0.177	0.177	0.177
2.0	0.000	0.051	0.179	0.177	0.177	0.177	0.177
2.5	0.000	0.077	0.178	0.177	0.177	0.177	0.177
3.0	0.000	0.119	0.177	0.177	0.177	0.177	0.177
3.5	0.000	0.117	0.177	0.177	0.177	0.177	0.177

Table A.3.11. Exact binomial test *p-values* for the predicted overall MSIs (simple sum), under various combinations of hill function shape parameters and $K_h = 1$, for WP-G Trip-7.

b_{CH}	n_{CH}						
	0.5	1.0	1.5	2.0	2.5	3.0	3.5
0.5	0.000	0.000	0.000	0.000	0.000	0.000	0.000
1.0	0.000	0.000	0.000	0.000	0.000	0.000	0.000
1.5	0.000	0.000	0.000	0.000	0.000	0.000	0.000
2.0	0.000	0.000	0.000	0.000	0.000	0.000	0.000
2.5	0.000	0.000	0.000	0.000	0.000	0.000	0.000
3.0	0.000	0.000	0.000	0.000	0.000	0.000	0.000
3.5	0.000	0.000	0.000	0.000	0.000	0.000	0.000

Table A.3.12. Exact binomial test *p-values* for the predicted overall MSIs (Pythagoras-type approach), under various combinations of hill function shape parameters and $K_h = 1$, for the WP-G Trip-7.

b_{CH}	n_{CH}						
	0.5	1.0	1.5	2.0	2.5	3.0	3.5
0.5	0.000	0.000	0.000	0.000	0.000	0.000	0.000
1.0	0.000	0.000	0.000	0.000	0.000	0.000	0.000

b_{CH}	n_{CH}						
	0.5	1.0	1.5	2.0	2.5	3.0	3.5
1.5	0.000	0.000	0.000	0.000	0.000	0.000	0.000
2.0	0.000	0.000	0.000	0.000	0.000	0.000	0.000
2.5	0.000	0.000	0.000	0.000	0.000	0.000	0.000
3.0	0.000	0.000	0.000	0.000	0.000	0.000	0.000
3.5	0.000	0.000	0.000	0.000	0.000	0.000	0.000

Table A.3.13. Exact binomial test *p-values* for the predicted overall MSIs (simple sum), under various combinations of hill function shape parameters and $K_h = 1$, for WP-G Trip-8.

b_{CH}	n_{CH}						
	0.5	1.0	1.5	2.0	2.5	3.0	3.5
0.5	0.000	0.000	0.000	0.003	0.018	0.049	0.092
1.0	0.000	0.000	0.018	0.090	0.164	0.219	0.293
1.5	0.000	0.002	0.066	0.164	0.295	0.291	0.290
2.0	0.000	0.009	0.123	0.219	0.291	0.290	0.290
2.5	0.000	0.018	0.165	0.295	0.290	0.290	0.290
3.0	0.000	0.025	0.164	0.292	0.290	0.290	0.290
3.5	0.000	0.050	0.221	0.291	0.290	0.290	0.290

Table A.3.14. Exact binomial test *p-values* for the predicted overall MSIs (Pythagoras-type approach), under various combinations of hill function shape parameters and $K_h = 1$, for the WP-G Trip-8.

b_{CH}	n_{CH}						
	0.5	1.0	1.5	2.0	2.5	3.0	3.5
0.5	0.000	0.000	0.004	0.048	0.122	0.221	0.219
1.0	0.000	0.006	0.168	0.294	0.290	0.290	0.290
1.5	0.000	0.049	0.219	0.290	0.290	0.290	0.290
2.0	0.000	0.090	0.292	0.290	0.290	0.290	0.290
2.5	0.000	0.122	0.290	0.290	0.290	0.290	0.290
3.0	0.000	0.164	0.290	0.290	0.290	0.290	0.290

b_{CH}	n_{CH}						
	0.5	1.0	1.5	2.0	2.5	3.0	3.5
3.5	0.000	0.222	0.290	0.290	0.290	0.290	0.290

Table A.3.15. Exact binomial test *p-values* for the predicted overall MSIs (simple sum), under various combinations of hill function shape parameters and $K_h = 1$, for WP-G Trip-9.

b_{CH}	n_{CH}						
	0.5	1.0	1.5	2.0	2.5	3.0	3.5
0.5	0.000	0.010	0.077	0.225	0.432	0.582	0.577
1.0	0.001	0.077	0.431	0.577	0.767	1.000	1.000
1.5	0.004	0.227	0.578	0.767	1.000	1.000	1.000
2.0	0.006	0.313	0.770	0.767	1.000	1.000	1.000
2.5	0.010	0.432	0.768	1.000	1.000	1.000	1.000
3.0	0.015	0.427	0.767	1.000	1.000	1.000	1.000
3.5	0.023	0.584	0.767	1.000	1.000	1.000	1.000

Table A.3.16. Exact binomial test *p-values* for the predicted overall MSIs (Pythagoras-type approach), under various combinations of hill function shape parameters and $K_h = 1$, for the WP-G Trip-9.

b_{CH}	n_{CH}						
	0.5	1.0	1.5	2.0	2.5	3.0	3.5
0.5	0.001	0.078	0.312	0.577	0.767	0.767	1.000
1.0	0.010	0.312	0.767	1.000	1.000	1.000	1.000
1.5	0.035	0.578	1.000	1.000	1.000	1.000	1.000
2.0	0.052	0.770	1.000	1.000	1.000	1.000	1.000
2.5	0.077	0.767	1.000	1.000	1.000	1.000	1.000
3.0	0.111	0.767	1.000	1.000	1.000	1.000	1.000
3.5	0.160	0.767	1.000	1.000	1.000	1.000	1.000

Table A.3.17. Exact binomial test *p-values* for the predicted overall MSIs (simple sum), under various combinations of hill function shape parameters and $K_h = 1$, for WP-G Trip-10.

b_{CH}	n_{CH}						
	0.5	1.0	1.5	2.0	2.5	3.0	3.5
0.5	0.000	0.040	0.465	1.000	0.822	0.481	0.449
1.0	0.003	0.461	0.821	0.316	0.273	0.160	0.149
1.5	0.015	0.842	0.457	0.184	0.154	0.145	0.142
2.0	0.029	1.000	0.300	0.163	0.147	0.142	0.140
2.5	0.055	0.822	0.281	0.154	0.144	0.141	0.140
3.0	0.100	0.645	0.273	0.149	0.142	0.141	0.140
3.5	0.132	0.634	0.175	0.147	0.141	0.140	0.140

Table A.3.18. Exact binomial test *p-values* for the predicted overall MSIs (Pythagoras-type approach), under various combinations of hill function shape parameters and $K_h = 1$, for the WP-G Trip-10.

b_{CH}	n_{CH}						
	0.5	1.0	1.5	2.0	2.5	3.0	3.5
0.5	0.002	0.225	1.000	0.475	0.291	0.175	0.157
1.0	0.029	1.000	0.288	0.152	0.142	0.140	0.140
1.5	0.100	0.634	0.161	0.142	0.140	0.140	0.140
2.0	0.174	0.324	0.148	0.141	0.140	0.140	0.140
2.5	0.290	0.291	0.144	0.140	0.140	0.140	0.140
3.0	0.368	0.277	0.142	0.140	0.140	0.140	0.140
3.5	0.462	0.179	0.142	0.140	0.140	0.140	0.140

Table A.3.19. Exact binomial test *p-values* for the predicted overall MSIs (simple sum), under various combinations of hill function shape parameters and $K_h = 1$, for WP-G Trip-11.

b_{CH}	n_{CH}						
	0.5	1.0	1.5	2.0	2.5	3.0	3.5
0.5	0.000	0.001	0.034	0.147	0.310	0.483	0.590
1.0	0.000	0.063	0.389	0.852	1.000	1.000	1.000

b_{CH}	n_{CH}						
	0.5	1.0	1.5	2.0	2.5	3.0	3.5
1.5	0.001	0.190	0.714	1.000	1.000	0.842	0.840
2.0	0.002	0.310	0.851	1.000	0.842	0.840	0.839
2.5	0.004	0.484	1.000	1.000	0.841	0.839	0.839
3.0	0.009	0.592	1.000	1.000	0.840	0.839	0.839
3.5	0.012	0.591	1.000	0.842	0.840	0.839	0.839

Table A.3.20. Exact binomial test *p-values* for the predicted overall MSIs (Pythagoras-type approach), under various combinations of hill function shape parameters and $K_h = 1$, for the WP-G Trip-11.

b_{CH}	n_{CH}						
	0.5	1.0	1.5	2.0	2.5	3.0	3.5
0.5	0.001	0.063	0.390	0.714	1.000	1.000	1.000
1.0	0.012	0.482	1.000	1.000	0.840	0.839	0.839
1.5	0.034	0.851	1.000	0.840	0.839	0.839	0.839
2.0	0.084	1.000	0.841	0.839	0.839	0.839	0.839
2.5	0.147	1.000	0.840	0.839	0.839	0.839	0.839
3.0	0.190	1.000	0.840	0.839	0.839	0.839	0.839
3.5	0.244	1.000	0.839	0.839	0.839	0.839	0.839

Table A.3.21. Exact binomial test *p-values* for the predicted overall MSIs (simple sum), under various combinations of hill function shape parameters and $K_h = 1$, for WP-G Trip-12.

b_{CH}	n_{CH}						
	0.5	1.0	1.5	2.0	2.5	3.0	3.5
0.5	0.000	0.000	0.001	0.004	0.014	0.030	0.063
1.0	0.000	0.001	0.031	0.088	0.174	0.243	0.239
1.5	0.000	0.007	0.090	0.173	0.240	0.238	0.237
2.0	0.000	0.021	0.124	0.242	0.238	0.237	0.237
2.5	0.000	0.030	0.175	0.239	0.237	0.237	0.238
3.0	0.000	0.044	0.173	0.238	0.237	0.237	0.238

b_{CH}	n_{CH}						
	0.5	1.0	1.5	2.0	2.5	3.0	3.5
3.5	0.000	0.063	0.172	0.238	0.237	0.238	0.238

Table A.3.22. Exact binomial test *p-values* for the predicted overall MSIs (Pythagoras-type approach), under various combinations of hill function shape parameters and $K_h = 1$, for the WP-G Trip-12.

b_{CH}	n_{CH}						
	0.5	1.0	1.5	2.0	2.5	3.0	3.5
0.5	0.000	0.001	0.015	0.063	0.124	0.173	0.243
1.0	0.000	0.021	0.175	0.238	0.237	0.238	0.238
1.5	0.000	0.090	0.240	0.237	0.238	0.238	0.238
2.0	0.001	0.124	0.238	0.237	0.238	0.238	0.238
2.5	0.001	0.174	0.237	0.238	0.238	0.238	0.238
3.0	0.003	0.172	0.237	0.238	0.238	0.238	0.238
3.5	0.004	0.243	0.237	0.238	0.238	0.238	0.238

Table A.3.23. Exact binomial test *p-values* for the predicted overall MSIs (simple sum), under various combinations of hill function shape parameters and $K_h = 1$, for WP-G Trip-13.

b_{CH}	n_{CH}						
	0.5	1.0	1.5	2.0	2.5	3.0	3.5
0.5	0.001	0.030	0.171	0.299	0.479	0.717	0.717
1.0	0.013	0.297	0.854	1.000	0.844	0.691	0.687
1.5	0.044	0.590	1.000	0.695	0.686	0.545	0.542
2.0	0.091	0.854	0.845	0.687	0.545	0.541	0.539
2.5	0.126	1.000	0.696	0.550	0.542	0.539	0.538
3.0	0.171	1.000	0.691	0.545	0.540	0.539	0.538
3.5	0.174	1.000	0.688	0.543	0.539	0.538	0.538

Table A.3.24. Exact binomial test *p-values* for the predicted overall MSIs (Pythagoras-type approach), under various combinations of hill function shape parameters and $K_h = 1$, for the WP-G Trip-13.

b_{CH}	n_{CH}						
	0.5	1.0	1.5	2.0	2.5	3.0	3.5
0.5	0.128	0.590	1.000	1.000	0.844	0.693	0.689
1.0	0.382	1.000	0.688	0.544	0.540	0.539	0.538
1.5	0.591	0.696	0.544	0.539	0.538	0.538	0.538
2.0	0.717	0.688	0.541	0.538	0.538	0.538	0.538
2.5	0.854	0.686	0.539	0.538	0.538	0.538	0.538
3.0	1.000	0.547	0.539	0.538	0.538	0.538	0.538
3.5	1.000	0.545	0.538	0.538	0.538	0.538	0.538

Table A.3.25. Exact binomial test *p-values* for the predicted overall MSIs (simple sum), under various combinations of hill function shape parameters and $K_h = 1$, for WP-G Trip-14.

b_{CH}	n_{CH}						
	0.5	1.0	1.5	2.0	2.5	3.0	3.5
0.5	0.000	0.026	0.189	0.424	0.829	1.000	1.000
1.0	0.008	0.329	1.000	0.803	0.595	0.417	0.401
1.5	0.026	0.674	0.806	0.591	0.404	0.392	0.388
2.0	0.037	0.828	0.610	0.412	0.393	0.387	0.385
2.5	0.074	1.000	0.595	0.401	0.389	0.385	0.384
3.0	0.102	1.000	0.432	0.395	0.387	0.385	0.384
3.5	0.140	0.813	0.420	0.392	0.386	0.384	0.384

Table A.3.26. Exact binomial test *p-values* for the predicted overall MSIs (Pythagoras-type approach), under various combinations of hill function shape parameters and $K_h = 1$, for the WP-G Trip-14.

b_{CH}	n_{CH}						
	0.5	1.0	1.5	2.0	2.5	3.0	3.5
0.5	0.008	0.189	0.673	1.000	0.801	0.599	0.430

b_{CH}	n_{CH}						
	0.5	1.0	1.5	2.0	2.5	3.0	3.5
1.0	0.074	1.000	0.599	0.401	0.388	0.385	0.384
1.5	0.141	0.808	0.405	0.387	0.384	0.384	0.384
2.0	0.251	0.609	0.392	0.385	0.384	0.384	0.384
2.5	0.426	0.593	0.388	0.384	0.384	0.384	0.384
3.0	0.541	0.425	0.386	0.384	0.384	0.384	0.384
3.5	0.538	0.414	0.385	0.384	0.384	0.384	0.384

Table A.3.27. Exact binomial test *p-values* for the predicted overall MSIs (simple sum), under various combinations of hill function shape parameters and $K_h = 1$, for WP-G Trip-15.

b_{CH}	n_{CH}						
	0.5	1.0	1.5	2.0	2.5	3.0	3.5
0.5	0.000	0.051	0.420	0.629	1.000	1.000	1.000
1.0	0.001	0.174	0.630	1.000	1.000	1.000	1.000
1.5	0.002	0.265	1.000	1.000	1.000	1.000	1.000
2.0	0.006	0.408	1.000	1.000	1.000	1.000	1.000
2.5	0.009	0.649	1.000	1.000	1.000	1.000	1.000
3.0	0.014	0.640	1.000	1.000	1.000	1.000	1.000
3.5	0.013	0.635	1.000	1.000	1.000	1.000	1.000

Table A.3.28. Exact binomial test *p-values* for the predicted overall MSIs (Pythagoras-type approach), under various combinations of hill function shape parameters and $K_h = 1$, for the WP-G Trip-15.

b_{CH}	n_{CH}						
	0.5	1.0	1.5	2.0	2.5	3.0	3.5
0.5	0.000	0.074	0.637	1.000	1.000	1.000	1.000
1.0	0.001	0.421	1.000	1.000	1.000	1.000	1.000
1.5	0.006	0.642	1.000	1.000	1.000	1.000	1.000
2.0	0.008	0.630	1.000	1.000	1.000	1.000	1.000
2.5	0.013	1.000	1.000	1.000	1.000	1.000	1.000

b_{CH}	n_{CH}						
	0.5	1.0	1.5	2.0	2.5	3.0	3.5
3.0	0.020	1.000	1.000	1.000	1.000	1.000	1.000
3.5	0.032	1.000	1.000	1.000	1.000	1.000	1.000

Table A.3.29. Exact binomial test *p-values* for the predicted overall MSIs (simple sum), under various combinations of hill function shape parameters and $K_h = 1$, for WP-G Trip-16.

b_{CH}	n_{CH}						
	0.5	1.0	1.5	2.0	2.5	3.0	3.5
0.5	0.000	0.065	1.000	0.515	0.346	0.282	0.265
1.0	0.000	0.530	0.546	0.323	0.268	0.261	0.260
1.5	0.001	1.000	0.427	0.282	0.262	0.261	0.260
2.0	0.002	1.000	0.368	0.269	0.261	0.260	0.260
2.5	0.005	1.000	0.335	0.265	0.261	0.260	0.260
3.0	0.007	1.000	0.314	0.263	0.260	0.260	0.260
3.5	0.010	1.000	0.300	0.262	0.260	0.260	0.260

Table A.3.30. Exact binomial test *p-values* for the predicted overall MSIs (Pythagoras-type approach), under various combinations of hill function shape parameters and $K_h = 1$, for the WP-G Trip-16.

b_{CH}	n_{CH}						
	0.5	1.0	1.5	2.0	2.5	3.0	3.5
0.5	0.000	0.094	1.000	0.409	0.274	0.261	0.260
1.0	0.000	0.524	0.441	0.266	0.260	0.260	0.260
1.5	0.001	1.000	0.326	0.261	0.260	0.260	0.260
2.0	0.002	1.000	0.284	0.260	0.260	0.260	0.260
2.5	0.005	1.000	0.269	0.260	0.260	0.260	0.260
3.0	0.010	0.587	0.264	0.260	0.260	0.260	0.260
3.5	0.015	0.537	0.262	0.260	0.260	0.260	0.260

A.4 Magnitude of the Objective Function for WP-G

Table A.4.1: Magnitude of the objective function for $K_h = 1/12$, while the total MSI being calculated as simple sum (minimum value in bold).

b_{CH}	n_{CH}						
	0.5	1.0	1.5	2.0	2.5	3.0	3.5
0.5	592.312	356.419	234.754	172.175	136.247	112.251	98.428
1.0	430.167	182.718	84.379	46.678	32.949	26.666	25.288
1.5	354.197	118.652	46.401	26.844	23.908	22.305	24.370
2.0	305.894	85.624	33.090	22.731	22.733	22.748	23.884
2.5	272.935	68.257	27.780	23.349	23.207	23.877	24.389
3.0	251.229	54.568	24.563	23.222	23.316	24.351	24.451
3.5	231.615	47.144	23.853	23.448	23.872	24.417	24.476

Table A.4.2: Magnitude of the objective function for $K_h = 1/12$, while the total MSI being calculated using Pythagoras-type approach (minimum value in bold).

b_{CH}	n_{CH}						
	0.5	1.0	1.5	2.0	2.5	3.0	3.5
0.5	474.589	260.704	155.779	101.482	73.059	57.738	49.049
1.0	332.066	113.121	38.822	24.454	23.257	23.214	23.325
1.5	262.845	63.314	23.368	23.316	24.252	24.437	24.484
2.0	221.323	40.761	22.423	24.168	24.451	24.500	24.511
2.5	192.603	31.071	22.776	24.375	24.495	24.510	24.513
3.0	173.326	27.689	22.832	24.448	24.506	24.512	24.515
3.5	156.643	24.218	23.545	24.478	24.513	24.515	24.512

Table A.4.3: Magnitude of the objective function for $K_h = 1/11$, while the total MSI being calculated as simple sum (minimum value in bold).

b_{CH}	n_{CH}						
	0.5	1.0	1.5	2.0	2.5	3.0	3.5
0.5	590.997	353.285	234.810	170.183	133.434	111.505	97.553
1.0	429.113	178.443	83.082	46.317	32.989	26.704	25.013

1.5	353.374	118.646	45.913	26.884	24.442	22.331	23.858
2.0	305.889	85.660	33.123	22.764	22.755	22.761	23.890
2.5	272.186	68.290	27.801	23.369	23.221	23.884	24.392
3.0	249.662	54.597	24.584	23.244	23.326	24.357	24.450
3.5	231.561	47.169	23.881	23.466	23.875	24.419	24.481

Table A.4.4. Magnitude of the objective function for $K_h = 1/11$, while the total MSI being calculated using Pythagoras-type approach (minimum value in bold).

b_{CH}	n_{CH}						
	0.5	1.0	1.5	2.0	2.5	3.0	3.5
0.5	473.507	258.019	153.181	100.088	73.176	56.957	47.402
1.0	330.128	111.643	38.320	23.825	23.814	23.164	23.342
1.5	261.878	62.823	23.408	23.258	24.267	24.441	24.487
2.0	221.348	40.816	22.451	24.176	24.453	24.500	24.510
2.5	192.021	31.096	22.809	24.382	24.495	24.510	24.512
3.0	171.467	27.012	22.852	24.450	24.506	24.514	24.512
3.5	156.684	24.234	23.560	24.480	24.510	24.515	24.516

Table A.4.5. Magnitude of the objective function for $K_h = 1/10$, while the total MSI being calculated as simple sum (minimum value in bold).

b_{CH}	n_{CH}						
	0.5	1.0	1.5	2.0	2.5	3.0	3.5
0.5	588.267	353.215	231.375	166.417	130.947	110.887	94.266
1.0	427.898	176.206	83.182	46.400	31.928	26.740	25.061
1.5	352.168	117.094	45.537	26.919	24.474	22.364	23.183
2.0	305.821	84.794	33.157	23.127	22.784	22.777	23.895
2.5	272.210	67.472	27.823	23.392	23.234	23.889	24.394
3.0	248.768	54.622	24.605	23.271	23.337	24.360	24.453
3.5	228.628	47.194	22.941	23.483	23.880	24.416	24.480

Table A.4.6. Magnitude of the objective function for $K_h = 1/10$, while the total MSI being calculated using Pythagoras-type approach (minimum value in bold).

b_{CH}	n_{CH}						
	0.5	1.0	1.5	2.0	2.5	3.0	3.5
0.5	469.935	256.389	151.826	98.116	71.390	55.719	46.505
1.0	328.035	110.068	37.962	23.892	23.847	23.195	23.361
1.5	261.159	62.884	22.405	23.291	24.273	24.444	24.488
2.0	220.440	40.870	22.484	24.189	24.459	24.501	24.507
2.5	191.123	31.120	22.847	24.387	24.495	24.508	24.511
3.0	170.667	26.064	22.875	24.454	24.507	24.513	24.512
3.5	156.113	24.250	23.575	24.481	24.509	24.510	24.514

Table A.4.7. Magnitude of the objective function for $K_h = 1/9$, while the total MSI being calculated as simple sum (minimum value in bold).

b_{CH}	n_{CH}						
	0.5	1.0	1.5	2.0	2.5	3.0	3.5
0.5	587.633	351.065	229.518	162.812	128.340	106.570	92.370
1.0	426.745	175.531	82.018	45.971	31.554	26.776	25.111
1.5	351.990	114.356	45.566	26.274	24.514	22.400	23.212
2.0	303.703	84.806	33.192	23.173	22.809	22.795	23.908
2.5	271.312	67.098	27.158	23.415	23.252	23.906	24.399
3.0	245.341	53.870	24.242	23.299	23.349	24.368	24.456
3.5	227.857	47.213	22.984	23.508	23.889	24.424	24.478

Table A.4.8. Magnitude of the objective function for $K_h = 1/9$, while the total MSI being calculated using Pythagoras-type approach (minimum value in bold).

b_{CH}	n_{CH}						
	0.5	1.0	1.5	2.0	2.5	3.0	3.5
0.5	468.086	254.035	147.228	94.122	68.984	52.227	45.824
1.0	326.105	107.637	38.030	23.967	23.883	23.235	23.818
1.5	259.220	62.292	22.467	23.342	24.289	24.451	24.492

2.0	217.004	40.360	22.520	24.204	24.461	24.504	24.510
2.5	189.469	31.553	22.889	24.393	24.498	24.516	24.511
3.0	168.931	26.107	22.905	24.457	24.509	24.517	24.513
3.5	154.548	24.266	23.592	24.484	24.510	24.515	24.511

Table A.4.9. Magnitude of the objective function for $K_h = 1/8$, while the total MSI being calculated as simple sum (minimum value in bold).

b_{CH}	n_{CH}						
	0.5	1.0	1.5	2.0	2.5	3.0	3.5
0.5	584.666	345.872	224.512	162.114	124.883	104.521	89.549
1.0	423.345	173.116	80.637	44.651	31.621	26.806	24.811
1.5	347.789	113.469	42.855	26.342	24.557	22.963	23.242
2.0	300.931	82.351	32.046	23.876	23.457	22.813	23.920
2.5	268.660	67.121	26.779	23.443	23.274	23.909	24.408
3.0	244.518	52.915	24.914	23.338	23.363	24.369	24.458
3.5	226.948	44.879	23.037	23.532	24.239	24.426	24.481

Table A.4.10. Magnitude of the objective function for $K_h = 1/8$, while the total MSI being calculated using Pythagoras-type approach (minimum value in bold).

b_{CH}	n_{CH}						
	0.5	1.0	1.5	2.0	2.5	3.0	3.5
0.5	465.835	252.163	145.671	92.310	66.220	50.763	44.513
1.0	324.202	105.776	37.694	24.041	22.973	23.280	23.847
1.5	259.188	60.044	23.181	23.393	24.299	24.451	24.492
2.0	216.475	40.417	22.562	24.219	24.460	24.500	24.510
2.5	189.575	29.359	22.938	24.396	24.497	24.508	24.515
3.0	169.053	26.155	22.940	24.461	24.508	24.512	24.513
3.5	152.940	23.866	23.616	24.484	24.508	24.513	24.512

Table A.4.11. Magnitude of the objective function for $K_h = 1/7$, while the total MSI being calculated as simple sum (minimum value in bold).

b_{CH}	n_{CH}						
	0.5	1.0	1.5	2.0	2.5	3.0	3.5
0.5	579.558	338.628	219.642	155.690	121.833	98.280	85.234
1.0	420.193	171.605	77.729	43.151	31.246	24.848	24.868
1.5	344.973	110.501	42.985	26.033	23.967	23.013	23.281
2.0	299.321	80.387	30.824	23.938	24.035	22.844	23.936
2.5	266.823	64.357	25.877	23.858	23.299	24.271	24.410
3.0	242.582	52.143	25.287	23.379	23.382	24.379	24.461
3.5	224.270	44.957	23.097	23.564	24.253	24.431	24.485

Table A.4.12. Magnitude of the objective function for $K_h = 1/7$, while the total MSI being calculated using Pythagoras-type approach (minimum value in bold).

b_{CH}	n_{CH}						
	0.5	1.0	1.5	2.0	2.5	3.0	3.5
0.5	463.249	246.424	142.042	88.986	62.515	50.405	40.977
1.0	323.076	103.518	35.618	24.778	23.218	22.731	23.882
1.5	255.918	57.618	22.889	23.457	24.319	24.457	24.496
2.0	214.948	39.689	22.613	24.239	24.471	24.507	24.512
2.5	188.787	29.424	23.006	24.409	24.501	24.515	24.511
3.0	167.529	26.206	22.984	24.465	24.510	24.515	24.514
3.5	152.072	23.755	23.640	24.485	24.510	24.514	24.515

Table A.4.13. Magnitude of the objective function for $K_h = 1/6$, while the total MSI being calculated as simple sum (minimum value in bold).

b_{CH}	n_{CH}						
	0.5	1.0	1.5	2.0	2.5	3.0	3.5
0.5	576.173	334.549	214.261	150.892	116.062	95.271	80.790
1.0	415.505	167.464	75.505	41.907	28.221	25.214	24.192
1.5	342.157	107.862	42.685	26.525	24.047	23.076	23.326
2.0	298.158	80.119	30.515	24.011	24.089	22.872	24.299

2.5	264.673	61.420	25.210	23.900	22.727	24.284	24.419
3.0	239.319	51.753	24.563	23.436	23.793	24.385	24.466
3.5	220.181	44.111	23.171	23.604	24.268	24.434	24.485

Table A.4.14. Magnitude of the objective function for $K_h = 1/6$, while the total MSI being calculated using Pythagoras-type approach (minimum value in bold).

b_{CH}	n_{CH}						
	0.5	1.0	1.5	2.0	2.5	3.0	3.5
0.5	457.467	238.710	136.720	84.496	60.546	45.777	38.956
1.0	317.256	102.269	34.094	23.830	23.327	23.189	24.262
1.5	251.621	56.362	23.509	23.530	24.337	24.466	24.499
2.0	211.577	38.597	22.538	24.260	24.470	24.505	24.514
2.5	186.389	29.062	23.085	24.413	24.499	24.512	24.513
3.0	163.442	25.491	23.375	24.469	24.507	24.512	24.515
3.5	148.389	22.855	23.672	24.487	24.512	24.512	24.513

Table A.4.15. Magnitude of the objective function for $K_h = 1/5$, while the total MSI being calculated as simple sum (minimum value in bold).

b_{CH}	n_{CH}						
	0.5	1.0	1.5	2.0	2.5	3.0	3.5
0.5	565.583	323.510	204.032	142.118	109.940	89.397	74.553
1.0	412.047	162.623	72.922	38.496	28.205	24.707	23.647
1.5	335.079	105.477	40.257	25.949	24.134	24.139	22.781
2.0	289.718	76.381	30.616	23.773	24.163	23.304	24.319
2.5	256.717	60.715	25.335	24.732	22.770	24.303	24.431
3.0	236.478	50.853	23.713	23.016	23.553	24.405	24.471
3.5	216.264	43.720	22.942	23.125	24.285	24.442	24.488

Table A.4.16. Magnitude of the objective function for $K_h = 1/5$, while the total MSI being calculated using Pythagoras-type approach (minimum value in bold).

b_{CH}	n_{CH}						
	0.5	1.0	1.5	2.0	2.5	3.0	3.5
0.5	450.812	233.596	128.385	80.158	55.492	43.023	36.362
1.0	314.494	97.974	33.754	22.705	23.460	23.702	24.301
1.5	247.198	53.639	23.497	23.628	24.357	24.470	24.497
2.0	208.921	36.969	23.851	24.290	24.477	24.507	24.512
2.5	181.880	27.728	23.187	24.426	24.499	24.511	24.516
3.0	160.689	22.775	24.372	24.512	24.518	24.516	24.514
3.5	144.099	22.944	23.712	24.490	24.510	24.514	24.513

Table A.4.17. Magnitude of the objective function for $K_h = 1/4$, while the total MSI being calculated as simple sum (minimum value in bold).

b_{CH}	n_{CH}						
	0.5	1.0	1.5	2.0	2.5	3.0	3.5
0.5	556.882	313.322	196.167	133.690	99.827	80.476	66.870
1.0	403.457	154.303	67.354	36.561	28.102	24.928	23.539
1.5	330.196	101.618	39.610	24.671	23.521	24.255	23.254
2.0	283.240	73.988	27.935	23.246	24.257	23.355	24.345
2.5	254.350	56.768	25.470	24.213	22.830	24.328	24.441
3.0	231.632	47.093	23.811	23.427	23.861	24.412	24.474
3.5	213.573	42.015	22.699	23.190	24.310	24.453	24.493

Table A.4.18. Magnitude of the objective function for $K_h = 1/4$, while the total MSI being calculated using Pythagoras-type approach (minimum value in bold).

b_{CH}	n_{CH}						
	0.5	1.0	1.5	2.0	2.5	3.0	3.5
0.5	442.753	222.165	119.534	72.126	48.375	38.407	33.723
1.0	306.125	92.124	29.594	23.877	23.697	23.804	24.354
1.5	241.716	51.492	23.712	23.139	24.389	24.479	24.502
2.0	203.886	35.395	24.057	24.325	24.485	24.508	24.511

2.5	176.604	27.954	23.321	24.439	24.504	24.511	24.514
3.0	157.494	24.187	23.524	24.479	24.510	24.514	24.512
3.5	141.284	22.809	24.160	24.493	24.511	24.516	24.515

Table A.4.19. Magnitude of the objective function for $K_h = 1/3$, while the total MSI being calculated as simple sum (minimum value in bold).

b_{CH}	n_{CH}						
	0.5	1.0	1.5	2.0	2.5	3.0	3.5
0.5	540.446	293.747	176.645	118.523	87.048	69.450	55.850
1.0	391.787	147.401	61.017	34.112	25.877	24.104	22.502
1.5	320.215	94.185	34.714	25.206	22.914	23.187	23.357
2.0	276.582	69.640	27.311	23.306	23.174	23.861	24.383
2.5	245.339	53.868	24.242	23.303	23.348	24.365	24.457
3.0	224.268	44.959	23.095	23.565	24.255	24.429	24.482
3.5	206.930	39.504	22.875	23.719	24.343	24.463	24.496

Table A.4.20. Magnitude of the objective function for $K_h = 1/3$, while the total MSI being calculated using Pythagoras-type approach (minimum value in bold).

b_{CH}	n_{CH}						
	0.5	1.0	1.5	2.0	2.5	3.0	3.5
0.5	429.459	206.079	106.918	60.161	41.089	32.719	29.226
1.0	295.636	84.028	28.855	23.481	23.241	24.264	24.410
1.5	232.568	46.780	22.021	23.294	24.425	24.490	24.508
2.0	195.400	32.685	23.236	24.369	24.490	24.509	24.513
2.5	168.922	26.106	22.905	24.457	24.508	24.513	24.514
3.0	152.068	23.755	23.639	24.485	24.512	24.512	24.512
3.5	123.181	21.626	24.340	24.503	24.510	24.513	24.515

Table A.4.21. Magnitude of the objective function for $K_h = 1/2$, while the total MSI being calculated as simple sum (minimum value in bold).

b_{CH}	n_{CH}						
	0.5	1.0	1.5	2.0	2.5	3.0	3.5
0.5	511.444	263.550	148.180	94.363	67.425	50.534	43.853
1.0	369.692	128.056	51.059	30.178	23.726	23.570	23.171
1.5	300.939	82.350	32.046	23.878	23.460	22.815	23.920
2.0	256.702	60.715	25.332	24.729	22.771	24.303	24.430
2.5	231.629	47.091	23.809	23.425	23.861	24.413	24.476
3.0	210.852	39.351	23.421	23.233	24.323	24.454	24.494
3.5	193.039	35.274	22.854	23.268	24.388	24.479	24.502

Table A.4.22. Magnitude of the objective function for $K_h = 1/2$, while the total MSI being calculated using Pythagoras-type approach (minimum value in bold).

b_{CH}	n_{CH}						
	0.5	1.0	1.5	2.0	2.5	3.0	3.5
0.5	403.532	179.182	84.511	44.608	31.076	26.820	23.509
1.0	274.677	70.768	25.610	23.961	23.775	24.390	24.465
1.5	216.475	40.417	22.562	24.222	24.463	24.501	24.510
2.0	181.874	27.727	23.184	24.424	24.502	24.511	24.514
2.5	157.491	24.187	23.524	24.478	24.510	24.515	24.514
3.0	139.616	22.173	24.191	24.496	24.510	24.512	24.513
3.5	124.573	20.965	24.331	24.502	24.512	24.515	24.513

Table A.4.23. Magnitude of the objective function for $K_h = 2$, while the total MSI being calculated as simple sum (minimum value in bold).

b_{CH}	n_{CH}						
	0.5	1.0	1.5	2.0	2.5	3.0	3.5
0.5	369.730	128.615	51.055	30.177	23.728	23.570	23.172
1.0	257.501	60.714	25.332	24.732	22.771	24.307	24.431
1.5	210.857	40.150	23.422	23.236	24.327	24.457	24.498
2.0	180.210	31.861	24.311	23.401	24.429	24.491	24.512

2.5	158.872	28.769	23.268	24.284	24.468	24.504	24.514
3.0	145.933	26.900	23.462	24.360	24.482	24.508	24.514
3.5	133.122	25.227	23.597	24.403	24.494	24.511	24.513

Table A.4.24. Magnitude of the objective function for $K_h = 2$, while the total MSI being calculated using Pythagoras-type approach (minimum value in bold).

b_{CH}	n_{CH}						
	0.5	1.0	1.5	2.0	2.5	3.0	3.5
0.5	275.417	70.765	25.608	23.965	23.779	24.390	24.467
1.0	181.873	27.722	23.184	24.427	24.503	24.516	24.516
1.5	139.609	22.170	24.194	24.500	24.515	24.515	24.518
2.0	115.437	22.776	24.397	24.510	24.517	24.516	24.519
2.5	97.571	22.175	24.458	24.512	24.517	24.516	24.518
3.0	85.369	22.328	24.484	24.514	24.513	24.515	24.515
3.5	76.797	22.484	24.495	24.514	24.515	24.515	24.514

Table A.4.25. Magnitude of the objective function for $K_h = 3$, while the total MSI being calculated as simple sum (minimum value in bold).

b_{CH}	n_{CH}						
	0.5	1.0	1.5	2.0	2.5	3.0	3.5
0.5	320.247	94.164	34.705	25.203	22.909	23.187	23.354
1.0	224.282	44.949	23.095	23.566	24.256	24.433	24.486
1.5	180.205	31.860	24.313	23.402	24.431	24.494	24.511
2.0	153.670	27.677	22.718	24.316	24.476	24.506	24.513
2.5	136.423	25.380	23.531	24.391	24.492	24.513	24.518
3.0	125.232	25.985	23.158	24.433	24.500	24.514	24.517
3.5	114.131	22.675	23.305	24.453	24.508	24.515	24.516

Table A.4.26. Magnitude of the objective function for $K_h = 3$, while the total MSI being calculated using Pythagoras-type approach (minimum value in bold).

b_{CH}	n_{CH}						
	0.5	1.0	1.5	2.0	2.5	3.0	3.5
0.5	233.261	46.776	22.013	23.296	24.424	24.493	24.509
1.0	152.071	23.751	23.642	24.489	24.514	24.517	24.517
1.5	115.432	22.774	24.399	24.512	24.519	24.518	24.518
2.0	94.437	22.357	24.473	24.515	24.518	24.517	24.516
2.5	80.552	22.620	24.493	24.515	24.516	24.518	24.519
3.0	69.203	22.796	24.503	24.517	24.515	24.517	24.518
3.5	62.896	23.087	24.508	24.514	24.518	24.517	24.516

Table A.4.27. Magnitude of the objective function for $K_h = 4$, while the total MSI being calculated as simple sum (minimum value in bold).

b_{CH}	n_{CH}						
	0.5	1.0	1.5	2.0	2.5	3.0	3.5
0.5	285.144	73.981	27.387	23.244	24.255	23.355	24.346
1.0	199.410	35.581	22.730	23.211	24.374	24.477	24.504
1.5	158.855	28.765	24.023	24.287	24.470	24.508	24.514
2.0	136.420	25.381	23.528	24.396	24.494	24.512	24.516
2.5	120.483	25.104	23.202	24.439	24.505	24.517	24.518
3.0	108.903	23.190	23.358	24.465	24.513	24.515	24.518
3.5	100.669	21.689	23.797	24.480	24.511	24.514	24.518

Table A.4.28. Magnitude of the objective function for $K_h = 4$, while the total MSI being calculated using Pythagoras-type approach (minimum value in bold).

b_{CH}	n_{CH}						
	0.5	1.0	1.5	2.0	2.5	3.0	3.5
0.5	203.846	35.382	24.047	24.329	24.487	24.511	24.515
1.0	131.858	21.089	24.298	24.506	24.516	24.519	24.517
1.5	97.552	22.170	24.459	24.517	24.519	24.520	24.517
2.0	80.547	22.621	24.493	24.519	24.518	24.517	24.517

2.5	68.722	22.880	24.505	24.516	24.519	24.520	24.519
3.0	60.569	23.202	24.511	24.518	24.521	24.516	24.518
3.5	54.196	23.423	24.512	24.519	24.517	24.515	24.519

Table A.4.29. Magnitude of the objective function for $K_h = 5$, while the total MSI being calculated as simple sum (minimum value in bold).

b_{CH}	n_{CH}						
	0.5	1.0	1.5	2.0	2.5	3.0	3.5
0.5	261.297	60.703	25.322	23.948	22.771	24.303	24.434
1.0	180.190	31.855	23.692	23.400	24.431	24.494	24.511
1.5	145.931	26.893	23.460	24.362	24.488	24.513	24.516
2.0	125.232	25.979	23.157	24.433	24.503	24.516	24.518
2.5	108.890	23.190	23.360	24.467	24.509	24.519	24.518
3.0	98.504	21.400	24.210	24.481	24.514	24.518	24.516
3.5	90.840	22.380	24.277	24.490	24.515	24.518	24.516

Table A.4.30. Magnitude of the objective function for $K_h = 5$, while the total MSI being calculated using Pythagoras-type approach (minimum value in bold).

b_{CH}	n_{CH}						
	0.5	1.0	1.5	2.0	2.5	3.0	3.5
0.5	181.837	27.702	23.179	24.427	24.506	24.515	24.521
1.0	115.414	22.769	24.397	24.512	24.519	24.518	24.519
1.5	85.340	22.329	24.487	24.517	24.519	24.520	24.517
2.0	69.525	22.791	24.505	24.518	24.518	24.519	24.518
2.5	61.198	23.205	24.512	24.521	24.518	24.521	24.518
3.0	53.494	23.855	24.517	24.518	24.520	24.519	24.517
3.5	49.128	24.028	24.515	24.517	24.519	24.519	24.516

Table A.4.31. Magnitude of the objective function for $K_h = 6$, while the total MSI being calculated as simple sum (minimum value in bold).

b_{CH}	n_{CH}						
	0.5	1.0	1.5	2.0	2.5	3.0	3.5
0.5	239.293	51.735	24.556	23.425	23.792	24.387	24.466
1.0	166.084	28.149	23.865	24.245	24.459	24.502	24.514
1.5	133.627	25.219	23.594	24.404	24.497	24.514	24.519
2.0	114.118	22.670	23.302	24.455	24.509	24.516	24.517
2.5	100.663	22.329	23.799	24.476	24.513	24.520	24.520
3.0	90.836	22.381	24.280	24.491	24.516	24.518	24.519
3.5	83.663	23.257	24.333	24.498	24.519	24.520	24.519

Table A.4.32. Magnitude of the objective function for $K_h = 6$, while the total MSI being calculated using Pythagoras-type approach (minimum value in bold).

b_{CH}	n_{CH}						
	0.5	1.0	1.5	2.0	2.5	3.0	3.5
0.5	164.143	25.802	23.372	24.470	24.513	24.517	24.517
1.0	104.660	22.701	24.446	24.515	24.519	24.518	24.519
1.5	78.098	22.476	24.498	24.517	24.518	24.518	24.520
2.0	62.882	23.090	24.507	24.517	24.519	24.518	24.517
2.5	54.187	23.423	24.515	24.516	24.518	24.521	24.520
3.0	49.124	24.031	24.518	24.518	24.520	24.518	24.519
3.5	44.527	24.169	24.519	24.518	24.521	24.520	24.520

Table A.4.33. Magnitude of the objective function for $K_h = 7$, while the total MSI being calculated as simple sum (minimum value in bold).

b_{CH}	n_{CH}						
	0.5	1.0	1.5	2.0	2.5	3.0	3.5
0.5	224.964	45.264	23.078	23.555	24.252	24.432	24.486
1.0	155.180	27.671	22.707	24.314	24.475	24.509	24.516
1.5	125.231	25.975	23.157	24.430	24.502	24.517	24.520
2.0	106.872	22.849	23.747	24.472	24.513	24.519	24.520

2.5	94.065	22.283	24.254	24.491	24.516	24.519	24.520
3.0	84.267	23.223	24.322	24.499	24.519	24.522	24.520
3.5	77.933	23.617	24.371	24.504	24.519	24.520	24.520

Table A.4.34. Magnitude of the objective function for $K_h = 7$, while the total MSI being calculated using Pythagoras-type approach (minimum value in bold).

b_{CH}	n_{CH}						
	0.5	1.0	1.5	2.0	2.5	3.0	3.5
0.5	152.978	23.096	23.638	24.490	24.517	24.519	24.518
1.0	94.426	22.350	24.470	24.516	24.518	24.519	24.519
1.5	69.880	22.791	24.507	24.515	24.518	24.520	24.521
2.0	58.055	23.302	24.515	24.519	24.520	24.520	24.520
2.5	49.952	23.979	24.514	24.521	24.520	24.519	24.520
3.0	44.456	24.153	24.515	24.519	24.521	24.522	24.520
3.5	40.865	24.263	24.521	24.519	24.521	24.520	24.520

Table A.4.35. Magnitude of the objective function for $K_h = 8$, while the total MSI being calculated as simple sum (minimum value in bold).

b_{CH}	n_{CH}						
	0.5	1.0	1.5	2.0	2.5	3.0	3.5
0.5	210.864	40.126	23.411	23.228	24.325	24.459	24.497
1.0	146.975	26.555	23.450	24.364	24.491	24.515	24.516
1.5	114.537	23.679	23.273	24.455	24.509	24.522	24.517
2.0	100.029	21.387	24.208	24.483	24.516	24.522	24.518
2.5	87.713	22.496	24.304	24.502	24.519	24.521	24.519
3.0	78.278	24.178	24.359	24.505	24.519	24.522	24.518
3.5	72.798	23.814	24.396	24.508	24.517	24.518	24.518

Table A.4.36. Magnitude of the objective function for $K_h = 8$, while the total MSI being calculated using Pythagoras-type approach (minimum value in bold).

b_{CH}	n_{CH}						
	0.5	1.0	1.5	2.0	2.5	3.0	3.5
0.5	0.5	1.0	1.5	2.0	2.5	3.0	3.5
1.0	141.397	22.864	24.192	24.502	24.518	24.520	24.518
1.5	85.992	22.316	24.485	24.522	24.523	24.523	24.518
2.0	64.716	23.021	24.512	24.522	24.521	24.524	24.518
2.5	53.477	23.849	24.519	24.521	24.522	24.523	24.518
3.0	46.739	24.094	24.520	24.526	24.522	24.521	24.519
3.5	41.734	24.241	24.520	24.521	24.521	24.522	24.518

Table A.4.37. Magnitude of the objective function for $K_h = 9$, while the total MSI being calculated as simple sum (minimum value in bold).

b_{CH}	n_{CH}						
	0.5	1.0	1.5	2.0	2.5	3.0	3.5
0.5	200.042	36.389	22.330	23.198	24.372	24.477	24.506
1.0	136.362	25.369	23.518	24.392	24.494	24.512	24.518
1.5	110.280	22.800	23.355	24.464	24.509	24.516	24.518
2.0	94.060	22.276	24.255	24.487	24.513	24.517	24.518
2.5	83.700	23.280	24.335	24.497	24.519	24.518	24.517
3.0	74.341	23.732	24.384	24.506	24.515	24.518	24.518
3.5	67.182	23.884	24.413	24.507	24.518	24.517	24.517

Table A.4.38. Magnitude of the objective function for $K_h = 9$, while the total MSI being calculated using Pythagoras-type approach (minimum value in bold).

b_{CH}	n_{CH}						
	0.5	1.0	1.5	2.0	2.5	3.0	3.5
0.5	132.392	21.071	24.294	24.507	24.520	24.521	24.521
1.0	80.501	22.609	24.494	24.519	24.518	24.517	24.520
1.5	61.166	23.198	24.513	24.518	24.517	24.518	24.518
2.0	49.938	23.979	24.516	24.517	24.517	24.518	24.518

2.5	43.825	24.181	24.516	24.517	24.522	24.518	24.517
3.0	38.952	24.301	24.519	24.519	24.517	24.518	24.518
3.5	34.790	24.373	24.518	24.517	24.519	24.517	24.517

Table A.4.39. Magnitude of the objective function for $K_h = 10$, while the total MSI being calculated as simple sum (minimum value in bold).

b_{CH}	n_{CH}						
	0.5	1.0	1.5	2.0	2.5	3.0	3.5
0.5	191.499	33.267	22.929	23.308	24.401	24.484	24.509
1.0	130.594	25.822	23.643	24.414	24.499	24.513	24.519
1.5	103.043	22.905	23.757	24.472	24.514	24.517	24.517
2.0	88.785	22.453	24.294	24.492	24.517	24.517	24.518
2.5	77.826	24.203	24.363	24.502	24.517	24.518	24.518
3.0	72.038	24.482	24.400	24.508	24.520	24.518	24.518
3.5	65.309	23.080	24.426	24.513	24.516	24.518	24.518

Table A.4.40. Magnitude of the objective function for $K_h = 10$, while the total MSI being calculated using Pythagoras-type approach (minimum value in bold).

b_{CH}	n_{CH}						
	0.5	1.0	1.5	2.0	2.5	3.0	3.5
0.5	122.765	21.698	24.356	24.511	24.517	24.518	24.520
1.0	75.611	22.586	24.500	24.518	24.518	24.517	24.520
1.5	56.483	23.340	24.511	24.518	24.521	24.518	24.517
2.0	47.170	24.072	24.519	24.517	24.521	24.518	24.518
2.5	40.808	24.253	24.519	24.518	24.519	24.518	24.518
3.0	36.265	24.349	24.517	24.519	24.521	24.518	24.518
3.5	35.003	24.408	24.517	24.521	24.517	24.518	24.518

Table A.4.41. Magnitude of the objective function for $K_h = 11$, while the total MSI being calculated as simple sum (minimum value in bold).

b_{CH}	n_{CH}						
	0.5	1.0	1.5	2.0	2.5	3.0	3.5
0.5	181.367	31.828	23.677	23.388	24.425	24.494	24.513
1.0	125.757	25.953	23.145	24.430	24.503	24.514	24.518
1.5	100.018	24.371	24.198	24.479	24.513	24.516	24.520
2.0	84.242	23.210	24.321	24.498	24.515	24.519	24.520
2.5	74.326	23.724	24.382	24.504	24.517	24.520	24.520
3.0	66.871	23.925	24.418	24.511	24.516	24.520	24.520
3.5	61.466	23.647	24.438	24.513	24.518	24.520	24.520

Table A.4.42. Magnitude of the objective function for $K_h = 11$, while the total MSI being calculated using Pythagoras-type approach (minimum value in bold).

b_{CH}	n_{CH}						
	0.5	1.0	1.5	2.0	2.5	3.0	3.5
0.5	115.791	22.737	24.395	24.514	24.518	24.520	24.521
1.0	70.322	22.778	24.506	24.517	24.519	24.518	24.519
1.5	54.251	23.848	24.512	24.517	24.519	24.517	24.520
2.0	44.011	24.150	24.517	24.519	24.517	24.519	24.520
2.5	38.940	24.300	24.518	24.518	24.519	24.520	24.520
3.0	34.334	24.384	24.519	24.521	24.517	24.520	24.520
3.5	33.425	24.426	24.517	24.520	24.519	24.520	24.520

Table A.4.43. Magnitude of the objective function for $K_h = 12$, while the total MSI being calculated as simple sum (minimum value in bold).

b_{CH}	n_{CH}						
	0.5	1.0	1.5	2.0	2.5	3.0	3.5
0.5	174.393	30.908	24.626	23.840	24.441	24.498	24.513
1.0	118.341	25.159	23.220	24.441	24.503	24.516	24.518
1.5	96.245	22.206	24.238	24.488	24.515	24.516	24.518
2.0	81.311	23.329	24.345	24.500	24.518	24.518	24.518

2.5	72.862	24.448	24.398	24.507	24.516	24.519	24.518
3.0	63.958	23.091	24.427	24.513	24.517	24.518	24.517
3.5	59.235	23.018	24.447	24.512	24.517	24.518	24.518

Table A.4.44. Magnitude of the objective function for $K_h = 12$, while the total MSI being calculated using Pythagoras-type approach (minimum value in bold).

b_{CH}	n_{CH}						
	0.5	1.0	1.5	2.0	2.5	3.0	3.5
0.5	109.486	22.967	24.421	24.513	24.517	24.519	24.520
1.0	67.338	22.939	24.504	24.516	24.517	24.518	24.519
1.5	49.955	23.941	24.514	24.521	24.519	24.517	24.518
2.0	42.679	24.210	24.517	24.519	24.520	24.518	24.518
2.5	36.199	24.340	24.518	24.519	24.518	24.519	24.518
3.0	35.014	24.409	24.517	24.521	24.518	24.518	24.517
3.5	30.501	24.446	24.518	24.518	24.518	24.518	24.518

Appendix B. Data Pertaining to Validation of SVH-Conflict Model

B.1 Raw and Filtered Motion Histories

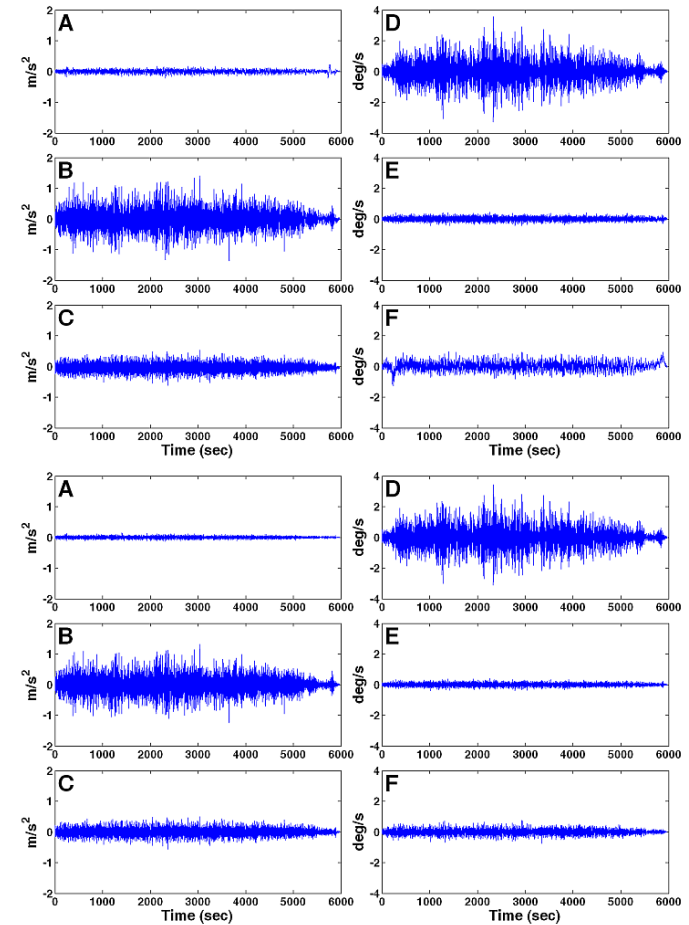


Figure B.1.1. Motion history (upper-row; lower-filtered) of Cat-A at MRU position during Trip-1; linear accelerations (A) longitudinal (B) lateral (C) vertical; angular velocities (D) roll (E) pitch (F) yaw.

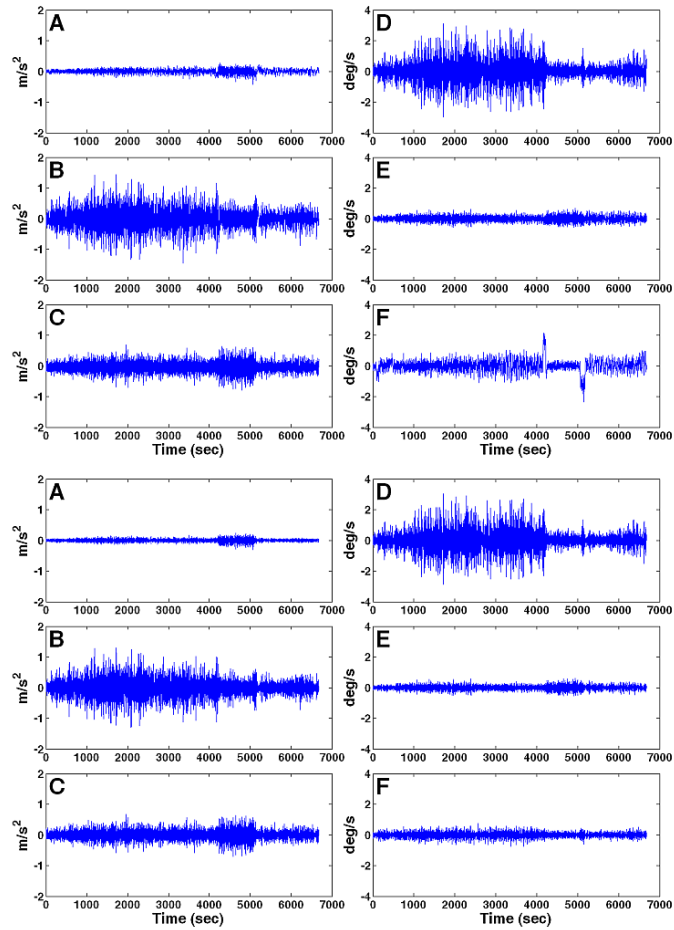


Figure B.1.2. Motion history (upper-row; lower-filtered) of Cat-A at MRU position during Trip-2; linear accelerations (A) longitudinal (B) lateral (C) vertical; angular velocities (D) roll (E) pitch (F) yaw.

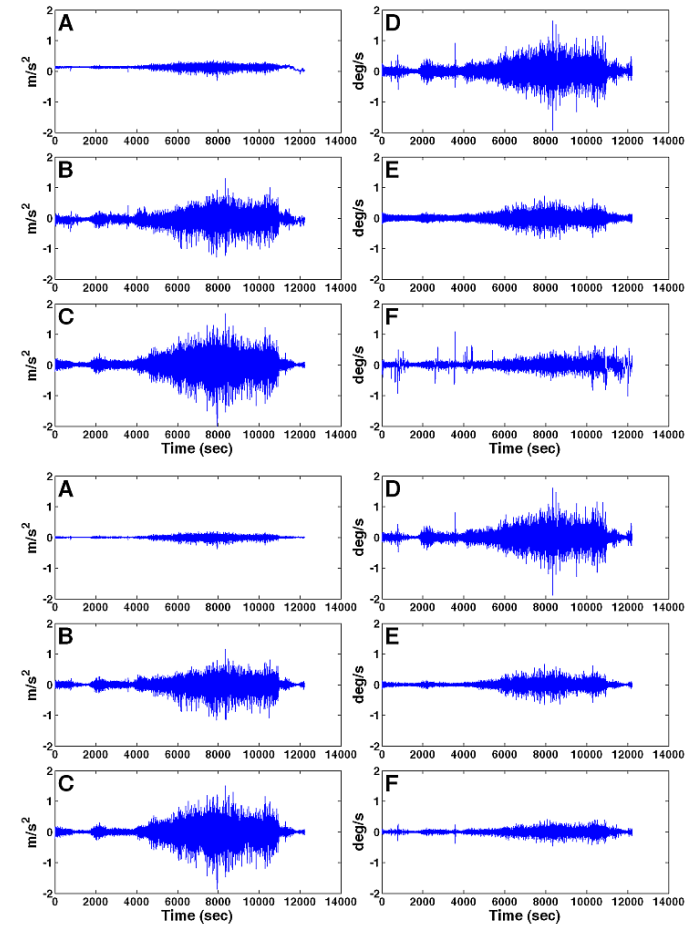


Figure B.1.3. Motion history (upper-row; lower-filtered) of DV-B at MRU position during Trip-1; linear accelerations (A) longitudinal (B) lateral (C) vertical; angular velocities (D) roll (E) pitch (F) yaw.

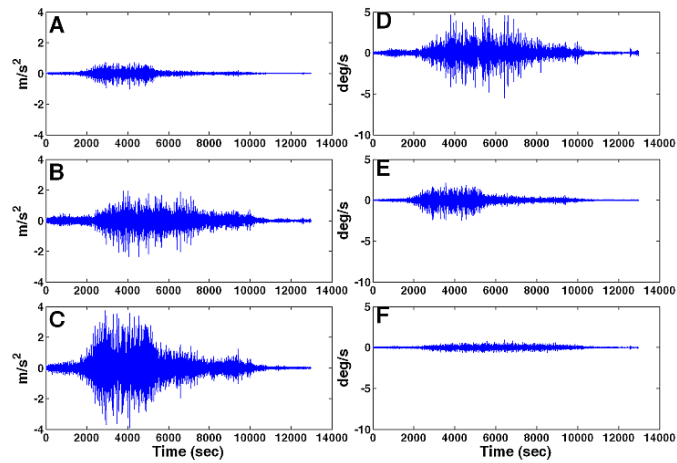
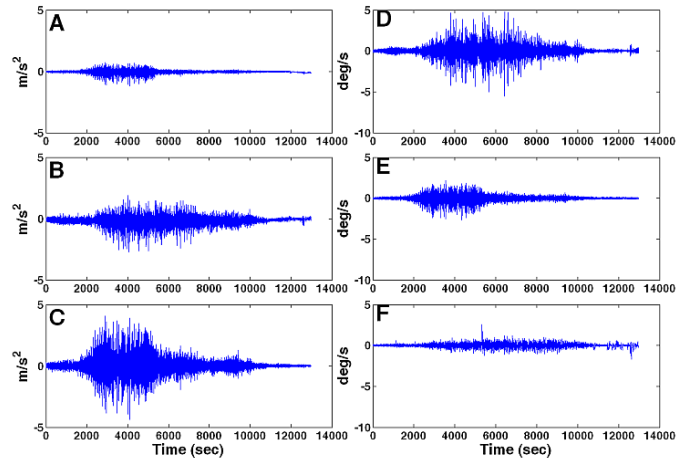


Figure B.1.4. Motion history (upper-row; lower-filtered) of DV-B at MRU position during Trip-2; linear accelerations (A) longitudinal (B) lateral (C) vertical; angular velocities (D) roll (E) pitch (F) yaw.

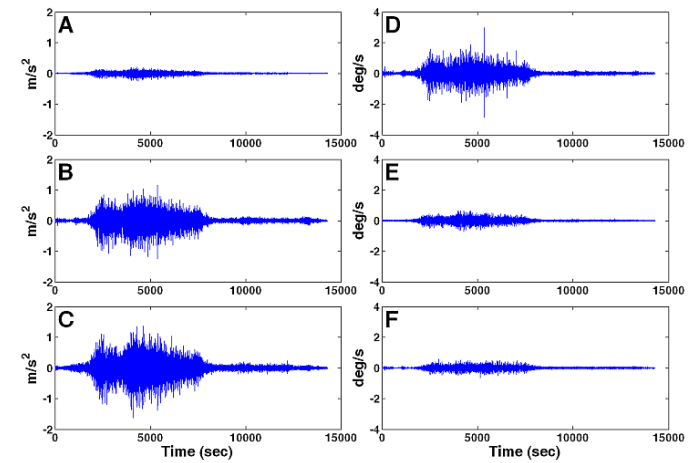
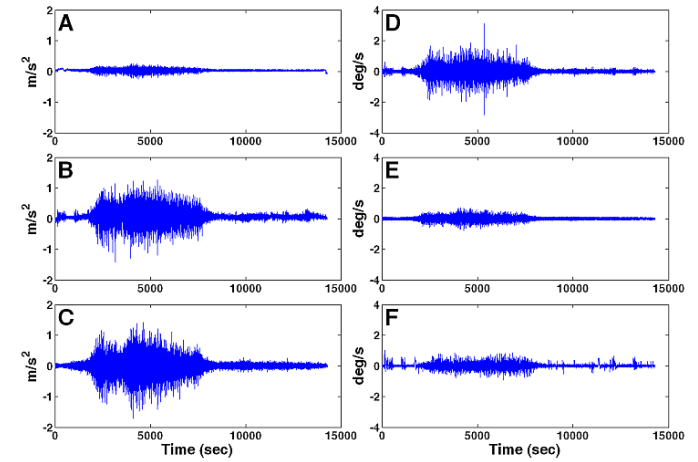


Figure B.1.5. Motion history (upper-row; lower-filtered) of DV-B at MRU position during Trip-3; linear accelerations (A) longitudinal (B) lateral (C) vertical; angular velocities (D) roll (E) pitch (F) yaw.

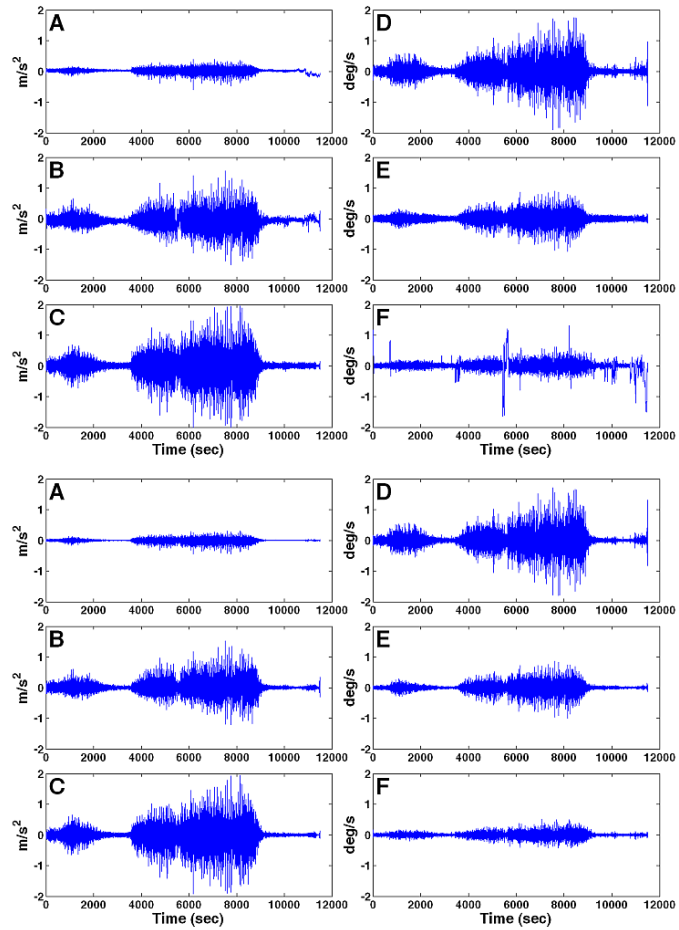


Figure B.1.6. Motion history (upper-row; lower-filtered) of DV-B at MRU position during Trip-4; linear accelerations (A) longitudinal (B) lateral (C) vertical; angular velocities (D) roll (E) pitch (F) yaw.

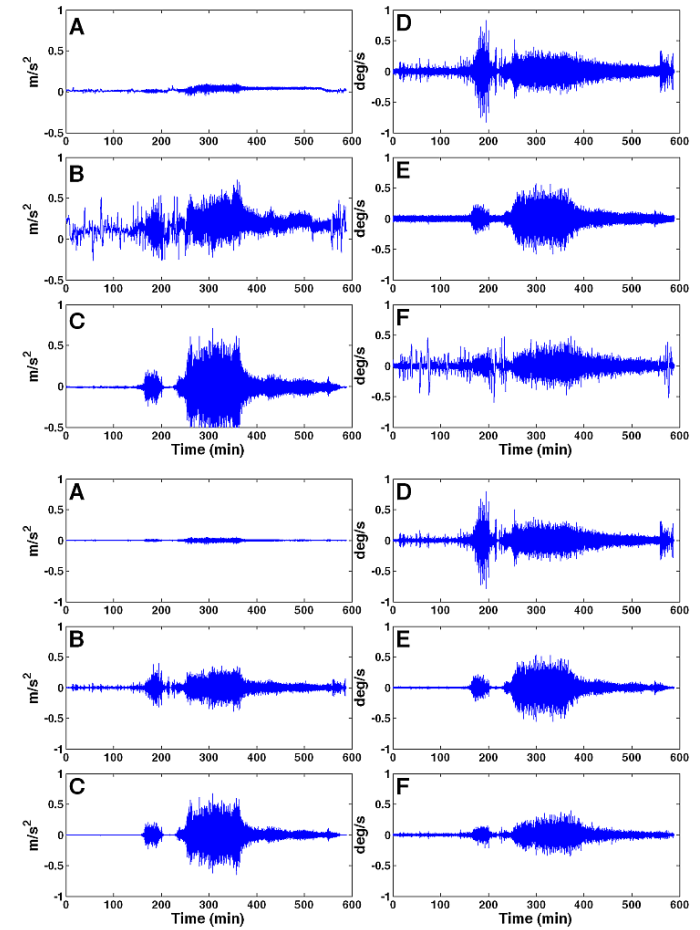


Figure B.1.7. Motion history (upper-row; lower-filtered) of MH-C at MRU position during Trip-1; linear accelerations (A) longitudinal (B) lateral (C) vertical; angular velocities (D) roll (E) pitch (F) yaw.

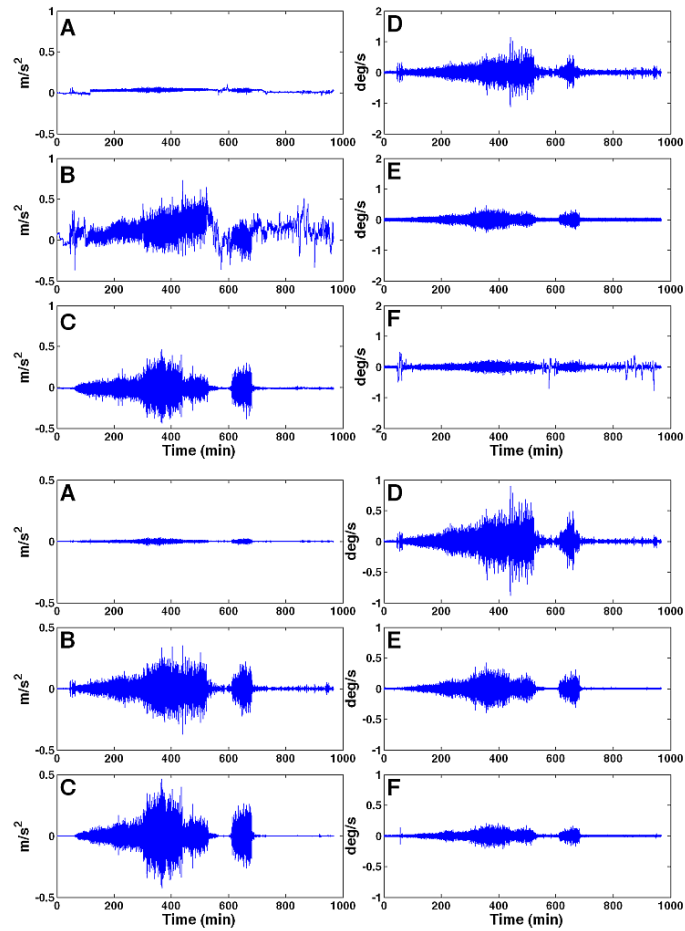


Figure B.1.8. Motion history (upper-row; lower-filtered) of MH-C at MRU position during Trip-2; linear accelerations (A) longitudinal (B) lateral (C) vertical; angular velocities (D) roll (E) pitch (F) yaw.

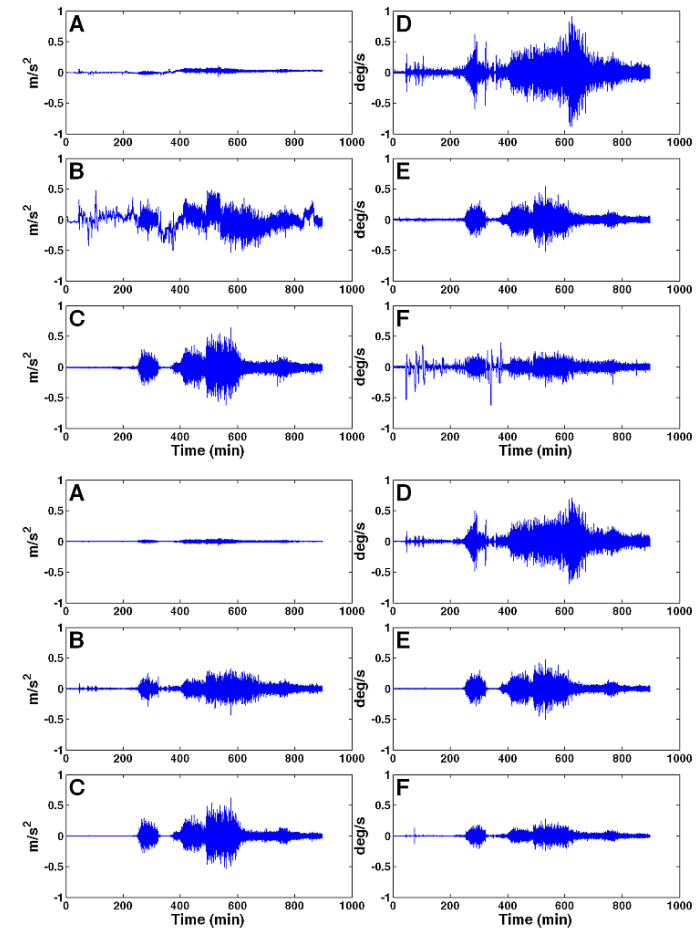


Figure B.1.9. Motion history (upper-row; lower-filtered) of MH-C at MRU position during Trip-3; linear accelerations (A) longitudinal (B) lateral (C) vertical; angular velocities (D) roll (E) pitch (F) yaw.

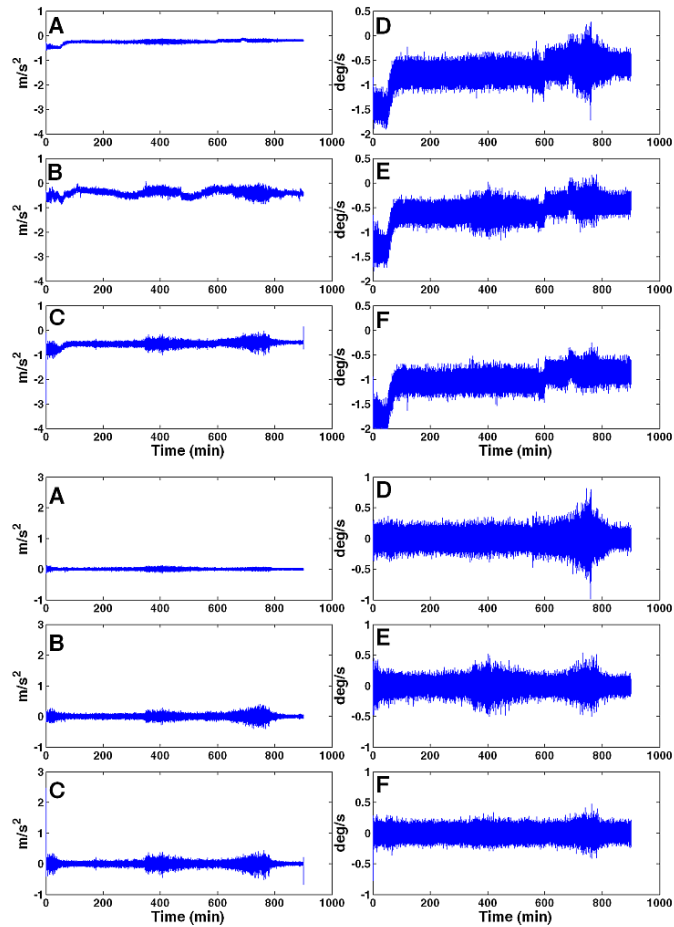


Figure B.1.10. Motion history (upper-row; lower-filtered) of MH-D at MRU position during Trip-1; linear accelerations (A) longitudinal (B) lateral (C) vertical; angular velocities (D) roll (E) pitch (F) yaw.

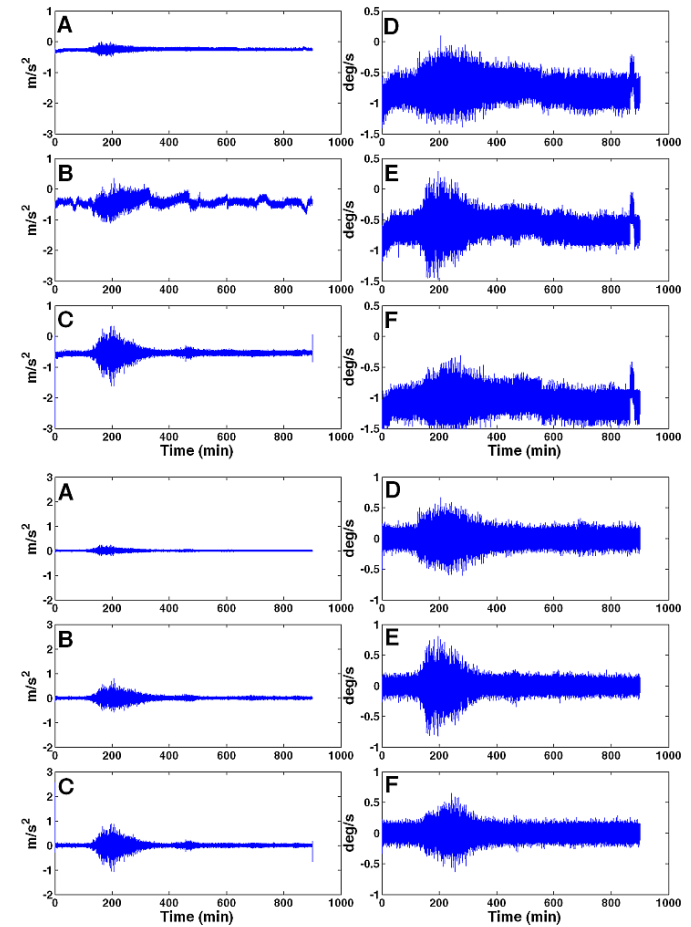


Figure B.1.11. Motion history (upper-row; lower-filtered) of MH-D at MRU position during Trip-2; linear accelerations (A) longitudinal (B) lateral (C) vertical; angular velocities (D) roll (E) pitch (F) yaw.

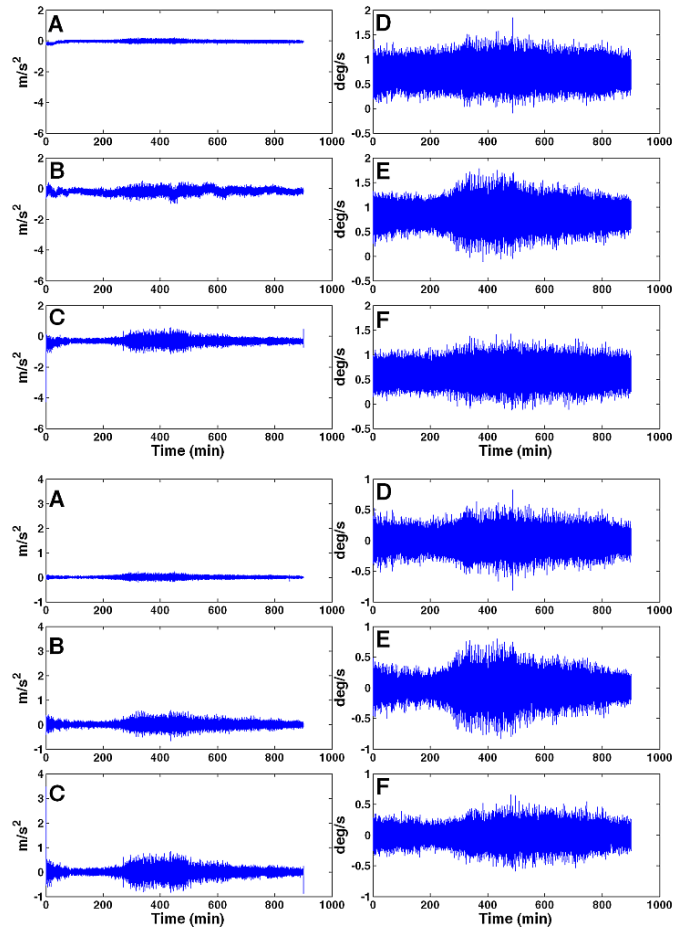


Figure B.1.12. Motion history (upper-row; lower-filtered) of MH-D at MRU position during Trip-3; linear accelerations (A) longitudinal (B) lateral (C) vertical; angular velocities (D) roll (E) pitch (F) yaw.

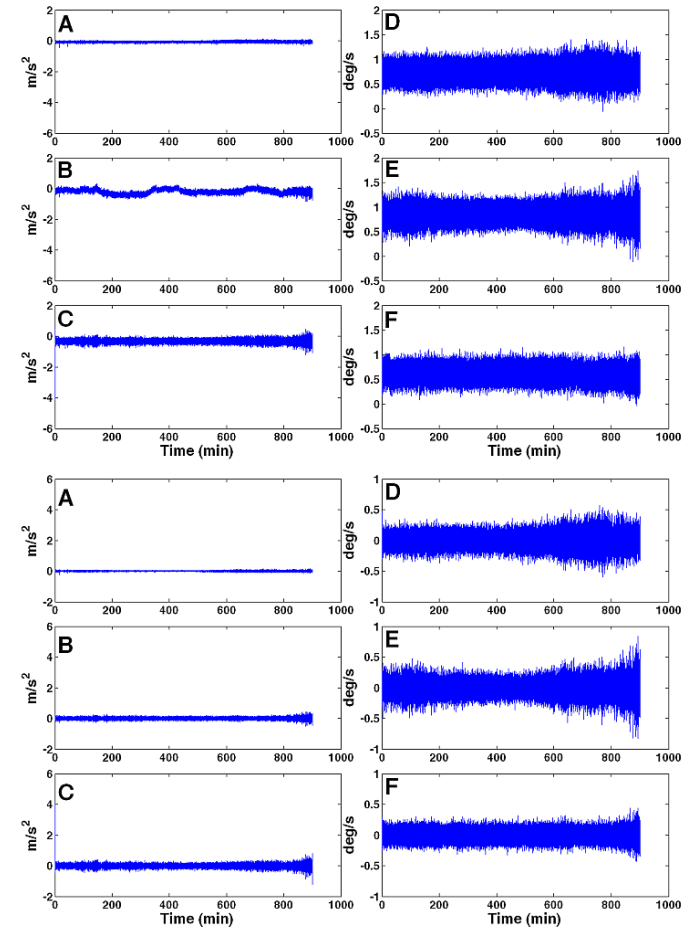


Figure B.1.13. Motion history (upper-row; lower-filtered) of MH-D at MRU position during Trip-4; linear accelerations (A) longitudinal (B) lateral (C) vertical; angular velocities (D) roll (E) pitch (F) yaw.

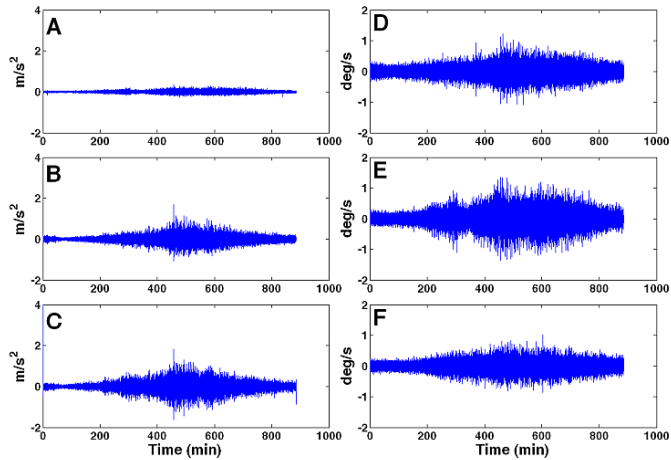
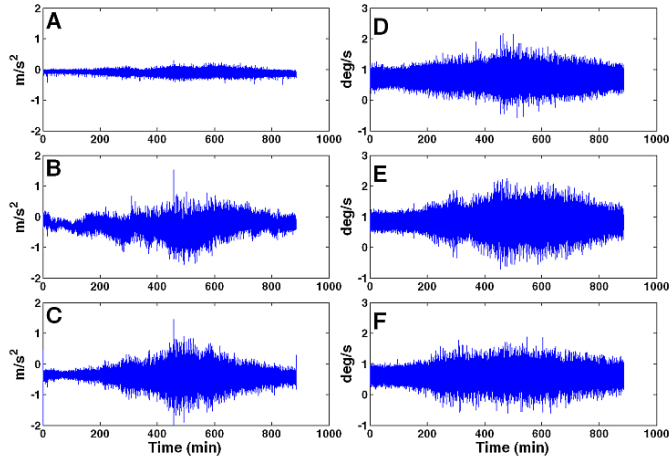


Figure B.1.14. Motion history (upper-row; lower-filtered) of MH-D at MRU position during Trip-5; linear accelerations (A) longitudinal (B) lateral (C) vertical; angular velocities (D) roll (E) pitch (F) yaw.

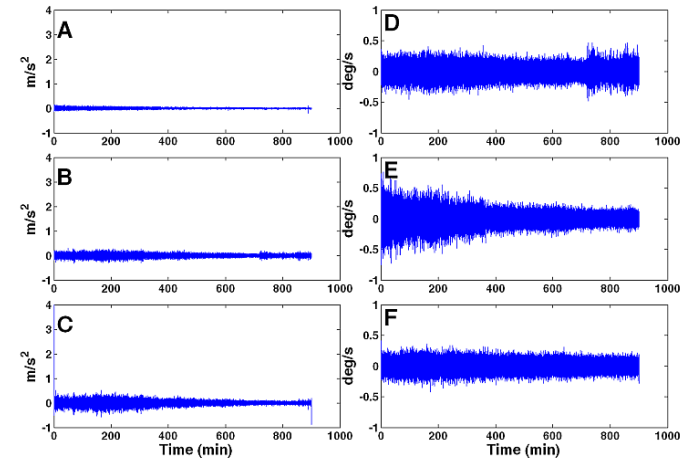
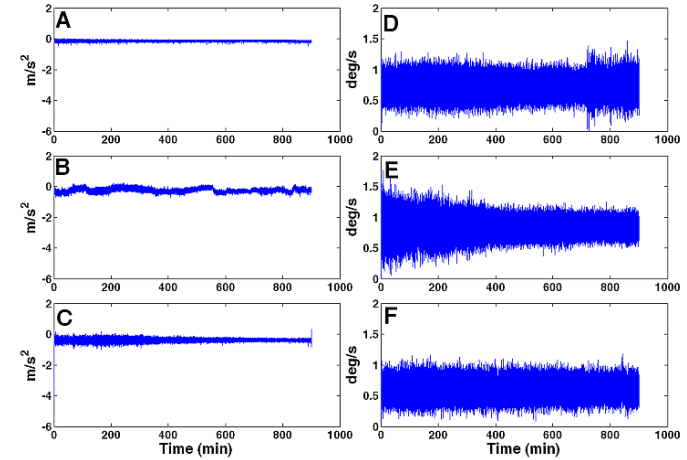


Figure B.1.15. Motion history (upper-row; lower-filtered) of MH-D at MRU position during Trip-6; linear accelerations (A) longitudinal (B) lateral (C) vertical; angular velocities (D) roll (E) pitch (F) yaw.

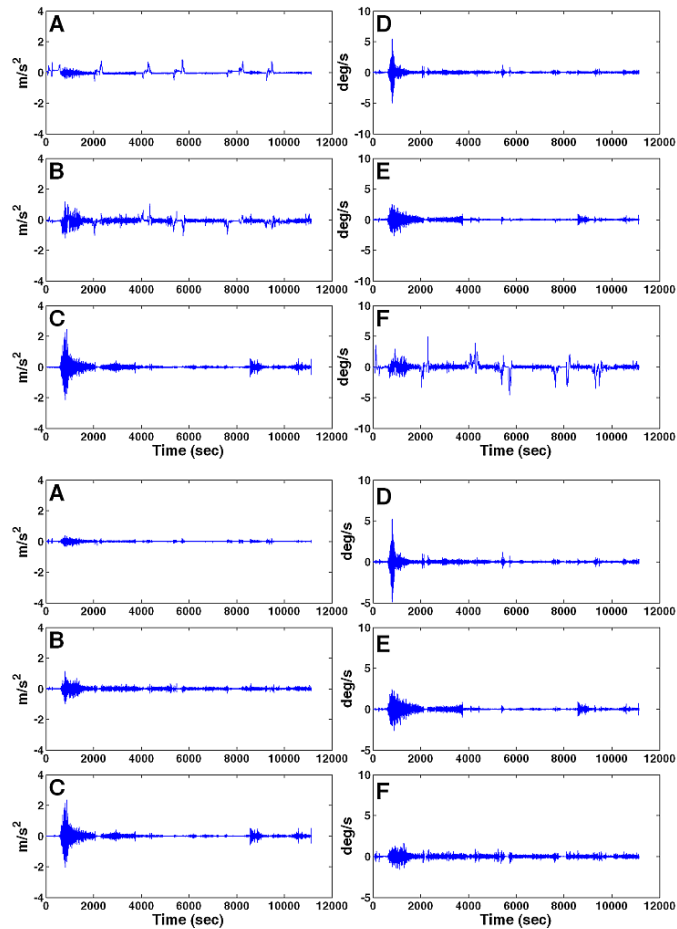


Figure B.1.16. Motion history (upper-row; lower-filtered) of Cat-E at MRU position during Trip-1; linear accelerations (A) longitudinal (B) lateral (C) vertical; angular velocities (D) roll (E) pitch (F) yaw.

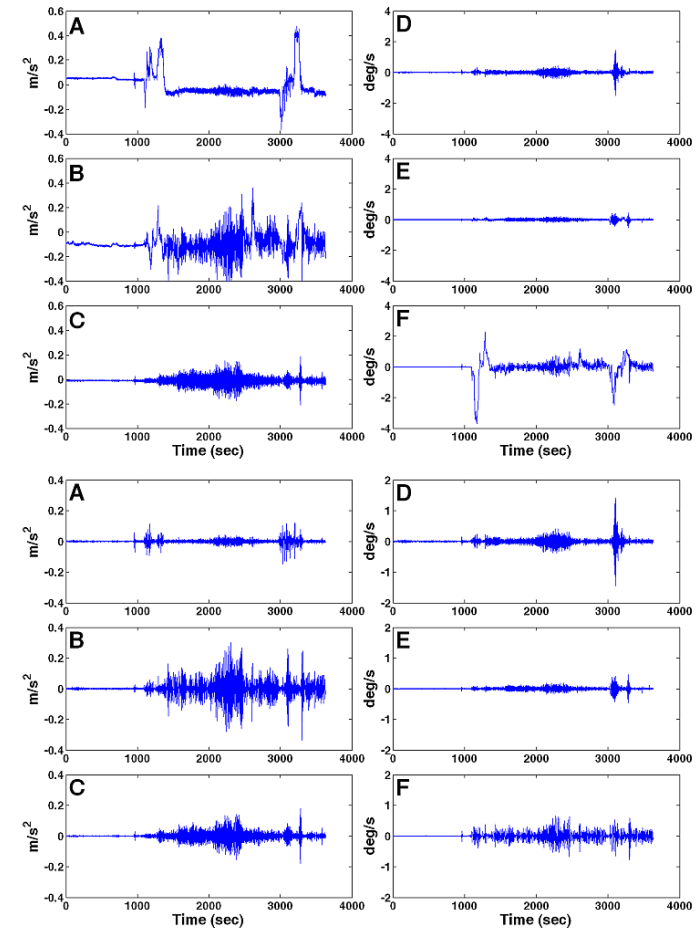


Figure B.1.17. Motion history (upper-row; lower-filtered) of Cat-E at MRU position during Trip-2; linear accelerations (A) longitudinal (B) lateral (C) vertical; angular velocities (D) roll (E) pitch (F) yaw.

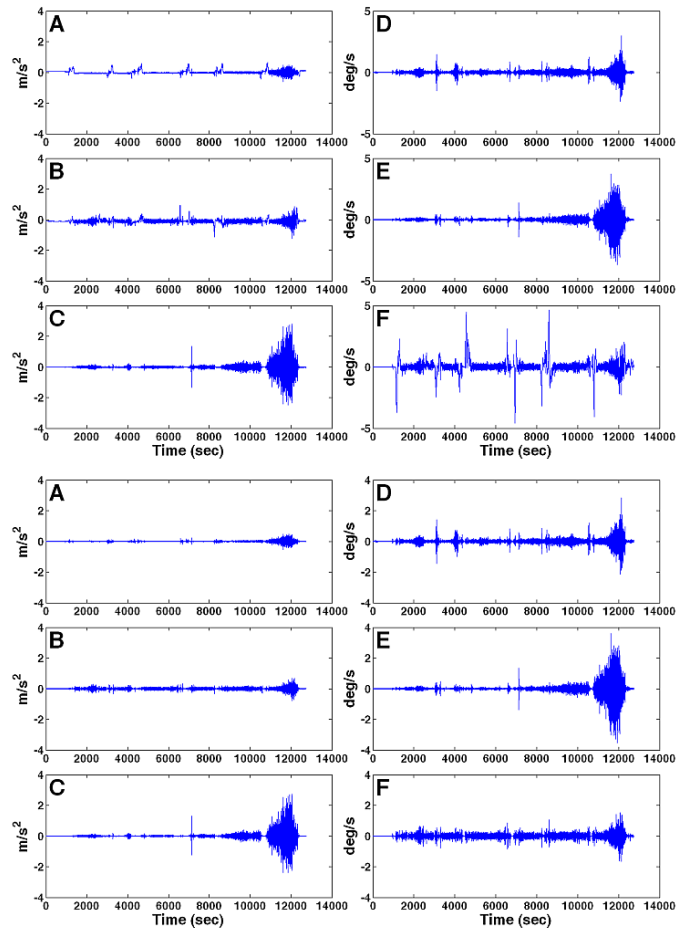


Figure B.1.18. Motion history (upper-row; lower-filtered) of Cat-E at MRU position during Trip-3; linear accelerations (A) longitudinal (B) lateral (C) vertical; angular velocities (D) roll (E) pitch (F) yaw.

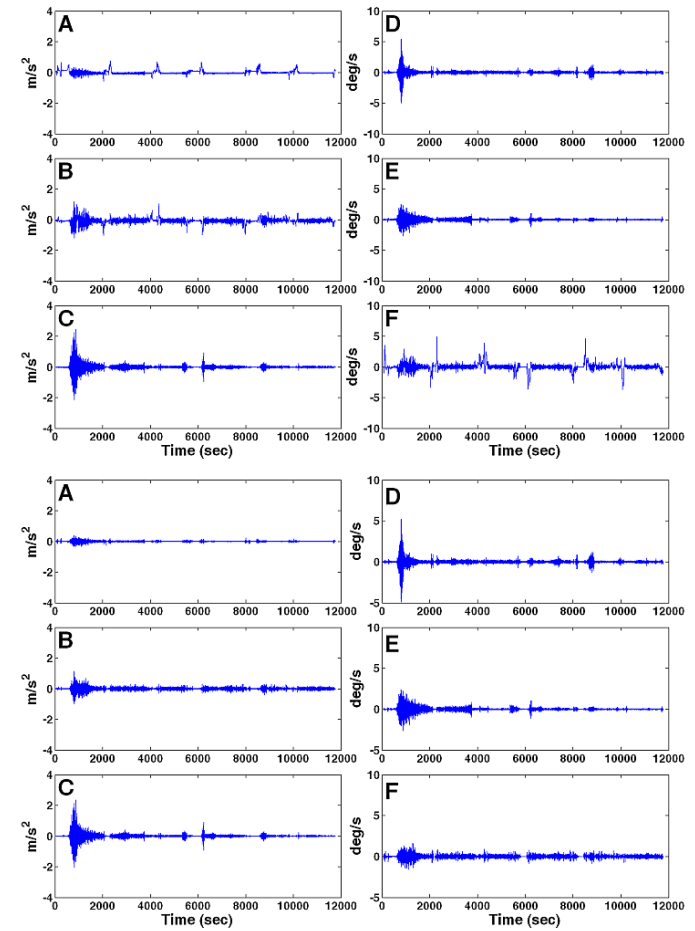


Figure B.1.19. Motion history (upper-row; lower-filtered) of Cat-E at MRU position during Trip-4; linear accelerations (A) longitudinal (B) lateral (C) vertical; angular velocities (D) roll (E) pitch (F) yaw.

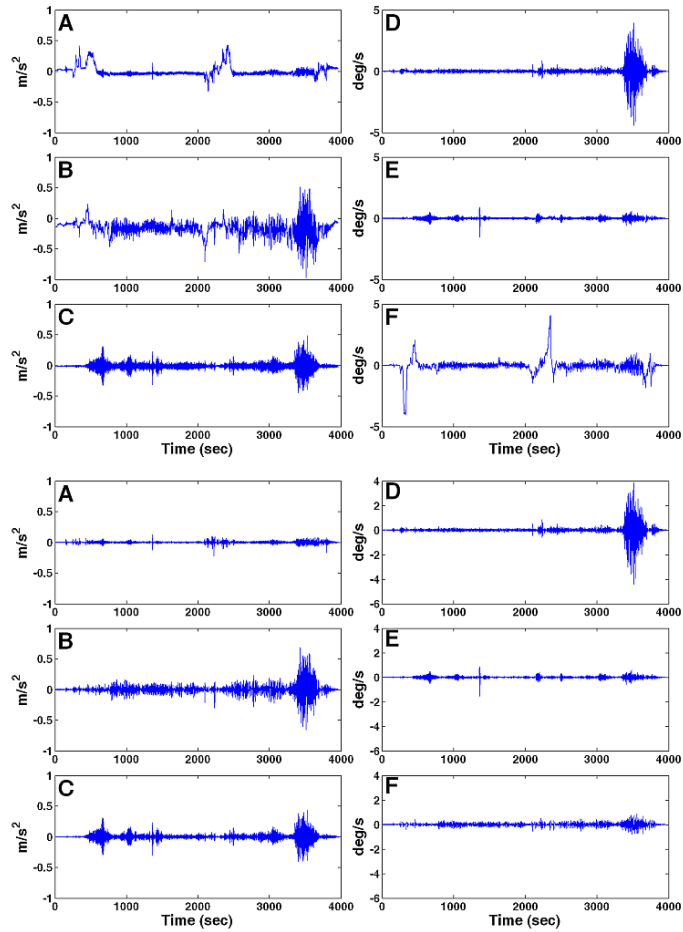


Figure B.1.20. Motion history (upper-row; lower-filtered) of Cat-E at MRU position during Trip-5; linear accelerations (A) longitudinal (B) lateral (C) vertical; angular velocities (D) roll (E) pitch (F) yaw.

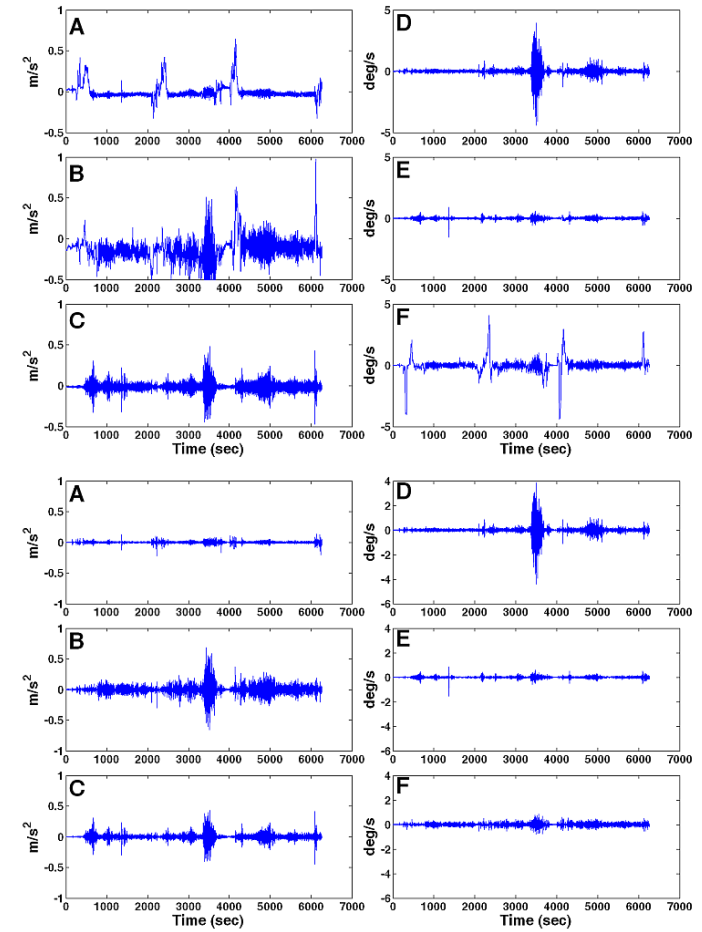


Figure B.1.21. Motion history (upper-row; lower-filtered) of Cat-E at MRU position during Trip-6; linear accelerations (A) longitudinal (B) lateral (C) vertical; angular velocities (D) roll (E) pitch (F) yaw.

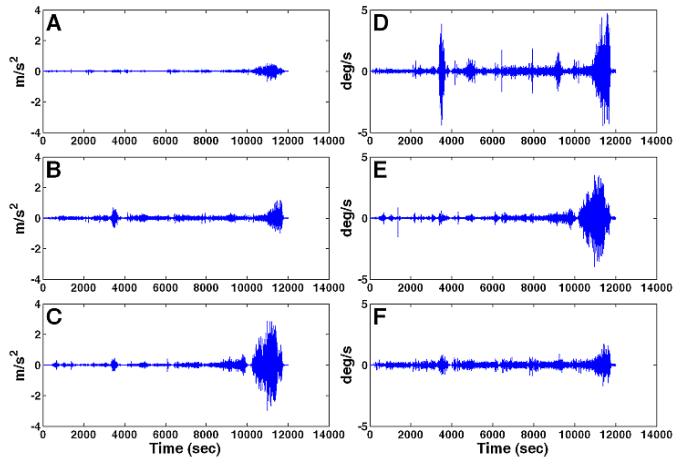
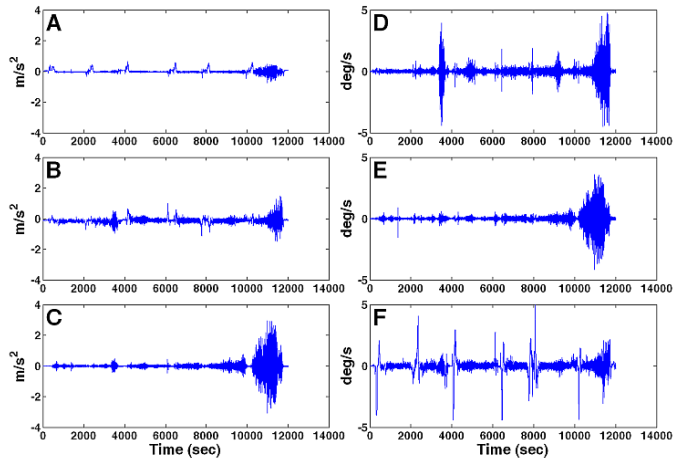


Figure B.1.22. Motion history (upper-row; lower-filtered) of Cat-E at MRU position during Trip-7; linear accelerations (A) longitudinal (B) lateral (C) vertical; angular velocities (D) roll (E) pitch (F) yaw.

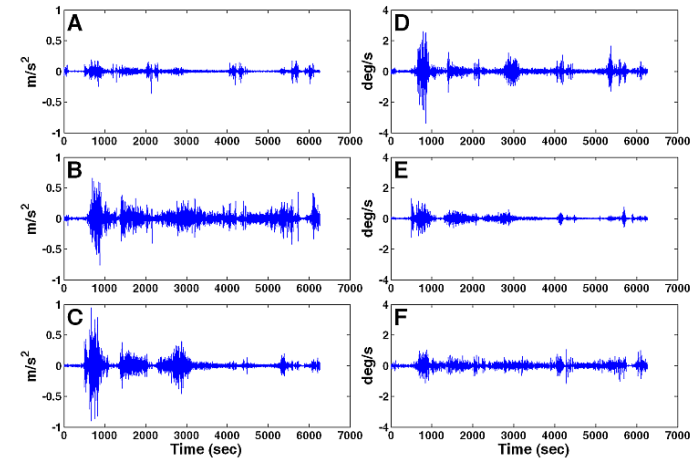
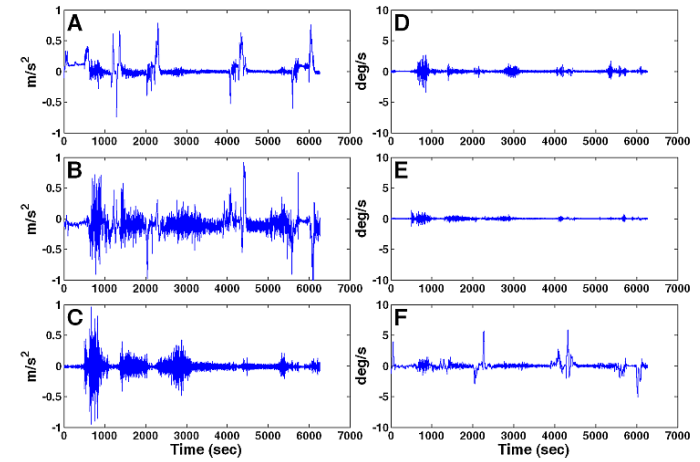


Figure B.1.23. Motion history (upper-row; lower-filtered) of Cat-E at MRU position during Trip-8; linear accelerations (A) longitudinal (B) lateral (C) vertical; angular velocities (D) roll (E) pitch (F) yaw.

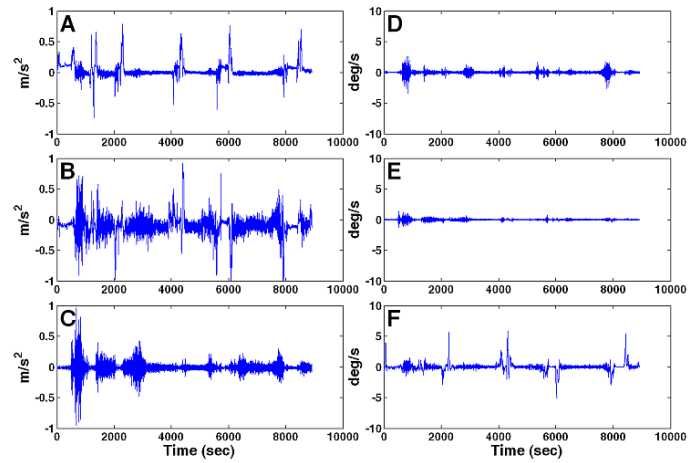


Figure B.1.24. Motion history (upper-row; lower-filtered) of Cat-E at MRU position during Trip-9; linear accelerations (A) longitudinal (B) lateral (C) vertical; angular velocities (D) roll (E) pitch (F) yaw.

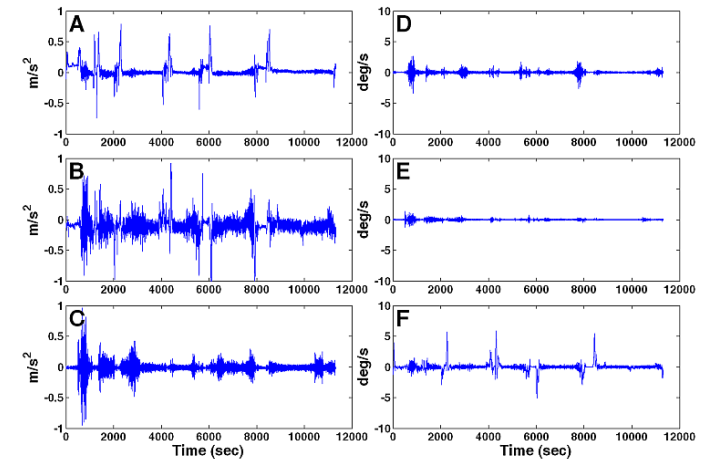


Figure B.1.25. Motion history (upper-row; lower-filtered) of Cat-E at MRU position during Trip-10; linear accelerations (A) longitudinal (B) lateral (C) vertical; angular velocities (D) roll (E) pitch (F) yaw.

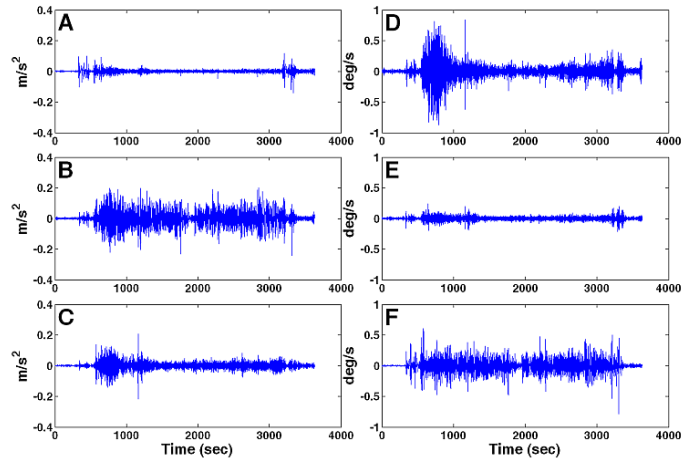
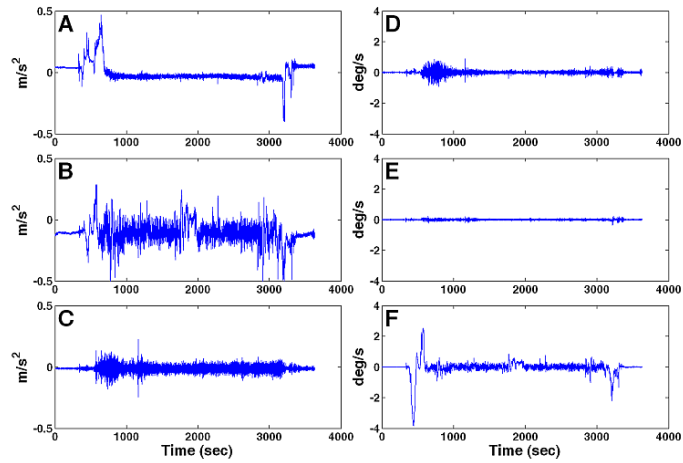


Figure B.1.26. Motion history (upper-row; lower-filtered) of Cat-E at MRU position during Trip-11; linear accelerations (A) longitudinal (B) lateral (C) vertical; angular velocities (D) roll (E) pitch (F) yaw.

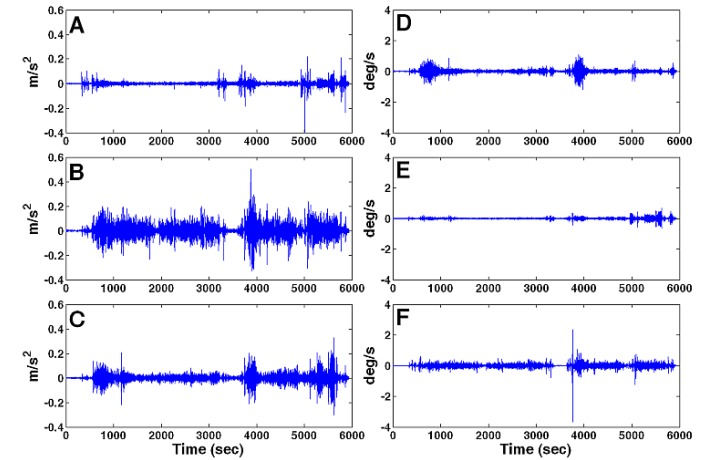
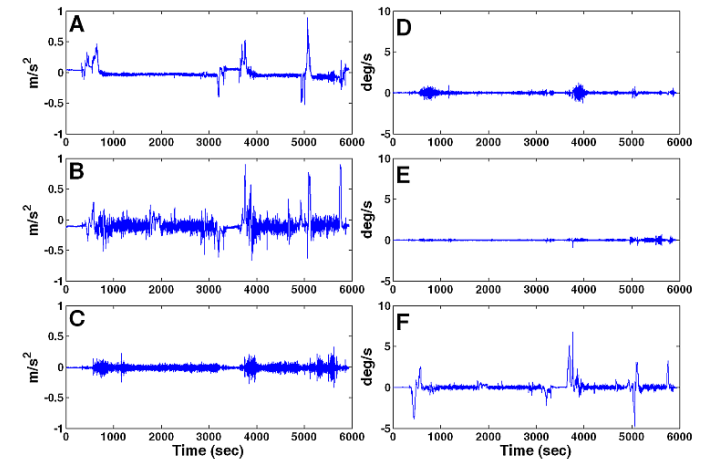


Figure B.1.27. Motion history (upper-row; lower-filtered) of Cat-E at MRU position during Trip-12; linear accelerations (A) longitudinal (B) lateral (C) vertical; angular velocities (D) roll (E) pitch (F) yaw.

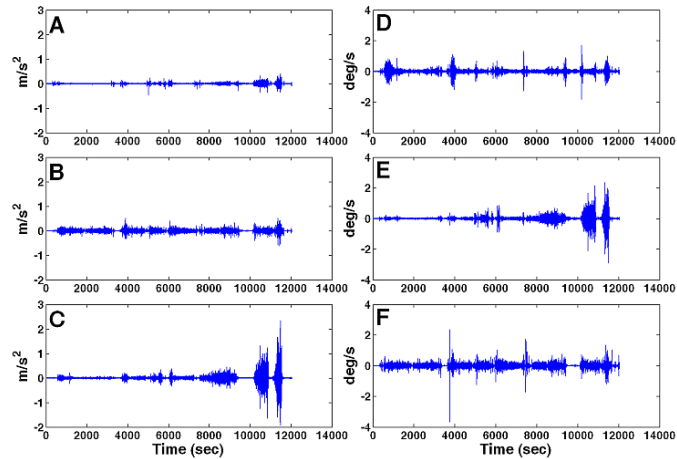
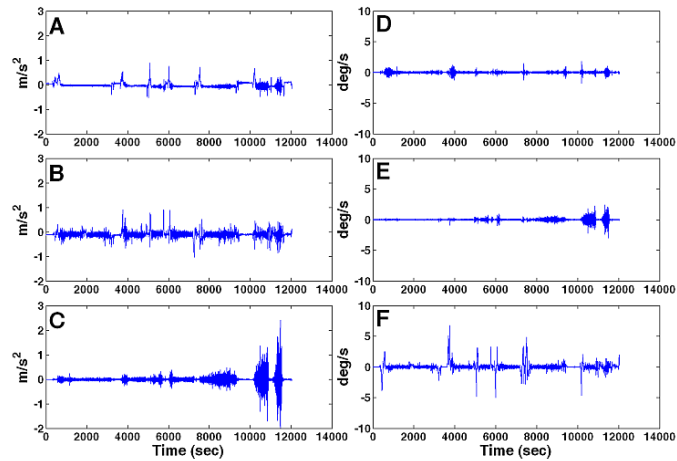


Figure B.1.28. Motion history (upper-row; lower-filtered) of Cat-E at MRU position during Trip-13; linear accelerations (A) longitudinal (B) lateral (C) vertical; angular velocities (D) roll (E) pitch (F) yaw.

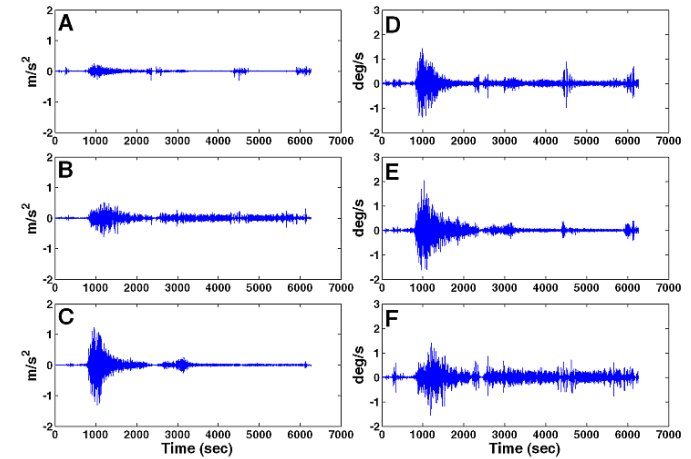
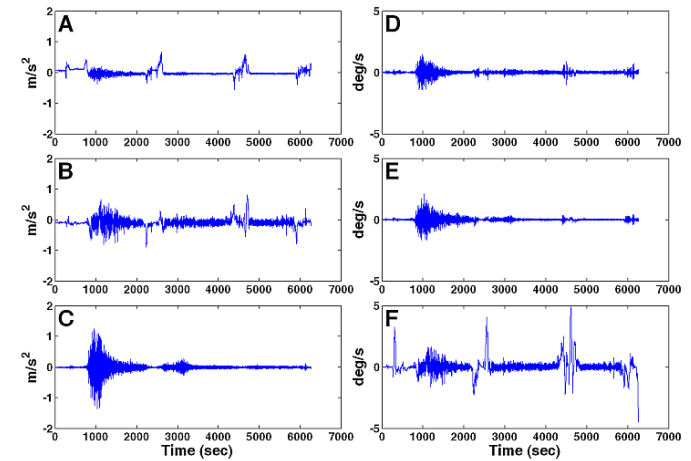


Figure B.1.29. Motion history (upper-row; lower-filtered) of Cat-E at MRU position during Trip-14; linear accelerations (A) longitudinal (B) lateral (C) vertical; angular velocities (D) roll (E) pitch (F) yaw.

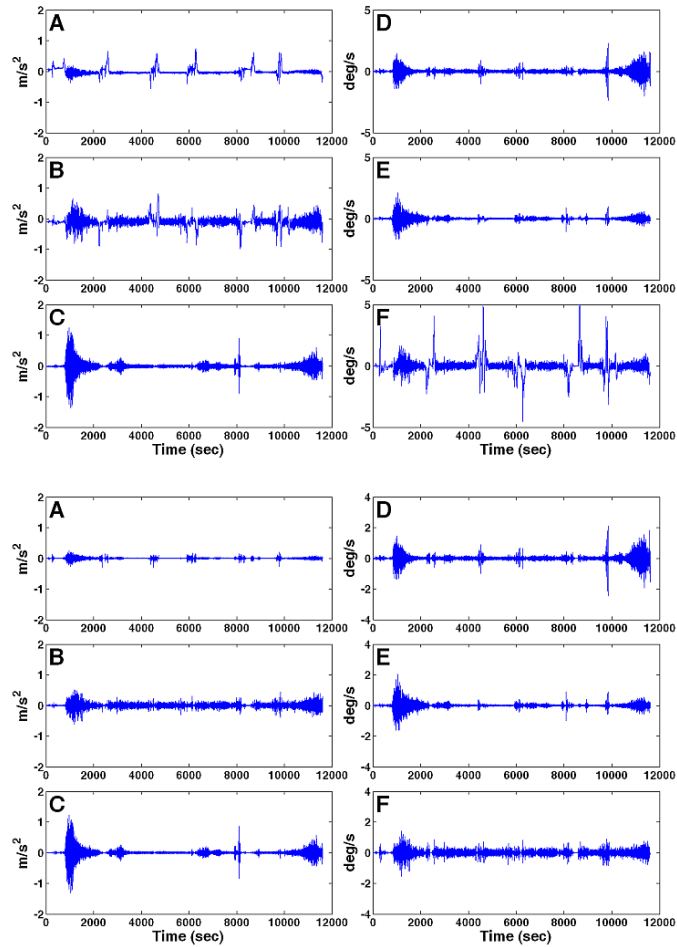


Figure B.1.30. Motion history (upper-row; lower-filtered) of Cat-E at MRU position during Trip-15; linear accelerations (A) longitudinal (B) lateral (C) vertical; angular velocities (D) roll (E) pitch (F) yaw.

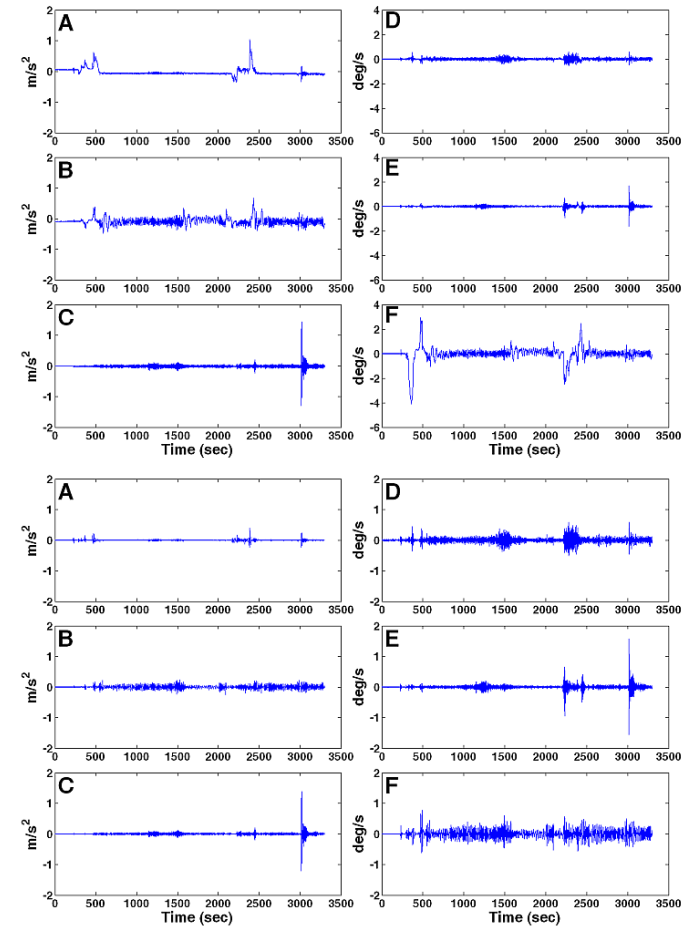


Figure B.1.31. Motion history (upper-row; lower-filtered) of Cat-E at MRU position during Trip-16; linear accelerations (A) longitudinal (B) lateral (C) vertical; angular velocities (D) roll (E) pitch (F) yaw.

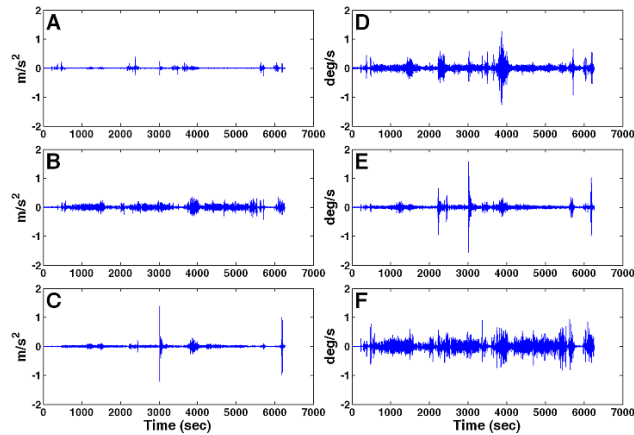
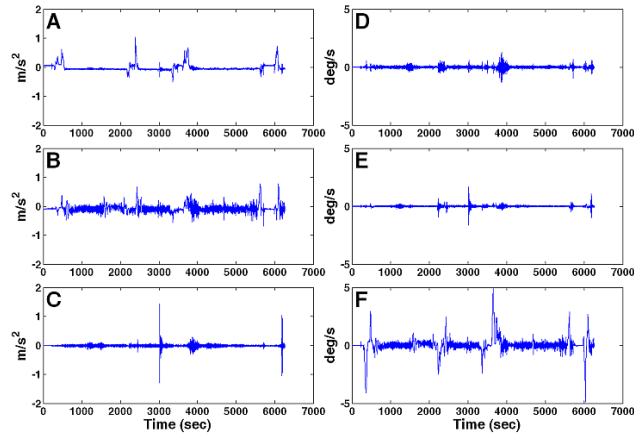


Figure B.1.32. Motion history (upper-row; lower-filtered) of Cat-E at MRU position during Trip-17; linear accelerations (A) longitudinal (B) lateral (C) vertical; angular velocities (D) roll (E) pitch (F) yaw.

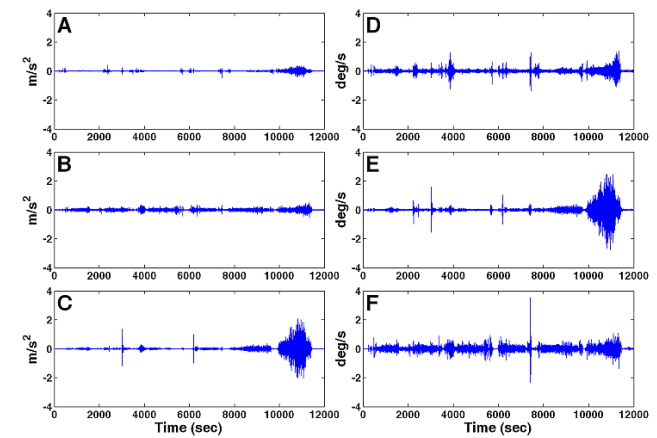
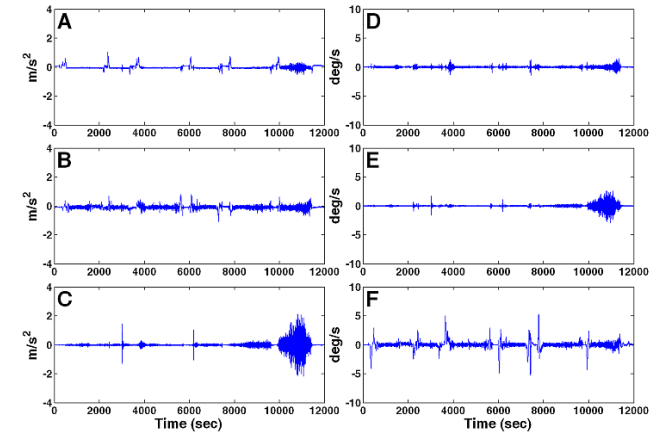


Figure B.1.33. Motion history (upper-row; lower-filtered) of Cat-E at MRU position during Trip-18; linear accelerations (A) longitudinal (B) lateral (C) vertical; angular velocities (D) roll (E) pitch (F) yaw.

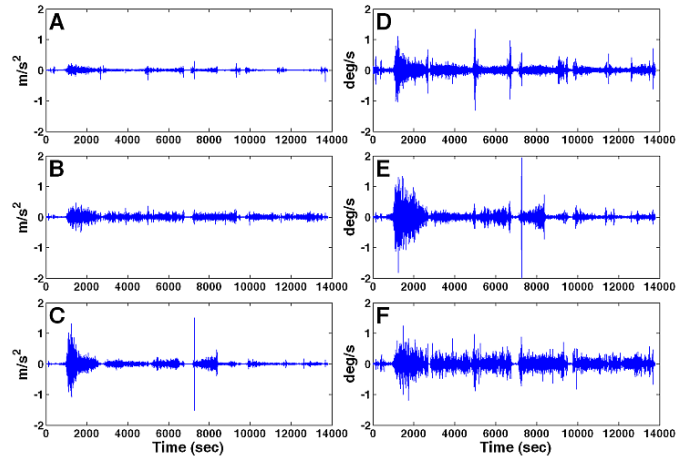
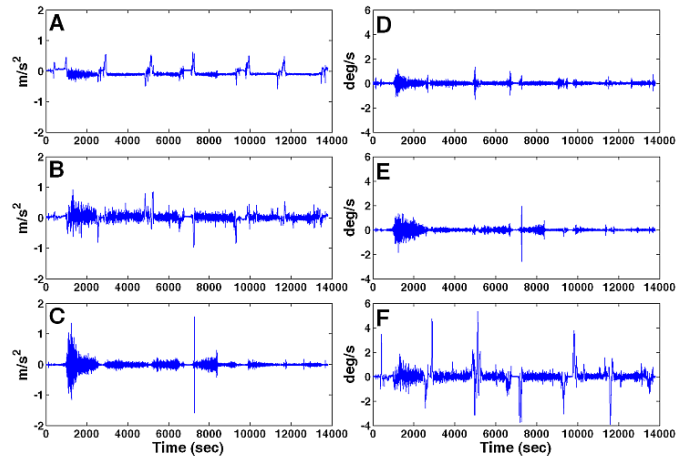


Figure B.1.34. Motion history (upper-row; lower-filtered) of Cat-E at MRU position during Trip-19; linear accelerations (A) longitudinal (B) lateral (C) vertical; angular velocities (D) roll (E) pitch (F) yaw.

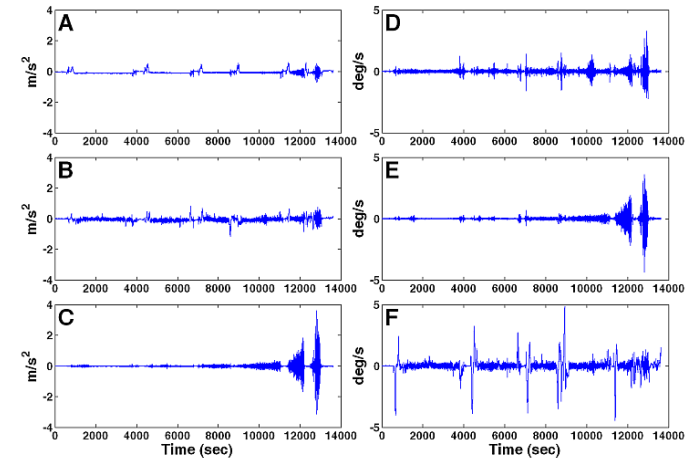


Figure B.1.35. Motion history (upper-row; lower-filtered) of Cat-E at MRU position during Trip-20; linear accelerations (A) longitudinal (B) lateral (C) vertical; angular velocities (D) roll (E) pitch (F) yaw.

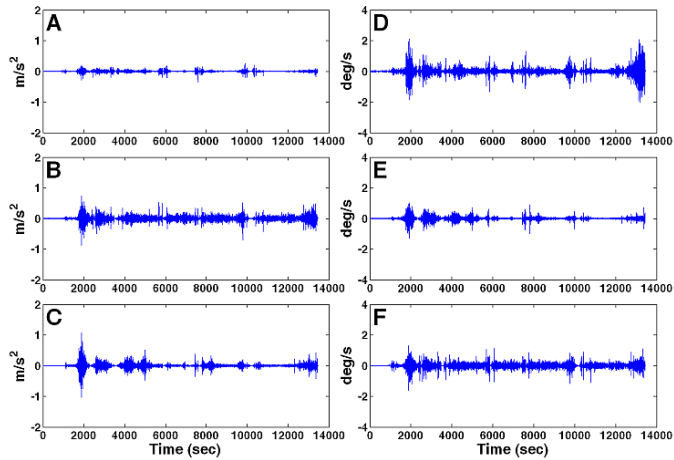
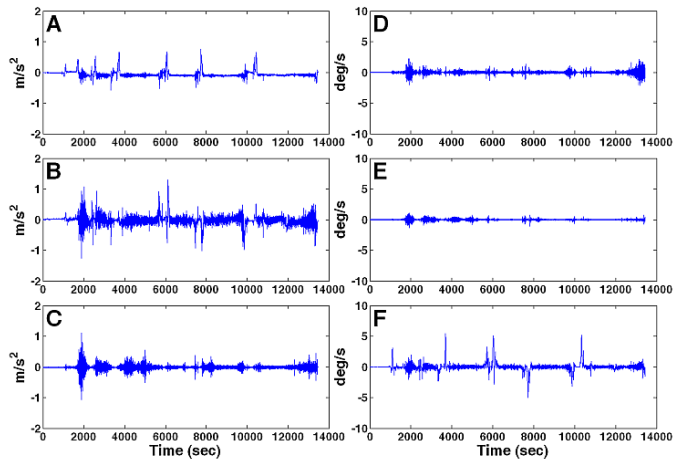


Figure B.1.36. Motion history (upper-row; lower-filtered) of Cat-E at MRU position during Trip-21; linear accelerations (A) longitudinal (B) lateral (C) vertical; angular velocities (D) roll (E) pitch (F) yaw.

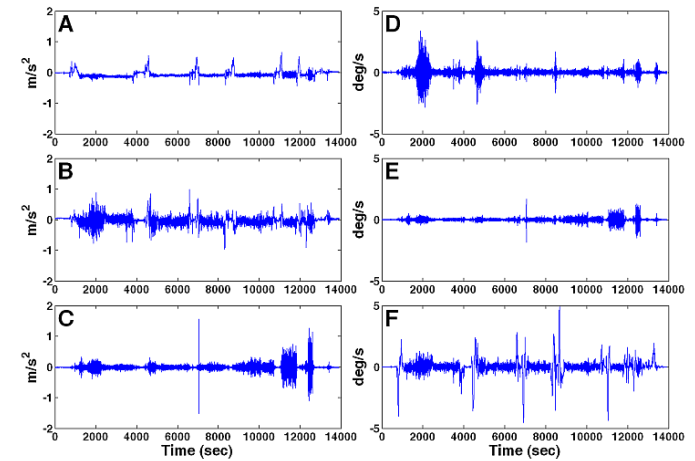


Figure B.1.37. Motion history (upper-row; lower-filtered) of Cat-E at MRU position during Trip-22; linear accelerations (A) longitudinal (B) lateral (C) vertical; angular velocities (D) roll (E) pitch (F) yaw.

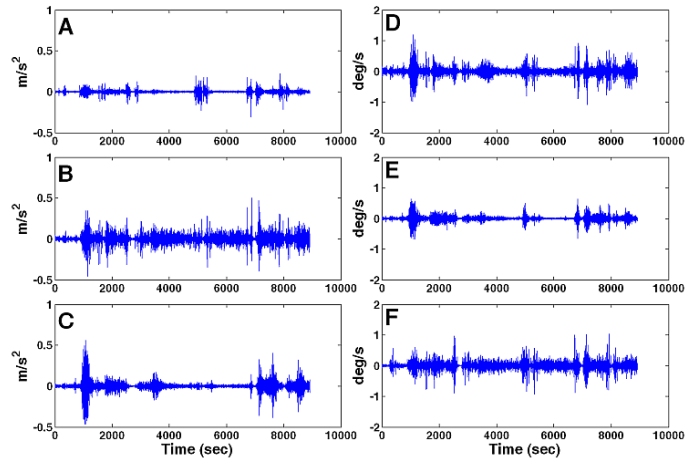
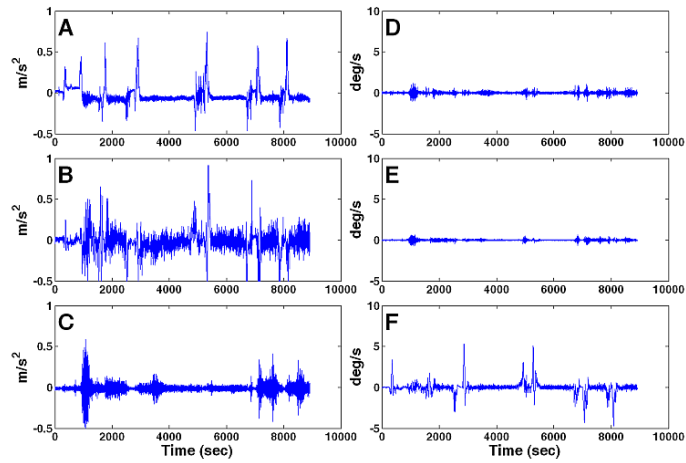


Figure B.1.38. Motion history (upper-row; lower-filtered) of Cat-E at MRU position during Trip-23; linear accelerations (A) longitudinal (B) lateral (C) vertical; angular velocities (D) roll (E) pitch (F) yaw.

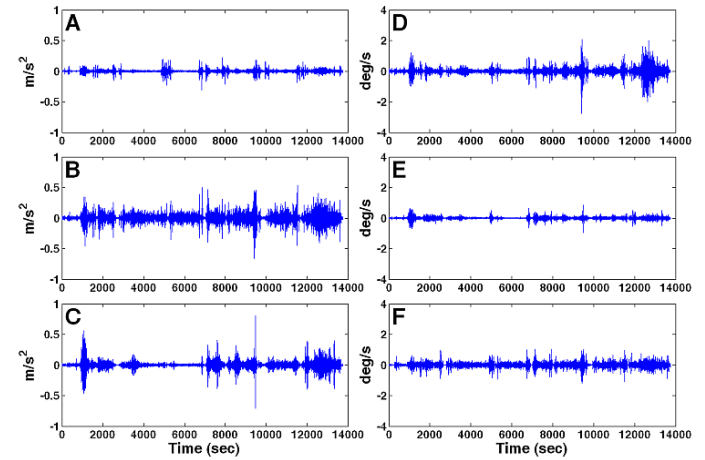
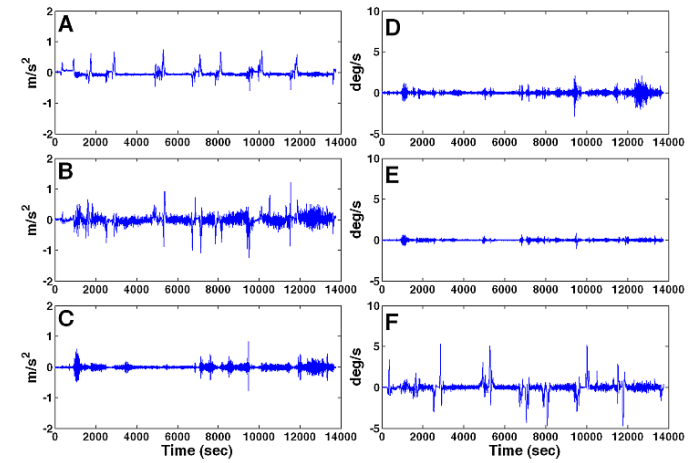


Figure B.1.39. Motion history (upper-row; lower-filtered) of Cat-E at MRU position during Trip-24; linear accelerations (A) longitudinal (B) lateral (C) vertical; angular velocities (D) roll (E) pitch (F) yaw.

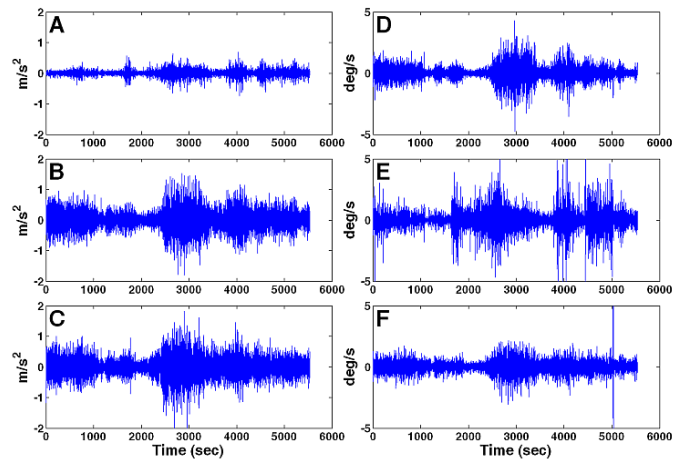
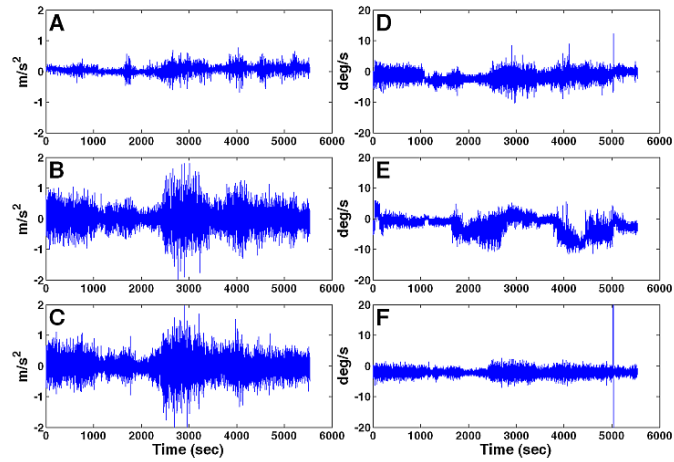


Figure B.1.40. Motion history (upper-row; lower-filtered) of Cat-F at MRU position during Trip-1; linear accelerations (A) longitudinal (B) lateral (C) vertical; angular velocities (D) roll (E) pitch (F) yaw.

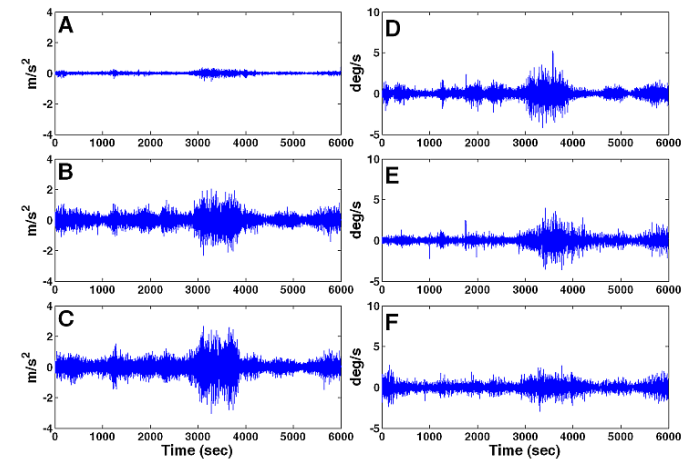
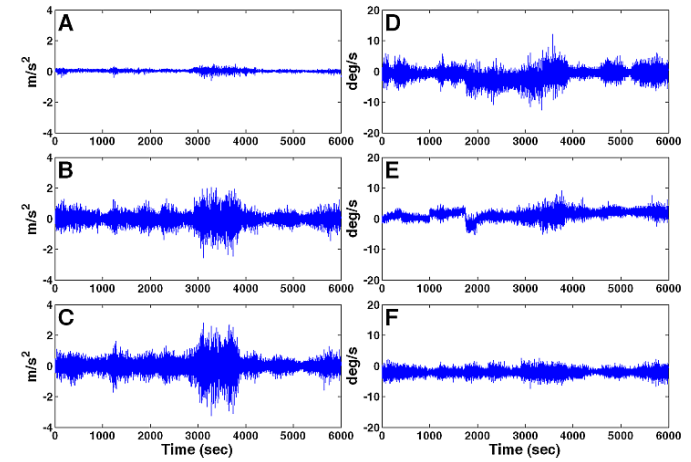


Figure B.1.41. Motion history (upper-row; lower-filtered) of Cat-F at MRU position during Trip-2; linear accelerations (A) longitudinal (B) lateral (C) vertical; angular velocities (D) roll (E) pitch (F) yaw.

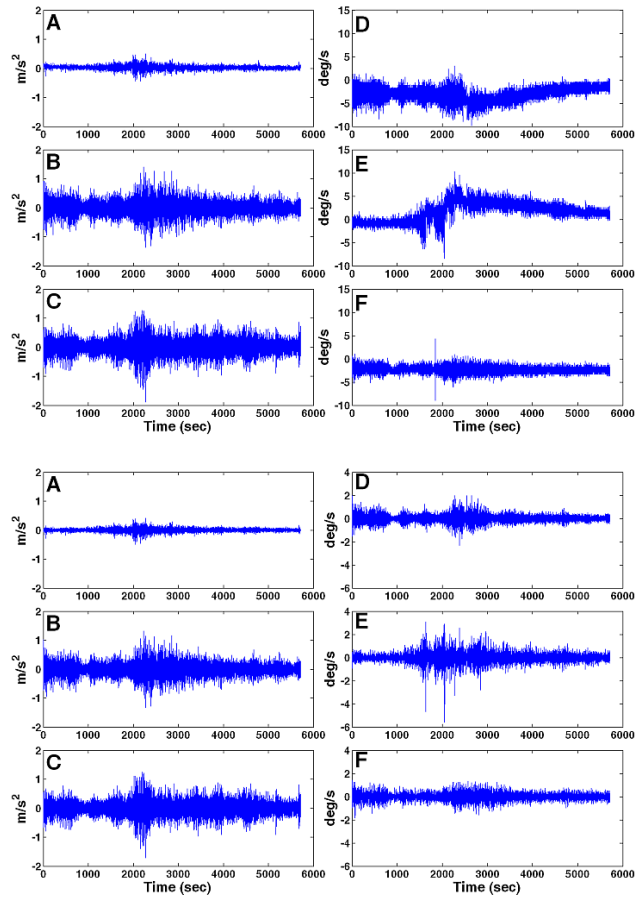


Figure B.1.42. Motion history (upper-row; lower-filtered) of Cat-F at MRU position during Trip-3; linear accelerations (A) longitudinal (B) lateral (C) vertical; angular velocities (D) roll (E) pitch (F) yaw.

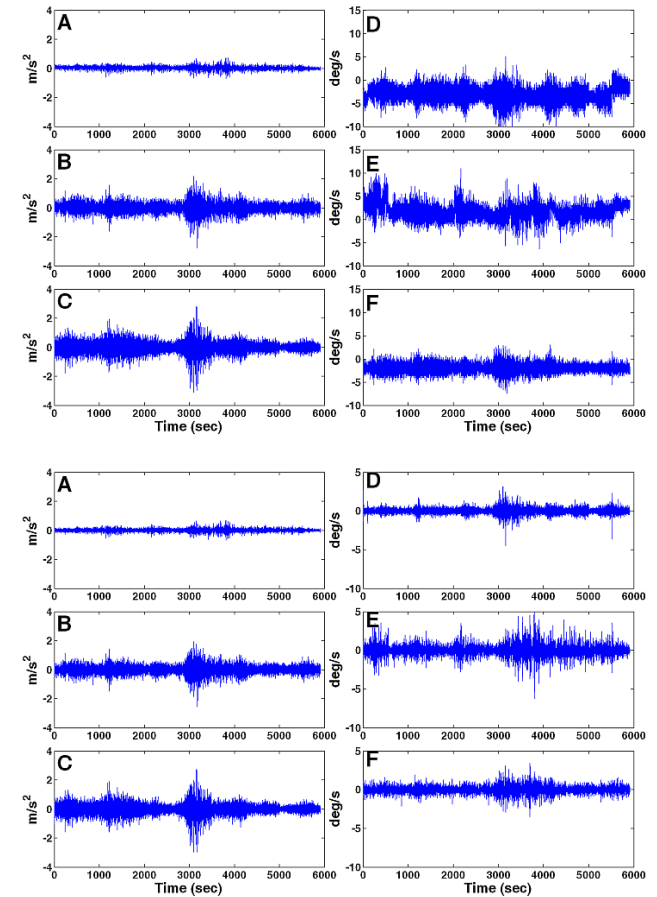


Figure B.1.43. Motion history (upper-row; lower-filtered) of Cat-F at MRU position during Trip-4; linear accelerations (A) longitudinal (B) lateral (C) vertical; angular velocities (D) roll (E) pitch (F) yaw

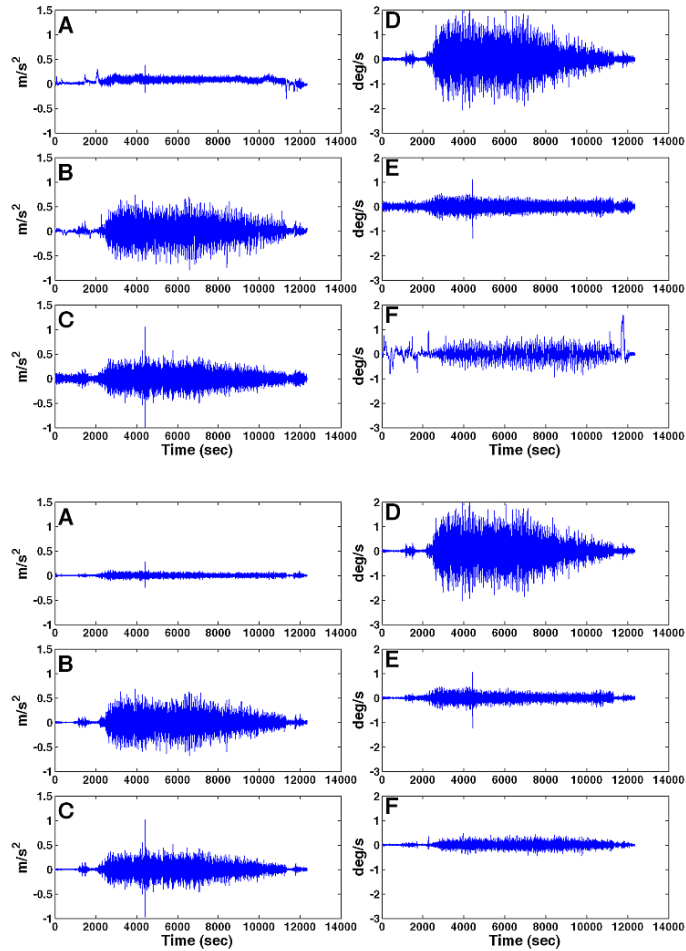


Figure B.1.44. Motion history (upper-row; lower-filtered) of WP-H at MRU position during Trip-1; linear accelerations (A) longitudinal (B) lateral (C) vertical; angular velocities (D) roll (E) pitch (F) yaw.

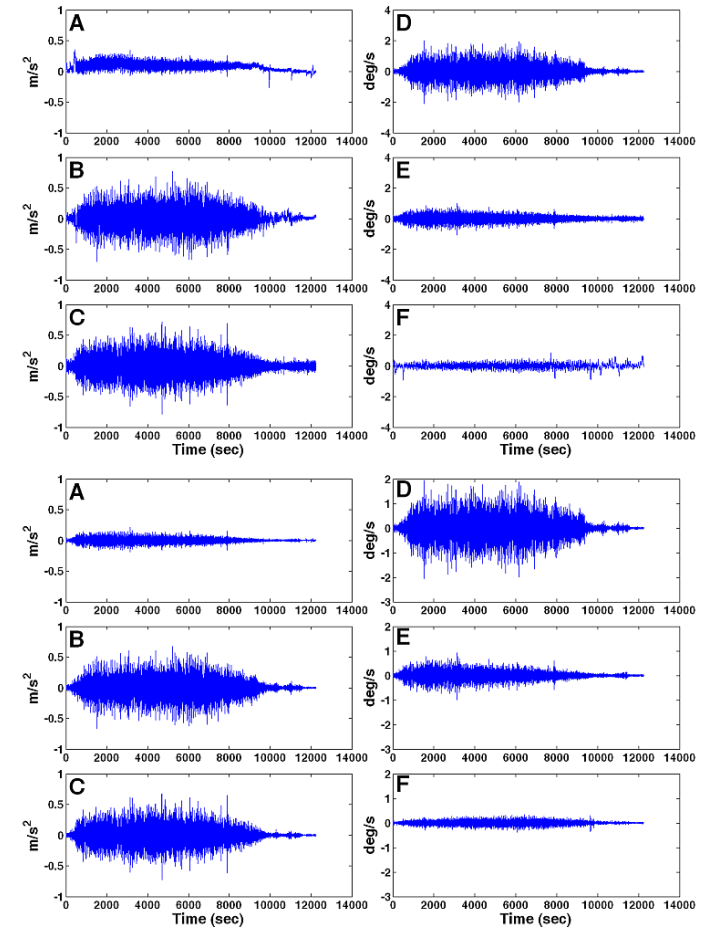


Figure B.1.45. Motion history (upper-row; lower-filtered) of WP-H at MRU position during Trip-2; linear accelerations (A) longitudinal (B) lateral (C) vertical; angular velocities (D) roll (E) pitch (F) yaw.

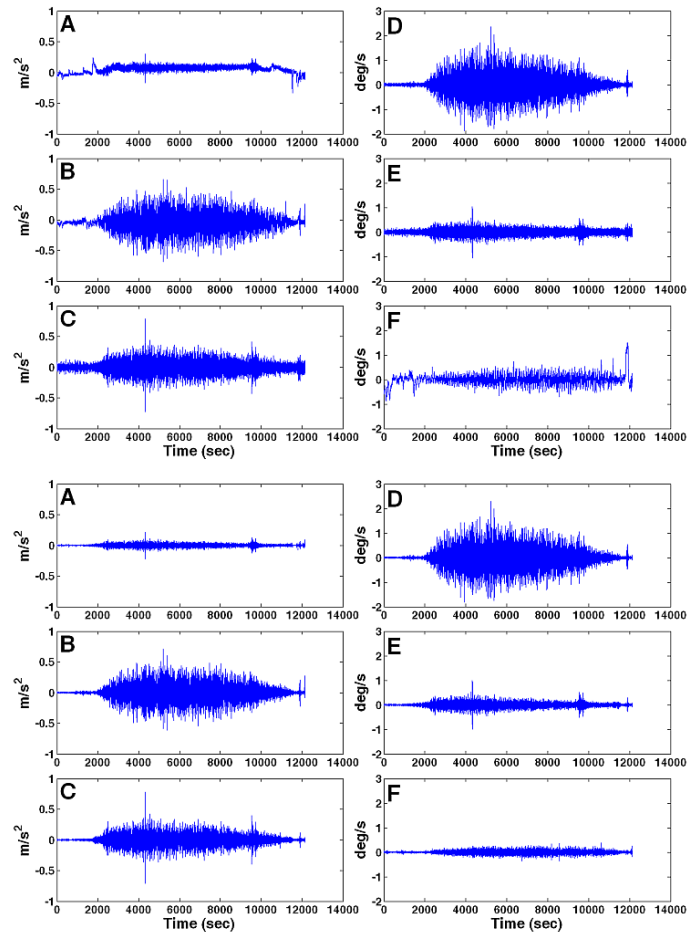


Figure B.1.46. Motion history (upper-row; lower-filtered) of WP-H at MRU position during Trip-3; linear accelerations (A) longitudinal (B) lateral (C) vertical; angular velocities (D) roll (E) pitch (F) yaw.

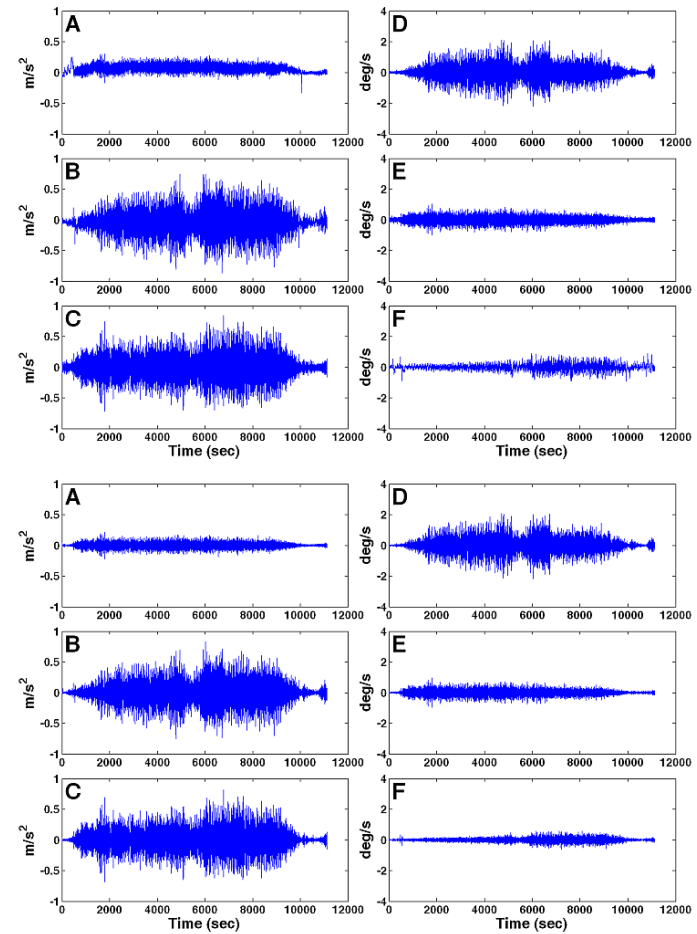


Figure B.1.47. Motion history (upper-row; lower-filtered) of WP-H at MRU position during Trip-4; linear accelerations (A) longitudinal (B) lateral (C) vertical; angular velocities (D) roll (E) pitch (F) yaw.

B.2 Passenger Zones Layout

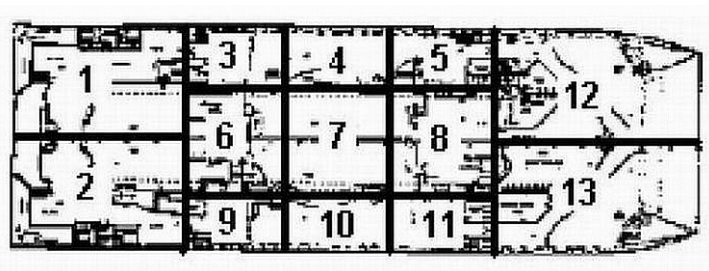
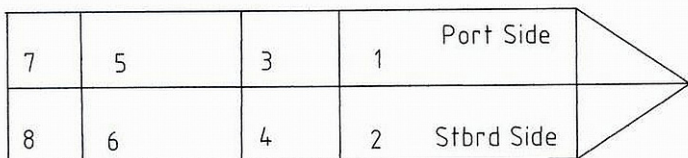
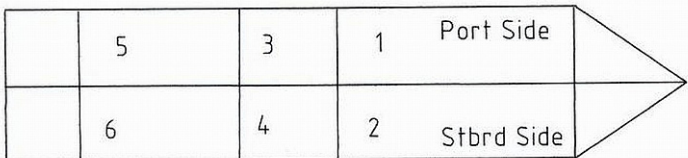


Figure B.2.1: Passenger zones layout of Cat-A



A Deck



B Deck

Figure B.2.2: Passenger zones layout of DV-B

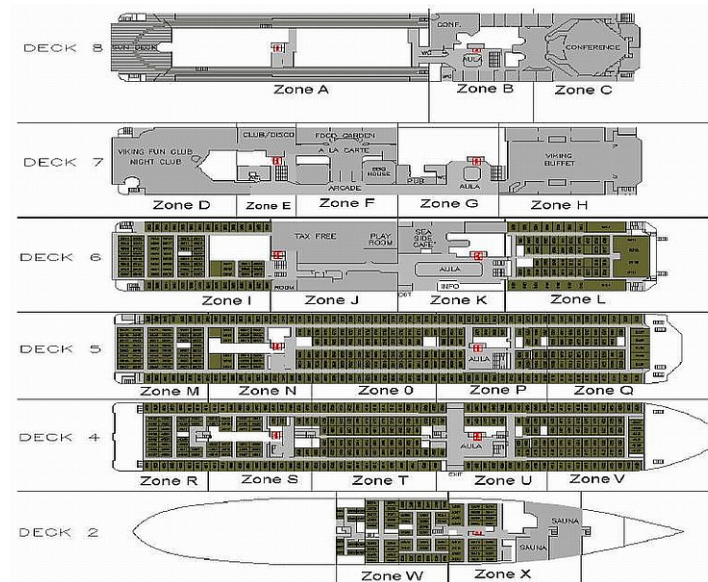


Figure B.2.3: Passenger zones layout of MH-C

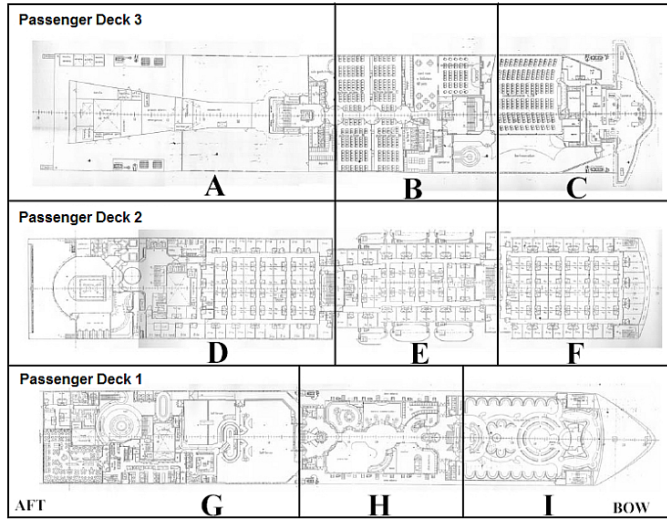


Figure B.2.4: Passenger zones layout of MH-D

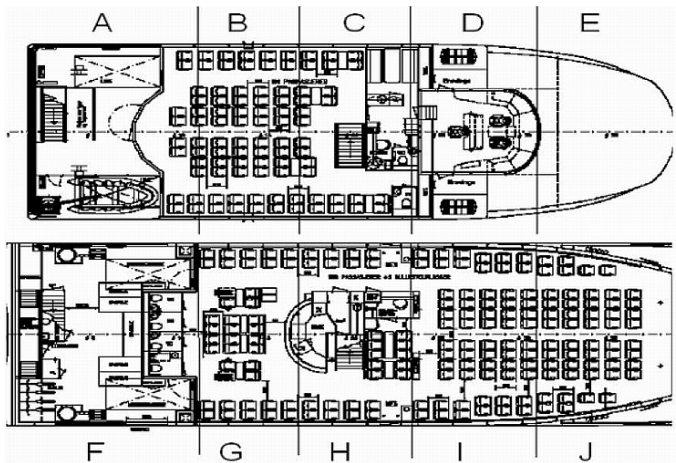


Figure B.2.5: Passenger zones layout of Cat-E

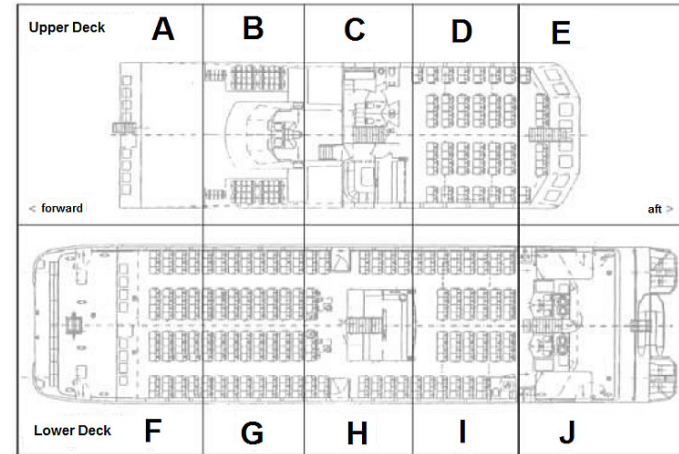


Figure B.2.6: Passenger zones layout of Cat-F

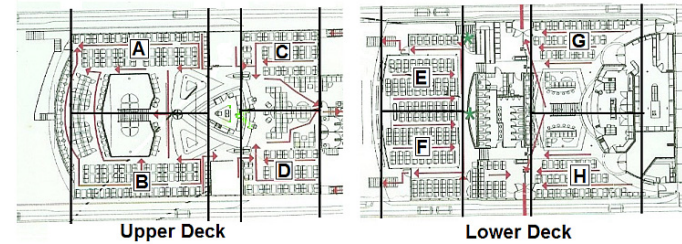


Figure B.2.7: Passenger zones layout of WP-H

B.3 Passenger Zones Position Vectors

Table B.3.1. Relative position vectors \mathbf{r} (meters) of Cat-A's passenger zones.

Zone	r_x	r_y	r_z
1	-88.0	-11.5	6.8
2	-88.0	17.9	6.8
3	-66.0	-11.5	6.8
4	-45.0	-11.5	6.8
5	-23.0	-11.5	6.8
6	-66.0	3.2	6.8
7	-45.0	3.2	6.8
8	-23.0	3.2	6.8
9	-66.0	17.9	6.8
10	-45.0	17.9	6.8
11	-23.0	17.9	6.8
12	-2.0	-8.8	6.8
13	-2.0	15.2	6.8

Table B.3.2. Relative position vectors \mathbf{r} (meters) of DV-B's passenger zones.

Zone	r_x	r_y	r_z
A1	-24.50	-8.00	-0.45
A2	-24.50	8.00	-0.45
A3,5	-60.50	-8.00	-0.45
A4,6	-60.50	8.00	-0.45
A7	-91.50	-8.00	-0.45
A8	-91.50	8.00	-0.45
B1	-24.50	-8.00	2.38
B2	-24.50	8.00	2.38
B3,5	-60.50	-8.00	2.38
B3,6	-60.50	8.00	2.38

Table B.3.3. Relative position vectors \mathbf{r} (meters) of MH-C's passenger zones.

Zone	r_x	r_y	r_z
B	35.8	0.0	-17.4
C	74.2	5.5	-17.4

Zone	r_x	r_y	r_z
D	-40.9	6.0	-14.4
E	-24.1	-6.0	-14.4
F	4.8	0.0	-14.4
G	35.9	9.0	-14.4
H	76.0	0.0	-14.4
I	-31.2	0.0	-11.4
J	4.8	-7.0	-11.4
K	35.9	-7.6	-11.4
L	76.7	0.0	-11.4
M	-50.0	0.0	-8.4
N	-14.3	-7.0	-8.4
O	16.9	0.0	-8.4
P	48.1	0.0	-8.4
Q	77.0	0.0	-8.4
R	-48.9	0.0	-6.4
S	-24.1	7.0	-6.4
T	18.9	0.0	-6.4
U	48.1	0.0	-6.4

Zone	r_x	r_y	r_z
V	74.7	0.0	-6.4
W	19.0	0.0	2.6
X	69.6	0.0	2.6

Table B.3.4. Relative position vectors \mathbf{r} (meters) of MH-D's passenger zones.

Zone	r_x	r_y	r_z
A	3.0	-6.5	-15.2
B	63.0	-6.5	-15.2
C	103.0	-6.5	-15.2
D	-2.0	-6.5	-11.2
E	54.0	-6.5	-11.2
F	96.0	-6.5	-11.2
G	-2.0	-6.5	-6.2
H	55.0	-6.5	-6.2
I	100.0	-6.5	-6.2

Table B.3.5. Relative position vectors \mathbf{r} (meters) of Cat-E's passenger zones.

Zone	r_x	r_y	r_z
A	-11.90	-5.39	-3.02
B	-5.50	3.61	-3.02
C	-0.60	-4.89	-3.02
D	4.50	-0.89	-3.02
E	10.25	-0.89	-3.02
F	-11.90	-0.89	-0.52
G	-5.50	3.61	-0.52
H	-0.60	-5.39	-0.52
I	4.50	1.61	-0.52
J	10.25	0.11	-0.52

Table B.3.6. Relative position vectors \mathbf{r} (meters) of Cat-F's passenger zones.

Zone	r_x	r_y	r_z
D	-22.25	0.00	-2.15
F	-3.13	0.00	0.00

Zone	r_x	r_y	r_z
G	-8.38	0.00	0.00
H	-15.50	0.00	0.00
I	-23.00	0.00	0.00

Table B.3.7. Relative position vectors \mathbf{r} (meters) of WP-H's passenger zones.

Zone	r_x	r_y	r_z
A	3.00	-7.50	-4.25
B	3.00	7.50	-4.25
C	22.00	-7.50	-4.25
D	22.00	7.50	-4.25
E	-16.00	-3.50	-1.25
F	-16.00	3.50	-1.25
G	3.00	-8.70	-1.25

Appendix C. Data Pertaining to Further Validation of SVH-Conflict Model

C.1 Raw and Filtered Motion Histories of MH-I

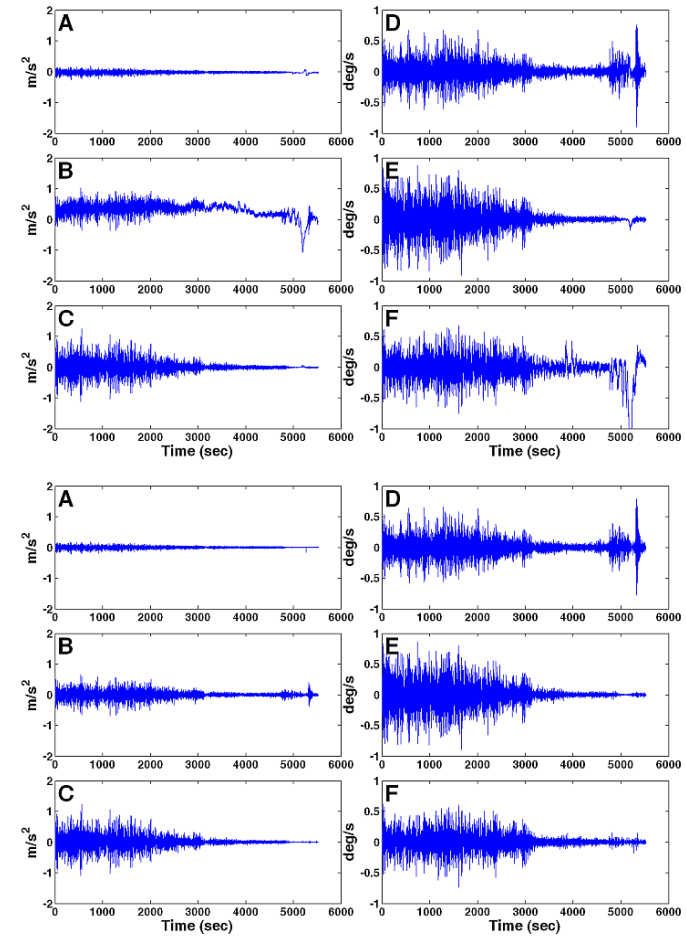


Figure C.1.1. Motion history (upper-row; lower-filtered) of MH-I at MRU position during Trip-2; linear accelerations (A) longitudinal (B) lateral (C) vertical; angular velocities (D) roll (E) pitch (F) yaw.

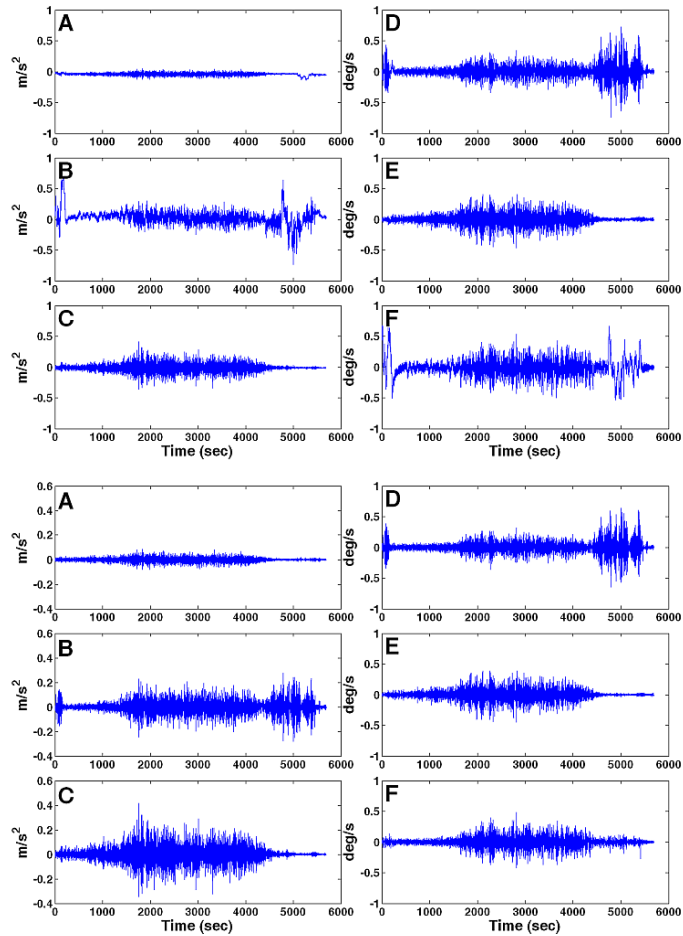


Figure C.1.2. Motion history (upper-row; lower-filtered) of MH-I at MRU position during Trip-3; linear accelerations (A) longitudinal (B) lateral (C) vertical; angular velocities (D) roll (E) pitch (F) yaw.

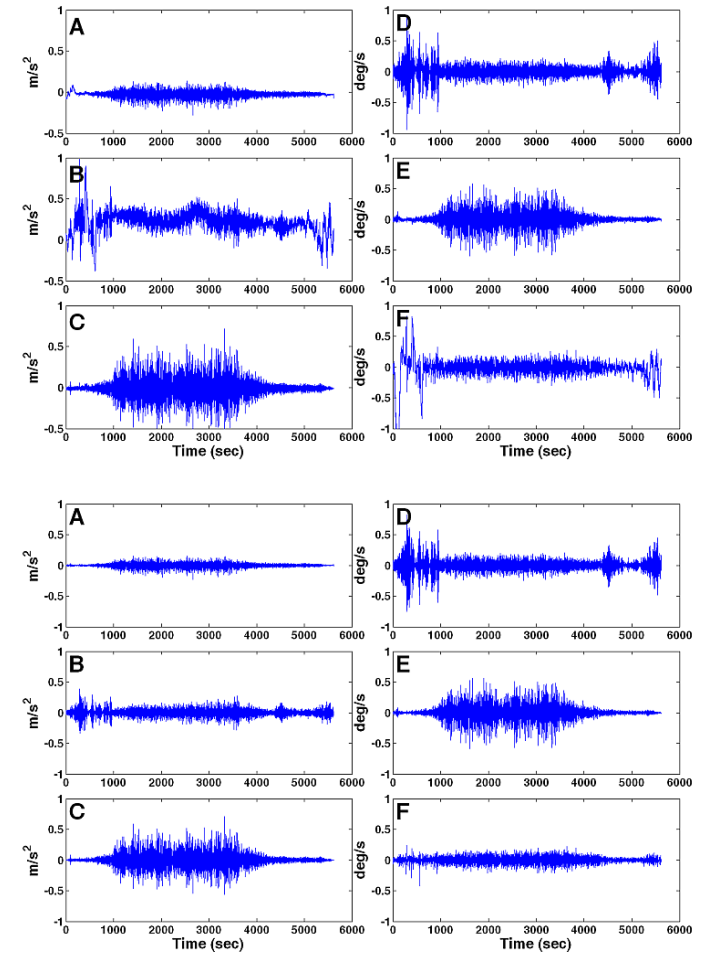


Figure C.1.3. Motion history (upper-row; lower-filtered) of MH-I at MRU position during Trip-4; linear accelerations (A) longitudinal (B) lateral (C) vertical; angular velocities (D) roll (E) pitch (F) yaw.

C.2 Cross Tabulation – MH-I

Table C.2.1: Type, categories and values of survey data collected aboard MH-I

Query	Description	Type	Category	Data Values
Q1	a. Gender	Qual.	Dichotomous	1-male; 0-female
	b. Age	Qty	Continuous	In years
Q2	Embarkation port	Qual.	Nominal	A, B and C is used for the three ports between which the ship operates.
Q3	Onboard location	Qual.	Nominal	Names of passenger zones are used
Q4	Activities			
	a. reading	Qual.	Dichotomous	1-yes; 0-no
	b. operating computer	-do-	-do-	-do-
	c. listening music	-do-	-do-	-do-
	d. talking	-do-	-do-	-do-
	e. no activity	-do-	-do-	-do-
	f. resting or sleeping	-do-	-do-	-do-
	g. in restaurant / shop	-do-	-do-	-do-
	h. looking outside	-do-	Nominal	as per the reply
	i. other			
Q5	a. Alcohol usage during the voyage	Qual.	Dichotomous	1-yes; 0-no
	b. 12 hrs before voyage	-do-	-do-	-do-
Q6	Sickness symptoms			
	a. hot or sweating	Qual.	Dichotomous	1-yes; 0-no
	b. headache	-do-	-do-	-do-
	c. skin colour	-do-	-do-	-do-
d. mouth watering	-do-	-do-	-do-	

Query	Description	Type	Category	Data Values
	f. drowsiness g. dizziness h. stomach awareness i. nausea j. vomiting	-do- -do- -do- -do- -do-	-do- -do- -do- -do- -do-	-do- -do- -do- -do- -do-
Q7	Sickness feelings	Qual.	Ordinal	0-all right; 1-unwell; 2-quite ill; 3-dreadful
Q8	Time to sickness a. felt unwell b. vomited	Qty -do-	Continuous -do-	In hours and minutes -do-
Q9	Anti-sickness tablets	Qual.	Dichotomous	1-Yes; 0-No
Q10	Travel frequency a. all types of vessel b. this vessel	Qual. -do-	Ordinal -do-	0-rare/never; 1-twice/year; 2-upto 6 times/year; 3-more than 6 times/year
Q11	Past history a. ships/boats b. coaches/buses c. cars d. aircraft e. trains	Qual. -do- -do- -do- -do-	Dichotomous -do- -do- -do- -do-	1-Yes; 0-No -do- -do- -do- -do-
Q12	Sitting comfort	Qual.	Ordinal	0-not; 1-little; 2-fairly; 3-uncomfortable; 4-very; 5-extremely uncomfortable
Q13	Steadiness	Qual.	Ordinal	0-not; 1-little; 2-fairly; 3-unsteady; 4-very; 5-extremely unsteady
Q14	Task difficulties a. eating/drinking b. reading c. writing	Qual. -do- -do-	Ordinal -do- -do-	0-not; 1-little; 2-fairly; 3-difficult; 4-very; 5-extremely difficult

Query	Description	Type	Category	Data Values
	d. others	-do-	-do-	as per the reply
Q15	Sources of discomfort a. primary b. secondary	Qual. -do-	Nominal -do-	as per the reply -do-
Q16	Expectations	Qual.	Ordinal	-1- less; 0-same; +1- more
Q17	Satisfaction	Qual.	Ordinal	0-extremely satisfied; 1-very; 2-satisfied; 3-fairly; 4-little; 5-not, may return; 6-not, will not return
Q18	Fatigue	Qual.	Ordinal	0-not; 1-little; 2-failry; 3-tiring; 4-very; 5-extremely tiring
Q19	Enjoyment	Qual.	Ordinal	0-extremely enjoyable; 1-very; 2-enjoyable; 3-fairly; 4-little; 5-not enjoyable

Example Cross Tables of the Dichotomous Variables

Table C.2.3: Example cross tabulation of dichotomous Q1a (gender) with Q6i (nausea)

		Gender		Total
		F	M	
Nausea No	Count	84	124	208
	Expected Count	94.9	113.1	208.0
	% within Gender	76.4%	94.7%	86.3%
Yes	Count	26	7	33
	Expected Count	15.1	17.9	33.0
	% within Gender	23.6%	5.3%	13.7%
Total	Count	110	131	241
	Expected Count	110.0	131.0	241.0
	% within Gender	100.0%	100.0%	100.0%

Table C.2.4: Example cross tabulation of dichotomous Q4a (reading) with Q1b (age)

		Reading		Total
		No	Yes	
Age <18	Count	28	7	35
	Expected Count	20.2	14.8	35.0
	% within Reading	21.5%	7.4%	15.6%
18-30	Count	22	8	30
	Expected Count	17.3	12.7	30.0
	% within Reading	16.9%	8.4%	13.3%
31-50	Count	43	35	78
	Expected Count	45.1	32.9	78.0
	% within Reading	33.1%	36.8%	34.7%
51-65	Count	25	28	53
	Expected Count	30.6	22.4	53.0
	% within Reading	19.2%	29.5%	23.6%

>65	Count	12	17	29
	Expected Count	16.8	12.2	29.0
	% within Reading	9.2%	17.9%	12.9%
Total	Count	130	95	225
	Expected Count	130.0	95.0	225.0
	% within Reading	100.0%	100.0%	100.0%

Table C.2.5: Example cross tabulation of dichotomous Q4c (listening to music) with Q6b (headache)

		Listening to Music		Total
		No	Yes	
Headache No	Count	209	12	221
	Expected Count	205.4	15.6	221.0
	% within Music	93.3%	70.6%	91.7%
Yes	Count	15	5	20
	Expected Count	18.6	1.4	20.0
	% within Music	6.7%	29.4%	8.3%
Total	Count	224	17	241
	Expected Count	224.0	17.0	241.0
	% within Music	100.0%	100.0%	100.0%

Table C.2.6: Example cross tabulation of dichotomous Q4d (talking) with Q6i (nausea)

		Talk		Total
		No	Yes	
Nausea No	Count	80	128	208
	Expected Count	74.2	133.8	208.0
	% within Talk	93.0%	82.6%	86.3%
Yes	Count	6	27	33
	Expected Count	11.8	21.2	33.0
	% within Talk	7.0%	17.4%	13.7%

Total	Count	86	155	241
	Expected Count	86.0	155.0	241.0
	% within Talk	100.0%	100.0%	100.0%

Table C.2.7: Example cross tabulation of dichotomous Q4e(no activity) with Q6c(pallor)

		Nothing		Total
		No	Yes	
Pallor No	Count	221	12	233
	Expected Count	218.5	14.5	233.0
	% within Nothing	97.8%	80.0%	96.7%
Yes	Count	5	3	8
	Expected Count	7.5	.5	8.0
	% within Nothing	2.2%	20.0%	3.3%
Total	Count	226	15	241
	Expected Count	226.0	15.0	241.0
	% within Nothing	100.0%	100.0%	100.0%

Table C.2.8: Example cross tabulation of dichotomous Q4f (resting) with Q6h (stomach awareness)

		Resting		Total
		No	Yes	
Stomach awareness No	Count	166	53	219
	Expected Count	159.0	60.0	219.0
	% within Resting	94.9%	80.3%	90.9%
Yes	Count	9	13	22
	Expected Count	16.0	6.0	22.0
	% within Resting	5.1%	19.7%	9.1%
Total	Count	175	66	241
	Expected Count	175.0	66.0	241.0
	% within Resting	100.0%	100.0%	100.0%

Table C.2.9: Example cross tabulation of dichotomous Q4g (visiting restaurant / bar/ shops) with Q1b (age)

		Restaurant/bar/shop		Total
		No	Yes	
Age <18	Count	12	23	35
	Expected Count	14.2	20.8	35.0
	% within Restaurant/bar/shop	13.2%	17.2%	15.6%
18-30	Count	3	27	30
	Expected Count	12.1	17.9	30.0
	% within Restaurant/bar/shop	3.3%	20.1%	13.3%
31-50	Count	36	42	78
	Expected Count	31.5	46.5	78.0
	% within Restaurant/bar/shop	39.6%	31.3%	34.7%
51-65	Count	25	28	53
	Expected Count	21.4	31.6	53.0
	% within Restaurant/bar/shop	27.5%	20.9%	23.6%
>65	Count	15	14	29
	Expected Count	11.7	17.3	29.0
	% within Restaurant/bar/shop	16.5%	10.4%	12.9%
Total	Count	91	134	225
	Expected Count	91.0	134.0	225.0
	% within Restaurant/bar/shop	100.0%	100.0%	100.0%

Table C.2.10: Example cross tabulation of Q4h (looking outside) with Q4d (talking)

		Looking out		Total	
		No	Yes		
Talk No	Count	53	33	86	
	Expected Count	41.4	44.6	86.0	
	% within Looking out	45.7%	26.4%	35.7%	
Yes		Count	63	92	155

	Expected Count	74.6	80.4	155.0
	% within Looking out	54.3%	73.6%	64.3%
Total	Count	116	125	241
	Expected Count	116.0	125.0	241.0
	% within Looking out	100.0%	100.0%	100.0%

Table C.2.11: Example cross tabulation of Q5a (use of alcohol) with Q12 (sitting discomfort)

		Alcohol during		Total
		No	Yes	
Sitting discomfort Not	Count	145	3	148
	Expected Count	144.1	3.9	148.0
	% within Alcohol during	65.0%	50.0%	64.6%
A little	Count	46	0	46
	Expected Count	44.8	1.2	46.0
	% within Alcohol during	20.6%	.0%	20.1%
Fairly	Count	9	2	11
	Expected Count	10.7	.3	11.0
	% within Alcohol during	4.0%	33.3%	4.8%
Uncomfortable	Count	11	0	11
	Expected Count	10.7	.3	11.0
	% within Alcohol during	4.9%	.0%	4.8%
Very	Count	11	0	11
	Expected Count	10.7	.3	11.0
	% within Alcohol during	4.9%	.0%	4.8%
Extremely	Count	1	1	2
	Expected Count	1.9	.1	2.0
	% within Alcohol during	.4%	16.7%	.9%
Total	Count	223	6	229
	Expected Count	223.0	6.0	229.0
	% within Alcohol during	100.0%	100.0%	100.0%

Table C.2.12: Example cross tabulation of dichotomous Q6a (feeling hot/sweating) with Q6e (cold sweating)

		Hot / sweating		Total
		No	Yes	
Cold sweat No	Count	209	29	238
	Expected Count	206.4	31.6	238.0
	% within Hot / sweating	100.0%	90.6%	98.8%
Yes	Count	0	3	3
	Expected Count	2.6	.4	3.0
	% within Hot / sweating	.0%	9.4%	1.2%
Total	Count	209	32	241
	Expected Count	209.0	32.0	241.0
	% within Hot / sweating	100.0%	100.0%	100.0%

Table C.2.13: Example cross tabulation of dichotomous Q6b (feeling headache) with Q4c (listening to music)

		Headache		Total
		No	Yes	
Music No	Count	209	15	224
	Expected Count	205.4	18.6	224.0
	% within Headache	94.6%	75.0%	92.9%
Yes	Count	12	5	17
	Expected Count	15.6	1.4	17.0
	% within Headache	5.4%	25.0%	7.1%
Total	Count	221	20	241
	Expected Count	221.0	20.0	241.0
	% within Headache	100.0%	100.0%	100.0%

Table C.2.14: Example cross tabulation of dichotomous Q6c (observing pallor) with Q6d (mouth watering)

		Pallor		Total
		No	Yes	
Mouth watering No	Count	229	4	233
	Expected Count	225.3	7.7	233.0
	% within Pallor	98.3%	50.0%	96.7%
Yes	Count	4	4	8
	Expected Count	7.7	.3	8.0
	% within Pallor	1.7%	50.0%	3.3%
Total	Count	233	8	241
	Expected Count	233.0	8.0	241.0
	% within Pallor	100.0%	100.0%	100.0%

Table C.2.15: Example cross tabulation of dichotomous Q6d (mouth watering) with Q6i (nausea)

		Mouth watering		Total
		No	Yes	
Nausea No	Count	205	3	208
	Expected Count	201.1	6.9	208.0
	% within Mouth watering	88.0%	37.5%	86.3%
Yes	Count	28	5	33
	Expected Count	31.9	1.1	33.0
	% within Mouth watering	12.0%	62.5%	13.7%
Total	Count	233	8	241
	Expected Count	233.0	8.0	241.0
	% within Mouth watering	100.0%	100.0%	100.0%

Table C.2.16: Example cross tabulation of dichotomous Q6e (cold sweating) with Q6i (nausea)

		Cold sweat		Total
		No	Yes	
Nausea No	Count	208	0	208
	Expected Count	205.4	2.6	208.0
	% within Cold sweat	87.4%	.0%	86.3%
Yes	Count	30	3	33
	Expected Count	32.6	.4	33.0
	% within Cold sweat	12.6%	100.0%	13.7%
Total	Count	238	3	241
	Expected Count	238.0	3.0	241.0
	% within Cold sweat	100.0%	100.0%	100.0%

Table C.2.17: Example cross tabulation of dichotomous Q6f (feeling drowsiness) with Q6i (nausea)

		Drowsiness		Total
		No	Yes	
Nausea No	Count	202	6	208
	Expected Count	199.4	8.6	208.0
	% within Drowsiness	87.4%	60.0%	86.3%
Yes	Count	29	4	33
	Expected Count	31.6	1.4	33.0
	% within Drowsiness	12.6%	40.0%	13.7%
Total	Count	231	10	241
	Expected Count	231.0	10.0	241.0
	% within Drowsiness	100.0%	100.0%	100.0%

Table C.2.18: Example cross tabulation of dichotomous Q6g (feeling dizzy) with Q6i (nausea)

		Dizziness		Total
		No	Yes	
Nausea No	Count	202	6	208
	Expected Count	195.9	12.1	208.0
	% within Dizziness	89.0%	42.9%	86.3%
Yes	Count	25	8	33
	Expected Count	31.1	1.9	33.0
	% within Dizziness	11.0%	57.1%	13.7%
Total	Count	227	14	241
	Expected Count	227.0	14.0	241.0
	% within Dizziness	100.0%	100.0%	100.0%

Table C.2.19: Example cross tabulation of dichotomous Q6h (stomach awareness) with Q6i (nausea)

		Stomach awareness		Total
		No	Yes	
Nausea No	Count	196	12	208
	Expected Count	189.0	19.0	208.0
	% within Stomach awareness	89.5%	54.5%	86.3%
Yes	Count	23	10	33
	Expected Count	30.0	3.0	33.0
	% within Stomach awareness	10.5%	45.5%	13.7%
Total	Count	219	22	241
	Expected Count	219.0	22.0	241.0
	% within Stomach awareness	100.0%	100.0%	100.0%

Table C.2.20: Example cross tabulation of dichotomous Q6i (nausea) with Q1a (gender)

		Nausea		Total
		No	Yes	
Gender F	Count	84	26	110
	Expected Count	94.9	15.1	110.0
	% within Nausea	40.4%	78.8%	45.6%
M	Count	124	7	131
	Expected Count	113.1	17.9	131.0
	% within Nausea	59.6%	21.2%	54.4%
Total	Count	208	33	241
	Expected Count	208.0	33.0	241.0
	% within Nausea	100.0%	100.0%	100.0%

Table C.2.21: Example cross tabulation of dichotomous Q6j (vomiting) with Q6i (nausea)

		Vomit		Total
		No	Yes	
Nausea No	Count	208	0	208
	Expected Count	204.5	3.5	208.0
	% within Vomit	87.8%	.0%	86.3%
Yes	Count	29	4	33
	Expected Count	32.5	.5	33.0
	% within Vomit	12.2%	100.0%	13.7%
Total	Count	237	4	241
	Expected Count	237.0	4.0	241.0
	% within Vomit	100.0%	100.0%	100.0%

Table C.2.22: Example cross tabulation of dichotomous Q9 (use of ant-sickness medicine) with Q14a (eating & drinking difficulties)

		Anti-Sickness Med		Total
		No	Yes	
Eating & drinking Not	Count	156	1	157
	Expected Count	152.8	4.2	157.0
	% within Anti-Sickness Med	84.8%	20.0%	83.1%
A little	Count	20	2	22
	Expected Count	21.4	.6	22.0
	% within Anti-Sickness Med	10.9%	40.0%	11.6%
Fairly	Count	4	1	5
	Expected Count	4.9	.1	5.0
	% within Anti-Sickness Med	2.2%	20.0%	2.6%
Difficult	Count	3	1	4
	Expected Count	3.9	.1	4.0
	% within Anti-Sickness Med	1.6%	20.0%	2.1%
Extremely	Count	1	0	1
	Expected Count	1.0	.0	1.0
	% within Anti-Sickness Med	.5%	.0%	.5%
Total	Count	184	5	189
	Expected Count	184.0	5.0	189.0
	% within Anti-Sickness Med	100.0%	100.0%	100.0%

Table C.2.23: Example cross tabulation of dichotomous Q11a (history of boat sickness) with Q1a (gender)

		Sickness boats		Total
		No	Yes	
Gender F	Count	50	60	110
	Expected Count	61.6	48.4	110.0
	% within Sickness boats	37.0%	56.6%	45.6%

M	Count	85	46	131
	Expected Count	73.4	57.6	131.0
	% within Sickness boats	63.0%	43.4%	54.4%
Total	Count	135	106	241
	Expected Count	135.0	106.0	241.0
	% within Sickness boats	100.0%	100.0%	100.0%

Table C.2.24: Example cross tabulation of dichotomous Q11b (history of bus sickness) with Q1a (gender)

		Sickness buses		Total
		No	Yes	
Gender F	Count	75	35	110
	Expected Count	87.2	22.8	110.0
	% within Sickness buses	39.3%	70.0%	45.6%
M	Count	116	15	131
	Expected Count	103.8	27.2	131.0
	% within Sickness buses	60.7%	30.0%	54.4%
Total	Count	191	50	241
	Expected Count	191.0	50.0	241.0
	% within Sickness buses	100.0%	100.0%	100.0%

Table C.2.25: Example cross tabulation of dichotomous Q11c (history of car sickness) with Q1a (gender)

		Sickness cars		Total
		No	Yes	
Gender F	Count	70	40	110
	Expected Count	79.4	30.6	110.0
	% within Sickness cars	40.2%	59.7%	45.6%
M	Count	104	27	131
	Expected Count	94.6	36.4	131.0

	% within Sickness cars	59.8%	40.3%	54.4%
Total	Count	174	67	241
	Expected Count	174.0	67.0	241.0
	% within Sickness cars	100.0%	100.0%	100.0%

Table C.2.26: Example cross tabulation of dichotomous Q11d (history of air sickness) with Q1a (gender)

		Sickness aircrafts		Total
		No	Yes	
Gender F	Count	88	22	110
	Expected Count	96.3	13.7	110.0
	% within Sickness aircrafts	41.7%	73.3%	45.6%
M	Count	123	8	131
	Expected Count	114.7	16.3	131.0
	% within Sickness aircrafts	58.3%	26.7%	54.4%
Total	Count	211	30	241
	Expected Count	211.0	30.0	241.0
	% within Sickness aircrafts	100.0%	100.0%	100.0%

Example Cross Tables of the Nominal Variables

Table C.2.27: Example cross tabulation of nominal Q3 (passenger zones) with Q15a (most discomforting factor)

		Passenger zone						Total	
		Missing	Open deck	Observation lounge	Restaurant / bar	Shops	Sitting area		
Most discomfort	Seasickness	Count	0	2	9	15	0	1	27
		Expected Count	1.0	3.8	5.8	9.4	.4	6.7	27.0
		% within Passenger zone	.0%	6.7%	19.6%	20.0%	.0%	1.9%	12.6%
Sitting discomfort		Count	2	0	2	4	0	1	9
		Expected Count	.3	1.3	1.9	3.1	.1	2.2	9.0
		% within Passenger zone	25.0%	.0%	4.3%	5.3%	.0%	1.9%	4.2%
Unsteadiness		Count	1	3	6	6	3	7	26
		Expected Count	1.0	3.6	5.6	9.1	.4	6.4	26.0
		% within Passenger zone	12.5%	10.0%	13.0%	8.0%	100.0%	13.2%	12.1%
Noise		Count	1	1	4	5	0	1	12
		Expected Count	.4	1.7	2.6	4.2	.2	3.0	12.0
		% within Passenger zone	12.5%	3.3%	8.7%	6.7%	.0%	1.9%	5.6%

Table C.2.28: Example cross tabulation of nominal Q15a (most discomforting factor) with Q7 (illness)

		Most discomfort								Total
		Seasickness	Sitting discmf	Unsteadiness	Noise	Vibration	Air quality	Others	None	
Illness All right	Count	3	4	17	12	13	7	5	104	165
	Expected Count	20.9	7.0	20.1	9.3	13.9	7.0	3.9	82.9	165.0
	% within Most discomfort	11.1%	44.4%	65.4%	100.0%	72.2%	77.8%	100.0%	97.2%	77.5%
Slightly unwell	Count	14	4	8	0	4	2	0	3	35
	Expected Count	4.4	1.5	4.3	2.0	3.0	1.5	.8	17.6	35.0
	% within Most discomfort	51.9%	44.4%	30.8%	.0%	22.2%	22.2%	.0%	2.8%	16.4%
Quite ill	Count	6	1	1	0	1	0	0	0	9
	Expected Count	1.1	.4	1.1	.5	.8	.4	.2	4.5	9.0
	% within Most discomfort	22.2%	11.1%	3.8%	.0%	5.6%	.0%	.0%	.0%	4.2%
Absolutely dreadful	Count	4	0	0	0	0	0	0	0	4
	Expected Count	.5	.2	.5	.2	.3	.2	.1	2.0	4.0
	% within Most discomfort	14.8%	.0%	.0%	.0%	.0%	.0%	.0%	.0%	1.9%

Total	Count	27	9	26	12	18	9	5	107	213
	Expected Count	27.0	9.0	26.0	12.0	18.0	9.0	5.0	107.0	213.0
	% within Most discomfort	100.0%	100.0%	100.0%	100.0%	100.0%	100.0%	100.0%	100.0%	100.0%

Table C.2.29: Example cross tabulation of nominal Q15b (2nd most discomforting factor) with Q17(illness)

			2nd most discomfort								Total	
			Missing	Seasickness	Sitting	Unsteadiness	Activities	Noise	Vibration	Air		None
Illness	All right	Count	108	1	4	5	3	7	17	3	41	189
		Expected Count	102.9	5.6	5.6	8.0	3.2	7.2	19.1	4.0	33.5	189.0
		% within 2nd most discomfort	83.7%	14.3%	57.1%	50.0%	75.0%	77.8%	70.8%	60.0%	97.6%	79.7%
Slightly unwell		Count	16	3	0	4	1	2	6	2	1	35
		Expected Count	19.1	1.0	1.0	1.5	.6	1.3	3.5	.7	6.2	35.0
		% within 2nd most discomfort	12.4%	42.9%	.0%	40.0%	25.0%	22.2%	25.0%	40.0%	2.4%	14.8%
Quite ill		Count	4	2	1	1	0	0	1	0	0	9
		Expected Count	4.9	.3	.3	.4	.2	.3	.9	.2	1.6	9.0

	% within 2nd most discomfort	3.1%	28.6%	14.3%	10.0%	.0%	.0%	4.2%	.0%	.0%	3.8%
Abs dreadful	Count	1	1	2	0	0	0	0	0	0	4
	Expected Count	2.2	.1	.1	.2	.1	.2	.4	.1	.7	4.0
	% within 2nd most discomfort	.8%	14.3%	28.6%	.0%	.0%	.0%	.0%	.0%	.0%	1.7%
Total	Count	129	7	7	10	4	9	24	5	42	237
	Expected Count	129.0	7.0	7.0	10.0	4.0	9.0	24.0	5.0	42.0	237.0
	% within 2nd most discomfort	100.0%	100.0%	100.0%	100.0%	100.0%	100.0%	100.0%	100.0%	100.0%	100.0%

Example Cross Tables of the Ordinal Variables

Table C.2.30: Example cross tabulation of ordinal Q1b (age) with Q7 (illness)

		Age					Total
		<18	18-30	31-50	51-65	>65	
Illness All right	Count	21	21	61	50	25	178
	Expected Count	28.1	24.1	60.9	42.5	22.5	178.0
	% within Age	60.0%	70.0%	80.3%	94.3%	89.3%	80.2%

Slightly unwell	Count	8	5	14	3	1	31
	Expected Count	4.9	4.2	10.6	7.4	3.9	31.0
	% within Age	22.9%	16.7%	18.4%	5.7%	3.6%	14.0%
Quite ill	Count	5	1	1	0	2	9
	Expected Count	1.4	1.2	3.1	2.1	1.1	9.0
	% within Age	14.3%	3.3%	1.3%	.0%	7.1%	4.1%
Absolutely dreadful	Count	1	3	0	0	0	4
	Expected Count	.6	.5	1.4	1.0	.5	4.0
	% within Age	2.9%	10.0%	.0%	.0%	.0%	1.8%
Total	Count	35	30	76	53	28	222
	Expected Count	35.0	30.0	76.0	53.0	28.0	222.0
	% within Age	100.0%	100.0%	100.0%	100.0%	100.0%	100.0%

Table C.2.31: Example cross tabulation of ordinal Q7 (illness) with Q12 (sitting discomfort)

			Illness				Total
			All right	Slightly unwell	Quite ill	Absolutely dreadful	
Sitting discomfort	Not	Count	142	6	0	0	148
		Expected Count	117.1	22.5	5.8	2.6	148.0

	% within Illness	78.0%	17.1%	.0%	.0%	64.3%
A little	Count	25	15	3	1	44
	Expected Count	34.8	6.7	1.7	.8	44.0
	% within Illness	13.7%	42.9%	33.3%	25.0%	19.1%
Fairly	Count	4	7	1	1	13
	Expected Count	10.3	2.0	.5	.2	13.0
	% within Illness	2.2%	20.0%	11.1%	25.0%	5.7%
Uncomfortable	Count	2	4	4	1	11
	Expected Count	8.7	1.7	.4	.2	11.0
	% within Illness	1.1%	11.4%	44.4%	25.0%	4.8%
Very	Count	7	3	1	1	12
	Expected Count	9.5	1.8	.5	.2	12.0
	% within Illness	3.8%	8.6%	11.1%	25.0%	5.2%
Extremely	Count	2	0	0	0	2
	Expected Count	1.6	.3	.1	.0	2.0
	% within Illness	1.1%	.0%	.0%	.0%	.9%
Total	Count	182	35	9	4	230

Table C.2.32: Example cross tabulation of ordinal Q10a (general travel frequency) with Q1b (age)

		Travel all				Total
		Rarely	Twice or less / year	Up to 6 times / year	More than 6 times / year	
Age <18	Count	6	7	4	8	25
	Expected Count	2.5	8.3	5.6	8.6	25.0
	% within Travel all	40.0%	14.0%	11.8%	15.4%	16.6%
18-30	Count	4	9	0	5	18
	Expected Count	1.8	6.0	4.1	6.2	18.0
	% within Travel all	26.7%	18.0%	.0%	9.6%	11.9%
31-50	Count	0	17	13	19	49
	Expected Count	4.9	16.2	11.0	16.9	49.0
	% within Travel all	.0%	34.0%	38.2%	36.5%	32.5%
51-65	Count	2	9	11	14	36
	Expected Count	3.6	11.9	8.1	12.4	36.0
	% within Travel all	13.3%	18.0%	32.4%	26.9%	23.8%
>65	Count	3	8	6	6	23
	Expected Count	2.3	7.6	5.2	7.9	23.0
	% within Travel all	20.0%	16.0%	17.6%	11.5%	15.2%

Total	Count	15	50	34	52	151
	Expected Count	15.0	50.0	34.0	52.0	151.0
	% within Travel all	100.0%	100.0%	100.0%	100.0%	100.0%

Table C.2.33: Example cross tabulation of ordinal Q10b (travel frequency aboard survey ship) with Q10a (general travel frequency)

		Travel this				Total
		Rarely	Twice or less / year	Up to 6 times / year	More than 6 times / year	
Travel all Rarely	Count	3	1	1	1	6
	Expected Count	.6	1.7	1.4	2.3	6.0
	% within Travel this	42.9%	5.3%	6.3%	3.7%	8.7%
Twice or less / year	Count	4	13	0	1	18
	Expected Count	1.8	5.0	4.2	7.0	18.0
	% within Travel this	57.1%	68.4%	.0%	3.7%	26.1%
Up to 6 times / year	Count	0	1	13	1	15
	Expected Count	1.5	4.1	3.5	5.9	15.0
	% within Travel this	.0%	5.3%	81.3%	3.7%	21.7%
More than 6 times / year	Count	0	4	2	24	30
	Expected Count	3.0	8.3	7.0	11.7	30.0

	% within Travel this	0.0%	21.1%	12.5%	88.9%	43.5%
Total	Count	7	19	16	27	69
	Expected Count	7.0	19.0	16.0	27.0	69.0
	% within Travel this	100.0%	100.0%	100.0%	100.0%	100.0%

Table C.2.34: Example cross tabulation of ordinal Q12 (sitting discomfort) with Q13 (unsteadiness)

		Sitting discomfort						Total
		Not	A little	Fairly	Uncomfortable	Very	Extremely	
Unsteadiness Not	Count	72	1	3	1	3	2	82
	Expected Count	53.4	15.8	4.3	3.9	3.9	.7	82.0
	% within Sitting discomfort	48.3%	2.3%	25.0%	9.1%	27.3%	100.0%	35.8%
A little	Count	63	30	2	1	6	0	102
	Expected Count	66.4	19.6	5.3	4.9	4.9	.9	102.0
	% within Sitting discomfort	42.3%	68.2%	16.7%	9.1%	54.5%	.0%	44.5%
Fairly	Count	9	5	1	0	0	0	15
	Expected Count	9.8	2.9	.8	.7	.7	.1	15.0
	% within Sitting discomfort	6.0%	11.4%	8.3%	.0%	.0%	.0%	6.6%
Unsteady	Count	5	6	5	3	2	0	21

	Expected Count	13.7	4.0	1.1	1.0	1.0	.2	21.0
	% within Sitting discomfort	3.4%	13.6%	41.7%	27.3%	18.2%	.0%	9.2%
Very	Count	0	2	0	4	0	0	6
	Expected Count	3.9	1.2	.3	.3	.3	.1	6.0
	% within Sitting discomfort	.0%	4.5%	.0%	36.4%	.0%	.0%	2.6%
Extremely	Count	0	0	1	2	0	0	3
	Expected Count	2.0	.6	.2	.1	.1	.0	3.0
	% within Sitting discomfort	.0%	.0%	8.3%	18.2%	.0%	.0%	1.3%
Total	Count	149	44	12	11	11	2	229

Table C.2.35: Example cross tabulation of ordinal Q13 (unsteadiness) with Q7 (illness)

		Unsteadiness						Total
		Not	A little	Fairly	Unsteady	Very	Extremely	
Illness All right	Count	82	89	7	6	1	0	185
	Expected Count	68.1	80.9	12.0	16.8	4.8	2.4	185.0
	% within Unsteadiness	96.5%	88.1%	46.7%	28.6%	16.7%	.0%	80.1%
Slightly unwell	Count	3	11	7	11	2	0	34
	Expected Count	12.5	14.9	2.2	3.1	.9	.4	34.0

	% within Unsteadiness	3.5%	10.9%	46.7%	52.4%	33.3%	.0%	14.7%
Quite ill	Count	0	1	1	2	3	2	9
	Expected Count	3.3	3.9	.6	.8	.2	.1	9.0
	% within Unsteadiness	.0%	1.0%	6.7%	9.5%	50.0%	66.7%	3.9%
Absolutely dreadful	Count	0	0	0	2	0	1	3
	Expected Count	1.1	1.3	.2	.3	.1	.0	3.0
	% within Unsteadiness	.0%	.0%	.0%	9.5%	.0%	33.3%	1.3%
Total	Count	85	101	15	21	6	3	231
	Expected Count	85.0	101.0	15.0	21.0	6.0	3.0	231.0
	% within Unsteadiness	100.0%	100.0%	100.0%	100.0%	100.0%	100.0%	100.0%

Table C.2.36: Example cross tabulation of ordinal Q14a (eating & drinking difficulties) with Q7 (illness)

		Eating & drinking					Total
		Not	A little	Fairly	Difficult	Extremely	
Illness All right	Count	143	12	0	0	0	155
	Expected Count	128.6	17.6	4.8	3.2	.8	155.0
	% within Eating & drinking	88.8%	54.5%	.0%	.0%	.0%	79.9%
Slightly unwell	Count	15	6	3	2	1	27

	Expected Count	22.4	3.1	.8	.6	.1	27.0
	% within Eating & drinking	9.3%	27.3%	50.0%	50.0%	100.0%	13.9%
Quite ill	Count	3	1	2	2	0	8
	Expected Count	6.6	.9	.2	.2	.0	8.0
	% within Eating & drinking	1.9%	4.5%	33.3%	50.0%	.0%	4.1%
Absolutely dreadful	Count	0	3	1	0	0	4
	Expected Count	3.3	.5	.1	.1	.0	4.0
	% within Eating & drinking	.0%	13.6%	16.7%	.0%	.0%	2.1%
Total	Count	161	22	6	4	1	194
	Expected Count	161.0	22.0	6.0	4.0	1.0	194.0
	% within Eating & drinking	100.0%	100.0%	100.0%	100.0%	100.0%	100.0%

Table C.2.37: Example cross tabulation of ordinal Q14b (reading difficulties) with Q7 (illness)

		Reading					Total
		Not	A little	Fairly	Difficult	Very	
Illness All right	Count	107	15	0	1	0	123
	Expected Count	101.6	17.1	1.7	1.7	.9	123.0
	% within Reading	89.9%	75.0%	.0%	50.0%	.0%	85.4%

Slightly unwell	Count	7	5	1	0	1	14
	Expected Count	11.6	1.9	.2	.2	.1	14.0
	% within Reading	5.9%	25.0%	50.0%	.0%	100.0%	9.7%
Quite ill	Count	4	0	0	1	0	5
	Expected Count	4.1	.7	.1	.1	.0	5.0
	% within Reading	3.4%	.0%	.0%	50.0%	.0%	3.5%
Absolutely dreadful	Count	1	0	1	0	0	2
	Expected Count	1.7	.3	.0	.0	.0	2.0
	% within Reading	.8%	.0%	50.0%	.0%	.0%	1.4%
Total	Count	119	20	2	2	1	144
	Expected Count	119.0	20.0	2.0	2.0	1.0	144.0
	% within Reading	100.0%	100.0%	100.0%	100.0%	100.0%	100.0%

Table C.2.38: Example cross tabulation of ordinal Q14c (writing difficulties) with Q3 (unsteadiness)

		Writing				Total
		Not	A little	Fairly	Difficult	
Unsteadiness Not	Count	44	4	0	0	48
	Expected Count	36.5	9.1	1.2	1.2	48.0

	% within Writing	47.8%	17.4%	.0%	.0%	39.7%
A little	Count	38	14	1	1	54
	Expected Count	41.1	10.3	1.3	1.3	54.0
	% within Writing	41.3%	60.9%	33.3%	33.3%	44.6%
Fairly	Count	4	3	0	0	7
	Expected Count	5.3	1.3	.2	.2	7.0
	% within Writing	4.3%	13.0%	.0%	.0%	5.8%
Unsteady	Count	3	2	1	1	7
	Expected Count	5.3	1.3	.2	.2	7.0
	% within Writing	3.3%	8.7%	33.3%	33.3%	5.8%
Very	Count	2	0	1	1	4
	Expected Count	3.0	.8	.1	.1	4.0
	% within Writing	2.2%	.0%	33.3%	33.3%	3.3%
Extremely	Count	1	0	0	0	1
	Expected Count	.8	.2	.0	.0	1.0
	% within Writing	1.1%	.0%	.0%	.0%	.8%
Total	Count	92	23	3	3	121

Table C.2.39: Example cross tabulation of ordinal Q16 (expectations) with Q7 (illness)

		Expectation			Total
		Worse	Same	Better	
Illness All right	Count	2	163	23	188
	Expected Count	6.4	160.8	20.8	188.0
	% within Expectation	25.0%	81.1%	88.5%	80.0%
Slightly unwell	Count	3	28	3	34
	Expected Count	1.2	29.1	3.8	34.0
	% within Expectation	37.5%	13.9%	11.5%	14.5%
Quite ill	Count	1	8	0	9
	Expected Count	.3	7.7	1.0	9.0
	% within Expectation	12.5%	4.0%	.0%	3.8%
Absolutely dreadful	Count	2	2	0	4
	Expected Count	.1	3.4	.4	4.0
	% within Expectation	25.0%	1.0%	.0%	1.7%
Total	Count	8	201	26	235
	Expected Count	8.0	201.0	26.0	235.0
	% within Expectation	100.0%	100.0%	100.0%	100.0%

Table C.2.40: Example cross tabulation of ordinal Q17 (satisfaction) with Q19 (enjoyment)

		Satisfaction					Total	
		Extremely	Very	Satisfied	Fairly	A little		Not
Enjoyment Extremely	Count	20	3	1	0	0	0	24
	Expected Count	4.7	7.5	9.3	1.4	.9	.3	24.0
	% within Satisfaction	42.6%	4.0%	1.1%	.0%	.0%	.0%	10.0%
Very	Count	15	31	7	0	0	1	54
	Expected Count	10.5	16.8	20.8	3.1	2.0	.7	54.0
	% within Satisfaction	31.9%	41.3%	7.5%	.0%	.0%	33.3%	22.4%
Enjoyable	Count	12	33	50	1	1	1	98
	Expected Count	19.1	30.5	37.8	5.7	3.7	1.2	98.0
	% within Satisfaction	25.5%	44.0%	53.8%	7.1%	11.1%	33.3%	40.7%
Fairly	Count	0	6	21	6	0	0	33
	Expected Count	6.4	10.3	12.7	1.9	1.2	.4	33.0
	% within Satisfaction	.0%	8.0%	22.6%	42.9%	.0%	.0%	13.7%
A little	Count	0	2	9	3	3	1	18
	Expected Count	3.5	5.6	6.9	1.0	.7	.2	18.0
	% within Satisfaction	.0%	2.7%	9.7%	21.4%	33.3%	33.3%	7.5%

Not	Count	0	0	5	4	5	0	14
	Expected Count	2.7	4.4	5.4	.8	.5	.2	14.0
	% within Satisfaction	.0%	.0%	5.4%	28.6%	55.6%	.0%	5.8%
Total	Count	47	75	93	14	9	3	241

Table C.2.41: Example cross tabulation of ordinal Q18 (fatigue) with Q7 (illness)

		Fatigue						Total
		Not	A little	Fairly	Tiring	Very	Extremely	
Illness All right	Count	147	30	4	3	2	1	187
	Expected Count	128.9	37.4	6.4	9.5	4.0	.8	187.0
	% within Fatigue	90.7%	63.8%	50.0%	25.0%	40.0%	100.0%	79.6%
Slightly unwell	Count	12	14	2	6	1	0	35
	Expected Count	24.1	7.0	1.2	1.8	.7	.1	35.0
	% within Fatigue	7.4%	29.8%	25.0%	50.0%	20.0%	.0%	14.9%
Quite ill	Count	2	2	2	3	0	0	9
	Expected Count	6.2	1.8	.3	.5	.2	.0	9.0
	% within Fatigue	1.2%	4.3%	25.0%	25.0%	.0%	.0%	3.8%
Absolutely dreadful	Count	1	1	0	0	2	0	4

	Expected Count	2.8	.8	.1	.2	.1	.0	4.0
	% within Fatigue	.6%	2.1%	.0%	.0%	40.0%	.0%	1.7%
Total	Count	162	47	8	12	5	1	235
	Expected Count	162.0	47.0	8.0	12.0	5.0	1.0	235.0
	% within Fatigue	100.0%	100.0%	100.0%	100.0%	100.0%	100.0%	100.0%

Table C.2.42: Example cross tabulation of ordinal Q19 (enjoyment) with Q7 (illness)

		Enjoyment						Total
		Extremely	Very	Enjoyable	Fairly	A little	Not	
Illness All right	Count	23	48	85	22	5	6	189
	Expected Count	19.1	42.3	78.2	23.9	14.4	11.2	189.0
	% within Enjoyment	95.8%	90.6%	86.7%	73.3%	27.8%	42.9%	79.7%
Slightly unwell	Count	1	4	9	8	9	4	35
	Expected Count	3.5	7.8	14.5	4.4	2.7	2.1	35.0
	% within Enjoyment	4.2%	7.5%	9.2%	26.7%	50.0%	28.6%	14.8%
Quite ill	Count	0	0	3	0	4	2	9
	Expected Count	.9	2.0	3.7	1.1	.7	.5	9.0
	% within Enjoyment	.0%	.0%	3.1%	.0%	22.2%	14.3%	3.8%

Absolutely dreadful Count	0	1	1	0	0	2	4
Expected Count	.4	.9	1.7	.5	.3	.2	4.0
% within Enjoyment	.0%	1.9%	1.0%	.0%	.0%	14.3%	1.7%
Total							
Count	24	53	98	30	18	14	237
Expected Count	24.0	53.0	98.0	30.0	18.0	14.0	237.0
% within Enjoyment	100.0%	100.0%	100.0%	100.0%	100.0%	100.0%	100.0%

C.3 Cross Tabulation – RHIB-J

Table C.3.1: Type, categories and values of survey data collected aboard RHIB-J

Query	Description	Type	Category	Data Values
Q1	Seat position	Qty	Nominal	1 to 10
Q2	Age	Qty	Continuous	In years
Q3	Gender	Qual.	Dichotomous	1-male; 0-female
Q4	Past history a. ships/boats b. coaches/buses c. cars d. aircraft e. trains	Qual. -do- -do- -do- -do-	Dichotomous -do- -do- -do- -do-	1-Yes; 0-No -do- -do- -do- -do-
Q5	Alcohol usage 12 hrs before voyage	Qual.	Dichotomous	1-yes; 0-no
Q6	Sickness feelings	Qual.	Ordinal	0-all right; 1-unwell; 2-quite ill; 3-very ill
Q7	Sitting comfort	Qual.	Ordinal	0-comfortable; 1-little uncomfortable; 2- fairly; 3-very; 4-extremely
Q8	Pain	Qual.	Nominal	as per the reply
Q9	Sources of discomfort	Qual.	Nominal	as per the reply
Q10	Sickness symptoms a. hot or sweating b. headache c. skin colour d. mouth watering f. drowsiness g. dizziness h. stomach awareness	Qual. -do- -do- -do- -do- -do- -do-	Dichotomous -do- -do- -do- -do- -do- -do-	1-yes; 0-no -do- -do- -do- -do- -do- -do-

Query	Description	Type	Category	Data Values
	i. nausea	-do-	-do-	-do-
	j. vomiting	-do-	-do-	-do-
Q11	Fatigue	Qual.	Ordinal	0-not; 1-little; 2-faily; 3-tiring; 4-very; 5-extremely tiring
Q12	Time to discomfort	Qty	Continuous	In hours and minutes

Table C.3.2: Fisher's Exact Test *P-values* of cross tabulations of the RHIB-J questionnaire survey

	Q3	Q4a	Q4b	Q4c	Q4d	Q4e	Q5	Q6	Q7	Q8a	Q8b	Q8c	Q8d	Q8e	Q9a	Q9b	Q10a	Q10b	Q10c	Q10d	Q10e	Q10f	Q10g	Q10h	Q10i	Q10j	Q11	
Q3		1.000	1.000	1.000	1.000			1.000	1.000	1.000	1.000		0.500	1.000	1.000	0.133	1.000	1.000		1.000		1.000		0.500				1.000
Q4a	1.000		0.444	0.048	0.444			1.000	0.524	1.000	1.000		0.524	0.444	0.444	0.810	1.000	1.000		0.444		1.000		1.000				1.000
Q4b	1.000	0.444		1.000	0.378			1.000	0.556	1.000	1.000		1.000	0.378	1.000	0.333	1.000	1.000		1.000		0.444		1.000				0.378
Q4c	1.000	0.048	1.000		0.133			1.000	0.714	1.000	1.000		0.190	1.000	1.000	0.886	1.000	0.500		0.133		1.000		1.000				0.667
Q4d	1.000	0.444	0.378	0.133				1.000	0.556	1.000	1.000		0.133	0.378	1.000	1.000	1.000	1.000		0.378		1.000		0.133				0.378
Q4e																												
Q5																												
Q6	1.000	1.000	1.000	1.000	1.000				0.200	0.378	1.000		0.467	1.000	1.000	1.000	1.000	1.000		1.000		0.444		0.467				1.000
Q7	1.000	0.524	0.556	0.714	0.556			0.200		0.089	0.500		1.000	0.556	0.333	0.119	0.500	1.000		1.000		1.000		0.714				1.000
Q8a	1.000	1.000	1.000	1.000	1.000			0.378	0.089		1.000		1.000	1.000	1.000	0.600	1.000	1.000		1.000		0.444		0.467				1.000
Q8b	1.000	1.000	1.000	1.000	1.000			1.000	0.500	1.000			1.000	1.000	0.200	0.700	1.000	1.000		1.000		1.000		1.000				0.200
Q8c																												
Q8d	0.500	0.524	1.000	0.190	0.133			0.467	1.000	1.000	1.000			1.000	1.000	0.190	1.000	0.500		0.133		1.000		1.000				0.667
Q8e	1.000	0.444	0.378	1.000	0.378			1.000	0.556	1.000	1.000		1.000		1.000	1.000	1.000	1.000		0.378		1.000		1.000				1.000
Q9a	1.000	0.444	1.000	1.000	1.000			1.000	0.333	1.000	0.200		1.000	1.000		0.200	0.200	1.000		1.000		1.000		0.667				0.378
Q9b	0.133	0.810	0.333	0.886	1.000			1.000	0.119	0.600	0.700		0.190	1.000	0.200		0.700	0.633	0.200	0.810	1.000	1.000						
Q10a	1.000	1.000	1.000	1.000	1.000			1.000	0.500	1.000	1.000		1.000	1.000	0.200	0.700		1.000		1.000		1.000		0.400				1.000
Q10b	1.000	1.000	1.000	0.500	1.000			1.000	1.000	1.000	1.000		0.500	1.000	1.000	0.633	1.000			0.067		1.000		1.000				1.000
Q10c																												
Q10d	1.000	0.444	1.000	0.133	0.378			1.000	1.000	1.000	1.000		0.133	0.378	1.000	0.200	1.000	0.067				1.000		1.000				1.000
Q10e																												
Q10f	1.000	1.000	0.444	1.000	1.000			0.444	1.000	0.444	1.000		1.000	1.000	1.000	0.810	1.000	1.000		1.000				0.524				1.000
Q10g																												
Q10h	0.500	1.000	1.000	1.000	0.133			0.467	0.714	0.467	1.000		1.000	1.000	0.667	1.000	0.400	1.000		1.000		0.524						0.667
Q10i																												
Q10j																												
Q11	1.000	1.000	0.378	0.667	0.378			1.000	1.000	1.000	0.200		0.667	1.000	0.378	1.000	1.000	1.000		1.000		1.000		0.667				

Appendix D. Details of Motion Reference Unit

D.1 Description of Motion Reference Unit (MRU)

The Seatex MRU5 is an inertial attitude reference system, capable of measuring orientation and dynamic linear motions. The unit is of very handy size (height = 204mm x diameter = 105mm) and weighs only 2.5Kg. It may virtually be installed at any location in a ship in any orientation of convenience. The unit may be fitted aboard a range of vessel types (from ROVs to large ships) to measure and record motion data of medium accuracy. The unit is not equivalent to a high performance gyro platform; however, it is highly reliable due to solid-state sensors with no moving parts (i.e. no inertial wheel). Typical marine applications of MRU5 include motion compensation for echo sounders, dynamic positioning systems, helideck monitoring systems and the motion damping systems of high speed craft.

D.1.1 Hardware Aspects

The schematic diagram as well as the physical dispositions of MRU's major components is shown in Figure D.1.1. Equipped with 3-axis angular rate sensors and 3-axis acceleration sensors, the unit is designed as a 'strap down' inertial system. The inertial sensors are 'strapped' to the housing of the unit (rather than to a turn-able mechanical platform i.e. no gimbals system is used), which in turn is rigidly fastened to the vehicle.

The angular rate sensors as well as the linear accelerometers are aligned with the three orthogonal sensor axes marked on the top lid of MRU. The orientation alignment of the unit is carried out using the software rather than the mechanical trimming, which allows the unit to be installed in any appropriate orientation. The raw sensor signals are scaled, linearized, orthogonalised and temperature compensated by the unit's hardware before being digitised.

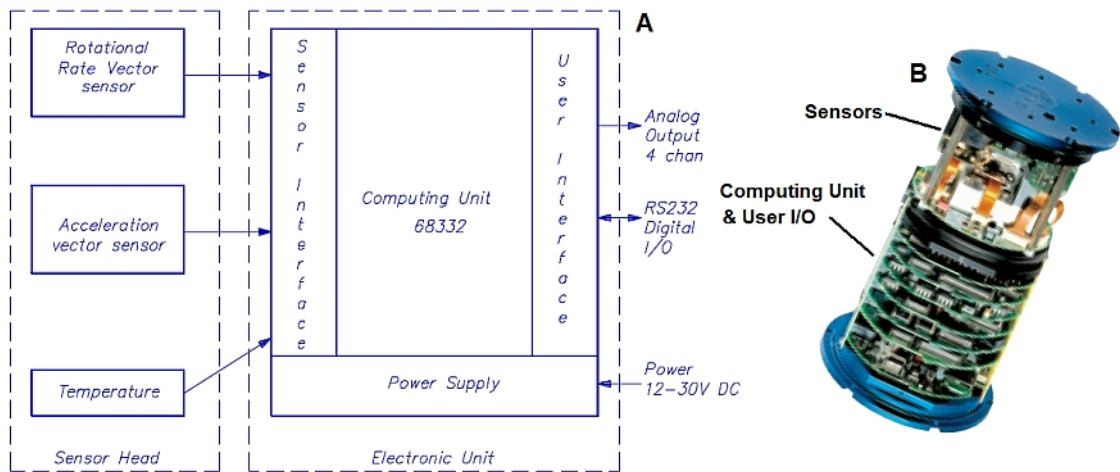


Figure D.1.1. Motion reference unit (MRU5): (A) schematic layout (B) physical arrangement.

Rotational rate sensors: MRU uses the 3-axis micromechanical vibrating cylinder gyroscopes, also known as ‘Coriolis vibratory gyros’, to measure the angular rate vector. Essentially, these devices are angular rate sensors measuring angular velocity, however, they are colloquially (though incorrectly) referred to as ‘gyroscopes’. These sensors are based on the micro-electromechanical system (MEMS) technologies (see Maluf & Williams 2004) and functionally mimic the halteres of insects (see Figure D.1.2). The angular rate sensors of MRU make use of the linear vibratory motions of a vibrating ring/cylinder to sense the Coriolis force originating from the rotational motions of the unit itself (Apostolyuk 2006).

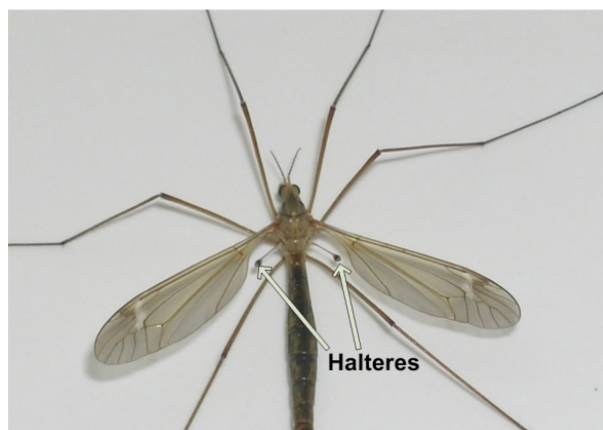


Figure D.1.2. Crane fly with a pair of visible halteres that are rapidly flapped to function like a Coriolis vibratory gyros (downloaded from http://en.wikivisual.com/images/d/d8/Crane_fly_halteres.jpg).

The vibratory gyros of MRU use the oscillation of a cylinder between two oval shaped paths as its primary modes of operation (see Figure D.1.3A). While the gyro is at rest, no vibration signals are observed at the nodes. As soon as the (body of) gyro is rotated around its axis of symmetry (normal to the plane of paper), the pickoff transducers that were at the nodes are rotated into the vibration zone producing signals proportional to the rotation rate (Watson 2006).

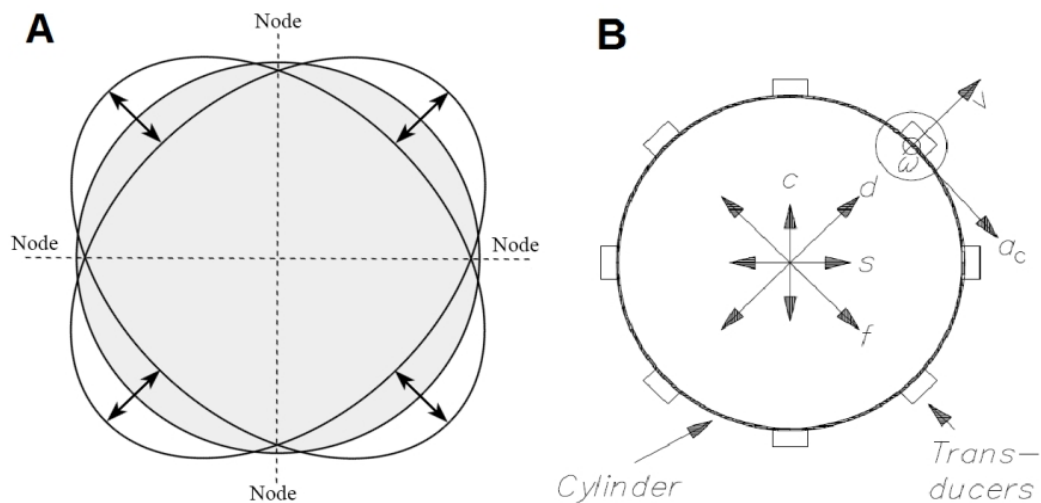


Figure D.1.3. MRU Coriolis gyroscope: (A) modes of operation [Watson 2006] (B) functional schematic [Kongsberg Seatex 2009].

As depicted in Figure D.1.3B, the Coriolis gyro of MRU has been implemented as a force feedback system utilizing eight transducers. Four transducers are used for the nodes or sense axes ('s' & 'c') and remaining four for the drive axes ('d' & 'f'). The two orthogonal nodes, as well as the two drive, axes have opposite phases for the sense and drive signals, respectively. The transducers installed along the drive axis ('d') are dedicated to produce the drive motion, oscillating the cylinder with velocity 'v', as an independent function. The other drive axis ('f') transducers are used for sensing the drive (cylinder) motion amplitude to control the excitation (along d-axis).

Upon rotation (ω) of MRU the transducers on sense axis ('s') sense the cylinder vibration signals. A measurement feedback loop is used to control the excitation along the other sense axis ('c', called compensation axis), producing a 'torquing' force on the cylinder. This excitation cancels the vibration set up along the sense s-

axis by the Coriolis acceleration (a_c). Thus the drive signal to c-axis is proportional to the angular rate of rotation of the unit about the axis normal to gyro. The main specifications of the MRU angular rate sensors are given in Table D.1.1.

Table D.1.1: Main specification of MRU Coriolis gyroscopes.

Description	Value
Angular orientation range	Unlimited
Angular rate range	± 150 degrees/sec
Scale factor error	0.08% RMS
Angle random walk in roll, pitch, yaw (angular rate noise)	0.025% RMS
Resolution in all axes	0.001 degree
Static accuracy of roll & pitch	0.02 degree RMS
Dynamic accuracy of roll & pitch (for $\pm 5^\circ$ amplitude)	0.02 degree RMS
Oscillation frequency of the cylinder	14.0kHz

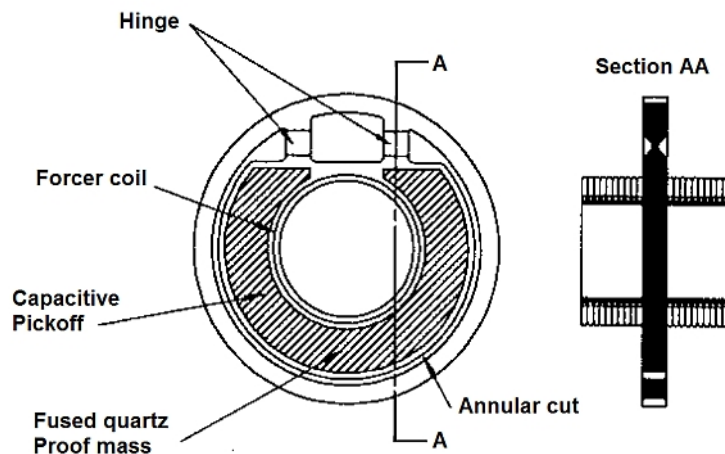


Figure D.1.4. MRU pendulum accelerometer construction [Kongsberg Seatex 2009].

Linear acceleration sensors: The 3-axis linear accelerometers used in MRU5 are of capacitive pendulum type. As shown in Figure D.1.4, each accelerometer consists of an inertia element (proof mass), a hinge, some damping, a capacitive pickoff, a

force and a servo loop. When exposed to static (tilt) and/or dynamic acceleration, the etched quartz proof mass of the accelerometer deflects from its neutral position. This deflection is compensated by the electronic servo loop, restraining the seismic element in its neutral position. The current required to hold the proof mass in its neutral position is directly proportional to the applied acceleration. The main specifications of MRU accelerometers are summarized in Table D.1.2.

Table D.1.2: MRU accelerometer specifications.

Description	Value
Acceleration range in all axes	$\pm 30 \text{ m/s}^2$
Acceleration noise	$0.002 \text{ m/s}^2 \text{ RMS}$
Acceleration accuracy	$0.01 \text{ m/s}^2 \text{ RMS}$
Scale factor error	0.02% RMS

The overall specifications concerning powering, operating environment and the internal signal processing by MRU are given in Table D.1.3.

Table D.1.3: General specifications of MRU5

Description	Value
Voltage input	12 to 30 volt DC
Maximum power consumption	8 Watts
Operating temperature range	-5 to +55°C
Maximum allowed vibration (in operation)	0.5 m/s^2
Maximum allowed vibration (not in operation)	20 m/s^2
Maximum shock immunity (not in operation)	1000 m/s^2
Internal update rate of the angular rate sensors	400Hz
Main processing frequency	100Hz

D.1.2 Software Interface

Hardware of MRU is accompanied by the system configuration software called MRC (see Figure D.1.5). MRC operates under Microsoft Windows environment and

communicates with the unit through a serial line (RS-232). It is designed to perform the following tasks:

- Configuring MRU for specific application.
- Checking internal status of the unit.
- Plotting the measured data on computer screen as well as logging it in a text file.
- Loading new software versions to the unit.

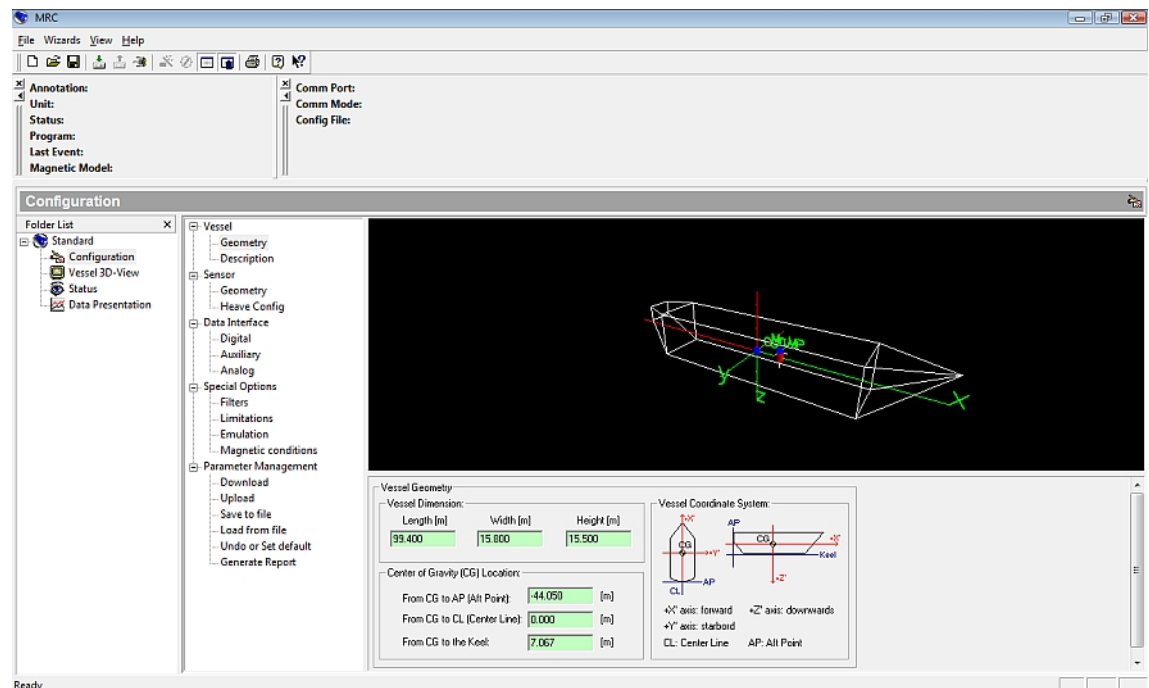


Figure D.1.5. MRC - the software interface of MRU.

Configuration: In the absence of pure gyroscopic devices (MRU has built in angular rate sensors to measure rotational velocities, see §D.1.1), MRU utilises gravity to locate the vertical direction. This is achieved by measuring the accelerations in the roll and pitch directions that are of tonical nature, representing static tilts. These accelerations are of transient type for the inertial motions. It is very important to install the unit as close to the centre of rotation (centre of gravity for a real ship) as much possible to minimise/avoid lever-arm effects. However, MRU's processing algorithms take account of the fact that it may not always be possible to install the

unit at the centre of gravity. It, therefore, compensates for the lever-arm effects while calculating the attitude of the vessel.

The configuration window of MRC allows users to provide the following information to the software:

- Principal dimensions of the vessel. These are used for the display purposes; see the line diagram of the ship in Figure D.1.5.
- Position of centre of gravity w.r.t to a frame of reference located at aft perpendicular on the centreline and at the keel level. This information is also used for displaying the location of CoG on computer screen.
- Position of MRU w.r.t to centre of gravity. This information is used in the calculation of MRU position vector (w.r.t CoG) for compensating the lever arm effects.

In addition to the lever arm effects' compensation, MRU uses a dedicated Kalman filter (hardware) based orientation observer to establish the attitude information. MRC allows the user to provide the time constant and damping characteristics of this filter. The other option would be to select 'automatic', wherein the algorithm calculates optimum filter parameters based on the characteristics (noise, error variance etc.) of current angular rate measurements. There are two other filters that the user may configure to, respectively, minimise the noise in surge and sway motions. In addition, one low pass filter attenuating structure borne vibration is also configurable by the user.

In this work, parameters of the abovementioned filters were adjusted as per the OEM recommendations given in Table D.1.4.

Table D.1.4: Selected parameter values of MRU filters.

Description	Value
Heave (Kalman) filter	Automatic
Surge filter	Time constant = 2.5sec

	Damping ratio = 0.6
Sway filter	Time constant = 2.5sec Damping ratio = 0.6
Vibration filter	Cut off frequency = 10Hz

Internal status: MRC provides the user with the current state (working status) of the MRU. In case of severe shock or excessive rotational motions the unit may lose track of the attitude information, which is conveyed to the user by the software as an online feature.

Plotting and logging of data: The user can plot and log a maximum of 16 output variables out of 189 available choices. Due to the limitation arising from internal processing frequency (see Table D.1.3), a maximum sampling frequency of 100Hz may be used for a single channel. However, the final sampling frequency depends on the number of variables being logged and the available baud rate of the computer port being used.

In this study, the MRU output variable enlisted in Table D.1.5, were logged at a sampling rate of 10Hz. This sampling frequency is far above the rate required by the sampling theorem (Nyquist 1928; Shannon 1949), as the rigid body motion of our interest (from seasickness view point) are far below 1Hz (see §7.8.3.1). It is important to note that the vessel motions were recorded in the body frame of reference depicted in Figure 7.4, at the MRU installation location(s).

Table D.1.5: MRU Channel logged during the field trails.

S.No.	Description	MRU Channel	
		Number	Designation
1.	Roll angle	63	Roll
2.	Ptich angle	64	Pitch
3.	Roll velocity	1	VelAngR
4.	Pitch velocity	2	VelAngP
5.	Yaw velocity	3	VelAngY

6.	Surge accelerations	11	AccMruGR
7.	Sway accelerations	12	AccMruGP
8.	Heave accelerations	13	AccMruGY
9.	Roll accelerations	60	AccAngR
10.	Pitch accelerations	61	AccAngP
11.	Yaw accelerations	62	AccAngY

In addition to the digitising and logging of vessel motions at MRU installation position, MRC (the software interface) provides the user with an option of estimating the rigid body motions at one more point anywhere inside/outside the vessel. This is referred to as ‘measuring point’ and the user is required to provide the position vector (w.r.t MRU installation position) as input to the software. However, this option was not used in this study and the vessel motions at other locations of interest, i.e. passenger-zone centres (see §7.8.3.2 & §7.9.2), were calculated using Equation(7.6).

New software version: This functionality of MRC is not available to the end user, but is meant to update the internal software used by MRU.

Appendix E. Model Comparison

E.1 Overview of the Appendix

This appendix statistically compares the physiologic (SV and SVH-conflict) and descriptive (ISO/BS, HFRI, & COMPASS) motion sickness models. Due to the random nature of MSI, this comparison is based on the statistical fitness characteristics of each model i.e. exact binomial test *p-values* for the individual trials as well as chi-square goodness-of-fit tests for the overall performance. The next section compares the considered models on individual field trial basis. The vessel-wise comparison is given in §E.3, prior concluding the appendix by comparing the models on overall (all trials of all ships) basis in §E.4.

E.2 Individual Field Trial Based Comparison

The observed and predicted MSIs are summarised in Table 7.16 for the validation and in Table 8.9 for the verification field trials of all (10) vessels (8 for the calibration & validation and 2 for the further validation). These tables are also depicting the exact binomial test *p-values* representing statistical fitness of the considered models [SVH (§6.6), SV (§5.11), ISO/BS (§3.7.5), HFRI (§3.7.1 & 3.7.2), and COMPASS (§3.8)] to the given field trial of a particular vessel. Statistically, *p-value* is just an indicator of the significance (i.e. likelihood of observing the occurrence) of an outcome. However, in our case we are using it to gauge the relative fitness of a particular motion sickness model. Thus, within the context of exact binomial tests presented in the aforementioned tables, a larger *p-value* indicates a greater probability of observing the field trial results (i.e. observed MSI) given the model predictions are statistically accurate i.e. a better fitness.

In order to assess the individual field trial's based performance of the abovementioned motion sickness models, their estimates are considered to be falling into one of the following three (assumed) fitness categories:

- **Statistically Not Fitting (NF):** The model MSI estimates with *p-value* of exact binomial test being less than 0.05 are assumed to be significant. Resultantly, the model is considered to be statistically not fitting.
- **Statistically Good Fitting (GF):** The model estimates are assumed to be insignificant when the exact binomial test *p-value* is between 0.05 and 0.5, inclusive. In such cases, the model is considered to be statistically good fitting.
- **Statistically Very Good Fitting (VGF):** In all cases, where the exact binomial test *p-values* are large than 0.5, the model estimates are assumed to be highly insignificant. Therefore, the model is considered to be showing very good statistical fitness.

In Table E.1, the results of all 68 field trials have been collated under the above outlined statistical fitness categories for each ship and motion sickness model. Also, Figure E.1 is depicting the model-wise summary of all trials falling under a specific fitness category. The following may be observed from Table 7.16, Table 8.9 and Table E.1, about the statistical fitness of each model:

E.2.1 SVH-Conflict Model

- This physiological model is estimating statistically accurate MSI for all but 2(2.9%) field trials [MH-D(#5) & WP-G(#7)]. It is displaying performance, better than all other models.
- The higher value of MSI estimates for the long duration field trial (No.5) of MH-D may be attributed to ‘habituation’ effects.
- However as far as trial No.7 of WP-G is concerned, it is evident that observed MSI of this specific field trial is significantly different ($p < 0.05$) from the high values predicted by all models (SVH, SV, ISO/BS, HFRI & COMPASS). Also, as already explained in §7.8.3.4 and §7.10.3, the outcome of this trial is inconsistent with other indicators of sickness (i.e. nausea). Therefore, the results of this specific field trials are discarded.

E2.2 SV-Conflict Model

- The SV-Conflict model is unable to estimate statistically accurate MSI for only 4 (5.9%) field trials [DV-B(#4); MH-D(#5); Cat-E(#14) & WP-G(#7)]. This makes it better than ISO/BS, HFRI and COMPASS models.
- Within the ‘non-fitted’ 4 trials, this model has under-predicted MSIs for the two field trials of high speed vessels DV-B & Cat-E.
- Alike SVH-Conflict model, a higher estimate of MSI for the long journey (No.5) of MH-D may be due to the habituation. Whereas, the higher estimates of MSI for the full scale trial (No.7) of vessel G are in line with all other models.

E2.3 ISO/BS (TD)

- This statistical model is statistically inaccurate for the 9 (13.2%) trials [Cat-A(#2); DV-B(#1, #2); MH-C(#1, #2, #3); MH-D(#4, #5) & WP-G(#7)], rendering it better than HFRI and COMPASS models.
- Considering the trials to which the model is unable to fit, it can be seen that it is predicting lower sickness events for the three field trials of high speed vessels (Cat-A & DV-B) and over estimating in rest of the cases (MH-C, MH-D, & WP-G).
- Significantly higher MSIs are calculated by the model for the long duration field trials of vessel MH-C & MH-D, which again, may be due to the habituation effects.

Table E.1: Vessel and model-wise summary of fitness categories for all field trials.

Vessel	Model	SVH-Conflict			SV-Conflict			ISO/BS (TD)			ISO/BS (FD)			HFRI			COMPASS		
		Statistical Fitness / Significance Level																	
	Trips	NF	GF	VGf	NF	GF	VGf	NF	GF	VGf	NF	GF	VGf	NF	GF	VGf	NF	GF	VGf
Cat-A	2	--	--	2	--	--	2	1	1	--	1	1	--	2	--	--	2	--	--
DV-B	4	--	2	2	1	--	3	2	--	2	2	--	2	4	--	--	3	--	1
MH-C	3	--	2	1	--	1	2	3	--	--	3	--	--	3	--	--	--	2	1
MH-D	6	1	2	3	1	2	3	2	4	--	2	4	--	--	5	1	1	5	--
Cat-E	24	--	2	22	1	--	23	--	2	22	--	2	22	1	--	23	1	--	23
Cat-F	4	--	2	2	--	2	2	--	1	3	--	1	3	3	--	1	--	3	1
WP-G	16	1	5	10	1	8	7	1	7	8	1	8	7	6	7	3	4	5	7
WP-H	4	--	1	3	--	3	1	--	1	3	--	1	3	2	1	1	--	1	3
MH-I	4	--	1	3	--	1	3	--	1	3	--	1	3	1	--	3	--	2	2
RHIB-J	1	--	--	1	--	--	1	--	--	1	--	--	1	--	--	1	--	--	1
Total	68	2	17	49	4	17	47	9	17	42	9	18	41	22	13	33	11	18	39
%age	100.0	2.9	25.0	72.1	5.9	25.0	69.1	13.2	25.0	61.8	13.2	26.5	60.3	32.4	19.1	48.5	16.2	26.5	57.4

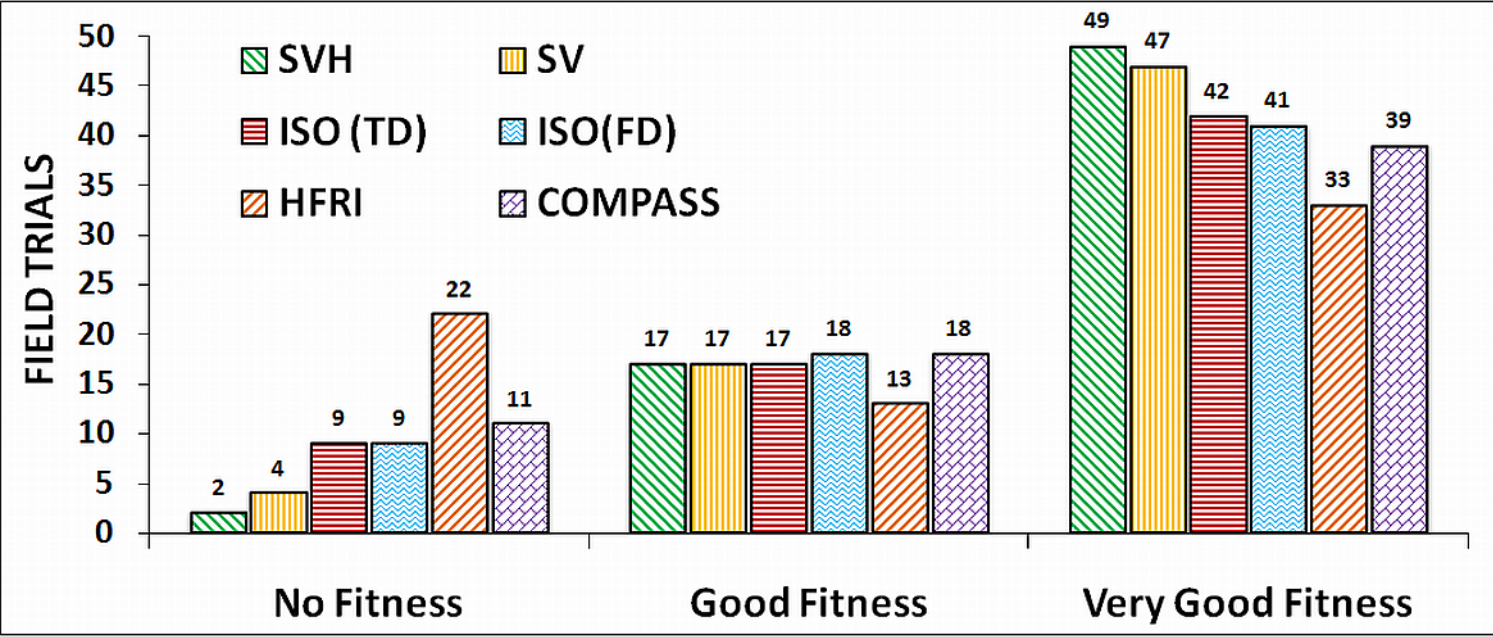


Figure E.1. Summary of trial-based model fitness.

E.2.4 ISO/BS (FD)

- Overall performance of frequency domain implementation of ISO/BS model is similar to its time domain counterpart.
- However, in 40 (58.8%) trials the fitness of frequency domain implementation is better (i.e. higher *p-value*) than the time domain approach. The two implementations are displaying identical (equal *p-value*) fitness in 13 (19.1%) field trials. Whereas, time domain methodology is predicting better estimates for the 15 (22.1%) trials.
- Thus, the frequency domain appears to be somewhat better than the time domain approach.

E.2.5 HFRI

- The HFRI statistical model is unable to predict accurate MSIs for the 22 (32.4%) field trials.
- It is predicting the smallest sickness incidences and is able to most successfully fit the sea trials with small or no vomiting incidences.
- With the exemption of Trip No.7 of WP-G, this model is predicting MSIs lower than the observed values in all field trials to which it is failing to fit.
- The model's inability to fit the long duration field trials of MH-C may be attributed to adaptation. However, it is surprising to see its good fitness to all the long journeys of MH-D (which also makes sense, as an underestimation overall may give a correct prediction some time during habituation).

E.2.6 COMPASS Model

- This motion sickness model is unable to predict statistically correct MSIs for the 11 (16.2%) field trials [Cat-A(#1, #2); DV-B (#2, #3, #4); MH-D(#5); Cat-E(#14); WP-G(#7, #10, #14, #16)].
- With the exceptions of MH-D's trail 5 and WP-G's trial 7, the model is under estimating the observed MSIs.
- As far as trial 5 of MH-D is concerned, the lower value of observed MSI may be attributed to 'habituation' effects.

- On the other hand, over estimations for WP-G's trial 7 is consistent with all other models.
- It is interesting to note that this model is showing discrepancies for the field trials of high speed vessels (Cat-A, DV-B, Cat-E, and WP-G), whereas, it was supposed to be more accurate for such type of vessels.

It can easily be gathered from above and Figure E.1 that the two physiological models (SVH & SV) are statistically more accurate than the three descriptive (ISO/BS, HFRI, & COMPASS) models. Moreover, with the least number of 'non-fitting' as well as the most of 'very good fitting' results, SVH conflict is apparently better than all other models. However, we need to verify this observation by an overarching statistical test for all field trials, irrespective of the vessel type, which is presented in §E.4.

E.3 Vessels-wise Comparison

The statistical fitness of the considered motion sickness models (SVH, SV, ISO/BS, HFRI, & COMPASS) may be assessed on vessel-wise basis by calculating the chi-square goodness-of-fit statistics. The exact binomial test *p-values* calculated for the individual trials (Table 7.16 & Table 8.9) may be used as input to Equation(7.4), which yields the desired statistics of the chi-square distribution (with degrees of freedom, d.o.f, being equal to the total field trials of the considered vessel).

The chi-square statistics may then be used to estimate the one-sided probability of chi-distribution. This probability is the overall likelihood (overall *p-value*) of observing the recorded MSIs for the multiple field trials of a specific vessel, given the estimates of the considered model are accurate. Once again, the larger the overall *p-value*, the better would be the statistical fitness of the model.

In the following sections, the statistical fitness of all considered models are presented and discussed on vessel-wise basis.

E.3.1 Comparison for Cat-A

The chi-square statistics along with the overall p -values for the multiple (2) field trials of Cat-A are summarised in Table E. 2. Assuming $p < 0.05$ as significant, it can be seen that only the physiological models (SVH and SV) are able to statistically fit the multiple trials of this vessel. Also in relative terms, the SVH-conflict model ($p=0.894$) is somewhat better than the SV-conflict model ($p=0.678$). The HFRI model has the largest value of chi statistics and is the most inaccurate model; this may be attributed to the under estimation characteristics of the model.

Table E. 2: χ^2 statistics and overall p -value for the (d.o.f =) 2 field trials of Cat-A

SVH-Conflict		SV-Conflict		ISO/BS (TD)		ISO/BS (FD)		HFRI		COMPASS	
χ^2	p	χ^2	p	χ^2	P	χ^2	P	χ^2	P	χ^2	p
0.223	0.894	0.678	0.713	11.255	0.004	10.481	0.005	90.162	0.000	34.452	0.000

(note: $p = 0.000$ indicates a value less than 0.0005)

Linear and rotational accelerations power spectral densities (PSDs) of the passengers zones (see Figure B.2.1 for layout) with the maximum and minimum estimated MSIs (using SVH) are plotted in Figure E.2, for the two field trials of Cat-A. Now by comparing these with the corresponding PSDs of a typical monohull, depicted in Figure 3.16, the following may be noticed:

- In contrast to a typical monohull, characterised with predominantly vertical accelerations, the lateral accelerations of Cat-A are either larger or of the same order as the vertical accelerations.
- Peak frequencies of the lateral accelerations of Cat-A are almost identical to its vertical accelerations' peak frequencies. Whereas, typical monohull vessels have the former to be lower than the latter.
- Typical monohull vessels have their pitch accelerations as the most significant, while the Cat-A is exhibiting the roll accelerations to be the largest.

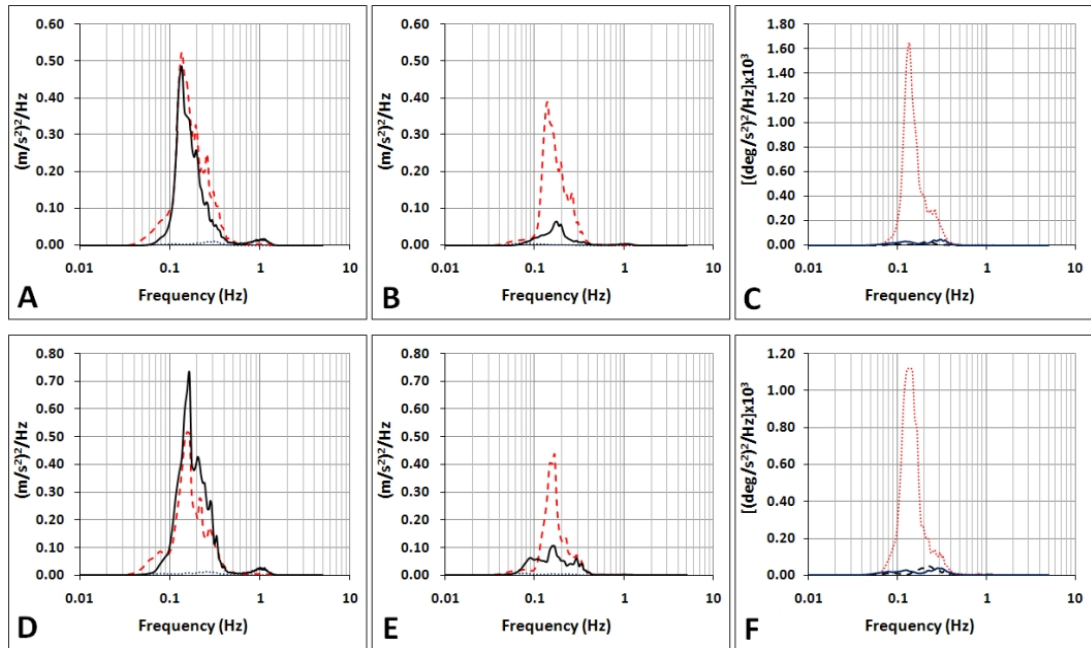


Figure E.2. Cat-A linear acceleration PSDs of (A Trip-1 & D Trip-2) max MSI zone-2, (B Trip-1 & E Trip-2) min MSI zone-7: dotted line longitudinal; dashed lateral; solid vertical. Rotational acceleration PSDs (C Trip-1 & F Trip-2): dotted line roll; dashed pitch; solid yaw.

Thus, the inability of ISO/BS motion sickness models in predicting statistically accurate MSIs of Cat-A may be attributed to the peculiar motions of the vessel (as compared to a typical monohull). It is worth recalling that these standards (ISO/BS) had been developed using field trial data (mainly) collected onboard monohull vessels (see §3.7).

However, the reasons for incorrect (lower) estimates by COMPASS model are not clear as the model is supposed to show better performance than the ISO/BS models for this type of vessels. One possibility could be the inaccurate estimates of the model parameters (Table 3.3). However, further field trials and detailed analysis would be necessary to conclude this.

E.3.2 Comparison for DV-B

Statistical feature of the considered models for the multiple (4) field trials of DV-B are summarised in Table E.3. Considering $p < 0.05$ to be significant, it is evident that only SVH and SV-conflict models are able to predict statistically accurate MSIs.

However, SV-conflict model is ‘just’ fitting ($p=0.05$) the trial results, while SVH is displaying ‘good’ fitness ($p=0.123$). This is because SV model was unable to estimate statistically accurate MSI for the 4th field trial of DV-B (see Table 7.16).

Table E.3: χ^2 statistics and overall p -value for the (d.o.f =) 4 field trials of DV-B

SVH-Conflict		SV-Conflict		ISO/BS (TD)		ISO/BS (FD)		HFRI		COMPASS	
χ^2	p	χ^2	p	χ^2	P	χ^2	P	χ^2	P	χ^2	p
7.263	0.123	9.469	0.050	19.986	0.001	20.217	0.000	156.850	0.000	46.309	0.000

(note: $p = 0.000$ indicates a value less than 0.0005)

The SV-conflict model is underestimating the MSI for the fourth field trial, the linear and rotational acceleration PSDs for this specific trial are shown in Figure E.3 below. The linear acceleration PSDs have been calculated for the zones with maximum and minimum MSIs predicted by SV and SVH-conflict models. It appears that SVH model is able to correctly estimate the MSIs for this trip due to the relatively large magnitudes of lateral accelerations in lower frequencies.

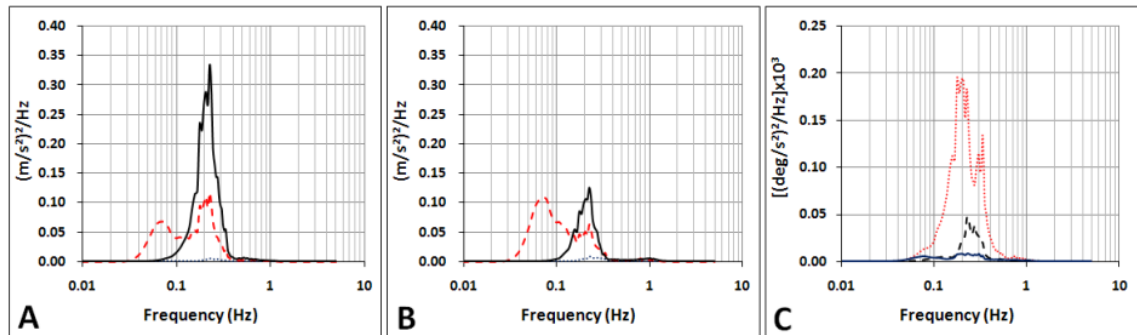


Figure E.3: DV-B trip-4: linear acceleration PSDs of A-max MSI zone-A2, B-min MSI zone-B3,5: dotted line longitudinal; dashed lateral; solid vertical. C-rotational acceleration PSDs: dotted line roll; dashed pitch; solid yaw.

From Table 7.16, it can be seen that ISO/BS models are overestimating MSI for the first field trial of DV-B. The motion history of DV-B for the first field trial at the passenger zone with maximum predicted MSI (using SVH) is shown in Figure E.4. The time domain MSI predictions of ISO/BS model as well as that of the SV and SVH-conflict models for this passenger zone are also shown in the same figure. The following may be observed from this figure:

- The vessel motions were moderate (e.g. vertical acceleration $< 0.5 \text{ m/sec}^2$) for almost half of the trip duration. These became severe for almost 1.25 hours and again restored to moderate values till the end of voyage.
- Due to the (relatively) short duration of provoking motion exposures, a small number of passengers are likely to reach the level of emesis, which is exactly what has been predicted by the physiological models(SVH & SV). Whereas, ISO/BS model is unable to capture the time characteristics of this belated exposure to severe vessel motions.
- Also, the physiological models are estimating increase as well as decrease in sensory conflict and thereby the MSI with the variation of motion severity, which is in accordance with general human response. However, ISO/BS model is continuously adding up the MSI, though at varying rates, hence it is has predicted higher MSI than the observed value.

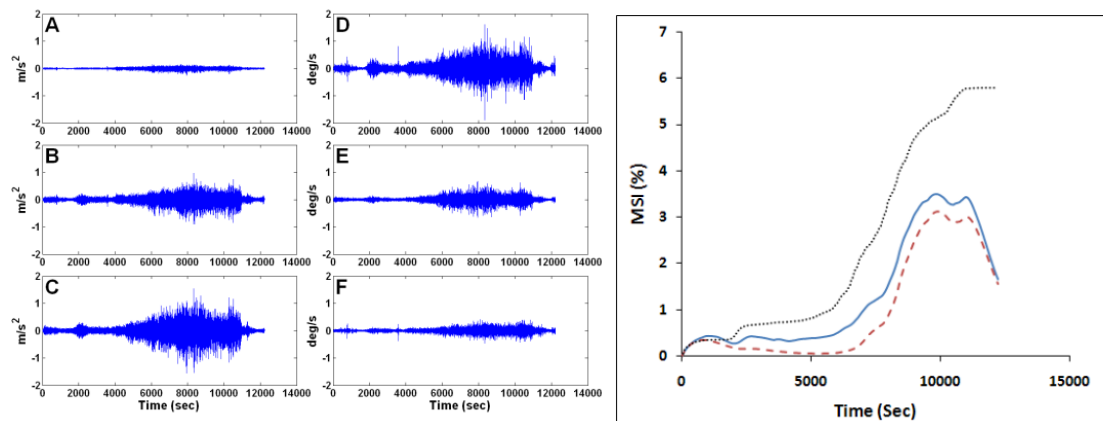


Figure E.4: (Left) DV-B trip-1 motion time history for zone-A2; A-longitudinal, B-lateral, & C-vertical accelerations; D-roll, E-pitch, & F-yaw velocities. (Right) MSI estimates for zone-A2; solid line-SVH conflict, dashed line SV-conflict, & dotted line ISO/BS models.

For the second field trip of DV-B, the ISO/BS models under-predicted the observed MSIs. The linear and rotation acceleration PSDs of the vessel for the zones with maximum and minimum predicted MSIs are shown in Figure E.5. It can be seen from the figure that the motion response of DV-B are atypical of a monohull, as explained for the Cat-A in §E3.1. Hence, inaccurate estimates of ISO/BS models

may be attributed to relatively large lateral and roll accelerations exhibited by the vessel.

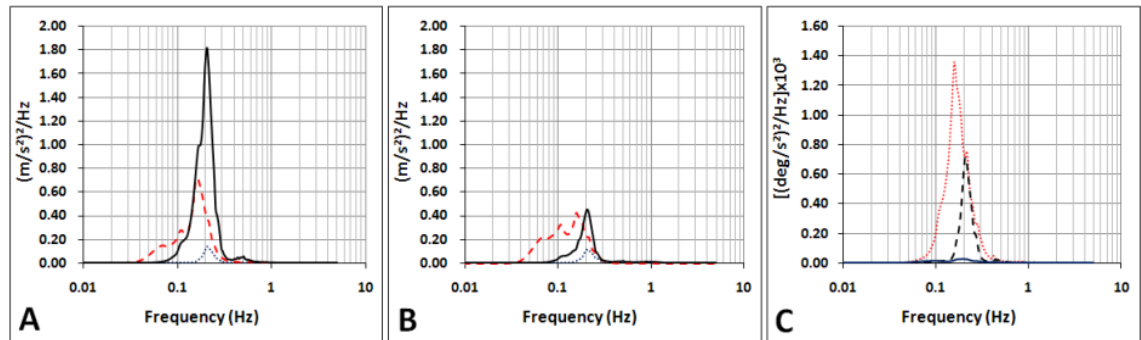


Figure E.5: DV-B trip-2: linear acceleration PSDs of A-max MSI zone-A1, B-min MSI zone-B3,6: dotted line longitudinal; dashed lateral; solid vertical. C-rotational acceleration PSDs: dotted line roll; dashed pitch; solid yaw.

The HFRI model with the largest value of chi statistics and is displaying the worst performance by underestimating the observed MSIs. Again, it is surprising to see that COMPASS model is under predicting MSIs for the three field trials (No.2 to 4) of vessel DV-B.

E.3.3 Comparison for MH-C

The fitness statistics for the multiple (3) field trials of MH-C are shown in Table E.4. The two physiological models (SV & SVH) as well as the COMPASS model are displaying good overall fitness for the field trials this vessel. HFRI model having the largest value of chi statistics is again unable to correctly estimate the MSIs (it is predicting much smaller values than observed, see Table 7.16). On the other hand the ISO/BS models are over estimating the proportion of passengers likely to get motion sick. The most likely reason for the inaccurate MSI estimates of ISO/BS is the habituation effects.

Table E.4: χ^2 statistics and overall p -value for the (d.o.f =) 3 field trials of MH-C

SVH-Conflict		SV-Conflict		ISO/BS (TD)		ISO/BS (FD)		HFRI		COMPASS	
χ^2	p	χ^2	p	χ^2	P	χ^2	P	χ^2	P	χ^2	p
3.701	0.296	4.209	0.240	32.004	0.000	32.519	0.000	43.442	0.000	5.772	0.123

(note: $p = 0.000$ indicates a value less than 0.0005)

As an example, the motion history and corresponding MSI estimates of SVH, SV and ISO/BS models for the first field trial of MH-C at the zone with maximum predicted MSI are shown in Figure E.6. It can be seen that ISO/BS models, similar to the first field trial of DV-B, keep on accumulating MSI, whereas the two physiological models are able to correctly follow the severity of vessel motions. Thus, the descriptive ISO/BS models are primarily affected by the long duration of the MH-C trials, wherein these models keep on integrating the motion effects with no decreasing effects (MSI only levels out when the vessel motions are small).

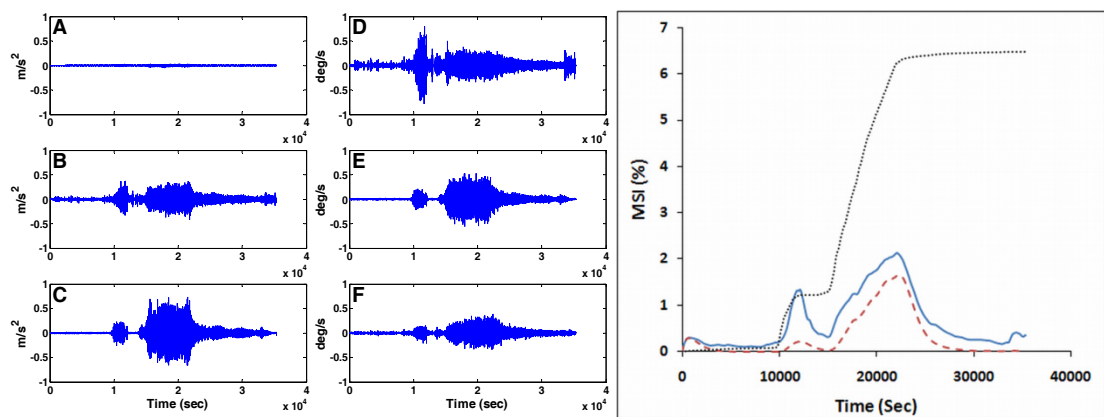


Figure E.6: (Left) MH-C trip-1 motion time history for zone-L; A-longitudinal, B-lateral, & C-vertical accelerations; D-roll, E-pitch, & F-yaw velocities. (Right) MSI estimates for zone-L; solid line-SVH conflict model, dashed line SV-conflict model, & dotted line ISO/BS models.

E.3.4 Comparison for MH-D

The statistical fitness characteristics of the considered models for the multiple (5) field trials of MH-D are summarised in Table E.5. This time (assuming $p < 0.05$ to be significant) none of the motion sickness prediction model is able to statistically fit the multiple full scale trials of MH-D, which may primarily be attributed to the ‘habituation’ effects (§3.5). A close look at Table 7.16 reveals that the physiological models (SVH, SV) as well as COMPASS model are unable to correctly estimate the results for the 5th field trial. ISO/BS models are predicting inaccurate MSIs for the 4th and 5th field trials. Surprisingly enough, the HFRI model is able to estimate statistically accurate MSIs for all individual field trials (underestimation characteristic of this model was able to offset the habituation effects).

Table E.5: χ^2 statistics and overall p -value for the (d.o.f =) 5 field trials of MH-D

SVH-Conflict		SV-Conflict		ISO/BS (TD)		ISO/BS (FD)		HFRI		COMPASS	
χ^2	p	χ^2	p	χ^2	P	χ^2	P	χ^2	P	χ^2	p
19.031	0.002	18.336	0.003	38.401	0.000	39.256	0.000	14.535	0.013	25.043	0.000

(note: $p = 0.000$ indicates a value less than 0.0005)

In order to appreciate the significance of adaptation, the motion time histories as well as the predicted MSIs (using SV, SVH and ISO/BS models) during the 5th field trial of MH-D (for the zone with maximum estimated MSI) are plotted in Figure E.7. By comparing this figure with Figure E.6, it can be seen that unlike MH-C, the motions of MH-D are quite severe from the very beginning till the end of voyage. Therefore, despite little difference between the journey times of MH-C and MH-D, it appears that the prevalence of severe motions throughout the journey led to the habituation of passengers. Resultantly, being unable to account for the adaptation, the physiological motion sickness overestimated MSIs.

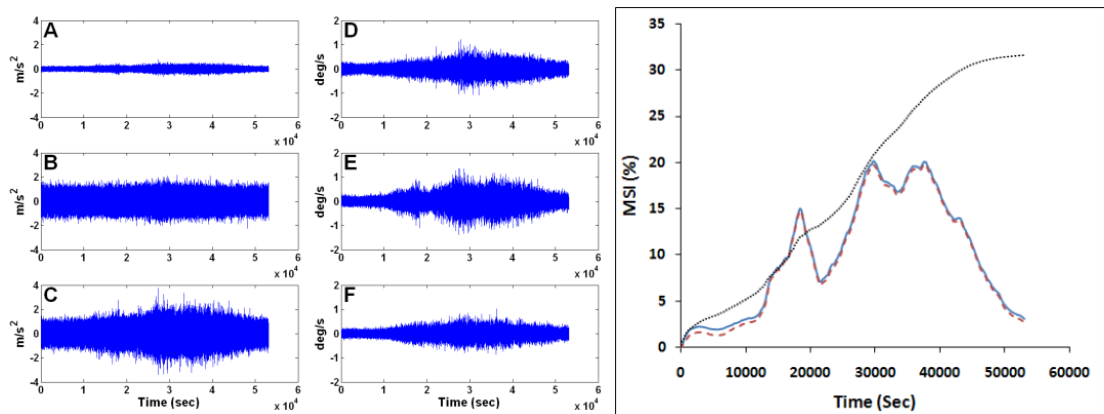


Figure E.7: (Left) MH-D trip-5 motion time history for zone-C; A-longitudinal, B-lateral, & C-vertical accelerations; D-roll, E-pitch, & F-yaw velocities. (Right) MSI estimates for zone-C; solid line-SVH conflict model, dashed line SV-conflict model, & dotted line ISO/BS models.

E.3.5 Comparison for Cat-E

The model fitness statistics for the multiple (24) field trials of Cat-E are given in Table E.6. As could be seen from Table 7.16, almost no sickness was reported during the full scale trials of this vessel. The motions' time history along with the MSI estimates of SVH, SV and ISO/BS models, for the zone with maximum predicted MSI, during the first trip of the vessel, are shown in Figure E.8.

Table E.6: χ^2 statistics and overall p -value for the (d.o.f =) 24 field trials of Cat-E

SVH-Conflict		SV-Conflict		ISO/BS (TD)		ISO/BS (FD)		HFRI		COMPASS	
χ^2	p	χ^2	p	χ^2	P	χ^2	P	χ^2	P	χ^2	p
10.753	0.991	7.378	1.000	14.430	0.936	14.355	0.938	21.095	0.633	11.046	0.989

It can be observed from Figure E.8 that the overall motions of the vessel had been relatively small (vertical and lateral accelerations $< 0.5 \text{ m/sec}^2$) for the most part of the trip. Hence, the accurate estimation of MSIs by all models may be attributed to the small amplitude motions of Cat-E. This vessel mostly operates in sheltered waters; hence the motion and MSI characteristics of all 24 trips had been very similar.

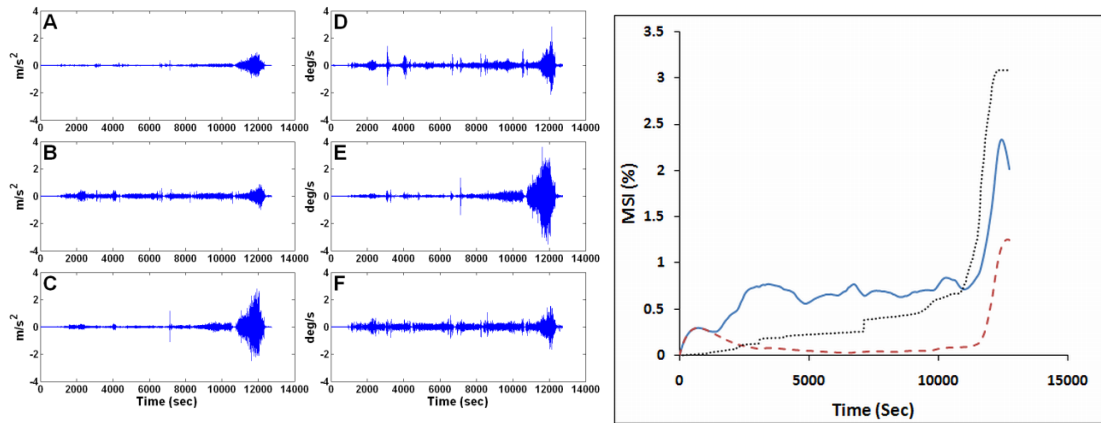


Figure E.8: (Left) Cat-E trip-1 motion time history for zone-A; A-longitudinal, B-lateral, & C-vertical accelerations; D-roll, E-pitch, & F-yaw velocities. (Right) MSI estimates for zone-A; solid line-SVH conflict model, dashed line SV-conflict model, & dotted line ISO/BS models.

E.3.6 Comparison for Cat-F

Table E.7 is summarising the fitness statistics of the considered motion sickness models for the multiple (4) field trials of catamaran vessel Cat-F. The HFRI and COMPASS models are unable to display overall statistical fitness (assuming $p < 0.05$ as significant). SVH, SV and ISO/BS models are displaying good statistical accuracy for multiple trials of the vessel. It is also interesting to note that in relative terms the SV-conflict model ($p=0.220$) is exhibiting performance superior to ISO/BS ($p=0.160$) as well as SVH-conflict ($p=0.105$) models.

Table E.7: χ^2 statistics and overall p -value for the (d.o.f =) 4 field trials of Cat-F

SVH-Conflict		SV-Conflict		ISO/BS (TD)		ISO/BS (FD)		HFRI		COMPASS	
χ^2	p	χ^2	p	χ^2	P	χ^2	P	χ^2	P	χ^2	p
7.647	0.105	5.731	0.220	6.583	0.160	6.527	0.163	29.684	0.000	10.186	0.037

(note: $p = 0.000$ indicates a value less than 0.0005)

The linear and rotation PSDs for the 3rd and 4th field trials, wherein SV is estimating somewhat better results than the SVH model (Table 7.16), are shown in Figure E.9. The SVH-conflict model is slightly overestimating MSIs for these two field trials, which, as it appears from Figure E.9, may be due to the presence of relatively high magnitudes of low frequency lateral and longitudinal accelerations.

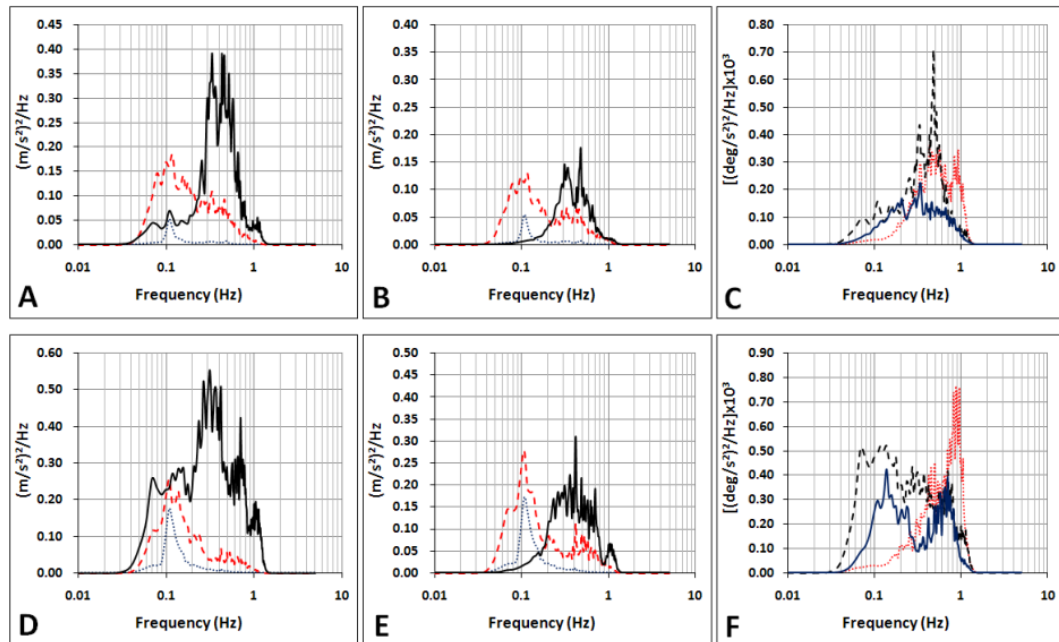


Figure E.9: Linear acceleration PSDs of (A Trip-3 & D Trip-4) max MSI zone-F/G, (B Trip-1 & E Trip-2) min MSI zone-I: dotted line longitudinal; dashed lateral; solid vertical.

Rotational acceleration PSDs (C Trip-3 & F Trip-4): dotted line roll; dashed pitch; solid yaw

E.3.7 Comparison for WP-G

The model-wise fitness statistics for the multiple (15) full scale trials of wave piercer, WP-G, are delineated in Table E.8. It is worth noting that trial No.7 of this specific vessel has been discarded due to experiment anomaly already discussed at length in Chapter 7 and Chapter 8. In this case, the SVH-conflict model ($p=0.134$) is

displaying overall statistical fitness superior to SV-conflict model ($p=0.057$). The latter is ‘just’ able to fit the multiple field trials of the vessel, while all descriptive models (ISO/BS, HFRI and COMPASS) are unable to show overall satisfactory statistical fitness. HFRI model, with the maximum value of chi statistic, is the most inaccurate model.

Table E.8: χ^2 statistics and overall p -value for the (d.o.f =) 15 field trials of WP-G

SVH-Conflict		SV-Conflict		ISO/BS (TD)		ISO/BS (FD)		HFRI		COMPASS	
χ^2	p	χ^2	p	χ^2	P	χ^2	P	χ^2	P	χ^2	p
21.090	0.134	24.511	0.057	28.262	0.020	29.637	0.013	126.157	0.000	39.280	0.001

(note: $p = 0.000$ indicates a value less than 0.0005)

Although, as summarised in Table 7.16, the ISO/BS models’ estimates for the individual trials of WP-G are statistically accurate (with $p > 0.05$); however, the overall fitness characteristics of these models are not good. The COMPASS model, on the other hand, is unable to estimate correct MSIs for the three (#10, #14 & #16) field trials. The linear and rotational accelerations PSDs for the field trial No.16 of WP-G [wherein SVH ($p=1.0$) is displaying much superior fitting than the SV model ($p=0.26$)] at the zones with maximum and minimum predicted MSIs are shown in Figure E.10. It can easily be gathered from this figure that the presence of low frequency lateral acceleration has caused the SVH-conflict model to estimate statistically better MSI than the SV-conflict model.

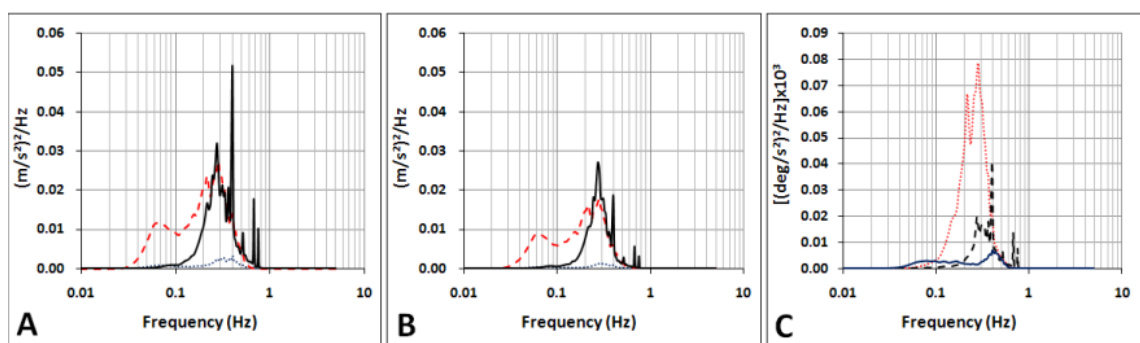


Figure E.10: WP-G trip-16: linear acceleration PSDs of A-max MSI zone-C, B-min MSI zone-O: dotted line longitudinal; dashed lateral; solid vertical. C-rotational acceleration PSDs: dotted line roll; dashed pitch; solid yaw.

E.3.8 Comparison for WP-H

As could be seen from the overall fitness statics summarised in Table E.9, the only model unable to estimate correct MSIs for the multiple (4) field trials of WP-H is the HFRI model. All other models are able to display good overall statistical fitness for the four full scale trials of this vessel. In relative terms, SVH-conflict with maximum overall *p-value* (0.437) is exhibiting performance better than all other models. COMPASS model is better than ISO/BS models, which in turn are superior to SV-conflict model.

Table E.9: χ^2 statistics and overall *p-value* for the (d.o.f =) 4 field trials of WP-H

SVH-Conflict		SV-Conflict		ISO/BS (TD)		ISO/BS (FD)		HFRI		COMPASS	
χ^2	<i>p</i>	χ^2	<i>p</i>	χ^2	<i>P</i>	χ^2	<i>P</i>	χ^2	<i>P</i>	χ^2	<i>p</i>
3.775	0.437	6.852	0.144	4.607	0.330	4.583	0.333	21.478	0.000	3.858	0.426

(note: *p* = 0.000 indicates a value less than 0.0005)

E.3.9 Comparison for MH-I

The overall fitness of the considered models for the multiple (4) full scale trials of MH-I are summarised in Table E.10. The linear and angular PSDs of the vessel during its first trip at the zones of maximum and minimum predicted MSIs are shown in Figure E.11.

Table E.10: χ^2 statistics and overall *p-value* for the (d.o.f =) 4 field trials of MH-I

SVH-Conflict		SV-Conflict		ISO/BS (TD)		ISO/BS (FD)		HFRI		COMPASS	
χ^2	<i>p</i>	χ^2	<i>p</i>	χ^2	<i>P</i>	χ^2	<i>P</i>	χ^2	<i>P</i>	χ^2	<i>p</i>
4.277	0.370	4.350	0.361	5.753	0.218	5.707	0.222	14.223	0.007	6.724	0.151

(note: *p* = 0.000 indicates a value less than 0.0005)

It is evident from Figure E.11 that the motion characteristics of MH-I are very similar to that of a typical monohull, as depicted in Figure 3.16. In the absence of significant lateral accelerations the SVH-conflict model is expected to display performance similar to SV-conflict model, which is the case here. Both of these physiological models are somewhat better than the descriptive (ISO/BS, HFRI, and

COMPASS) models. Once again, HFRI model is unable to display overall statistical fitness for the multiple trials of MH-I.

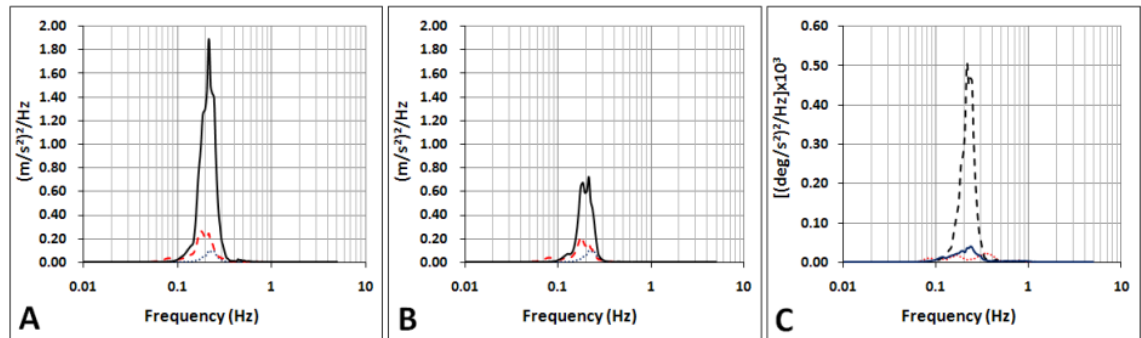


Figure E.11: MH-I trip-1: linear acceleration PSDs of A-max MSI zone-N, B-min MSI zone-J: dotted line longitudinal; dashed lateral; solid vertical. C-rotational acceleration PSDs: dotted line roll; dashed pitch; solid yaw.

E.3.10 Comparison for RHIB-J

A single field trial was carried out onboard the rigid hull inflatable boat (RHIB-J). It could be seen from Table 8.9 that all motion sickness models are able to predict statistically accurate MSI for this vessel.

E.3.11 Summary of Vessel-wise Comparison

Assuming similar fitness categories could be applied to the vessel-wise statistical comparison as used for the field trial-wise comparison in §E.2, we can summarise the overall fitness characteristics of the considered models. This summary is depicted in Figure E.12, which is showing the following:

- The two physiological models i.e. SVH-conflict and SV-conflict have the minimum of ‘no fit’ cases. In fact the only case pertains to the long journey field trials of MH-D, wherein the ‘habituation’ effects appear to play the detrimental role.
- HFRI model is unable to display overall fitness for the 80% of cases; hence it is the worst model.
- ISO/BS and COMPASS models are showing similar trends i.e. 50% ‘no fit’, 30% ‘good fit’ and 20% ‘very good fit’ cases.

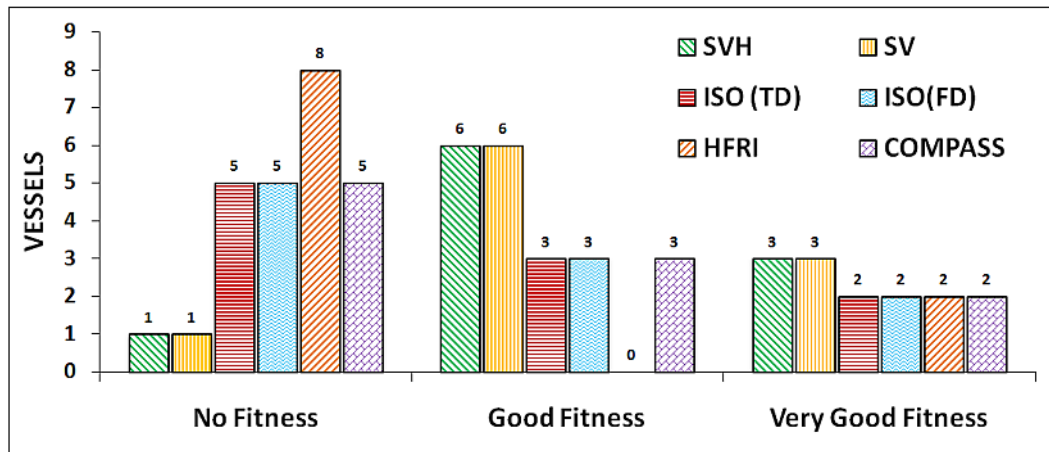


Figure E.12: Summary of vessel-based model fitness.

With 90% cases in either ‘good fit’ or ‘very good fit’ category, the SVH-conflict and SV-conflict models are exhibiting overall fitness characteristics much superior to the descriptive models.

E.4 Overall Comparison of the Motion Sickness Models

The physiological (SV & SVH-conflict) and descriptive (BS/ISO, HFRI, & COMPASS) motion sickness models have been compared on individual trial (§E.2) and ship-wise (§E.3 & §E.3.11) basis in this appendix. This comparison clearly indicates that the physiological models in general and the SVH-conflict in particular, are able to show good statistical fitness. However, it is important to verify this observation through an overarching statistical test for all field trials, irrespective of the vessel type. Therefore, the chi-square goodness-of-fit test statistics for the considered models (SVH, SV, ISO/BS, HFRI, & COMPASS) have been calculated using Equation(7.4). These statistics for the 67 field trials (trial No.7 of WP-G has been discarded) of the 10 vessels are summarised in Table E.11 below.

Table E.11: Overall fitness statistics of the considered model to 67 field trials of 10 vessels.

Model	d.o.f	χ^2	Overall p-value	Improvement
SVH	67	77.761	0.1734	Reference Chi
SV	67	81.513	0.1094	approx. 5%
ISO/BS (TD)	67	161.281	9.59E-10	approx. 200%

ISO/BS (FD)	67	163.281	5.23E-10	approx . 200%
HFRI	67	517.627	7.96E-71	approx . 670%
COMPASS	67	182.670	1.16E-12	approx . 230%

It can be seen from the above table that only the two physiological models (SVH and SV) are showing overall statistical fitness ($p > 0.05$) for the multiple (67) full scale trials of the 10 vessels. Whereas, all the considered descriptive models (ISO/BS, HFRI and COMPASS) are highly significant (*overall p-values* $\ll 0.05$), exhibiting the lack of statistical fitness. The ratio of the overall chi-square statistics for the SVH and SV conflict models is 0.954, which indicates an overall improvement of about 5%. This implies that the overall statistical fitness of SVH-conflict model is reasonably better than that of the SV-conflict model. However, further sea trials, in particular aboard contemporary high speed craft, would be necessary to conclude the superiority of SVH over SV-conflict model.

E.5 Summary

This appendix has presented detailed statistical comparisons of the motion sickness model developed in this work, with the existing physiologic (SV-conflict) and descriptive (BS/ISO, HFRI, & COMPASS) models. The overall statistical fitness of the new model to the multiple (67) field trials of several (10) vessels, is much superior to the existing regression-based models (Table E.11). Also, the SVH-conflict is also somewhat better ($p = 0.1734$; $\chi^2 = 77.76$; $d.o.f = 67$) than the SV-conflict model ($p = 0.1094$; $\chi^2 = 81.513$; $d.o.f = 67$).